THE SIMPSONITE PARAGENESIS

The Crystal Chemistry and Geochemistry of Extreme Ta Fractionation

by

T. Scott Ercit

A thesis
presented to the University of Manitoba
in partial fulfillment of the
requirements for the degree of
Ph.D.
in
Geological Sciences

Winnipeg, Manitoba, 1986

THE SIMPSONITE PARAGENESIS

THE CRYSTAL CHEMISTRY AND GEOCHEMISTRY OF EXTREME Ta FRACTIONATION

BY

T. SCOTT ERCIT

A thesis submitted to the Faculty of Graduate Studies of
the University of Manitoba in partial fulfillment of the requirements
of the degree of
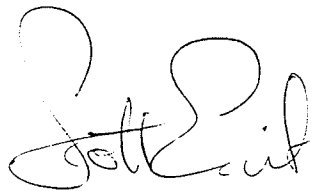
DOCTOR OF PHILOSOPHY

© 1986

I hereby declare that I am the sole author of this thesis. I authorize the University of Manitoba to lend this thesis to other institutions or individuals for the purpose of scholarly research.

T.S. Ercit

I further authorize the University of Manitoba to reproduce this thesis by photocopying or by other means, in total or in part, at the request of other institutions or individuals for the purpose of scholarly research.

T.S. Ercit

The University of Manitoba requires the signatures of all persons using or photocopying this thesis. Please sign below, and give address and date.

ABSTRACT

The simpsonite paragenesis, the suite of all oxide minerals associated with simpsonite, comprises 30% of all Ta-oxide minerals in a mere 9 occurrences, and shows some of the greatest degrees of Ta fractionation; thus from a mineralogic viewpoint, it is one of the most important parageneses of Ta-oxide minerals.

The members of the simpsonite paragenesis are: alumotantite, cassiterite, cesstibtantite, ferrotapiolite, manganocolumbite, manganotantalite, microlite, natrotantite, parabariomicrolite, plumbomicrolite, rankamaite, simpsonite, sosedkoite, stibiomicrolite, stibiotantalite, tantalowodginite and wodginite. Of these, three are new mineral species (parabariomicrolite, stibiomicrolite, and tantalowodginite), and alumotantite, cesstibtantite and natrotantite are redefined. The crystal structures of alumotantite, cesstibtantite and parabariomicrolite have been solved, and structure refinements have been done for microlite, natrotantite, simpsonite and partially-ordered wodginite. In addition to the study of the crystal chemistry of the simpsonite paragenesis, the crystal chemistry of wodginite-group minerals has been done, establishing (1) the ranges in chemistry for wodginite-group minerals, (2) two additional new species: titanowodginite and ferrowodginite, and (3) the style of cation disorder in wodginite.

Simpsonite localities are: the Tanco pegmatite, Canada; the Alto do Giz and Onça pegmatites, Brazil; the Bikita and Benson no. 3 pegmatites, Zimbabwe; the Leshaia pegmatite, USSR; the Tabba Tabba pegmatite, Australia;

Lake Kivu and the Manono pegmatite, Zaire. A study of the geochemistry of the paragenesis shows remarkable similarities amongst occurrences, despite their wide geographical separation. The oxide mineralogy of the Tanco pegmatite has been studied as background to the setting of the simpsonite paragenesis, and shows that enrichment in Ta coupled with depletion in common transition-metal cations (e.g. Mn,Fe,Sn) is necessary for formation of the simpsonite paragenesis. Crystallization histories of all occurrences of the simpsonite paragenesis can be explained on the basis of either increasing $\mu(Ta/\underline{A})$ or increasing acidity of the parental melt/fluid.

ACKNOWLEDGEMENTS

FREQUENTLY USED ABBREVIATIONS AND SYMBOLS

D: density
ED: energy-dispersive
|F|: structure factor
H: hardness
I: X-ray diffraction intensity
n: refractive index
O(eff): effective number of oxygen atoms for charge balance
p.f.u.: per formula unit

P: pressure
r: effective ionic radius
s: bond valence
SQI: spodumene-quartz intergrowth
T: temperature
VHN: Vickers hardness number
WD: wavelength-dispersive

□: site vacancy
δ: isomer shift (Mössbauer)
ΔE: quadrupole splitting "
Γ: line width "

∅: anion
μ: linear absorption coefficient (X-ray)
μ(Z): chemical potential of element Z

CONTENTS

FIGURES

- xiii -

Part 1

GENERAL INTRODUCTION

Chapter I

1.1 CRYSTAL CHEMISTRY OF TANTALUM AND NIOBIUM OXIDES

Tantalum and niobium are Group $\underline{Va}$ transition metal elements, separated by the lanthanide contraction in the periodic table, so Ta (180.948 a.m.u.) has approximately two times the mass of Nb (92.906 a.m.u.) associated with it. Otherwise, the two elements are extremely similar. Ions of both elements strongly prefer the +5 valence state, they have identical radii of 0.64 Å (Shannon, 1976), they have similar electronegativities (Nb: 1.6, Ta: 1.5) and ionization potentials (1st ionization potentials are Nb: 159, Ta: 182 kcal/m), both have d^0 configurations, and both show an extremely strong preference for octahedral coordination. Consequently, Ta-Nb isomorphism is quite widespread.

Although various exotica such as Ta- and Nb-chalcogenides are readily synthesized, Ta and Nb only form oxygen-based minerals. The slight differences in the electronegativities of Nb and Ta often play an important role in the crystal chemistry of Ta,Nb-oxides (Blasse, 1964). Nb-O bonding tends to be more covalent than Ta-O bonding, which accounts for the generally greater degrees of polyhedral distortion observed for Nb-oxides as compared to isomorphous Ta-oxides (Ercit, unpublished data), for greater stereochemical activity of lone-pair cations in Ta-oxides than Nb-oxides (Sleight & Jones, 1973), and for the significantly lower energy of charge transfer (oxygen-to-metal) bands for Nb-oxide compounds than Ta-oxide compounds (Phillips, 1970).

The radius ratios of Ta and Nb compared to O (both 0.47) are optimal for octahedral coordination of the cations. Until the solution of the natrotantite structure in this thesis, it was thought that all Ta and Nb in minerals was octahedrally coordinated; it is now known that [7]-coordination is also possible. Exclusive preference for the pentavalent state, coupled with octahedral and septahedral coordination results in Pauling bond strengths of 5/6 and 5/7 v.u. for both Ta-O and Nb-O bonds, allowing polymerization of both or either of $[MO_6]^{7-}$, $[MO_7]^{9-}$ (M=Ta,Nb) polyhedra. Ta- and Nb-oxide minerals tend to be highly polymerized (finite cluster$\rightarrow$framework structures).

Because of the high charge on Ta^{5+} and Nb^{5+}, few cations substitute for these elements in significant quantities in nature. The list of confirmed substituents is Ti^{4+}, W^{6+}, Sn^{4+}, Al^{3+}, Fe^{3+}, U^{4+}.

1.2 GEOCHEMISTRY OF TANTALUM AND NIOBIUM IN GRANITIC ROCKS

As a consequence of the strong crystal-chemical similarities of Ta and Nb, the two elements show a close geochemical relationship. On the basis of the lower electronegativity and ionization potential of Ta^{5+} compared to Nb^{5+}, Ta^{5+} might be expected to be concentrated into early generations of (Nb,Ta)-oxide minerals. However, this is not the case; during the main course of gabbro-to-granite differentiation, the Ta/(Ta+Nb) ratio is practically invariant, remaining close to 0.09, typical of upper-crustal rocks (Flörke et al., 1974). Late differentiates (silicic leucogranites, pegmatitic granites and granitic pegmatites) are the first to show significant changes in the Ta/(Ta+Nb) ratio, and contrary to predictions, it is Nb, not Ta, that is preferred by the early generations of oxide minerals. To

explain this phenomenon, most investigators have suggested that it is the complexing behaviour of Ta and Nb with respect to liquid fractionation, and transport in a (diffuse or exsolved) hydrous phase that are responsible (e.g. Parker & Fleischer, 1968; Hildreth, 1981; Černý et al., 1985). Specifically, Ta-fluoride complexes are generally stable to lower temperatures than Nb-fluoride complexes (Wang et al., 1982). If Ta and Nb exist as fluoride complexes in granitic melts or derived supercritical fluids, then the fractionation of Nb into early crystallization products may be due to its decreased stability in solution with decreasing temperature.

Concomitant with increasing Ta/(Ta+Nb) in late granitic differentiates is an increase in the absolute contents of Ta and Nb. The mean upper crustal abundances of Nb and Ta in calc-alkaline igneous rocks are 23 and 2 ppm, respectively (Flörke et al., 1974). These figures increase to approximately 150 and 40 ppm for Nb and Ta in silicic leucogranites and pegmatitic granites (Beus et al., 1968) and have been recorded to reach 500 ppm and 4500 ppm for Nb and Ta in rare-element granitic pegmatites (Černý et al., 1985). Increased rare-metal abundances in granites and pegmatites have conventionally been attributed to the effects of fractionation and volatile-related transport (e.g. as described above, a F-rich supercritical fluid in coexistence with the silicate melt) (Černý et al., 1985). However, the fluid inclusion studies of London (1986) show that (some) pegmatitic melts are homogeneous at the time of Ta,Nb-oxide mineral precipitation, and that the fluxing properties of an alkali borate component of the melt could play an important role in concentrating Ta, Nb and other rare elements in these systems. However, until the speciation of boron in hydrous alkali borosilicate liquids is better understood, it is difficult to elaborate further on its role in Ta,Nb accumulation.

Ta,Nb-oxide minerals in granites and granitic pegmatites are predictably more enriched in Nb than Ta. Ta-dominant species are restricted to highly-fractionated, complex-type rare-element granitic pegmatites. Exclusive of exsolution relationships, multiphase Ta,Nb-oxide mineral assemblages are uncommon to rare; usually only a single phase is present, or much less commonly, two phases coexist. The mineralogy of Ta,Nb-oxides in granitic pegmatites is complex; the reader is referred to Foord (1982) and Černý & Ercit (1985) for detailed reviews. To generalize on the rare-element class of granitic pegmatites, the columbite-group minerals (usually disordered to partially ordered) are the most common Ta,Nb-oxide minerals, excepting the REE-subtype, where REE,Nb,Ta-oxides (aeschynite, fergusonite, euxenite, polycrase) can be the most common species, and the lepidolite subtype with dominant microlite.

1.3 THE SIMPSONITE PARAGENESIS

Prior to the start of this thesis (1980), a maximum of three oxide mineral species were known to coexist with simpsonite (Alto do Giz, Brazil occurrence). The works of the present author and of A.V. Voloshin et al. (198-) have extended this number to ten; in general, simpsonite-bearing assemblages are the most diverse of all Ta-oxide mineral assemblages. Defining the simpsonite paragenesis as the suite of all oxide mineral species associated with simpsonite, 17 mineral species are members of this paragenesis, 16 of which are Ta-oxide minerals proper (30 % of all Ta-oxide minerals known to 1986). Ta-oxide mineral paragenesis.

With only one exception, all members of the simpsonite paragenesis have Ta>Nb, and generally average Ta/(Ta+Nb)>0.9, indicative of extreme Ta frac-

tionation. Furthermore, many of the members of the paragenesis are the Ta-richest examples of their species (e.g. manganotantalite from Bikita).

The purpose of this thesis is to examine the crystal chemistry and geochemistry of the simpsonite paragenesis. Part 3 of the thesis describes the crystal chemistry of the simpsonite paragenesis, and includes first descriptions of two new mineral species, and structure solutions/ refinements of six species. Part 4 describes the geochemistry of the various occurrences of the paragenesis, and elaborates on the origin of the paragenesis. A re-investigation of the oxide mineralogy of the Tanco pegmatite, Manitoba is provided (Chapter 18) as a background study to the setting of the simpsonite paragenesis.

Part 2

EXPERIMENTAL METHODS

Chapter II

MINERAL SEPARATION

Several of the oxide mineral samples from the Tanco pegmatite were of low grade and/or extremely fine-grained. Manual separation, both inefficient and highly subjective, was inadequate for these samples, and heavy liquid separation was used. Bulk samples were first crushed and ground by hand; to prevent overgrinding, samples were ground in small batches and regularly sieved (approximately three times per batch). Approximately 100 cm^3 of each sample was ground by this procedure, except for samples of extremely low grade, for which twice the normal quantity was ground.

Pure bromoform (CHBr$_3$) was used in the separations because of its high specific gravity (G=2.88 g/ml), its efficient recovery, and lesser toxicity than other available heavy liquids of comparable density (e.g. methylene iodide). Because of the low average grade and fine grain size, a centrifuge was used to improve settling rates. The test-tubes available (50 ml) required the use of small batches of sample in each separation. Samples were placed in bromoform-filled tubes, mixed and centrifuged for 3 minutes; the lighter separate was remixed with the upper parts of the bromoform to reduce drying and caking. After 5 more minutes of centrifuging, the hard cake of light gangue minerals (dominantly albite + quartz + muscovite) was removed with a spatula. This waste material was discarded in a large, water-filled beaker, and saved for later bromoform recovery.

After washing in acetone, the heavy separate was examined under a microscope. One or two of the largest grains plus a random sampling of 20 to 100 grains were used for microprobe mounts. Any remaining material was reground to a coarse powder and centrifuged to remove bits of silicate gangue still attached to the oxide minerals. After this second phase of separation, samples were relatively pure, except for occasional contamination by minor amounts of albite and micas contained as inclusions in some of the larger oxide mineral fragments. This fraction was used in X-ray powder diffractometry.

Upon completion of each work period, contents of the waste beaker were vigorously mixed and filtered, twice for their solid contents and a third time to separate reclaimed bromoform from water. With this treatment, bromoform recovery was found to be about 80% effective.

Chapter III

ELECTRON MICROPROBE ANALYSIS

In the first $1\frac{1}{2}$ years of study, only manual operation by wavelength-dispersive (WD) spectroscopy was possible. After this period, purchase of an energy-dispersive (ED) spectrometer made rapid quantitative analysis possible, superceding the wavelength-dispersive mode of operation. Most work on the simpsonite paragenesis proper was done by WD spectrometry; nearly all work on the oxide minerals of the Tanco pegmatite was done by ED spectrometry. All analyses presented here were done by the author, unless otherwise indicated.

3.1 WAVELENGTH-DISPERSIVE SPECTROMETRY

Analyses were done with a Materials Analysis Company electron microprobe, model MAC 5. Crystals used in analysis were thallium acid phthalate (TAP), pentaerythritol (PET) and lithium fluoride (LiF), which when considered with the operating ranges of the spectrometers of the MAC 5, allows for analysis of all elements from $\underline{Z}=11$ (Na) to $\underline{Z}=92$ (U).

Standard operating conditions were 20 kV and 40 nA (measured on ZnS), a 10 s collection time and a beam diameter of 1-3 μm. Non-standard conditions of operation were necessary for the analysis of some elements in order to improve counting statistics and to minimize high absorption. Data were reduced with the program EMPADR VII (Rucklidge & Gasparrini, 1969).

First attempts at analysis were met with failure: simpsonite analyses had oxide sums 3-4 % higher than ideal, and the recalculated formulae were grossly non-stoichiometric. The situation was eventually remedied by: (1) improved analyses of selected microprobe standards, (2) operation at low kV's, thereby lowering absorption, (3) improvement of the ZAF routine of EMPADR VII (Appendix A). The most significant improvement under point (1) was a re-analysis of the manganotantalite standard used in Ta and Mn analysis. Analysis of several wodginites, tantalites, tapiolites and simpsonites using the standard, and cross-analysis against synthetic calciotantite (Ta) and manganocolumbite (Mn,Nb) showed the analysis accompanying the standard (Nb=3.9, Ta=65.8, Mn=10.9, O=19.4 %) to be wrong. Assuming ideal $Mn(Ta,Nb)_2O_6$ stoichiometry, and repeatedly analyzing for Nb, which could be more precisely determined than Ta at the time, a new composition was determined for the standard (Nb=5.7, Ta=63.3, Mn=11.3, O=19.7 %). This composition has been used in all analyses involving the manganotantalite standard which are reported in this thesis, and has given consistently good results (both cation and oxide sums scatter about their ideal values) for a wide range of species and of compositions within species.

3.2   ENERGY-DISPERSIVE SPECTROMETRY

The MAC 5 used here is equipped with a KEVEX Micro-X 7000 analytical spectrometer. The ED spectrometer uses a Si(Li) detector with a Be window of 0.008 mm thickness, and a 1024 multichannel analyzer. Resolution is 144.6 eV for Mn Kα at 1000 Hz.

All ED analyses were done at an accelerating potential of 15 kV, chosen so as to minimize absorption, yet still provide good peak-to-background

ratios of all lines analyzed.   All sample currents were 5 nA, measured on fayalite or ZnS; however,   ilmenite samples were analyzed at 10 nA to improve dead-time correction.   Under standard conditions of operation, the beam diameter was 1-2 μm.

In all cases, the multichannel analyzer was set for operation at 10 eV/ channel, which made for a detection range of 1→10 keV. For this range, at least one α-line for all elements from Z=11 (Na) to Z=92 (U) was potentially available for analysis.

The data were reduced using KEVEX software based on the MAGIC V program (Colby, 1980).   Techniques for routine quantitative analysis of REE-free Ta-Nb-Sn-Ti oxide minerals using this software were developed by the author and are described in Appendix B.

3.3   STANDARDS

Standards used in analysis were chosen primarily to minimize ZAF correc- tions. Table 1 lists the standards used in analysis, and which elements of each standard were used in analyzing each mineral or mineral group.   Spec- tral lines used in analysis are given in Table 2.

<u>Table 1</u>: Standards Used in Electron Microprobe Analyses

Standard	Sample												
	WD	CT	TP	RU	CS	IL	PY	CB	PB	NT	SP	AL	ST
Mangano-tantalite	Ta Mn	Ta Mn	Ta Mn	Ta Mn	Ta Mn	Mn	Mn		Ta	Ta	Ta	Ta	Ta
CoNb$_2$O$_6$	Nb	Nb	Nb	Nb	Nb		Nb	Nb					Nb
Stibio-tantalite	(Nb)		(Nb)				Sb Bi	Nb Sb Bi	Nb	Nb	Nb	Nb	Sb Bi
Rutile	Ti	Ti	Ti	Ti	Ti		Ti						
Ilmenite	(Ti)	(Ti)	(Ti)	(Ti)	(Ti)	Ti							
Fayalite	Fe	Fe	Fe	Fe	Fe	Fe	Fe						
Cassiterite	Sn	Sn	Sn	Sn	Sn		Sn	Sn			Sn	Sn	
Scandium	Sc	Sc		Sc									
ZrO$_2$	Zr												
Microlite	Ca	Ca					Na Ca Ta Nb	Na Ca Ta	Na Ca	Na Ca			
PbTe							Pb	Pb			Pb		
Pollucite							Cs	Cs					
Orthoclase								K	K	K			
UO$_2$							U						
Ba$_2$NaNb$_5$O$_{15}$									Ba				
SrTiO$_3$									Sr				
Sphene											Ca	Fe Ti	
YAG											Al	Al	

<u>WD</u>: wodginite group minerals, <u>CT</u>: columbite-tantalite group minerals,
<u>TP</u>: tapiolite series minerals, <u>RU</u>: rutile, <u>CS</u>: cassiterite, <u>IL</u>: ilmenite,
<u>PY</u>: pyrochlore group minerals, <u>CB</u>: cesstibtantite, <u>PB</u>: parabariomicrolite,
<u>NT</u>: natrotantite, <u>SP</u>: simpsonite, <u>AL</u>: alumotantite, <u>ST</u>: stibiotantalite

- elements in parentheses mark infrequently used standards

Table 2: X-ray Spectral Lines Used in Analysis

Line	Elements
Kα	Na, Al, K, Ca, Sc, Ti, Mn, Fe, Sr
Lα	Zr, Nb, Sn, Sb, Cs, Ba, Ta (WDS)
Mα	Ta (EDS), Pb, Bi, U

3.4 PRECISION OF MICROPROBE ANALYSES

The program MAGIC V gives estimates of the standard deviation in the weight percentages of elements analyzed. All such estimates are based solely on count statistics for the line analyzed (of both the standard and the sample). The standard composition itself is assumed to be free of error, and other systematic errors are disregarded (e.g. errors in drift corrections). As such, the estimated precision of analysis tends to be optimistic.

The standard deviations in the oxide weights of the sample are simply propagated from those of the element weights; the standard deviations of atomic proportions were propagated using:

$$sQ^2 = \frac{\Sigma\{s(i)\cdot[A(i)-B(i)]/M(i)\}^2}{C^2} \tag{1}$$

(LeMaitre, 1982). The various terms of (1) are defined as follows:

$$A(i)=N_0\cdot a(i)\cdot w(i) \tag{2}$$

$$B(i)=Q\cdot b(i) \tag{3}$$

$$C=\Sigma x(i)\cdot b(i)/M(i) \tag{4}$$

N_0 is the number of anions used in normalization, $a(i)$ is the number of cations in the ith oxide formula, $b(i)$ is the number of anions in the ith oxide formula, $M(i)$ is the molecular weight of the ith oxide formula, $x(i)$ is the ith oxide weight, and $s(i)$ is the standard deviation of $x(i)$.

Q is the quantity of atoms for which the standard deviation is being estimated. If the standard deviation of a single cationic constituent is desired, Q is equal to the number of these cations per N_0 anions. If the standard deviation of a site sum or of the total cation sum is desired, then Q is equal to the sum of all cations in the site, or in the total.

The term $w(i)$ is a weighting factor. It has a value of 1 for all cations involved in Q, and of 0 for all other cations.

The quantity calculated in equation (1), sQ^2, is the variance of Q; note that traditionally, $2sQ$ is reported with microprobe analyses (Dunham & Wilkinson, 1978).

A sample calculation is shown in Table 3 for an ED analysis of synthetic manganocolumbite, analyzed under the standard conditions outlined earlier.

The procedure outlined here was applied to typical ED analyses of typical compositions of minerals most frequently encountered in this study. Results of the calculations for site sums and cation sums of these minerals are given in Table 4. The WD analyses of this study do not readily lend themselves to statistical analysis. Because of vacuum instability when WD analyses were done, and because of focussing errors (which can be large with microprobes with inclined stages), reliable estimates of the precision of WD analyses are possible only through repeated analysis. Because of the small proportion of WD data presented here, no such estimates were made; however, standard deviations reported for ED analyses should serve as approximate (lower?) estimates of the precision of WD analyses.

Table 3: Propagation of Errors for Atomic Proportions - $MnNb_2O_6$

Oxide	$\underline{x}$	$\underline{2s}$	Cations per 24(O)
MnO	20.98	0.42	3.97
Nb_2O_5	79.34	0.80	8.01
	100.32		11.98

$\underline{C} = \Sigma x(i) \cdot b(i)/M(i)$
$= 0.296 + 1.492 = \underline{1.788}$

		Calculation for Mn^{2-}			Calculation for Nb^{5+}		
Oxide	$\underline{M}$	$\underline{A}$	$\underline{B}$	$[s \cdot (A-B)/M]^2$	$\underline{A}$	$\underline{B}$	$[s \cdot (A-B)/M]^2$
MnO	70.94	24	3.97	.00352	0	8.01	.00056
Nb_2O_5	265.81	0	19.85	.00089	48	40.06	.00014

$sQ^2 \cdot C^2 = .00441$
$2sQ = .074$

$sQ^2 \cdot C^2 = .00070$
$2sQ = .030$

Calculation for Cation Sum

Oxide	$\underline{M}$	$\underline{A}$	$\underline{B}$	$[s \cdot (A-B)/M]^2$
MnO	70.94	24	11.98	.00127
Nb_2O_5	265.81	48	59.91	.00032

$sQ^2 \cdot C^2 = .00159$
$2sQ = .044$

Table 4: Precision of ED Analyses (Atomic Proportions)

Mineral or Group	N_0	A-site		B-site		C-site		Cation Sum	
		Q	2sQ	Q	2sQ	Q	2sQ	Q	2sQ
Columbite-tantalite	24	4	.08	8	.03			12	.04
Tapiolite	12	2	.04	4	.02			6	.02
Wodginite	32	4	.09	4	.05	8	.06	16	.05
Cassiterite	4							2	.001
Rutile	4							2	.003
Microlite	$6\frac{1}{2}$	1	.07	2	.01			3	.05

Chapter IV

ROUTINE X-RAY DIFFRACTION EXPERIMENTS

4.1 POWDER METHODS

Due to major equipment purchases during the course of this study, and to
the variable amounts of sample involved in the experiments, a number of
X-ray powder methods and instruments were used. Most work involved powder
diffractometers, but for small samples, film methods were used.

4.1.1 Diffractometry

Initially a Philips X-ray powder diffractometer (PW1050 goniometer) was
available, and about one-quarter to one-third of all diffractometry was
done with this instrument. Purchase of an automated Philips PW1710 X-ray
powder diffractometer in 1982 provided a means of rapid and precise data
collection, a great improvement over the older model. Most work done on
minerals of the simpsonite paragenesis was done with the old equipment;
most work done on Tanco pegmatite oxide minerals involved the newer instru-
ment.

Low detector efficiency of the PW1050 necessitated slow scanning speeds.
Each sample was run at a goniometer speed of $1/4°$ 2θ per minute, using a
chart speed of 10X; this provided diffractograms that could be read to
within $\pm0.02°$ 2θ. All data were measured from diffractograms. In all
experiments, Ni-filtered CuKα radiation was used.

The PW1710, with its improved detector and goniometer drive, and its automated recording system, could be operated at speeds of 0.01° 2θ/s, yet still produce data of better precision than the PW1050 (by a factor of 1.5 to 2). In all experiments, graphite-monochromated CuKα radiation was used. The PW1710 uses an "automatic divergence slit" - the divergence of the slit is coupled to the θ-2θ drive so as to irradiate a constant area of the sample over all 2θ. This has the effect of intensifying high angle diffractions (>40° 2θ CuKα) as compared to diffractometers with slits of fixed divergence.

Diffractograms were produced at a scale of 1/2° 2θ per cm; however, diffractograms were only used qualitatively. Gross peak intensities and positions were determined with the PW1710 hardware routine CSP. CSP is a continuous scanning routine which also searches for the tops of diffraction peaks. The position of each peak top is determined by fitting a parabola to seven datapoints about the most intense point of each peak. The routine provides the fitted peak-top position (in °2θ) and gross intensity (in counts) as printed output. These positions do not correspond exactly to $K\alpha_1$, $K\alpha_2$, or even $K\alpha$ peak positions in the range where the $K\alpha_1$ and $K\alpha_2$ components of a pattern are at best incompletely resolved (0°→65° 2θ for moderately to well-crystallized samples), and, consequently, are of little use in this form. For the data to be of immediate use, internal standards with regular and small diffraction spacings (e.g. every 10° 2θ) must be used. Often this is not practical; standards with only 3 to 5 strong diffractions in the range of investigation and of irregular 2θ distribution are more typical. Consequently, systematic errors in individual peak positions as large as ±0.02° 2θ (all with the same bias) can result from indiscriminant use of uncorrected data with CSP.

To correct this problem, a FORTRAN program, FIX, was written by the author to convert CSP-measured peak tops to true $CuK\alpha_1$ peak locations. FIX using the empirical equation

$$\Delta = A \cdot x^4 + B \cdot x^3 + C \cdot x^2$$

corrects the data, where $\underline{x}$ is the CSP-measured peak top position (in $°2\theta$, $CuK\alpha$) and Δ is the deviation of $\underline{x}$ from the expected $K\alpha_1$ position. The order of the polynomial and the values of the coefficients were determined with the SAS least-squares linear regression routine GLM, using hand-measured $K\alpha$ positions and CSP-measured top positions of peaks in CaF_2, BaF_2 and LiF as input. The results were:

$$A = -3.4(5) \times 10^{-8}$$
$$B = 3.9(3) \times 10^{-6}$$
$$C = -1.1(6) \times 10^{-4}$$

The use of FIX reduces systematic errors in positional data to $\pm 0.01°$ 2θ, and is intended for samples of moderate to excellent crystallinity. Use of the PW1710, with its data reduced by FIX, cut down on the time involved in unit cell refinement by a factor of 3 to 4 over the older diffractometer.

Internal standards used in data calibration were annealed CaF_2 ($\underline{a}$=5.46379(4) Å), annealed BaF_2 ($\underline{a}$=6.19896(8) Å), and LiF ($\underline{a}$=4.0280(1) Å). The unit cell parameters for the standards themselves were refined from resolved $K\alpha_1$ peak positions ($80° \rightarrow 130°$ 2θ), calibrated against NBS reference standard Si (batch 640a; $\underline{a}$=5.430825 Å). This not only resulted in extremely precise unit cell parameters for each standard, but also eliminated the possibility of systematic error due to the use of different stan-

dards in different samples. In a few early experiments, unannealed CaF_2 ($\underline{a}$=5.4620 Å) was used in place of the much more crystalline annealed material. Its use is not considered to have lowered the precision of the results because it was used only in experiments involving the less precise PW1050.

4.1.2 Film Methods

Conventional 114.6 mm diameter Debye-Scherrer and Gandolfi cameras (various makes) were used to obtain powder-type diffraction patterns of samples too small to examine by diffractometry. Most work was qualitative, but occasionally film methods were used in collecting data for unit cell refinement. In all cases Ni-filtered, $CuK\alpha$ radiation was used in the experiment.

Patterns were measured with a Supper precision film reader; with this instrument, the 2θ angles of sharp patterns can be determined to about $\pm0.06°$ 2θ. Intensities were estimated visually. Data used in unit cell refinement were corrected for "film shrinkage", but not for absorption.

4.1.3 Unit Cell Refinement

The 2θ angles measured by diffractometry and film methods were used for unit cell refinement by the CELREF program of Appleman & Evans (1973). Weights were assigned to each measurement according to the following scheme. Sharp peaks of normal width at half height were assigned weights of 1; all ragged, or abnormally broad peaks (indicating possible overlap of two or more reflections) were subjectively assigned weights of 0.1 to 0.5, depending upon the quality of the peak. Peaks which were obviously overlapped were omitted from refinement. When this weighting scheme was used,

the majority of peaks of unit weight were found to fit the refined model to within the level of precision expected from the method and equipment used.

4.2   SINGLE CRYSTAL METHODS

All photographic work with single crystals involved Gandolfi and precession cameras.   Gandolfi photography produces powder-like patterns; consequently, this method is described in the preceding section, and only precession photography is described here.

Charles Supper Co.,   Model 3000 and Model 3532 precession cameras were used in the study.   All precession photography used Mo Kα radiation, both Zr-filtered and unfiltered.   In all cases, a crystal-to-film distance of 60 mm and a precession angle of 25° were used.   High-speed Type 57 Polaroid film was used for setting photographs, while Kodak NS-5T and DEF-5, and CEX Reflex 25 X-ray film were used for the final photographs.

At least one crystal of all minerals of the simpsonite paragenesis which were large enough for precession photography were studied with this method.

Chapter V

CRYSTAL STRUCTURE ANALYSIS

5.1 SINGLE CRYSTAL METHODS

5.1.1 Data Collection

All intensity data collections were done by automatic single crystal diffractometry using graphite-monochromated MoKα X-radiation. All intensity datasets were collected with Syntex/Nicolet 4-circle diffractometers. One dataset collected on alumotantite was done with a $P2_1$ model at McMaster University; all other datasets were collected with an R3m model at the University of Manitoba.

Although X-ray methods are inferior to neutron diffraction experiments for strong X-ray absorbers like Ta, careful shaping of crystals coupled with the efficient empirical absorption correction routine used here provided high-quality data, resulting in refinements of good to excellent quality. Bond length standard deviations of 0.02 to 0.005 Å are typical of these refinements.

Data collection with Syntex/Nicolet diffractometers involves four preliminary steps: (1) mounting and optical alignment of the crystal, (2) centring, (3) automatic reflection indexing and (4) least-squares refinement of the orientation matrix and unit cell parameters. These steps are described below.

After shaping, each crystal was mounted on a glass rod with epoxy. Crystals were crudely oriented on the glass rod such that their two most-similar semi-axes were approximately in the collimator-detector plane (horizontal), thus minimizing differential absorption. Crystals were optically aligned on the goniometer head such that their centre of mass approximately coincided with the centre of rotation of the goniometer assembly. This condition was inspected by rotating the crystal about $\emptyset$ at selected settings of χ, and vice-versa.

After optical alignment, a random orientation rotation photograph of the crystal was taken. Using vertical and horizontal components of the spacings between equivalent diffractions in the photograph as input, the diffractometer computer centred on each diffraction, thereby refining 2θ, ω and χ ($\emptyset$ is held constant). A subset of 15 to 25 reflections was used in centring.

The indexing program uses the refined angles from the centring routine to set up a list of up to 60 axial vectors and 59 inter-vector angles. By either automatic selection of a vector set, or by user-intervention in the solution, unrefined values of $\underline{a}$, $\underline{b}$, $\underline{c}$, α, β and γ were chosen and the reflections indexed.

After indexing, the selected unit cell parameters and orientation matrix were refined using a least-squares procedure. When the starting cell was not appropriate (e.g. if a subcell, or pseudo-symmetric cell were chosen), a second program involving index and axis transformation was used to carry out both the desired transformation, and re-refinement of the orientation matrix and unit cell parameters.

All intensity datasets were collected using 96-step $2\theta:\theta$ scans, with scan ranges from 2-2.5° 2θ, plus the $\alpha_1-\alpha_2$ separation. Scanning speeds were variable and ranged from 4°/m for weak diffractions to 29.3°/m for intense diffractions, and were adjusted automatically. Two to three standard reflections were monitored every 46 reflections for changes in beam intensity or crystal orientation during data collection. All such changes were insignificant. In each case, all unique data to $\sin\theta/\lambda=0.7035$ were collected. Background corrections were made during data collection.

Subsequent to formal intensity data collection, additional data, for calculating an absorption correction, were collected on a subset of an average of 11 strong diffractions. These data were collected every 10° while rotating each reflection 360° about its diffraction vector (ψ). The ψ-scan collection used the same set of scan parameters (e.g. scan range, speed) as the main collection.

5.1.2   Data Reduction

Data reduction was carried out with the SHELXTL package of programs. The main dataset and ψ-scan dataset were first processed with the program XTAPE which rejects bad data (judged on bases of peak symmetry, centroid location in the scan range, and background balance), scales on the standard reflection data, and calculates L·p corrections.

The program XEMP was used for empirical absorption correction (spherical absorption + shape correction). The program uses the ψ-scan data as a calibration dataset for correction of absorption in the main dataset, after the approach of North et al. (1968). One of two approaches is taken in the correction, depending upon the shape of the crystal. If the crystal is plate-like, a thin plate model is used for the shape, and the product of

the linear absorption coefficient (μ) times the crystal thickness (t) is refined (plus two "edge effect" fudge factors). If the crystal is not plate-like, a pseudo-ellipsoid is used as the shape model in the calculations. The average value of $\mu \cdot R$ is input, where R is the crystal radius. The lengths and orientations of the semi-axes of the ellipsoid are refined, holding $<\mu R>$ constant. Although this approach works moderately well even with irregularly-shaped crystals, in practice it was found that a good absorption correction could only be had for strong absorbers like Ta-oxides if crystals were first shaped to be as close to ellipsoidal as possible.

5.1.3 Structure Refinement

Structure solution/refinement was carried out with the program X in the SHELXTL package, or with the program RFINE (Finger, 1969). Prior to acquisition of the four-circle diffractometer, RFINE was the only program locally available. One of the alumotantite datasets was refined with RFINE; all other datasets involved the use of X. Scattering curves for neutral atoms from Cromer & Mann (1968) and anomalous dispersion coefficients from Cromer & Liberman (1970) were used in both programs. Both use full-matrix least squares methods in refinement. The program X, however, uses a blocked cascade procedure if the number of refined parameters exceeds 103; this situation was not encountered in any of the refinements done here.

The R-indices used here are of the form:

$$R = \frac{\Sigma[|F(obs)|-|F(calc)|]}{\Sigma|F(obs)|} \qquad wR = \frac{\{\Sigma w[|F(obs)|-|F(calc)|]^2\}^{1/2}}{\{\Sigma w|F(obs)|^2\}^{1/2}}$$

All refinements involving RFINE and those involving X but with no extinction correction use w=1. Refinements involving the use of an extinction correction with the program X are limited to using $w=\sigma^{-2}|F(obs)|$.

The steps involved in a given solution or refinement are unique to each situation, thus are described in later chapters.

5.2   POWDER METHODS

Powder diffraction data were used only once in this study for structure refinement (Rietveld method).   Consequently, experimental methods used in Rietveld refinement are described in a later chapter (Natrotantite), in conjunction with the results of the study.

Chapter VI

HEATING EXPERIMENTS AND MINERAL SYNTHESES

Most heating experiments were done in air, in a Fisher Isotemp muffle furnace, Model 186. The temperature gauge was periodically calibrated by monitoring the melting point of NaCl (T(fusion)=801°C). Temperature regulation by the furnace is precise to ±20°C.

Some heatings were done in controlled atmospheres in furnaces designed and constructed by Dr. A.C. Turnock of the Department of Earth Sciences. Temperature control with these furnaces is precise to ±10°C.

All mineral syntheses were done anhydrously at atmospheric pressures. Starting products were reagent-grade pure oxide compounds. Starting powders were weighed to produce 0.3 to 0.5 g samples, and were mixed by light hand-grinding in acetone for 20 minutes. The mixed powders were then pressed into pellets under a 1500 psi load, to optimize reactivity. After 4 to 10 hours of heating, samples were removed from the furnace, reground, and subjected to continued heating. In most cases reactions were complete after 4 to 20 hours; however, some samples required repeated grinding and heating (up to 40 hours).

Ag-Pd foil was used as a substrate or sample holder for runs at 1000°C or lower. Runs at higher temperatures and some runs at 1000°C used Pt-foil, which was iron-soaked where necessary.

Specific run conditions for each set of experiments are outlined in later chapters.

Chapter VII

MISCELLANEOUS METHODS

7.1 DENSITY DETERMINATIONS

Densities were measured with a Roller-Smith Berman balance (model B).
Toluene was used as the immersion liquid. All samples used in the experi-
ments were between 15 and 25 mg in weight (air). Five repeated weighings
were done on each crystal fragment. In the case of the simpsonites, this
procedure was repeated on three separate days to test the reproducibility
of the results.

7.2 MINERAL OPTICS

Refractive index determinations were done using the Becke line method.
Cargille oils were used as immersion liquids in all cases. Studies at the
University of Manitoba involved uncalibrated liquids, due to the inavail-
ability of a suitable refractometer. Studies at the Royal Ontario Museum
(simpsonites) involved liquids calibrated using a two-circle goniometer and
the minimum deviation method (D. Sturman, pers. comm.).

All extinction measurements were made with a Charles Supper Co. spindle
stage using Cargille oils as an immersion medium. The program EXCALIBR
(Bloss, 1981) was used to calculate 2V from the extinction data.

Na-light was used in all studies, except where otherwise indicated.

Part 3

CRYSTAL CHEMISTRY OF THE SIMPSONITE PARAGENESIS

Chapter VIII

SIMPSONITE

8.1 INTRODUCTION

Simpsonite (Figure 1) was discovered in a granitic pegmatite at Tabba Tabba, Western Australia by Bowley (1939) [1]. Bowley enumerated the physical, optical and chemical properties of the mineral; X-ray crystallography was given in a companion paper by Taylor (1939 [2]. Eleven independent studies of simpsonite from eight additional localities (Table 5) have since been carried out: Guimarães (1944) [3], Pough (1945) [4], Kerr & Holmes (1945) [5], Macgregor (1946) [6], Sosedko & Denisov (1957) [7], Safiannikoff & van Wambeke (1961) [8], von Knorring & Hornung (1963) [9], Borisov & Belov (1963) [10], Černý et al. (1981) [11], Voloshin & Pakhomovskii (1983) [12], Sarp & Deferne (1983) [13]. (The numbers in brackets are assigned reference numbers to be referred to in later tables).

Table 5: Simpsonite Localities

---

1. Tabba Tabba, Western Australia.
2. Alto do Giz, Rio Grande do Norte, Brazil.
3. Onça Mine, Rio Grande do Norte, Brazil.
4. Mdara Mine, Bikita, Zimbabwe.
5. Leshaia, northern Kola Peninsula, USSR.
6. Benson Mine, Mtoko, Zimbabwe.
7. Mumba, Lake Kivu, Zaire.
8. Tanco Pegmatite, Bernic Lake, Manitoba, Canada.
9. Manono Mine, Shaba, Zaire.
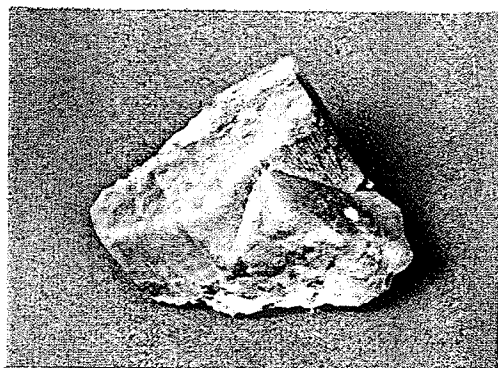
Figure 1: Simpsonite crystals from Alto do Giz, Brazil (from Pough, 1945).

Table 6: Published Simpsonite Analyses

	1	2	3	4	5	6	7	8	9
Al_2O_3	16.75	18.64	26.15	26.15	25.20	25.06	22.58	23.79	23.52
Fe_2O_3	0.14	0.48	---	---	---	---	0.11	0.0	0.88
TiO_2	---	---	---	---	0.02	0.05	---	0.10	0.08
SnO_2	2.00	1.19	---	---	0.10	0.47	0.42	1.45	1.31
Nb_2O_5	0.33	0.32	---	---	1.82	1.61	6.05	1.84	1.80
Ta_2O_5	72.31	71.48	73.45	73.80	71.54	67.92	60.01	69.46	66.20
Li_2O	---	---	---	---	---	---	---	---	---
Na_2O	1.16	0.68	---	---	---	---	0.39	0.35	0.46
K_2O	0.24	0.42	---	---	---	---	0.23	0.13	0.44
MgO	---	---	---	---	0.0	0.01	0.0	0.0	0.0
CaO	3.40	3.19	---	---	0.12	0.12	0.32	0.41	1.40
FeO	0.16	0.44	---	---	0.16	3.65	0.82	0.60	0.69
MnO	0.08	0.04	---	---	0.0	0.44	0.03	0.32	0.38
PbO	0.42	---	---	---	---	---	0.0	0.0	0.0
SiO_2	1.78	2.34	---	---	1.00	0.50	8.01	1.60	2.40
ZrO_2	---	---	---	---	---	---	0.05	0.0	0.0
P_2O_5	---	---	---	---	---	---	0.55	0.0	0.0
H_2O^+	1.35	1.39	---	---	---	---	0.19	0.12	0.62
H_2O^-	0.20	0.03	---	---	---	---	0.27	0.32	0.03
F	0.21	0.38	---	---	0.0	0.0	0.0	0.0	0.0
O=F	-0.09	-0.16	---	---	0.0	0.0	0.0	0.0	0.0
	100.44	100.86	99.60	99.95	99.96	99.83	100.03	100.49	100.21

1,2. Tabba Tabba. Contaminated with microlite, quartz, and mica. Bowley (1939).
3,4. Alto do Giz. Guimarães (1944).
5. Alto do Giz. Kerr & Holmes (1945).
6. Bikita. Kerr & Holmes (1945).
7-9. Bikita. Macgregor (1946).

"0.0": not detected
"---": not analyzed

Table 6 (cont.)

	10	11	12	13	14	15	16	17
Al_2O_3	24.47	23.00	23.30	22.70	23.30	24.00	23.89	20.89
Fe_2O_3	---	0.0	0.0	0.0	0.0	0.0	0.0	---
TiO_2	---	---	---	---	---	---	0.0	---
SnO_2	0.0	0.20	0.79	0.92	1.58	2.35	1.00	---
Nb_2O_5	3.65	0.96	1.02	1.82	1.14	1.52	2.10	---
Ta_2O_5	68.32	74.90	73.90	73.00	72.00	69.90	70.48	78.10
Li_2O	---	---	---	---	---	---	0.04	---
Na_2O	---	0.0	0.0	0.0	0.0	0.0	0.07	---
K_2O	---	0.0	0.0	0.0	0.0	0.0	0.16	---
MgO	---	---	---	---	---	---	---	---
CaO	---	0.0	0.0	0.0	0.0	0.02	0.00	---
FeO	---	---	---	---	---	---	---	---
MnO	---	---	---	---	---	---	---	---
PbO	---	0.0	0.0	0.0	0.0	0.0	---	---
SiO_2	---	---	---	---	---	---	0.85	---
ZrO_2	---	---	---	---	---	---	---	---
P_2O_5	---	---	---	---	---	---	---	---
H_2O^+	---	---	---	---	---	---	1.20	0.90
H_2O^-	---	---	---	---	---	---	0.06	---
F	---	---	---	---	---	---	0.25	---
O=F	---	---	---	---	---	---	-0.10	---
	96.44	99.06	99.01	98.44	98.02	97.79	100.06	98.89

10.   Leshaia. Sosedko & Denisov (1957).
11-15. Leshaia. Voloshin & Pakhomovskii (1983).
16.   Mtoko. von Knorring & Hornung (1963). Contaminated
        with mica.
17.   Manono. Sarp & Deferne (1983).

All published chemical data for simpsonite (Table 6) are variable; on the basis of these data the following ideal formulae for simpsonite have been proposed: $CaO \cdot 5Al_2O_3 \cdot 4Ta_2O_5 \cdot 2H_2O$ (Bowley, 1939), $Al_6Ta_4O_{19}$ (Guimarães, 1944; Kerr & Holmes, 1945), $Al_8Ta_6O_{27}$ (Macgregor, 1946), $AlTaO_4$ (Dana, 1944) and $Al_4Ta_3O_{13}(OH)$ (von Knorring & Hornung, 1963, and all subsequent studies).

A summary of all crystallographic data is given in Table 7. These data are more similar than the chemical data. Only Taylor's (1939) data differ from those of the other studies; however, re-interpretation of her data (Kerr & Holmes, 1945) shows that the $\underline{a}$ period that she reports is actually $\underline{d}(110)$. Subsequent recalculation of $\underline{a}$ gives results consistent with the other studies.

Published physical and optical properties are given in Table 8. The data are reasonably similar with only a few exceptions. An apparent change of optic sign reported for simpsonite from the Benson pegmatite (von Knorring & Hornung, 1963) was due to a misprint, and a positive optic sign reported by Bowley (1939) for simpsonite from Tabba Tabba was unsubstantiated by later studies (Macgregor, 1946; von Knorring & Hornung, 1963).

It is surprising that the structural, physical and optical properties of simpsonite are so similar in light of the apparent variability of the chemical data. Contamination, as shown for example by the presence of SiO_2, and considerable error in the chemical analyses, as shown by comparing analyses of samples from the same locality but analyzed by different laboratories, are certainly two sources for the variability. Unfortunately, few of the studies involved samples from a number of localities, thus the degree of true chemical variability cannot be assessed. A study of the

crystal chemistry of simpsonite was undertaken largely for this reason; samples from as many localities as possible were examined by modern mineralogical methods.

Table 7: Published Crystallographic Data for Simpsonite

Crystal System	a (Å)	c (Å)	Space Group	Reference
Hexagonal	6.2	4.5	P6/m	[2]
Hexagonal	7.377	4.514	----	[5]
Hexagonal	7.377	4.516	----	[7]
Hexagonal	7.38	4.51	P3	[10]
Hexagonal	7.39	4.50	----	[13]

Table 8: Published Physical and Optical Properties of Simpsonites

Locality	ω	ϵ	Optic Sign	D (g/cm^3)	H	Colour	Fluor-escence	Clea-vage	Ref.
Tabba Tabba	2.06		–	5.92	---	CL	---	none	[1]
Alto do Giz	2.045	2.005	–	6.77 to 6.81	7½	W to Y	B-W to Y	none	[4]
Onça	---	---	---	6.60 to 6.70	---	W to Y	B-W	none	[4]
Bikita	2.035	1.995	–	6.68 to 6.84	7½	Y	B-W	none	[6]
Leshaia	2.034	1.976	–	6.61	7	W to Y	Y-B	none	[7]
Mtoko	2.036	2.004	–	6.72	>7	W	B-W	none	[9]
Manono		2	–	---	---	Y	---	none	[13]

CL: colourless,   W: white,   Y: yellow,   B: blue

8.2   SAMPLES

Samples were obtained from all known simpsonite localities except Manono and Mtoko (see Table 5).   Except for the Leshaia sample, there was enough material for powder diffractometry and for physical property determination. For most localities only one sample was available, with the exception of Mumba and Tabba Tabba (2 samples each) and Alto do Giz (>20 samples). Samples and their sources are given in Table 9.

<p align="center">Table 9: Simpsonite Samples</p>

Sample	Locality	Source
F-8,9	Tanco	Dr. P. Černý
GSC-1	Mumba	Geological Survey of Canada (NMC 62089)
KO-1,2	Leshaia	Dr. A.V. Voloshin
L-12	Alto do Giz	Harvard University (97557A.1)
L-13	Bikita	Smithsonian Institute (NMNH 105760)
L-14	Mumba	" " (NMNH 136445)
L-15	Alto do Giz	" " (NMNH 104738)
L-16	Onça	" " (NMNH 104739)
L-17	Alto do Giz	" " (NMNH 105002)
L-18	Tabba Tabba	" " (NMNH 103440)
ROM-1	Alto do Giz	Royal Ontario Museum (M22607)
ROM-2	Tabba Tabba	" " " (M19325)
RVG series	Alto do Giz	Dr. R.V. Gaines
SMP series	Tanco	Collected by T.S. Ercit, Dr. P. Černý

8.3   PHYSICAL AND OPTICAL PROPERTIES

Physical and optical properties of simpsonites examined in this study are summarized in Table 10.

All simpsonites investigated range from yellow to white in colour. They do not fluoresce under long-wave ultraviolet light, but under short-wave ultraviolet light, they fluoresce blue-white to yellow (Alto do Giz only).

Table 10: Physical, Optical and Structural Properties of Simpsonites

Sample	Colour	ω	Optic Sign	D (g/cm^3)	H	a (Å)	c (Å)
L-12	yellow	2.040	–	6.73(5)	$7\frac{1}{2}$	7.385	4.516
L-13	yellow	2.030	–	6.59(3)	$7\frac{1}{2}$	7.387	4.515
L-14	yellow	2.035	–	----	$7\frac{1}{2}$	7.387	4.515
L-15	yellow	2.035	–	6.82(4)	$7\frac{1}{2}$	7.385	4.516
L-16	yellow	2.035	–	6.76(5)	$7\frac{1}{2}$	7.385	4.515
L-17	yellow	2.040	–	6.79(2)	$7\frac{1}{2}$	7.386	4.516
L-18	white	2.025	–	6.31(1)	$7\frac{1}{2}$	---	---
ROM-2	white	2.025	–	----	$7\frac{1}{2}$	7.387	4.515
SMP-2	white	2.025	–	6.68(1)	$7\frac{1}{2}$	7.387	4.515

All refractive index determinations are ±.005
For unit cell parameters, σ=0.001 Å

All have a prominent blue-white cathodoluminescence under the electron beam. Powdered simpsonite is always white. In thin section, simpsonite is colourless; all simpsonite is optically negative. As a test of variability in terms of optical properties, ω's were measured for 10 simpsonites; ω shows little variability: 2.025 to 2.040 (±.005).

The simpsonites have no cleavage, but have a conchoidal fracture. All have a Moh's hardness of $7\frac{1}{2}$. Their densities range from 6.31 to 6.82 g/cm^3; however, macroscopically unaltered material has a tighter range of 6.68 to 6.82 g/cm^3.

Simpsonite shows subhedral to euhedral crystal development. Euhedral crystals most frequently consist of a hexagonal prism plus basal pinacoid; however, more complex forms have been found (Pough, 1945). Prism faces are always striated parallel to Z and frequently show parallel growth features.

<u>8.4</u>   <u>CHEMISTRY</u>

Electron microprobe analyses of the simpsonites are given in Table 11. The simpsonites are all similar in chemistry and stoichiometry, in contrast with the results of the earlier studies. Al and Ta are the dominant cationic constituents of simpsonite, Nb can be a major constituent(to 8.6 oxide %) and Sn, a minor constituent (to 1.9 oxide %); Ti (to 0.02 oxide %) and Fe (to 0.03 oxide %) are at most only present in trace quantities. Ca, Mn and Si were not detected.

On the basis of charge and size considerations, Fe should reside at the Al-site, and Nb, at the Ta-site. The ratio of (Al+Fe):(Ta+Nb) is close to 4:3 in all samples; the apparent large variations indicated by earlier studies must have been due to problems in wet chemical analysis and to contamination. The cation sums are tightly distributed about 7 (mean cation sum=6.997, mean absolute deviation=0.011) when formulae are calculated on a basis of 27 negative charges per formula unit. This suggests that the fourteenth anion in the formula unit is exclusively monovalent. The ideal formula for simpsonite is thus $Al_4Ta_3O_{13}(OH)$. Using this formula and the measured densities (Table 10), $\underline{Z}$, the number of formula units per unit cell is 1.

The behaviour of Sn and Ti is unknown and is difficult to assess given the minor amounts that tend to occur in simpsonites. Two possibilities exist: either Sn and Ti are disordered over the Al- and Ta-sites, or they are ordered at the Ta-site, and charge balance is achieved by substitution of hydroxyl at the O-sites. The lack of correlation between the cation sum per 13(O)+1(OH) and Sn,Ti contents, and the more ideal sites sums for the disordered model (mean ΣAl-site:ΣTa-site = 3.992:3.005) versus the ordered

<u>Table 11</u>: Electron Microprobe Analyses of Simpsonites

	F-8	F-9	L-12	L-13	L-14	L-15	L-16	L-17	L-18
Al_2O_3	23.0	22.9	23.3	23.3	24.3	22.8	23.0	22.8	22.6
Fe_2O_3	0.0	0.0	0.0	0.0	0.01	0.0	0.03	0.0	0.0
TiO_2	0.0	0.0	0.01	0.01	0.0	0.0	0.02	0.02	0.03
SnO_2	1.5	0.9	0.05	1.0	0.9	0.0	0.1	0.02	1.9
Nb_2O_5	0.9	0.8	1.1	0.0	8.6	0.0	0.2	0.7	1.0
Ta_2O_5	71.9	72.6	73.3	74.9	64.6	76.4	74.8	74.6	72.4
H_2O	1.0	1.0	1.0	1.0	1.1	1.0	1.0	1.0	1.0
	98.3	98.2	98.8	100.2	99.5	100.2	99.2	99.1	98.9

<center>Cations per 13(O)+1(OH)</center>

	F-8	F-9	L-12	L-13	L-14	L-15	L-16	L-17	L-18
Al^{3+}	3.99	3.99	4.02	3.99	3.97	3.93	3.98	3.95	3.92
Fe^{3+}	0.00	0.00	0.00	0.00	0.00	0.00	0.00	0.00	0.00
Ti^{4+}	0.00	0.00	0.00	0.00	0.00	0.00	0.00	0.00	0.00
Sn^{4+}	0.09	0.05	0.07	0.06	0.05	0.00	0.01	0.00	0.11
Nb^{5+}	0.06	0.06	0.00	0.00	0.54	0.00	0.02	0.05	0.06
Ta^{5+}	2.87	2.91	2.91	2.96	2.44	3.04	2.99	2.98	2.89
	7.01	7.00	7.01	7.01	7.00	6.97	7.00	6.98	6.99

All analyses by WDS. All H_2O calculated for 1(OH) per unit cell.

Sample L-15 was analyzed against YAG (Al) and manganotantalite (Ta).
All other samples were analyzed against L-15 (Al,Ta) assuming ideal
$Al_4Ta_3O_{13}(OH)$ stoichiometry for simpsonite L-15.

one (mean ΣAl-site:ΣTa-site = 3.971:3.026) suggest that the disordered model is to be preferred.

A part of the infrared absorption spectrum for simpsonite L-15, covering the range 3000-3800 cm^{-1} is given in Figure 2. The spectrum is characterized by a strong absorption at the low frequency of 3300 cm^{-1}, indicative of the presence of substantial hydroxyl in the structure. The low frequency of the O-H stretch further indicates that strong hydrogen bonds exist, which makes the hydroxyl site in simpsonite an extremely unlikely locus for (OH)$\rightarrow$F substitution. To this effect, F has only been reported in samples contaminated with microlite and micas (muscovite and lepidolite). A fair correlation (R=+73%) exists between F and $Na_2O+K_2O+Li_2O+CaO$ contents (= alkali plus alkaline earth parts of the F-bearing contaminants); it is probable that most, if not all F is contained in the typically F-rich contaminant phases.
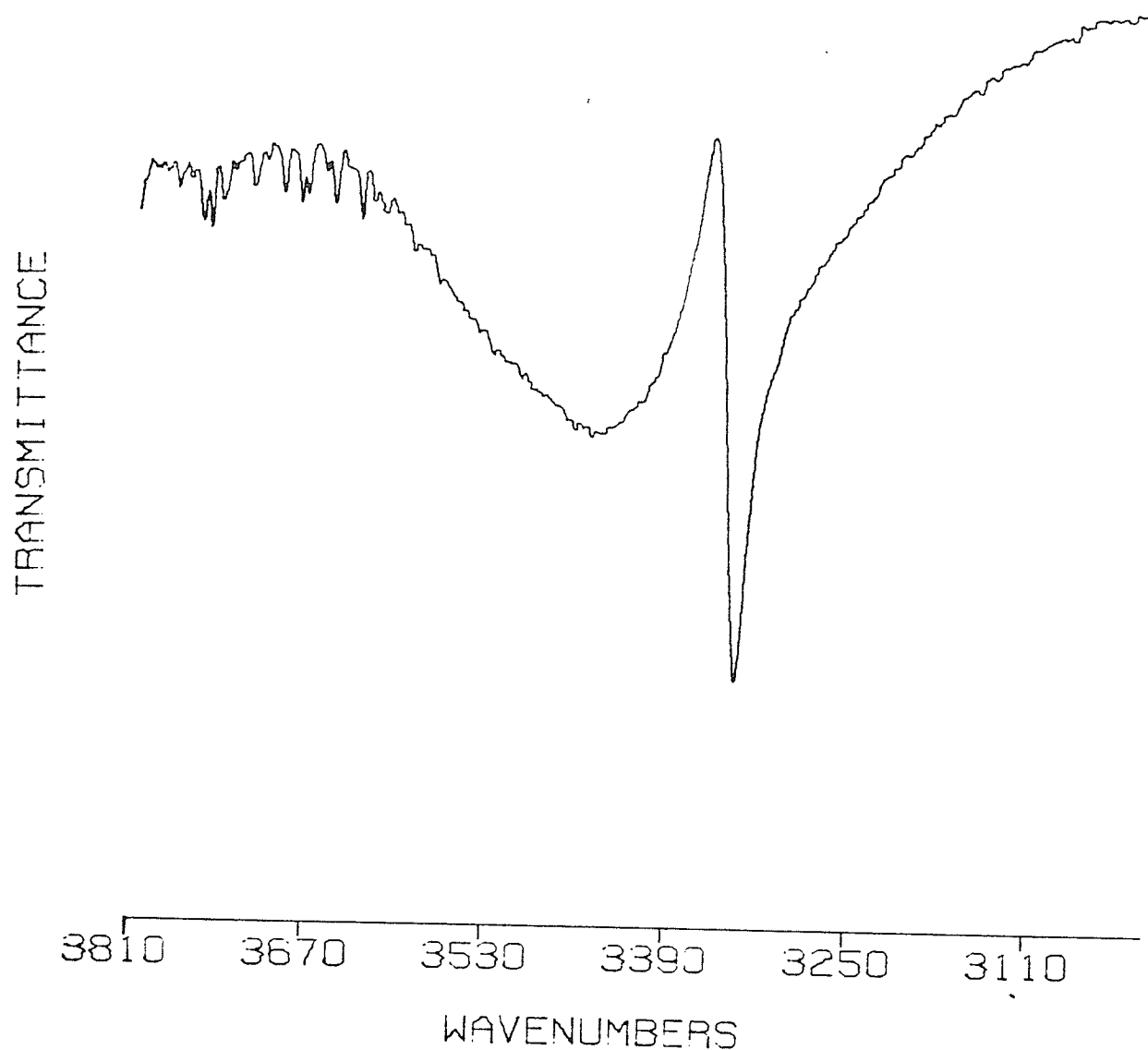
Figure 2: Simpsonite L-15: Infrared absorption spectrum in the O-H stretching region. The sharp absorption at 3300 cm^{-1} is assigned to O-H stretching in simpsonite. The broad absorption at 3450 cm^{-1} is due to adsorbed water in the pellet.

8.5   CRYSTAL STRUCTURE

8.5.1   X-ray Crystallography

X-ray powder diffraction data for all simpsonites are identical, as are
the cell parameters (Table 10).   Consequently, powder diffraction data for
sample L-17 (Table 12) are representative of all simpsonites. The diffrac-
tion pattern consists of groups of strong diffractions which regularly
repeat themselves with increasing 2θ.   This repetative character implies
that simpsonite possesses a layer structure.

Precession photographs were taken for three simpsonites: L-13, L-15 and
L-17.   The photographs show $P\bar{3}$ diffraction symmetry, giving $P3$ or $P\bar{3}$ as
possible space groups.   The diffraction pattern has a strong pseudo-$P6/m$
diffraction symmetry which accounts for the earlier assignment of $P6/m$ as
the space group (Taylor, 1939).   (Note: a reconstruction of Taylor's data
by Kerr & Holmes, 1945 shows the true 3-fold character of the unique axis,
although the authors did not recognize it).

8.5.2   Structure Refinement

The crystal structure of simpsonite was solved by Borisov & Belov
(1962).   Their work confirmed $Al_4Ta_3O_{13}(OH)$ stoichiometry and $P\bar{3}$ diffrac-
tion symmetry for the mineral as well as correctly determining the atom
positions (Table 13).   Because their model was refined from projections
using photographic data, resulting in high R-indices ($\bar{R}=15.2\%$), a structure
refinement was required.

Sample L-15 was chosen for the refinement because it most closely
approaches ideal simpsonite in cation chemistry and was wanted as a micro-
probe standard for the other simpsonites.

Table 12: Powder Diffraction Data for Simpsonite L-17

d(obs)	I	d(calc)	hkl	d(obs)	I	d(calc)	hkl
6.40	13	6.40	10.0	1.362	6	1.362	20.3
4.52	19	4.52	00.1	1.333	10	1.334	41.1
3.69	62	3.69	11.0	1.305	2	1.305	40.2
		3.69	10.1	1.278	7	1.278	21.3
3.196	30	3.198	20.0	1.230	10	1.230	32.2
2.859	67	2.859	11.1	1.209	3	1.209	42.0
2.609	37	2.610	20.1	1.187	9	1.188	33.1
2.417	40	2.418	21.0			1.187	41.2
2.257	6	2.258	00.2	1.168	3	1.168	42.1
2.131	59	2.132	30.0	1.148	9	1.148	31.3
		2.131	21.1	1.129	2	1.129	00.4
1.926	25	1.926	11.2	1.113	2	1.113	51.1
		1.926	30.1			1.113	50.2
1.844	10	1.844	20.2	1.096	2	1.096	40.3
1.773	16	1.774	31.0	1.079	2	1.080	11.4
1.651	100	1.651	31.1	1.066	10	1.066	60.0
1.599	3	1.599	40.0			1.066	42.2
1.550	2	1.550	30.2	1.051	11	1.051	32.3
1.507	12	1.507	40.1	1.038	7	1.038	60.1
1.468	5	1.467	32.0	1.024	10	1.024	52.0
1.395	54	1.396	41.0			1.024	43.1
		1.396	32.1			1.024	51.2

Philips powder diffractometer, Ni-filtered CuKα radiation.
LiF internal standard.

A crystal fragment 0.12 X 0.14 X 0.10 mm was used for data collection. A set of 25 strong diffractions was collected by the diffractometer for calculation of the cell parameters which were: a=7.381(1) and c=4.516(1) Å, in excellent agreement with powder data for this sample (Table 10). Data were collected over two asymmetric units, empirically corrected for absorption (μ=385 cm^{-1}, Mo Kα) by approximating the crystal shape to an ellipsoid and were merged to give 867 unique reflections. The criterion, I>3σ was used to decide whether or not a reflection was observed; this resulted in the suppression of only 1 reflection from the dataset. E-statistics for the total dataset strongly supported an asymmetric model ($<E^2-1>$=0.735 for reflections with $\sin(\theta)/\lambda$>0.1), so refinement was carried out in P3.

Patterson synthesis indicated only 1 heavy atom site (Ta) at x=0.113, y=0.394. These parameters were used to refine the Ta position; the origin was fixed by setting z(Ta)=0. At this stage, a difference Fourier synthesis showed the two Al positions. Refinement of the cation positions and isotropic temperature factors resulted in an R-index of 9.5%, and a subsequent difference Fourier map gave the six anion sites. Refinement of all atom positions and anisotropic temperature factors, and of an extinction correction, resulted in final values of R=5.3%, wR=6.9% for this fully-ordered model. An attempt to disorder Ta and Al resulted in divergence, showing that the assumption of full cation order was valid . Observed and calculated structure factors are given in Appendix G. Final positional and temperature parameters for the atoms are given in Table 13 and Table 14. Bond lengths and angles are given in Table 15.

Table 13: Positional Parameters for Simpsonite

		This Study			Borisov & Belov (1962)	
Atom	x	y	z	x	y	z
Ta	0.1118(1)	0.3910(1)	0	0.112	0.391	0.000
Al(1)	0.423(2)	0.303(2)	0.496(2)	0.423	0.297	0.500
Al(2)	0	0	0.499(4)	0	0	0.500
O1	0.246(5)	0.062(4)	0.730(7)	0.237	0.067	0.720
O2	0.392(5)	0.472(5)	0.777(8)	0.376	0.474	0.765
O3	0.192(4)	0.238(5)	0.274(7)	0.183	0.227	0.274
O4	0.482(5)	0.111(5)	0.265(7)	0.481	0.113	0.266
O5	1/3	2/3	0.194(9)	1/3	2/3	0.204
O6	2/3	1/3	0.691(10)	2/3	1/3	0.703

Table 14: Thermal Parameters (Å^2) for Simpsonite

Atom	U_{11}	U_{22}	U_{33}	U_{12}	U_{13}	U_{23}	$U(eq)$
Ta	85(5)	88(5)	119(5)	42(4)	0(3)	3(3)	98(4)
Al(1)	120(34)	149(37)	139(34)	59(26)	14(23)	7(28)	139(28)
Al(2)	87(32)	87(32)	159(66)	0	0	0	131(30)
O1	77(100)	125(102)	148(103)	-2(81)	20(65)	7(76)	140(80)
O2	261(139)	464(213)	154(122)	295(147)	-55(88)	-70(93)	242(137)
O3	231(123)	146(101)	111(101)	102(103)	-67(85)	-24(73)	159(91)
O4	112(110)	239(125)	210(121)	-3(115)	63(102)	46(95)	227(99)
O5	95(104)	95(104)	53(148)	48(52)	0	0	81(85)
O6	354(170)	354(170)	98(171)	0	0	177(85)	269(127)

All U's are x 10^4

Table 15: Selected Bond Lengths (Å) and Angles (°) in Simpsonite

Ta Octahedron

Ta-O1b:	1.87(3)	O1b-Ta-O2a:	96(1)	O2a-Ta-O5a:	75(1)
-O2a:	2.10(4)	-O2b:	91(1)	O2b-Ta-O4b:	87(1)
-O2b:	2.00(4)	-O3a:	103(1)	-O5a:	77(1)
-O3a:	1.96(4)	-O4b:	97(1)	O3a-Ta-O4b:	93(1)
-O4b:	1.98(3)	O2a-Ta-O2b:	92(2)	-O5a:	89(1)
-O5a:	2.06(2)	-O3a:	86(1)	O4b-Ta-O5a:	92(1)

\<Ta-O>:   2.00   \<O-Ta-O>: 89.8

Al(1) Octahedron

Al(1)-O1a:	1.91(3)	O1a-Al(1)-O2a:	89(2)	O2a-Al(1)-O6a:	92(2)
-O2a:	1.88(4)	-O3a:	85(2)	O3a-Al(1)-O4b:	92(2)
-O3a:	1.83(3)	-O4b:	85(2)	-O4c:	100(2)
-O4b:	1.97(4)	-O6a:	91(1)	O4b-Al(1)-O4c:	87(2)
-O4c:	1.87(3)	O2a-Al(1)-O3a:	98(2)	-O6a:	78(2)
-O6a:	1.91(3)	-O4c:	97(2)	O4c-Al(1)-O6a:	81(2)

\<Al(1)-O>:   1.90   \<O-Al(1)-O>: 89.6

Al(2) Octahedron

Al(2)-O1 x3:	1.94(3)	O1-Al(2)-O1 x3:	94(1)
-O3 x3:	1.91(3)	-O3 x3:	88(2)
		-O3 x3:	84(1)
		O3-Al(2)-O3 x3:	94(1)

\<Al(2)-O>:   1.93   \<O-Al(2)-O>: 90.0

Equivalent Positions

a: x, y, z   b: -y, x-y, z   c: y-x, -x, z

8.5.3   Description of the Structure

The gross structural details (Figure 3 and Table 13) are the same as those reported by Borisov and Belov (1962).   Ta and Al occur in octahedral interstices in an approximately hexagonal closest-packing of oxygen atoms. All Ta atoms occupy one layer in the packing and all Al atoms, adjacent layers.   Each Ta octahedron shares two edges with adjacent octahedra forming dense $[Ta_3O_{13}]^{11-}$ trimers.   Al occupies interstices which, in projection, correspond to unoccupied octahedra of the Ta layer.   As such, the Al-layer consists of a sheet of Al octahedra,   each octahedron sharing three edges with adjacent Al octahedra.   The inter-relationship of the Al and Ta layers is such that they connect via corner-sharing of their polyhedra.

Details of the structure are illustrated in Figure 4.   All polyhedra show features in good agreement with Pauling's rules.   The shared edges of each polyhedron are shorter than the unshared ones.   The Al(1) polyhedron has three shared and nine unshared edges.   The shared edges are not symmetrically disposed about the polyhedron, so cation-cation repulsion displaces the Al(1) cation toward the side of the polyhedron with the fewest shared edges.   On the other hand,   the Al(2) polyhedron has three shared edges symmetrically disposed about the polyhedron (threefold symmetry), resulting in balanced repulsive forces;   consequently, Al(2) sits at the centre of its polyhedron.   The Ta polyhedron has two adjacent shared edges; Ta-Ta repulsion across the shared edges displaces the Ta cation well toward the opposing corner of the polyhedron.

Empirical bond valences are given in Table 16. All bond valence sums to the cations and anions approach their ideal values closely, except for O6 and, to a lesser degree, O4.   The sum at O6 (1.50 v.u.) implies that much,
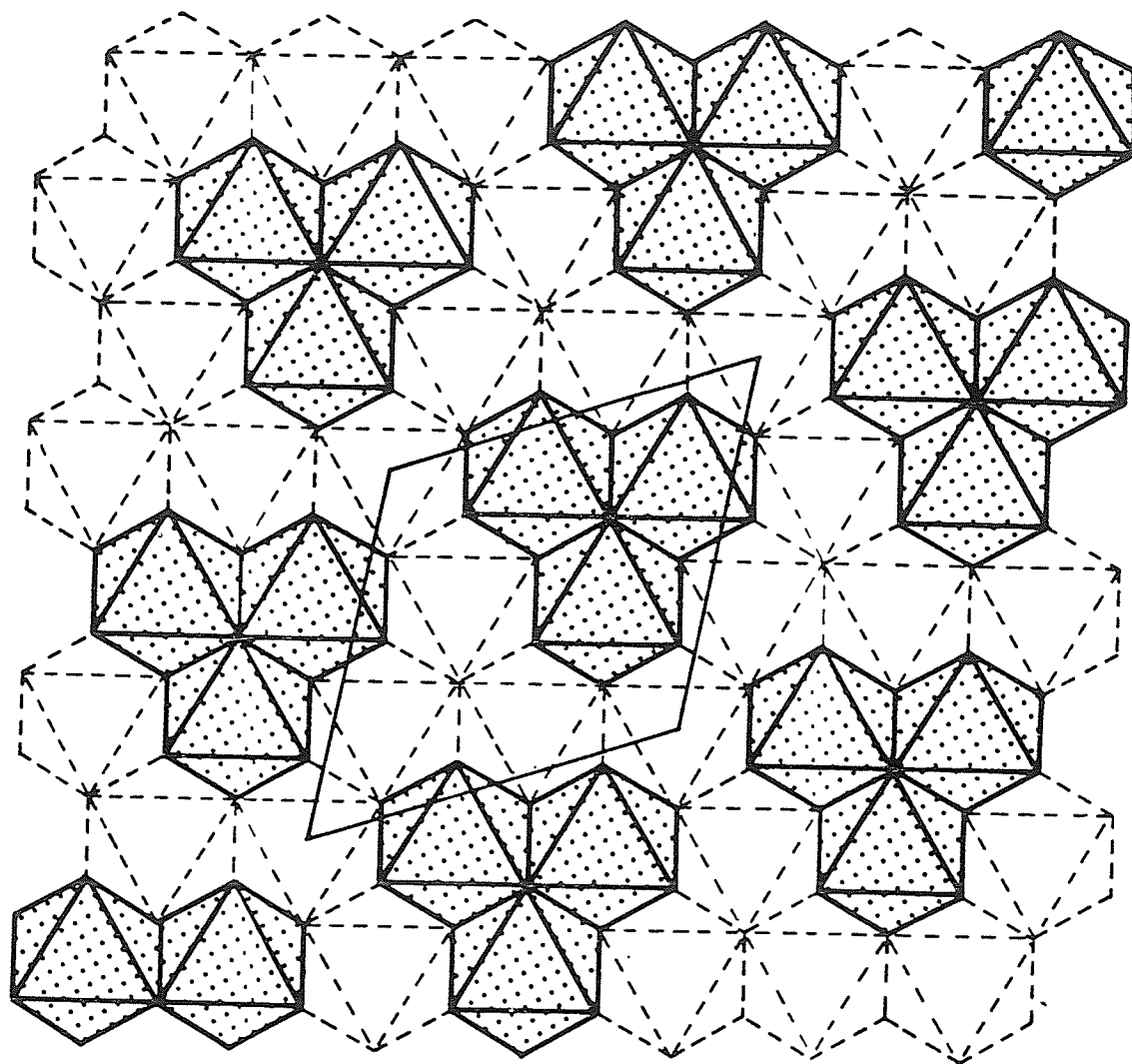
Figure 3: The ideal simpsonite structure as projected along Z. Solid lines represent polyhedra of one level, broken lines, those of adjacent levels. Ta polyhedra are shaded, Al polyhedra, unshaded. One unit cell is two layers of polyhedra deep; the outline of one unit cell is shown in fine rule.
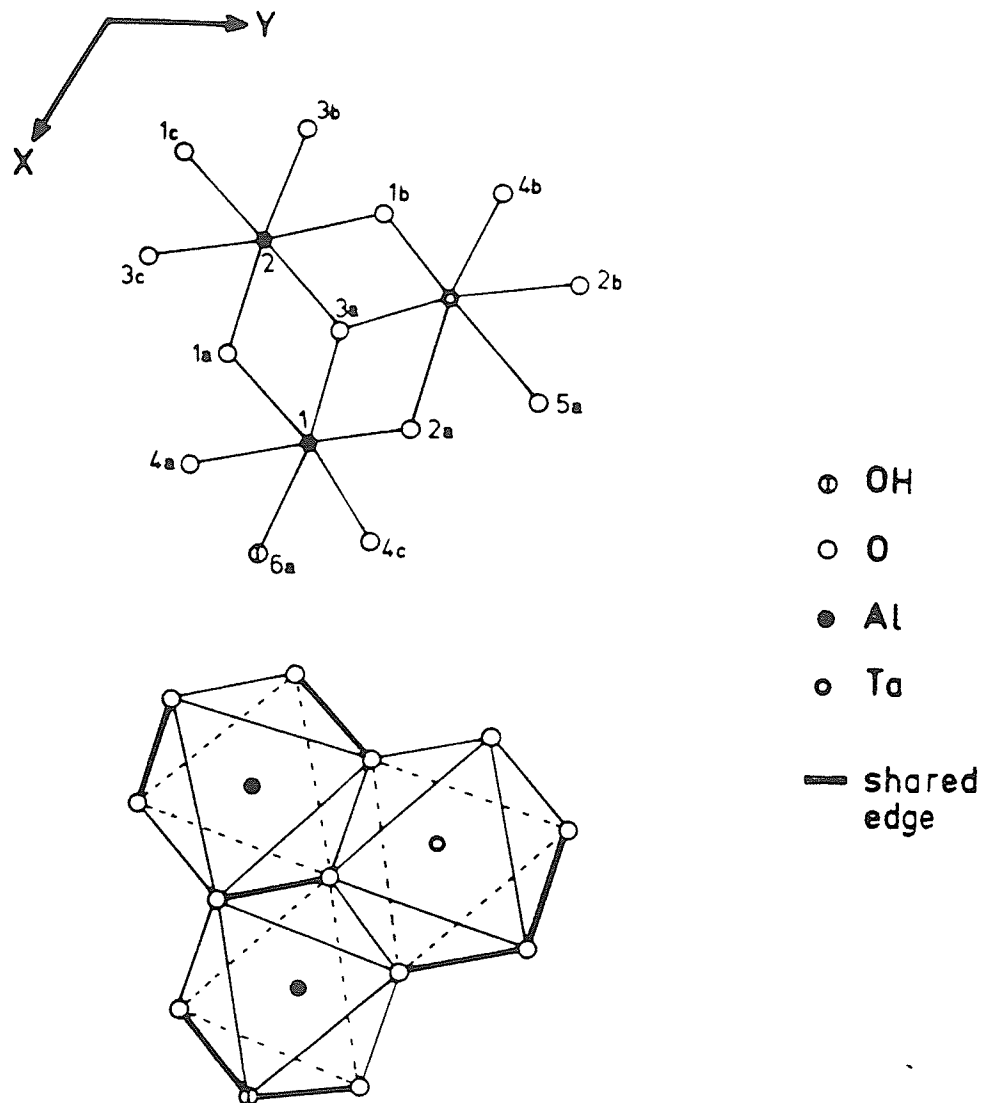
Figure 4: Coordination polyhedra in simpsonite. See Table 15 for the coding of the oxygen atoms.

if not all, of the hydroxyl is located at this position in the structure. A bond valence of 2-1.50 = 0.50 v.u. is assigned to the O-H bond, which corresponds to a bond length of 1.19 Å. The low bond valence sum (1.81 v.u.) to nearby O4 suggests that hydrogen bonding between the proposed H atom and O4 exists, which explains why the bond valence sum to O6 is higher than ideal for an oxygen atom of an OH group (i.e. 1).

Because O6 marks the common corner of three edge-sharing Al(1) octahedra, the H atom bonded to it must lie above or below the plane of Al octahedra, but not within it. Furthermore, because O6 lies on a triad axis, the O-H bond must be perpendicular to this plane. Whether the H atom were to lie above or below O6, the OH bond would protrude into a tetrahedral interstice (Figure 5). The lower tetrahedron is bound by three shared, and one unshared face between three symmetrically equivalent O4 atoms and O6. For this location, the calculated O6-H distance of 1.19 Å gives an O4-H distance of 1.71 Å. Each O4-H bond would have 0.23 v.u. associated with it, resulting in a bond valence sum of 1.20 v.u. at the proposed H atom position and of 2.05 v.u. at O4. The upper tetrahedral interstice has no shared faces between its bounding anions (O6 and 3-O4's) – a much more favourable location for the H atom than in the first model. Here the 1.19 Å O6-H distance gives an O4-H separation of 2.08 Å. Each O4-H bond would have 0.15 v.u. associated with it, resulting in a sum of 0.96 v.u. to the proposed H atom position and of 1.97 v.u. to O4, clearly superior to the first model.

On the basis of both steric and bond valence considerations, it is concluded that the undetected H atom lies 1.19 Å above O4. The O6-H bond has approximately 0.50 v.u. associated with it; hydrogen bonding to three nearby O4 atoms accounts for the remaining 0.50 v.u. .

Table 16: Bond Valences (v.u.) in Simpsonite

Ta Octahedron		Al(1) Octahedron		Al(2) Octahedron	
Bond	s	Bond	s	Bond	s
Ta–01b	1.21	Al(1)–01a	0.50	Al(2)–01	0.46 (x 3)
–02a	0.58	–02a	0.54	–03	0.50 (x 3)
–02b	0.79	–03a	0.61		
–03a	0.90	–04b	0.42		
–04b	0.84	–04c	0.55		
–05a	0.65	–06a	0.50		

Sums to Atoms

Ta: 4.97

Al(1): 3.12
Al(2): 2.88

01: 2.17
02: 1.91
03: 2.01
04: 1.81
05: 1.95
06: 1.50

Figure 5: Simpsonite: geometry about potential sites for the H-atom. Solid lines: potential O-H bonds. Dashed lines: polyhedron edges.

The bond valence sum of 1.50 v.u. to O6 (ignoring H) is 50% in excess of the ideal value expected if F occurred at that location. This environment is extremely unfavourable for F substitution. Consequently, simpsonites should not show much F=OH substitution and, as indicated previously (Chemistry subsection), F reported in early analyses is probably due to contamination.

Chapter IX

ALUMOTANTITE

9.1 INTRODUCTION

Alumotantite has only been found as a member of the simpsonite paragenesis. It was first described as a new mineral by Voloshin et al. (1981) from granitic pegmatites of the Kola Peninsula. They assigned the formula $AlTaO_4$ and orthorhombic symmetry, and inferred an isomorphous relationship between it and stibiotantalite group minerals. Some of their results are given in Table 17.

About the time Voloshin et al. (1981) described their mineral, I found a mineral resembling alumotantite from the Bikita pegmatite, Zimbabwe. A literature review showed that this mineral had actually been encountered 35 years earlier by Macgregor (1946). Microprobe analyses and X-ray diffraction studies confirmed it as alumotantite. Close inspection of other simpsonite paragenesis samples showed a third locality for alumotantite, Alto do Giz, Brazil (sample L-15).

Table 17: Data for Type Alumotantite

Composition: $Al_{0.98}Ta_{0.99}Nb_{0.02}O_4$

Orthorhombic, a=4.90(1)
b=11.58(2)
c=5.66(1) Å

Anisotropic
Colourless, transparent, fluoresces blue-white
in UV light.
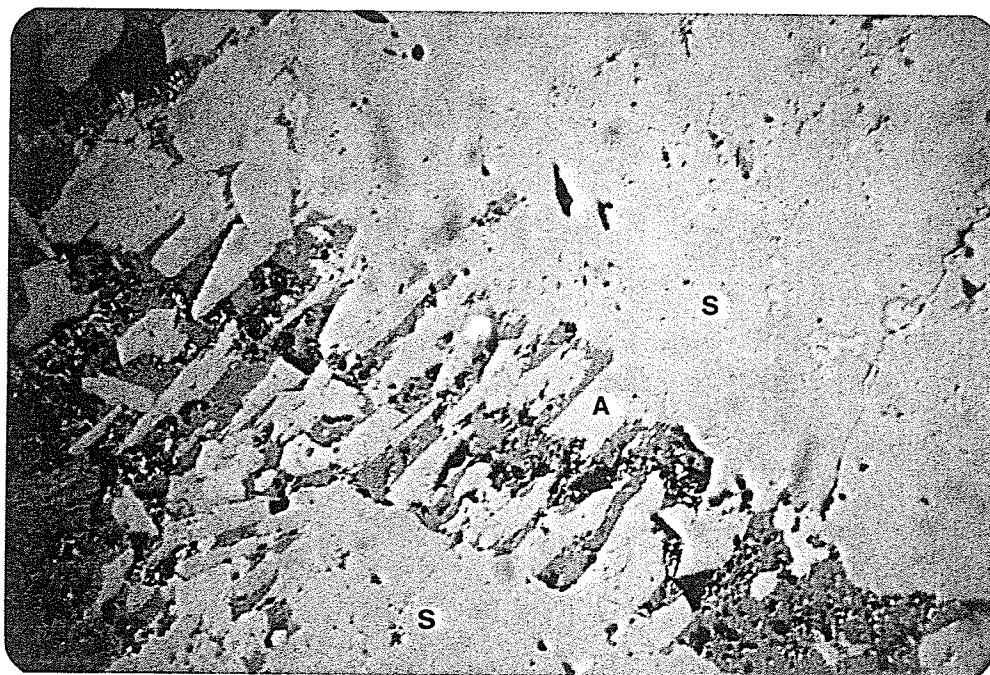
Figure 6: Alumotantite (A) in a muscovite vein cutting simpsonite (S),
Bikita pegmatite. Reflected light, 200x magnification.

9.2   PHYSICAL AND OPTICAL PROPERTIES

Alumotantite ranges from colourless (Bikita, Kola) to translucent white (Alto do Giz). Similarly, the lustre ranges from adamantine to greasy with increasing opacity. Crystals are subhedral to euhedral, elongate and are rectangular to rhombic in cross-section (Figure 6). Crystals are always small. Alumotantite from Bikita is typically less than 0.1 mm in length, much like the type material (Voloshin et al. 1981); that from Alto do Giz is up to 1 mm in length. Crystals of the Bikita material often occur as oriented parallel growths on simpsonite, with the axis of elongation of the alumotantite parallel to Z of simpsonite (Macgregor 1946). None of the samples examined show any cleavage. Because of the small crystal size, no density determinations were possible. The X-ray study, however, gives a calculated density of 7.48 gm/cm³.

In reflected light, alumotantite has higher reflectivity than simpsonite and is also markedly more bireflectant. In transmitted light, alumotantite is biaxial negative; refinement of extinction data obtained with the spindle stage gives 2V=66(2)° (sample L-15). None of the refractive indices of alumotantite is less than 2.00. This is consistent with Gladstone-Dale calculations ($\bar{n}$=2.21; constants from Mandarino, 1976) and MacGregor's assignment of a birefringence of 0.12 to alumotantite.

9.3   CHEMISTRY

Table 18 gives all available analyses of alumotantite; for comparative purposes, the ideal composition of alumotantite is also given. Voloshin et al. (1981) proposed the formula $AlTaO_4$ for alumotantite; all analyzed alumotantites conform well to this stoichiometry. Alumotantite may possess

minor amounts of SnO_2 (up to 1.0 wt.%, Bikita) and Nb_2O_5 (up to 0.8 wt.%, Kola) in addition to Ta_2O_5 and Al_2O_3. In the present study, manganese, iron and titanium were sought but not detected.

Although the data are not precise enough to be conclusive, Sn^{4+} probably substitutes for equal amounts of Al^{3+} and Ta^{5+} as charge balance considerations would dictate. Niobium-tantalum isomorphism is very minor to undetectable, most probably due to a geochemical, not a crystal-chemical control.

Table 18: Electron Microprobe Analyses and
Ideal Composition of Alumotantite

	1	2	3	4
Al_2O_3	18.6	18.9	18.5	18.7
SnO_2	0.2	1.0	----	0.0
Nb_2O_5	0.0	0.0	0.8	0.0
Ta_2O_5	81.6	80.9	81.1	81.3
	100.4	100.8	100.4	100.0

Cations per 16(O)

	1	2	3	4
Al^{3+}	3.96	3.99	3.93	4.00
Sn^{4+}	0.01	0.07	----	0.00
Nb^{5+}	0.00	0.00	0.07	0.00
Ta^{5+}	4.01	3.95	3.98	4.00
	7.98	8.01	7.98	8.00

1. Alto do Giz, Brazil (L-15).
2. Bikita, Zimbabwe (L-13).
3. Kola Peninsula, USSR - Voloshin et al.
   (1981).
4. Ideal composition of alumotantite.

9.4   STRUCTURE ANALYSIS

9.4.1   X-Ray Crystallography

Powder-type patterns for alumotantite crystal fragments were recorded by the Gandolfi method.   An uncontaminated pattern was obtained for the Alto do Giz material but only simpsonite-contaminated patterns could be recorded for the Bikita material.   Initially, an attempt was made to index the pattern for the Brazilian alumotantite on the cell proposed by Voloshin et al. (1981) for the type material, but this failed. In addition, several of the lines reported in the indexing of the type material were not present in the uncontaminated pattern but were present in the simpsonite-contaminated one, suggesting that the type pattern was contaminated with simpsonite diffractions.   Precession photographs of the Alto do Giz crystal fragment showed that the cell proposed by Voloshin et al. (1981) was not truly orthogonal; however, the diffraction pattern possessed mmm symmetry. From the diffraction symmetry, a new set of axes was located and the diffraction patterns were indexed on this cell.   Systematic absences of the types 0kl with k=2n+1, h0l with l=2n+1 and hk0 with h+k=2n+1 uniquely determined the space group as Pbcn.   The data for the type material were re-indexed on the new cell resulting in cell parameters in good agreement with the Brazilian material and standard deviations an order of magnitude better than before. The indexed patterns of the Brazilian and type alumotantite are given in Table 19.   Cell parameters for all three alumotantites are given in Table 20.

Table 19: X-Ray Powder Diffraction Data for Alumotantite

| | ALUMOTANTITE NMNH 104738 (Brazil) | | | | TYPE ALUMOTANTITE (USSR) | |
| | 1 | | 2 | | 3 | |
hkl	I (calc)	d (calc)	I (obs)	d (obs)	I (obs)	d (obs)
020	17	5.65	30	5.63	50	5.66
110	10	4.16	20	4.16		
021	42	3.65	50	3.64	70	3.64
111	100	3.14	100	3.13	100	3.13
130	47	2.88	60	2.88	80	2.89
040	4	2.83	10	2.82	10	2.83
131	1	2.468				
041	20	2.433	40	2.427	50	2.439
002	11	2.388	30	2.381	30	2.389
200	7	2.237	10	2.234	30	2.238
022	4	2.199	10	2.192	10	2.195
141	4	2.137	10	2.133	20	2.142
102	2	2.106	10	2.102		
220	3	2.080				
112	4	2.071	10	2.072	10	2.068
150	5	2.018	10	2.012	30	2.022
221	14	1.907	30	1.904	40	1.904
060	5	1.885	10	1.881	20	1.884
151	11	1.859	20	1.855	30	1.861
132	24	1.839 ⎫	40	1.834	50	1.837
042	3	1.824 ⎭				
240	2	1.754	10	1.752	10	1.754
241	21	1.646	40	1.644	50	1.649
202	12	1.632	30	1.629	40	1.633
222	2	1.568	10	1.566	10	1.563
152	4	1.541	10	1.539	20	1.543
023	3	1.532	10	1.526	20	1.528
170	2	1.519	10	1.516		
113	8	1.487 ⎫				
062	4	1.479 ⎬	20	1.475	30	1.483
310	1	1.478 ⎭				
171	8	1.448 ⎫	30	1.444	30	1.448
260	3	1.441 ⎭				
242	2	1.414 ⎫				
080	2	1.414 ⎬				
311	6	1.412 ⎭	20	1.410	40	1.413
043	7	1.387 ⎫	20	1.382	40	1.388
330	5	1.386 ⎭				
081	3	1.355	10	1.352	20	1.357
172	2	1.282	10	1.278	10	1.281
223	3	1.264	10	1.262	20	1.264
153	2	1.250 ⎫	10	1.246	10	1.249
350	1	1.245 ⎭				
262	4	1.234	10	1.231	30	1.235
082	1	1.216 ⎫				
190	2	1.210 ⎬	10	1.207	10	1.212
351	2	1.205 ⎭				
332	5	1.199	10	1.197	20	1.200

1. Calculated (from the refined structure with the program DBW 2.9, Wiles & Young, 1981) for a powder diffractometer equipped with an automatic divergence slit. Only reflections with I>1 are reported.
2. 114.6 mm Gandolfi camera; Ni-filtered Cu radiation. Corrected for shrinkage but not absorption.
3. Voloshin et al (1981). Powder camera, 114.6 mm, unfiltered Fe radiation.

Table 20: Unit Cell Parameters (Å) for Alumotantite

	1	2	3
a	4.471(1)	4.46	4.477(1)
b	11.302(4)	11.29	11.309(3)
c	4.766(1)	4.76	4.767(1)

1. Alto do Giz, Brazil (L-15). Four-circle diffractometer, MoKα radiation, C monochromator.
2. Bikita, Zimbabwe (L-13). Precession camera, Zr-filtered MoKα radiation.
3. Kola Peninsula, USSR. Refined from the data of Voloshin et al.(1981).

9.4.2 Structure Solution and Refinement

A search of the literature showed no compounds isostructural with alumotantite, so a structure analysis was undertaken. An equant fragment with dimensions 0.10 X 0.12 X 0.14 mm was used for the intensity data collection. Data were collected with the four-circle diffractometer of the Materials Research Institute of McMaster University.

A total of 563 reflections was measured, of which 288 were considered observed (I > 3σ). Of these, four very weak reflections (I only slightly > 3σ) violating Pbcn group symmetry were removed from the set. The highly absorbing characteristic of the material (μ = 480 cm^{-1}, Mo Kα) necessitated absorption correction; an empirical correction was used, based on an ellipsoidal approximation to the shape of the crystal. Cell dimensions were obtained from least squares refinement of a set of reflections automatically aligned on the diffractometer.

Consideration of the proposed stoichiometry and possible densities for alumotantite indicated that its true cell contains 4 formula units. Assuming complete cation order, Al and Ta were assigned to separate 4c sites (Wyckoff notation). While the diffractometer intensity data were being collected, an hk0 Patterson projection was made from precession camera intensities; Ta-Ta vectors were located giving y(Ta)=0.17.

The composition of the sample used in the refinement was approximated as AlTaO$_4$. In the first stage of the solution, the Ta-atom position was refined. A difference Fourier map was then constructed from which the Al position was located. The cation positions were refined and a Δ(Ta,Al) map was constructed. The map suggested that oxygen atoms occupied four general positions, not the two expected from the stoichiometry. Nevertheless, the

positions of all four sites were entered in the refinement. The isotropic temperature factors of the oxygen atoms clearly indicated the spurious oxygens (B=4.5); these were discarded from the refinement. Two more cycles of refinement with isotropic temperature factors reduced the R index from 13.9% to 5.0%. A difference Fourier map at this stage showed no unexpected anomalies. The thermal vibrations of the tantalum and oxygen atoms were modelled as anisotropic (the analogous parameters for Al were non-positive definite, so an isotropic model was retained for Al) and a secondary extinction correction was applied, resulting in final R-indices of $\underline{R}$=4.4%, w$\underline{R}$=5.5%.

Bond valence calculations showed that the sums to the cations differed significantly from their ideal values. The sum to Ta was low (Σ=4.7 v.u.) and to Al was high (Σ=3.2 v.u.) suggesting possible cation disorder. An attempt was made to refine cation site order according to the constraint, no. Al atoms = no. Ta atoms = 4 cations/cell, suggested from microprobe analyses. The model converged on a fully-ordered scheme (0 Al in the Ta-site and vice versa) indicating that cation disorder was not cause for the deviant bond valence sums. Errors in the absorption correction were suspected, and the experiment was repeated.

The second data collection followed the same procedure as the first, except that data were collected with the R3m diffractometer at the University of Manitoba. Starting with atom positions from the first experiment, the second refinement converged on improved R-indices of $\underline{R}$=3.9% and w$\underline{R}$=4.2%. Unlike the first experiment, all sets of anisotropic temperature factors were positive definite; hence all atoms were modelled with aniso-tropic thermal parameters. An extinction correction was not applied because it did not make a significant contribution to the model.

Observed and calculated structure factors for both experiments are given in Appendix G. Final positional and thermal parameters are given in Table 21.

Table 21: Positional and Thermal Parameters for Alumotantite

Atom	Experiment	x	y	z	$U(eq)Å^2$
Ta	1	0	0.16817(9)	1/4	52(4)
	2	0	0.16813(7)	1/4	146(2)
Al	1	0	0.4346(7)	1/4	56(14)
	2	0	0.4344(5)	1/4	163(16)
O1	1	0.222(4)	0.312(1)	0.086(4)	68(29)
	2	0.223(3)	0.315(1)	0.083(3)	203(32)
O2	1	0.266(4)	0.058(1)	0.073(4)	84(32)
	2	0.264(2)	0.055(1)	0.073(2)	135(26)

Anisotropic Temperature Parameters (Experiment 2)

Atom	U_{11}	U_{22}	U_{33}	U_{12}	U_{13}	U_{23}
Ta	144(4)	129(4)	165(4)	0	5(5)	0
Al	152(27)	129(26)	208(30)	0	4(37)	0
O1	259(61)	125(47)	224(57)	51(45)	-32(60)	19(47)
O2	176(47)	135(46)	96(44)	53(42)	-38(47)	-37(42)

All U's are x 10^4

9.4.3 Description of the Structure

The oxygen array of the alumotantite structure is approximately hexagonally closest-packed (Figure 7), with cations occupying half of the octahedral interstices of the array. The closest-packed layering is perpendicular to $\underline{X}$. Considered in terms of polyhedra, each level perpendicular to $\underline{X}$ consists of branched, zig-zag chains of edge-sharing, slightly distorted octahedra running parallel to $\underline{Z}$. Aluminum octahedra make up the backbone of these chains; tantalum octahedra are attached laterally to this backbone. Gross chain configuration is the same for all levels.

Projection along $\underline{Y}$ (Figure 8) illustrates the interrelationship of the tantalum polyhedra. Each octahedron shares four corners with two octahedra above and two below it. The result is a perforated, corrugated sheet of tantalum polyhedra normal to $\underline{Y}$. Each sheet is linked to neighbouring sheets by edge-sharing with the backbone of aluminum polyhedra.

Interatomic distances and angles for the second refinement are presented in Table 22. Details of the two types of polyhedron in alumotantite are given in Figure 9. <Ta-O> and <Al-O> distances compare well with calculated values from Shannon (1976) (<Ta-O>obs = 2.013, <Ta-O>calc = 2.00; <Al-O>obs = 1.883, <Al-O>calc = 1.895 Å) supporting the assumption of full cation ordering. Deviations of the coordination polyhedra from ideal octahedral geometry are slight. Most deviations can be rationalized in terms of cation-cation repulsions and the number and location of shared edges. The aluminum octahedron possesses three shared edges regularly disposed about the polyhedron. Two of these edges are shared with adjacent aluminum octahedra and one with an adjacent tantalum octahedron. Because of this immediate environment of nearly balanced repulsions, the aluminum atom lies
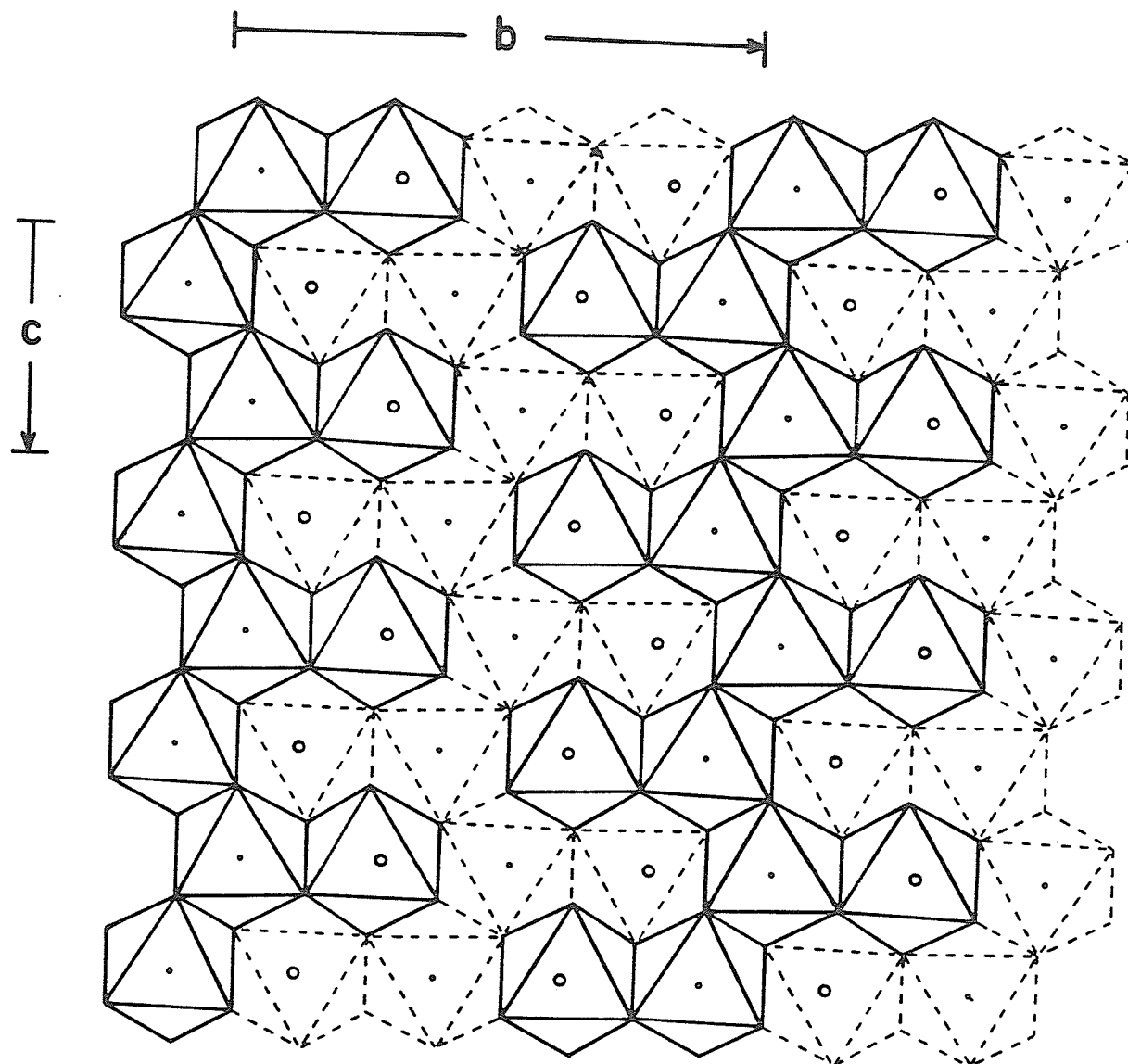
Figure 7: Structure of alumotantite projected along X. Solid lines represent polyhedra of one level; broken lines, those of adjacent levels. Ta atoms are shown as open circles, Al atoms, filled circles.
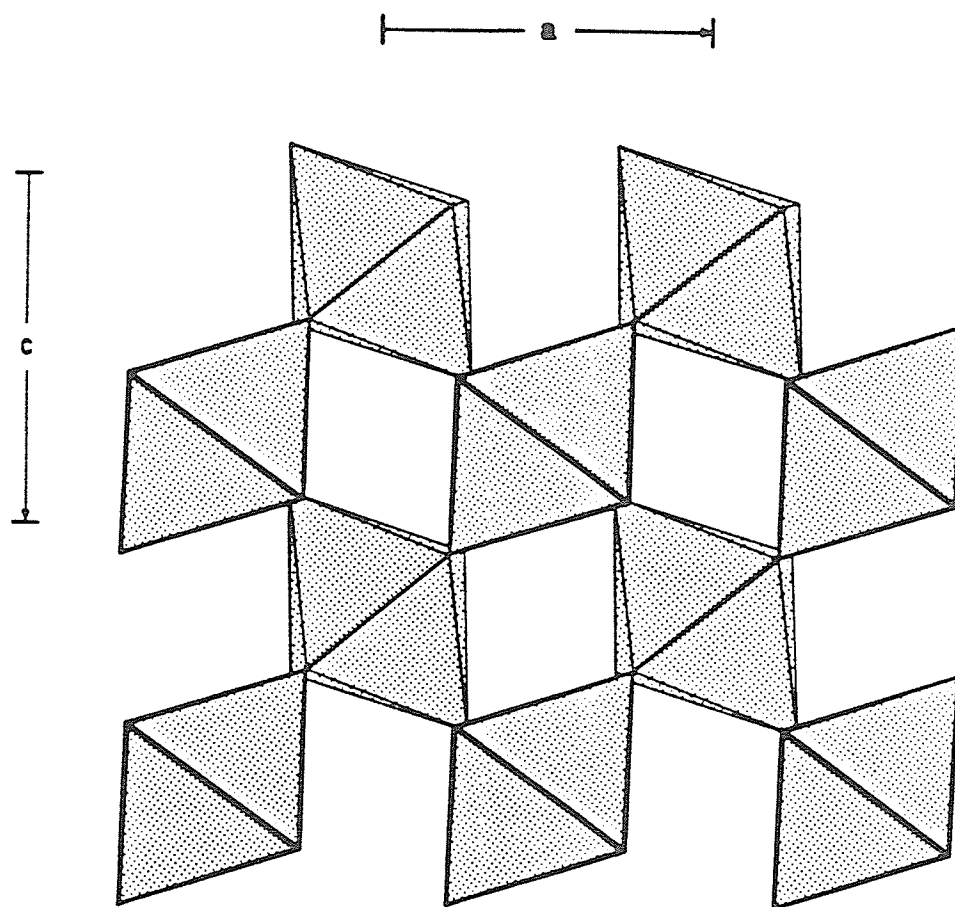
Figure 8:   Alumotantite: Ta-sheet projected along Y.
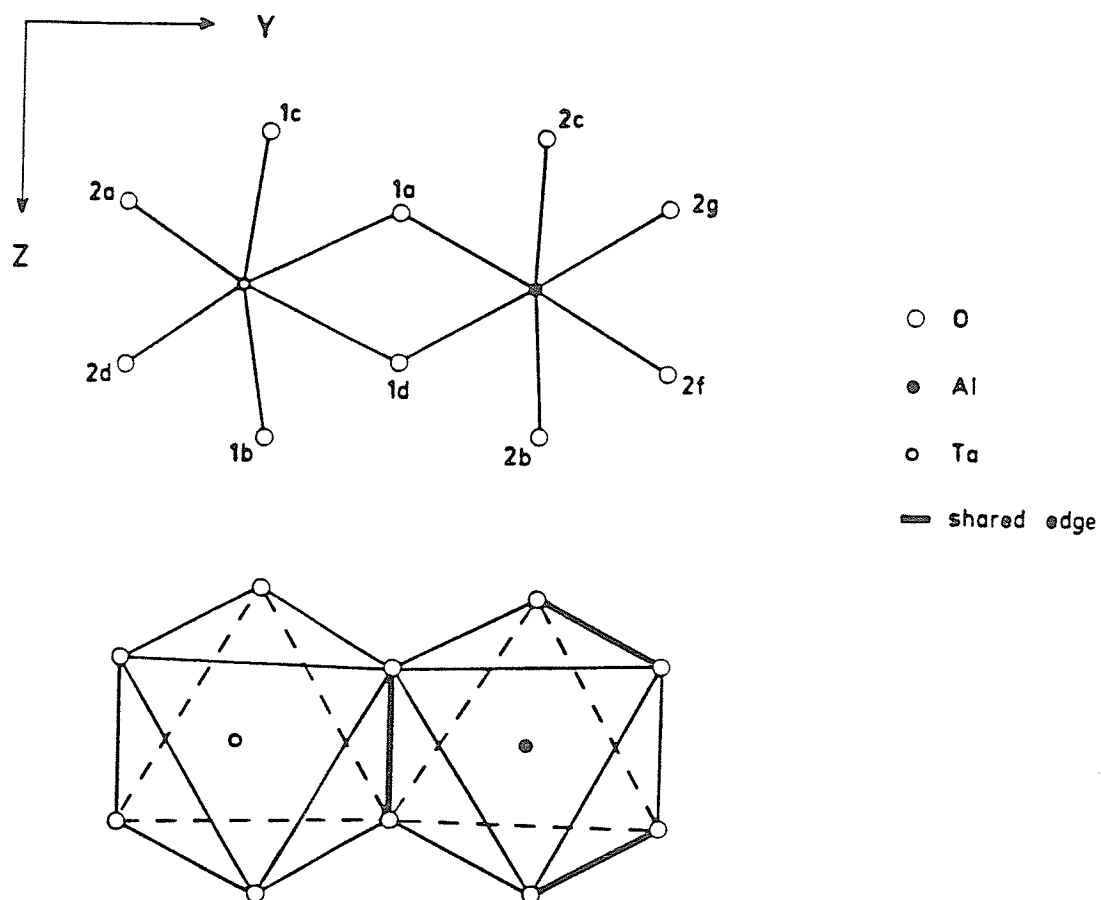
Figure 9: Polyhedra in Alumotantite

Table 22: Selected Interatomic Distances (Å) and Angles (°) in Alumotantite

	Ta Octahedron				Al Octahedron		
Ta	– O1a	x 2	2.09(1)	Al	– O1a	x 2	1.86(1)
	– O1b	x 2	2.02(1)		– O2b	x 2	1.87(1)
	– O2a	x 2	1.93(1)		– O2f	x 2	1.92(1)
	< Ta – O >		2.013		< Al – O >		1.883

O1a	– O1b	x 2	2.779(17)	O1a	– O1d	x 1	2.527(36)
	– O1c	x 2	2.763(20)		– O2b	x 2	2.752(30)
	– O1d	x 1	2.527(36)		– O2g	x 2	2.783(22)
	– O2a	x 2	2.880(22)		– O2c	x 2	2.628(25)
O1b	– O2a	x 2	2.861(30)	O2b	– O2f	x 2	2.564(38)
	– O2d	x 2	2.944(24)		– O2g	x 2	2.722(14)
O2d	– O2a	x 1	2.920(42)	O2f	– O2g	x 1	2.693(37)
	< O – O >		2.825		< O – O >		2.677

O1a	– Ta – O1b	x 2	85.3(4)	O1a	– Al – O1d	x 1	84.6(11)
	– Ta – O1c	x 2	84.7(4)		– Al – O2b	x 2	94.7(8)
	– Ta – O1d	x 1	75.7(10)		– Al – O2c	x 2	89.2(8)
	– Ta – O2a	x 2	92.7(7)		– Al – O2g	x 2	93.7(7)
O1b	– Ta – O2a	x 2	92.3(7)	O2b	– Al – O2f	x 2	84.8(9)
	– Ta – O2d	x 2	95.9(8)		– Al – O2g	x 2	91.4(8)
O2a	– Ta – O2d	x 1	99.0(11)	O2f	– Al – O2g	x 1	88.0(11)
	< O – Ta – O >		89.7		< O – Al – O >		90.0

Equivalent Positions

a: x, y, z
d: x, y, 1/2-z

b: 1/2-x, 1/2-y, 1/2+z
f: 1/2+x, 1/2+y, 1/2-z

c: 1/2+x, 1/2-y, z
g: x, y, 1/2+z

near the geometric centre of its coordination polyhedron. Because the tantalum octahedron shares only one edge and because the Ta-Al interatomic vector lies along Y (the only positional variable for the tantalum atom), tantalum-aluminum repulsion distorts the tantalum octahedron more than the aluminum octahedron. As a result, interatomic distances and angles in the tantalum polyhedron show greater variability than those in the aluminum polyhedron.

Examination of Table 21 shows that the atomic positions of each experiment agree well; however, the temperature factors differ significantly. A half-normal probability plot (Abrahams, 1974) was constructed to compare the results of the two experiments (Figure 10). For such plots, the differences in the values of identical parameters of each experiment ($\Delta(i)$) divided by their pooled standard deviation ($\sigma(i)$) are plotted against expected values of $\Delta(i)/\sigma(i)$, which can be obtained from tables (e.g. Hamilton, 1972). For sets of experiments with only random error, the points should scatter about a straight line of unit slope and zero intercept. Distributions which are non-linear, have non-unit slope, or non-zero intercept contain systematic error in one or both of the datasets. As can be seen from the point distributions, there is no indication of systematic error with the positional parameters; however, the equivalent isotropic thermal parameters show a large systematic error. The most obvious source of this error is incorrect absorption correction; because of the lower R-indices of the second experiment and because the experiment was done by the author with absorption correction in mind, the error described above is expected to belong to the first dataset.
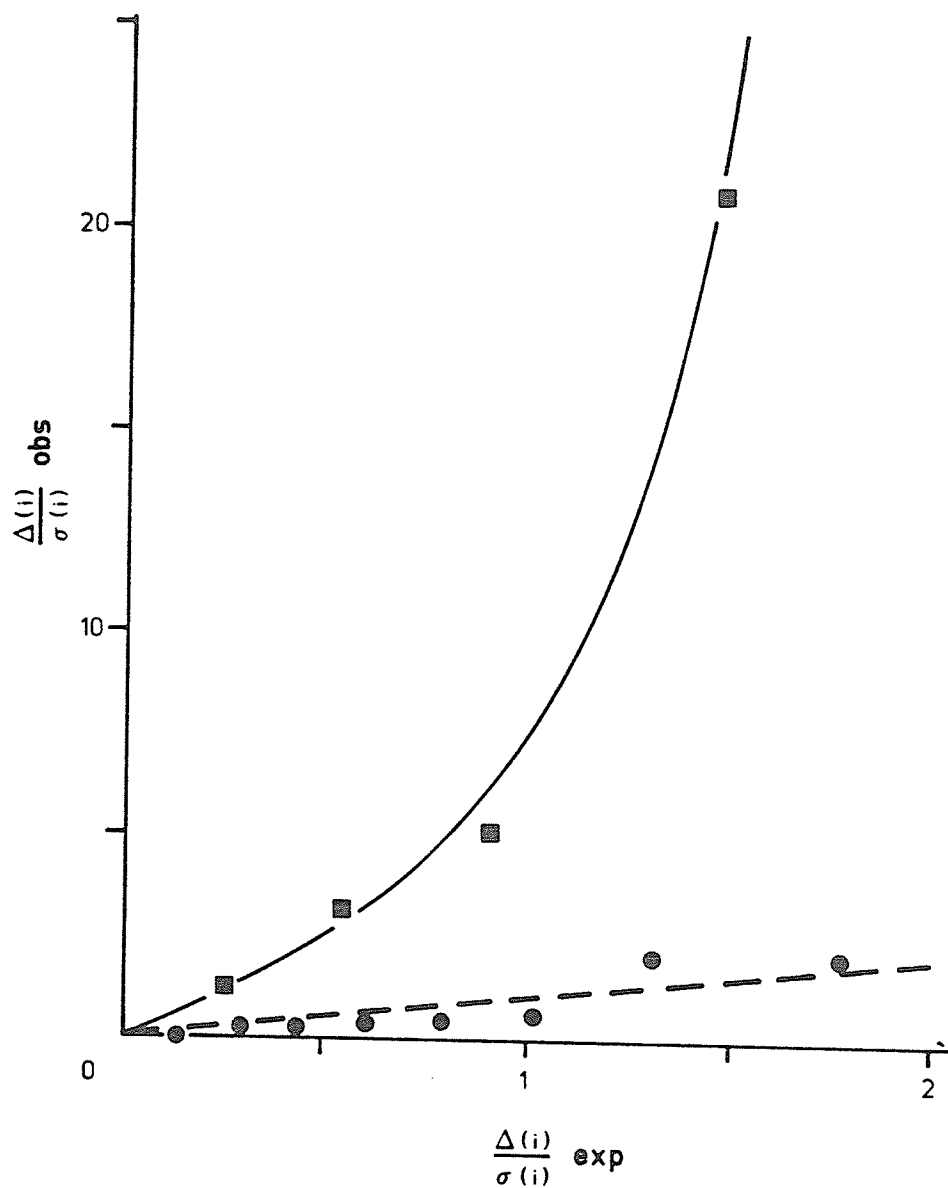
Figure 10: Half-normal probability plot for alumotantite. Circles: positional parameters, squares: equivalent isotropic temperature parameters. The dashed line marks the ideal curve for distributions with only random error; the unbroken line, an approximate fit to the temperature parameter data.

Bond valences and bond valence sums are given in Table 23. The good agreement between positional parameters of both experiments produced insignificantly different results in terms of bond valences; consequently, only those calculations for the second dataset are given. As mentioned in the previous section, the bond valence sums deviate significantly from their ideal values. Ruling out inadequate absorption correction and cation disorder as causes, it is difficult to explain the deviations. One possibility is that the deviant sums may be due to nearest-neighbour effects upon the bond lengths, from which the bond valences are derived (i.e. the Ta-O bond valence curve is derived largely from Ta-oxide structures with large, low-valence $\underline{A}$-cations, and alumotantite hosts small, highly-charged cations).

Table 23: Bond Valences (v.u.) in Alumotantite

Ta Octahedron		Al Octahedron	
Bond	s	Bond	s
Ta-O1a	0.60	Al-O1a	0.57
-O1b	0.74	-O2a	0.56
-O2a	0.99	-O3a	0.48

Sums to Atoms

Ta: 4.66	O1: 1.91
Al: 3.22	O2: 2.03

9.5   SIMPSONITE-ALUMOTANTITE TOPOTAXY

In addition to prismatic alumotantite crystals, isolated patches of a "cloudy alteration" in Bikita simpsonite (Figure 11) can be observed (Macgregor 1946). Gandolfi photos of this opaque, white material showed both simpsonite and alumotantite. Qualitative microprobe analysis also showed a minor third phase with only detectable Al. These data and paragenetic considerations suggest the phase to be a hydroxide, perhaps gibbsite.

On the basis of the similarity of several of the interplanar spacings of simpsonite to alumotantite, a topotaxic relationship between these minerals was suspected. To investigate this, a fragment of the opaque region was studied by the precession method. The topotaxic relationship was confirmed in the photographs taken, with

$$\underline{X}(a) \ || \ \underline{Z}(s)$$

$$\underline{Y}(a) \ || \ [210](s)$$

$$\underline{Z}(a) \ || \ [410](s)$$

where the letters in parentheses refer to alumotantite and simpsonite. This alumotantite is twinned; topotaxic control on the twinning has produced threefold rotation twins of alumotantite about $\underline{Z}(s)$ in the partially consumed simpsonite. No additional diffractions indicative of a third phase were observed in the precession photos.

Comparison of the simpsonite structure to that of alumotantite in light of the above relationships shows that the hexagonal closest-packing of oxygens in simpsonite is preserved through the topotaxic reaction generating

alumotantite (Figure 12). Hence, the reaction is marked by cation migration through an essentially unchanged oxygen array.

Optical examination of the Bikita sample shows that both the prismatic alumotantite and the alumotantite in the white patches possess (at least) parallel X axes. By inference, the same crystallographic relationship (less twinning) exists between simpsonite and both alumotantite textural varieties. However, important differences between the two varieties do exist:

(1) The prismatic variety occurs as partial replacements of, and overgrowths on simpsonite, whereas the patchy variety occurs as replacements only.

(2) The prismatic variety occurs along fractures and rims of the simpsonite, whereas the other variety occurs as isolated patches in the interior of simpsonite crystals.

(3) Aluminum silicates (muscovite and albite) and not aluminum hydroxides occur with the prismatic variety.

Although the two varieties differ greatly in occurrence and paragenesis, the rarity of alumotantite, the similar paragenetic timing of the varieties, and the same topotaxic relationship between simpsonite and both alumotantite varieties suggest a single reaction mechanism. The observations outlined above suggest the reaction of simpsonite with minor volumes of late fluids with which it is no longer in equilibrium. In particular, an increase in $\mu(Ta)$ is the most feasible cause for the breakdown of simpsonite. A generalized equation describing this reaction is:

$$Ta^{5+} + 2Al_4Ta_3O_{13}(OH) = 7AlTaO_4 + 2H^+ + Al^{3+}$$
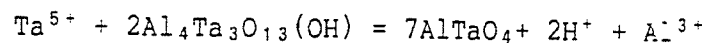
In the interiors of alumotantite crystals, the aluminum released in this reaction is bound up as a hydroxide (i.e. in the white patches). At the rims of, and along fractures in the simpsonite crystal, $\mu(Si)$ (and $\mu(Na)$, $\mu(K)$) is great enough to result in the incorporation of the liberated Al^{3+} in aluminum silicates. Quite clearly, the phases formed from the liberated Al^{3+} do not play an active role in simpsonite-alumotantite topotaxy -- the same topotaxic relationship between simpsonite and alumotantite is shown by both parageneses despite their differences in mineralogy.
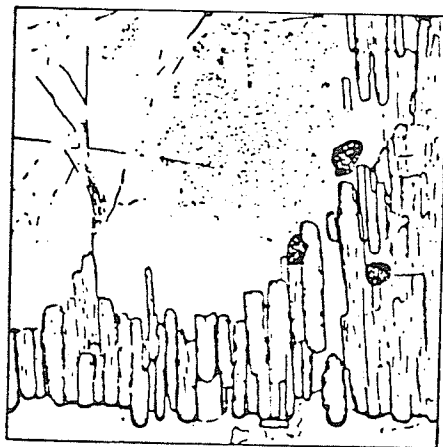
<u>Figure 11</u>: Alumotantite replacing simpsonite, Bikita pegmatite (from Macgregor, 1946). Laths are alumotantite crystals. The stippled region is a pervasive alteration of simpsonite to alumotantite.
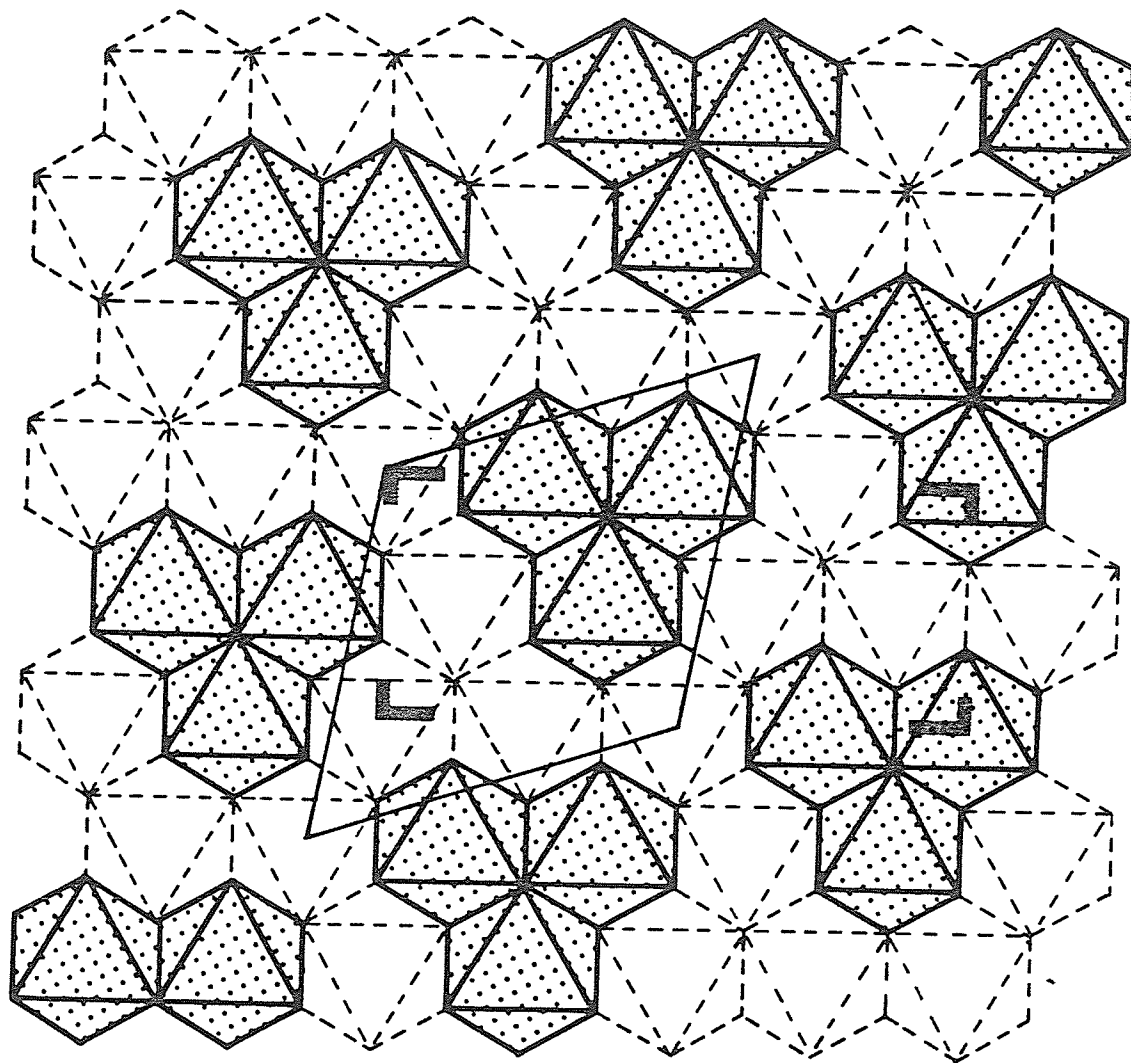
Figure 12: Topotaxy between simpsonite and alumotantite. Background: simpsonite structure. The simpsonite cell is in narrow rule; the corners of the alumotantite cell are shown in bold rule.

Chapter X

NATROTANTITE

10.1 INTRODUCTION

Natrotantite is only known as a member of the simpsonite paragenesis. It was first encountered by Voloshin et al. (1981) in granitic pegmatites of the Kola Peninsula. On the basis of microprobe and powder X-ray diffraction data, they described it as monoclinic $NaTa_3O_8$. While examining simpsonite-bearing samples of the Alto do Giz pegmatite, Brazil, I found a mineral similar in chemistry and optical properties to natrotantite (sample L-17). Although agreement between chemical data for this sample and type natrotantite (Voloshin et al., 1981) was only fair, I concluded that the two minerals were the same on the basis of identical powder diffraction patterns.

In an attempt to resolve the problem of the chemical differences between the samples, a literature search was done for data on syntheses in the system $NaTaO_3-Ta_2O_5$. Interestingly, poor agreement exists between the different studies, and no firm conclusions regarding the true composition of natrotantite could be derived from these data. However, more recent syntheses indicate a strong dependence of the results upon temperature (Chaminade et al., 1972). With the intent to synthesize a compound isostructural with natrotantite, the join $NaTaO_3-Ta_2O_5$ was investigated at 850°C.

10.2   NATROTANTITE

10.2.1   Physical and Optical Properties

Natrotantite from Brazil is colourless; that from the USSR is colourless to pale yellow.   Natrotantite has an adamantine lustre and is transparent to translucent.   Under reflected light, natrotantite has a relatively high reflectivity (> simpsonite).   Crystals of Brazilian natrotantite are bladed; ones from the USSR are irregular in shape.   Crystals occur in patchy aggregates or as veinlets in simpsonite (Figure 13).   Crystals are always very small; samples from Alto do Giz are typically less than 0.05 mm in diameter, but can range up to 0.5 mm in length. Because of the small crystal size,   the density of the mineral has never been measured; however, D(calc)=6.0 g/cm^3.
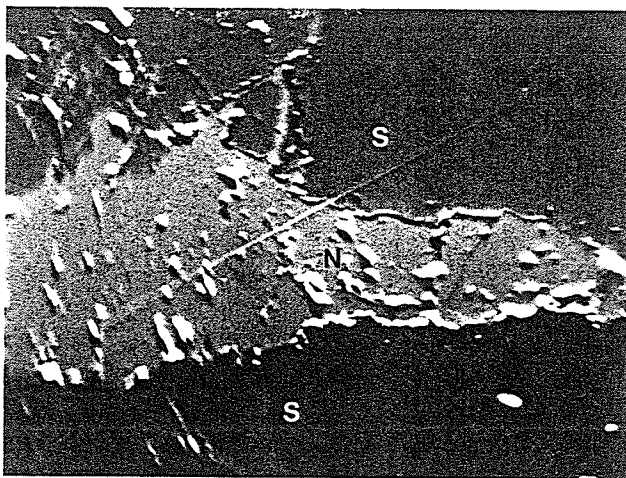
Figure 13:   Backscattered electron image of a natrotantite vein (N)   in simpsonite (S), Alto do Giz.   200 X magnification.

10.2.2 Chemistry

All available analyses of natrotantite are given in Table 24, as well as calculated oxide contents of the compounds $NaTa_3O_8$, $Na_2Ta_4O_{11}$ and $Na_2Ta_8O_{21}$. Immediately obvious from Table 24 is that analyses of the Brazilian material (this study) do not agree well with those of the type material (Voloshin et al., 1981). Furthermore, although the analysis of the type sample closely approximates $NaTa_3O_8$, the analyses of the Brazilian samples most closely approach $Na_2Ta_8O_{21}$ in composition.

To evaluate the precision of the results of this study, sample L-17 was analyzed twice, using two different sodium standards (microlite and synthetic $NaInSi_2O_6$). In terms of reproducibility of results, the precision was good. The analyses with microlite as a Na standard are averaged in Table 24. Use of $NaInSi_2O_6$ produces similar results (<Na_2O>=3.6%), suggesting adequate absorption correction of the data. Voloshin et al. (1981) also analyzed their sample several times to evaluate the precision of their results. If the difference in composition between the two analyses is not real, it must be due to errors in ZAF correction of the microprobe data. However, the difference in Na_2O between the samples is approximately 50%; as it is improbable that the ZAF-type corrections of the two data-reduction routines differ by this amount, much of the difference should be real.

Natrotantites typically contain minor amounts of Nb_2O_5, PbO, and CaO and can also contain trace amounts of K_2O. In the Brazilian samples, Pb/(Na+K+Ca) increases with Ta/(Ta+Nb), indicating that solutions responsible for natrotantite formation became richer in Pb with respect to smaller alkali cations, with fractionation.

Table 24: Composition of Natrotantite and Similar Compounds

	1	2	3	4	5	6	7
Na_2O	3.1	3.2	3.3	4.7	6.6	4.5	3.4
K_2O	0.06	0.2	---	---	0.0	0.0	0.0
CaO	0.3	0.4	0.1	0.08	0.0	0.0	0.0
PbO	0.6	1.8	3.2	0.9	0.0	0.0	0.0
Nb_2O_5	1.0	1.0	0.4	2.7	0.0	0.0	0.0
Ta_2O_5	94.3	93.1	91.7	91.3	93.5	95.5	96.6
	99.4	99.7	98.7	99.7	100.0	100.0	100.0

1. Natrotantite (L-17), Alto do Giz, Brazil.
2. Natrotantite (RVG-1C-6), Alto do Giz, Brazil.
3. Natrotantite (RVG-1C-5), Alto do Giz, Brazil.
4. Natrotantite, Leshaia, Kola Peninsula, USSR
   (Voloshin et al., 1981).
5. Ideal $Na_2Ta_4O_{11}$.
6. Ideal $NaTa_3O_8$.
7. Ideal $Na_2Ta_8O_{21}$.

10.2.3 X-Ray Crystallography

A 2 x 10^{-6} mm^3 crystal fragment was extracted from the microprobe mount for X-ray studies. Gandolfi patterns (Table 25), although weak, agree completely with the pattern reported for type natrotantite (Voloshin et al., 1981).

Voloshin et al. (1981) pointed out the correspondence between the X-ray powder diffraction patterns of synthetic $Na_2Ta_4O_{11}$ and natrotantite. They proposed the space group C2/c for the mineral; however, all data for it and that of Chaminade et al. (1972) for $Na_2Ta_4O_{11}$ can be completely indexed on a hexagonal-R cell of dimensions a=6.21, c=36.6 Å. Long-exposure precession photographs of sample L-17 fragment confirm this assignment; all aspects of the diffraction data indicate R3c or R$\bar{3}$c as possible space groups.

Late in this study, the unit cell parameters of a natrotantite fragment from sample RVG-1C (Brazil) were refined from single crystal diffractometer data (15 reflections). The unconstrained unit cell parameters are:

$$a=6.210(1) \quad b=6.207(1) \quad c=37.026(6) \text{ Å}$$
$$\alpha=89.99(1) \quad \beta=89.99(1) \quad \gamma=120.03(2) \text{ °}$$

which indicate that natrotantite is metrically hexagonal even at a high level of precision.

Table 25: Powder Diffraction Data for Natrotantite

| | Natrotantite | | | | $Na_2Ta_4O_{11}$ | | |
| | USSR | | Brazil | | | | |
hkl	I (obs)	d (obs)	I (obs)	d (obs)	I (obs)	d (obs)	d (calc)
006	4	6.12	6	6.14	30	6.09	6.10
012	3	5.19	5	5.17	31	5.15	5.16
104	1	4.66	1	4.63	5	4.64	4.64
018	1	3.50	1	3.52	4	3.49	3.49
110					1	3.10	3.10
00$\overline{12}$	7	3.06	4	3.07	49	3.051	3.052
10$\overline{10}$			1	3.04	10	3.025	3.027
11$\overline{3}$	10	3.02	10	3.01	100	3.010	3.009
116	9	2.778	9	2.772	81	2.766	2.767
024	2	2.601	1	2.580	9	2.579	2.579
119	6	2.474	5	2.477	34	2.467	2.468
01$\overline{14}$					3	2.351	2.352
20$\overline{8}$			1	2.324	8	2.318	2.318
02$\overline{10}$					1	2.167	2.167
00$\overline{18}$,	4	2.038	3	2.042	15	2.032	2.034
21$\overline{1}$							2.029
122			2	2.022	4	2.023	2.020
214					1	1.984	1.984
125	1	1.973	1	1.958	8	1.958	1.958
11$\overline{15}$	5	1.926	4	1.934	31	1.919	1.919
21$\overline{7}$	1	1.884			1	1.894	1.894
128	3	1.849	1	1.858	3	1.858	1.857
300	6	1.799	6	1.791	46	1.792	1.792
21$\overline{10}$	1	1.783			5	1.778	1.777
02$\overline{16}$					5	1.743	1.743
12$\overline{11}$					1	1.735	1.735
306	1	1.727			11	1.720	1.720
11$\overline{18}$	6	1.707	5	1.717	35	1.701	1.702
21$\overline{13}$	1	1.648			3	1.648	1.648
12$\overline{14}$	1	1.595			3	1.605	1.605
10$\overline{22}$					1	1.590	1.590
30$\overline{12}$	8	1.556	5	1.549	48	1.547	1.552
22$\overline{3}$	8	1.548			15	1.543	1.540
00$\overline{24}$	3	1.527			10	1.527	1.526
11$\overline{21}$			3	1.535	20	1.520	1.520
226	2	1.509	2	1.504	16	1.504	1.504
131,	1	1.493	2	1.484	12	1.487	1.490
312							1.486
12$\overline{17}$					2	1.480	1.478
315	2	1.466			2	1.463	1.461
229	3	1.453	1	1.451	10	1.450	1.450
137	1	1.421			2	1.434	1.434
21$\overline{19}$	2	1.404			2	1.399	1.398
a		6.224 (2)		6.199 (2)		6.2086 (3)	
c		36.76 (1)		37.08 (2)		36.618 (2)	Å

USSR sample: data from Voloshin et al. (1981).
Brazilian sample: 114.6 mm Gandolfi camera, Ni-filtered
            Cu radiation. Corrected for shrinkage.
$Na_2Ta_4O_{11}$: Philips PW1710 powder diffractometer, automatic
            divergence slit, graphite-monochromated, Cu $K\alpha$
            radiation.

10.3 THE JOIN $NaTaO_3$-Ta_2O_5

Because of the diversity of results of separate studies of the join $NaTaO_3$-Ta_2O_5, each study is summarized in Table 26. To date, the phases $NaTaO_3$, $NaTa_3O_8$, $Na_2Ta_4O_{11}$, $Na_2Ta_8O_{21}$ and L-Ta_2O_5 have been reported for the system. Of these phases, $Na_2Ta_4O_{11}$ of Chaminade et al. (1972) and Jahnberg (1970) most closely resembles natrotantite in terms of its X-ray powder diffraction pattern.

For the present study, the following starting materials were used: Ta_2O_5 (Puratronic, 99.99%), Na_2CO_3 (Fisher, 99.99%) and $NaHCO_3$ (Fisher, 100.2%). The components were dried, weighed, thoroughly mixed and pressed into pellets prior to firing in an electric furnace. Heatings were done in a platinum crucible at 850°C for 4, 10 and 20 hours. All run products were characterized by X-ray powder diffractometry. Annealed reagent-grade BaF_2 and CaF_2, calibrated against U.S. National Bureau of Standards silicon (batch 640a) were used as internal standards in unit cell refinements.

The run results are shown in Figure 14. Three phases exist at 850°C: $NaTaO_3$, $Na_2Ta_4O_{11}$ and Ta_2O_5. Compositions more sodic than $Na_2Ta_4O_{11}$ produced mixtures of $Na_2Ta_4O_{11}$ and $NaTaO_3$; less sodic compositions produced mixtures of $Na_2Ta_4O_{11}$ and Ta_2O_5. The results of this study confirm the findings of Chaminade et al. (1972) for the join at low temperature (700-900°C). Unit cell parameters of all phases are given in Table 27.

Table 26: Results of Previous Investigations of the Join $NaTaO_3-Ta_2O_5$

Reference	$Na_2Ta_4O_{11}$	$NaTa_3O_8$	$Na_2Ta_8O_{21}$	T (°C)
King et al.(1956)	T a=16.40 c=16.81	T a=7.806 c=7.66	---	from melt
Reisman (1962)	O a=6.00 b=7.66 c=5.08	O a=7.74 b=7.74 c=5.97	---	1300
Whiston & Smith (1965)	T a=7.86 c=7.152	---	T a=12.5 c= 3.92	1000
Jahnberg (1970)	R a= 6.209 c=36.618			1000
Chaminade et al.(1972)	---	---	O a=12.430 b=37.290 c= 3.900	1300
	H a= 6.208 b=36.659	---	---	900

T: tetragonal, O: orthorhombic, H: hexagonal P, R: hexagonal R
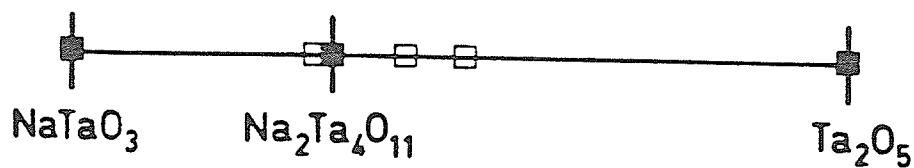
Figure 14: The Join $NaTaO_3$-Ta_2O_5 at 850°C. Squares mark compositions investigated. Filled squares: single phase. Open squares: two phases.

Table 27: Unit Cell Parameters (Å) for Phases of the Join $NaTaO_3$-Ta_2O_5

$NaTaO_3$	$Na_2Ta_4O_{11}$	L-Ta_2O_5
a: 3.8913(1)	a: 6.2086(3)	a: 6.231(3)
	c: 36.618(2)	b: 40.18(2)
		c: 3.8890(4)
V: 58.923(5)	V: 1222.4(1)	V: 973.7(3)
Cubic	Hexagonal	Orthorhombic

Philips powder diffractometer, graphite-monochromated CuKα radiation.

10.4 $Na_2Ta_4O_{11}$

10.4.1 Structure Analysis and Refinement

Powder diffraction data for the compound $Na_2Ta_4O_{11}$ are given in Table 25. These data confirm that $Na_2Ta_4O_{11}$ is isostructural with natrotantite. This is surprising: chemical analyses (Table 24) suggest either $NaTa_3O_8$ or $Na_2Ta_8O_{21}$ as possible compositions for natrotantite.

As shown earlier, the X-ray powder diffraction data for both natrotantite and $Na_2Ta_4O_{11}$ can be completely indexed on a R-centred cell, despite suggestions of Chaminade et al. (1972) and Voloshin et al.(1981) to the contrary. The content of this cell is six formula units, i.e. $Na_{12}Ta_{24}O_{66}$. The true cell is related to the monoclinic pseudo-cell proposed by Voloshin et al. (1981) by

$$\underline{a}(hex) = 1/\sqrt{3}\ \underline{a}(mon)$$

$$\underline{b}(hex) = \underline{b}(mon)$$

$$\underline{c}(hex) = 3\underline{c}\ sin\beta(mon)$$

The relationship is shown in Figure 15. The pseudocell is nearly identical to the true cell of the compound $Na_2Nb_4O_{11}$; comparison of the diffraction patterns of these compounds strongly suggests that the $Na_2Nb_4O_{11}$ structure is merely a monoclinic distortion of the $Na_2Ta_4O_{11}$ structure (Jahnberg, 1970). In order to assess the validity of this model, a structure refinement of $Na_2Ta_4O_{11}$ was done.

Because of the strong structural similarities between $Na_2Nb_4O_{11}$ and $Na_2Ta_4O_{11}$, the data of Jahnberg (1970) for $Na_2Nb_4O_{11}$ were used to generate the starting model for $Na_2Ta_4O_{11}$. Because $Na_2Nb_4O_{11}$ has a centric structure, the space group $R\overline{3}c$ was chosen for the refinement. The equation,
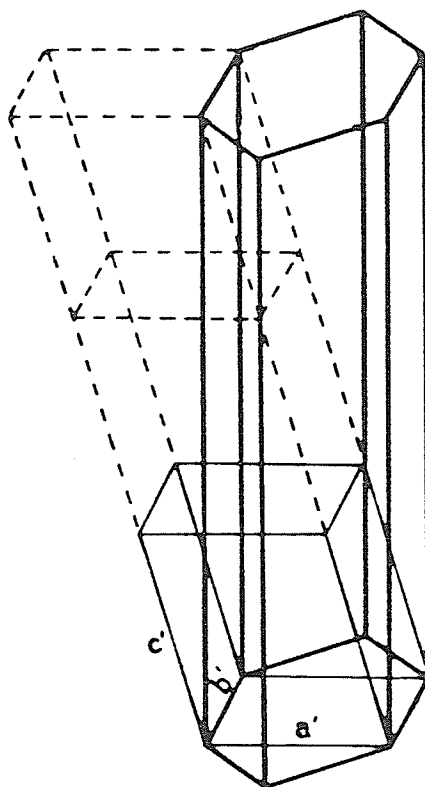
<u>Figure 15</u>: Relationship between the hexagonal cell of natrotantite (bold
rule) and its monoclinic pseudo-cell (light rule and dashed).

$$\underline{H} = \underline{AM} + \underline{C},$$

where $\underline{A} = [\ 2,\ 0,\ -2/3\ \ /\ \ 1,\ 1,\ -1/3\ \ \ /\ \ 0,\ 0,\ -1/3\ ]$

$\underline{C} = [\ -1/2,\ 0,\ 0\ ]$

$\underline{M} = [\ x,\ y,\ z\ ]$ monoclinic

$\underline{H} = [\ x,\ y,\ z\ ]$ hexagonal

was used to transform the coordinates of $Na_2Nb_4O_{11}$ to R3c-compatible ones. The transformation placed Na at a 12c site (Wyckoff notation) with z= 1/6, Ta at both an 18e site with x=0.364 and the 6b site and O at three sites: 36f (x=0.055, y=0.413, z=0.197), 18e (x=3/4), 12c (z=0.406).

For the data collection, the sample of $Na_2Ta_4O_{11}$ (powder) from the 20 hour run was used. Data were collected with the PW1710 powder diffractometer over the range 10°-150° 2θ (CuKα) with a step size of .01° 2θ and a counting time of 5 s per step.

Refinement was carried out using the Rietveld method with a slightly modified version of the program DBW 2.9 (Wiles and Young, 1981). The program has problems with rhombohedral space groups, so the structure was refined in the subgroup P3c1, with all shifts constrained to comply with R3c. Thus, the refinement was effectively done in R3c. Data used in the refinement covered the interval 12-78° 2θ in 0.04° increments, chosen on the basis of space restrictions of the program. A small region in this range (21.5 - 24.9°) was excluded from refinement due to the presence of the (001) peak of minor (<1%) contaminant Ta_2O_5. The profile function used was the modified Lorentzian of Khattak & Cox (1977), which gave a better fit to the data than a conventional Lorentzian or Gaussian function. The

preferred orientation parameter was fixed at 0.0 because of the uncertainty of the morphology and cleavage of crystallites in the powder and because of the absence of any such data for the compound or natrotantite.

Refinement was done in three steps. First, the scale factor, cell parameters and 0° 2θ position were refined, with all structural parameters fixed at values for the transformed $Na_2Nb_4O_{11}$ starting model, and with a fixed background model based on visual estimation. In the second step, the half-width parameters, background (a quadratic function of 2θ), peak asymmetry parameter and overall isotropic temperature factor were included as variables. In the final step, all structural parameters were eventually allowed to vary, including individual isotropic temperature factors of the atoms, and the background model was expanded to a fourth order polynomial of 2θ.

The temperature factors of the atoms all converged on values higher than expected (i.e. those of $Na_2Nb_4O_{11}$) by a factor of 2 to 3; this may be due to absorption, which is not modelled by the program. In an attempt to evaluate the effect of the problem on the positional parameters, the temperature factors were fixed at expected values and the data were re-refined. Although the pattern R's increased by a factor of 1.5 and the Bràgg R by a factor of 3, the positional parameters of the atoms showed insignificant shift (mean absolute shift =1.5 σ, maximum absolute shift = 2.5 σ). Thus, the problem does not affect the positional parameters significantly.

In the last cycle, 26 parameters (profile, lattice and structural) were refined simultaneously until all shifts were less than 0.1 σ. Final values of the important profile parameters are given in Table 28. Lattice and structural parameters and final R-indices are given in Table 29. A plot of the observed and calculated profiles is given in Figure 16.

Table 28: Profile Information for Synthetic Natrotantite

Preferred orientation parameter: 0.0 (fixed)

Asymmetry parameter: 1.04(4)

Halfwidth parameters:
    U=0.127(9), V=-0.064(6), W=0.0263(9)

2θ(initial): 12.0°, 2θ(final): 78.0°, step: 0.04°

Number of datapoints: 1565

Table 29: Structural Parameters for Synthetic Natrotantite

Atom	x	y	z	B (Å)^2
Na	0	0	0.3323(3)	3.1(3)
Ta(1)	0.3641(2)	0	1/4	3.14(4)
Ta(2)	0	0	0	3.36(7)
O(1)	0.052(1)	0.414(1)	0.1975(1)	2.2(2)
O(2)	0.750(2)	0	1/4	3.6(3)
O(3)	0	0	0.4074(4)	1.8(4)

Space group: R3c,   a=6.2092(1) c=36.619(1) Å

Rp = 8.7, Rwp = 9.2, RB = 2.3 %

$Rp = \Sigma|y_i(o)-y_i(c)| / \Sigma y_i(o)$

$Rwp = \{\Sigma w_i [y_i(o)-y_i(c)]^2 / \Sigma w_i [y_i(o)]^2\}^{1/2}$
        $w_i = 1/(y_i + y_{bi})$

$RB = \Sigma|I_\kappa(o)-I_\kappa(c)| / \Sigma I_\kappa(o)$
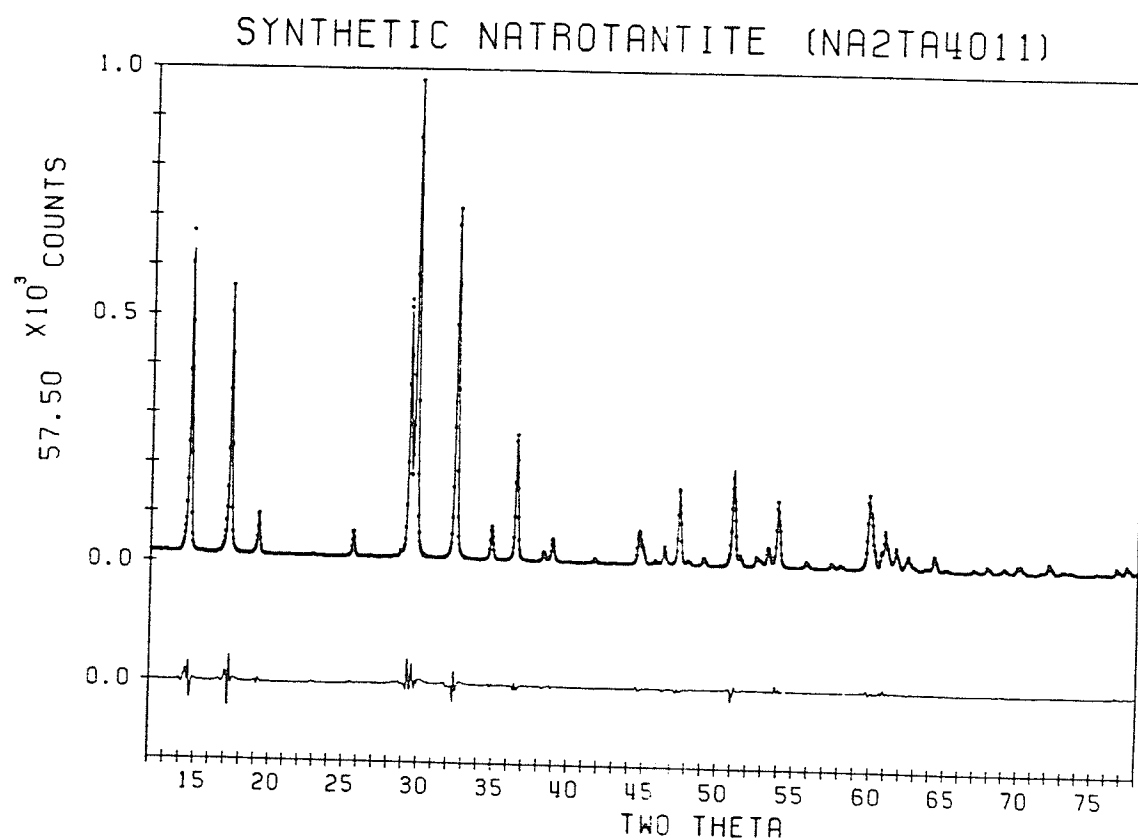
Figure 16: X-ray powder diffractometer profile (CuKα) of natrotantite. Above, squares: datapoints, curve: calculated profile. Below, difference plot.

10.5   DESCRIPTION OF THE STRUCTURE

The general topology of the $Na_2Ta_4O_{11}$ structure is the same as that of $Na_2Nb_4O_{11}$; the two structures differ only in geometric detail. The structure consists of alternations of two types of layer along $\underline{Z}$ (Figure 17). Each layer has edge-sharing arrangements, with adjacent layers connected via corners and edges. One layer consists of isolated TaO_6 octahedra in a sheet of NaO_7 capped octahedra. The other layer consists solely of TaO_7 pentagonal bipyramids. These shall be referred to as the octahedral and pentagonal bipyramidal layers respectively.

Bond lengths and angles are given in Table 30. The Ta octahedron is regular. All Ta-O bond lengths are equal and all O-Ta-O angles are within $1.1°$ of the mean $(90°)$. Conversely, the Ta pentagonal bipyramid is quite distorted. Axial Ta-O bonds $(Ta(1)-O(1))$ are shorter than equatorial bonds $(Ta(1)-O(2), Ta(1)-O(3))$, as is to be expected for this type of coordination polyhedron. However, there is considerable variation in equatorial bond angles and lengths, a consequence of repulsion due to crowding of Ta-O bonds in the equatorial plane ($<O-Ta-O>eq. = 78.2°$), in conjunction with the high degree of edge-sharing of the bipyramids in the plane.

The Na polyhedron is also highly distorted. Each Na polyhedron shares three edges with three Ta bipyramids of one of the adjacent pentagonal bipyramidal layers. The capping-oxygen bond is the longest of the polyhedron. Because this bond points alternately upward and downward from Na polyhedron to Na polyhedron within an octahedral layer, adjacent Na polyhedra link via edge-sharing to different pentagonal bipyramidal layers.

Comparison of the details of the $Na_2Ta_4O_{11}$ structure with those of $Na_2Nb_4O_{11}$ gives predictable results (Table 31). $Na_2Ta_4O_{11}$ and $Na_2Nb_4O_{11}$ show no real differences in terms of polyhedral bond length distortion. In

A

B
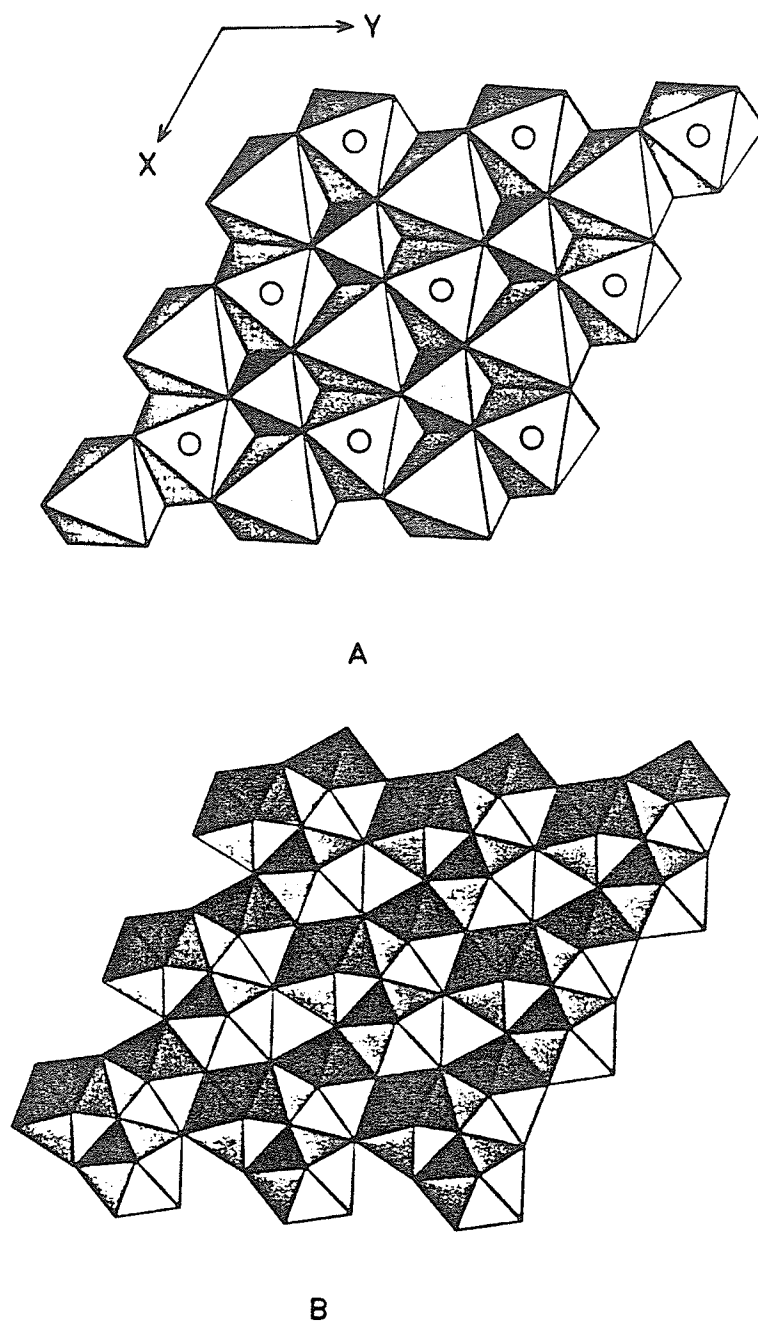
Figure 17: Natrotantite structure. (a) "Octahedral" layer. The small octahedra contain Ta, the large octahedra, sodium. Circles over the Na polyhedra mark the seventh oxygen in the true Na coordination polyhedron; Na polyhedra without circles have their seventh oxygen below the plane of the figure. (b) Pentagonal bipyramidal layer.

Table 30: Selected Interatomic Distances (Å) and Angles (°)

Ta(1) Pentagonal Bipyramid

Ta(1) - O(1)	x 2	1.95
- O(2)	x 2	2.00
- O(2)	x 1	2.40
- O(3)	x 2	2.01

< Ta(1) - O >	2.05

Equatorial Angles

O(2) - Ta(1) - O(2)	x 1	84.3
- O(3)	x 2	78.0
- O(3)	x 2	75.6

< O(eq) - Ta - O(eq) >	78.3

O(1) - O(2)	x 2	3.00
- O(2)	x 2	2.97
- O(2)	x 2	2.74
- O(3)	x 2	2.81
- O(3)	x 2	2.70
O(2) - O(2)	x 1	2.69
- O(3)	x 4	2.40

< O - O >	2.72

Axial-Equatorial Angles

O(1) - Ta(1) - O(2)	x 2	85.7
- O(2)	x 2	98.8
- O(2)	x 2	87.7
- O(3)	x 2	86.0
- O(3)	x 2	90.4

< O(ax) - Ta - O(eq) >	89.7

Ta(2) Octahedron

Ta(2) - O(1)	x 6	2.01

O(1) - Ta(2) - O(1)	x 6	91.1
- O(1)	x 6	88.9

O(1) - O(1)	x 6	2.81
O(1) - O(1)	x 6	2.88

< O - O >	2.85

< O - Ta - O >	90.0

Na Polyhedron

Na - O(1)	x 3	2.48
- O(1)	x 3	2.66
- O(3)	x 1	2.75

< Na - O >	2.60

O(1) - Na - O(1)	x 3	91.4
- O(1)	x 3	94.0
- O(1)	x 3	84.1
- O(1)	x 3	94.8
- O(3)	x 3	61.9

O(1) - O(1)	x 6	2.81
- O(1)	x 6	2.88
- O(3)	x 3	2.70

< O - O >	2.82

terms of bond angles, the M^{5-} polyhedra of $Na_2Ta_4O_{11}$ are marginally less distorted than those of $Na_2Nb_4O_{11}$, at the expense of additional distortion in the Na polyhedron. Why the lower symmetry exists for this niobium oxide, and for niobium oxides versus tantalum oxides in general, is not understood.

As pointed out by Jahnberg (1970), the structure of natrotantite $(Na_2Ta_4O_{11})$ is similar to that of calciotantite $(CaTa_4O_{11})$, as calciotantite possesses alternating "octahedral" and pentagonal bipyramidal layers like natrotantite. The pentagonal bipyramidal layer of calciotantite is topologically identical to that of natrotantite. The octahedral layer (Figure 18) is similar to that of natrotantite, except that only one out of every two of the potential large-cation sites is occupied (in an ordered manner), and that the large-cation polyhedron is 8-coordinated. The difference in coordination of the large cation between the two structures is responsible for their different layer-stacking sequences. Seven-coordination of the large cation in natrotantite introduces an additional translation in the layer stacking that calciotantite does not have, resulting in a 36.6 Å $\underline{c}$ period in the latter compared to 12.3 Å in the former.

Table 31: Polyhedral Distortion in $Na_2M_4O_{11}$ (M=Ta,Nb)

	$Na_2Ta_4O_{11}$			$Na_2Nb_4O_{11}$		
	Δ	σ^2		Δ	σ^2	
$^{VI}[M^{5+}]$	0	1		2	2	
$^{VII}[M^{5+}]$	51	10	[O(eq)-M-O(eq)]	45,48	9,18	[O(eq)-M-O(eq)]
		23	[O(eq)-M-O(ax)]		27,25	[O(eq)-M-O(ax)]
$^{VIII}[Na]$	3	150		3	104	

$\Delta = 1/n \sum_{}^{n}[(l_i - l_0)/l_0]^2 \times 10^4$ where $l_0 = 1/n \sum_{}^{n} l_i$

$\sigma^2 = 1/n \sum_{}^{n}(\theta_i - \theta_0)^2$ where $\theta_0 = 1/n \sum_{}^{n}\theta_i$

eq: equatorial, ax: axial
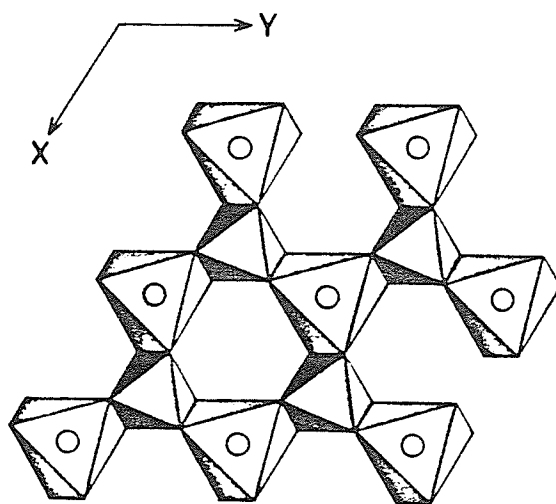
Figure 18: The octahedral layer of calciotantite. All symbols have the same significance as in Figure 17. The eighth oxygen of the Ca polyhedron lies directly under the polyhedron, with the same lateral coordinates as the seventh oxygen.

10.6   DISCUSSION: THE CRYSTAL CHEMISTRY OF NATROTANTITE

All samples of natrotantite and synthetic $Na_2Ta_4O_{11}$ are isomorphous, indicating that natrotantite ideally possesses $A^+_2B^{5+}_4O_{11}$ stoichiometry. The natural samples are all non-stoichiometric; variable Na_2O and near-constant $Ta_2O_5 + Nb_2O_5$ of these samples suggest that partial A-cation vacancy, and perhaps anion vacancy is the norm for natrotantites. By analogy with behaviour in the pyrochlore group (Hogarth, 1977), Ta-Nb analogues of "tungsten"-bronze structured compounds, and defect sodium "oxyfluorotantalates" (Chaminade et al., 1972), it is expected that the B-cation sites should be fully occupied. Table 32 contains the contents per formula unit of natrotantites, calculated assuming full B-cation site occupancies. On the basis of these calculations, the A-cation site of Alto do Giz samples is approximately 50-60 % occupied, and of the Leshaia sample, 70 % occupied. Space group restrictions indicate the A-cation site vacancies to be distributed in a disordered manner.

The matter of anion vacancies is not easily resolved. The recalculations allow for the possibility of vacancies; however, synthesis studies suggest the opposite. Consequently, it is most likely that charge balance in A-cation deficient natrotantites is brought about by hydroxyl or fluorine substitution for oxygen. Unfortunately, this model has yet to be directly tested experimentally. Samples of natural natrotantites are less than 0.1 mm^3 in total volume, precluding powder IR spectroscopic examinations. Chaminade et al. (1972) did not detect O = F substitution in $Na_2Ta_4O_{11}$; however, the join needed to evaluate such substitutions, $Na_2Ta_4O_{11}-Ta_4O_9F_2$, was not investigated in his study. Andersson (1967) suggested O = OH substitution in $Na_2Nb_4O_{11}$, but did not test this model.

Table 32: Formula Contents of Natrotantites

	1	2	3	4
Na^+	0.93	0.95	1.03	1.40
K^+	0.01	0.04	----	----
Ca^{2+}	0.04	0.07	0.02	0.01
Pb^{2+}	0.03	0.07	0.14	0.04
Nb^{5+}	0.07	0.07	0.03	0.19
Ta^{5+}	3.93	3.93	3.97	3.81

Σ A-site:	1.01	1.13	1.19	1.45
O(eff):	10.54	10.63	10.68	10.75

Calculated on 4(Ta+Nb)

1. L-17   (Alto do Giz, Brazil).
2. RVG-1C-6   "
3. RVG-1C-5   "
4. Leshaia, Kola Peninsula, USSR.

- see Table 24 for references

In light of these conclusions, it is instructive to re-examine the X-ray data for the natural and synthetic natrotantites. In Figure 19, a plot of the c period of natural and synthetic natrotantites is shown plotted against $\underline{A}$-site occupancies. An excellent negative correlation (R=-95%) exists between the layer stacking period ($\underline{c}$) and $\underline{A}$-site occupancy; that is, as the $\underline{A}$-site occupancies decrease, the $\underline{c}$ period increases. No correlation exists, however, between the $\underline{a}$ period and $\underline{A}$-site occupancies (Figure 20).

As $\underline{A}$-site occupancy decreases, the polyhedron size of the site should probably increase (Shannon, 1976), which would be reflected in increased cell parameters. Because natrotantite consists of strongly-bonded layers which are sodium-free (pentagonal bipyramidal layer), alternating along $\underline{Z}$ with layers with a Na-polyhedron framework, the $\underline{c}$ period is quite sensitive to $\underline{A}$-site occupancy. The lack of vacancies in the pentagonal bipyramidal layers and high relative strength of B-O bonds in the layers ($\underline{X}$-$\underline{Y}$ plane) make $\underline{a}$ relatively insensitive to $\underline{A}$-site occupancy.

Thus, on the basis of the present understanding of natural and synthetic natrotantites, the formula of natrotantite is best written as:

$$(M^+_x M^{2+}_y) M^{5+}_4 O_{11-z} (OH,F)_z$$
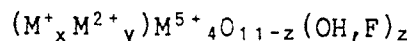
where $z = 2-(x+y)$. In natural samples, $1 < x+y < 1.5$ and $x \gg y$.
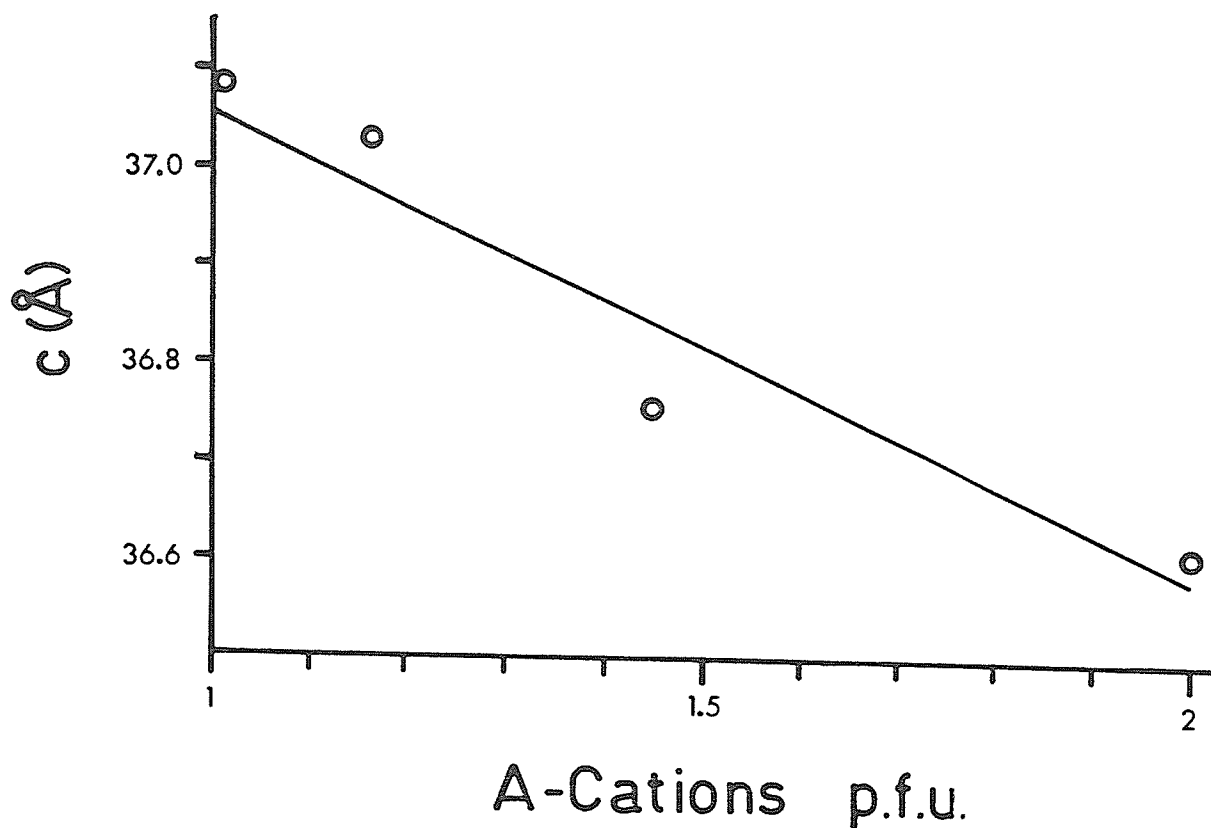
Figure 19: Layer stacking period (c) versus A-site occupancy in natrotantites.
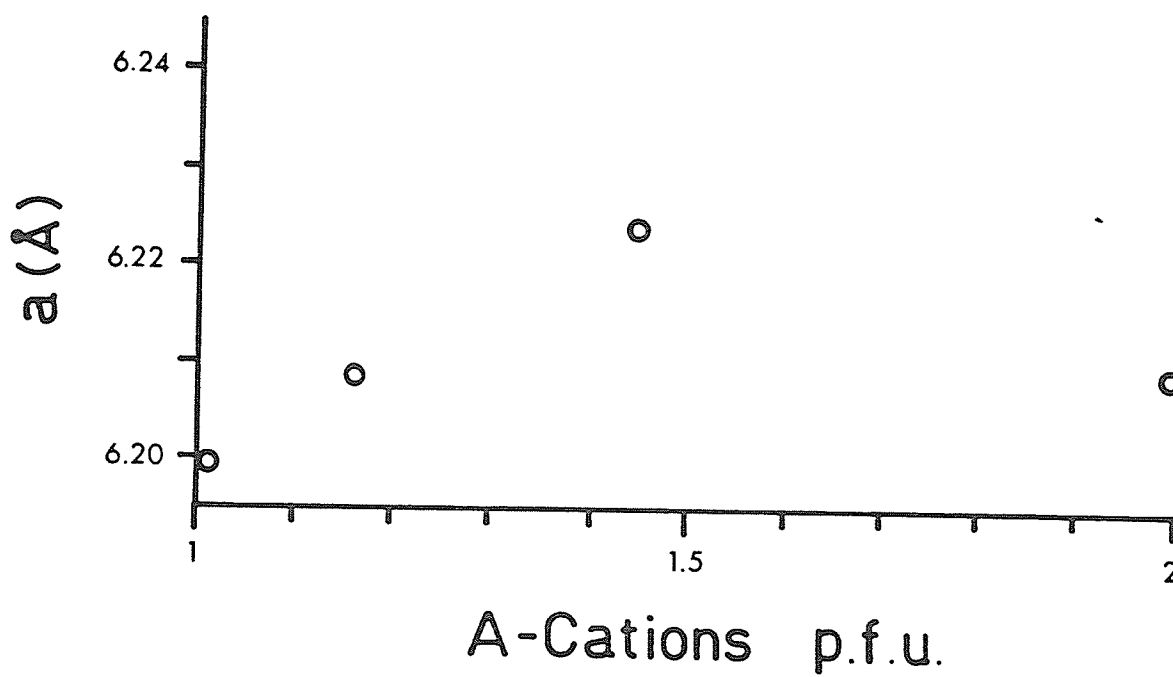
Figure 20: a cell edge versus A-site occupancy in natrotantites.

Chapter XI

RANKAMAITE AND SOSEDKOITE

11.1   INTRODUCTION

Rankamaite, a sodium-bearing tantalum oxide of complex chemistry, was discovered by von Knorring et al. (1969). At the type locality, Mumba, at Lake Kivu, Zaire, it occurs as soft, white, fibrous replacements of simpsonite and other oxide minerals which together occur as alluvial pebbles. The potassium analogue of rankamaite was discovered by Voloshin et al. (1982) and was named sosedkoite. At the type locality at Leshaia in the Kola Peninsula, USSR, it occurs as late (post-simpsonite) acicular crystals. Rankamaite and sosedkoite are assumed to form a continuous solid solution series (Voloshin et al., 1982) on the basis of the intermediate Na:K ratios shown by both species. Rankamaite and sosedkoite have only been found at these two localities, and as such are unique to the simpsonite paragenesis.

Although samples from both Mumba and Leshaia were obtained for the study, rankamaite-sosedkoite was only found in the Mumba samples. Consequently, all new data for the mineral presented here are based on study of this occurrence only.
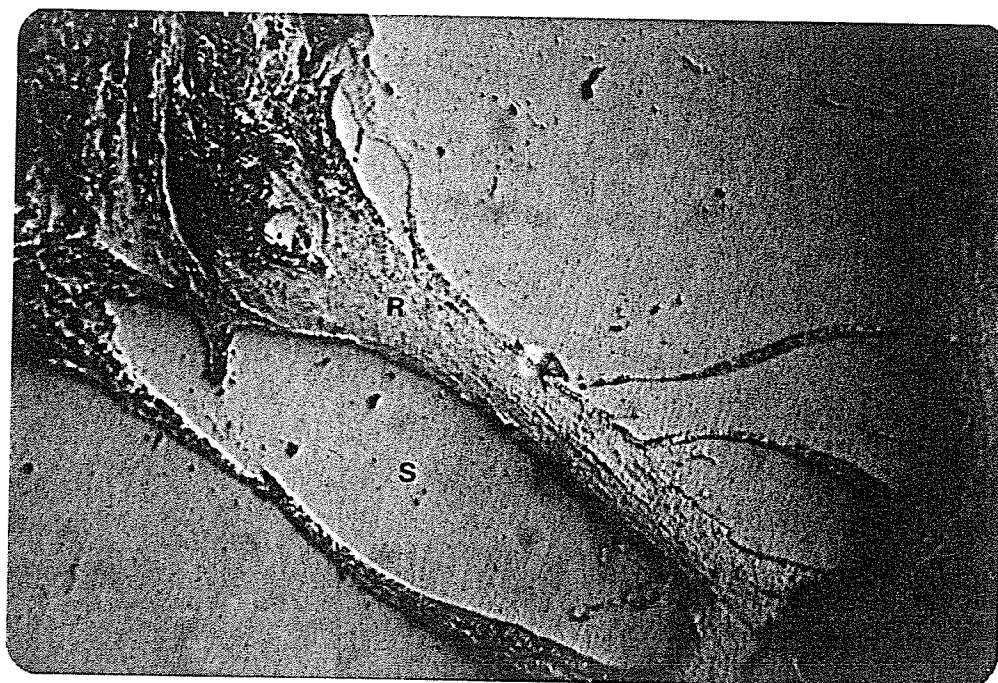
Figure 21: Rankamaite (fibrous) replacing simpsonite (rounded crystals). Reflected light, 100 X magnification.

11.2   PHYSICAL AND OPTICAL PROPERTIES

Rankamaite-sosedkoite always occurs as acicular crystals, elongated along $\underline{Z}$. The style of aggregation varies from deposit to deposit: at Mumba, the aggregation is always fibrous, almost asbestiform (Figure 21), whereas at Leshaia it only forms single crystals.

The mineral is colourless to white, but may appear yellow because of iron staining due to weathering or to relict simpsonite in the rankamaite-sosedkoite fibres. In transmitted light, it is biaxial negative with $\underline{Z}$ || $\underline{c}$. In reflected light, it has a high relative reflectivity (> simpsonite). It is relatively soft (H<4) and has variable but high density (5.5-6.9 g/cm^3: von Knorring et al., 1969; Voloshin et al., 1982), which increases with increasing Ta:Nb ratio.

11.3   CHEMISTRY

All chemical analyses of rankamaite-sosedkoite from this study and from previous investigations are given in Table 33. Analysis (2) (from von Knorring et al., 1969) has been corrected for muscovite impurities. Rankamaite-sosedkoite has a complex chemistry: Na, K, P, Al, Fe^{3+}, Nb, Ta, OH, O are all major constituents of the mineral, and the ratios of these elements to one another, particularly Na:K and Nb:Ta are quite variable. Because all but one analysis are electron microprobe analyses, H_2O determination has been done for only one sample to date. Li is of questionable origin, and may be due to "mica" contamination (e.g. atomic absorption analysis of sosedkoite by Voloshin et al., 1982 gave no detectable Li_2O).

Table 33:   Rankamaite and Sosedkoite Analyses

	1	2	3	4
Na_2O	2.3	2.36	1.9	1.2
K_2O	1.9	1.63	2.2	2.8
PbO	2.2	2.69	1.8	---
CaO	---	----	0.05	0.1
Al_2O_3	2.7	2.64	2.2	2.0
Fe_2O_3	1.2	----	1.1	---
Sb_2O_3	---	----	---	0.5
Nb_2O_5	19.8	17.77	15.7	2.7
Ta_2O_5	69.4	70.94	73.6	91.3
H_2O^+	---	1.48	---	---
	99.6	99.52	98.4	100.4

Ions per $24(Ta+Nb+Al+Fe+Sb)$

	1	2	3	4
Na^+	3.41	3.61	2.84	1.88
K^+	1.84	1.64	2.17	2.99
Pb^{2+}	0.43	0.57	0.38	----
Ca^{2+}	----	----	0.04	0.09
Σ	5.68	5.82	5.43	4.96
Al^{3+}	2.42	2.45	2.02	1.94
Fe^{3+}	0.67	----	0.63	----
Sb^{3+}	----	----	----	0.16
Nb^{5+}	6.73	6.34	5.59	1.03
Ta^{5+}	14.18	15.21	15.76	20.87
OH^-	----	7.79	----	----
O	----	56.85	----	----
O(eff)	59.96	60.74	60.28	60.42

1. Rankamaite (this study).
2. Rankamaite (von Knorring et al.,
   1969). Corrected for muscovite
   impurities.
3. Rankamaite (Voloshin et al., 1982).
4. Sosedkoite (Voloshin et al., 1982).

O(eff): effective oxygen for charge
        balance.

11.4   X-RAY CRYSTALLOGRAPHY

X-ray powder diffraction data for rankamaite and sosedkoite are given in Table 34.   The diffraction patterns are complex, but can be indexed on an orthorhombic unit cell of dimensions $\underline{a}$=17.2, $\underline{b}$=17.7, $\underline{c}$=3.9 Å.   Precise cell parameters are given in Table 34.

Because of the fibrous nature of rankamaite, single crystal diffraction photographs could not be taken.   All attempts at taking precession photographs gave multiple diffraction maxima or smeared, arcuate maxima indicative of subparallel orientation of fibre-like crystals in the fragments photographed.   However, a photograph taken parallel to the length of one clump of fibres was of good enough quality to confirm the long axis of the fibres to be $\underline{Z}$.

As a consequence of the lack of suitable single crystals for study, all conclusions regarding the space group of rankamaite-sosedkoite had to be derived from systematic absences in powder diffraction data.   The data follow a pseudo C-centred distribution,   with the condition h+k=2n satisified for all diffractions except one: (121)   (and perhaps another: (210) of sosedkoite?). A check for possible contamination was made by comparing the rankamaite pattern to its only possible contaminant: simpsonite.   The unambiguous absence of many of the strong lines of simpsonite in the rankamaite pattern indicated that there was no detectable contamination at all. Consequently, the space lattice of rankamaite must be P-centred.   From the data of this study, the following systematic absences hold:

Table 34: X-Ray Powder Diffraction Data for Rankamaite and Sosedkoite

	Rankamaite (L-14)			Sosedkoite*	
hkl	d(calc)	d(obs)	I	d(obs)	I
020	8.84	8.81	2	8.8	2
?				7.2	1
220	6.16	6.19	2	6.1	5
130	5.73	5.58	<1		
310	5.45	5.46	3	5.47	2
040	4.42	4.43	3	4.42	3
400	4.30	4.30	2	4.24	2
330	4.11	4.11	3	4.12	2
001,	3.94				
240	3.93	3.94	5	3.95	10
420	3.86	3.86	2		
201	3.58	3.59	<1		
150	3.47	3.46	5	3.47	5
510	3.37	3.37	5	3.28	2
311	3.194	3.193	<1	3.15	1
440	3.081	3.078	1		
350	3.010	3.014	7	3.03	9
530,	2.969	2.962	10	2.99	2
060,	2.948				
041	2.942			2.95	2
600,	2.864				
331	2.844	2.853	2	2.85	1
260	2.789	2.787	4	2.79	5
421	2.759	2.755	1		
620	2.725	2.722	1		
151	2.602	2.607	<1	2.611	2
511	2.563	2.564	1	2.574	3
460	2.431	2.427	<1		
351	2.392	2.394	1	2.396	1
531	2.371	2.369	2	2.374	1

a = 17.184(5) Å
b = 17.689(8)
c = 3.942(2)

* from Voloshin et. al (1982)

hk0 with h+k=2n+1

h0l with h=2n+1

0kl with k=2n+1

which indicate the space group to be Pban.

11.5 DISCUSSION: THE CRYSTAL CHEMISTRY OF RANKAMAITE-SOSEDKOITE

Rankamaite-sosedkoite shows diffraction patterns and unit cell dimen-sions which indicate that its structure is derived from that of the tetrag-onal tungsten bronzes. The a:b ratio of rankamaite-sosedkoite ranges from 0.973 to 0.983, very close to the ideal value of 1 for tetragonal symmetry. The similarity of its powder data to those of orthorhombically distorted "tetragonal tungsten bronze"-derived structures (von Knorring et al., 1969) indicates it to be a close relative of these compounds. Rankamaite-sosedkoite is proposed to be an orthorhombic superstructure of the simple tetragonal tungsten bronze structure (Figure 22).

Synthetic tungsten bronzes are typically alkali-cation deficient, yet do not have any vacancies at the octahedral sites. Although the anion sites are not typically anion-deficient, the possibility of O=OH substitution without previous knowledge of the O:OH ratio or of the ideal number of anions per unit cell makes normalization on an anion basis impossible.

Consideration of the measured density and unit cell volumes of rankamaite-sosedkoite in conjunction with its chemistry indicates that there are approximately 28-30 cations and 60 anions (= effective oxygen for charge balance) per unit cell. Using a basis of 60 anions per formula unit, von Knorring et al. (1969) proposed
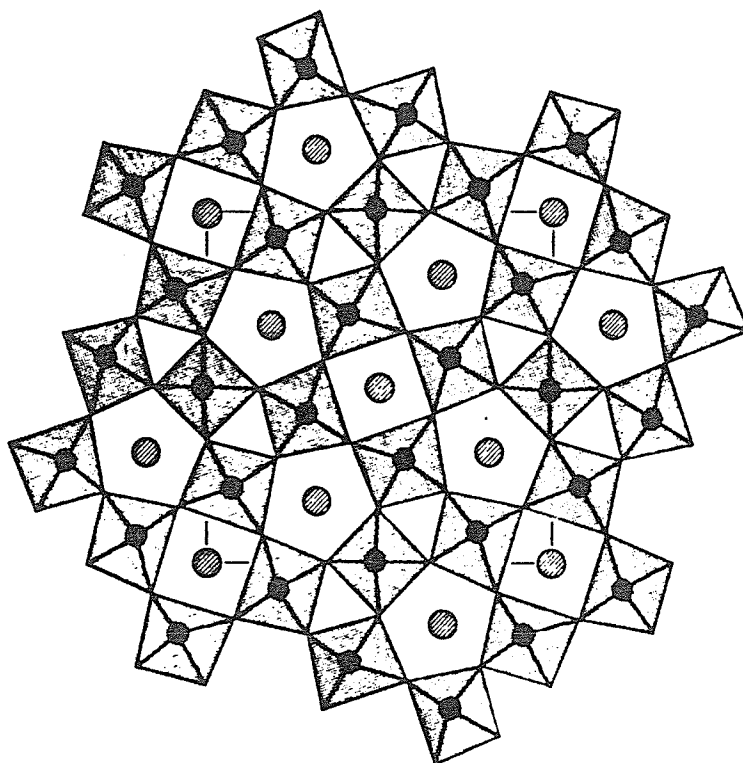
Tetragonal tungsten bronze structure as typified by $K_x WO_3$ (from Lundberg, 1971). The tungsten polyhedra (shaded) corner-link to form 3-, 4-, and 5-sided holes. Alkali cations occupy the 4- and 5-sided interstices. Nb and Ta analogues have octahedra of these cations in place of W. The unit cell volume of rankamaite-sosedkoite is 2x that of the tetragonal tungsten bronze structure.

$$(Na,K,Pb,Li)_{5.86}(Ta,Nb,Al)_{22.18}(O,OH)_{60}$$
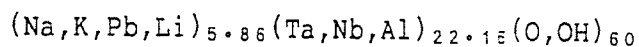
as the formula for rankamaite. Along a similar line, Voloshin gave

$$(Na,K)_5Al_2(Ta,Nb)_{22}(O,OH)_{60}$$
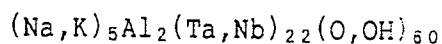
as the ideal formula for rankamaite-sosedkoite, whereby Na>K for rankamaite and K>Na for sosedkoite.   The problems with the above formulations are numerous:

1. von Knorring et al. (1969) made errors in calculating the formula of rankamaite which result in an underestimation of the anion:cation ratio.

2. Voloshin et al. (1982) incorrectly calculated the formula of rankamaite on a basis of 60 oxygens, not 60 anions, which has the effect of artificially lowering the cation:anion ratio.

3. Voloshin et al.'s (1982) ideal formula underestimates "observed" site occupancies (inferred from chemistry) by as much as 17%.

4. Fe^{3+} is assumed to substitute for Ta in the model of Voloshin et al. (1982), whereas from both size and charge considerations, it should prefer the Al-site instead. Transfer of Fe^{3+} to the proposed Al-site causes an overfilling of the site by 32%.

5. An ideal site occupancy of 5 cations (for the Na+K site) is not possible on the basis of site multiplicities for the space group Pban (note: nor is it possible for any of the C-centred space groups proposed by von Knorring et al., 1969), invalidating Voloshin et al.'s (1982) ideal formula.

From the above and previous discussions, it is obvious that one must consider O=OH substitution, the ideal anion:cation ratio, the possibility of variable alkali contents, and possible octahedral cation ordering before proposing a formula for these minerals. With very little data available on H_2O contents of rankamaite-sosedkoite, all of these aspects of rankamaite-sosedkoite chemistry are difficult to assess.

Variable (Na+K) contents make normalization on the total cation sum impossible. However, the improbability of vacancies at the octahedral cation sites allows normalization on the octahedral cation sum. Assuming Al, Fe^{3+}, Sb^{3+}, Ta and Nb to be in octahedral coordination, rankamaite has 24 octahedral cations per unit cell (on the basis of the measured density of rankamaite). Unit cell contents for rankamaite and sosedkoite on a basis of 24 octahedral cations are given in Table 33. From this calculation, it can be seen that the alkali cation site sum is variable, ranging from 5 to 6 cations per unit cell. The maximum of 6 cations is the best estimate to date of the ideal full occupancy of this site. The number of effective oxygens is only slightly variable, ranging from 60 to 60.75; however, the total number of anions for the one analysis with H_2O determined, is 64.6. The ratios of $(Ta+Nb)^{5+}:(Al+Fe+Sb)^{3+}$ are variable, ranging from 7:1 to 11:1. Looking at Al alone, although Voloshin et al.'s (1969) analyses give 2 Al per unit cell, the analyses of von Knorring et al. (1969) and of this study give significantly more than 2 Al per unit cell (Table 33). No ideal Al:(Fe+Sb+Nb+Ta) or (Al+Fe+Sb):(Ta+Nb) ratio exists for this mineral, and full trivalent cation - pentavalent cation order is unlikely.

Of all the tetragonal tungsten-bronze derivative compounds, the X-ray powder diffraction patterns of $PbNb_4O_{11}$ and $Na_2Ta_8O_{21}$ are most similar to

rankamaite-sosedkoite. For the only rankamaite-sosedkoite on which an estimate of the total number of anions can be made (analysis (2) of Table 33), the nearest integral number of anions is 65. However, site multiplicities for Pban dictate that ideal rankamaite-sosedkoite should have an even number of anions per unit cell. In terms of both the alkali cation to octahedral cation to anion ratio and powder diffraction data, rankamaite-sosedkoite is most similar to $PbNb_4O_{11}$. Ideal natrotantite probably has $AB_4\emptyset_{11}$ stoichiometry (i.e. unit cell content of $A_6B_{24}\emptyset_{66}$). The observed number of anions per unit cell for the Mumba rankamaite is only 1.5% below the ideal number for this stoichiometry, which can easily be ascribed to analytical error, or to minor anion vacancies. That the number of effective oxygens (for charge balance) varies only slightly between all analyses, suggests that the O:OH ratio is similarly only slightly variable. As Voloshin et al. (1982) noted, most rankamaite-sosedkoites give reasonably stoichiometric-looking formulae when calculated on 60 effective oxygens. This corresponds to 54 O + 12 OH, a result somewhat at odds with von Knorring et al.'s analytical results (57 O + 8 OH).

Without better data on the behaviour of Al and without more water determinations, the ideal formula of rankamaite-sosedkoite is best given as:

$$(Na,K)_{1-x}(Ta,Nb,Al)_4(O,OH)_{11} \quad (Z=6)$$
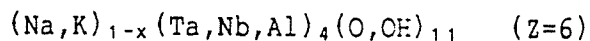
whereby positive charge deficiency brought about by alkali cation site vacancies and Ta,Nb $\rightarrow$ Al substitution is offset by increased O $\rightarrow$ OH substitution. Results from the structural studies of simpsonite and alumotantite make complete Al - Ta disorder seem unlikely which, considered with

the persistence of Al in the mineral, suggests at least partial order between these elements. It is possible that the ideal formula may take the form

$$(Na,K)_{1-x}(Al,Ta)(Ta,Nb)_3(O,OH)_{11}$$
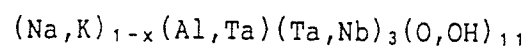
but in the absence of material suitable for structure analysis, this cannot be tested.

Chapter XII

WODGINITE

12.1 INTRODUCTION

Although wodginite was first encountered by Simpson (1909) at Wodgina, Western Australia, recognition of its status as a new mineral species came only when the work of Nickel et al. (1963) on oxide minerals of the Tanco pegmatite showed it to be distinct from tantalite. Wodginite is much more common than initially realized; since 1963, it has been recognized at thirty other localities (Table 35), over half of which were found in the last decade.

Nickel et al. (1963b) correctly inferred wodginite to be a superstructure of ixiolite; however, it was not until much later that its details were deduced. The first published structure of wodginite was that of Grice (1973). Grice and Ferguson (1974) orally presented the results of this study at the same time as Graham and Thornber (1974b) published the results of their analysis of the wodginite structure. Later, Ferguson et al. (1976) showed that all earlier studies of the structure were in error due to incorrectly chosen origins or space groups. They re-refined the data of Grice (1973) and obtained the currently accepted model for the structure. As such, the ideal formula of wodginite was proposed to be $MnSnTa_2O_8$, $Z=4$, and space group $C2/c$.

Although the existence of partially disordered wodginites was suggested in early studies, proof was not established until recently (Lahti, 1982).

Table 35: Wodginite Localities

Locality	Sample Obtained	Sample No.
1. Alto do Giz pegmatite, Brazil	Y	L-15
2. Ankole, Uganda	Y	A-17
3. Annie Claim pegmatite, Manitoba	Y	AC2-79
4. Benson pegmatite, Zimbabwe	N	
5. Coosa County, Alabama	Y	CX-1
6. Cross Lake, Manitoba	Y	CL-1
7. Eräjärvi pegmatite area, Finland	N	
8. Greenbushes pegmatite, W. Australia	Y	GB-1 to -4
9. Herbb No. 2 pegmatite, Virginia	Y	H2-1
10. Kalbin Range, USSR	N	
11. Karibib, Namibia	Y	MC-1
12. Kazakhstan, USSR	Y	KZ-1
13. Kola Peninsula, USSR	Y	KO-1
14. Krasonice, Moravia, Czechoslovakia	Y	CZ-1
15. Lavra Jabuti, Minas Gerais, Brazil	Y	LJ-1
16. Marble Bar, W. Australia	Y	MB-1
17. Mt. Matthew, W. Australia	Y	MM-1
18. Muhembe River, Rwanda	Y	A-17
19. Odd West pegmatite, Manitoba	Y	OW-102
20. Peerless pegmatite, S. Dakota	Y	A-29,-30
21. Eastern Sayan, USSR	N	
22. Seridozinho, Paraiba, Brazil	N	
23. Eastern Siberia, USSR	N	
24. Strickland Quarry, Connecticut	Y	SQ-1
25. Sukula pegmatite, Tammela, Finland	Y	SK-1
26. Tabba Tabba, W. Australia	Y	TT-1
27. Tanco pegmatite, Manitoba	Y	Various (G69-, SMP-,TSE-series)
28. Lower Tanco pegmatite, Manitoba	Y	
29. Transbaikal region, USSR	Y	TB-1
30. Viitaniemi pegmatite, Finland	Y	VII-1
31. Wodgina, W. Australia	Y	WD-1
32. Yellowknife, NWT	Y	YKF-series

Several models for order-disorder in wodginite have been proposed (e.g. Maksimova & Khvostova, 1970; Khvostova et al., 1982); however, all have been speculative, and little experimental work has been done.

Work on the chemistry of the mineral has principally appeared in descriptive reports of its occurrence; there are few studies with the chemistry of the mineral as a primary objective. Chemical data from synthesis studies is the exception to this trend. Turnock (1966) was the first to synthesize wodginite, showing that ferric iron played a similar role to tin in the structure. Komkov (1970) was the first to grow tin-bearing wodginites similar in chemistry to natural wodginites. Sidorenko et al. (1974) showed that synthetic wodginites could be non-stoichiometric by growing wodginites with variable Sn:Mn+Ta ratios. Gatehouse et al. (1976) showed that cations as small as Li^+ could stabilize the wodginite structure. Komkov & Dubik (1983) proved Sn$\leftrightarrow$Ti isomorphism in synthetic wodginites.

The discovery of wodginite in four of the simpsonite-bearing assemblages, together with its great abundance at the Tanco pegmatite (Part 4) makes wodginite an important mineral in this study. For this reason, the crystal chemistry of wodginite is a major theme of this work, and extends past the confines of the simpsonite paragenesis.

Samples were obtained from all but six of the known localities for wodginite (Table 35). As such, most extremes in chemistry and structure shown by wodginite were examined (as recorded in the literature). The main exception was the Fe^{3+}-rich wodginite from the Transbaikal territory of the USSR (Kornetova et al., 1978), from which samples were obtained, but no wodginite was found. However, Fe^{3+}-rich synthetic wodginites were donated for study by Dr. A.C. Turnock, which completed the dataset from the point of view of chemistry.

12.2 CRYSTALLOGRAPHY

Wodginite typically occurs as irregular aggregates of crystals or as parallel to subparallel groups of crystals. Twinning is a common feature of wodginite; all apparently "isolated" crystals of wodginite are actually twins. Penetration twins with {001} or {100} as the composition planes are the most common. Predominance of the form {111} in combination with this style of twinning produces the characteristic diamond-shaped pseudo-orthorhombic morphology of wodginite; when present, this readily distinguishes it from columbite-tantalite and tapiolite (Figure 23). Wodginites can also be polysynthetically twinned across {100} (e.g. sample SK-1); however, this style of twinning is much less frequent than the penetration twinning.

Powder diffraction data for several wodginites are given in Table 36. All samples studied show the following systematic absence conditions when indexed on the cell of Ferguson et al. (1976):

$$hkl, \quad h+k = 2n+1$$
$$h0l, \quad l = 2n+1$$

Some show additional systematic absence conditions suggesting either a subcell or increased symmetry; these are discussed in a later section (Order-Disorder). The conditions listed above are compatible with the space groups C2/c and Cc. Ferguson et al. (1976) showed the former to be the correct choice; hence wodginite is centric with space group C2/c. This is at odds with the results of second harmonic generation (SHG) tests by Gatehouse et al. (1976) on synthetic $M-LiTa_3O_8$, in which they got a positive
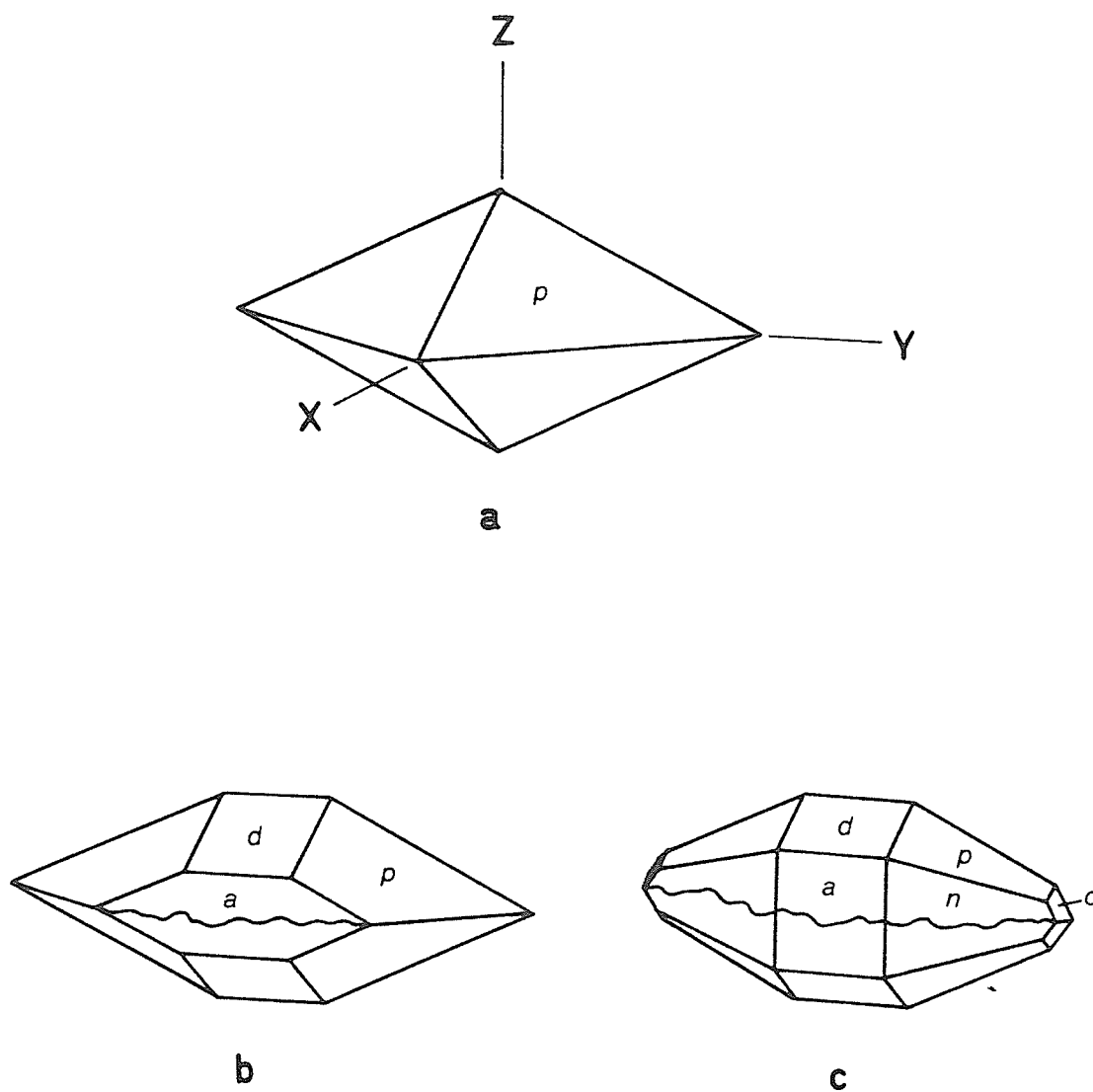
Figure 23: The morphology of penetration-twinned wodginite. (a) tantalo-wodginite, Tanco, (b) ferrowodginite, Ankole, (c) wodginite, Muhembe. Irregular lines mark composition planes. Forms are a: {100}, d: {101}, n: {310}, p: {111}, q: {131}.

result (indicating non-centrosymmetry). However, both this, and a later neutron refinement of M-LiTa$_3$O$_8$ by them (Santoro et al., 1977) were done in C2/c. Given these circumstances, together with the strong pseudo-centric character of the acentric model (Graham and Thornber, 1974b), and the significantly higher R-indices of the acentric model (Ferguson et al., 1976), there is little cause to reject the centric model.

Unit cell parameters of wodginites from this study are given in Table 37. Variation in the cell parameters can be substantial; maximum variations are:

$\underline{a}$: 0.12 Å   (1.2 %)

$\underline{b}$: 0.09 Å   (0.7 %)

$\underline{c}$: 0.06 Å   (1.2 %)

$\underline{\beta}$: 1.1 °   (1.2 %)

where the values in parentheses are relative variations. As in the columbite-tantalite group minerals (Černý and Turnock, 1971), $\underline{a}$ and $\underline{c}$ are the most variable. The angle $\underline{\beta}$ shows similar relative magnitudes of variation as $\underline{a}$ and $\underline{c}$. By comparison with columbite-tantalite group minerals, it is tempting to predict at this point that high variability of $\underline{a}$ and $\underline{c}$ (and $\underline{\beta}$) and much lesser variability of $\underline{b}$ is principally due to order-disorder effects; this question will be dealt with later.

Table 36: Powder Diffraction Data for Selected Wodginites

hkl	Wodginite (A-30) d (obs)	d (calc)	I	Tantalowodginite (TSE-76) d (obs)	d (calc)	I	Ferrowodginite (A-17) d (obs)	d (calc)	I	Titanowodginite (TSE-126) d (obs)	d (calc)	I
110	7.33	7.33	2	7.31	7.31	5	7.29	7.30	3	7.28	7.28	<1
020	5.74	5.75	3	5.75	5.76	2	5.71	5.72	1	5.71	5.71	<1
200	4.77	4.76	12	4.73	4.74	12	4.73	4.72	3	4.72	4.72	1
11̄1	4.23	4.22	4	4.20	4.20	13	4.20 } 4.18 }	4.19	2	4.19 } 4.19 }	4.19	1
111	4.16	4.16	4	4.14	4.15	12						
021	3.818	3.818	17	3.808	3.810	13	3.813	3.810	6	3.812	3.808	2
220	3.665	3.669	53	3.654	3.652	65	3.643	3.642	49	3.640	3.642	44
130	3.549	3.548	5	3.554	3.555	13	3.533	3.528	2	3.530	3.533	1
310	---	--		3.043	3.040	5	---	--		---	---	--
22̄1	3.003	3.003	100	2.987	2.984	100	2.978	2.978	100	2.969 } 2.964 }	2.967	100
221	2.957	2.957	96	2.947	2.945	86	2.959	2.962	100			
040	2.868	2.868	19	2.876	2.877	15	2.857	2.854	15	2.855	2.855	13
31̄1	---	--		2.631	2.633	4	---	--		---	---	--
311	---	--		2.590	2.592	4	---	--		---	---	--
002	2.558	2.557	24	2.541	2.543	23	2.560	2.559	21	2.560	2.561	21
041	2.501	2.501	41	2.503	2.504	38	2.495	2.493	37	2.493	2.493	31
240	2.457	2.457	5	2.458	2.460	5	---	--		---	---	--
330	---	--		2.436	2.438	6	---	--		---	---	--
400	2.382	2.382	15	2.366	2.365	17	2.365	2.364	13	2.362	2.362	16
202	2.274	2.273	6	2.255	2.256	8	2.260	2.260	5	2.253	2.254	3
241	2.205	2.204	11	2.204	2.203	16	2.203	2.202	8	2.204	2.203	7
222	2.114	2.112	9	2.100	2.100	12	2.102	2.102	8	2.096 } 2.096 }	2.096	11
222	2.082	2.081	9	2.072	2.072	11	2.088	2.087	8			
42̄1	---	--		2.022	2.022	3	---	--		---	---	--
421	---	--		1.998	1.996	5	---	--		---	---	--
042	1.909	1.909	16	1.904	1.904	10	1.907	1.907	10	1.906	1.906	8
440	1.833	1.833	12	1.827	1.827	13	1.822	1.822	10	1.820	1.820	9
260	1.774	1.774	31	1.777	1.777	30	1.767	1.766	32	1.765	1.765	28
402	1.762	1.763	23	1.747	1.747	20	1.745	1.746	20	1.738 } 1.716 }	1.740	14
44̄1	1.734	1.734	23	1.727	1.726	28	1.720	1.720	28			
402	1.725	1.726	20	1.716 } 1.712 }	1.712	31	1.729	1.729	30	1.734 } 1.714 }	1.715	36
441	1.716	1.717	20				1.712	1.713	15			
223	1.557	1.556	13	1.545	1.544	13	1.550	1.549	11	1.546	1.546	12
223	1.537	1.537	10	1.529	1.528	12	1.542	1.541	11	1.544	1.542	9
442	1.501	1.500	6	1.493	1.492	5	---	--		1.484 } 1.456 }	1.465	13
442	---	--		1.474	1.474	4	---	--		---		
62̄1	1.475	1.475	15	1.464 } 1.461 }	1.461	29	1.460	1.460	28			
262	1.463	1.464	18				1.456	1.457	27	1.454 } 1.453 }	1.454	31
262	1.453	1.453	15	1.452	1.451	21	1.452	1.452	27			
080	---	--		1.438	1.439	3	---	--		---	---	--
081	1.381	1.381	10	1.384	1.384	10	1.376	1.376	7	1.375	1.375	7

-Philips PW1710 diffractometer, automatic divergence slit with Cu Kα radiation and a graphite monochromator.
-all intensities are peak heights.
-samples A-30, TSE-76 are fully ordered, A-17 and TSE-126 are partially ordered

Table 37: Unit Cell Parameters for Wodginites

Sample	a	b	c (Å)	β °	V
A-17	9.459(1)	11.427(2)	5.121(1)	90.51(2)	553.5(1)
A-25	9.466(1)	11.431(1)	5.126(1)	90.31(2)	554.6(1)
A-29	9.533(1)	11.472(1)	5.117(1)	91.17(1)	559.4(1)
A-30	9.533(2)	11.471(1)	5.117(1)	91.21(2)	559.4(1)
AC2-79-1	9.523(3)	11.476(3)	5.142(1)	90.78(3)	561.9(2)
BLM-1A	9.498(3)	11.451(3)	5.112(2)	90.99(3)	558.6(2)
G69-2	9.496(2)	11.455(2)	5.109(1)	91.07(3)	555.6(1)
G69-13	9.497(4)	11.452(4)	5.116(2)	90.94(3)	556.4(2)
G69-14	9.491(1)	11.453(1)	5.114(1)	90.95(1)	555.9(1)
G69-17	9.517(2)	11.452(3)	5.112(2)	91.10(3)	557.0(1)
G69-23	9.487(3)	11.449(2)	5.106(1)	91.04(3)	554.5(1)
G69-39	9.498(3)	11.454(2)	5.118(1)	90.93(3)	556.7(1)
G69-42	9.492(1)	11.451(1)	5.113(1)	90.97(1)	555.7(1)
G69-46A	9.492(1)	11.452(1)	5.118(1)	90.90(1)	556.2(1)
GB-1	9.468(1)	11.441(2)	5.108(1)	90.78(2)	553.2(1)
GB-2	9.480(2)	11.444(1)	5.110(1)	90.80(2)	554.3(1)
GB-3	9.506(1)	11.459(1)	5.113(1)	90.97(1)	557.0(1)
GB-4	9.469(2)	11.436(2)	5.120(3)	90.66(4)	554.4(2)
H2-1	9.472(1)	11.427(2)	5.109(1)	90.75(1)	553.0(1)
KZ-1	9.489(1)	11.491(1)	5.094(1)	91.08(1)	555.3(1)
LJ-1	9.500(1)	11.457(1)	5.138(1)	90.60(1)	559.1(1)
LJ-2	9.505(1)	11.456(1)	5.126(1)	90.82(2)	558.1(1)
MC-1	9.530(2)	11.474(1)	5.119(1)	91.14(2)	559.6(1)
OW-102	9.529(1)	11.463(1)	5.114(1)	91.20(1)	558.5(1)
SMP-12	9.520(1)	11.471(1)	5.105(1)	91.19(1)	557.4(1)
SQ-1	9.522(1)	11.467(1)	5.115(1)	91.18(2)	558.3(1)
TL-45	9.481(3)	11.444(2)	5.113(1)	90.90(3)	554.7(2)
TSE-5	9.508(2)	11.476(2)	5.102(1)	91.12(3)	556.6(1)
TSE-7	9.519(1)	11.467(1)	5.112(1)	91.21(1)	557.9(1)
TSE-16	9.486(2)	11.448(2)	5.106(1)	91.01(2)	554.4(1)
TSE-28	9.523(2)	11.477(1)	5.110(1)	91.11(2)	558.3(1)
TSE-30	9.478(1)	11.446(2)	5.116(1)	90.77(2)	555.0(1)
TSE-31	9.483(2)	11.438(2)	5.103(1)	90.91(2)	553.4(1)
TSE-32	9.489(2)	11.446(2)	5.111(1)	90.99(3)	555.0(1)
TSE-40	9.503(2)	11.458(1)	5.109(1)	91.06(2)	556.2(1)
TSE-45	9.469(2)	11.441(2)	5.108(1)	90.86(2)	553.4(1)
TSE-48	9.491(1)	11.452(1)	5.109(1)	91.03(2)	555.2(1)
TSE-65	9.480(4)	11.442(6)	5.114(2)	90.94(4)	554.7(4)
TSE-76	9.446(2)	11.504(2)	5.082(1)	91.04(2)	553.3(1)
TSE-77	9.481(2)	11.442(1)	5.116(1)	90.82(3)	555.0(1)
TSE-90	9.471(5)	11.434(2)	5.125(1)	90.40(6)	554.9(3)
TSE-97	9.483(3)	11.448(1)	5.108(1)	90.87(2)	554.5(1)
TSE-100	9.484(6)	11.441(3)	5.116(3)	90.89(9)	555.1(5)
TSE-107	9.453(2)	11.426(1)	5.097(1)	90.71(2)	550.5(1)
TSE-109	9.464(4)	11.427(3)	5.106(4)	90.62(5)	552.1(3)
TSE-122	9.417(5)	11.394(5)	5.112(2)	90.18(2)	548.5(5)
TSE-126	9.449(1)	11.418(1)	5.120(1)	90.13(3)	552.4(1)
TSE-130	9.446(3)	11.413(2)	5.115(1)	90.00(5)	551.5(1)
TSE-132	9.486(2)	11.446(1)	5.108(1)	90.93(2)	554.5(1)
TSE-134	9.462(3)	11.429(1)	5.106(1)	90.72(3)	552.1(2)
TSE-136	9.475(3)	11.441(3)	5.108(1)	90.80(3)	553.7(2)
TSE-137	9.489(2)	11.446(2)	5.121(1)	90.71(3)	556.1(1)
TSE-138	9.507(2)	11.461(1)	5.115(1)	91.05(2)	557.2(1)
TT-1	9.509(2)	11.472(1)	5.109(1)	91.14(2)	557.3(1)
VII	9.532(2)	11.466(1)	5.123(1)	91.04(2)	559.8(1)
WD-1	9.526(1)	11.474(1)	5.111(1)	91.15(1)	558.5(1)

12.3 CRYSTAL STRUCTURE

Wodginite from the Tanco pegmatite (sample G69-17) was used in the structure analysis of Ferguson et al. (1976). On the basis of criteria discussed later (see Order-Disorder), the wodginite is fully ordered, thus the effects of disorder can be ignored when considering the results of this structure analysis.

Polyhedral representations of the wodginite structure are shown in Figure 24. Oxygen atoms form approximately hexagonally closest-packed layers perpendicular to $\underline{X}$. Cations occupy $\frac{1}{2}$ of the octahedral interstices at each level in the closest-packing. Coordination polyhedra form a-PbO_2-like zigzag chains via edge-sharing along $\underline{Z}$. Chains are inter-connected by corner-sharing linkages between levels of the closest-packed layering.

In the mineral ixiolite, there is no cation ordering. In wodginite, cations order into three distinct sites, one site consisting predominantly of Mn, one of Sn, and one of Ta, which causes a quadrupling of the unit cell volume of the parent ixiolite subcell ($\underline{a}(w)=2\underline{a}(i)$, $\underline{b}(w)=2\underline{b}(i)$, $\underline{c}(w)=\underline{c}(i)$). The site with Mn is designated "A"; however, a break is made here from the nomenclature of Ferguson et al. (1976) by designating the Sn-site as "B" and the Ta-site as "C" (these are reversed in the above reference). Coordination polyhedra of the $\underline{A}$-, and $\underline{B}$-sites alternate along one type of chain in the structure. The other chain consists solely of edge-sharing $\underline{C}$-site coordination polyhedra. Chains of any given level in the closest-packed layering consist only of one of these two types. Consequently, two types of layers exist (Figure 24), one with only $\underline{C}$-cation polyhedra, the other with only $\underline{A},\underline{B}$-cation polyhedra. In the repeat period along $\underline{X}$, there are two of each type of layer (Figure 25).
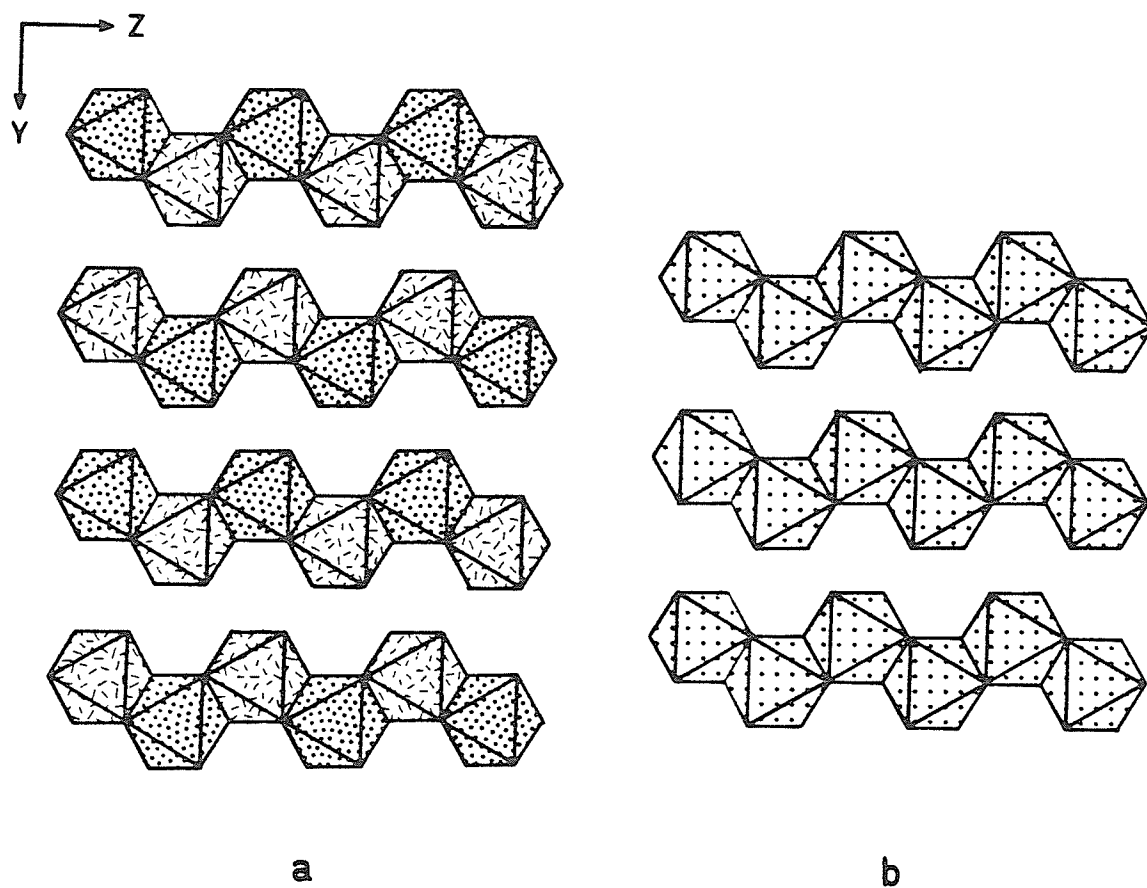
Figure 24: The ideal wodginite structure as projected along X. (a) The layer of Mn,Sn-polyhedra. (b) The layer of Ta-polyhedra. Mn polyhedra: hatch-stippled, Sn polyhedra: densely stippled, Ta polyhedra: lightly stippled.
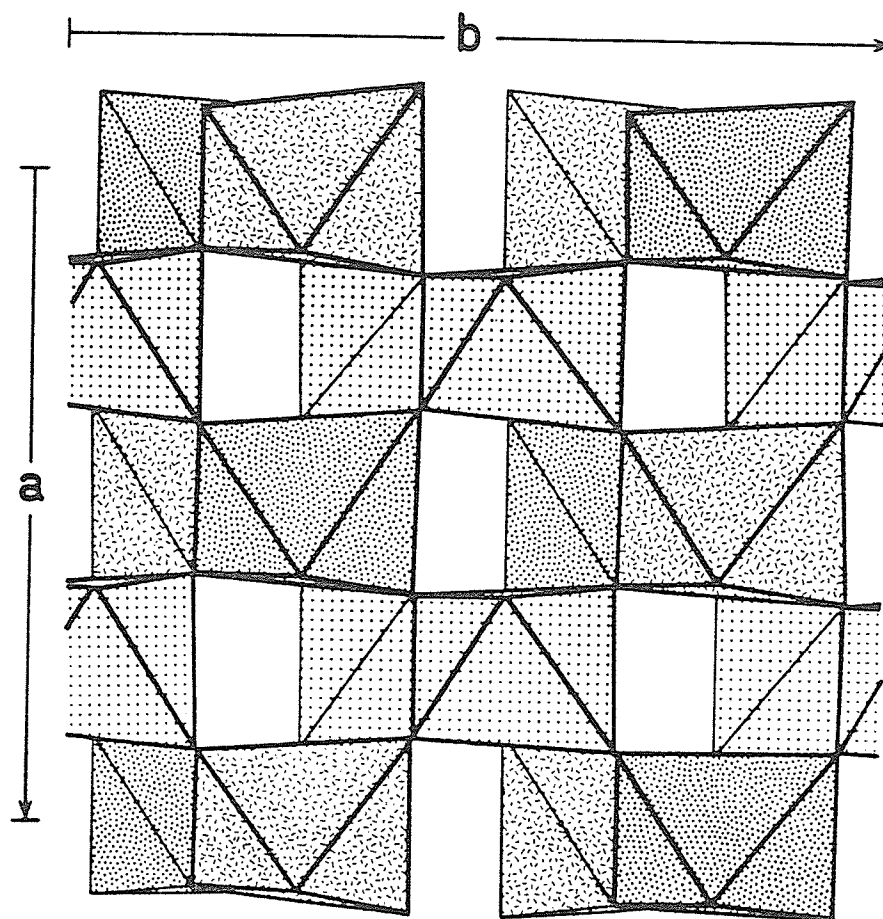
Figure 25: The wodginite structure as projected along z. The zig-zag chains of the structure are perpendicular to the plane of the page.

12.4 CHEMISTRY

12.4.1 Electron Microprobe Analyses

On the basis of their structure analysis, Ferguson et al. (1976) gave the formula of wodginite as ABC_2O_8, with $\underline{A}$=Mn, $\underline{B}$=Sn^{4+},Ta,(Fe^{3+},Ti) and $\underline{C}$=Ta,Nb; ideally, wodginite is $MnSnTa_2O_8$.

Ta is the smallest cation in the ideal structure (0.64 Å), and Mn the largest (0.83 Å), with Sn intermediate, yet closer to Ta in size (0.69 Å) (all effective ionic radii from Shannon, 1976). Because of the similar cation sizes, it is presumed that cation ordering is regulated principally by charge differences between the cations, especially between the $\underline{B}$-, and $\underline{C}$-sites. To this effect, because of the similarity of Sn and Ta in both charge and size, it is not too surprising that the structure tolerates excess amounts of Ta by incorporation of the Ta at the $\underline{B}$-site.

Electron microprobe analyses obtained for all of the samples of this study are given in Appendices C and D, the latter containing all analyses of Tanco wodginites. A cursory glance at the appendices shows that wodginite is quite non-ideal. Wodginites are typically Mn, Sn and Ta rich; however, there are several samples which contain either drastically diminished amounts of some of these elements, or major amounts of other elements. Maximum variations of each element for all wodginites are given in Table 38.

The main substituents for Mn, Sn and Ta are Fe, Ti and Nb. Trace amounts of Sn^{2+} (E.E. Foord, pers. comm.) Zr, Sc and Ca have been detected.

Selected cation-cation correlation plots based on unit cell contents are shown in Figure 26.

Table 38: Variation in Main Element Chemistry

Element	Maximum	Minimum	Ideal
Mn	9.0	2.1	8.3
Fe	8.7	0.0	0.0
Ti	6.0	0.0	0.0
Sn	15.1	0.5	17.9
Nb	10.6	0.5	0.0
Ta	75.5	46.0	54.5

- all figures are wt. %'s of the element

Figure 26a is a plot of total Fe (as Fe^{2+}) versus Mn. The strong, linear negative correlation between total Fe and Mn (R=-.85) indicates that the presence of most iron in wodginite can be accounted for by Mn→Fe substitution. Several of the datapoints of the plot fall off the main trend, particularly at very low Fe contents. This indicates that significant substitution mechanisms not involving Fe also operate at the A-site. Examination of the chemistry of these wodginites (e.g. samples KZ-1, L-15 and several samples of the SMP-series) shows no anomalous amounts of substituents which could feasibly be located at the A-site. The only feature that these wodginites have in common are high Ta+Nb contents and anomalously low cation sums, some by as much as 12.5%.

Figure 26b is a plot of total Ta+Nb versus the cation sum. The excellent negative correlation between these variables (R=-.91) indicates that (1) the low sums are not "accidental" - not due to poor analytical conditions such as bad carbon coats, improper correction for current drift, et
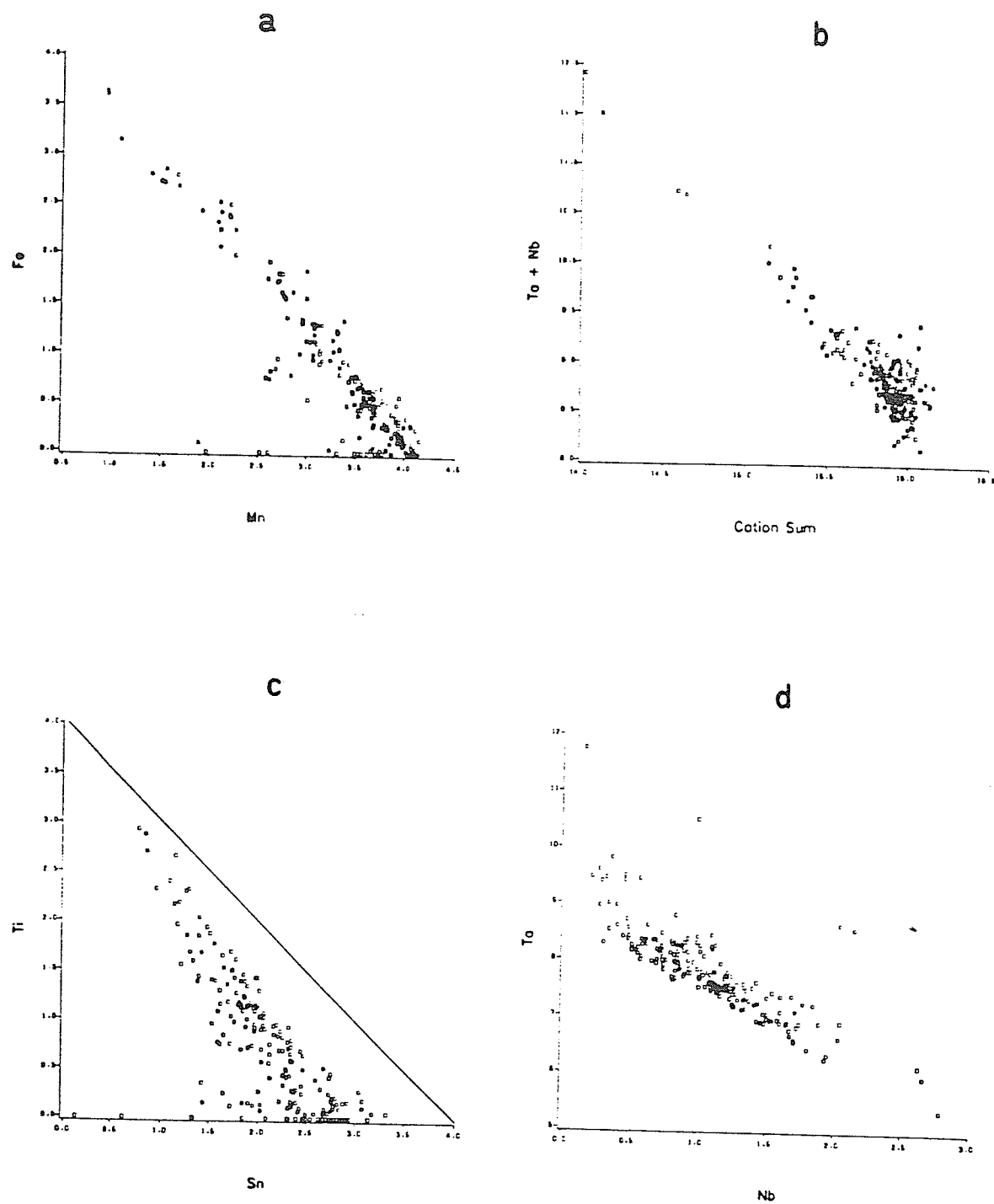
Figure 26: Wodginites: cation-cation plots. (a) Total Fe versus Mn. (b) Ta+Nb versus cation sum. (c) Ti versus Sn. (d) Ta versus Nb.

cetera, (2) the cause for the low cation sums lies with the pentavalent cations. The strong correlation of the deviant sums with excessive contents of the highest-charged cations indicates that vacancies are required in (Ta,Nb)-rich wodginites to maintain charge balance, unattainable even by means of coupled cation substitutions. Specifically, it must be difficult for the structure to balance the excess positive charge introduced by Ta at, most likely, the B-site. That the Mn-deficient compositions of Figure 26a are also the tantalum-richest compositions of Figure 26b, suggests that vacancies are preferentially located at the A-site.

A good negative correlation exists between Sn and Ti (Figure 26c); however, only 52% of the variation in Sn can be accounted for by Sn→Ti substitution. As is apparent from this plot, substantial Sn→Ti substitution is possible in natural wodginites: samples with up to 75% Ti in the B-site have been found. Despite the linear trend, all datapoints plot well below the curve for ideal Sn⇔Ti substitution (bold line in Figure 26c), indicating that constitutents other than Ti and Sn often occur at the B-site. The deviation of datapoints from the trend increases as Ti content decreases; some samples with no detectable Ti deviate from the ideal Sn⇔Ti isomorphism curve by nearly 100%. These points mark analyses with Ta+Nb far in excess of 8 cations per unit cell (the maximum amount of these cations that can be accomodated at the C-site), and often correspond to samples with high numbers of cation vacancies. This indicates that much of the spread in the distribution of the datapoints of Figure 26c is due to the presence of B-site Ta.

Ta⇔Nb isomorphism (Figure 26d) is fairly extensive: wodginites show Nb:Ta as high as 0.35:1, although they typically have lower ratios. The

high degree of scatter in this plot is due to the presence of excess Ta at the B-site.

To summarize, at this stage it can be concluded that (1) all Mn and most Fe occur at the A-site, (2) Sn and Ti occur at the B-site, (3) Ta occurs at both the B-, and C-sites, (4) Nb occurs at the C-site and (5) vacancies are present and are concentrated at the A-site.

12.4.2 Mössbauer Spectroscopy

Although preliminary cation-cation plots (Figure 26a) suggest that much of the Fe in wodginite is ferrous and resides at the A-site, electron microprobe data cannot give conclusive information about the valence and location of iron when high proportions of vacancies can be present in the structure. To answer these questions, an independent determination of the $Fe^{2+}:Fe^{3+}$ ratios of wodginites was required. Mössbauer spectroscopy was used because it has the potential of giving not only information on the valence of the iron present in the mineral, but also information about the location of iron in the structure.

From earlier studies, some preliminary conclusions can be drawn about the valence and location in the structure. Turnock (1966) was able to synthesize Sn-free wodginites with Fe^{3+}-bearing, Ta-excess compositions. Turnock found the wodginites to be unstable at relatively low fO_2, indicating that the trivalent state of iron was essential for stabilizing these tin-free compositions. From the chemistry of his samples, the A-site is occupied only by Mn, the C-site, by Ta, and the B-site, by Fe^{3+} and Ta (and in some cases, minor amounts of Mn^{3+} or Mn^{2+}). Turnock's (1966) wodginites fall close to a hypothetical $Mn(Fe^{3+}Ta)Ta_2O_8$ end-member in composition. The instability of these wodginites at lower fO_2's indicates that Fe^{2+} can-

not be stabilized at the B-site. According to Turnock's phase diagram for the system $MnTa_2O_6$-$FeTa_2O_6$-$FeTaO_4$, the minimum Mn content of these wodginites is 1 atom per formula unit. When the Fe^{3+}:Mn ratio of the system increases beyond this value, other phases form (i.e. $FeTaO_4$); wodginites with less than full occupancy of the A-site by Mn will not form if Fe^{3+} is the available substituent.

Natural wodginites show considerable Mn→Fe substitution (Figure 26a). On the basis of Turnock's (1966) work, the iron substituting for Mn must be divalent. To test the validity of this assumption, ^{57}Fe-Mössbauer spectroscopy was done on seven samples, five of which were relatively iron-rich natural samples and two of which were synthetic Fe^{3+}-bearing wodginites from Turnock's study.

The ^{57}Fe-Mössbauer spectra are shown in Figure 27. The synthetic wodginites (TR1-1 and TR3-1) are characterized by a single absorption doublet with an isomer shift of about 0.4 mm/s and a quadrupole splitting of 0.5 mm/s. This is undoubtedly due to Fe^{3+}. The absence of any other doublets in their spectra confirms that all the iron is ferric, as Turnock (1966) inferred from the fO_2 conditions of synthesis.

All natural wodginites have ^{57}Fe-Mössbauer spectra which are different from the synthetic samples. The absorption envelope near the Fe^{3+} doublet is more complex, and there is a substantial second absorption with a transmission minimum at approximately 2 mm/s. Both features are consistent with a doublet with an isomer shift of about 1.1 mm/s and a quadrupole splitting of about 2 mm/s, characteristic of Fe^{2+}.

Individual isomer shifts, quadrupole splittings, line widths and Fe^{2+}:Fe^{3+} ratios (Table 39) were obtained by Dr. C.A. McCammon of the Dept. of Physics by fitting Lorentzian functions to the data.
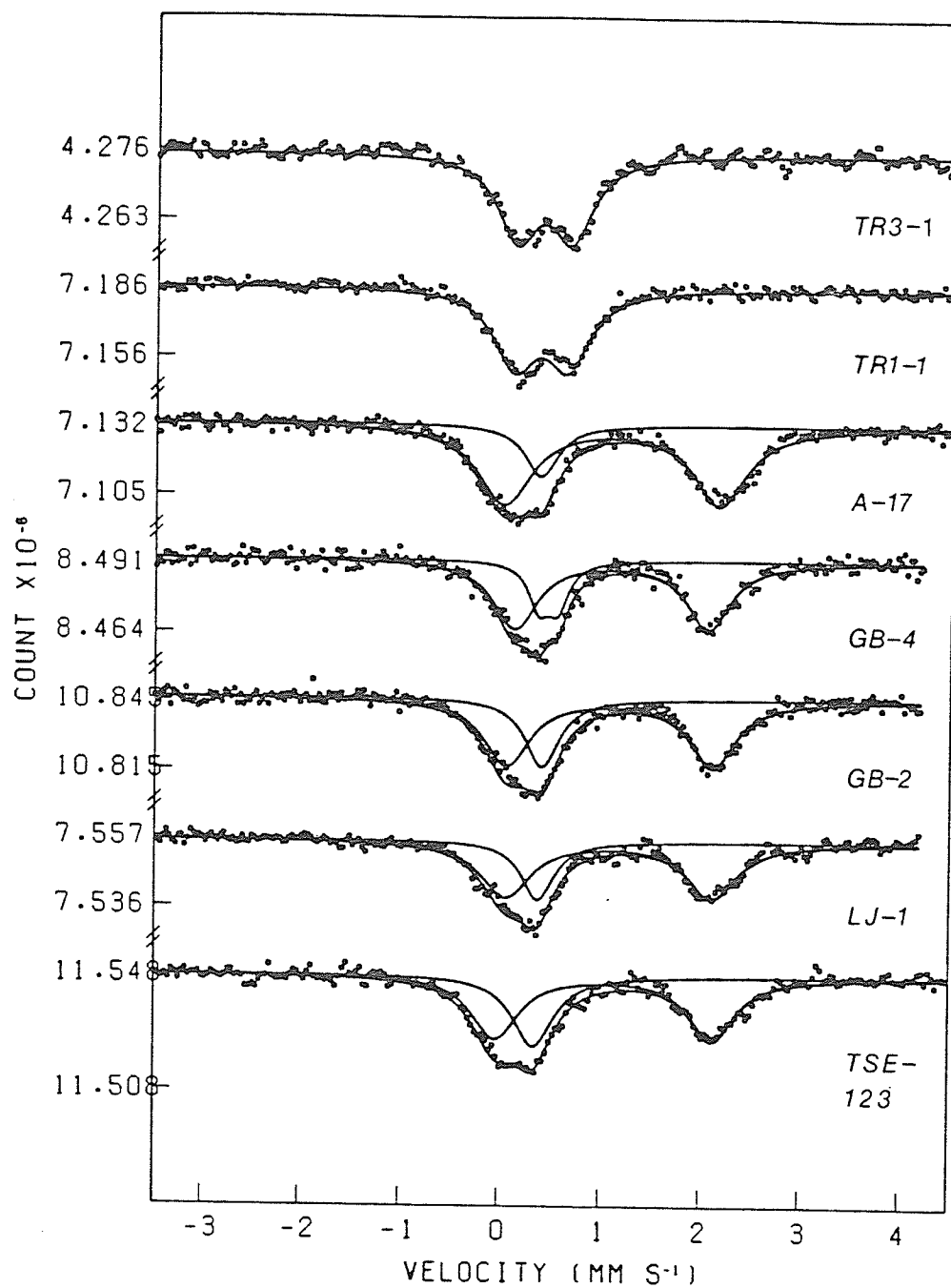
Figure 27: ^{57}Fe-Mössbauer spectra of selected wodginites.

In the natural iron-rich samples studied here, the proportion of Fe^{2+} varies from 68% to 83%. Natural wodginites tend not only to be Fe^{2+}-bearing, but are typically Fe^{2+}-dominant, confirming expectations from the microprobe data.

Formula contents for the five natural wodginites on which Mössbauer data were obtained were recalculated using the $Fe^{2+}:Fe^{3+}$ ratios of the Mössbauer experiments (Table 40). There is an excellent negative correlation between Fe^{2+} and Mn (Figure 28), supporting the earlier assertion that all A-site iron is divalent.

Dr. E.E. Foord of the U.S. Geological Survey (pers. comm.) carried out a ^{119}Sn-Mössbauer experiment on a wodginite from the same batch as sample CX-1. He found that a small proportion of the tin in the sample was in the divalent state (7 ± 3%). Divalent tin is a large cation; six-coordinated Sn^{2+} has an effective ionic radius of 1.10 Å (from calculations by the author). Sn^{2+} undoubtedly substitutes for Mn^{2-}, the largest and lowest-valent cation in ideal wodginite. Sn^{2+} is scarce in the high-fO_2 environments in which wodginite occurs, as evidenced by frequent association of wodginite and cassiterite (a Sn^{4+}-excess phase), contrasted with the rare association of wodginite and Sn^{2+}-excess phases (e.g. stannomicrolite and thoreaulite). Consequently, Sn^{2+} contents of all wodginites are expected to be extremely low, and in this study, all Sn in wodginite is considered to be quadrivalent.

Table 39: ^{57}Fe-Mössbauer Parameters*

Sample	Fe^{2+}			Fe^{3+}			$\dfrac{Fe^{3+}}{Fe}$
	Γ	$\delta**$	ΔE	Γ	$\delta**$	ΔE	
A-17	0.66(7)	1.08(3)	2.16(7)	0.32(8)	0.37(4)	0.15(11)	0.17(7)
GB-2	0.57(6)	1.09(4)	2.05(7)	0.33(5)	0.42(4)	0.17(10)	0.26(3)
GB-4	0.54(6)	1.10(4)	1.92(7)	0.27(12)	0.47(4)	0.18(9)	0.23(4)
LJ-2	0.64(11)	1.06(14)	2.05(25)	0.34(46)	0.38(11)	0.15(78)	0.25(7)
TSE-126	0.58(15)	1.16(6)	1.94(17)	0.44(15)	0.15(13)	0.54(24)	0.32(9)
TR1-1	----	----	----	0.52(6)	0.37(4)	0.53(6)	1.0
TR3-1	----	----	----	0.49(5)	0.39(5)	0.54(6)	1.0

* mm/s, ** relative to Fe-foil

Table 40: Compositional Data for Wodginites used in Mössbauer Experiments

	A-17		GB-2	GB-4	LJ-2		TSE-126	
	core	rim			core	rim	core	rim
MnO	5.4	4.7	6.4	6.2	7.5	7.1	10.2	10.0
FeO	5.8	6.4	4.7	4.6	3.6	3.7	1.5	1.5
Fe_2O_3	1.3	1.5	1.6	1.8	1.3	1.4	0.8	0.8
TiO_2	2.2	3.3	0.7	1.4	0.0	0.0	7.7	4.6
SnO_2	11.0	10.4	14.6	13.2	15.3	15.6	7.9	10.6
Nb_2O_5	7.5	8.0	6.3	5.6	6.9	7.2	9.5	7.9
Ta_2O_5	66.9	64.8	64.5	66.5	65.0	64.2	61.1	62.6
	100.1	99.0	98.8	99.4	99.8	99.2	98.6	98.0

Cations per 32(O)

	A-17		GB-2	GB-4	LJ-2		TSE-126	
	core	rim			core	rim	core	rim
Mn^{2+}	1.89	1.66	2.33	2.24	2.69	2.57	3.42	3.49
Fe^{2+}	2.01	2.22	1.69	1.65	1.30	1.31	0.49	0.53
Fe^{3+}	0.41	0.45	0.51	0.58	0.43	0.43	0.23	0.25
Ti^{4+}	0.69	1.03	0.23	0.44	0.00	0.00	2.29	1.42
Sn^{4+}	1.82	1.71	2.49	2.24	2.61	2.66	1.25	1.75
Nb^{5+}	1.41	1.49	1.21	1.08	1.32	1.39	1.69	1.47
Ta^{5+}	7.57	7.30	7.50	7.68	7.54	7.47	6.57	7.03
	15.81	15.85	15.96	15.90	15.89	15.84	15.95	15.95
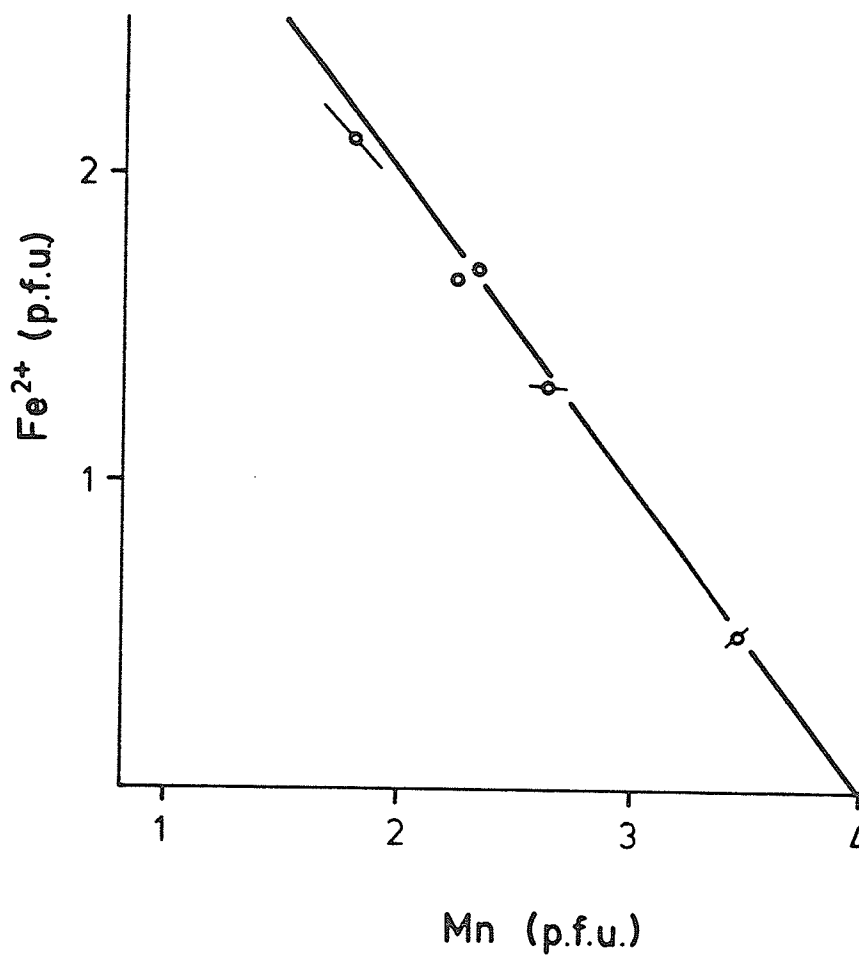
<u>Figure 28</u>: Fe^{2+} versus Mn for the wodginites of Table 40. Bars mark core-to-rim compositional ranges. The solid line marks ideal $Mn^{2+} \Leftrightarrow Fe^{2+}$ isomorphism.

12.4.3   Lithium Determinations

In their study of the polymorphs of LiTa$_3$O$_8$, Gatehouse et al. (1976) found that the medium temperature polymorph had the wodginite structure. In this compound, Li occupies the A-site and Ta occupies the B-, and C-sites.   As shown earlier, several of the wodginites of the present study were found to have substantial amounts of Ta at the B-site. As many of the natural wodginites occur in Li-rich environments, (Li+Ta)⟷(Mn+Sn) substitution was considered to be a possible substitution.

Li determinations were done by atomic absorption spectroscopy by Mr. V. Kubat of the Ecole Polytechnique.   Two wodginites were analyzed for Li. One sample (VII-1) was a wodginite with a composition close to MnSnTa$_2$O$_8$, the other was a Ta-rich, Sn-poor wodginite (KZ-1).   The results of the analyses were as follows: sample VII-1 has 87 ppm Li and sample KZ-1 has 1643 ppm Li.   Although the Ta-rich sample contains substantially more Li than the the Ta-poorer one, the amount of Li is far too low to make Mn→Li substitution a significant mechanism for balancing Sn→Ta substitution. Consequently, Li contents of natural wodginites are expected to be negligible.

12.5   FORMULA CALCULATION

The calculation of wodginite formulae from electron microprobe data is complicated by (1) the large number of elements substituting for Mn, Sn and Ta, (2) the presence of vacancies in the structure, (3) the existence of iron in two valence states and (4) the possibility of various degrees of order.   The first three points have been addressed in preceeding discussions; however, without quantitative data on the degree of order, only ful-

ly ordered formulae can be calculated. Because Fe^{2+} is more abundant than Fe^{3+} in wodginites, for the formula calculation it is initially assumed that all iron is Fe^{2+}.

The chemically most simple site is the C-site. The C-site contains only tantalum and niobium. Moreover, all Nb in fully-ordered wodginite is contained at that site. To calculate the C-site contents, first all Nb is assigned to the site, followed by Ta to (Nb+Ta)=8. Inherent in this is the assumption that vacancies do not occur at the C-site. Vacancies should be preferentially located at the sites with weaker bond strength sums, and bond strength sums to the C-site are the highest in the structure. Furthermore, as indicated earlier, Figure 26 suggests that vacancies are concentrated at the A-site.

Excess Ta (total Ta minus C-site Ta) is assigned to the B-site; Sn and Ti (and Zr and Sc) are assigned to this site also, all Sn being considered as Sn^{4+}.

All Mn is assigned to the A-site. Although some of Turnock's wodginites possibly contain Mn^{3+} at the B-site, fO_2 conditions of natural wodginites inferred from observed $Fe^{2+}:Fe^{3+}$ ratios do not support the possibility of Mn^{3+} in natural wodginites. Furthermore, in the formulae that result from the calculations, Mn has never significantly exceeded 4 cations/unit cell, suggesting it is restricted to the A-site.

At this point in the assignment, some decisions must be made about the role of vacancies and iron in the structure. The data presented so far indicate that vacancies are concentrated at the A-site; initially in the calculations it is assumed that the B-site is fully occupied. All Fe needed to fill the B-site (= 4-[Sn+Ti+Ta(B-site)+Zr+Sc]) is assigned to that

site. The excess is assigned to the A-site. From earlier discussions, it
follows that the B-site iron will be ferric and the A-site iron will be
ferrous. However, in calculating the formula, all Fe was assumed to be
Fe^{2+}; therefore, the results of the formula calculation necessarily do not
agree with the initial assumption used in the calculation; hence the calcu-
lation must be repeated until the initial and final iron ratios agree. For
this reason, formula and $Fe^{2+}:Fe^{3+}$ calculation is an iterative procedure
with a convergence criterion of $Fe^{2+}:Fe^{3+}$ = Fe(A-site):Fe(B-site).

Using this approach, $Fe^{2+}:Fe^{3+}$ ratios were determined and formulae were
calculated for all of the wodginites examined in the present study, using a
FORTRAN program written by the author; the results are reported in Append-
ices C and D.

The validity of the $Fe^{2+}:Fe^{3+}$ calculations is shown by Figure 29, a plot
of the calculated and observed $Fe^{3+}/(Fe^{3+}+Fe^{2+})$ ratios. A reference line
is shown for the case of perfect agreement between calculated (microprobe),
and observed (Mössbauer spectroscopic) data. The datapoints scatter close-
ly about the ideal curve; therefore the approach taken in formula calcula-
tion (assumption of full order) gives satisfactory estimates of the
$Fe^{2+}:Fe^{3+}$ ratio.
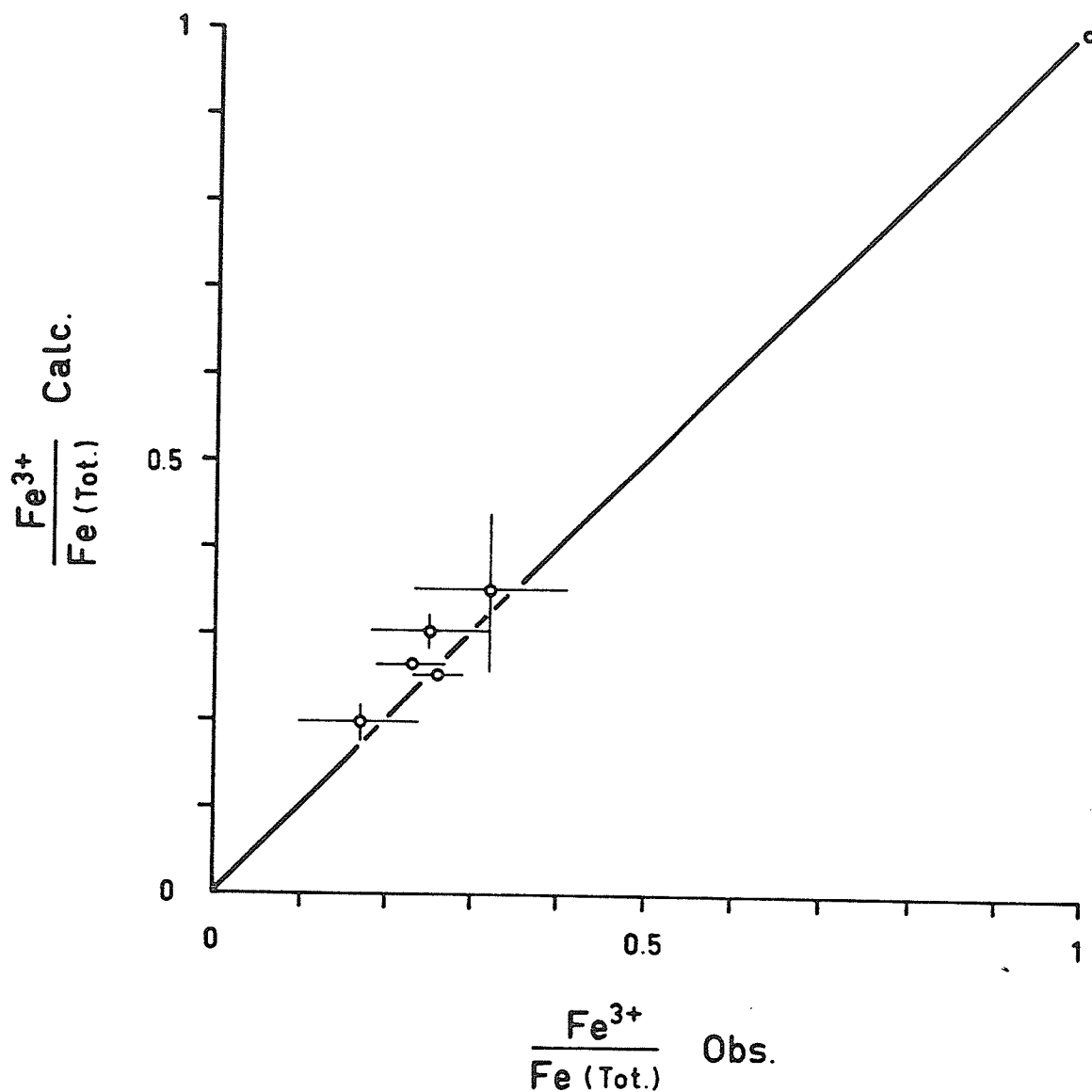
Figure 29: Wodginite-group minerals: calculated versus observed $Fe^{3+}/(Fe^{3+}+Fe^{2+})$. The "calculated" value comes from microprobe data, the "observed" value, from Mössbauer data. The reference line marks perfect agreement between calculated and observed data.

12.6   STRUCTURAL CHEMISTRY

In the fully-ordered model (no mixing between the A, B and C sites; e.g. all Mn at A, all Sn at B, all Nb at C), the A-site contains only Mn, Fe^{2+} and vacancies.   In Figure 30, compositions cluster near the Mn apex, along either the Mn-Fe sideline or the Mn-◻ sideline.   Wodginites moderately to extremely enriched in Fe^{2+} tend to have few A-site vacancies, whereas Mn-rich compositions can have up to 50% of their A-sites vacant.   There seems to be no crystal-chemical reason for such a correlation.   The phenomenon is controlled geochemically: wodginites with low A-site occupancies tend to form in relatively transition-metal depleted environments which only develop very late in pegmatite fractionation, i.e. when Fe/Mn is typically very low (see Part 4).   Interesting from a taxonomic point of view is that six of the wodginites actually have Fe>Mn; that is, these samples have A-site chemistries which deviate from ideality by more than 50%.

B-site chemistry is more complex than that of the A-site.   Sn, Ti, Fe^{3+} and Ta are major constituents.   As well, Zr and Sc are trace constituents, and the formula calculation even suggests that minor amounts of vacancies are tolerated at this site.   Of the major constituents, Fe^{3+} is the least significant; the maximum proportion of Fe^{3+} observed at the site is 21%, and the average proportion is only 7%.   However, Turnock's (1966) synthetic wodginites have as much as 50% Fe^{3+} at this site.   By analogy, natural wodginites with proportions of B-site Fe^{3+} greater than 21% should be possible under conditions of higher relative $\mu(Ta)$ with respect to $\mu(Sn,Ti)$, and of high fO_2.

Figure 30 also shows the B-site Sn-Ta-Ti population, as projected from the Fe^{3+} apex of a tetrahedral four-component representation.   Unlike the
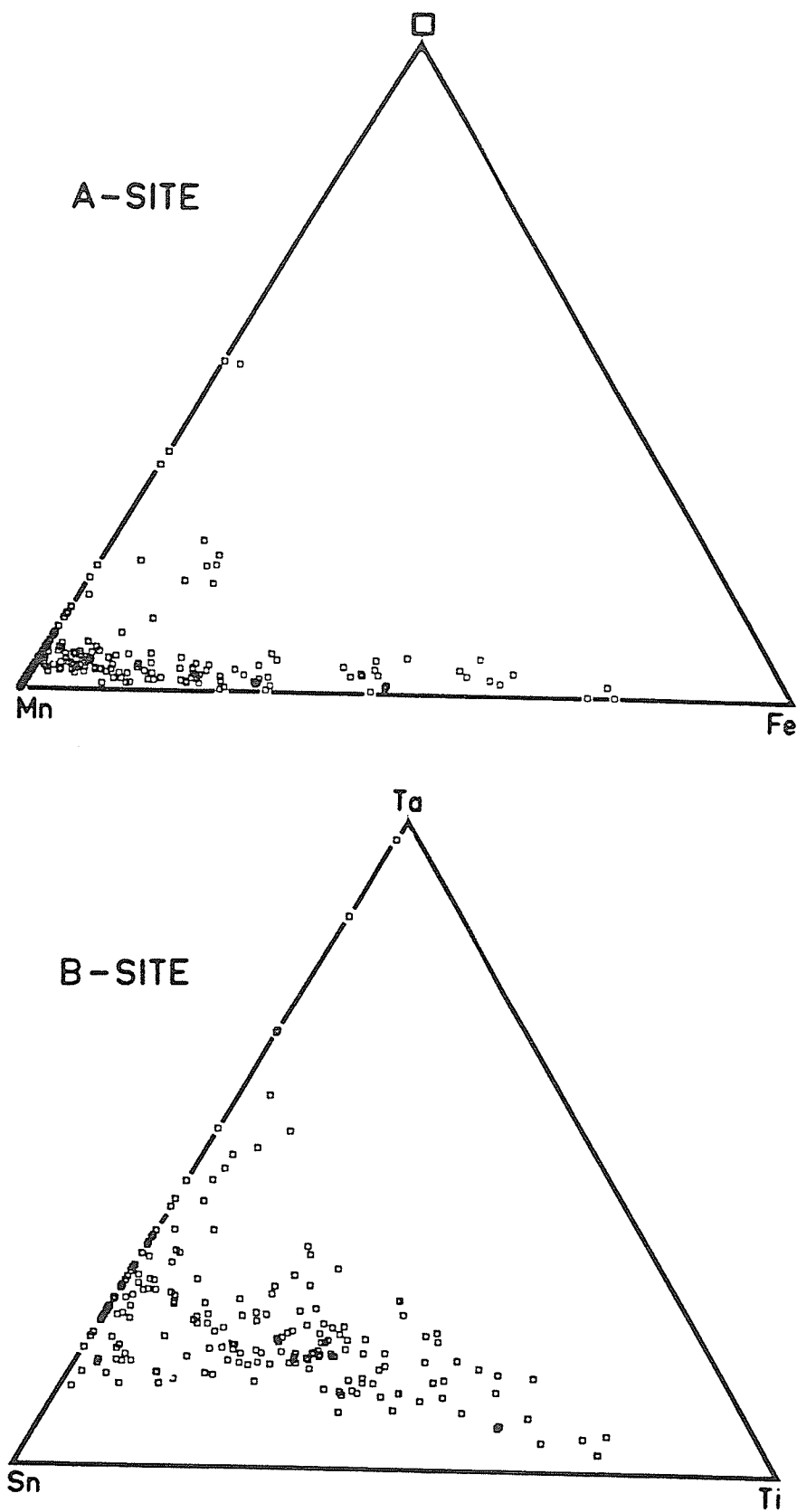
Figure 30: Wodginites: A-site and B-site main element chemistries. The diagram for the B-site is projected from the Fe^{3+} apex.

A-site, B-site chemistries are never ideal. Sn dominates in most of the compositions observed; however, Sn→Ta substitution can be substantial, and no wodginite is known with greater than 90% Sn at the B-site. Although Ti-free compositions are known, wodginites without B-site tantalum are not known. Furthermore, as the Ti content of wodginites decreases, the proportion of B-site Ta increases, suggesting that the proportion of B-site Ta is controlled geochemically: as fractionation progresses in granitic pegmatites, $\mu(Ta)/[\mu(Nb)+\mu(Ti)]$ typically increases. The compositional gap along the Ta-Ti sideline indicates that if the control is geochemical, then granitic pegmatites hosting wodginites typically become enriched in Sn with respect to Ti prior to significant increases in the relative potential of Ta. Several features of the diagram are interesting from a taxonomic viewpoint: (1) most wodginites have Sn-dominant B-site chemistries, (2) several wodginites have Ti-dominant B-site chemistries and (3) some compositions have Ta-dominant B-sites.

Figure 31 shows the total number of vacancies versus B-site Ta. The presence of vacancies in the structure is clearly due to the presence of Ta at the B-site. The slope of the trend is approximately +0.5; for every two Ta atoms introduced at the B-site, one vacancy occurs at the A-site. Full occupancy of the B-site by Ta marks the maximum amount of non C-site Ta possible in the structure (4 atoms per unit cell). From the 1:2 slope of Figure 31, and the realization of the maximum amount of Ta in the structure, the upper limit on the number of vacancies in wodginite is predicted to be 2 per unit cell, which corresponds to a 50% A-site occupancy, in agreement with the lower limit to A-site occupancy apparent from Figure 30.

The reference line drawn in Figure 31 is the ideal curve for the relationship between $\underline{A}$-site vacancies and $\underline{B}$-site Ta in the absence of other substitutions involving either of these variables. The location of most of the datapoints below this curve indicates that wodginites typically contain more $\underline{B}$-site Ta than can be accounted for by the $\underline{A}$-site vacancy model alone.

Figure 32 is a plot of all $\underline{B}$-site tantalum which cannot be accounted for by the $\underline{A}$-site vacancy model, versus Fe^{3+}. Much of the correlation between these variables is due to the constraint that the $\underline{B}$-site contents sum to 4; nevertheless, it serves to show that most of the deviation in Figure 31 is due to the balancing of excess positive charge associated with $\underline{B}$-site Ta by equal amounts of Fe^{3+}. The 1:1 Fe^{3+}:Ta line representing ideal $2Sn \rightarrow Fe^{3+}+Ta$ substitution is shown in Figure 32. The datapoints which fall below the curve cannot be fully accounted for by this mechanism and the $\underline{A}$-site vacancy model. No other substituents occur at the $\underline{B}$-site to explain these deviations. It is assumed that the deviations are due to the incorporation of vacancies at the $\underline{B}$-site to balance part of the positive charge introduced by this excess Ta^{5+}. As such, the method of formula calculation necessarily gives a minimum estimate of these vacancies.

For the fully-ordered model, $\underline{C}$-site chemistry involves only simple homovalent isomorphism between Ta and Nb, and warrants no further discussion at present.
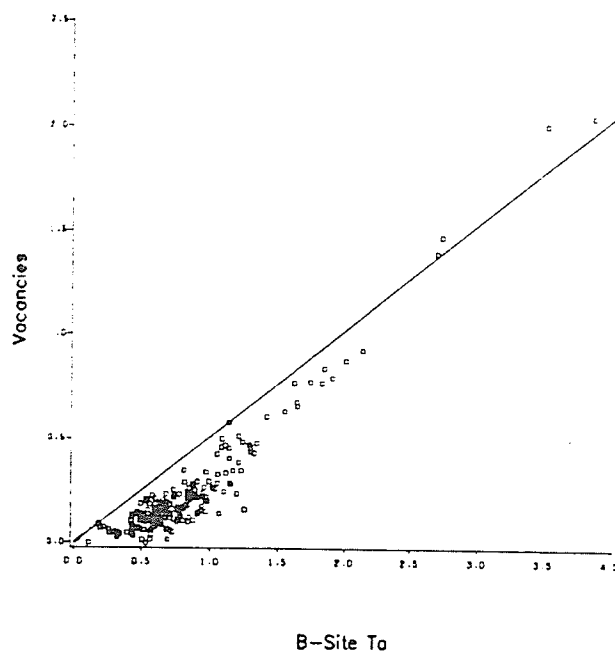
Figure 31: Wodginites: total cation-site vacancies versus B-site Ta.
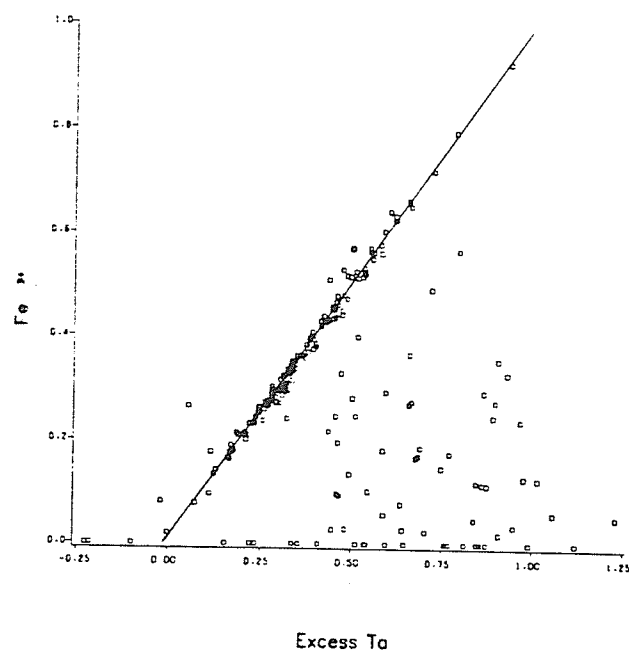
Figure 32: Wodginites: excess B-site Ta (= B-site Ta - 2 x A-site vacancies) versus Fe^{3+} from formula calculation.

12.7 SUBSTITUTION MECHANISMS

On the basis of arguments in the previous section, the operators of Table 41 are proposed to account for substitutions observed in wodginites. With these operators, all variations in major element chemistry in wodginite can be related back to ideal $MnSnTa_2O_8$.

Table 41: Substitution Operators

Operator	Type
1. $Fe^{2+}Mn^{2+}_{-1}$	Homovalent
2. $Ti^{4+}Sn^{4+}_{-1}$	"
3. $Nb^{5+C}Ta^{5+}_{-1}$	"
4. $^A\square^BTa^{5+}_2Mn^{2+}_{-1}Sn^{4+}_{-2}$	Heterovalent
5. $Fe^{3+B}Ta^{5+}Sn^{4+}_{-2}$	"
6. $^B\square^BTa^{5+}_4Sn^{4+}_{-5}$	"

The fourth operator of the table defines charge compensation involving $\underline{A}$-site vacancies and $\underline{B}$-site Ta. For every two tantalum atoms introduced at the $\underline{B}$-site by substitution for an equal amount of Sn, one vacancy is introduced at the $\underline{A}$-site.

Operator (5) of Table 41 defines Fe^{3+} substitution in wodginite, whereby one Fe^{3+} and one Ta^{5+} replace every two Sn^{4+} at the $\underline{B}$-site.

The last operator of Table 41 defines charge compensation by the incorporation of vacancies at the $\underline{B}$-site. Only one vacancy per five Ta^{5+} need be introduced to the site to preserve charge balance.

Of the operators of Table 41, one affects the A-site only, one affects the C-site only and four involve the B-site. Complete efficiency of the operators would result in 32 hypothetical end-members bounding compositional space for natural wodginites. However, only two of the homovalent (numbers 1 and 2), and one of the heterovalent operators (number 4) are more than 50% effective in natural wodginites.

Operators involving Ca, Zr and Sc are not ennumerated because they are nearly always insignificant (except for Zr in sample CX-1), but are expected to be similar to (1), (2) and (5) respectively in operation.

12.8 SUBDIVISION AND CLASSIFICATION

The name "wodginite", as introduced by Nickel et al. (1963b) and precisely defined by Ferguson et al. (1976), is associated with the composition $MnSnTa_2O_8$. As such, the name is inappropriate for several natural wodginites which deviate by more than 50% from this ideal composition at individual cation sites. These wodginites most closely approach the hypothetical end-members $FeSnTa_2O_8$, $MnTiTa_2O_8$ and $(\square_{0.5}Mn_{0.5})TaTa_2O_8$.

Subdivision and classification of the wodginites is complicated by a number of factors. Cation substitutions involve three distinct sites, making a nomenclature based on the generic name "wodginite" difficult. Coupled substitutions involving more than one site further complicate the matter, as does the introduction of some substituents by more than one mechanism (e.g. B-site Ta). Furthermore, the degree of order has not been considered so far, and the fully-ordered formulae may not exactly reflect the disorder-modified site occupancies of some samples. However, for the sake of practicality, classification is necessarily based on the fully-

ordered formulae because of the difficulty involved in obtaining actual site occupancies by means other than crystal structure analysis.

Because of the limited amount of Nb substitution at the $\underline{C}$-site ($<\underline{C}$-site Nb$>$ = 15%, max. $\underline{C}$-site Nb = 35%), substitutions at this site can be ignored from the point of view of developing a working nomenclature. Classification can be based on the chemistry of the $\underline{A}$-, and $\underline{B}$-sites only; the reduced dimensionality of the problem makes a nomenclature involving a generic name plus chemical prefixes possible.

Taking all of the above into consideration, the following guidelines are proposed for a classification and nomenclature of wodginites based on $\underline{A}$-, and $\underline{B}$-site chemistries:

1. The set of species with the wodginite structure (partially to completely ordered) is to be referred to as the "wodginite group".

2. For historical reasons, the name "wodginite" is to be preserved for end-member $MnSnTa_2O_8$, which is closest to the composition of most natural wodginite-group minerals.

3. Species names are to consist of the root "wodginite" modified by prefixes reflecting $\underline{A}$-, and $\underline{B}$-site chemistries.

4. Such prefixes are to be used only in cases where one or more of the operators in Table 41 are more than 50% effective.

5. No more than one prefix per site should be used to construct the name, in which case the $\underline{A}$-site prefix should always precede the $\underline{B}$-site prefix. In cases where more than one constituent is introduced to a single site by the operation, the prefix chosen should reflect the unique constituent only.

e.g., Ta is a non-unique B-site constituent in that it can be introduced to the site by as many as three different substitution mechanisms (operators 4,5,6 of Table 41). One of these operators is always insignificant from a taxonomic point of view, thus it can be ignored (operator 6). Of the remaining operators, (5) represents the only one by which Fe^{3+} can be introduced to the B-site. Fe^{3+} is the unique constituent of this operation, thus the appropriate prefix for >50% efficiency of (5) is "ferri". This leaves the prefix "tantalo" as the one to be assigned for >50% efficiency of operator (4).

To summarize, only operators (1), (2) and (4) are effective enough in natural wodginites described to date to generate new species. On the basis of the results of Turnock's (1966) synthesis work, and because some natural samples have Fe^{3+} contents indicating nearly 50% efficiency of operator (5), (5) could also be effective enough to generate new species.

Table 42 simplifies the classification of natural wodginites. This table gives species names and end-members for all compositions generated by operators (1), (2), (4) and (5). Criteria for classification follow the rules given above. The table is divided into two halves by a horizontal line, separating the Mn-dominant species above and the Fe dominant species below the line. Species names not enclosed by parentheses indicate compositions which have been found to occur naturally. Three new wodginite group members are recognized: titanowodginite, tantalowodginite and ferrowodginite. Type samples for the new species are marked in Table 43. Species names in Table 42 in parentheses are merely examples of the nomenclature for compositions not yet known.

Two samples (TSE-82 and TSE-94) have more than 50% of the end-member $FeTiTa_2O_8$; however, because of the minute size of each sample, adequate material was not available for characterization of the hypothetical species "ferrotitanowodginite".

The new species and classification scheme have been approved for publication by the International Mineralogical Association, Commission for New Minerals and New Mineral Names.

Table 42: Wodginite Classification

Criteria		Name	End Member Composition
A-site	B-site		
$Mn \gtrsim Fe^{2+}$			
≤25% ¤	≤50% Ti ≤25% Fe^{3+}	Wodginite	$Mn_4Sn_4Ta_8O_{32}$
"	>50% Ti	Titanowodginite	$Mn_4Ti_4Ta_8O_{32}$
"	>25% Fe^{3+} (>25% Ta)	(Ferriwodginite)	$Mn_4(Fe^{3+}_2Ta_2)Ta_8O_{32}$
>25% ¤	>50% Ta	Tantalowodginite	$Mn_2Ta_4Ta_8O_{32}$
$Fe^{2+} > Mn$			
≤25% ¤	≤50% Ti ≤25% Fe^{3+}	Ferrowodginite	$Fe^{2+}_4Sn_4Ta_8O_{32}$
"	>50% Ti	(Ferrotitanowodginite)	$Fe^{2+}_4Ti_4Ta_8O_{32}$
"	>25% Fe^{3+} (>25% Ta)	(Ferroferriwodginite)	$Fe^{2+}_4(Fe^{3+}_2Ta_2)Ta_8O_{32}$
>25% ¤	>50% Ta	(Ferrotantalowodginite)	$Fe^{2+}_2Ta_4Ta_8O_{32}$

Table 43: New Members of the Wodginite Group

Titanowodqinites

A-25
TSE-63*, -86, -90, -109, -122, -126

Tantalowodqinites

KZ-1*, L-15, TSE-76*

Ferrowodqinites

A-17,-26
SK-1*
TSE-112, -117, -136

-asterisks mark type samples

12.9 ORDER-DISORDER

In disordered to partially ordered columbite-tantalite group minerals, heating at 1000°C for 16 hours induces order (Černý & Turnock, 1971). In these samples, an increase in order is noted qualitatively by increased intensity of supercell diffractions. Komkov (1970) and Černý & Turnock (1971) have quantified order-disorder to an extent by monitoring changes in the $\underline{a}$ and $\underline{c}$ parameters of the columbites-tantalites. The heating of disordered columbite-tantalite decreases $\underline{c}$ and increases $\underline{a}$. Samples which are fully ordered prior to heating show no change in the relative intensities of supercell diffractions, nor in the values of $\underline{a}$ or $\underline{c}$.

Several of the wodginites studied by X-ray diffraction have powder patterns intermediate to ixiolite and the fully-ordered wodginite of Ferguson et al. (1976) (sample G69-17). They have diminished supercell diffraction intensities compared to sample G69-17; some samples are so extreme in this respect that only a few supercell diffractions in their patterns can be detected. In these samples, $\underline{\beta}$ approaches 90° as the supercell diffractions diminish in intensity (Figure 33). These features imply that the wodginites with intermediate structural properties are partially disordered.

On the basis of the chemical and structural similarities of columbite-tantalite group and wodginite group minerals, it would seem likely that heating experiments should give information about the degree of order in wodginites. Heating experiments were done under the same set of conditions standardized for columbites-tantalites by Černý and Turnock (1971), 1000°C/16 h. Heatings were done in air rather than in fO_2-controlled atmospheres because at the time of the experiment (1981), all iron was assumed to be ferric, based on the results of Turnock's (1966) synthesis
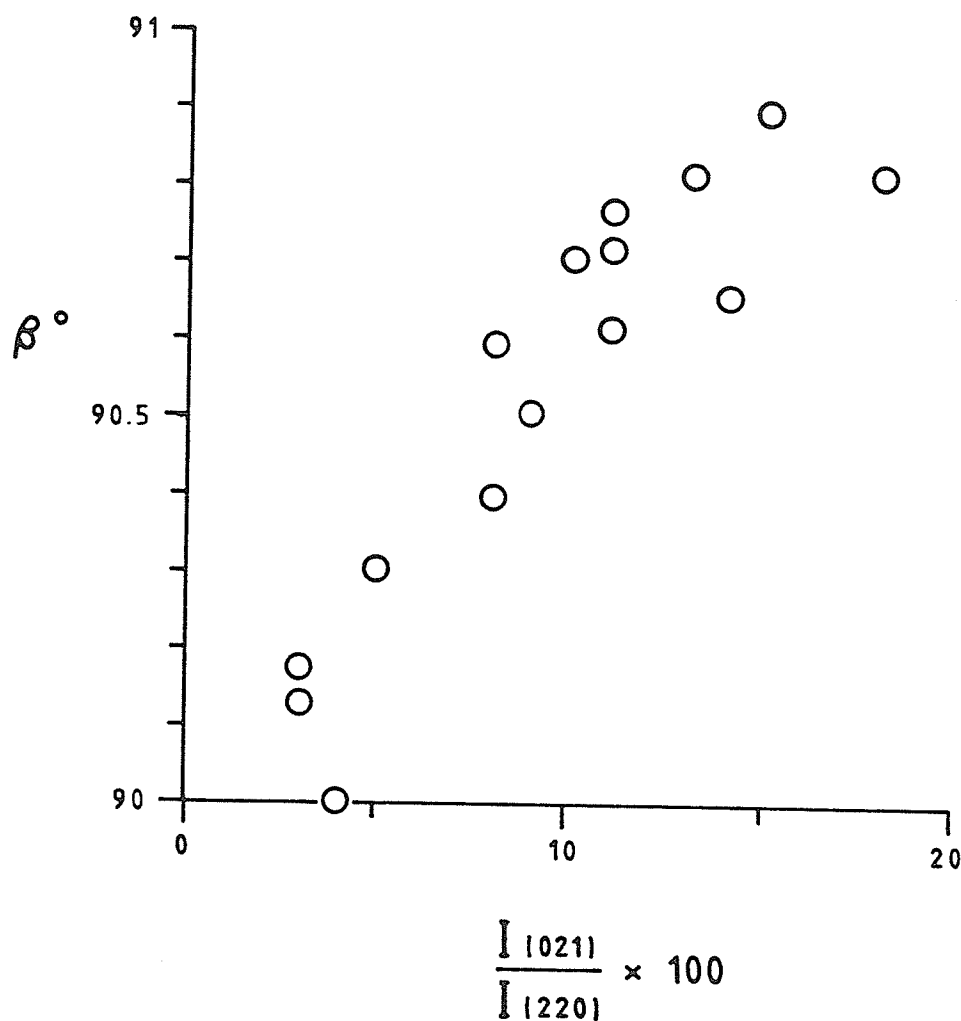
Figure 33: Wodginite-group minerals: correlation of β and supercell diffraction intensity. (021) is a supercell diffraction and (220) is a subcell diffraction. I(021)/I(220) is a normalized measure of supercell diffraction intensity. All intensities are peak heights and were measured 3 times for each sample. All intensity data were collected with a Philips PW1710 powder diffractometer with an automatic divergence slit. All samples in Table 55 are used in this plot except for H2-1, which was not examined with the above instrument.

work.   This is not considered to be too serious an error for the following
reasons:

1. All heated samples were crystal fragments, not powders, minimizing the
   surface area available for oxidation.

2. Most samples were Mn-rich (Figure 26a).   Oxidation of minor iron due to
   heating should not significantly modify ordering trends in these sam-
   ples.

3. Oxidation-reduction reactions at this temperature are slow (Turnock,
   1966).   It was shown by Černý and Turnock (1971) that unit cell dimen-
   sions of even Fe-rich columbite-tantalite group minerals are statisti-
   cally identical for granular samples heated in air and in mixed CO_2/CO
   atmospheres.   Similar behaviour is expected for wodginites because of
   their compositional and structural similarity to columbite-tantalite
   group minerals.

4. To quantify the problem, a series of heating experiments were done on
   the only abundant iron-rich wodginite sample (A-25)   in atmospheres of
   different fO_2.   A single wodginite crystal was ground to a powder which
   was then divided into two batches for the experiment. Powders were used
   instead of crystal fragments to ensure homogeneity and to optimize
   oxidation/reduction conditions.   One batch of powder was heated in CO
   ($fO_2=10^{-17}$ atm), the other in CO_2 ($fO_2=10^{-2.5}$ atm), both for 16 hours.
   Heatings resulted in different colours of powder (CO_2: brown, CO: brown-
   black); however, no significant differences in relative peak intensities
   or in unit cell parameters could be detected (Table 44, sample A-25H2),
   nor did extra phases form. Grice (1970) observed the same behaviour for
   the cell parameters of fully-ordered Fe-poor wodginites.

I conclude that in terms of unit cell parameters, and at conditions used here (1000 °C, 16 hr., air), oxidation does not affect ordering trends significantly.

Upon heating, many of the wodginites showed greatly altered unit cell parameters (Table 44) and greatly increased supercell diffraction intensities (Figure 34). However, many also showed no significant change upon heating. By comparison with the heating behaviour of columbite-tantalite group minerals, the wodginites which showed no change must be fully-ordered; those which showed change were incompletely ordered prior to heating.

The unit cell parameters β and V showed the most change upon heating, thus are the most sensitive to order-disorder effects. Figure 35 is a plot of heating vectors for the wodginites as reflected by changes in β and V. Most vectors are subparallel, and indicate that β increases and V decreases with order. In two cases (samples OW-102 and WD-1), V was actually observed to increase upon heating. Powder diffraction patterns of the starting materials indicate that both samples were slightly contaminated with cassiterite; disappearance of cassiterite peaks from the diffraction pattern of the heated samples suggests that the cassiterite reacted with the wodginite which, in turn, may be the cause of the volume increases.

Although diagrams like Figure 35 help to semi-quantify disorder in wodginite, little can be done to fully quantify the phenomenon without a structural model for fully disordered (and partially ordered) wodginite. Is fully disordered wodginite monoclinic with a structure like that of another α-PbO_2 structural derivative, wolframite? Or is fully disordered
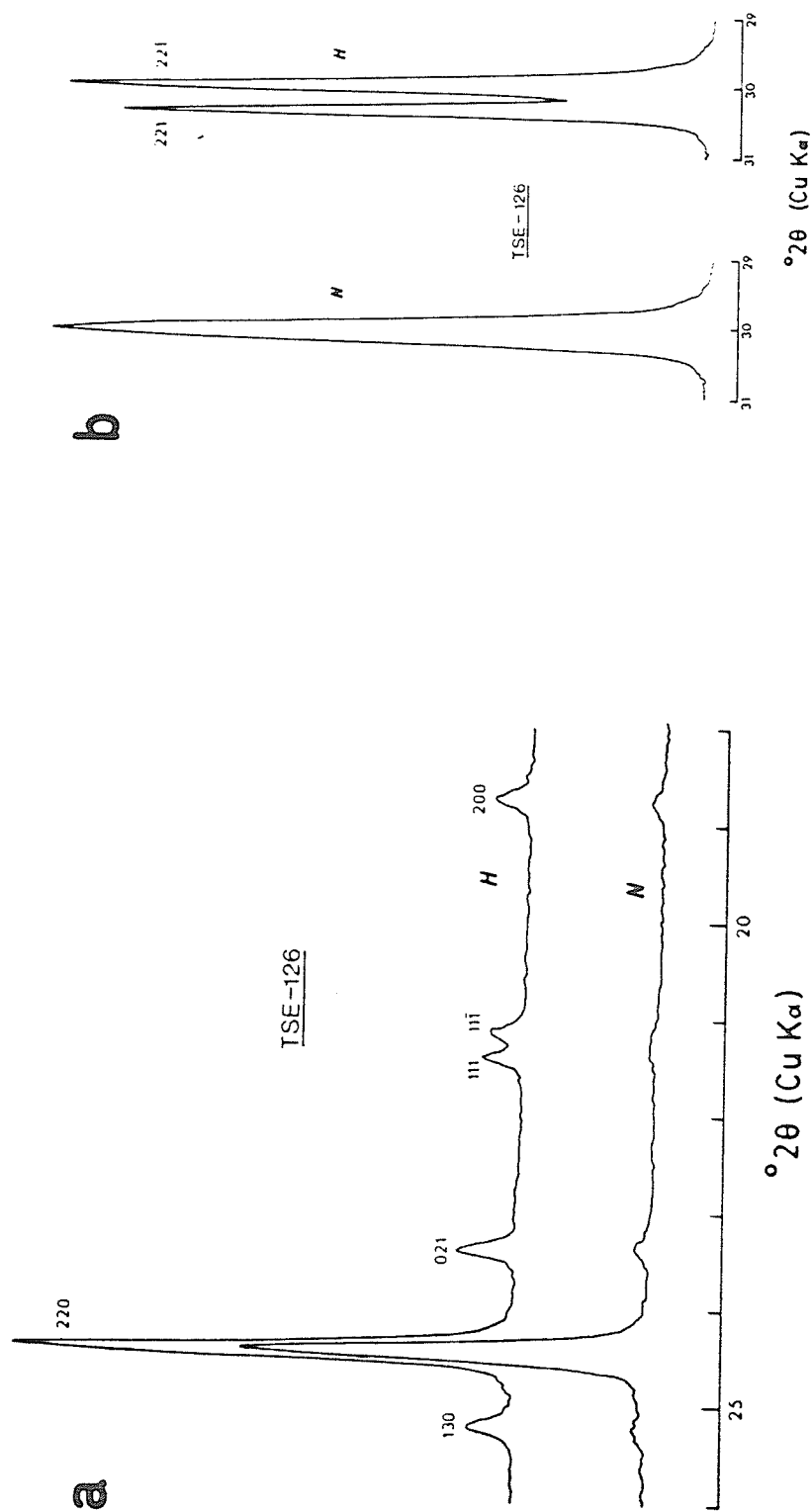
Figure 34: Change in x-ray diffraction patterns of partially-ordered wodginites with heating, as typified by sample TSE-126. (a) In the range, 18°-26° 2θ (CuKα), intensities of the supercell diffractions'(200), (11Ī), (111), (021), and (130) increase relative to the subcell diffraction (220) upon heating. (b) The separation of the diffractions (221) and (22Ī) increases upon heating, indicative of an increase in β. N: natural, H: heated.

wodginite merely identical to ixiolite, a chemically similar, but ortho-
rhombic relative of wodginite? Could the ordering path go from an
ixiolite-structure starting point to an intermediate wolframite structure
to a final, fully-ordered wodginite? Only through structure analyses of
disordered to partially ordered wodginite can such questions be answered.

Table 44: Unit Cell Parameters for Heated Wodginites

Sample	a	b	c	β	V
A-17H	9.453(1)	11.429(1)	5.098(1)	90.78(2)	550.8(1)
A-25H1	9.456(2)	11.429(2)	5.094(1)	90.86(2)	550.4(1)
A-25H2(CO)	9.457(3)	11.431(3)	5.093(1)	91.01(4)	550.5(2)
A-25H2(CO2)	9.458(2)	11.426(2)	5.093(1)	91.04(2)	550.3(1)
A-29H	9.531(3)	11.465(2)	5.118(1)	91.22(2)	559.2(1)
A-30H	9.526(2)	11.474(2)	5.116(1)	91.19(2)	559.1(1)
AC2-79-1H	9.527(2)	11.471(2)	5.119(1)	91.15(2)	559.4(1)
G69-2H(CO)	9.492(3)	11.452(2)	5.108(2)	91.07(3)	555.1(1)
G69-2H(CO2)	9.491(2)	11.449(2)	5.106(1)	91.06(2)	554.8(1)
G69-23H	9.485(1)	11.449(1)	5.108(1)	91.05(1)	554.6(1)
GB-2H	9.467(2)	11.434(1)	5.105(1)	90.78(2)	552.5(1)
H2-1H	9.457(2)	11.427(3)	5.098(2)	90.92(2)	550.8(2)
KZ-1H	9.484(2)	11.493(2)	5.095(1)	91.02(2)	555.3(1)
LJ-1H	9.507(1)	11.463(1)	5.116(1)	90.93(1)	557.4(1)
OW-102H	9.531(1)	11.475(1)	5.125(1)	91.12(2)	560.4(1)
TSE-7H	9.517(1)	11.469(1)	5.114(1)	91.14(2)	558.1(1)
TSE-40H	9.498(2)	11.457(2)	5.110(1)	91.11(3)	555.9(1)
TSE-45H	9.461(2)	11.432(1)	5.101(1)	91.01(2)	551.6(1)
TSE-76H	9.458(1)	11.506(1)	5.083(1)	91.04(1)	553.0(1)
TSE-126H	9.441(2)	11.414(2)	5.088(1)	90.93(2)	548.2(1)
WD-1H	9.529(2)	11.477(1)	5.121(2)	91.19(3)	560.0(2)

-all heatings are in air unless otherwise indicated
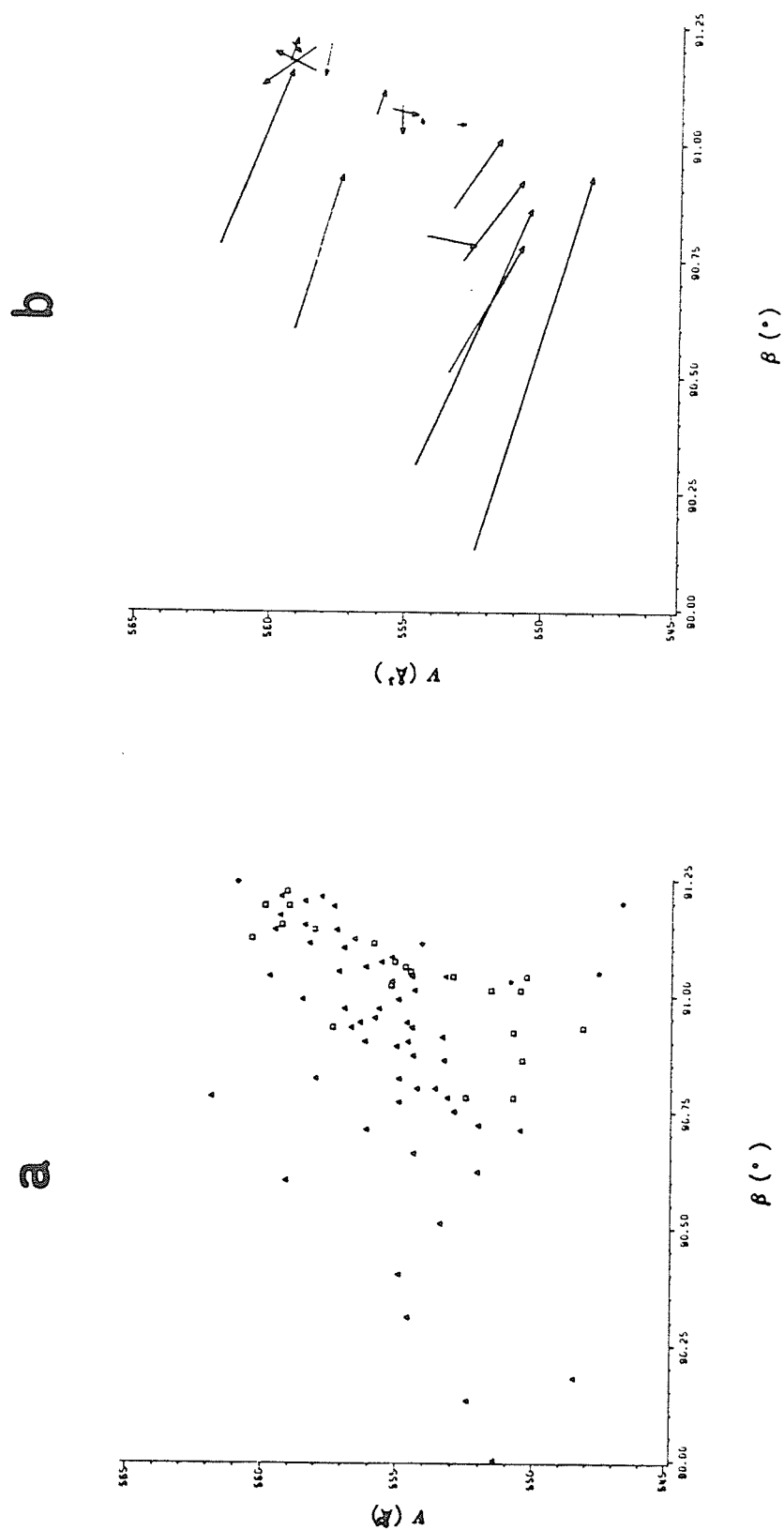
Figure 35: Wodginite-group minerals: plots of V versus β. (a) All wodginites. (b) natural and heated pairs of wodginites. In (a), triangles denote natural samples, squares denote heated samples and asterisks denote synthetic wodginites. In (b), the tail of each vector marks the natural (unheated) sample; the tip, the heated sample.

12.10   THE CRYSTAL STRUCTURE OF PARTIALLY-ORDERED WODGINITE

In spring of 1984, Dr. E.E. Foord approached me on the matter of solving the structure of a mineral which was similar to wodginite, but with apparent ABO_4 stoichiometry. The mineral was supposed to have a monoclinic cell with ixiolite-like dimensions, not with wodginite-like dimensions. These properties suggested that the mineral might be a new species with a wodginite composition but the wolframite structure.

Crystals of the mineral were initially examined by the precession method. All are sector-twinned, with $\underline{Y}$ as the twin axis. A fragment from one sector of a large twinned crystal (1 mm long) was isolated and shaped into an ellipsoid with a mean radius of 0.08 mm. Precession photographs of this fragment showed it to be untwinned. Long-exposure photographs showed wodginite-supercell diffractions, indicating that this mineral was structurally intermediate to ixiolite and wodginite, or to wolframite and wodginite.

Intensity data were collected on the crystal using the four circle diffractometer with $MoK\alpha$ radiation. A set of 25 strong diffractions collected with the centring routine of the diffractometer was used for the calculation of unit cell parameters giving $\underline{a}=9.500(5)$, $\underline{b}=11.465(6)$, $\underline{c}=5.133(3)$ Å, $\underline{\beta}=90.51(4)°$ in excellent agreement with parameters from powder diffractometry obtained by Dr. Foord: $\underline{a}=9.490(4)$, $\underline{b}=11.456(4)$, $\underline{c}=5.139(3)$ Å, $\underline{\beta}=90.56(4)°$.

Data were collected over one asymmetric unit on a wodginite cell. A total of 946 relections was measured, of which only 652 were considered as observed ($I>3\sigma$), attesting to the extreme weakness of the wodginite supercell diffractions. An empirical absorption correction was made by approximating the shape of the crystal to an ellipsoid, using ψ-scan data ($\mu=430$

cm^{-1}). To eliminate compositional uncertainty as a variable, the remaining fragments of the starting crystal were analyzed with the electron microprobe. $Fe^{2+}:Fe^{3-}$ was calculated for the starting model using the wodginite formula calculation program, and it agreed reasonably well with [57]Fe-Mössbauer results obtained by Dr. Foord on another sample of the mineral. $Sn^{2+}:Sn^{4+}$ was taken from the [119]Sn-Mössbauer analysis by Dr. Foord. Averaged microprobe analyses and the resulting formula are given in Table 45.

Table 45: Compositional Data for Sample CX-1

	Oxide wt. %		Cations per 32(O)
MnO	7.7	Mn^{2+}	2.71
FeO	2.6	Fe^{2+}	0.90
SnO	0.7	Sn^{2+}	0.13
Fe_2O_3	2.3	Fe^{3+}	0.73
ZrO_2	1.5	Zr^{4+}	0.31
SnO_2	10.3	Sn^{4+}	1.71
Nb_2O_5	7.5	Nb^{5+}	1.42
Ta_2O_5	69.1	Ta^{5+}	7.84
	101.6		15.74

The large number of constituents (8) coupled with an uncertain degree of order made model-independent refinement of the intensity data an impossibility for this sample. Consequently, refinement involved testing of the two structural models discussed above, namely of whether the mineral was structurally intermediate to ixiolite and wodginite, or wolframite and wodginite.

In terms of wodginite site designations, each of the possible structural end-members has the following ordering scheme. A wodginite with full cation order has the structural formula ABC_2O_8. If the identity of the C-site is maintained and mixing occurs between the A-, and B-sites, a wolframite structure results; it has the structural formula $(AB)C_2O_8$. If all cation sites lose their crystallographic identities, an ixiolite structure results; its structural formula is $(ABC_2)O_8$.

Refinement involved a starting model with a wodginite-like fully-ordered cation distribution. Starting positions were taken from Ferguson et al. (1976). In the first stage of refinement, mixing at only the A- and B-sites was allowed. In the second stage, all sites were mixed according to an ixiolite model. Refinement of the first model (fully anisotropic) resulted in R-indices of $\underline{R}=8.0\%$, $w\underline{R}=7.6\%$. There were several unsuitable features of this model. Difference maps indicated that the A-, and B-sites were scattering more strongly, and the C-site less strongly than the model could account for, indicative of disorder between the stronger scatterers of the C-site (e.g. Ta) and the weaker scatterers of the A-, and B-sites (e.g. Mn and Sn). True to this indication, refinement of the second model gave significantly lower R-indices than the first model: $\underline{R}=6.0\%$; $w\underline{R}=5.7\%$. The success of the latter model was further shown by difference Fourier maps: electron differences at the cation sites were two times lower than those of the first model and were much less spherical, to not-at-all spherical in shape.

Observed and calculated structure factors for the second model are given in Appendix G. Final positional and thermal parameters are given in Table 46. Large equivalent isotropic temperature factors for all sites reflect the high degree of positional disorder at all cation sites.

From the refined degree of site mixing, the sample is 60(1)% ordered. The resulting site occupancies are given in Table 47. Bond lengths and angles are given in Table 48. Differences in the mean bond lengths between the sites are less than those for fully ordered wodginite, which reflects the high degree of cation mixing (Table 49). Using the site occupancies of Table 47, the bond lengths calculated from the effective ionic radii of Shannon (1976) agree well with the observed lengths (Table 49).

Table 50 gives empirical bond valences for the various sites using the compositional data of Table 47. Bond valence sums to all cation and anion sites are lower than expected from the occupancies of Table 47. That all sums are uniformly low suggests that the problem does not exist with the refinement, but rather that the method of Brown and Shannon (1973) does not work well in cases of extreme positional disorder.

To conclude, there is overwhelming evidence that partially disordered wodginites are simply structurally intermediate to wodginite and ixiolite. There is no need to propose new compounds such as a wolframite-structured phase (e.g. Maksimova & Khvostova, 1970; Polyakov & Cherepivskaya, 1981; Khvostova et al., 1982).

Table 46: Positional and Thermal Parameters for Wodginite CX-1

Site	x	y	z	U(eq)$\mathring{A}^2$
A	0	0.6637(3)	1/4	237(8)
B	0	0.1682(2)	1/4	236(5)
C	0.2492(2)	0.4146(1)	0.2497(3)	221(3)
O1	0.137(2)	0.058(2)	0.075(4)	367(58)
O2	0.139(2)	0.446(2)	0.574(4)	318(52)
O3	0.115(2)	0.305(1)	0.098(3)	253(44)
O4	0.114(2)	0.187(2)	0.584(3)	328(50)

Anisotropic Temperature Parameters

Site	U_{11}	U_{22}	U_{33}	U_{12}	U_{13}	U_{23}
A	244(14)	213(15)	256(14)	0	39(10)	0
B	246(8)	238(8)	225(8)	0	42(6)	0
C	241(5)	227(5)	195(4)	-9(4)	40(3)	2(4)
O1	515(119)	259(80)	334(100)	19(77)	271(84)	-42(74)
O2	377(99)	289(80)	287(91)	106(74)	-105(70)	-138(74)
O3	246(70)	230(82)	282(75)	110(59)	-22(59)	-67(62)
O4	302(79)	327(94)	358(86)	63(73)	54(67)	-117(80)

All U's are x 10^4

Table 47: Refined Site Contents

	A-site	B-site	C-site
Mn^{2+}	1.89	0.27	0.54
Sn^{2+}	0.09	0.01	0.03
Fe^{2+}	0.63	0.09	0.18
Fe^{3+}	0.07	0.51	0.15
Sn^{4+}	0.17	1.19	0.34
Zr^{4+}	0.03	0.21	0.06
Nb^{5+}	0.14	0.14	1.14
Ta^{5+}	0.78	1.54	5.51

-site contents refined by mixing
 a fully ordered wodginite model
 with an ixiolite model

Table 48: Selected Distances and Angles in Wodginite CX-1

BOND LENGTHS

A Octahedron	B Octahedron	C Octahedron
A – O2 x2 2.05(2)	B – O1 x2 2.04(2)	C – O1 c 2.02(2)
– O3 x2 2.12(2)	– O3 x2 2.07(2)	– O1 d 2.16(2)
– O4 x2 2.20(2)	– O4 x2 2.03(2)	– O2 a 2.00(2)
		– O2 e 2.11(2)
		– O3 a 1.95(2)
		– O4 f 1.94(2)

ANGLES

A Octahedron

O2 – A – O2	104.0(10)	
– O3 x2	98.3(6)	
– O3 x2	93.6(7)	
– O4 x2	89.1(7)	
O3 – A – O4 x2	86.6(6)	
– O4 x2	78.3(6)	
O4 – A – O4	77.9(9)	

B Octahedron

O1 – B – O1	102.9(10)	
– O3 x2	87.9(7)	
– O4 x2	95.7(7)	
– O4 x2	91.9(7)	
O3 – B – O3	81.4(9)	
– O4 x2	83.2(7)	
– O4 x2	87.6(7)	

C Octahedron

O1c – C – O1d	87.5(7)	O1d – C – O4f	86.7(7)
– O2e	78.0(7)	O2a – C – O2e	87.7(6)
– O3a	97.1(7)	– O3a	96.1(7)
– O4f	95.6(7)	– O4f	95.4(7)
O1d – C – O2a	77.2(7)	O2e – C – O3a	89.9(7)
– O2e	81.2(7)	O3a – C – O4f	102.8(7)

Table 49: Mean Bond Lengths (Å) in Wodginites

	CX-1		G69-17
	obs.	calc.	
A-site	2.121	2.131	2.185
B-site	2.047	2.038	2.027
C-site	2.027	2.021	2.003
% order:	60		100

-data for G69-17 from Ferguson et al. (1976)

Table 50: Bond Valences in Wodginite CX-1

A Octahedron		B Octahedron		C Octahedron	
Bond	s	Bond	s	Bond	s
A-O2 x2	0.52	B-O1 x2	0.66	C-O1c	0.75
-O3 x2	0.43	-O3 x2	0.59	-O1d	0.49
-O4 x2	0.34	-O4 x2	0.67	-O2a	0.75
				-O2e	0.56
				-O3a	0.90
				-O4f	0.93

Site Sums

	Obs.	Exp.		Obs.	Exp.
A:	2.58	2.72	O1:	1.87	2.00
B:	3.84	4.07	O2:	1.83	2.00
C:	4.35	4.60	O3:	1.91	2.00
			O4:	1.93	2.00

-all bond valences in valence units (v.u.)

12.11   UNIT CELL PARAMETERS AND CRYSTAL CHEMISTRY

Because of the relatively large number of substitution mechanisms involved in wodginite-group minerals, coupled with the variable degrees of order, data on mineral chemistry and order-disorder are difficult to derive from unit cell parameters.

The use of heating vectors, such as in Figure 35, allows for semi-quantitative assessments of order-disorder; the larger the magnitude of the vector, the less ordered the mineral is in its natural state. In Figure 35, individual heating vectors cover a large range of the space occupied by the data; obviously, plots like this emphasize structural variability within the group (order-disorder). Heating vectors in a plot of $\underline{a}$ versus $\underline{b}$ (Figure 36) are much less extensive than in the $\underline{V}$ versus $\underline{\beta}$ plot; $\underline{a}$ and $\underline{b}$ are relatively insensitive to order-disorder, and as such, an $\underline{a}$ versus $\underline{b}$ plot might be useful for gleaning compositional information. In Figure 36, Fe- and Ti-rich compositions plot closest to the lower left-hand corner of the diagram, Mn- and Sn-rich compositions plot in the upper parts of the diagram, and compositions rich in $\underline{B}$-site Ta (and $\underline{A}$-site vacancies) plot near the lower right-hand corner of the diagram. The low degree of scatter in the plot attests to (1) the ineffectiveness of $\underline{B}$-site Ta enrichment in environments which are not Mn-rich – note that samples plot from the Fe,Ti-rich corner to the Mn,Sn-rich corner, then to the $\underline{B}$-site Ta-rich corner, but not from the Fe,Ti-rich corner to the $\underline{B}$-site Ta-rich corner, and (2) the subparallelism in this plot of several operator vectors, e.g. $TiSn_{-1} \parallel FeMn_{-1}$.

A multiple regression analysis using the SAS program GLM (General Linear Models) was carried out on 22 fully-ordered natural and heated wodginites to assess compositional controls on unit cell parameters. To improve the
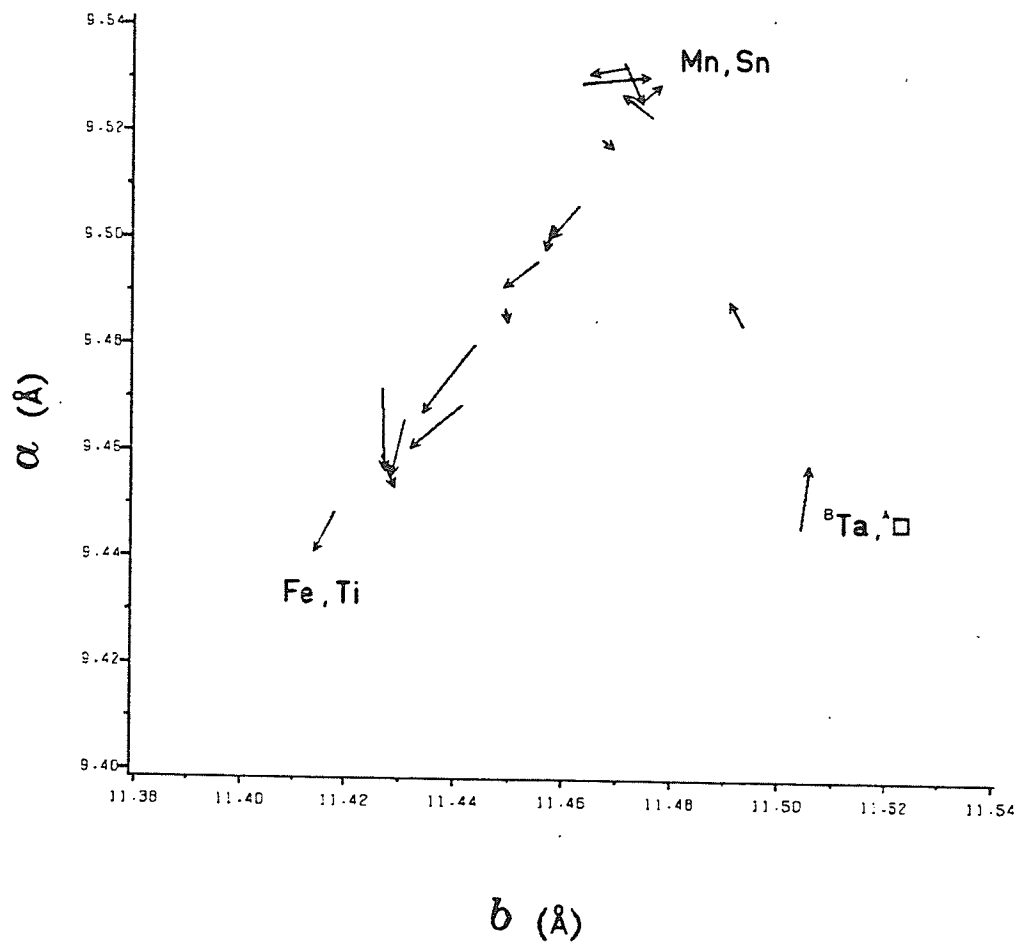
Figure 36: Wodginite-group minerals: heating vectors in a-b space.

spread of data, unit cell parameters were added for two synthetic wodginites grown in the present study ($MnSnTa_2O_8$ and $MnTiTa_2O_8$) and one from Turnock (1966) ($Mn_2Fe^{3+}Ta_5O_{16}$, with cell parameters determined by TSE). Run conditions and cell parameters for these wodginites are given in Table 51.

The independent variables of the analysis were chosen on the basis of the operators of Table 41. Each variable represents the unique part of each operator. Compositional variation was thus considered as a deviation from $MnSnTa_2O_8$. The results of the analysis are given in Table 52, and some statistical data are given in Table 53. The coefficients and intercepts of equations for each unit cell parameter are given across each row of the table. The order of each equation was determined by stepwise addition, with a maximum R^2 improvement, using the SAS program STEPWISE. All six compositional variables were necessary for modelling $\underline{b}$, $\underline{c}$, $\underline{\beta}$ and $\underline{V}$, whereas $\underline{a}$ could be modelled with only five variables. Because of the nature of the independent variables, the intercepts of the five equations necessarily represent the lattice parameters of $MnSnTa_2O_8$. Input to the equations consists of the number of atoms per unit cell of each independent variable, based on the calculations of the fully-ordered formulae. As an example, the calculated $\underline{a}$ cell edge of hypothetical "ferrotitanowodginite" ($Fe_4Ti_4Ta_8O_{32}$) would be $9.539 - (.011 \times 4) - (.030 \times 4) = \underline{9.38}$ Å. Calculated unit cell parameters for the samples used in the regression analysis are given in Table 54.

Table 51: Synthetic Wodginites used in Cell Parameter Calculation

Composition	Starting Mixture	T (°C)	Atmosphere	Run Time (h)
$MnSnTa_2O_8$	$MnCO_3 + SnO_2 + Ta_2O_5$	1050	air/1 atm	10+10
$MnTiTa_2O_8$	$MnCO_3 + TiO_2 + Ta_2O_5$	1050	air/1 atm	10+10
$Mn_2Fe^{3+}Ta_5O_{16}$	$2MnTa_2O_6 + FeTaO_4$	1225	air/1 atm*	

CELL PARAMETERS

	$MnSnTa_2O_8$	$MnTiTa_2O_8$	$Mn_2Fe^{3+}Ta_5O_{16}$
a	9.537(1)	9.428(2)	9.450(1)
b	11.482(1)	11.410(1)	11.426(1)
c	5.124(1)	5.084(1)	5.094(1)
β	91.24(1)	91.20(1)	90.89(1)
V	561.0(1)	546.7(1)	549.7(1)

* from Turnock (1966)

Table 52:   Results of the Multiple Regression Analysis

Lattice Parameter	Inter-cept	Coefficients						R^2
		Fe^{2+}	Ti	A_H	B_H	Fe^{3+}	Nb	
a	9.539	-.011	-.030	-.035	0	-.044	-.005	.93
b	11.481	-.007	-.019	+.015	-.05	-.030	-.006	.94
c	5.126	-.002	-.011	-.020	-.05	-.015	-.002	.90
ß	91.25	-.09	-.02	-.02	+.4	-.19	-.12	.91
V	561.3	-1.3	-3.9	-3.5	-8	-5.6	-0.8	.93

Table 53:   Statistical Data for Table 52

	Inter-cept	Fe^{2+}	Ti	A_H	B_H	Fe^{3+}	Nb
a	6(0.0)	5(3.2)	2(0.0)	5(0.0)	–	6(0.0)	5(29)
b	5(0.0)	4(6.6)	2(0.0)	4(0.1)	3(14)	4(0.0)	4(13)
c	3(0.0)	2(28)	1(0.0)	2(0.0)	2(2.9)	3(0.0)	2(37)
ß	3(0.0)	2(0.1)	1(5.9)	2(37)	2(8.0)	3(0.0)	2(0.0)
V	9(0.0)	6(6.0)	3(0.0)	7(0.0)	6(18)	7(0.0)	6(22)

Numbers out of parentheses are standard deviations on the last signi-
ficant figure of the parameters of Table 52.
Numbers enclosed in parentheses are % probabilities for Ho$|t|$=0.

Table 54: Calculated Cell Parameters for Samples Used in the
           Multiple Regression Analysis

Sample	a	b	c (Å)	$\beta°$	V
G69-23	9.492	11.450	5.106	91.08	555.0
G69-42	9.491	11.448	5.106	91.05	554.7
OW-102	9.518	11.468	5.114	91.14	558.2
SMP-12	9.514	11.481	5.108	91.14	557.9
TSE-7	9.524	11.477	5.114	91.17	559.0
TSE-16	9.478	11.441	5.103	90.98	553.2
TSE-28	9.510	11.482	5.106	91.13	557.5
TSE-32	9.492	11.448	5.106	91.05	554.7
TSE-48	9.492	11.448	5.107	91.06	555.0
TSE-138	9.506	11.454	5.112	91.09	556.7
WD-1	9.523	11.470	5.115	91.09	558.4
A-17H	9.452	11.434	5.098	90.77	551.0
A-25H2	9.449	11.419	5.094	90.88	549.4
A-29H	9.519	11.474	5.113	91.16	558.4
A-30H	9.530	11.469	5.119	91.16	559.3
G69-23H	9.492	11.450	5.106	91.08	555.0
H2-1H	9.465	11.438	5.100	90.93	552.1
KZ-1H	9.484	11.488	5.092	90.98	554.5
LJ-1H	9.497	11.450	5.112	90.92	555.8
TSE-45H	9.486	11.446	5.105	91.04	554.1
TSE-76H	9.465	11.502	5.083	91.09	553.6
TSE-126H	9.456	11.422	5.097	90.91	550.2
$MnSnTa_2O_8$	9.544	11.473	5.125	91.29	561.4
$MnTiTa_2O_8$	9.412	11.405	5.081	91.13	545.8
$Mn_2FeTa_5O_{16}$	9.448	11.423	5.095	90.87	550.0

It must be pointed out that problems with the calibration dataset and the method were not trivial:

1. Powder diffraction data represent structural data for a bulk sample. Estimation of the bulk composition of the sample from microprobe data is difficult due to strong compositional zoning of some samples. In cases where core and rim analyses of a crystal were available, the assigned bulk composition was a weighted mean of 2/3 x core composition + 1/3 x rim composition.

2. In nearly all cases, separate parts of crystals or batches of crystals were used for microprobe analysis versus powder diffractometry. As such, the bulk compositions of the powders may deviate significantly from the microprobe-derived composition.

3. The multiple regression model is a linear one, whereas solid-solution in minerals may result in non-linear correspondence between compositional data and unit cell parameters (Newton & Wood, 1980).

4. The precision of $Fe^{2+}:Fe^{3+}$ calculation from microprobe data is necessarily low (Le Maitre, 1982). Furthermore, the possibility of oxidation affecting the cell parameters of some heated wodginites cannot be entirely ruled out.

5. The low degree of efficiency observed for some of the substitution operators in natural wodginites (which make up most of the dataset), results in substitution vectors with short magnitudes in compositional - structure space. These will have a lot of angular uncertainty associated with them. (Better definition of the vectors should be possible if their magnitudes can be extended with data from synthesis studies).

Despite the above points, the equations of Table 52 predicted the unit cell parameters of wodginite-group minerals reasonably precisely: the root mean square errors in $\underline{a}$, $\underline{b}$, and $\underline{c}$ are 0.01, 0.01 and 0.004 Å respectively, in $\underline{\beta}$, is 0.05° (comparable to the precision of $\underline{\beta}$ measurement from precession photographs!), and in $\underline{V}$, is 1.1 Å³.

One of the advantages of the equations of Table 52 is that the bounds for fully-ordered wodginites in structure space can be readily defined. Figure 37 is a plot, once again, of $\underline{V}$ versus $\underline{\beta}$; the solid line with positive slope divides a region with only incompletely ordered wodginites (to the left) from one with ordered wodginites (to the right) (some slightly disordered compositions can also plot in this field). With this plot, most wodginites with only partial cation order can be discerned from those which are mainly ordered, without the need for heating experiments. As a rule of thumb, samples which plot furthest to the left of the line are the most disordered; those which plot closest to the line are the least disordered.

On a more quantitative level, one can now take a microprobe analysis of a wodginite and calculate its fully-ordered unit cell parameters. The result of such a calculation compared to the actual cell parameters of the wodginite (unheated) should show whether the sample is fully or partially ordered. The "ordering index" (Δ) of the wodginite, defined as

$$\Delta = \frac{[\beta(obs)-90]}{[\beta(calc)-90]}$$

should serve as a measure of the degree of order for the sample. Samples for which $\underline{\beta}$(obs)=90° have the ixiolite structure and are fully disordered. Samples for which $\underline{\beta}$(obs)=$\underline{\beta}$(calc) have the fully ordered wodginite struc-
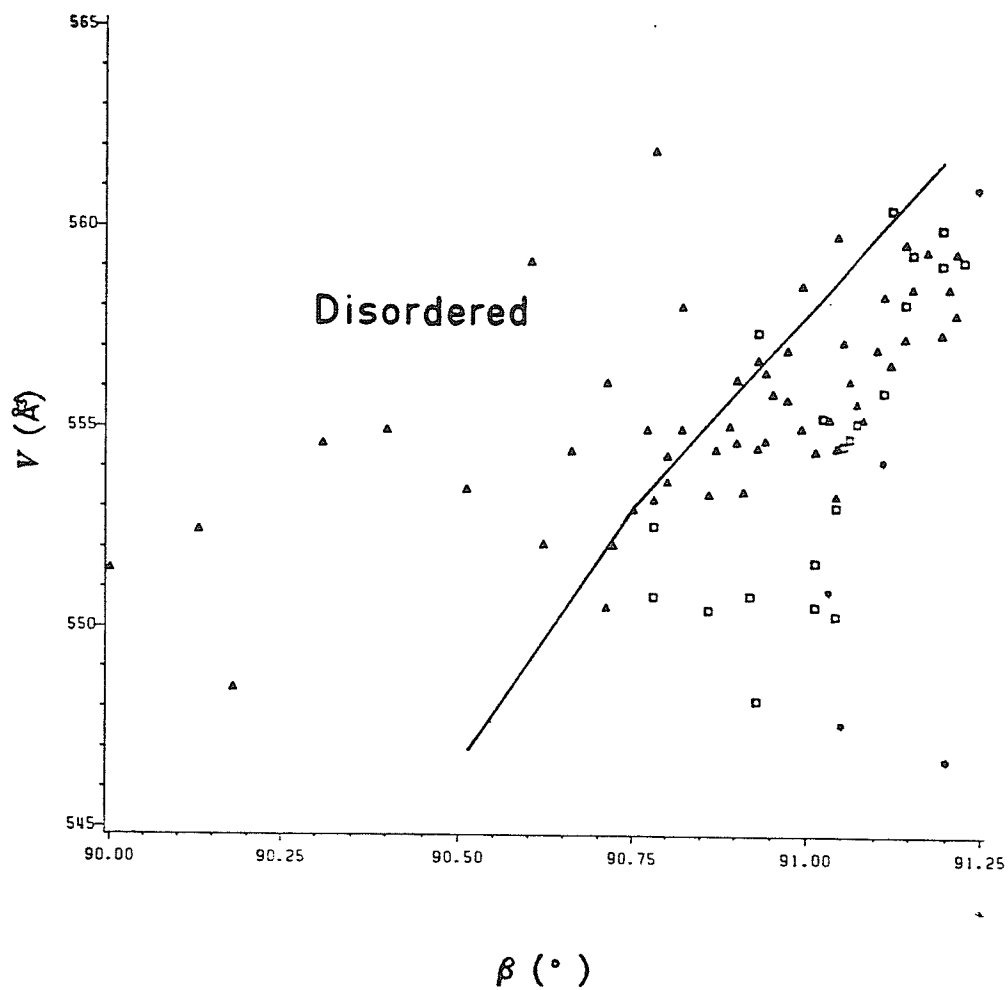
Figure 37: Wodginite-group minerals: subdivision of $\underline{V}$-$\underline{\beta}$ space. Incompletely ordered wodginites plot to the left of the line; samples to the right of the line are largely ordered. Sample symbols are as in Figure 35.

ture. Δ x100 gives the degree of order, and from what is known of the precision of $\underline{\beta}$ measurement and $\underline{\beta}$ calculation, it should be precise to within 10% of the actual value. On the basis of earlier discussions (Unit Cell Parameters and Crystal Chemistry), better precision would be difficult to obtain without a considerable amount of synthesis work.

It must also be noted that the assumption inherent in this approach is that the order-disorder transformation from ixiolite to wodginite is continuous; the relationship between Δ and the degree of order is taken to be continuous and linear. The possibility of the transformation being discontinuous cannot be ruled out; however, plots like Figure 33 suggest that at this low level of precision (±10%), the assumption of a continuous transformation is probably acceptable.

Estimates of the degree of order of all wodginites in the "disordered" field of Figure 37 are given in Table 55. In addition to these calculations, the method was applied to sample CX-1, on which the structure refinement was done. On the basis of its fully-ordered formula, sample CX-1 has a calculated $\underline{\beta}$ of 90.87°. The observed value of $\underline{\beta}$ is 90.51°, which results in a ordering index of 0.6, or a degree of order of 60 %. This figure is in excellent agreement with the results of the structure analysis, where the degree of order is 60(1)%, despite the fact that Sn^{2+} and Zr^{4+} were ignored in the calculation of $\underline{\beta}$.

The above approach has even greater potential in that the degree of order can be estimated for wodginites in which either too little sample exists for heating experiments, or for which contamination with potential reactants (e.g. cassiterite) is far too intimate. A great many wodginites fall into this last category. Previous studies of wodginite rarely

involved heating experiments; the present method allows data from these studies to be more completely evaluated from a structural point of view.

Table 55: Ordering Data for Selected Wodginites

Sample	β(obs)°	β(calc)°	Δ	% Order
TSE-130	90.00	90.90	0.00	0
TSE-126	90.13	90.92	0.14	15
TSE-122	90.18	90.87	0.21	20
A-25	90.31	90.88	0.35	35
TSE-90	90.40	90.93	0.43	45
TSE-109	90.62	90.99	0.63	65
A-17	90.51	90.78	0.65	65
LJ-1	90.60	90.91	0.66	65
TSE-137	90.71	91.07	0.66	65
TSE-134	90.72	91.00	0.72	70
GB-4	90.66	90.86	0.77	75
TSE-30	90.77	90.97	0.79	80
TSE-77	90.82	91.01	0.81	80
H2-1	90.75	90.93	0.81	80
G69-46a	90.90	91.02	0.88	90
LJ-2	90.82	90.88	0.93	95
G69-17	91.10	91.14	0.96	95

All degrees of order rounded to the nearest 5%

Chapter XIII

PYROCHLORE GROUP MINERALS

13.1   INTRODUCTION

Pyrochlore group minerals are the second most-common group of Ta-Nb oxide minerals in granitic pegmatites.   This high degree of abundance persists even to the simpsonite paragenesis, in which pyrochlore group minerals are second only to simpsonite in frequency of occurrence.

The general formula of pyrochlore group minerals (Hogarth, 1977) is:

$$A_{2-m}B_2O_6\emptyset_{1-n} \cdot pH_2O \qquad (Z=8)$$
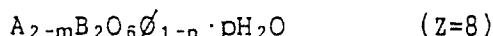
$\underline{A}$-cations range from monovalent to trivalent.   The most typical $\underline{A}$-cations are Na and Ca; less common $\underline{A}$-cations are Ba, Bi, Ce, K, Pb, Sb^{3+}, Sn^{2-}, Sr, Th, U, Y, Zr.   The smaller, $\underline{B}$-cations are either quadrivalent or pentavalent.   Typical $\underline{B}$-cations are Nb, Ta and Ti; atypical ones such as Sn^{4+} and Fe^{3+} only occur in trace to minor quantities.   In the IMA-recommended formula given here, a distinction is made between the six oxygens which coordinate each $\underline{B}$-cation, and the other anion which is bonded only to the $\underline{A}$-cation.   This anion, denoted $\emptyset$ here, can be OH, F or O.   Some pyrochlore group minerals also contain structural water; the upper limit is not well-established, but is in the neighbourhood of one molecule per formula unit.

Vacancies, indicated in the formula by the subscripts $\underline{m}$ and $\underline{n}$, can occur at the $\underline{A}$-site and the $\underline{\emptyset}$-site.   Observed ranges of these variables for natural pyrochlores are: $\underline{m}=0 \rightarrow 1.75$, $\underline{n}=0 \rightarrow 1$.

Structure refinements of natural and synthetic pyrochlores show that the B-site is always fully occupied. Although the IMA-recommended formula for pyrochlore-group minerals indicates that the O-site is also fully occupied, some recent refinements of synthetic pyrochlores of unusual composition (Groult et al., 1982) show that it is possible to have vacancies at this site. Consequently, the only acceptable basis for formula calculation is normalization of the B-cation sum to 2 cations per formula unit, despite the fact that previous studies mostly use 14 anions, or in the absence of F and OH determinations, 13 oxygens for the calculation.

The pyrochlore group is divided into three subgroups on the basis of B-site chemistry (Hogarth, 1977). The pyrochlore subgroup has Nb+Ta>2Ti and Nb>Ta. The microlite subgroup has Nb+Ta>2Ti and Ta≥Nb. The betafite subgroup has 2Ti≥Nb+Ta. Further division of each subgroup into species is based on A-site chemistry (Table 56): the subgroup name plus a prefix reflecting the A-site chemistry make up the species name.

The pyrochlore structure is a fluorite-derivative structure with ordered anion vacancies. The fluorite structure consists of cubic cation coordination polyhedra such that each edge of each polyhedron is shared with an adjacent polyhedron (Figure 38a). The ideal pyrochlore structure is derived from the fluorite structure by replacing one half of the cubes of this structure with octahedra, which is done by removing oxygens at two opposing corners of the cubes involved. In the structure that results (Figure 38b), B-cations occur at the centres of the octahedra and are coordinated by 6 oxygens. A-cations occur near the centres of the cubes and are coordinated by 6 oxygens and 2 $\emptyset$-anions. Water, when present, occurs at the same location as the $\emptyset$-anions (Groult et al., 1982).

Table 56: Classification of Pyrochlore Group Minerals

(modified from Hogarth, 1977)

SUBGROUP:		PYROCHLORE Nb+Ta>2Ti & Nb>Ta	MICROLITE Nb+Ta>2Ti & Ta≥Nb	BETAFITE 2Ti≥Nb+Ta
No A-cation other than Na or Ca >20% total A-cations		pyrochlore	microlite	calciobetafite (Ca>Na)
Any A-cation, other than Na or Ca, >20% of total A-cations. Name is for the dominant non-(Na,Ca) cation.	K	kalipyrochlore		
	Sn		stannomicrolite	
	Ba	bariopyrochlore	bariomicrolite	
	Pb	plumbopyrochlore	plumbomicrolite	plumbobetafite
	Sb			stibiobetafite
	Bi		bismutomicrolite	
	Y*	yttropyrochlore		yttrobetafite
	Ce*	ceriopyrochlore		
	U	uranpyrochlore	uranmicrolite	betafite

Ce* = La → Eu , Y* = Y + Gd → Lu

- the prefixes "cerio" or "yttro" are applied if Y* + Ce* >20% total A-cations, not just if Y* >20% or if Ce* >20%.

Pyrochlore-group minerals are typically non-ideal in that they have incomplete A- and ϕ-site occupancies. If this were taken to extremes by removing all cations from the A-sites and all anions from the ϕ-sites, a framework of only BO_6 octahedra would result (Figure 39b). This structure is shown by the compound $TaWO_{5.5}$ (Groult et al., 1982) and is called the defect pyrochlore structure. Pyrochlore group minerals have structures which are intermediate to the ideal and defect pyrochlore structures; although some with the ideal structure have been found, none with the full defect structure are known.

Solid-state chemists refer to the group of all pyrochlores with structures ranging from the ideal to defect types as normal pyrochlores; this nomenclature is used here.
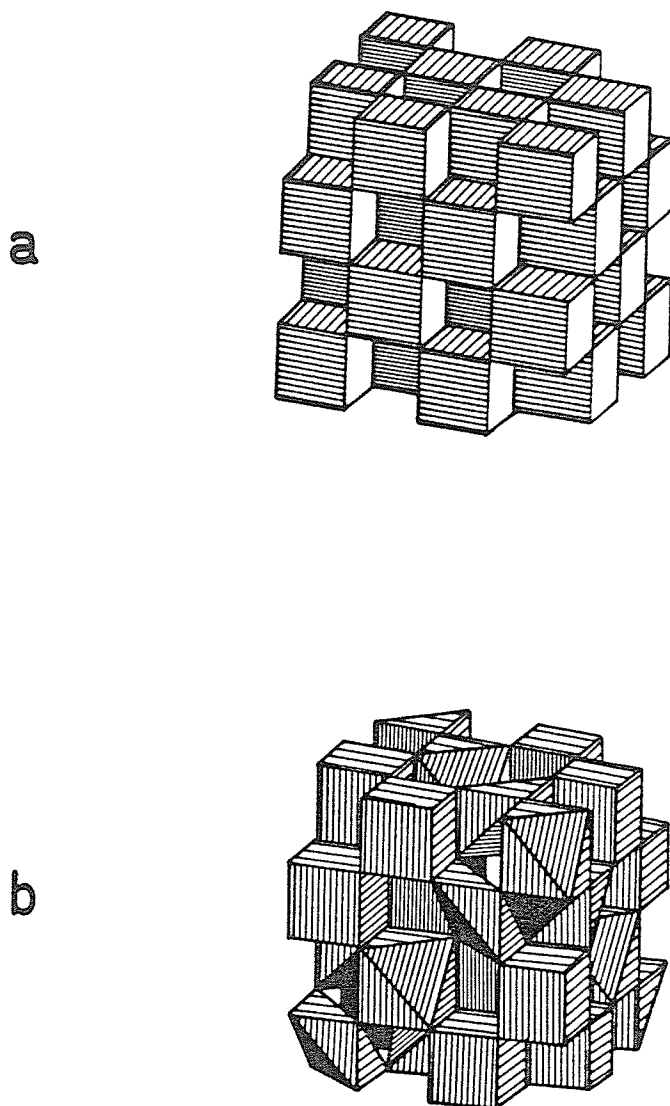
Figure 38: Derivation of the ideal pyrochlore structure from the fluorite
structure. (a) Fluorite structure, (b) ideal pyrochlore struc-
ture. The ideal pyrochlore structure can be derived from the
fluorite structure by replacing $\frac{1}{2}$ of the cubic coordination
polyhedra of the fluorite structure with octahedra. In the
resulting structure, the A-cation polyhedra are the remaining
cubes, the B-cation polyhedra are the octahedra.
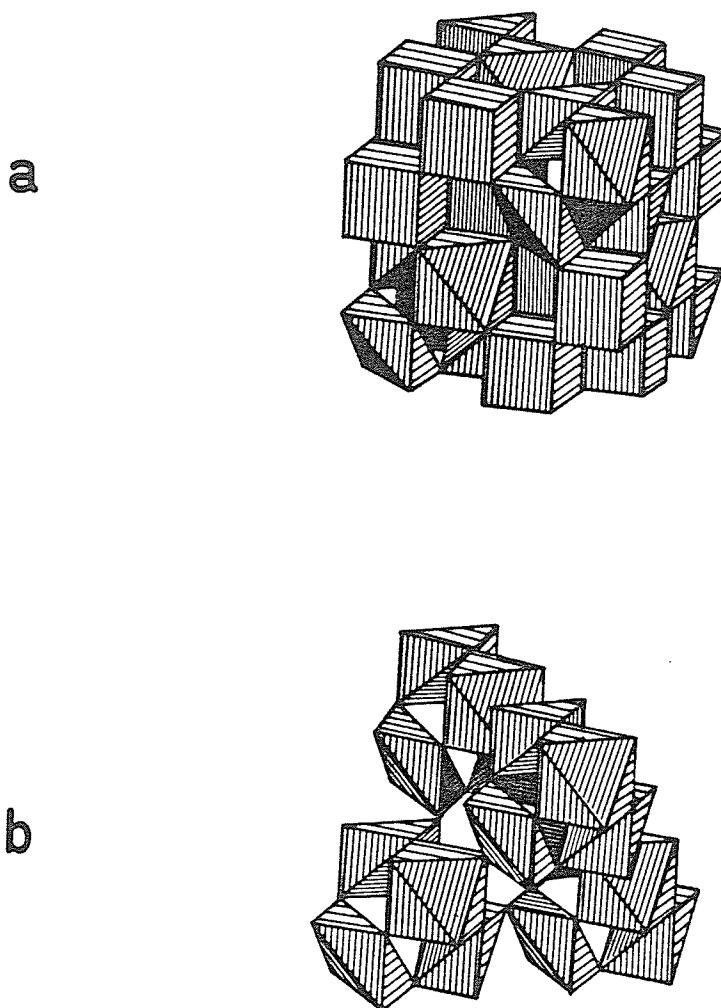
Figure 39: Derivation of the defect pyrochlore structure. (a) Ideal pyrochlore structure, (b) defect pyrochlore structure. The defect structure is derived from the ideal structure by removing all A-cation polyhedra, resulting in a framework of BO_6 octahedra with large cavities.

13.2 CHEMISTRY

Electron microprobe analyses of all normal pyrochlore group minerals of the simpsonite paragenesis are given in Table 57. Low oxide sums are due to undetermined H_2O and F, which together typically account for 2 or more wt.% of the sum.

The following assumptions were made in formula calculation:

1. The B-site is always fully occupied. Formulae were calculated on a basis of 2 B-cations.

2. Ta^{5+}, Nb^{5+}, Ti^{4-}, Sn^{4+} are B-cations; all other cations are assumed to be A-cations.

3. All Sn is assumed to Sn^{2+} and to reside at the A-site, unless the A-site occupancy is greater than the B-site occupancy. For the latter case, enough Sn^{2+} is converted to Sn^{4+} for the condition ΣA-site = ΣB-site to be met. As such, formula calculation gives a maximum estimate of $Sn^{2+}:Sn^{4+}$.

All pyrochlore group minerals in the simpsonite paragenesis belong to the microlite subgroup: all have Ta+Nb>2Ti and Ta$\geq$Nb. They are particularly interesting in that they have no detectable Ti and typically have very high Ta:Nb ratios. Pb is a trace to major element in most of the microlite subgroup minerals from the simpsonite paragenesis. Minor-to-trace elements other than Pb (e.g. Sn, U, Sb) are typically variable in their occurrence.

Three species of microlite-subgroup minerals occur in the simpsonite paragenesis: microlite, plumbomicrolite and stibiomicrolite. Of these,

only plumbomicrolite is unique to the paragenesis; microlite is a common species of the subgroup in several different parageneses and stibiomicrolite, a new member (Groat et al., in prep.), has been found in other Sb-enriched parageneses. Most of the microlites are common varieties (no significant $\underline{A}$-cation other than Na, Ca); however, uranian and antimonian varieties are found at Tanco, and a stannian variety is found at Tabba Tabba. The stibiomicrolite of the simpsonite paragenesis is distinctive for its high Pb content, showing that considerable solid solution exists between plumbo- and stibiomicrolite. Note that the effective number of oxygens per formula unit for this sample (Table 57) is less than the minimum of 6 reported in the IMA-approved formula for the group. The implication is that either vacancies occur at the $\underline{O}$-site of this sample, or, more probably, that minor $O \rightarrow OH,F$ substitution occurs.

Table 57: Chemistry of Simpsonite Paragenesis Microlites

	1	2	3	4	5	6	7	8	9	10
Na_2O	5.5	3.8	5.5	4.6	2.9	5.3	0.7	3.4	5.3	0.0
Cs_2O	0.0	0.0	0.0	0.0	0.0	0.0	1.9	0.0	0.0	0.0
CaO	9.2	7.6	10.2	8.8	8.2	10.3	0.0	12.2	8.1	3.3
MnO	0.0	0.0	0.0	0.0	0.0	0.0	0.0	0.2	0.0	0.9
FeO	0.0	0.0	0.0	0.0	0.1	0.0	0.0	0.0	0.0	0.0
SnO	0.0	0.0	0.0	0.0	0.0	0.0	0.5	1.9	0.0	0.0
PbO	0.5	0.8	0.0	0.0	1.3	1.3	32.1	0.0	1.2	5.3
Sb_2O_3	0.0	0.5	0.0	2.3	0.0	0.0	2.2	0.3	0.0	3.9
Bi_2O_3	0.0	0.0	0.0	0.0	0.0	0.0	0.0	0.0	0.0	0.3
UO_2	0.0	3.2	0.0	0.3	2.4	0.0	0.0	0.0	0.0	0.0
Nb_2O_5	2.0	1.1	0.4	0.6	1.1	10.1	14.1	1.4	1.7	0.4
Ta_2O_5	<u>81.0</u>	<u>81.5</u>	<u>81.2</u>	<u>80.0</u>	<u>80.0</u>	<u>70.3</u>	<u>47.5</u>	<u>78.0</u>	<u>81.7</u>	<u>81.8</u>
	98.2	98.5	97.3	96.6	96.0	97.3	99.0	97.2	98.0	95.9

Ions per 2 $\underline{B}$-Cations

	1	2	3	4	5	6	7	8	9	10
Na^+	0.93	0.65	0.96	0.82	0.51	0.86	0.14	0.60	0.89	0.0
Cs^+	0.0	0.0	0.0	0.0	0.0	0.0	0.17	0.0	0.0	0.0
Ca^{2+}	0.86	0.72	0.98	0.86	0.79	0.93	0.0	1.19	0.76	0.31
Mn^{2+}	0.0	0.0	0.0	0.0	0.0	0.0	0.0	0.01	0.0	0.07
Fe^{2+}	0.0	0.0	0.0	0.0	0.01	0.0	0.0	0.0	0.0	0.0
Sn^{2+}	0.0	0.0	0.0	0.0	0.0	0.0	0.02	0.08	0.0	0.0
Pb^{2+}	0.01	0.02	0.0	0.0	0.03	0.03	0.90	0.01	0.03	0.13
Sb^{3+}	0.0	0.02	0.0	0.09	0.0	0.0	0.09	0.0	0.0	0.14
Bi^{3+}	0.0	0.0	0.0	0.0	0.0	0.0	0.0	0.0	0.0	0.01
U^{4+}	0.0	0.06	0.0	0.01	0.05	0.0	0.0	0.0	0.0	0.0
Nb^{5+}	0.08	0.05	0.02	0.02	0.04	0.39	0.66	0.06	0.07	0.01
Ta^{5+}	1.92	1.95	1.98	1.98	1.96	1.61	1.34	1.94	1.93	1.99
O(eff)	6.33	6.22	6.46	6.41	6.18	6.39	6.17	6.59	6.23	5.73

1: Microlite, Tanco pegmatite (SMP-4).
2: Uranian microlite, Tanco (SMP-6).
3: Microlite, Tanco (SMP-51). Average of 5 analyses.
4: Antimonian microlite, Tanco (SMP-51). Average of 3 analyses.
5: Uranian microlite, Tanco (SMP-51). Average of 5 analyses.
6: Microlite, Mumba, Zaire (L-14).
7: Plumbomicrolite, Mumba (L-14).
8: Stannian microlite, Tabba Tabba, Australia (L-18).
9: Microlite, Alto do Giz, Brazil (ROM-1).
10: Plumboan stibiomicrolite, Alto do Giz, Brazil (RVG-1C).

- O(eff) is effective oxygen for charge balance
- analyses 1,2,8,9 are WD analyses, all others are ED

13.3   X-RAY CRYSTALLOGRAPHY

By definition, members of the pyrochlore group are cubic and have the space group Fd3m. The unit cell averages 10.4 Å along an edge and is sensitive only to extreme changes in chemistry.

Unit cell edges for microlites from the simpsonite paragenesis are given in Table 58. All unit cell edges measured are typical for microlite, and on the basis of sharpness of diffractions, non-uranian varieties are all well crystallized. Uranian varieties (e.g. SMP-6) show various degrees of metamictization, although none of the samples examined were completely metamict. Because of the extremely small size of the plumbomicrolite and stibiomicrolite crystals, unit cell parameters for these species could not be measured.

Table 58:   Unit Cell Edges for Microlites
from the Simpsonite Paragenesis

Sample	Locality	Description	a (Å)
L-15	Alto do Giz	microlite	10.431(1)
L-18	Tabba Tabba	stannian microlite	10.423(1)
KO-1	Leshaia	microlite	10.436(2)
SMP-4	Tanco	microlite	10.435(1)
SMP-6	Tanco	uranian microlite	10.433(2)
SMP-51	Tanco	antimonian microlite	10.426(4)

13.4   A CRYSTAL STRUCTURE REFINEMENT OF MICROLITE

To date no crystal structure refinement has ever been done on a member of the microlite subgroup, much less on the species microlite. For this reason, and to assess the quality of electron microprobe analyses of microlites of this study, a structure refinement of microlite SMP-4 was carried out.

A small fragment of the sample was plucked out from the area analyzed with the electron microprobe, and hand-shaped into a subsphere with a radius of 0.05 mm. Intensity data were collected with the R3m four circle diffractometer using graphite-monochromated MoKα radiation. A set of 25 strong diffractions used in centring was also used for unit cell refinement: $\underline{a}$=10.428(1) Å. Data were collected over 3 asymmetric units (1 octant of reciprocal space) and merged to give a total of 105 reflections, of which 94 were considered observed (I>3σ). An empirical absorption correction was done by approximating the shape of the crystal as an ellipsoid, using ψ-scan data (μ=403 cm^{-1}).

Starting positional parameters for the refinement were ideal values for the pyrochlore structure. The positional parameters for all cations and the $\emptyset$-anion are invariant. Only $\underline{x}$ for the $\underline{O}$-site can vary; the initial value used for $\underline{x}$ was 0.4375, which makes the $\underline{B}$-cation coordination polyhedron a regular octahedron.

Initial site occupancies were taken from the microprobe results. The $\underline{B}$-site was assumed to be fully occupied, and the Ta:Nb ratio was fixed at the value determined from microprobe analysis. The constraint Ca:Na:Pb = 0.93:1:0.01 (from microprobe analysis) was used for the $\underline{A}$-site, and the total occupancy of the site was refined. The $\underline{O}$- and $\emptyset$-site total

occupancies were also refined; the scattering curve for neutral O was used for the $\underline{O}$-site, and a 50:50 F:O curve was used for the $\emptyset$-site.

Refinement of a fully anisotropic model converged on R-indices of $\underline{R}$=2.3%, w$\underline{R}$=1.9%, and included an extinction correction (which necessitated use of a weighting scheme of $\sigma^{-2}|F|$). Observed and calculated structure factors are given in Appendix G. Positional and thermal parameters are given in Table 59, and selected distances and angles are given in Table 60.

The total occupancy of the $\underline{A}$-site is 0.96(4), in good agreement with the result from microprobe analysis of 0.90, based on $\underline{B}$-site normalization. The occupancy of the $\underline{O}$-site is 0.99(3), and of the $\emptyset$-site is 0.98(6), indicating full occupancy for both sites.

The formula resulting from microprobe analysis plus site occupancy refinement is:

$$(Na_{0.97}Ca_{0.94}Pb_{0.01})_{\Sigma 1.92}(Ta_{1.92}Nb_{0.08})_{\Sigma 2}O_{5.94}\emptyset_{0.98}$$
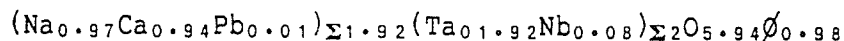
The sum of the positive charges per formula unit is 12.87 . If $\emptyset$ consists only of monovalent anions, the sum of the negative charges is 12.86; if $\emptyset$ is only divalent, the sum is 13.84. Thus, for charge balance, $\emptyset$ must be completely monovalent. The validity of the formula calculation procedure (normalization on 2 $\underline{B}$-cations) is confirmed by $\underline{A}$:$\underline{B}$:O ratios from the structure refinement in good agreement with microprobe results.

Crystal structure refinement is an extremely rapid procedure for pyrochlore group minerals; with only 90+ unique reflections to a limit of d=0.890 Å, a complete intensity dataset can be collected in a matter of a few hours with an automatic single-crystal diffractometer. Structure refinement pro-

vides valuable information about the quantity and types of anions present in pyrochlore group minerals. The relative softness makes hand-shaping of crystals a simple and rapid task. Crystals shaped to spheres can give reasonably precise site-occupancy information, comparable to electron microprobe data in precision. For these reasons, structure refinement may be used for chemical analysis of microlites, and is a good complement to electron microprobe analysis.

Table 59: Atomic Positional and Thermal Parameters for Microlite SMP-4

Site	x	y	z	U(eq)$Å^2$
A	1/2	1/2	1/2	316(12)
B	0	0	0	171(2)
O	0.3160(7)	1/8	1/8	233(18)
$\emptyset$	3/8	3/8	3/8	174(28)

Anisotropic Temperature Parameters

Site	U_{11}	U_{22}	U_{33}	U_{12}	U_{13}	U_{23}
A	316(21)	316(21)	316(21)	−91(13)	−91(13)	−91(13)
B	171(4)	171(4)	171(4)	−10(2)	−10(2)	−10(2)
O	184(39)	257(28)	257(28)	−54(32)	0	0
$\emptyset$	174(49)	174(49)	174(49)	0	0	0

All U's are x 10^4

Table 60: Bond Lengths (Å) and Angles (°) for Microlite SMP-4

A Polyhedron	B Polyhedron

BOND LENGTHS

A − O x6 2.660(5)	B − O x6 1.968(3)
− $\emptyset$ x2 2.258	
mean: 2.560	

ANGLES

O − A − O x6 117.8(1)	O − B − O x6 91.5(3)
− O x6 62.2(1)	− O x6 88.5(3)
− $\emptyset$ x6 98.6(1)	
− $\emptyset$ x6 81.4(1)	mean: 90.0
mean: 90.0	

Chapter XIV

CESSTIBTANTITE

14.1   INTRODUCTION

Cesstibtantite was discovered by Voloshin et al. (1981) in the simpsonite-bearing pegmatite at Leshaia, Kola Peninsula, USSR. On the basis of X-ray crystallography, chemical and physical properties, they concluded that its structure is derived from the microlite structure and that it has the ideal formula $(Cs,Na)SbTa_4O_{12}$. A summary of data for type cesstibtantite is given in Table 61.

In late 1980, I encountered a mineral at the Tanco pegmatite, Bernic Lake, Manitoba with properties similar to those of cesstibtantite. Because of some important differences between the Tanco mineral and the description of cesstibtantite in Voloshin et al. (1981), a complete investigation of both minerals was undertaken. The properties of type cesstibtantite were reinvestigated and were found to be much more similar to the Tanco mineral than initially inferred; it was concluded that the Tanco mineral was also cesstibtantite.

Cesstibtantite has since been found at a third locality, in Australia (E.H. Nickel, pers. comm.). The description of this occurrence is currently in preparation (Nickel & Robinson, 1986), consequently it is not discussed here.

Table 61: Summary of Data for Type Cesstibtantite
(from Voloshin et al. (1981)

Ideal formula: $(Cs,Na)SbTa_4O_{12}$, $\underline{Z}=4$

Symmetry: Cubic, $\underline{a}=10.526(5)$ Å

Optics: Isotropic, $\underline{n}>1.8$. Colourless to grey, transparent.

Density: obs.=6.4-6.6 g/cm^3, calc.=6.49 g/cm^3

Hardness: VHN=670-780 (100 g load)

Strongest diffraction lines ($\underline{d}$, $\underline{I}$): 3.17 (9), 3.04 (10),
1.860 (10), 1.587 (10), 1.370 (9), 1.017 (9), 1.012 (10)

14.2   PHYSICAL AND OPTICAL PROPERTIES

Cesstibtantite (Figure 40) is colourless to grey to yellow-orange, and ranges in opacity from transparent to translucent; the lustre similarly ranges from vitreous to adamantine. Cesstibtantite fluoresces yellow-orange to orange under UV light. It is brittle with a hardness of about 5. Voloshin et al. (1981) report a range of densities of 6.4 to 6.6 g/cm^3 for the Leshaia sample; Tanco samples were too small and too few in number for density determination.

Cesstibtantite from Leshaia is reported to be isotropic with $\bar{n}>1.8$ (Voloshin et al., 1981). Cesstibtantite from the Tanco pegmatite is not always isotropic; in thin section, some crystals are anisotropic with a weak birefringence (1st order grey). Anisotropic crystals have vermiform optical domains; to date, no optically continuous anisotropic crystals have been found.
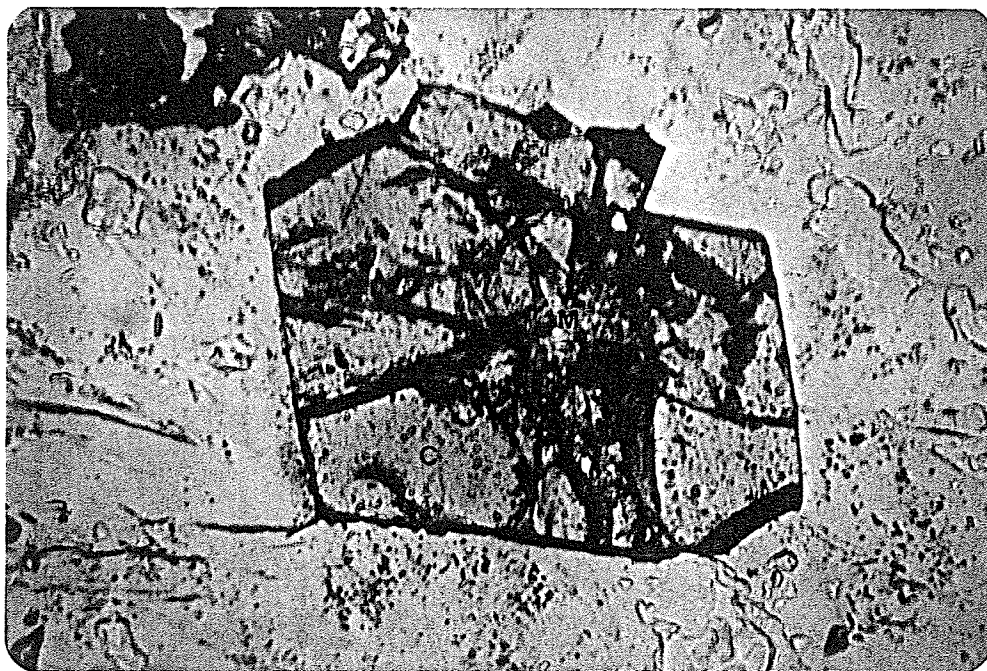
Figure 40: Cesstibtantite from the Tanco pegmatite.   Euhedral cuboctahe-
dral cesstibtantite (C)   is shown here overgrowing an earlier
generation of uranian microlite (M).   100 X magnification.

Crystals are always very small, typically 0.1-0.5 mm in diameter. At Tanco, cesstibtantite occurs as isolated crystals or as overgrowths on antimonian and uranian varieties of microlite. At Leshaia, it occurs as irregularly-shaped aggregates along simpsonite and stibiotantalite grain boundaries, in fractures in these minerals, and in fine intergrowths with microlite (Voloshin et al., 1981) as with the sample investigated in this study.

14.3 X-RAY CRYSTALLOGRAPHY

X-ray powder diffraction patterns were obtained with a Gandolfi camera using CuKα radiation. Powder diffraction data for cesstibtantites from both occurrences are given in Table 62. Both diffraction patterns can be completely indexed on a cubic cell with a=10.5 Å, space group Fd3m. Refined unit cell parameters (Table 62) show the cell of cesstibtantite from Leshaia to be slightly larger than that of the Tanco specimen.

Powder diffraction data for type cesstibtantite (Voloshin et al., 1981) are given in Table 63. The pattern reported by Voloshin et al. (1981) is different from the ones obtained in the present study: (1) there are diffractions which violate the F-centring (e.g. at 2.415 Å), and (2) several high-angle diffractions are "split" (e.g. the 1.156 Å diffraction seems to be split into two diffractions at 1.156 and 1.155 Å). Regarding the first point, the diffractions which violate the F-centring can all be indexed on a cubic F-centred cell with a=10.436(2) Å. This is a typical cell edge for common microlite (see Pyrochlore Group Minerals, Table 58). Because of the fine intergrowth of type cesstibtantite and microlite, as described by Voloshin et al. (1981), it is concluded that all such diffractions result

Table 62: Powder Diffraction Data for Cesstibtantites

hkl	KO-1		SMP-6	
	d	I	d	I
111	6.07	8	6.07	8
311	3.17	9	3.16	9
222	3.03	10	3.03	10
400	2.632	7	2.625	8
331	2.417	1	2.406	1
511,333	2.026	7	2.021	6
440	1.861	9	1.856	9
531	1.776	4	1.774	3
533	1.606	2	1.600	1
622	1.586	8	1.582	9
444	1.518	2	1.514	2
711,551	1.472	4	1.470	3
731,553	1.370	6	1.367	4
800	1.315	1	1.311	3
751,555	1.214	1	1.212	1
662	1.206	3	1.204	3
840	1.177	3	1.175	3
911,753	1.155	2	1.154	1
931	1.1017	2	1.1005	1
844	1.0734	2	1.0713	2
933,771	1.0565	<1		
951,773	1.0168	1	1.0151	2
1022,666	1.0123	4	1.0102	4
a (Å)	10.522(3)		10.497(1)	

114.6 mm dia. Gandolfi camera, Ni-
filtered CuKα radiation. Corrected
for shrinkage.

KO-1: Leshaia, Kola Peninsula, USSR.
SMP-6: Tanco Pegmatite, Manitoba.

Table 63: Reinterpretation of the Type Diffraction
            Pattern for Cesstibtantite

I	1	2	3
6	6.06	6.06	6.06
9	3.17	3.17	3.17
10	3.04	3.04	3.04
7	2.631	2.631	2.63˙
3	2.415	2.415	
8	2.024	2.024	2.024
10	1.860	1.860	
1	1.846		1.846
5	1.779	1.779	
1	1.662	1.662	
5	1.605	1.605	
10	1.587	1.587	
1	1.574		1.574
3	1.520	1.520	
8	1.474	1.474	
1	1.461		1.46˙
9	1.370	1.370	
1d	1.358		1.358
6	1.317	1.317	
1d	1.305		1.305
3	1.287	1.287	
7	1.216	1.216	
3	1.216 *		
8	1.208	1.208	
3	1.208 *		
1d	1.197		1.197
6	1.177	1.177	
3	1.176 *		
6	1.156	1.156	
3	1.155 *		
7	1.1032	1.1032	
4	1.1027 *		
8	1.0738	1.0738	
5	1.0738 *		
1	1.0644		1.0644
1	1.0644 †		
6	1.0572	1.0572	
3	1.0571 *		
1d	1.0460		1.0460
1d	1.0258 ?		
9	1.0173	1.0173	
5	1.0169 *		
10	1.0123	1.0123	
7	1.0121 *		
2	1.0035		1.0035
1	1.0035 †		
3	0.9840 ?		
5	0.9811	0.9811	
3	0.9810 *		

1. Type pattern (Voloshin et al. 1981).
2. Cesstibtantite component: $a=10.525(1)$ Å.
3. Microlite component: $a=10.436(2)$ Å.

KEY: d - diffuse
     * - Fe $K\alpha_2$ component of cesstibtantite
     † - Fe $K\alpha_2$ component of microlite
     ? - unexplained contaminant

from microlite contamination. Regarding point (2), the higher-d member of each split diffraction corresponds reasonably well to d's reported for Leshaia cesstibtantite examined in the present study (Table 62). Also, the lower-d members are consistently $\frac{1}{2}$ as intense as their higher-d counterparts. It is probable that the doublets reported by Voloshin et al. (1981) result from unrecognized Ka_1-Ka_2 resolution. Different d's for each component result from the use of incorrect values of λ in Bragg's equation for one or both members of each doublet. Because Voloshin et al. (1981) do not report the type or wavelength of radiation used in their d-calculations, this probability cannot be further explored.

Precession photographs were taken of cesstibtantites from both localities (0 to 3rd levels, MoKa radiation), and conform completely to Fd3m symmetry; intensity distributions obey Fd3m symmetry, and there are no metric deviations from cubic symmetry. However, both cesstibtantites were found to have some weak diffractions in their precession photographs ($I \leq 1\%$) which are not shown by normal pyrochlores (Table 64). Although these do not violate Fd3m symmetry, they do violate extinction conditions for the pyrochlore structure (all atoms in the pyrochlore structure are at special positions).

Table 64: Forbidden Diffractions of Cesstibtantite

$(I/I_0 \leq 1)$
244, 446, 248, 468, 288, 688, 4410, 4810, 2412, 4612, 2812

14.4 CHEMISTRY

Electron microprobe analyses of cesstibtantites of this study and an average of the analyses of Voloshin et al. (1981) are given in Table 65. The average analysis of Voloshin et al. (1981) for cesstibtantite agrees reasonably well with the analyses of this study for Leshaia cesstibtantites. However, the Tanco sample differs from the Leshaia samples in having higher Ta_2O_5, PbO, Na_2O and lower Nb_2O_5, Sb_2O_3, Cs_2O.

Formula contents on a basis of 12 oxygens, as suggested by Voloshin et al. (1981), are given in Table 65. Voloshin et al. (1981) observed a nearly 1:1:4:12 ratio for (Cs+Na+Ca):(Sb+Bi+Pb):(Ta+Nb):O of their analyses and proposed that cesstibtantite had the structural formula $AA'B_4O_{12}$, where $\underline{A}$ = Cs, Na, Ca, (K), $\underline{A}'$ = Sb^{3+}, Bi, Pb, (Sn^{2+}), and $\underline{B}$=Ta, Nb. Actual ratios on a basis of 12(O) are:

1.09 : 1.18 : 3.89 : 12   (Leshaia, Voloshin et al., 1981)

1.22 : 1.16 : 3.87 : 12   (Leshaia, KC-3, present study)

1.46 : 1.08 : 3.89 : 12   (Tanco, SMP-6, present study)

1.39 : 1.18 : 3.88 : 12   (Tanco, SMP-51B, present study)

The actual ratios are quite non-ideal, indicating that $AA'B_4O_{12}$ stoichiometry is not shown by this mineral.

The IR spectrum of Leshaia cesstibtantite (Voloshin et al., 1981) is reproduced in Figure 41. The absorptions at 1625 and 3625 cm^{-1} indicate the presence of both H_2O and OH, the former of uncertain origin and role because the authors do not discuss sample preparation. Quite clearly, a basis of 12(O) is not suitable for formula calculation if appreciable OH is

Table 65: Electron Microprobe Analyses of Cesstibtantites

	1	2	3	4
Na_2O	1.3	1.7	2.4	2.1
K_2O	---	---	0.05	0.0
Cs_2O	7.3	7.4	5.4	5.3
CaO	0.1	---	0.6	0.6
SnO	---	---	0.1	0.0
PbO	1.6	0.8	5.3	8.0
Sb_2O_3	13.6	14.2	9.7	8.5
Bi_2O_3	0.7	0.3	0.6	1.0
Nb_2O_5	2.3	2.8	1.2	0.8
Ta_2O_5	72.0	70.8	72.5	70.6
	98.9	97.9	97.8	96.9

Cations per 12(O)

	1	2	3	4
Na^+	0.48	0.62	0.89	0.81
K^+	----	0.00	0.01	0.00
Cs^+	0.59	0.60	0.44	0.45
Ca^{2-}	0.02	0.00	0.12	0.13
Sn^{2-}	----	0.00	0.01	0.00
Pb^{2-}	0.08	0.04	0.27	0.43
Sb^{3-}	1.06	1.10	0.77	0.70
Bi^{3-}	0.04	0.02	0.03	0.05
Nb^{5-}	0.20	0.24	0.10	0.07
Ta^{5-}	3.69	3.63	3.79	3.81
	6.16	6.24	6.43	6.45

1. Leshaia, USSR. Average of analyses of Voloshin et al. (1981).
2. Leshaia, USSR. Average of 2 analyses. Sample KO-1.
3. Tanco pegmatite. Average of 2 analyses. Sample SMP-6.
4. Tanco pegmatite. Average of 2 analyses. Sample TSE-51B.

present.   Furthermore, no F determination has yet been done on cesstibtan-
tite; with microlites as rich in F as they typically are (e.g. Eid & von
Knorring, 1981), it would be unusual if cesstibtantite were devoid of F.

As with   pyrochlore-group minerals,   natrotantite and   rankamaite-
sosedkoite, when OH+F contents are not known, formula contents are best
calculated by normalizing on the B-site sum.   The results of this calcula-
tion (for $\Sigma\underline{B}$=2 by analogy with pyrochlore-group minerals) are given in
Table 66.   The cesstibtantites show an excess of effective oxygen (for
charge balance) over the number proposed by Voloshin et al. (1981), which
for this basis should be 6.   It is tempting to assign two times the excess
to be (OH,F) by analogy with pyrochlore group minerals, but quantitative F
and OH determinations and a structure determination are needed before this
can be done with any confidence.
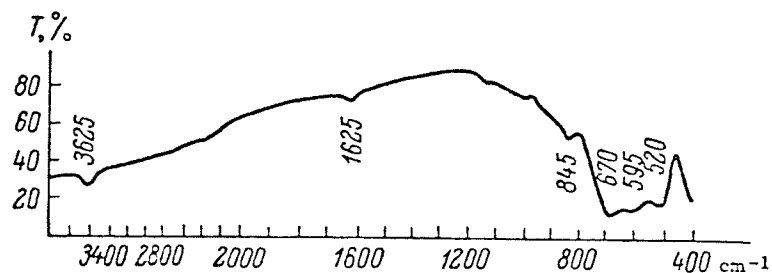
Figure 41: IR spectrum of type cesstibtantite (from Voloshin et al., 1981).

Table 66: Formula contents of Cesstibtantites

	1	2	3	4
K^+	-----	0.000	0.007	0.000
Cs^+	0.300	0.308	0.219	0.233
$\Sigma A'$	0.300	0.308	0.226	0.233
Na^+	0.244	0.312	0.451	0.417
Ca^{2+}	0.014	0.000	0.063	0.063
Sn^{2+}	-----	0.000	0.009	0.000
Pb^{2+}	0.042	0.021	0.141	0.222
Sb^{3+}	0.543	0.571	0.393	0.358
Bi^{3+}	0.017	0.007	0.016	0.026
ΣA	0.860	0.911	1.073	1.086
Nb^{5+}	0.102	0.124	0.052	0.035
Ta^{5+}	1.898	1.876	1.948	1.965
ΣB	2.000	2.000	2.000	2.000
$O(eff)$	6.168	6.202	6.160	6.185

Ions on a basis of 2 (Ta+Nb).

Analysis numbers are as in Table 65.

14.5   STRUCTURE ANALYSIS AND REFINEMENT

With the intent of testing the validity of Voloshin et al.'s (1981) structural model for cesstibtantite, and to eliminate ambiguities discussed in the previous section, a structure analysis of Leshaia cesstibtantite was undertaken.   Because of the dissimilarity of cation ratios for Tanco and Leshaia cesstibtantites, a refinement was also done on the Tanco sample, to outline solid solution in the species.   At the time of data collection, cesstibtantite SMP-6 was the best characterized of the Tanco samples, so it was chosen for the refinement.

Fragments of crystals containing the microprobe-analyzed spots were used for the study.   The Tanco sample was cut cleanly from its thin section with a razor blade to produce a 0.12 x 0.13 x 0.03 mm fragment.   The Leshaia sample (0.09 x 0.06 x 0.04 mm) was plucked from a circular mount with a needle, and suffered minor crushing on extraction.   Precession photographs of each fragment, taken before intensity data were collected, indicated that the Tanco sample was a monocrystal, but that the Leshaia fragment had a slight mosaic character.

Intensity data were collected with the four-circle diffractometer using MoKα radiation.   Unit cell refinement based on a set of 25 reflections used in centring gave the following unconstrained unit cell parameters:

	Tanco	Leshaia	
a	10.500(2)	10.519(5)	Å
b	10.497(2)	10.514(4)	
c	10.494(2)	10.511(3)	
α	90.05(2)	89.98(3)	°
β	89.96(2)	89.99(3)	
γ	90.01(2)	90.06(3)	

indicating that both samples are metrically cubic. Constrained refinement gave $\underline{a}$=10.515(2) Å for the Leshaia sample and $\underline{a}$=10.496(1) Å for the Tanco sample, in excellent agreement with cell dimensions refined from powder data (Table 62). Intensity data were collected over one quadrant of reciprocal space (6 asymmetric units) and merged to give totals of 104 observed reflections (I>3σ) for the Tanco sample and 96 observed reflections for the Leshaia sample.

An empirical absorption correction (μ=465 cm^{-1}, Mo$\underline{K}a$) was made to the Tanco sample data by approximating the shape of the fragment to a thin plate which was bound by the polished surfaces of the fragment. The index of the polished surface of the plate was estimated from precession photographs, and was refined by minimizing on the merging $\underline{R}$ of the absorption correction. Inaccuracy in the indexing and errors in the absorption correction due to diffraction at small angles to the surface of the plate were eliminated by excluding all diffractions within a glancing angle of 4° to the plate. Because of the large number of asymmetric units of data collected, no reflections were lost from the dataset due to this exclusion. An empirical absorption correction (μ=430 cm^{-1}, Mo$\underline{K}a$) was done for the Leshaia sample by assuming an ellipsoidal shape for the crystal, and involved no data exclusion.

Starting parameters for each refinement were taken from the microlite structure refinement (see Pyrochlore Group Minerals). The starting model had all Na, Cs, Sb, Bi, Sn, Pb, Ca at the $\underline{A}$-site and all Ta, Nb at the $\underline{B}$-site, based on Ta+Nb=16 cations per unit cell. The O-site occupancy was fixed at 1; initially the $\emptyset$-site was set at $\frac{1}{2}$ occupancy. Isotropic temperature factors were refined for each site, and the total occupancy of the $\emptyset$-

and A-sites were refined.   Refinement converged at R=5.6%, wR=5.4% for the
Tanco sample and R=6.5%, wR=7.1% for the Leshaia sample.   Despite the rea-
sonable R-indices , both models had the following undesirable features:

1. The A-site had large U's of 0.074 for the Tanco sample and 0.186 Å^2 for
   the Leshaia sample.   In addition,   the A-site occupancy refined to 20%
   (Tanco) and 25% (Leshaia), much lower than expected from microprobe
   analyses.

2. The occupancy of the $\emptyset$-site refined to 2 and 2.5 times the allowable
   maximum for the site (8 atoms/unit cell) for the Tanco and Leshaia sam-
   ples respectively, using neutral O as the scattering curve for the site.
   Furthermore, difference Fourier maps showed a single large maximum (3
   $e^-/\text{Å}^3$ for the Tanco sample and 6 $e^-/\text{Å}^3$ for the Leshaia sample) at the
   same location as the $\emptyset$-site.

These features indicated that there was too little scattering at the
A-site and too much scattering at the $\emptyset$-site to be accounted for by a nor-
mal pyrochlore structural model.   On the basis of arguments presented in
the next subsection, the A-site constituents Cs and K were transferred to
the $\emptyset$-site and the data were re-refined.   The B- and O-sites were modelled
as vibrating anisotropically; the $\emptyset$-site is constrained by symmetry to
vibrate isotropically.   At this stage,   the A-site temperature factor was
still large (Tanco: U=0.072, Leshaia: U=0.168 Å^2).   A difference map in
the region of the A-site showed an elongated football-shaped maximum for
the Tanco sample, and a dumbell-shaped maximum for the Leshaia sample,
indicating that the A-cations were not located at their ideal position
(Wyckoff notation: 16d, site symmetry 3m).   The observed electron density

distributions indicated that the A-cations actually occupy a 96g position near the ideal 16d position, producing a sixfold increase in site multipl- icity, which is necessarily accompanied by a sixfold decrease in the site occupancy. Consequently, positional constraints for the A-site were relaxed to conform with the symmetry of the 96g position, and the position of the A-cation was refined. Because of high covariance between the posi- tion and temperature factor for the A-site, the temperature factor was fixed at a value of U=0.015 $Å^2$, comparable to U(A-site) of microlites.

An attempt was made to refine the anion occupancy of the $\emptyset$-site while using microprobe-constrained cation proportions. Refinement converged at over twice the calculated number of effective oxygens for the site, conseq- uently the anion content of the $\emptyset$-site was considered to be all OH+F, and was set to a value suitable for charge balance.

In the final stages of refinement, microprobe-constrained occupancies were used for the various sites, and refinement converged at R=3.9, wR=3.7% for the Tanco sample, and R=3.8, wR=4.3% for the Leshaia sample. Final positional and thermal parameters are given in Table 67, selected bond lengths in Table 68, polyhedral angles in Table 69, and structure factors in Appendix G.

Table 67: Atomic Positional and Thermal Parameters
for Cesstibtantites

Site	Parameter	KO-1	SMP-6
A	x	0.518(1)	0.513(2)
	y	x	x
	z	0.455(1)	0.471(2)
	U	150*	150*
B	x	0	0
	y	0	0
	z	0	0
	U_{11}	202(5)	98(4)
	U_{12}	−40(4)	−26(3)
O	x	0.314(2)	0.311(1)
	y	1/8	1/8
	z	1/8	1/8
	U_{11}	212(82)	162(74)
	U_{22}	233(50)	255(48)
	U_{12}	0	0
	U_{23}	43(67)	81(66)
Ø	x	3/8	3/8
	y	3/8	3/8
	z	3/8	3/8
	U	580(45)	370(37)

For $\underline{B}$, $U_{11}=U_{22}=U_{33}$ and $U_{12}=U_{13}=U_{23}$
For $\underline{O}$, $U_{22}=U_{33}$ and $U_{12}=U_{13}=0$

All U's are $Å^2 \times 10^4$

* fixed value

Table 68: Bond Lengths (Å) for Cesstibtantites

	KO-1	SMP-6
A-Polyhedron		
A – O x 2	2.47(1)	2.55(1)
– O x 2	3.01(1)	2.91(1)
– O x 1	2.18(2)	2.37(3)
– O x 1	3.22(2)	3.06(3)
– Ø x 1	2.29(2)	2.28(3)
– Ø x 1	2.39(2)	2.32(3)
A'-Polyhedron		
A'– O x6	3.27(2)	3.29(2)
– O x12	3.772(3)	3.771(3)
B-Polyhedron		
B – O x 6	1.978(5)	1.963(5)

Table 69: Selected Polyhedral Angles (°) for Cesstibtantites

	KO-1	SMP-6		KO-1	SMP-6
A Polyhedron			**A' Polyhedron**		
O - A - O x2	60.1(2)	61.0(1)	O - A' - O x24	134.1(0)	134.2(0)
- O x2	73.2(4)	68.9(6)	- O x24	119.0(0)	119.1(0)
- O x2	52.9(3)	55.6(4)	- O x24	45.9(0)	45.8(0)
- O x2	125.4(4)	123.6(6)	- O x12	100.2(2)	99.7(2)
- O x2	107.9(4)	111.7(6)	- O x12	91.8(1)	91.6(1)
- O x1	139.0(7)	131.5(10)	- O x12	90.0(0)	90.0(0)
- O x1	100.4(5)	106.3(8)	- O x12	79.8(2)	80.3(2)
- Ø x2	73.5(4)	77.1(6)	- O x12	76.3(3)	75.5(4)
- Ø x2	89.9(5)	92.4(8)	- O x12	43.0(4)	43.8(4)
- Ø x2	86.8(5)	85.7(7)	- O x6	159.5(4)	154.5(2)
- Ø x2	101.8(5)	101.2(8)			
- Ø x1	70.4(5)	74.5(9)	**B Polyhedron**		
- Ø x1	83.0(5)	87.7(7)			
- Ø x1	91.2(8)	89.3(11)	O - B - O x6	89.5(6)	89.3(6)
- Ø x1	115.4(8)	108.5(9)	- O x6	90.5(6)	90.7(6)

14.6 INVERSE PYROCHLORES AND THE CESSTIBTANTITE STRUCTURE

As described in previous sections of this chapter, cesstibtantite is similar to the pyrochlore group minerals; however, there are several features of its chemistry and structure which no pyrochlore group mineral shows, and they warrant further discussion here.

The unique feature of cesstibtantite is its high Cs content, with Cs present at the $\emptyset$-site. Synthetic Cs-bearing compounds with pyrochlore-like structures have been known for forty years (Schrewelius, 1943); however, there has been widespread recognition of this earlier work only in the last 15 years. These, and related compounds have the structural formula,

$$\square B_2 \emptyset_6 A'$$
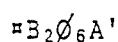
where $\underline{A}'$ is a large monovalent cation

$\underline{B}$ is a relatively small tri- to hexavalent cation

$\emptyset$ is O, OH or F

In these compounds, the $\underline{B}$-cations play the same structural role as do $\underline{B}$-cations of the pyrochlore structure; however, both O and $\emptyset$-anions are located at the $\underline{O}$-sites of the pyrochlore structure, and the $\underline{A}$-cations are located at the $\emptyset$-sites of the pyrochlore structure. What were $\underline{A}$-cation sites of the pyrochlore structure are vacant sites in these compounds.

Some synthetic normal pyrochlores have the general structural formula,

$$AB_2O_6 \square$$
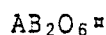
with half-occupied A-sites and completely vacant ϕ-sites. The compositions of the A- and ϕ-sites of the Cs-bearing compounds are inverted compared to this formula, hence the Cs-bearing and related compounds are referred to as inverse pyrochlores by solid-state chemists; this is analogous to a vaguely similar nomenclature used for spinels.

Whether a given A-cation adopts a normal or inverse distribution depends upon the radius ratio A:B. For B=Nb, Ta, Ti or W, cations larger than Tl$^+$ (r=1.59 Å in 8-coordination; Shannon, 1976) cannot be stabilized at the A-site, and reside instead at the ϕ-site (Fourquet et al., 1973). Of these cations, only Cs is large enough to be properly stabilized at the ϕ-site. Smaller cations are displaced from the ideal ϕ-site position (Wyckoff notation: 8b) along the threefold axis passing through the 8b site, the magnitude of the displacement varying inversely with ionic radius (Fourquet et al., 1973).

Cations with 8-coordinated radii in the range r=1.50→1.60 Å (i.e. K,Tl) can be stabilized at either or both of the ϕ- and A-sites (Fourquet et al., 1970; Grins et al., 1980) depending upon the ratio of A-cations to B-cations. For A:B=1:1, the A-cations adopt a normal distribution; for A:B=1:2, they take an inverse distribution. Intermediate A:B ratios produce either single phases with A-cations at both the A- and ϕ-sites or two-phase mixtures, depending upon the exact A:B ratio and temperature (Figure 42). Cesstibtantite is similar to this last group of compounds in that it has A-cations distributed over both the A- and ϕ-sites, yet is dissimilar in that it necessarily also has ϕ-site anions (needed for charge balance).

$$Tl_xNb_2O_{4+x}F_{2-x}$$
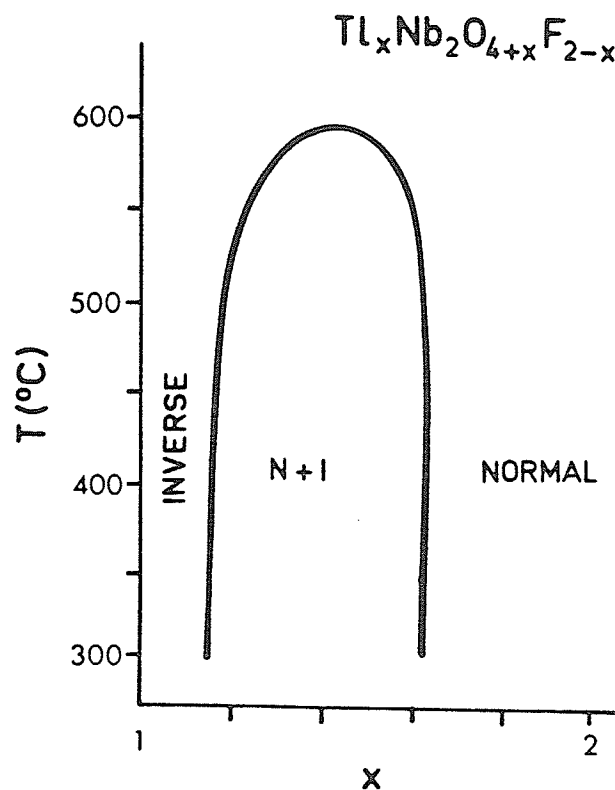
Figure 42: Solid solution in Tl pyrochlore (after English & Sleight, 1980). Although considerable inverse pyrochlore (I) is soluble in normal pyrochlore (N), the reverse is not true. The large field in the centre of the diagram marks a two-phase region where both phases are stable.

Figure 43 is a simplification of the environment of the ϕ-site of cesst-ibtantite. The ϕ-site is occupied by Cs, and is surrounded by six oxygens, each at a distance of approximately 3.28 Å from the site, and by 12 more oxygens at a distance of approximately 3.77 Å from the site (Figure 44). Were the A-cations in cesstibtantite to be located at their ideal position (16d, symmetry 3m), there would be four A-cations about each Cs at a distance of only 2.3 Å. Instead, the A-cations are located off the 3-axis (at 96g, symmetry m), and fractionally occupy 6 symmetrically equivalent positions about the ideal position. This results in 24 fractionally occupied A-cation positions about each A'-cation, each A-cation only marginally displaced from its ideal 16d position. Consequently, half of these positions are closer-than-ideal to the ϕ-site (A-A'=2.28 Å, Tanco and 2.39 Å, Leshaia), and half are more distant than ideal (A-A'=2.32 Å, Tanco and 2.39 Å, Leshaia). All such distances, however, are far too short to represent stable Cs-Sb separations, indicating that the refined structure is an average.

The cause of the positional disorder of the A-cations is not known. Although it is tempting to suggest that A'-A cation repulsion is responsible, similar behaviour has been observed in the (A'-cation free) synthetic normal pyrochlores $Sn^{2+}_{2-x}(M_{2-y}Sn^{4+}_y)O_{7-x-y/2}$ where M=Nb,Ta (Birchall & Sleight, 1975). In these compounds, Sn^{2+} is displaced from the 16d position toward a 96g position with x=0.518(1) and z=0.474(1), showing identical behaviour as the A-cations of cesstibtantite (Table 67). The similarity is too close to be coincidental. Consequently, it is unlikely that A-A' cation repulsion is the cause for the A-cation displacements in cesstibtantite; the phenomenon is more likely related to some as-of-yet undefined characteristic of the A-cations themselves.
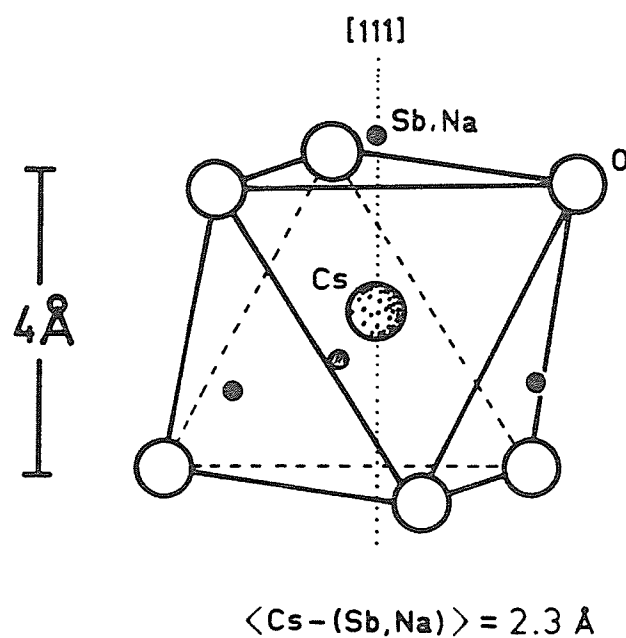
Figure 43: Cesstibtantite: idealized first nearest-neighbour environment about the A'- cation. Twelve O-site oxygens at 3.77 Å from the A'-cation are not shown, for simplicity.
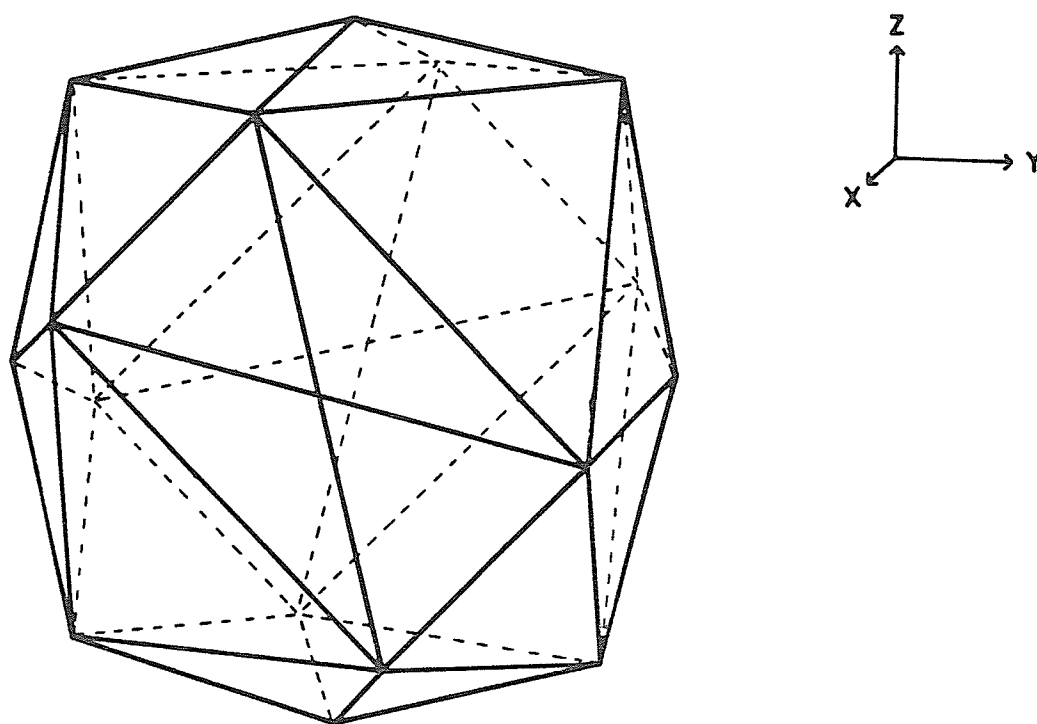
Figure 44: Cesstibtantite: coordination polyhedron of the A'-cation. The A'-cation is 18-coordinated, with 6 oxygens at 3.3 Å, and 12 at 3.8 Å, resulting in a coordination polyhedron with 32 faces (distorted trapezohedron with octahedral modifications).

It can be seen that the Leshaia cesstibtantite has A-cations which are more displaced from the 16d position than the Tanco sample (Table 67). In terms of A-cation composition, the Leshaia sample differs most from the Tanco sample in having a higher $Sb^{3+}:Na^+$ ratio; the positional deviations seem to be related to Sb^{3+} content. Another coincidence emerges: Sb^{3+} and Sn^{2+} are typical lone-pair cations. It may be that the positional disorder of A-cations in Sn^{2+}- and Sb^{3+}-pyrochlores is related to bonding tendencies of the A-cation. If the lone pair of electrons of the Sb^{3+} and Sn^{2+} is stereochemically active, then these cations should prefer acentric environments, accounting for why they are not located at the 16d position (symmetry 3m); location at the proposed 96g position (symmetry m) is compatible with this model.

If the above model is correct, then normal pyrochlores with Sb^{3+} as their sole A-site constituent must have similar A-cation behaviour as cesstibtantite. To date, only one structure refinement of a normal Sb^{3+}-pyrochlore has been done: synthetic Sb_6O_{13} (Stewart et al., 1972). The formula of this compound is better represented as $Sb^{3+}Sb^{5+}_2O_{6.5}$ to compare with the IMA-recommended one for the pyrochlore-group minerals. The compound has the normal pyrochlore structure, with Sb^{5+} at the B-site, O at the O- and $\emptyset$-sites and Sb^{3+} at the A-site (Stewart et al., 1972). The model of Stewart et al. (1972) has Sb^{3+} at the ideal position (16d); however, the temperature factor (B) of 6.3 $Å^2$ is clearly unacceptable (cf. B=5.8 $Å^2$ for the Tanco cesstibtantite before positional disorder was modelled). The Sb^{3+} in this compound shows the same sort of behaviour as the A-cations in cesstibtantite; there is strong evidence that this A'-cation free pyrochlore has positionally disordered cations, which would indicate that A-site

positional disorder in cesstibtantite is due to bonding preferences of Sb^{3-}, not to Cs-Sb repulsion.

Only one structure analysis has been done on a synthetic "inverse" Sb-pyrochlore, which quite coincidentally is the only synthetic pyrochlore with non-isochemical $\underline{A}$- and $\underline{A}'$-site populations, and with cation-anion $\emptyset$-site disorder, like cesstibtantite. This compound is $K_{0.51}Sb^{3+}_{0.67}Sb^{5+}_2O_{6.26}$ (Piffard et al., 1978). It has Sb^{5+} at the $\underline{B}$-site and O at the $\underline{O}$- and $\emptyset$-sites; however, Sb^{3+} shows positional disorder about the $\underline{A}$-site, and K shows positional disorder about the $\emptyset$-site. The behaviour of Sb^{3+} is identical to that observed for $\underline{A}$-cations in cesstibtantite: Sb^{3-} fractionally occupies a 96g position. The behaviour of K in this pyrochlore is not identical to that of Cs in cesstibtantite; because of its small size, K fractionally occupies both a 32e position and a 96g position about the ideal 8b position. Although the study of this synthetic, mixed normal-inverse pyrochlore adds no further insights into the crystal chemistry of mixed normal-inverse pyrochlores, it does confirm the assignment of Sb^{3-} to the 96g position, and confirms the possibility of $\underline{A}'$-cation versus $\emptyset$-anion disorder.

Other possible candidates for non-ideal behaviour are Pb^{2+} and Bi^{3-}-pyrochlores. The structure of the normal pyrochlore $Pb_{1.5}Nb_2O_{6.5}$ (synthetic plumbopyrochlore) has been refined (Bernotat-Wulf & Hoffmann, 1982). The Pb^{2+} was found to be located at the ideal 16d position, and to have a normal temperature factor ($\underline{B}=1.71(3)$ $Å^2$). The extra electron pair of Pb^{2+} would seem to be stereochemically inactive in pyrochlores. Unfortunately, the only structure refinements done on Bi^{3+}-pyrochlores (Jeanne et al., 1974) did not involve refinement of individual temperature factors

of the atoms, and assumed ideal behaviour for Bi^{3+}, so no data is available for the bonding tendencies of Bi^{3+} in pyrochlores.

To conclude, the following set of points lists the important features of the cesstibtantite structure:

1. All compositions have anions in excess of 6 per formula unit. By analogy with the inverse pyrochlore $CsNb_2O_5F$ (Fourquet et al., 1973), if there is 1 (OH+F) in the O-site per Cs atom, then, for local charge balance, there are 0.23 effective oxygens per formula unit at the $\emptyset$-site of the Tanco cesstibtantite and 0.31 effective oxygens p.f.u. at the $\emptyset$-site of the Leshaia sample. Refinement showed the $\emptyset$-site occupancy to be in excess of twice these values for both samples, hence monovalent anions are more probable for this site. On this basis, there would be 1.5 wt.% and 1.2 wt.% H_2O for the Leshaia (KO-1) and Tanco (SMP-6) samples respectively, assuming all $\emptyset^-$ to be OH for the comparative purposes of the calculation. Both figures compare reasonably well with the observed analysis deficits of Table 65.

2. A-cations, perhaps only Sb^{3+} (and minor Sn^{2+} and Bi^{3-}), are positionally disordered, fractionally occupying a 96g position, not the ideal 16d position. A'-cations are not positionally disordered, and occupy the ideal position for the $\emptyset$-site (8b).

3. The structural formula of cesstibtantite is:

$$A_{2-m}B_2O'_6(\emptyset,A')_{1-n}$$
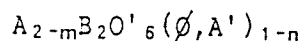
where A = Na, Sb^{3+}, Pb, Bi^{3+}, Ca, Sn^{2+}
        B = Ta, Nb
       O'= O, OH, F
       $\emptyset$ = OH,F
       A'= Cs, K

Actual formulae for cesstibtantites are:

(1) Leshaia (KO-1):

$$A_{0.91}B_2O'_6(\emptyset,A')_{1.00}$$
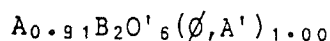
where A = 0.57 Sb^{3+} + 0.31 Na + 0.02 Pb + 0.01 Bi^{3+}
       B = 1.88 Ta + 0.12 Nb
       O'= 5.69 O + 0.31 (OH+F)
       $\emptyset$ = 0.69 (OH+F)
       A'= 0.31 Cs

(2) Tanco (SMP-6):

$$A_{1.06}B_2O'_6(\emptyset,A')_{0.78}$$
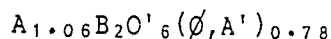
where A = 0.45 Na + 0.39 Sb^{3+} + 0.14 Pb + 0.06 Ca + 0.02 Bi^{3+}
       B = 1.95 Ta + 0.05 Nb
       O'= 5.78 O + 0.22 (OH+F)
       $\emptyset$ = 0.55 (OH+F)
       A'= 0.22 Cs + 0.01 K

4. The mean separation of the A- and A'-sites is too short to represent a stable Sb-Cs separation. This indicates that the refined structure is an average. Two possibilities exist for the real structure, and depend upon the range of A- and A'-cation versus vacancy ordering. (1) Short-range order. The low fractional cation occupancies of the A- and $\emptyset$-sites permit a model in which the mineral consists of domains with

A'-cations but no A-cations, and vice-versa. In this case the mineral would consist of both normal and inverse pyrochlore-structured domains. (2) Long-range order. The structure would consist of a pyrochlore-like BO_6 octahedral framework with as-of-yet undefined cation-vacancy ordering at what are presently termed the A- and A'-sites.

5. Cesstibtantite possesses a small subset of X-ray diffractions which normal pyrochlores do not typically have. Specifically, the systematic absence conditions for a pyrochlore structure with all atoms at ideal positions do not allow such diffractions. Displacement of the A-cations to 96g positions relaxes these conditions, and constructive scattering is observed from the planes given in Table 64. These diffractions should be indigeneous to all pyrochlores with A-cations having stereochemically active lone-pair electrons, and conversely should be useful indicators of the presence of stereochemically active lone-pair cations in pyrochlores. Because the A-cation displacements are not due to A'-A cation repulsion, they cannot be used as an indirect indication of inverse-pyrochlore character, as suggested earlier (Ercit et al., 1985).

Chapter XV

PARABARIOMICROLITE

15.1   INTRODUCTION

Investigation of the Alto do Giz occurrence of the simpsonite paragene-
sis showed microlite to be an abundant member of that assemblage.   The
microlite at Alto do Giz is a characteristic transparent green, and occurs
as isolated octahedra at the bases of simpsonite crystals and as loose,
isolated crystals (Pough, 1945).   The chemistry and X-ray constants of this
microlite are described in Chapter XIII.

The microlite is sometimes fresh, but most frequently is slightly to
heavily replaced by a translucent white mineral along {111} cleavage planes
and crystal margins.   Pough (1945) was the first to take note of the miner-
al,   referring to it as "altered microlite",   but did not carry out X-ray,
chemical or optical investigations.   The mineral has been characterized for
the first time here and has been found to be a new mineral, closely related
to bariomicrolite in chemistry.   The mineral has been named parabariomi-
crolite in allusion to this relationship;   the species and name have been
approved for publication by the IMA Commission on New Minerals and New Min-
eral Names.

15.2   PHYSICAL AND OPTICAL PROPERTIES

Parabariomicrolite is translucent, white to pale pink and has a white streak. The lustre ranges from vitreous to pearly.   The mineral is non-fluorescent under both short- and long-wave ultraviolet light.   It is anisotropic and has all $n > 2.0$.   Parabariomicrolite is slightly softer than its associated microlite; it has a hardness of 4 and is very brittle. This, coupled with well-developed {001} and {101} cleavages causes the mineral to splinter under even the slightest pressure.   Samples were either too small or too contaminated with microlite for a density determination; however, the density calculated from the proposed formula is 5.97 g/cm^3, in good agreement with a measured density of 6.03 g/cm^3 for a parabariomicrolite plus microlite mixture (Pough, 1945).

Parabariomicrolite typically occurs as topotaxic replacements of microlite; however, some RVG-series samples seem to be open-space fillings. Individual crystal size is in the range of 0.01 to 0.1 mm; aggregates of crystals are up to 2 mm across.

A mineral chemically similar to parabariomicrolite was found in sample L-14 from Lake Kivu, Zaire.   On the basis of arguments to be presented in later sections, this mineral is almost certainly a parabariomicrolite; however, because of the small crystal size (appx. 30 μm), no X-ray diffraction data could be collected for confirmation of its identity.

15.3   X-RAY CRYSTALLOGRAPHY

X-ray powder diffraction patterns were obtained by Debye-Scherrer and Gandolfi camera methods on powders and crystal fragments respectively, and by powder diffractometry.   Extreme variability of the first Debye-Scherrer

and Gandolfi patterns indicated contamination by a second phase. However, the variability made identification and characterization of each phase easier. The contaminant phase was microlite, which by later inspection of polished sections was found as minute relicts in areas initially suspected to be pure parabariomicrolite (Figure 45).

Precise d-values were determined by powder diffractometry using the PW1030 diffractometer and CuKα radiation. After calibration against quartz, diffraction maxima corresponding to the microlite contaminant were eliminated from the dataset. The remaining pattern resembles those of the pyrochlore-group minerals, except that several diffraction maxima in the pattern seem to be "split", starting at large values of d. The splitting suggests a lower than cubic symmetry; by trial-and-error the pattern was eventually found to obey rhombohedral symmetry. Although microlite contamination complicated the diffraction pattern, comparison with a pattern for pure Alto do Giz microlite made peak assignment unambiguous; consequently, unit cell parameters for both phases of the pattern could be determined.

Initially the parabariomicrolite was indexed on a rhombohedrally-distorted F-centred pyrochlore cell. This gave:

$$a = 10.5657(5) \text{ Å}, \quad \alpha = 89.358(6) \text{ °}$$

No diffractions violated the F-centring of this setting.

The pattern was then re-indexed on a conventional R-centred cell with hexagonal axes, giving:

$$a = 7.4290(6), \quad c = 18.505(2) \text{ Å}$$

Figure 45: Relict microlite (M) in a parabariomicrolite (P) matrix, Alto
do Giz. The greater polishing hardness of the microlite gives
it a positive relief with respect to the parabariomicrolite.
Reflected light.

Indexed powder diffraction data for this setting are given in Table 70.

Precession photographs (0 to 2nd levels) of parabariomicrolite strongly resemble those of microlite. No reflections were found that violated the F-centring of the pyrochlore-like setting. However, precession photography had its problems. Of the five sets of photographs collected on five apparently single parabariomicrolite crystals, two showed evidence of microlite contamination, and these plus two more showed large, elongated diffraction maxima characteristic of twinning or mosaic structure. The photographs with microlite contamination showed that a topotaxic relationship exists between parabariomicrolite and microlite with {001} and {101} of parabariomicrolite || {111} of microlite.

Measurements on the four photographs with smeared diffraction maxima show a metrically cubic cell, but Gandolfi photographs of the same fragments gave patterns with line splitting characteristic of rhombohedral parabariomicrolite. The remaining set of precession photographs was found to show evidence of rhombohedral symmetry in terms of reciprocal $\underline{d}$'s, interreciprocal axial angles, and intensities. For the 10.5 Å F-centred microlite-like cell, an α-angle of 89.26±0.10° was measured, close to the value refined from powder data of 89.358(6)°. However, smearing of the diffractions of the sample within planes of constant $\sin\theta/\lambda$ suggested that this sample was slightly twinned or showed slight mosaic character.

Twinning is the likely cause of most smeared diffraction maxima. Topotaxic control over parabariomicrolite replacement of microlite should produce four-fold parabariomicrolite twins: the $\underline{Z}$-axis of parabariomicrolite corresponds to the body diagonal {111} of microlite; there are four symmetrically equivalent body diagonals in microlite; hence, four-fold

Table 70: X-Ray Powder Diffraction Data for Parabariomicrolite

hkl	d (calc)	d (obs)	I	hkl	d (calc)	d (obs)	I
00.3	6.17	6.18	50	10.10	1.778	1.778	20
10.1	6.08	6.08	35	22.3	1.778		
01.2	5.28	5.28	6	12.8	1.676	1.675	3
10.4	3.76	3.76	3	01.11	1.628	1.628	3
11.0	3.71	3.71	2	02.10	1.604	1.603	24
01.5	3.208	3.207	7	40.1	1.602		
02.1	3.169	3.172	65	22.6	1.591	1.591	42
00.6	3.084	3.085	41	40.4	1.519	1.519	14
20.2	3.038	3.040	100	20.11	1.491	1.491	4
02.4	2.641	2.641	50	30.9	1.484	1.484	2
20.5	2.428	2.426	13	04.5	1.475	1.474	6
11.6	2.373	2.371	3	21.10	1.473		
12.2	2.352	2.353	1	22.9	1.378	1.379	8
21.4	2.152	2.152	5	04.8	1.321	1.320	7
00.9	2.056	2.056	7	20.14	1.223	1.223	4
02.7	2.042	2.043	10	40.10	1.214	1.214	9
30.3	2.026	2.025	10	33.3	1.214		
20.8	1.878	1.878	38	42.2	1.205	1.205	14
22.0	1.857	1.857	39	22.12	1.186	1.187	10
11.9	1.799	1.798	5	24.4	1.176	1.176	10
21.7	1.790	1.789	3				

a = 7.4290(6)   c = 18.505(2) Å

Philips powder diffractometer, 1° divergence slit, Ni-filtered CuKα radiation. Internal standard: quartz. Integrated intensities.

twinning should result in parabariomicrolite which topotaxically replaces microlite. With only a 90-89.36 = 0.64° angular deviation from cubic symmetry, twinning coupled with the poor crystallinity of the sample might easily produce oversized, elongate maxima, rather than the resolved multiple diffractions normally expected in a twinned pattern.

According to powder diffraction and precession photographic data, systematic absence conditions for parabariomicrolite are hkl with -h+k+l=3n+1, giving R3m, R3m, R32, R3 and R3 as possible space groups (all are subgroups of Fd3m). Even the diffraction pattern of the crystal of parabariomicrolite with the sharp diffraction maxima has 3m diffraction symmetry; thus R3m, R3m and R32 are the most probable choices for the space group of parabariomicrolite.

15.4 CHEMISTRY

A wavelength-dispersive electron microprobe analysis of type parabariomicrolite is given in Table 71. In addition, analyses of an unreplaced microlite relic in the parabariomicrolite (WD) and the parabariomicrolite-like mineral from Kivu (ED) are given.

Microlites typically contain 2-3 wt.% H_2O+F, thus the analytical sum for the microlite, in absence of H_2O and F determinations, namely 98.0 wt.%, is well within expectations. The total for the parabariomicrolite analysis is 3.5 wt.% lower than that of the microlite; because data for both analyses were obtained at the same time, the same operating conditions apply to both analyses; thus the 3.5 wt.% difference should be a reasonable estimate of the difference in volatile content of the two minerals. Furthermore, with the reasonable microlite analysis available as a check, some confidence can

Table 71: Electron Microprobe Analyses of Parabario-
microlite and Associated Microlite

	1	2	3
Na_2O	0.4	0.0	5.3
K_2O	0.3	0.0	0.0
CaO	0.0	1.7	8.1
SrO	0.8	0.0	0.0
BaO	10.5	7.3	0.0
PbO	0.4	3.4	1.2
Nb_2O_5	1.5	9.0	1.7
Ta_2O_5	.80.6	70.9	81.7
	94.5	92.3	98.0

Unit Cell Contents
(on 12 B-cations)

Na^+	0.40	0.00	5.37
K^+	0.22	0.00	0.00
Ca^{2+}	0.00	0.91	4.53
Sr^{2+}	0.23	0.00	0.00
Ba^{2+}	2.19	1.48	0.00
Pb^{2+}	0.06	0.47	0.17
Nb^{5+}	0.36	2.09	0.40
Ta^{5+}	11.64	9.91	11.60
	15.10	14.86	22.06
O(eff)	32.82	32.86	37.39

1. Parabariomicrolite, Alto
   do Giz, Brazil (ROM-1).
2. Parabariomicrolite, Lake
   Kivu, Zaire (L-14).
3. Microlite, Alto do Giz,
   Brazil (ROM-1).

be placed on the estimate of the H_2O+F content of parabariomicrolite as 5.5 wt.% by difference.

The work of Eid & von Knorring (1976) on microlite geochemistry has shown that the $F:(OH+H_2O)$ ratio of pegmatitic microlite is strongly geochemically controlled. Primary pegmatite-hosted microlites are the F-richest class of microlites, with secondary microlites typically F-impoverished, and often enriched in H_2O as opposed to OH. Textural evidence shows parabariomicrolite to be a secondary microlite-like mineral, hence it is reasonable to assume that most, if not all of the undetected constituents of the parabariomicrolite analysis is H_2O plus OH. Water-rich (as opposed to hydroxyl-rich) microlites are typically poorly crystalline; the poor crystallinity of parabariomicrolite may indicate that much of the H_2O is actually structural water. Alternately, the poor crystallinity may be due to metamictization; however, (1) no uranium has been detected in any of the minerals of the Alto do Giz paragenesis and (2) none of the microlites of the simpsonite paragenesis, including the microlite relicts in the parabariomicrolite, show poor crystallinity. It is concluded that the poor crystallinity of the mineral is most likely related to a high water content.

Parabariomicrolite is essentially a barium tantalum oxide mineral; however, minor amounts of Pb, Sr, Na and K substitute for Ba, and Nb substitutes for Ta. The trace-to-minor element chemistry of the mineral is similar to that of microlites of the simpsonite paragenesis, especially the Pb-enrichment and lack of Ti.

In the absence of a good measured density for parabariomicrolite, the unit cell contents of the mineral were determined by assuming a pyrochlore-

like structure for the mineral. More specifically, a BO_6 octahedral framework topologically identical to that of pyrochlore-group minerals is expected, on the basis of (1) the topotaxic relationship of parabariomicrolite and the microlite it replaces, and (2) the strong similarity of the X-ray diffraction patterns of parabariomicrolite and pyrochlore-group minerals. The unit cell volume of parabariomicrolite is 3/4 times that of the pyrochlore structure, thus parabariomicrolite has 16 x 3/4 = <u>12</u> B-cations per unit cell. The unit cell contents of Table 71 were calculated on this basis.

The sum of the mono- and divalent cations, which shall hereafter be called <u>A</u>-cations after a similar nomenclature used in other sections of this thesis, is equal to 3. From Table 71, the effective number of oxygens for charge balance is 32.82; however, to meet the expectation of a pyrochlore-like octahedral framework, there must be at least 48 x 3/4 = <u>36</u> anions (with a possibility of 8 x 3/4 = <u>6</u> more at the $\emptyset$-site). Thus, an appreciable amount of OH must be present even at the former <u>O</u>-site in order to raise the number of anions to 36. This is in line with the high H_2O+F content of the parabariomicrolite suggested by the analysis sum of 94.5%.

15.5   THE CRYSTAL STRUCTURE AND CRYSTAL CHEMISTRY OF PARABARIOMICROLITE

15.5.1   Structure Analysis

The limited data available for parabariomicrolite leave the discussion of the crystal chemistry of the mineral at an unsatisfactory point. The exact relationship of the structure of the mineral to that of pyrochlore, and the conditions for the stable crystallization of parabariomicrolite versus bariomicrolite are unknown. Based on extinction conditions for powder diffraction data, there are as many as five possible space groups for

parabariomicrolite. Group-subgroup relationships do not help to reduce this number; all possible space groups are subgroups of Fd3m. With no suitable single crystals available for structure analysis, nor enough powder available for quantitative Rietveld refinement, neither single-crystal nor powder diffraction methods of structure analysis were possible. Consequently, a trial-and-error approach was taken to structure solution.

The first step of the solution involved the transformation of coordinates of the pyrochlore structure (F-centred, cubic) to a hexagonal-R basis. The following transformation matrix was derived:

$$[\quad -4/3 \quad -2/3 \quad 2/3 \quad / \quad -2/3 \quad -2/3 \quad 4/3 \quad / \quad 1/3 \quad 1/3 \quad 1/3 \quad]$$

Because of the high symmetry of the pyrochlore structure, and of the relatively simple cation chemistry of parabariomicrolite, the highest-symmetry space group possible for parabariomicrolite (R3m) was initially chosen for the analysis, with the intention of using lower symmetry space groups only if necessary. Site correlations for the pyrochlore structure in its Fd3m setting and in the transformed setting (R3m) are given in Table 72.

The Fd3m→R3m transformation causes each site of the cubic pyrochlore structure to split into two non-equivalent sites, except for the ∅-site. The splitting of the A- and B-sites produces, for each, one site with a multiplicity of 9, and one with a multiplicity of 3. With an A-cation sum of 3 per unit cell, it is possible that all A-cations have ordered into the threefold site (denoted A) and all (pyrochlore) A-site vacancies into the ninefold site (denoted A*). Alternately, it may be that the A-cations remain disordered over both sites with a fractional occupancy of 0.25 .

Table 72: Site Correlation Between Fd3m and R3m Pyrochlore

Atom	Fd3m Pyrochlore					R3m Pyrochlore				
	Site	Position	x	y	z	Site	Position	x	y	z
Ba	A	16d	1/2	1/2	1/2	A A*	3b 9e	0 1/2	0 0	1/2 0
Ta	B	16c	0	0	0	B1 B2	3a 9d	0 1/2	0 0	0 1/2
O	O	48f	x	1/8	1/8	O1 O2	18h 18h	x x	-x -x	z z
OH,F, H_2O	$\emptyset$	8b	3/8	3/8	3/8	$\emptyset$	6c	0	0	z

However, unlike the former model, the latter model does not account for the rhombohedral symmetry of the mineral. Furthermore, for isotropically vibrating atoms, the latter model predicts zero intensity for reflections such as (012), (104), (110), (116) and (122); however, these diffractions have readily observable intensities (e.g. $\underline{I}$(01.2)=6%, Table 70). It would seem that even at this early stage of the discussion, the disordered $\underline{A}$-cation model is unsatisfactory.

An attempt was made to refine the positional parameters of the structure initially from bond-valence considerations, and subsequently by comparison with the diffraction intensities of the powder data listed in Table 70. Because of the paucity of data, the oxygen atom sites were assigned the same symmetry as corresponding oxygen sites in the pyrochlore structure. This places constraints on $\underline{x}$ and $\underline{z}$ of $\underline{O1}$ and $\underline{O2}$. From the Fd3m→R3m transformation matrix,

$$\underline{x}(O1) = \underline{x}(O2) = 2/3 \cdot \underline{x}(O*) - 1/12 \qquad (1)$$

$$\underline{z}(O1) = 1/3 \cdot \underline{x}(O*) + 1/12 \qquad (2)$$

$$\underline{z}(O2) = 1/3 \cdot \underline{x}(O*) + 5/6 \qquad (3)$$

$$\text{thus:} \quad \underline{x}(O1) = \underline{x}(O2) = 2 \cdot \underline{z}(O1) - 1/4 = 2 \cdot \underline{z}(O2) - 7/4 \qquad (4)$$

where the sites marked by asterisks are for the pyrochlore structure and those without asterisks are for the parabariomicrolite structure. The above assumption reduces the number of independent positional variables for O1 and O2 of the parabariomicrolite structure from 4 to 1. Because the B-cation polyhedra of parabariomicrolite are coordinated by only O1 and O2, $\underline{x}(O1)$ can be refined by minimizing the differences between the expected and observed bond valences at B1 and B2. Refinement gave $\underline{x}(O1)=0.1253$ for $\Sigma \underline{s}(B1)=5.00$ v.u., $\Sigma \underline{s}(B2)=5.00$ v.u., thus $\underline{x}(O2)=0.1253$, $\underline{z}(O1)=0.1877$, and $\underline{z}(O2)=0.9377$, from equation (4).

The only other positional parameter $\underline{z}(\emptyset)$ is model-dependent, thus different criteria were used to determine its value for the different models. In the case of the ordered-Ba model, that is with all Ba at A, $\underline{z}(\emptyset)$ was determined by normalizing the bond valence sum for A to a value of 2. This gave $\underline{z}(\emptyset)=0.315$. For the model with disordered Ba, the $\emptyset$-site was set at the ideal location for the pyrochlore structure, i.e. at $\underline{z}(\emptyset)=3/8$.

Diffraction intensities for each model were calculated using the program DBW 2.9 (Wiles & Young, 1981), and are compared to the observed intensities in Table 73. Casual examination of Table 73 shows the ordered model (1) to be greatly superior to the disordered model (3). The reflections with zero calculated intensity alluded to earlier are given in this table, and fur-

ther emphasize the problems of the disordered model. On a more objective level, Bragg R-indices were calculated for each model by:

$$R = \frac{\Sigma |I_0 - I_c|}{\Sigma I_0} \qquad (5)$$

The resulting indices are R=16% for the ordered model and R=36% for the disordered model. Because of the small sample size coupled with great incident X-ray beam divergence at low 2θ angles, the incident beam was much larger than the sample at low angles, thus the models significantly overestimate the intensities of high-d diffractions. The effect of this unavoidable systematic error was reduced by repeating the calculation using only reflections with d<4.0 Å. The resulting values were R=11% and R=29% for the ordered and disordered models respectively. For both approaches to the calculation, the disordered model is clearly inferior to the ordered model.

Bond lengths, angles and O-O separations for the ordered model are given in Table 74. Bond valences are given in Table 75. The bond valence sum to O1 of 2.0 v.u. indicates that O1 is occupied only by O. The sum to O2 of 1.6 v.u. indicates that all of the OH in the BO_6 framework is located at this site. The sum to $\emptyset$ of 0.1 v.u. is instructive. A typical bond valence for O-H bonds in solids is 0.8 v.u. (Brown, 1981); thus, neglecting the contribution of O-H bonds, the sum to an oxygen of an H_2O molecule is 2 - (2 x 0.8) = 0.4 v.u., whereas it is 2 - 0.8 = 1.2 v.u. for the O of a hydroxyl molecule. The low sum to $\emptyset$ indicates that either $\emptyset$ is occupied by H_2O, or not occupied at all. Important in this regard is the observation that parabariomicrolite has a total volatile content of 5.5 wt.%. With the expectation of full occupancy of the O-sites, the effective number of oxy-

Table 73: Observed and Calculated Intensities
for Parabariomicrolite

hkl	I(obs)	I(calc)		
		1	2	3
00.3	50	73	81	26
10.1	35	53	57	76
01.2	6	8	11	0
10.4	3	7	7	0
11.0	2	5	3	0
01.5	7	6	8	16
11.3	65	66	55	38
00.6	41	40	35	35
20.2	100	100	100	100
02.4	50	49	47	42
20.5	13	16	13	3
11.6	3	4	3	0
12.2	1	2	3	0
21.4	5	5	6	0
00.9	7	6	6	3
02.7	10	8	8	2
30.3	10	8	3	11
20.8	38	28	28	30
22.0	39	31	27	14
11.9	5	4	3	5
21.7	3	4	3	2
10.10	20	18	18	9
12.8	3	2	2	0
01.11	3	1	1	3
31.5	24	24	23	21
22.6	42	45	42	42
40.4	14	12	12	11
20.11	4	6	5	2
30.9	2	3	2	3
13.7	6	6	5	2
22.9	8	6	6	3
04.8	7	8	8	8

1: All Ba ordered into A-site.
   $\emptyset$-site fully occupied.
2: All Ba ordered into A-site.
   $\emptyset$ vacant.
3: Ba disordered over A- & A*-
   sites. $\emptyset$-site fully occu-
   pied.

gens per unit cell of 32.82 gives 18 O at the O1-site and 11.64 O + 6.36 OH at the O2-site. This OH corresponds to 1.8% H_2O by weight, significantly less than the amount expected from the analysis deficit. Only by introducing H_2O molecules at the $\emptyset$-site can this figure be increased. If the $\emptyset$-site is fully occupied by H_2O, then 5.2 wt.% H_2O results, which would give an excellent analytical sum of 99.7 wt.%.

As a further test of $\emptyset$-site occupancy, a second intensity calculation was carried out, this time modelling $\emptyset$ as vacant (column 2 of Table 73). R-indices were R=21% for all diffractions and R=14% for those diffractions with d<4.0Å, giving 5% and 3% poorer fits, respectively, than the same calculations with $\emptyset$ fully occupied by H_2O.

It is concluded that for the site labels of Table 72, A is occupied by Ba (and Na, Pb, Sr, K), A* is vacant, B1 and B2 are occupied by Ta (and Nb), O1 by O, O2 by O+OH and $\emptyset$ by H_2O. The ideal formula for parabariomicrolite is:

$$BaTa_4O_{10}OH_2 \cdot 2H_2O \qquad (Z=3)$$
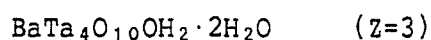
If the O plus OH of the O2-site are ordered, instead of disordered, then the space group symmetry must be lower than R3m. With approximately 6 OH and 12 O at O2, a 1:2 splitting of the site would be expected. None of the R-centred subgroups of R3m allow splitting of O2 in this fashion; it is concluded that R3m is the best candidate for the space group of parabariomicrolite and that O and OH are disordered over O2.

Table 74: Selected Distances (Å) and Angles (°) for the
Parabariomicrolite Structure

A Polyhedron	B1 Polyhedron	B2 Polyhedron

BOND LENGTHS

```
A - O1 x6  2.71      B1 - O2 x6   1.98      B2 - O1 x4  1.97
  - ∅  x2  3.33                               - O2 x2  2.00
< A - O >  2.87                             < B2 - O >  1.98
```

ANGLES

```
O1 - A - O1 x6  118    O2 - B1 - O2 x6  90    O1 - B2 - O1 x2  90
      - O1 x6   62            - O2 x6  90          - O1 x2  90
      - ∅  x6   98      < O - B1 - O >   90          - O2 x4  89
      - ∅  x6   82                                   - O2 x4  91
  < O - A - O >  90                             < O - B2 - O >  90
```

O-O DISTANCES

```
O1 - O1 x6  2.79*     O2 - O2 x6  2.79     O1 - O1 x2  2.79*
   - ∅  x6  3.98              x6  2.81        - O1 x2  2.79*
 < O - O >  3.39      < O - O >  2.80        - O2 x4  2.80
                                             - O2 x4  2.83
                                           < O - O >  2.81
```

"*" denotes shared polyhedral edges

Table 75: Bond Valences (v.u.) for Parabariomicrolite

A Octahedron		B1 Octahedron		B2 Octahedron	
Bond	s	Bond	s	Bond	s
A-O1 x6	0.32	B1-O2 x6	0.84	B2-O1 x4	0.86
-∅ x2	0.05			-O2 x2	0.78

Site Sums

A: 2.0   B1: 5.0   B2: 5.0
O1: 2.0   O2: 1.6   ∅: 0.1

15.5.2   Description of the Structure

The parabariomicrolite structure is represented polyhedrally in Figure 46. It is best described as a layer structure, consisting of alternations of two topologically distinct layers along Z, as has been done previously for the pyrochlore structure along {111} (Yagi & Roth, 1978). One layer (Figure 46a) has corner-sharing BO_6 octahedra (B2-site) which form 6- and 3-membered rings within the layer. This layer has a topologically identical counterpart in the pyrochlore structure. A-cations are located at the geometric centre of the 6-membered rings. A-cation polyhedra are cubes; six vertices of each cube lie within the layer; the other two lie directly above and below the A-cation. The six anions within the plane of the layering are oxygens of the O1-site; the two anions above and below the A-cation are water molecules. From a steric viewpoint, this is an excellent location for the water molecule; a large, open space lies above and below each A-cation polyhedron. From the viewpoint of R3m symmetry, the

location is somewhat less than ideal: the oxygen atom of each molecule has site symmetry 3m; the two H-atoms of the molecule must, therefore, be positionally disordered.

The second layer is shown by Figure 46b. In parabariomicrolite, this layer is occupied only by B1-cation octahedra. The B1-O bonds of these octahedra serve as the sole links between layers of the first type. The second layer has an analogous counterpart in the pyrochlore structure, except that the unoccupied polyhedra of the layer (denoted by the dotted outlines in Figure 46b) are occupied by A-cations in the pyrochlores. Thus the pyrochlore structure has extra bonding along Z which parabariomicrolite does not have, which might well account for the lower hardness of parabariomicrolite as compared to microlite. The ∅-site anions occur at the triple junction of the A-cation polyhedra of this layer. In the pyrochlore structure with its occupied layer 2 A-cation polyhedra, each ∅-site has bond valence-contributions from one A-cation in layer 1 plus three A-cations in layer 2, thus has a Pauling bond strength sum of 4 x 2/8 = 1 v.u. . The ∅-site of parabariomicrolite receives bond valence contributions from the layer 1 A-cation only; its Pauling bond strength sum is only 1 x 2/8 = 0.25 v.u. . This is the reason why OH and F are typical ∅-site occupants in pyrochlores, whereas H_2O is the sole ∅-site occupant in parabariomicrolite.

Several features of the refined structure are quite noteworthy:

1. Shared polyhedral edges are typically shorter than unshared edges (Table 74).
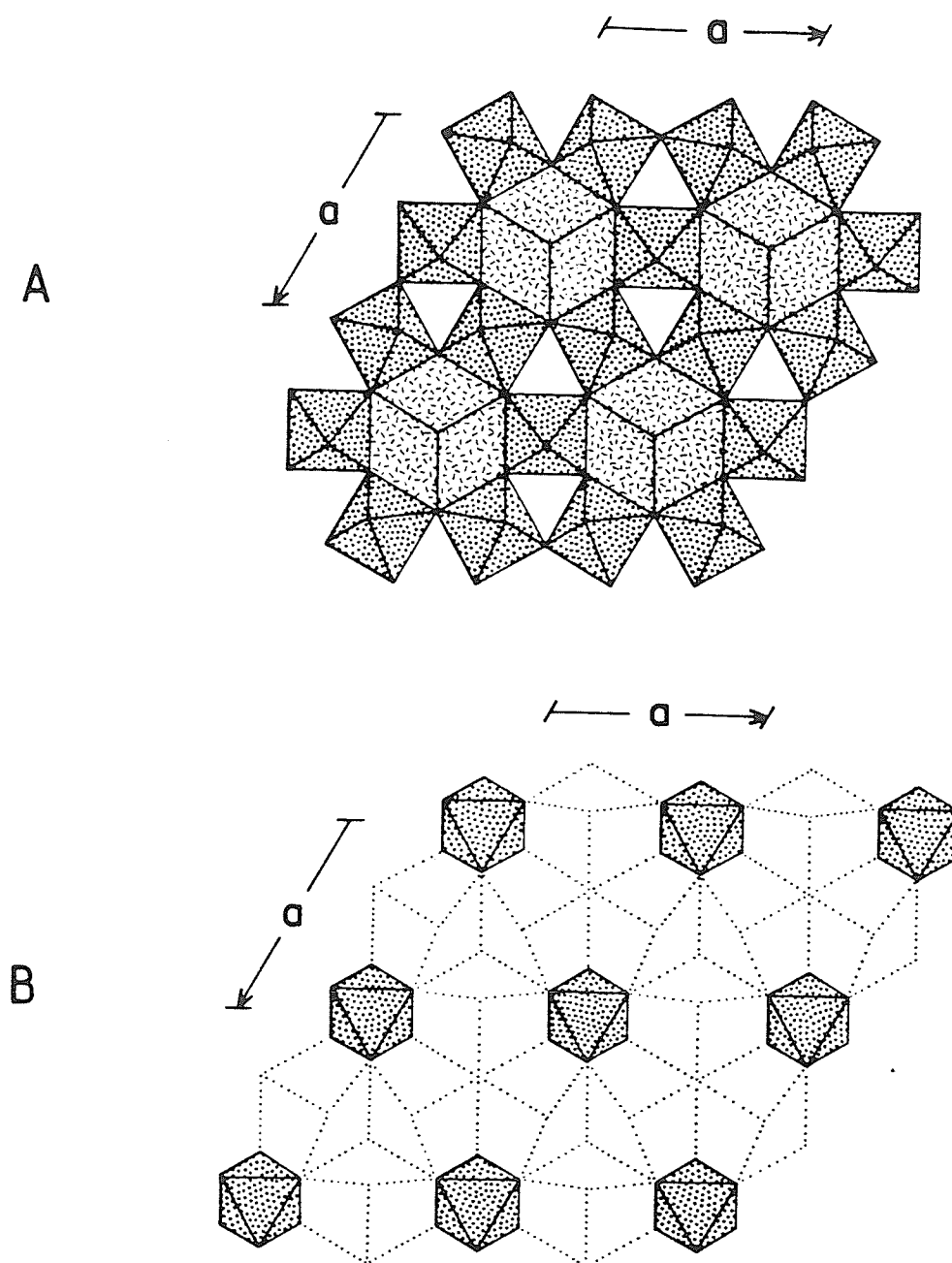
Figure 46: The layer structure of parabariomicrolite. (A) Layer 1: B2-cation polyhedra are stippled; A-cation polyhedra are hatch-stippled. (B) Layer 2: B1-cation polyhedra are stippled; unoccupied polyhedra are represented with a dotted outline.

2. The H_2O molecule is quite displaced from the ideal position for the ∅-site of the cubic pyrochlore structure: z(obs.)=0.315, z(ideal)=0.375. This conforms with recent refinements of H_2O-bearing pyrochlores (e.g. Groult et al., 1982) which claim that H_2O in the pyrochlore structure is positionally disordered off the ideal 8b position.

3. The presence of A-cation versus vacancy ordering, which is not compatible with the pyrochlore structure, explains the non-cubic symmetry of this mineral. Two criteria for the formation of parabariomicrolite as opposed to bariomicrolite are (1) an A:B ratio of 1:4, and (2) growth at (low) temperatures conducive to the incorporation of major amounts of H_2O in the structure. Unlike parabariomicrolite, bariomicrolite should have A:B ratios in excess of 0.25, crystallizing as either a primary or a secondary pegmatite mineral (i.e. with or without structural water).

On the basis of these two criteria, the Kivu mineral with a 1:4 A:B ratio, and with an analysis deficit of 7.7 wt.% is certainly a parabariomicrolite.

Chapter XVI

COLUMBITE-GROUP AND TAPIOLITE-GROUP MINERALS

16.1 INTRODUCTION

Unlike their occurrence in most Ta-Nb oxide mineral parageneses (cf. Černý & Ercit, 1985), the columbite-group minerals are uncommon members of the simpsonite paragenesis. However, they are persistent members of the paragenesis; they have been found in the Alto do Giz, Kivu, Leshaia, Bikita and Tanco associations. Tapiolite-group minerals are rarer. They are uncommon-to-rare members of three associations: Tanco, Alto do Giz and Bikita. Although tapiolites have been reported from Onça, they were not observed nor have ever been reported as associates of simpsonite at this locality.

Columbite-group minerals have the general formula:

$$AB_2O_6$$

where
$$\underline{A} = Mn, Fe^{2+}, Ca, Mg$$
$$\underline{B} = Nb, Ta$$
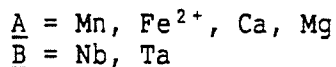
describes the major element chemistry of the group. Species names usually consist of the root "columbite" for $Nb \geq Ta$ or "tantalite" for $Ta > Nb$, modified by a prefix indicating the dominant $\underline{A}$-site cation, e.g. "ferro-" for Fe^{2+}, "mangano-" for Mn^{2+} and "magno-" for Mg^{2+}. Fersmite, $CaNb_2O_6$, is the sole exception to this otherwise coherent nomenclature. Known species are

- 241 -

manganocolumbite, manganotantalite, ferrocolumbite, ferrotantalite, magno-columbite and fersmite. Typical minor-to-trace elements in columbite-group minerals are Sc^{3+}, Fe^{3+}, REE^{3+}, Ti^{4+}, Sn^{4+} and W^{6+}.

The vast majority of occurrences of columbite-group minerals is of Fe^{2+}- or Mn^{2+}-dominant species. In all types of the rare-element class of grani-tic pegmatites of orogenic association, except the rare-earth type, these are the only compositions to form (Černý & Ercit, 1985); consequently, com-positional data for the columbite-group minerals are commonly represented in a quadrilateral (the "columbite quadrilateral") bound by the end-members $MnTa_2O_6$, $FeTa_2O_6$, $MnNb_2O_6$ and $FeNb_2O_6$ (Figure 47). Furthermore, the columbite-group minerals of these classes of rare-element pegmatites are typically poor in the minor elements listed above; hence the columbite quadrilateral adequately represents all major compositional variations.

The columbite structure was solved by Sturdivant (1930); Grice et al. (1976) and Foord (1976) refined the structures of selected columbite-group minerals, and Cummings & Simonsen (1970), Weitzel (1976), Wichmann & Müller-Buschbaum (1983) and Waburg & Müller-Buschbaum (1984) refined the structures of several synthetic columbites and tantalites. Like wodginite, the columbite structure is an ordered derivative of the ixiolite structure. The dominant structural units are zig-zag chains of edge-sharing octahedra (Figure 48); the reader is referred to Chapter XII for details of the ixiolite structure and its derivatives.

Cation ordering in the columbite structure produces layers perpendicular to $\underline{X}$ which contain only one type of cation. Along $\underline{X}$, the cation layering sequence is ...-A̱-Ḇ-Ḇ-A̱-Ḇ-Ḇ-..., whereas in ixiolite it is ...-A̱-A̱-... (there is only one type of cation site in ixiolite). Disorder in
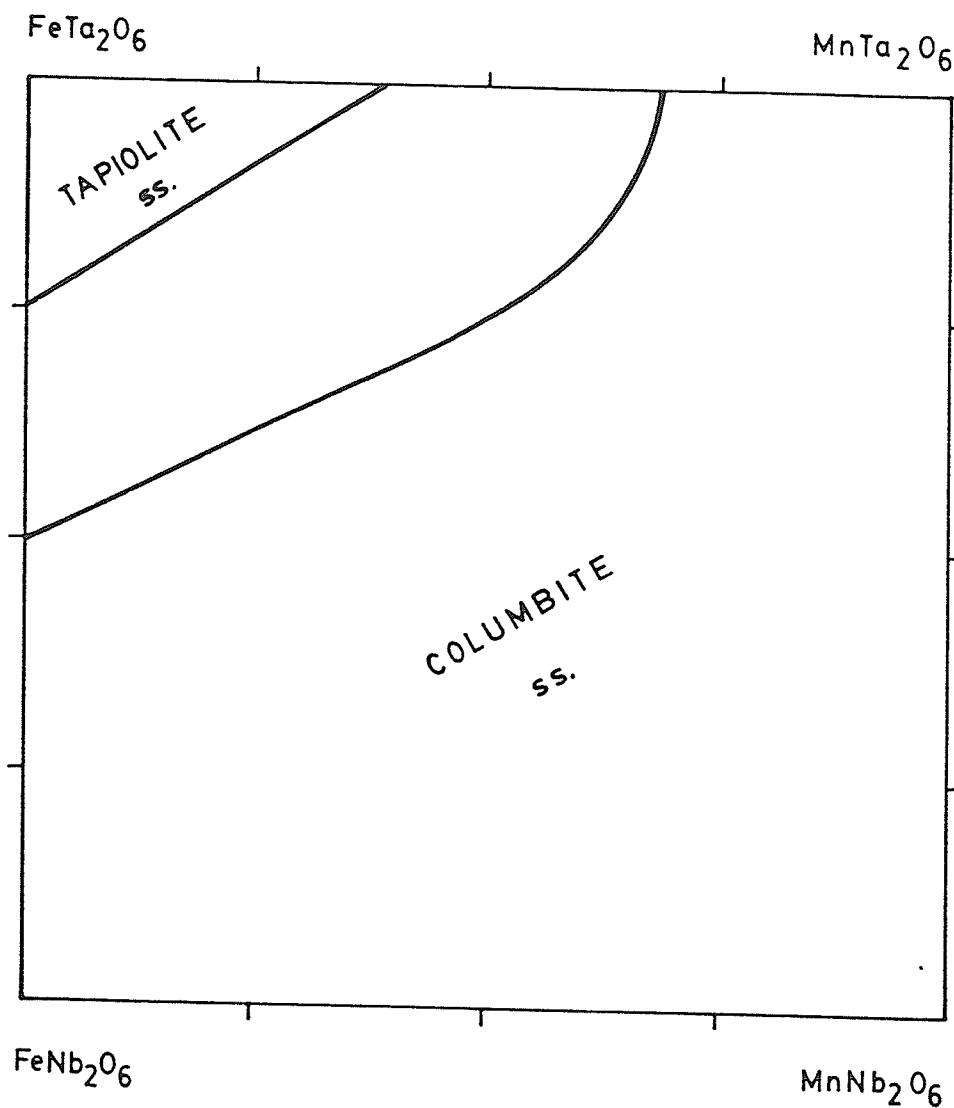
Figure 47: The columbite quadrilateral. Columbites plot in the centre to right-hand side of the diagram; tapiolites plot in the upper left-hand corner. A large composition gap (bound by the two bold lines) exists between the tapiolite-stable and columbite-stable regions (modified from Černý & Ercit, 1985).
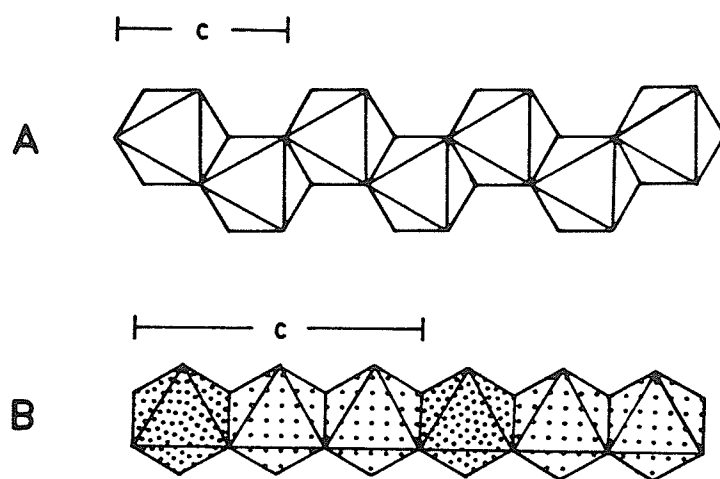
Figure 48: Octahedral chains in the columbite (A) and tapiolite (B) structures. The columbite structure has no intra-chain cation ordering; all chains have either M^{2+} or M^{5+} octahedra. In the tapiolite structure, ordering of M^{2+} (densely stippled) versus M^{5+} (lightly stippled polyhedra) cations takes place within the chains.

columbite-group minerals is marked by mixing of the A- and B-site contents; fully disordered columbite-tantalite has the ixiolite structure, has the structural formula $(A_{.33}B_{.67})O_2$ for $\underline{Z}=12$, and has $\underline{a}=1/3\cdot\underline{a}$ of ordered columbite.

Columbite-group minerals have structures intermediate to the fully-ordered and fully-disordered models. From the data of Černý & Ercit (1985), the average columbite-group mineral is only about 40-50% ordered. This creates an interesting nomenclature problem: the names columbite and tantalite are traditionally applied to group members which have, or are assumed to have, the fully-ordered columbite structure. Pseudoixiolite was the name given by Nickel et al. (1963a) to disordered tantalite, in allusion to its structural identity with ixiolite. Pseudoixiolite is not, however recognized by the IMA as being distinct from ixiolite, which is the name applied to disordered wodginite. Zhang et al. (1980) named disordered columbite ashanite, yet this doubtful species (E.E. Foord, pers. comm.) is recognized by the IMA. To avoid misrepresentation and confusion, only the names for the ordered species are used in this thesis, modified by adjectives such as "disordered" (0-25% order), "partially ordered" (26-75% order), and "ordered" (76-100% order).

Unit cell parameters of the columbite-group minerals are sensitive to order-disorder effects: for samples with identical chemistry but different degrees of order, the more ordered samples have larger $\underline{a}$ and smaller $\underline{c}$ than their disordered equivalents. Černý & Turnock (1971) have used $\underline{a}$ versus $\underline{c}$ plots to represent structural and chemical variations in columbite-group minerals. Figure 49 shows such a plot and outlines the compositional and structural trends in $\underline{a}$-$\underline{c}$ space. By extrapolating the trends to the ordinate and abscissa of this plot, the degree of order and mole fraction of Mn

can be estimated. Using the cell parameters of Wise et al. (1985) for columbite-tantalite end-members, the average slope of a line marking 100% order was obtained. Assuming that all lines of equal order in the a-c plot are parallel, and taking disordered Tanco tantalite TSE-42 (P. Černý, pers. comm.) as the best example for fully-disordered columbite-tantalite, the following equations were derived:

$$y = c - 0.2329 \cdot a \tag{1}$$
$$\% \text{ order} = 1727 - 941.6 \cdot y \tag{2}$$

which give the degree of order by linear interpolation between the ordinate intercepts of the lines with 0 and 100% order (y_0 and y_{100}). The accuracy of the calculation is impossible to assess at the present time because of the lack of available data to test the necessary assumption that the lines of equal order are parallel in a-c space. However, based on the precision of a and c determinations by powder diffractometer methods, the degree of order calculated from equations (1) and (2) should be precise to within ±5%. The effect of impurities upon a and c was not considered in the calculations, so this estimate of precision holds only for Fe-Mn columbite-group minerals low in impurity elements (W, Sn, Ti, Sc, Fe^{3+}, Ca, Mg).

The tapiolite-group minerals are identical in stoichiometry to columbite-group minerals: AB_2O_6, but with Z=2. Tapiolites always have Ta>Nb and range from Fe^{2+}-dominant (ferrotapiolite) to Mn-dominant (manganotapiolite); however, the vast majority are ferrotapiolites with $Mn/(Mn+Fe^{2+}) \leq 0.35$, and textural evidence suggests the Mn-dominant species
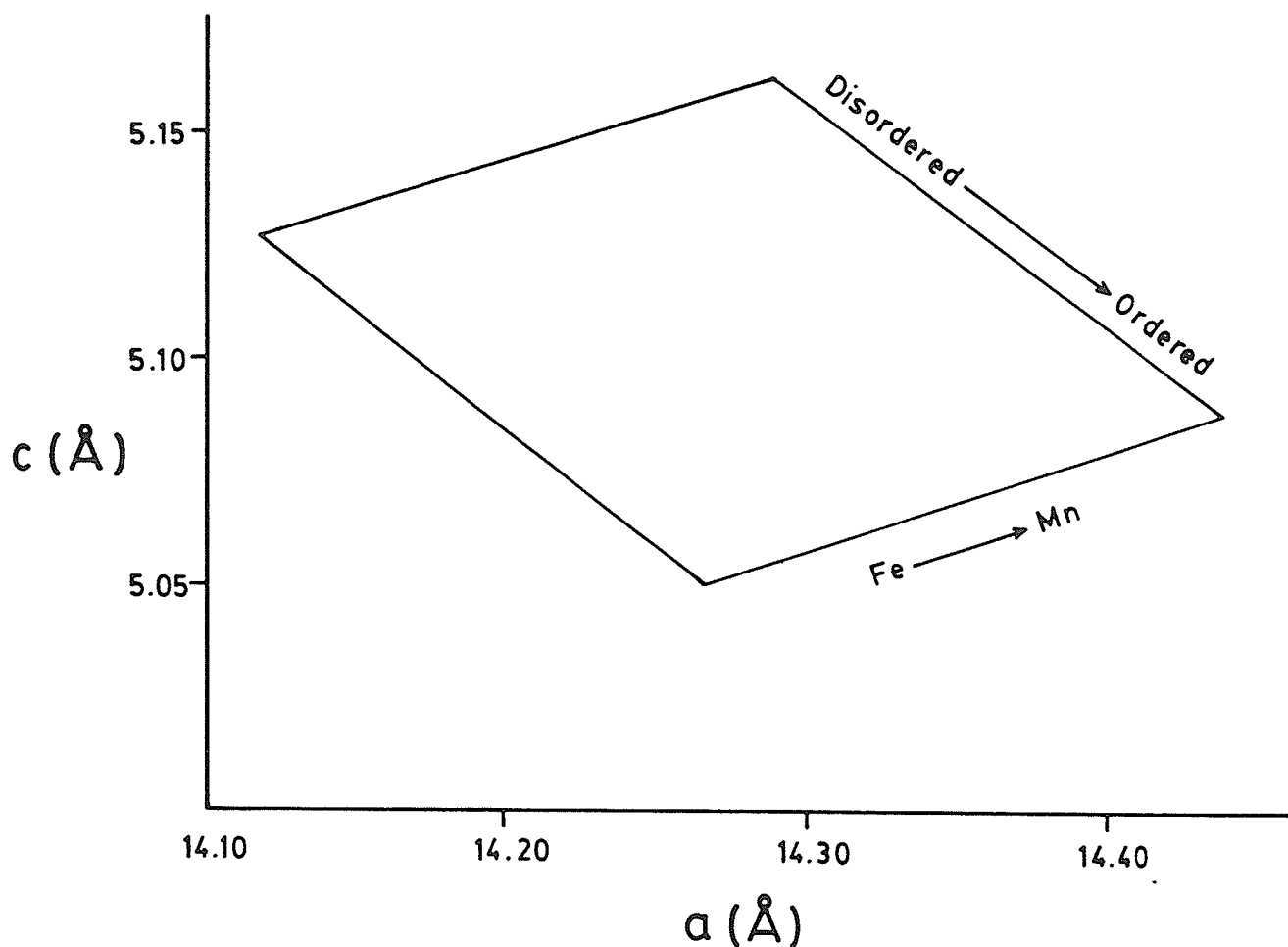
Figure 49: Compositional and structural variations of columbite-group minerals in a-c space. All members plot within the marked bounds. Disordered columbite-group minerals plot near the upper bound of the parallelogram; ordered ones plot near the lower bound. Fe-rich members plot near the left-hand bound; Mn-rich ones plot near the right-hand bound (modified from Wise et al., 1985).

to be metastable (Černý & Ercit, 1985). Typical minor-to-trace elements include Sc^{3+}, Fe^{3+}, Sn^{4+}, Ti^{4+} and W^{6+}. Because of the strong similarity of $\underline{A}$- and $\underline{B}$-site chemistries of tapiolite-group and columbite-group minerals, and because of their identical stoichiometries, compositional data for tapiolites are plotted in the same way as for columbite-group minerals, i.e. upon the plane of the columbite quadrilateral (Figure 47).

Figure 47 shows that compositional fields for columbite-group and tapiolite-group minerals do not overlap, as confirmed by synthesis studies (e.g. Turnock, 1966; Schröcke, 1966). The relationship between tapiolite-group and columbite-group minerals is not polymorphic; for natural systems, the stability of the columbite and tapiolite structures is compositionally controlled; the tapiolite structure is stable for Fe+Ta rich compositions, and the columbite structure is stable for most other compositions of the columbite quadrilateral. Synthetic columbites and tapiolites also are found to occupy different regions of compositional space. Figure 50 is a stability diagram for the columbite and tapiolite structures. The diagram shows that the columbite structure is generally stable at lower Ta/(Ta+Nb), and prefers larger and more electropositive $\underline{A}$-cations than the tapiolite structure. This explains why natural tapiolites cluster at the Fė (smaller and more electronegative than Mn) plus Ta-rich corner of the columbite quadrilateral.

The tapiolite structure was solved by Byström et al. (1941) and has been refined by Weitzel & Klein (1974). It has an approximately hexagonal closest-packing of oxygens and has cations in 1/2 of the octahedral interstices of the packing like ixiolite and its derivative structures; however, the tapiolite structure differs from these structures in its cation
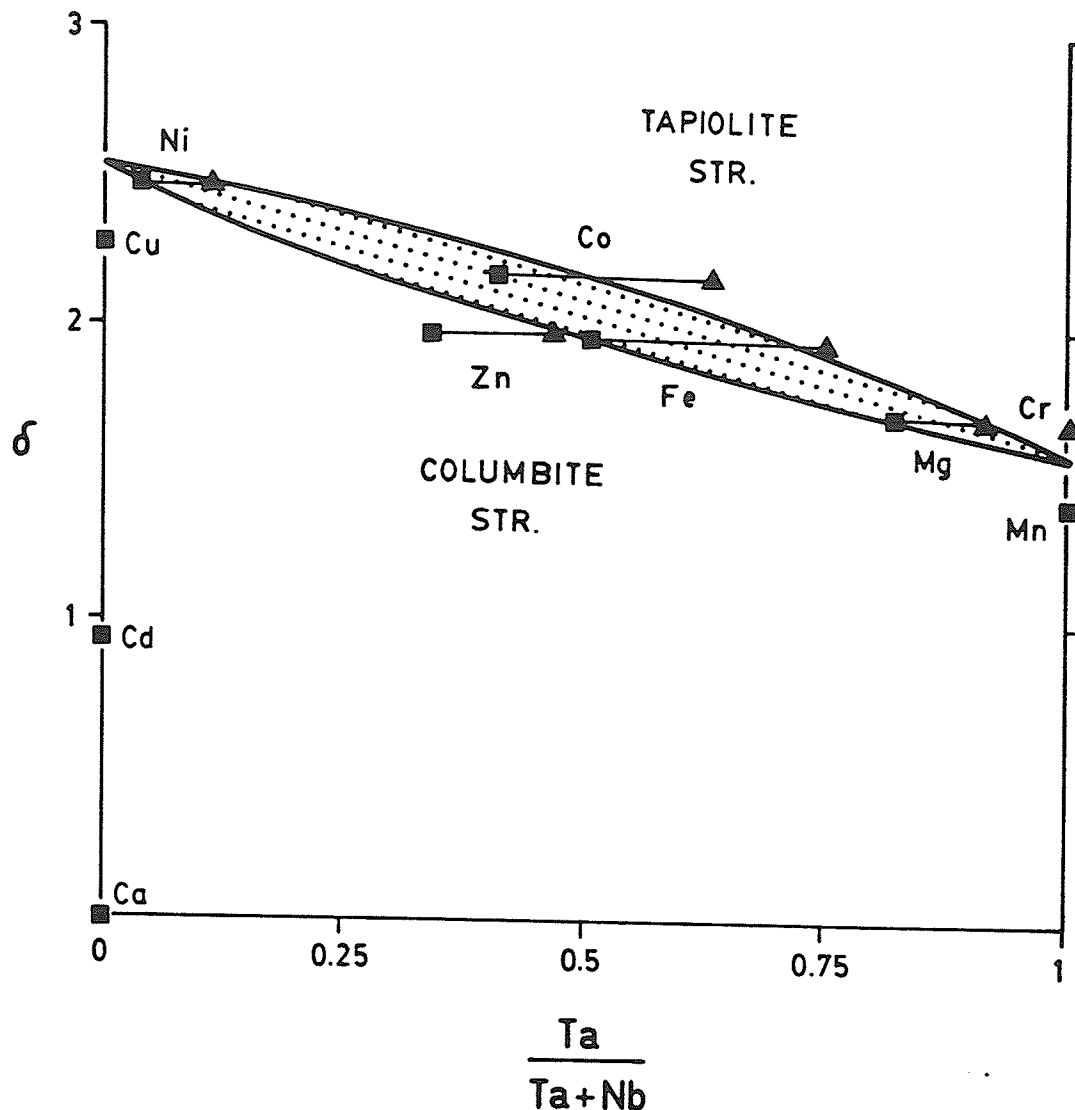
Figure 50: Stability diagram for the columbite and tapiolite structures. The parameter δ is a simple function of the effective ionic radius (r) and the Pauling electronegativity (Δ) of the A-cation, which was best fit to the data to give δ=4 +Δ -5·r. Experimental data are taken mainly from Felton (1967) and Sugitani et al. (1985). Only the columbite structure is stable to the left of the squares; only the tapiolite structure is stable to the right of triangles; bars mark two-phase regions for individual A-cations. The stippling marks an approximate fit to data for the two-phase region.

arrangement. The tapiolite structure is an ordered derivative of the rutile structure, which has straight chains of octahedra as its structural basis, not the zig-zag chains of the ixiolite structure (Figure 48). Tapiolite has an intra-chain ordering sequence ...-A-B-B-A-B-B-... whereas rutile has ...-A-A-... . The chains in tapiolite and rutile parallel $\underline{z}$, so the cation ordering in tapiolite results in a tripled $\underline{c}$-period relative to rutile. From the descriptions given here, the tapiolite ordering sequence may seem similar to that of columbite; however, tapiolite has intra-chain ordering whereas columbite has inter-chain ordering.

As in columbite-group minerals, the degree of order of tapiolites is variable (Clark & Fejer, 1978). However, the effects of composition and structure upon unit cell parameters of tapiolite-group minerals are poorly documented, and there is no quantitative measure of the degree of order of tapiolites at the present time.

16.2   CHEMISTRY

Electron microprobe analyses for columbite-group and tapiolite-group minerals of the simpsonite paragenesis are given in Table 76 and Table 77, respectively. All $\underline{A}$-site chemistries are Mn^{2+}- or Fe^{2+}-dominant, typical for the general type (complex) of rare-element pegmatite from which they come.

Unlike other minerals of the simpsonite paragenesis, the columbite-group and tapiolite-group members frequently contain detectable Ti, suggesting that Ti is preferentially partitioned into these phases. Sn^{4+} is a persistent minor-to-trace element; only the Alto do Giz samples are Sn-free. Tapiolites, unlike columbite-group minerals, can contain significant Fe^{3+}

Table 76: Electron Microprobe Analyses of Columbite-Group
Minerals of the Simpsonite Paragenesis.

	1	2	3	4	5	6	7	8	9	10
MnO	14.6	12.3	12.1	13.9	12.0	13.5	11.6	10.9	13.5	14.2
FeO	0.3	1.5	1.6	0.4	2.0	0.9	2.2	2.1	2.8	2.6
TiO_2	0.3	0.0	0.0	0.0	0.2	0.1	0.0	0.0	0.0	0.0
SnO_2	0.4	0.6	0.0	0.0	0.5	0.2	0.0	1.2	0.9	0.8
Nb_2O_5	13.6	0.2	0.3	6.1	2.3	8.9	0.4	4.5	43.6	45.3
Ta_2O_5	70.7	84.5	86.2	79.8	83.1	75.7	85.4	81.1	40.6	37.3
	99.9	99.1	100.1	100.2	100.1	99.2	99.6	99.8	101.4	100.2

Cations per 24(O)

	1	2	3	4	5	6	7	8	9	10
Mn^{2+}	3.86	3.58	3.49	3.86	3.41	3.71	3.36	3.07	3.00	3.16
Fe^{2+}	0.08	0.43	0.46	0.11	0.56	0.24	0.63	0.58	0.62	0.57
Ti^{4+}	0.07	0.00	0.00	0.00	0.05	0.02	0.00	0.00	0.00	0.00
Sn^{4+}	0.05	0.08	0.00	0.00	0.07	0.03	0.00	0.16	0.09	0.08
Nb^{5+}	1.92	0.03	0.05	0.90	0.35	1.30	0.06	0.68	5.18	5.38
Ta^{5+}	6.01	7.90	7.98	7.11	7.57	6.67	7.94	7.33	2.90	2.66
	11.99	12.02	11.98	11.98	12.01	11.97	11.99	11.82	11.79	11.85
ΣA	3.98	4.04	3.95	3.97	4.01	3.97	3.99	3.70	3.65	3.76
ΣB	8.01	7.98	8.03	8.01	8.00	8.00	8.00	8.12	8.14	8.09

1. Manganotantalite, Leshaia, USSR (KO-2).
2. Manganotantalite (yellow), Bikita, Zimbabwe (L-13).
3. Manganotantalite (yellow), Alto do Giz, Brazil (RVG-1C).
4. Manganotantalite (red), Alto do Giz (RVG-1C).
5. Manganotantalite (brown), Tanco, Manitoba (SMP-6).
6. Manganotantalite (yellow), Tanco (SMP-6).
7. Manganotantalite (brown), Tanco (SMP-51B).
8. Manganotantalite (?), aver. of 2 analyses, Tanco (SMP-51B).
9. Manganocolumbite (altered, rim), Lake Kivu, Zaire (L-14).
10. Manganocolumbite (altered, core), Lake Kivu (L-14).

- all analyses are ED except no. 6 (WD)

Table 77: Electron Microprobe Analyses of Tapiolite-Series
Minerals of the Simpsonite Paragenesis

	1	2	3	4	5	6	7	8
MnO	4.4	5.0	4.3	3.2	2.3	2.1	2.9	2.2
FeO	9.2	8.6	9.4	10.3	11.3	11.5	10.9	11.4
Fe_2O_3	0.0	0.0	0.5	0.0	0.0	0.0	0.1	0.9
TiO_2	0.0	0.0	0.0	0.0	0.0	0.3	0.0	0.3
SnO_2	1.0	0.0	0.0	0.7	0.8	0.6	0.7	0.8
Nb_2O_5	0.2	0.3	0.0	0.6	0.8	0.8	0.6	1.9
Ta_2O_5	83.7	85.6	86.0	85.3	82.8	84.6	85.1	83.0
	98.5	99.5	100.2	100.2	98.1	99.7	100.2	100.4

Cations per 12(O)

	1	2	3	4	5	6	7	8
Mn^{2+}	0.64	0.73	0.62	0.46	0.34	0.30	0.42	0.31
Fe^{2+}	1.33	1.23	1.34	1.47	1.64	1.63	1.55	1.59
Fe^{3+}	0.00	0.00	0.06	0.00	0.00	0.00	0.01	0.11
Ti^{4+}	0.00	0.00	0.00	0.00	0.00	0.04	0.00	0.04
Sn^{4+}	0.07	0.00	0.00	0.05	0.06	0.04	0.05	0.05
Nb^{5+}	0.02	0.02	0.00	0.05	0.06	0.06	0.05	0.14
Ta^{5+}	3.94	3.99	3.98	3.95	3.90	3.90	3.92	3.76
	6.00	5.97	6.00	5.98	6.00	5.97	6.00	6.00
ΣA	1.99	1.96	2.00	1.95	2.00	1.96	2.00	2.00
ΣB	4.01	4.01	4.00	4.03	4.00	4.01	4.00	4.00

1. Ferrotapiolite, Bikita, Zimbabwe (L-13).
2. Ferrotapiolite, Alto do Giz, Brazil (RVG-1C).
3. Ferrotapiolite, Alto do Giz (RVG-1C).
4. Ferrotapiolite, Tanco, Manitoba (SMP-6).
5. Ferrotapiolite (core), Tanco (SMP-51A).
6. Ferrotapiolite (rim), Tanco (SMP-51A).
7. Ferrotapiolite (aver. of 2), Tanco (SMP-51B).
8. Ferrotapiolite, Tanco (SMP-51D).

- all analyses are ED except no. 4 (WD)

(Turnock, 1966), so Fe^{3+} was calculated for all tapiolites with cation sums greater than 6.00 by normalizing on sums of 12 anions and 6 cations. Site sums for both mineral groups were calculated by assigning all M^{2+} to the A-site and all M^{5+} to the B-site, and by disordering all M^{3+} and M^{4+} between these sites for charge balance: 2/3 M^{3+} plus 1/3 M^{4+} to A, 1/3 M^{3+} plus 2/3 M^{4+} to B).

All columbite-group minerals of the simpsonite paragenesis have Mn^{2+}-dominant A-site chemistries (Figure 51). They are typically greatly enriched in Ta over Nb (tantalites), thus tend to plot near the $MnTa_2O_6$ corner of the columbite quadrilateral. The Kivu sample is atypical, having Nb>Ta (columbite). Analysis 2 of manganotantalite from Bikita marks the highest recorded Ta/(Ta+Nb) for any columbite-group mineral (cf. Zelt, 1975; Foord, 1976; Sahama, 1980; von Knorring & Fadipe, 1981).

Analyses 1-7 of Table 76 are reasonably well-behaved: their total cation sums and individual site sums fall within $\pm 2\sigma$ of the ideal values. Analyses 8-10 are quite non-ideal: the total cation sums are low by 4-5 σ, the A-site sums are low by 6-9 σ and the B-site sums are high by 6-9 σ. Analyses 9 and 10 are of a visibly altered manganotantalite, partially replaced by rankamaite at the rims. The low A-site sums and high B-site sums of these analyses indicate that both differential cation leaching (A-cations in preference to B-cations) and anion leaching (or replacement of O by OH) have taken place. As expected, rim analyses are the most non-ideal, indicating greater alteration of the rims over the cores. A structure analysis of this sample has been initiated to assess the exact mechanism of alteration.
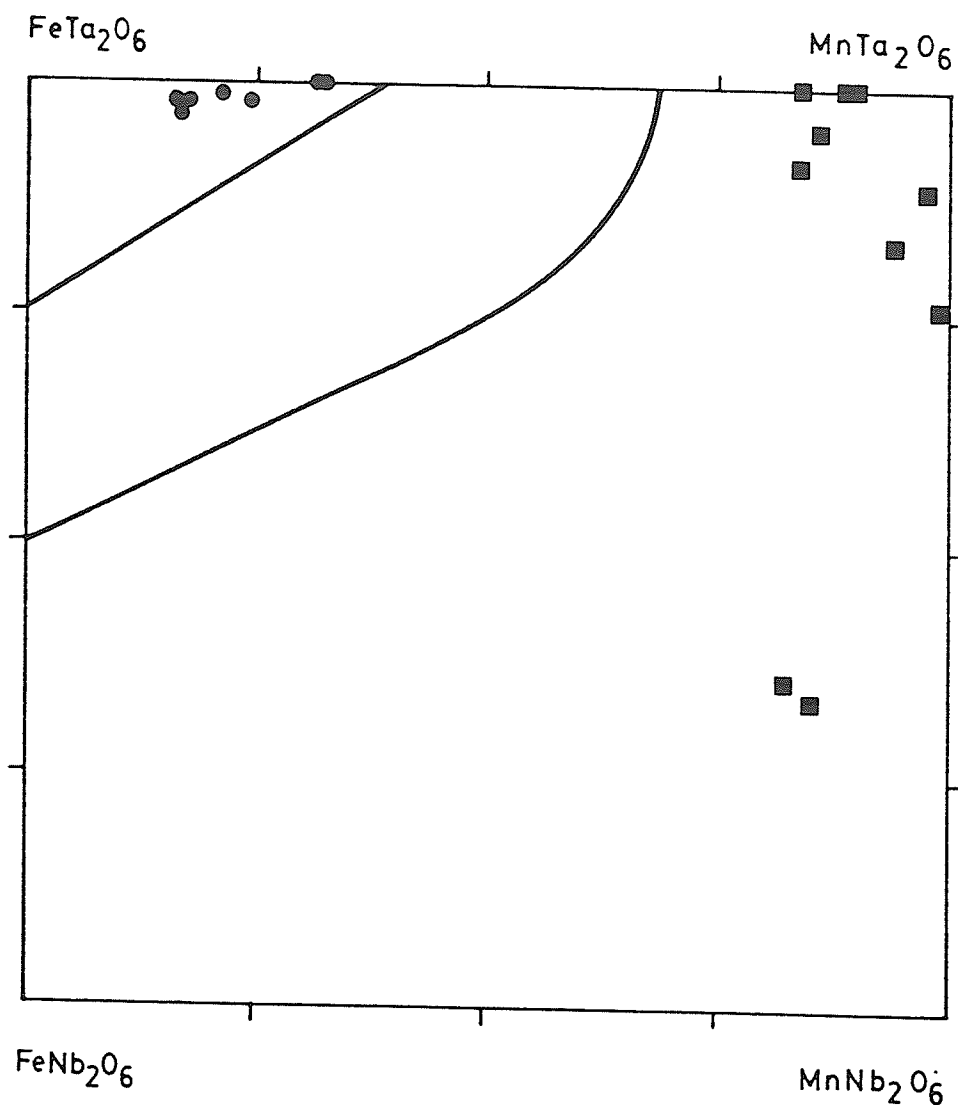
<u>Figure 51</u>: Plot of chemical data for tapiolite-group minerals (circles) and columbite-group minerals (squares) of the simpsonite para-genesis. The two squares near the bottom of the diagram are analyses of the Kivu manganocolumbite.

The Tanco manganotantalite of analysis 8 is similar to the Kivu mangano-columbites in terms of its non-stoichiometry: it has low $\underline{A}$-site and total cation sums and a high $\underline{B}$-site sum. It differs in that it is fresh and unaltered. It is no different from other manganotantalites of the same sample (e.g. analysis 7) in terms of colour or opacity, but has a slightly different morphology (less elongated than the other Tanco manganotantal-ites, and is somewhat diamond-shaped in cross-section). Initially an ana-lytical error was suspected, and the sample was cleaned, re-carbon-coated and re-analyzed. A virtually identical analysis resulted; the average of the two is given in Table 76. An attempt was made to extract the crystal for X-ray diffraction studies, but it proved to be too small (0.01 mm) for successful extraction. There are, however, two features of the chemistry of the mineral which may provide some clue to the problem of its non-ideality: (1) it has 5 times more Sn^{4+} than the average Tanco manganotan-talite associated with simpsonite, and (2) although its Fe-content is com-parable to this average manganotantalite, it has 12% less Mn. It is very possible, if not probable, that the mineral may actually be a tantalowodgi-nite; calculating the formula contents in the manner outlined in Chapter XII gives a wodginite-like result:

$$Mn_{1.01}(Ta_{.64}Fe^{3+}_{.19}Sn^{4+}_{.05}\square_{.12})(Ta_{1.78}Nb_{.22})O_8$$
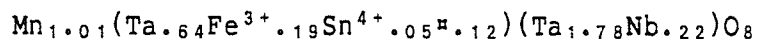
The tapiolite-group members of the simpsonite paragenesis are typically quite depleted in Nb^{5+}, to the extent that the ferrotapiolite of analysis 3 has no detectable Nb (<0.2 wt.%). Although all are ferrotapiolites, they

have atypically high Mn/(Mn+Fe^{2+}); consequently, the analyses plot along the FeTa$_2$O$_6$-MnTa$_2$O$_6$ sideline of the columbite quadrilateral (Figure 51). All ferrotapiolites from the simpsonite paragenesis form remarkably well-crystallized euhedral, transparent red crystals. Samples L-13 and RVG-1C coexist with equally well-crystallized manganotantalites. Because the maximum Mn content of tapiolites increases with Ta/(Ta+Nb), the tapiolites of L-13 and RVG-1C have extremely high Ta/(Ta+Nb): 0.995 and 0.997 respectively. As these tapiolites coexist with manganotantalites, the Mn-contents of these tapiolites should mark the maximum amount of Mn stable in the tapiolite structure under the conditions of formation of complex rare-element granitic pegmatites.

16.3   X-RAY CRYSTALLOGRAPHY

Unit cell parameters for the columbite-group and tapiolite-group minerals were determined by X-ray powder diffractometry, complemented by single-crystal diffractometry and precession photography where necessary. For the powder studies, Ni-filtered or graphite-monochromated Cu$\underline{K}\alpha$ radiation was used; for the single crystal studies, Zr-filtered or graphite-monochromated Mo$\underline{K}\alpha$ radiation was used. In most cases, the columbite-group and tapiolite-group minerals were too scarce, too finely crystalline and too intimately associated with other Ta-oxide minerals to permit quantitative XRD studies. Consequently, X-ray crystallographic data for these minerals are much more incomplete than for the other minerals of the simpsonite paragenesis.

Unit cell parameters for both mineral groups are given in Table 78. Order estimates for the columbite-group minerals are given there as well, and indicate all such members of the simpsonite paragenesis to be fully-

ordered, even the Kivu manganocolumbite.   Order-disorder in tapiolites has not yet been fully modelled,   hence an estimate of the degree of order cannot be made.   However, Clark & Fejer (1978) found that "ordered" tapiolites had c cell-edges less than 9.24 Å.   By this criterion, all tapiolites of the present study are ordered.

Table 78:   Unit Cell Parameters (Å) for Columbite-Group and Tapiolite-Group Minerals

Sample	Locality	a	b	c	V	% order
			Columbite-Group Minerals			
L-14	Kivu	14.389(3)	5.759(1)	5.080(1)	421.0(2)	100
RVG-2 (red)	Alto do Giz	14.424(2)	5.762(1)	5.089(1)	422.9(1)	100
SMP-12	Tanco	14.41	5.76	5.09	423	95
			Tapiolite-Group Minerals			
RVG-1C	Alto do Giz	4.7604(1)		9.2397(5)	209.38(1)	
SMP-8	Tanco	4.7610(2)		9.2321(5)	209.26(2)	

Cell parameters for RVG-1C, RVG-2, SMP-8 by powder diffractometry, for L-14 by single crystal diffractometry, for SMP-12 by precession photography.

Chapter XVII

OTHER SPECIES

17.1   CASSITERITE

Cassiterite is a rare member of the simpsonite paragenesis, despite its common abundance in other parts of some simpsonite-bearing pegmatites, for example, the Tanco pegmatite. Cassiterite was found only in the Kivu and Kola associations, and is reported by Sarp & Deferne (1983) to occur in the Manono association.

Although cassiterite is ideally SnO_2, most pegmatitic cassiterites contain trace to major amounts of $(Ta_2O_5+Nb_2O_5)$ and $(FeO+MnO)$ (Foord, 1982). Cassiterites from the simpsonite paragenesis have up to $5\frac{1}{2}$ wt.% $(Ta_2O_5+Nb_2O_5)$ with Ta>>Nb (Table 79). The Kola Peninsula sample has $\frac{1}{2}$ wt.% $(FeO+MnO)$ with Mn>>Fe; the Kivu sample has no detectable Mn or Fe. The $M^{2+}:M^{5+}$ ratio of the Kola sample indicates charge balance was achieved by a $2M^{2+}+2M^{5+}=3M^{4+}$ mechanism; it would seem that a model such as $\square+4Ta^{5+}=5Sn^{4+}$ holds for the Kivu sample.

Because of the extreme scarcity and small size of available material, unit cell dimensions could not be determined for the cassiterites. However, the work of Clark et al. (1976) showed that the unit cell dimensions of cassiterites are insensitive to the substitutions outlined above, so unit cell dimensions would provide no additional information on the crystal chemistry of this species.

Table 79: Cassiterite Analyses

	KO-2	L-14
MnO	0.5	0.0
FeO	0.2	0.0
SnO_2	96.0	94.3
Nb_2O_5	0.0	0.3
Ta_2O_5	3.7	5.3
	100.3	100.0

Cations per 4(O)

	KO-2	L-14
Mn^{2+}	0.020	0.000
Fe^{2+}	0.006	0.000
Sn^{4+}	1.924	1.900
Nb^{5+}	0.000	0.007
Ta^{5+}	0.050	0.073
	2.001	1.980

KO-2: Leshaia, Kola Pen-
    insula, USSR.
L-14: Kivu, Zaire.

17.2   STIBIOTANTALITE

In terms of number of occurrences, stibiotantalite is an uncommon member of the simpsonite paragenesis, found only at Leshaia and Alto do Giz. With regard to abundance, it is typically rare; it is only common in the Leshaia association.

Stibiotantalite is a member of the stibiotantalite group, which has the general formula:

$$ABO_4$$

where $\underline{A}$ = Sb^{3-}, Bi^{3+}
       $\underline{B}$ = Ta, Nb

Species names consist of the root "columbite" (Nb≥Ta) or "tantalite" (Ta>Nb), modified by either "stibio-" or "bismuto-" to reflect the dominant A-site chemistry. The Bi-Nb (hypothetical "bismutocolumbite") end-member has not been found, nor are group members with appreciable amounts of this end-member known. There is no apparent crystal-chemical reason for why this should be: $BiNbO_4$ is easily synthesized (Jeitschko & Sleight 1974); thus the composition gap is probably a geochemical phenomenon.

Electron microprobe analyses for stibiotantalites of the Leshaia and Alto do Giz occurrences are shown in Table 80. Because material from the Benson pegmatite could not be obtained, no analysis of the stibiotantalite from this locality could be done. Consequently, an analysis of the mineral from von Knorring & Hornung (1963) is presented in Table 80. The Nb:Ta ratios of the stibiotantalites are similar to those of the columbite-group members of each association, which are higher than most other members of the association, yet the ratios are the lowest for published analyses of stibiotantalites (c.f. Foord, 1982).

Table 80: Stibiotantalite Analyses

	KO-1	RVG-7	BENSON
Sb_2O_3	39.8	38.8	39.0
Bi_2O_3	0.6	0.5	0.9
Nb_2O_5	3.5	2.1	1.9
Ta_2O_5	56.1	57.6	57.0
	100.0	99.0	98.8

Cations per 16(O)

	KO-1	RVG-7	BENSON
Sb^{3+}	3.92	3.90	3.93
Bi^{3+}	0.03	0.03	0.06
Nb^{5+}	0.38	0.23	0.22
Ta^{5+}	3.65	3.81	3.79
	7.98	7.97	8.00

KO-1: Leshaia, Kola Peninsula,
      USSR.
RVG-7: Alto do Giz, Brazil.
BENSON: Benson pegmatite,
        Zimbabwe (von Knorring
        & Hornung, 1963).

GEOCHEMISTRY OF THE SIMPSONITE PARAGENESIS

Chapter XVIII

THE TANCO PEGMATITE

18.1   LOCATION AND GEOLOGY

The Tanco pegmatite is located on the northeast shore of Bernic Lake, 180 km ENE of Winnipeg, Manitoba (Figure 52).   It occurs in the Bird River Greenstone Belt, which is situated in the English River Subprovince of the Superior Province of the Canadian Shield.   Much of the following descrip- tion of the geology of the region, and of the Tanco pegmatite is taken from Crouse & Černý (1972) and Crouse et al. (1979).

The Bird River Greenstone Belt consists of six formations of metavolcan- ic and related metasedimentary rocks plus synvolcanic to late tectonic intrusive rocks.   Two major episodes of folding and faulting have acted upon the belt, the second of which corresponds to the peak of regional metamorphism which reached greenschist facies in most parts, but amphibol- ite facies in eastern to northeastern parts of the belt.   Emplacement of batholithic masses was also contemporaneous with the second folding event; tonalitic diapirs and biotite granite intrusions are most typical.   Post- metamorphic E-W faulting produced channelways for late leucogranites and pegmatitic granites, parental to the pegmatites of the Winnipeg River dis- trict.   However, it seems that the granitic source of the Tanco deposit and related pegmatites in its vicinity is hidden.

The Tanco pegmatite was forcibly emplaced (Brisbin, 1986) into subhori- zontal joints and fractures in the metagabbro which now encloses it.   The
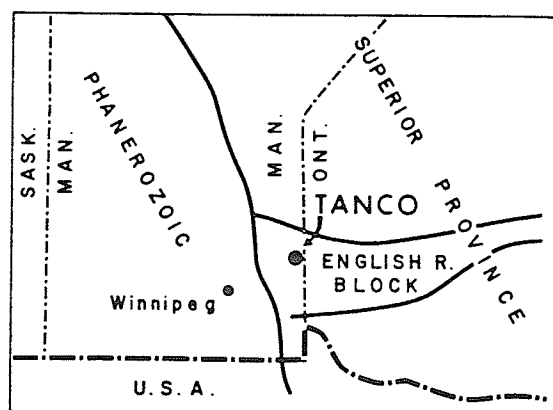
<u>Figure 52</u>: Location of the Tanco pegmatite (from Crouse et al., 1979).

pegmatite is bilobate: it dips shallowly to the north and plunges both to the east and west (Figure 53); the crest lies near the centre of the pegmatite. Its dimensions are 1440 m (strike) by 820 m (width) by a maximum thickness of 100 m.

The primary crystallization range of the pegmatite has been bracketed at 600 to 400°C and 3.3 to 2.6 kbar on the basis of Li-aluminosilicate phase relations and fluid inclusion microthermometry (London, 1986); however, Thomas & Spooner (1985) propose lower temperatures (to 265°C) based on their fluid inclusion microthermometric work.

The Tanco pegmatite belongs to the petalite subtype of the complex type of rare-element granitic pegmatites of orogenic association (Černý, 1986). Černý (1982) has outlined the extremes in geochemistry of this remarkably fractionated granitic pegmatite. A few notable examples are: K/Rb as low as 2.1 and Rb/Cs as low as 4.5 (lepidolite); Nb/Ta as low as 0.01 (simpsonite); Zr/Hf as low as 5 (zircon).
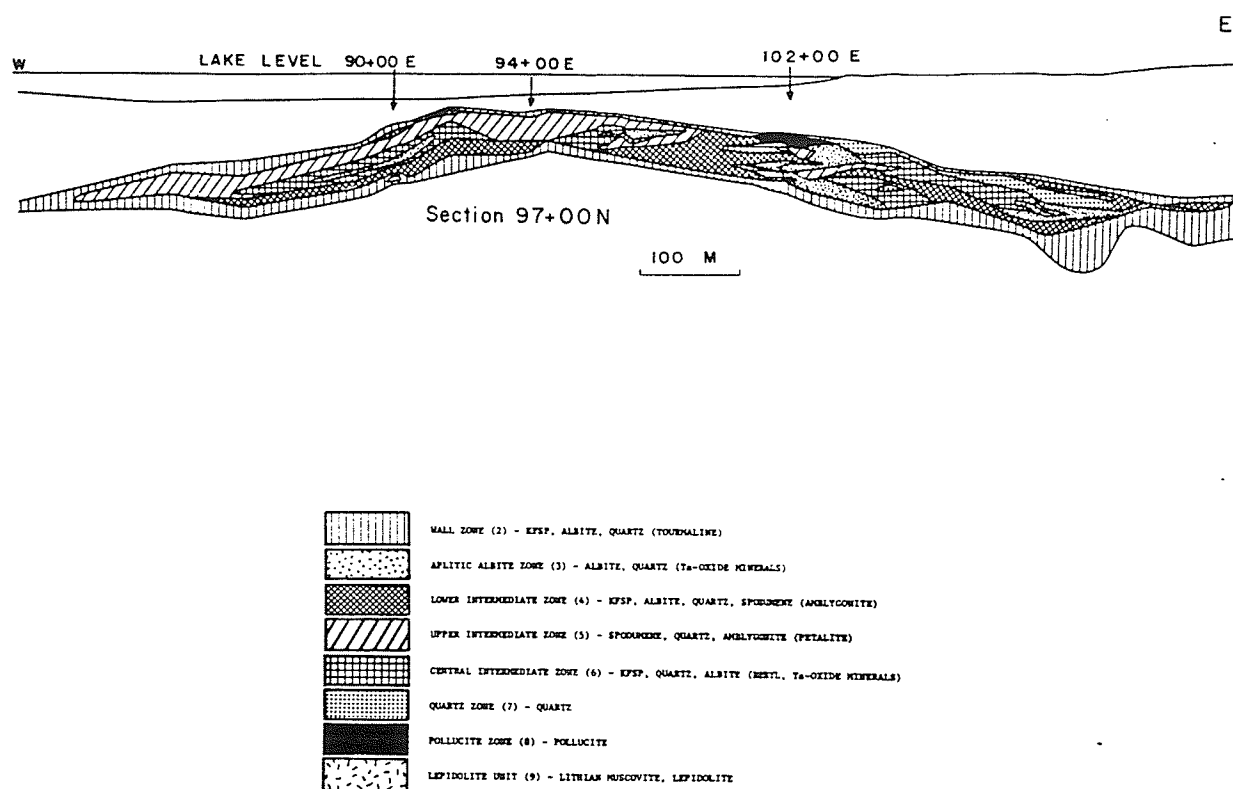
Figure 53: Section and internal zoning of the Tanco pegmatite (from Crouse et al., 1979).

18.2   INTERNAL STRUCTURE

The Tanco pegmatite consists of nine units of different mineralogy, texture and location.

The border unit (1) forms a fine-grained aplitic shell-like envelope about the pegmatite. The wall unit (2) is concentric with unit (1), but consists of medium to coarse-grained albite, quartz, muscovite and microcline-perthite. Both units tend to be thicker in their footwall segments.

The saccharoidal albite unit (3) tends to occupy basal parts of the pegmatite between unit (2) and other units of the pegmatite, most often units (7),(6) and (4). Unit (3) is only developed in sizeable homogeneous masses in the eastern flank of the pegmatite (up to 16 m thick); however, the central and western flanks of the pegmatite contain abundant but dispersed occurrences of saccharoidal albite. Unit (3) consists mainly of fine-grained albite plus quartz with accessory amounts of muscovite, oxide minerals and beryl, which accentuate the typically layered fabric of the unit.

The lower (4) and upper (5) intermediate units together form another concentric shell within the envelopes of units (1) and (2) (Figure 53). The contact between units (4) and (5) is gradational, and their mineralogy differs mainly in terms of mode and texture. Unit (4), as its name implies, is in the lower to central parts of the pegmatite. It is texturally and compositionally inhomogeneous, consisting of these assemblages: (i) mixtures of large crystals of microcline-perthite and spodumene plus quartz pseudomorphs after petalite ("SQI") in a medium-grained quartz, albite, mica matrix; (ii) amblygonite-montebrasite and SQI in quartz pods (to 2 m). Unit (5) occupies upper to central parts of the pegmatite, and

differs from (4) in having greater and more homogeneous proportions of giant crystals (SQI, microcline-perthite, amblygonite-montebrasite), and by the scarcity of micas and appreciable albite.

The central intermediate unit (6) is largely enclosed within the shell of units (4) and (5). Because the inner hangingwall and footwall contacts of this shell meet near the centre of the pegmatite, unit (6) does not extend continuously from the western flank to the eastern flank of the pegmatite. The contacts of unit (6) with other units are typically sharp, except for contacts with the lepidolite units (9) which are often gradational. The mineralogy of the central intermediate unit consists of giant microcline-perthite and quartz crystals with minor to major, but discontinuous amounts of SQI, unit (3)-like saccharoidal albite, and unit (9)-like muscovite plus lepidolite as incomplete replacements of the microcline-perthite.

The quartz unit (7) is located at the core in the eastern flank of the pegmatite, but is discontinuous and occupies upper parts of other parts of the pegmatite.

The pollucite unit (8) forms a large, almost monomineralic body at the unit (5) - hanging wall unit (2) contact in the upper parts of the central to eastern parts of the pegmatite, and several smaller bodies at similar levels in other parts of the pegmatite. Its contact with unit (5) is gradational, and with unit (2), sharp.

The lepidolite unit (9) typically occurs as replacements of the microcline-perthite of unit (6). Unit (9) consists of two lenticular sheets to 18 m thick near the centre of the pegmatite plus several smaller bodies; fine-grained lithian muscovite to lepidolite is the main constituent.

On the basis of the spatial setting of the units, the textural relationships described above, $\delta^{18}O$ and δD studies of quartz, muscovite and K-feldspar of units (1),(2) and (4)-(6) (Taylor & Friedrichsen, 1983), and preliminary fluid inclusion data (Thomas & Spooner, 1985; London, 1986), the sequence of crystallization of the units is (1)→(2)→(3)→(4,5,8)→ (6)?(7)→(9).

18.3 SAMPLING AND OXIDE MINERAL DISTRIBUTION

The works of Grice (1972) and subsequent work of Černý et al. (1981) and other unpublished data of Černý have shown Ta-Nb-Sn-Ti oxide minerals to occur in several of the units of the Tanco pegmatite, most notably units (6),(3),(4) and (5) (roughly in order of decreasing abundance). At the time of this study (1980-1985), all units of the pegmatite were exposed in the underground workings of the mine; consequently, all units could be investigated for the presence of oxide minerals. Attempts were made to sample every accessible pillar and back of the workings, which resulted in approximately 220 samples, 95% of which were found to contain one or more Ta-Nb-Ti-Sn oxide mineral grains. The high success rate should not be taken wholly as an indication of the richness of oxide mineralization as there was a distinct bias in sampling: for the most part, only samples with visible oxide mineral grains, or failing this, samples resembling ore material in other parts of the mine were taken.

A time-averaged map of the mine workings for the period 1980-1985 showing sample locations is given in Figure 54. A corresponding map with the floor geology compiled from mine sections and modified by the author's observations is given in Figure 55. The list of samples and pertinent data is given in Appendix E.
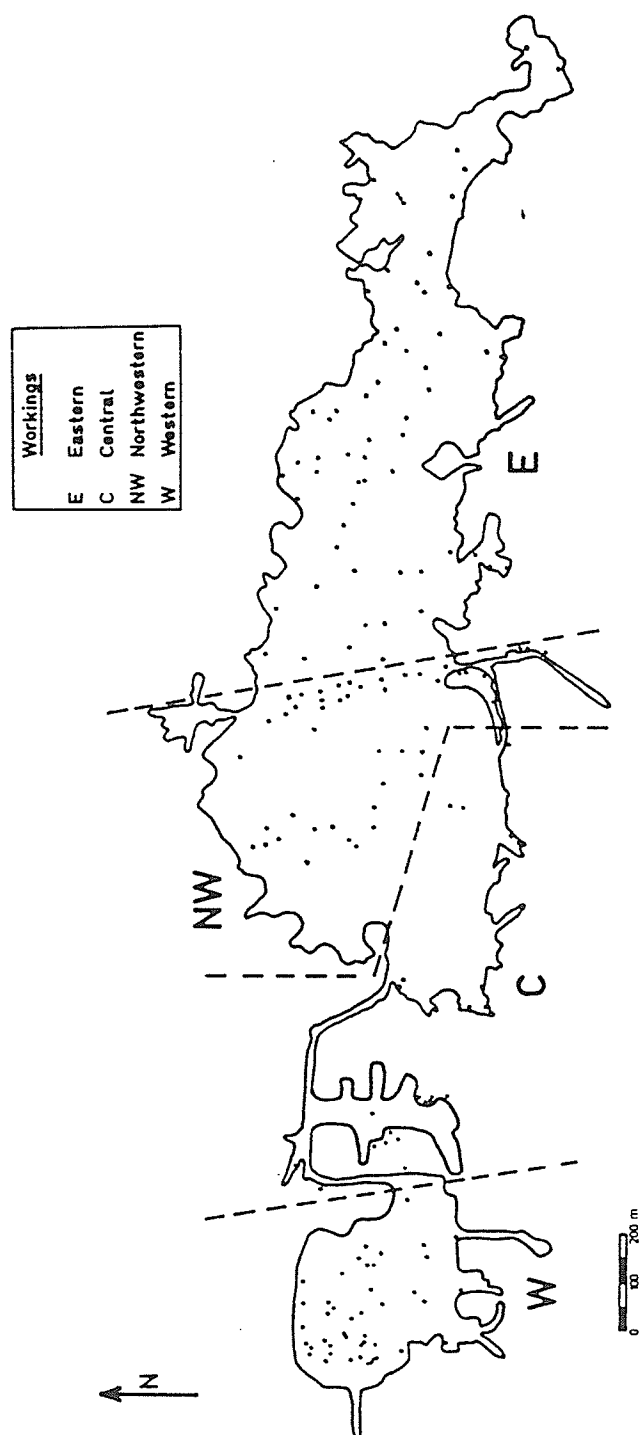
Figure 54: Tanco mine workings and sample locations.

271
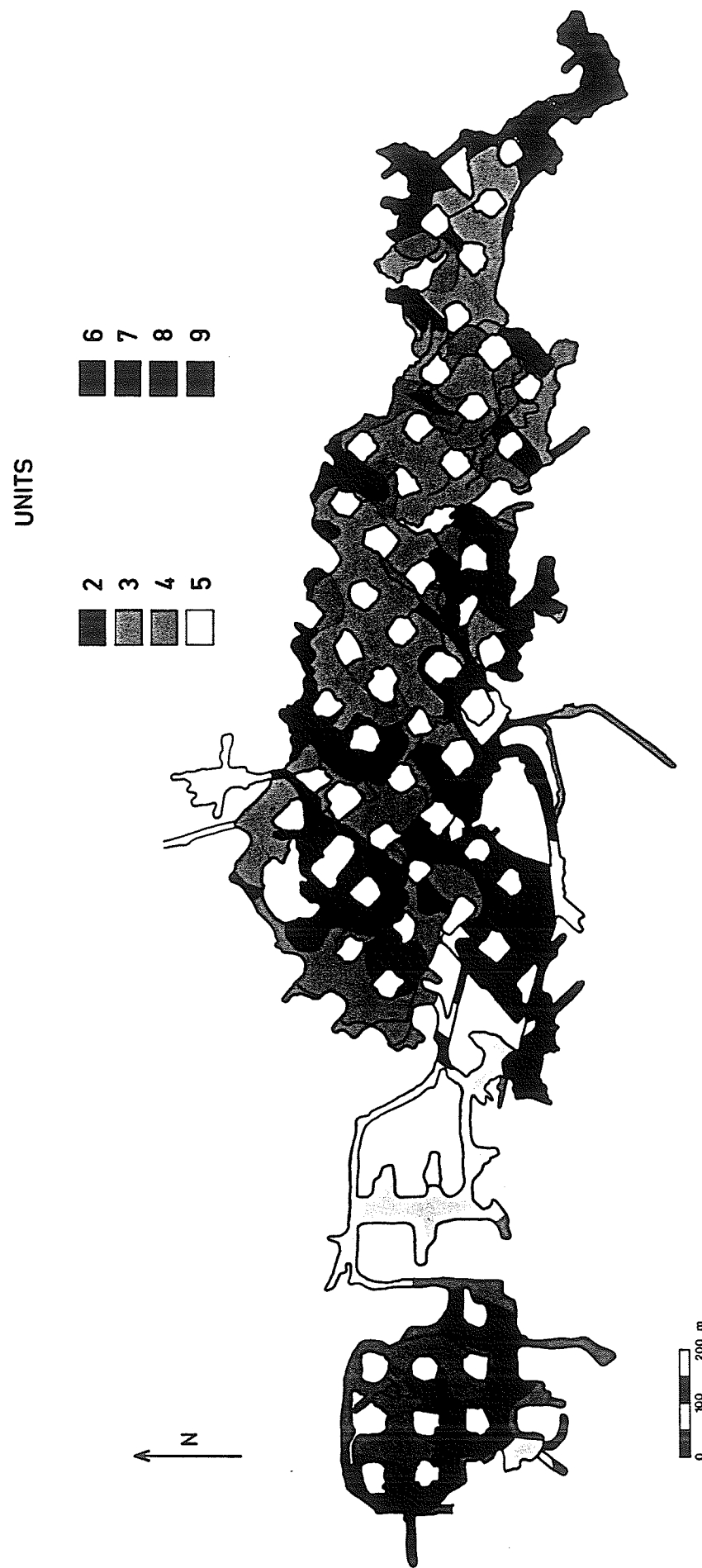
Figure 55: Floor geology of the Tanco pegmatite.

Through these sampling procedures, and by the methods of sample preparation described in Part 2, oxide minerals were found in units (2)-(6), (8) and (9) of the pegmatite. A total of 13 oxide minerals were found: wodginite, tantalowodginite, titanowodginite, ferrocolumbite, manganocolumbite, manganotantalite, microlite, uranmicrolite, cesstibtantite, ferrotapiolite, simpsonite, tantalian rutile and cassiterite. Their distribution amongst the units is outlined in Table 81. Even in this highly simplified tabulation, a correlation between internal zoning of the pegmatite and oxide mineralogy can be seen.

Table 81: Summary of Oxide Mineral Distribution

Internal Unit	Wd	Mc	Tn	Ct	Ru	Tp	Ur	Sm	Cs
Wall			u	u					
Saccharoidal Albite	a	c	c	c	u	r			
Lower Intermediate		r	a	u					
Upper Intermediate	r	u	a	u	r		r		
Central Intermediate	a	c	r	u			u	r	r
Pollucite	r	r							
Lepidolite	r	c	u	c					

Wd: wodginite-group minerals, Mc: microlite subgroup minerals, Tn: columbite-group minerals, Ct: cassiterite, Ru: rutile, Tp: ferrotapiolite, Ur: uraninite, Sm: simpsonite, Cs: cesstibtantite.

a: abundant, c: common, u: uncommon, r: rare
The most abundant mineral of each zone is underlined.

Wodginite-group minerals are the most abundant oxide minerals of the pegmatite. This, coupled with their typically high Ta:Nb ratios makes them the main Ta-ore minerals of the pegmatite. As a cursory examination of

Appendix E will show, the wodginite-group minerals are nearly confined to the central intermediate and saccharoidal albite units.

Pyrochlore-group minerals (microlite varieties) are the next most-abundant oxide minerals, and are concentrated in the same units as the wodginites; however, they tend to be more abundant in albitic associations. Often concentrated at the upper margins of unit (3), their uranian varieties are probably responsible for smoky quartz halos at unit (7) – unit (3) contacts (Figure 56).

Columbite-group minerals are the most widely-distributed oxide minerals, and are most concentrated in the wodginite-poor upper and lower intermediate units. Despite their wide distribution, their scarcity in the central intermediate and saccharoidal albite units makes them only the third-most abundant of the oxide minerals.

Rutile was found only in Ti-rich associations of the saccharoidal albite unit; however, unpublished work by Černý on triphylite nodules has shown rutiles to be present in some similarly Ti-rich associations of the upper and lower intermediate units.

Ferrotapiolite is found only in uncommon Fe-rich associations, and except for one occurrence, all such associations are contained within the central intermediate unit.

Simpsonite, although a rare mineral for the pegmatite, is common in some parts of the central intermediate unit of the western flank of the pegmatite. Cesstibtantite, although always associated with simpsonite, is much rarer, and is found only in a few of the simpsonite occurrences.

Cassiterite is uncommon, but not rare, and is present as a minor phase in most units. Relative to other oxide minerals, it is most abundant in

Figure 56: Saccharoidal albite unit (3) - quartz unit (7) contact, eastern
flank of the Tanco pegmatite. The dark colouration of the
quartz at the contact is most likely due to radiation damage
originating from U-bearing microlite in the albite.

the lepidolite unit, and is more abundant than columbite-group minerals in the wall unit.

Uraninite was only identified in one sample (TRT-42). It comes from a triphylite-lithiophilite nodule from either the upper or lower intermediate unit. Nearly all U in the pegmatite is contained within uranian microlite – uranmicrolite; presumably the one uraninite occurrence represents an unusual circumstance of high $\mu(U)$ and relatively low $\mu(Ta)$, $\mu(Ca)$ and $\mu(Na)$.

Ilmenite has only ever been found in mill concentrates, and as later discussions will show, it is probably non-pegmatitic in origin.

18.4   ASSOCIATIONS

For the most part, the silicate and phosphate associates of the oxide minerals are defined by the unit in which the minerals occur. However, it is not unusual to find small bodies within larger units that are atypical in mineralogy for the unit, for example, small (1 to 3 m) lepidolite bodies in the central intermediate unit, and small to extensive saccharoidal albite bodies in all of the intermediate units. In cataloguing, when a sample was found to have a silicate mineralogy atypical for the unit (and mapping errors were ruled out), it was assigned the unit number of the observed or inferred enclosing unit, yet a note was made of the mineralogy of the association.

The associated silicate matrix was categorized as either
(1) Coarse-grained K-feldspar plus quartz with lesser amounts of saccharoidal or cleavelanditic albite with or without muscovite, apatite, beryl, or in the case of units (4) and (5), amblygonite and SQI. These associations

are typical of units (2),(4) and (5), the distinctions between which are described in the previous sections. Oxide minerals in these units are normally associated with the albite.

(2) Saccharoidal albite plus quartz with lesser amounts of muscovite-lepidolite, tourmaline, beryl and apatite. This association is typical of unit (3), but, at least on a small scale, it is found in most units of the pegmatite. Typical occurrences of this association are layered: variations in the modes of silicate and oxide minerals produce well-defined mm- to cm-scale layering. The layering is typical of saccharoidal albites in many granitic pegmatites. Its origin is unknown; rhythmic crystallization (Jahns & Tuttle, 1963), metasomatic front progression (Crouse et al., 1979) and crystallization from a gel medium (Stone, 1969) are possible mechanisms.

(3) Coarse-grained K-feldspar (plus quartz) partially to completely hydrolized to muscovite. This association is typical of unit (6) of the eastern flank (to central regions) of the pegmatite. Wodginite is a frequent oxide member of this association. Smaller occurrences of this association overlie or rim saccharoidal albite, perhaps marking a hydrolized precursor to Na-metasomatism, or perhaps instead marking a reaction rim between a corrosive Na,F-rich primary melt parental to the saccharoidal albite, and adjacent crystalline material.

(4) Lepidolite to lithian muscovite plus quartz which largely replaces K-feldspar plus quartz. This assemblage can be recognized by its violet to violet-grey colour, and is the assemblage typical of unit (9). Smaller bodies are often found in units (4) to (6). The assemblage is typically less rich in oxide minerals than the other three.

18.5 WODGINITE GROUP MINERALS

At Tanco, wodginite-group minerals range in colour from black (ferroan titanowodginites) to orange-yellow (tantalowodginites). Crystals range from less than 1/10 mm to 2 cm in size, and are usually subhedral. Wodginite-group minerals are readily distinguishable in hand-sample from ferrotapiolites by their yellow to brown streak, as opposed to red streak. Well-developed crystals of wodginite-group minerals can be distinguished from those of columbite-group minerals by their dominantly bipyramidal, as opposed to tabular morphologies. Ambiguities can be further resolved by optical examination: wodginite-group minerals are usually sector-twinned, unlike columbite-group minerals. Failing this, X-ray identification, coupled with microprobe analysis is exact.

Compositional data for Tanco wodginites are presented in Appendix D, Table 106. Cursory examination of this table shows that wodginite-group minerals of the Tanco pegmatite vary considerably in composition: wodginites, titanowodginites, ferrowodginites and tantalowodginites are all present. The extent of this variability is shown in Figure 57, which illustrates the result of a principal component analysis of compositional data for all non-Tanco wodginites. The first and second principal components were calculated from the eigenvectors taken from the variance-covariance matrix, and together account for 87% of all of the variability in the chemistry of non-Tanco wodginites. The eigenvectors of Table 82 show that the first principal component corresponds mainly to Mn$\Leftrightarrow$Fe substitution, with Fe increasing as the principal component does. The second principal component corresponds mainly to Sn$\Leftrightarrow$Ta substitution, with Ta increasing as the principal component does. As can be seen from Figure 57,

Tanco wodginites show even more variability in their chemistry than the global sample, indicative of how extensive changes in transition metal geochemistry were during crystallization of the Tanco pegmatite.

In addition to crystal-chemical trends of the wodginites outlined in Part 3, the Tanco wodginite-group minerals also show geochemical trends. The strongest of these (R = -0.80) is an antipathetic decrease in the Ti contents of the wodginites and increase in their Ta/(Ta+Nb) ratios (Figure 58). From what is known of normal chemical zonation in Ta-Nb oxide minerals from granitic pegmatites, earliest-formed oxide minerals tend to be Ti-enriched and Nb-enriched (with respect to Ta) (Černý & Ercit, 1985); efficient fractionation results in Ta-enriched compositions. Wodginite-group minerals of the saccharoidal albite unit (3) cluster near the Ti-rich and Ta/(Ta+Nb)-low end of the plot, whereas intermediate unit (4,5,6) wodginite-group minerals cluster near the low-Ti, Ta/(Ta+Nb)-high end of the plot. Wodginite-group minerals from the saccharoidal albite unit seem to represent a less-fractionated source than those from the intermediate units, a conclusion compatible with the results of other studies of the internal zoning of the Tanco pegmatite.

Structural data for Tanco wodginites were presented in Chapter XII. There it was shown that $\underline{a}$ and $\underline{b}$ are strongly compositionally dependent, $\underline{c}$ is in part composition and order dependent, and $\underline{V}$ and β are strongly order-dependent. The degree of order of Tanco pegmatite wodginite-group minerals was calculated for samples in which either compositional plus structural data, or structural data for both the heated and unheated states were available. Figure 59 is a plot of the degree of order of these wodginite-group minerals, showing the ranges and means for each unit of the pegma-
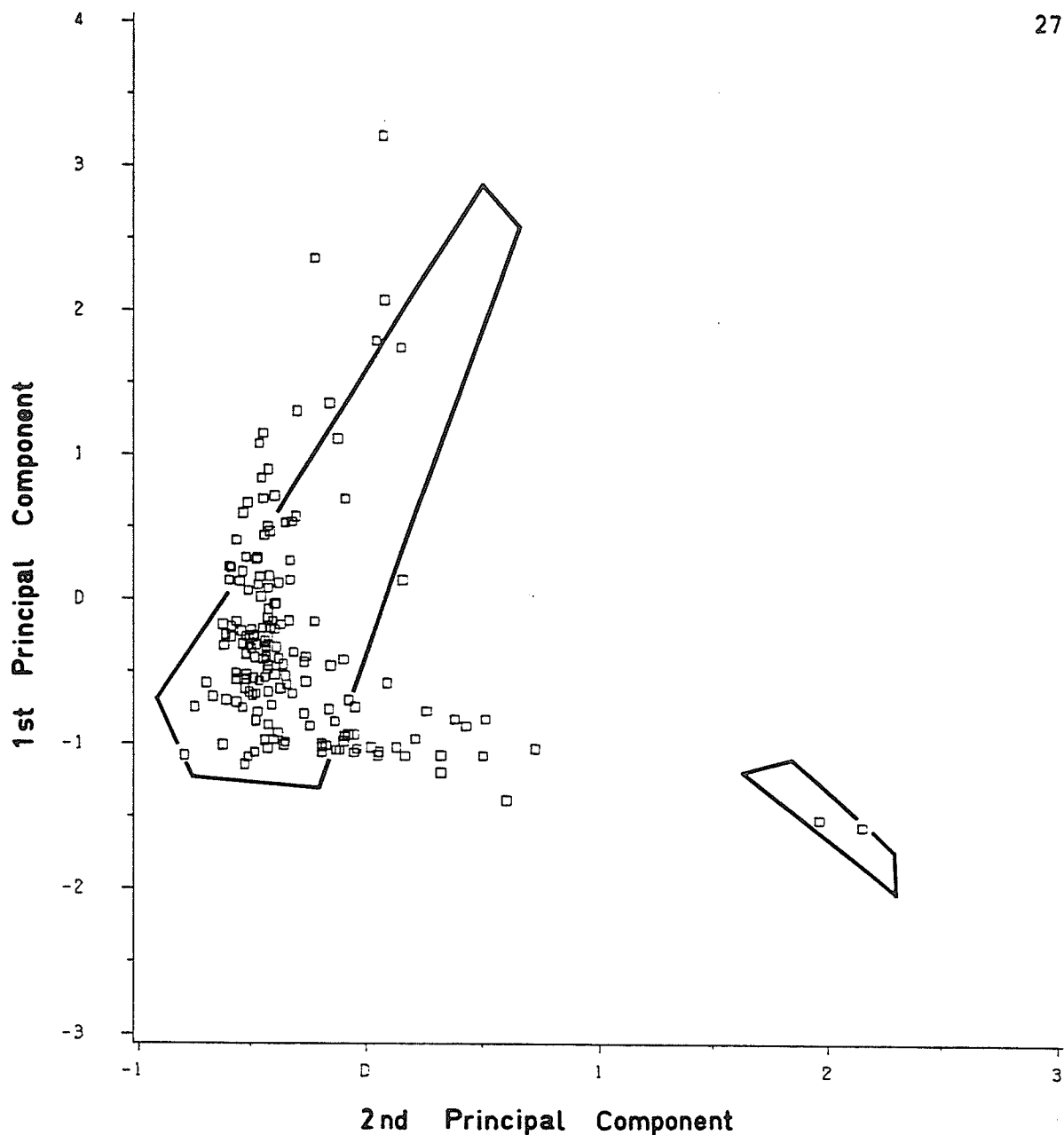
<u>Figure 57</u>: Principal component analysis   of wodginite-group minerals.
Principal components were calculated from chemical data for
non-Tanco wodginites, and eigenvectors are given in Table 82.
The 1st principal component corresponds mainly to Mn→Fe sub-
stitution, and the 2nd p.c. corresponds mainly to Sn→Ta sub-
stitution.   Datapoints are Tanco pegmatite samples; the out-
lined field, all other wodginite-group minerals.

Table 82: Principal Component Analysis of Wodginite-Group
Minerals: Eigenvectors

	Principal Component				
	1st	2nd	3rd	4th	5th
Fe^{2+}	0.834	0.173	-0.414	-0.176	-0.268
Ti	0.278	0.032	0.022	0.928	0.244
Fe^{3+}	0.158	-0.057	-0.186	-0.284	0.926
Ta(B)	-0.268	0.937	-0.210	0.034	0.071
Nb	0.360	0.297	0.866	-0.161	0.817
$\Sigma\ s^2$	0.66	0.87	0.94	0.99	1.00

$\Sigma\ s^2$: cumulative proportion of variance (1st→5th
principal component).

tite. Means for the units were as follows: saccharoidal albite unit –
62%, lower intermediate unit – 80%, upper intermediate and pollucite units
– 92%, central intermediate unit – 98% order. To generalize, the saccharoidal albite unit shows lower degrees of order than all other intermediate units plus the pollucite unit; it is concluded that the degree of order of the wodginite-group minerals increased with crystallization of the pegmatite.
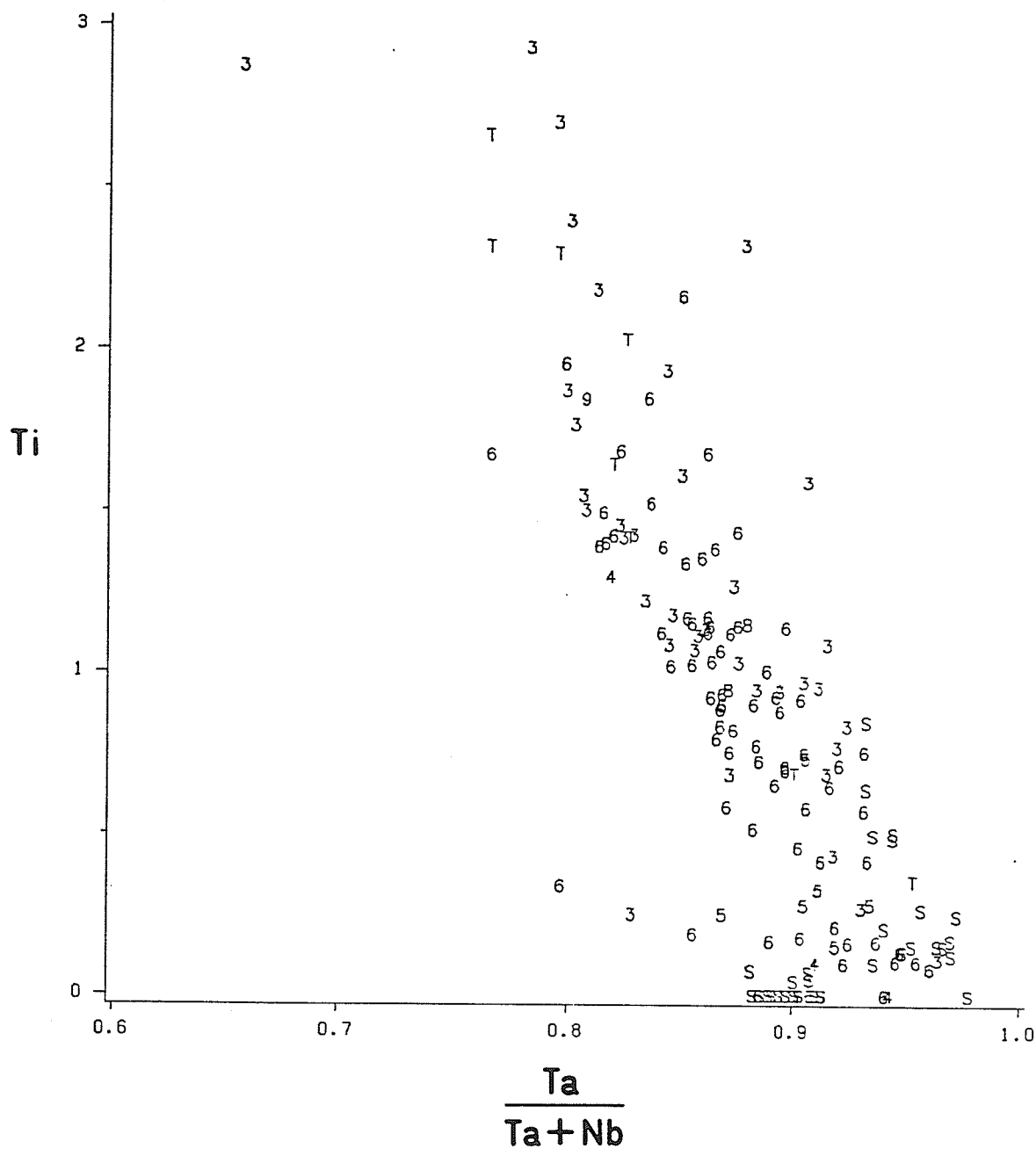
Figure 58: Plot of Ti versus Ta/(Ta+Nb) for Tanco wodginite-group miner-
als.   Numbers refer to units of the pegmatite, "S" refers to
members of the simpsonite paragenesis and "T" means undesignat-
ed.
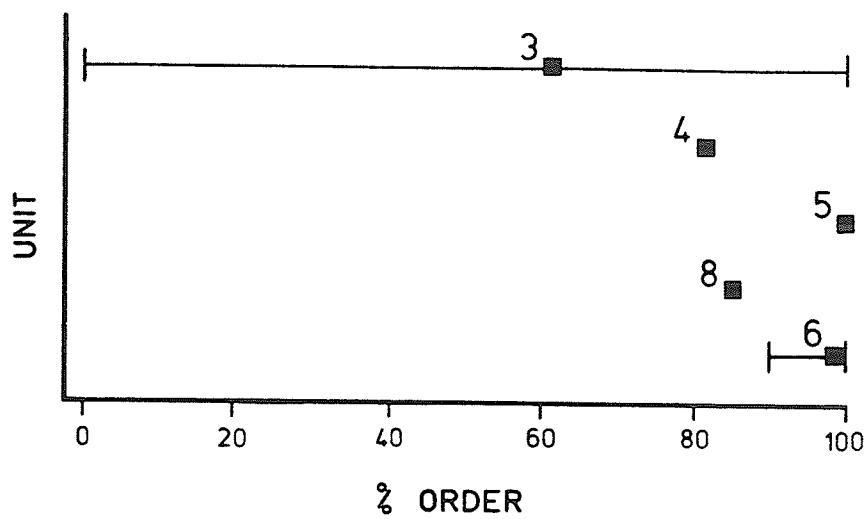
Figure 59: Relationship of the degree of order of wodginite-group minerals to zoning of the Tanco pegmatite. Squares are means, and bars are ranges of the degree of order for each unit.

18.6 COLUMBITE-GROUP MINERALS

The physical properties of columbite-group minerals of the Tanco pegmatite vary considerably. Columbite-group minerals from the wall unit are intergrown with cassiterite and form coarse-grained ($\geq$ 5 mm) radiating aggregates of tabular crystals. Crystals from the saccharoidal albite unit are most typically anhedral, as partially replaced relicts and inclusions in microlite. Those from the lower and upper intermediate units are typically euhedral to subhedral, tabular subparallel growths of crystals, often to 5mm or more in size. In the central intermediate and lepidolite units, columbite-group minerals are much finer-grained (typically less than 1 mm), and are equant to bladed and subhedral to euhedral. Most varieties of columbite-group minerals throughout the pegmatite are dark brown to black with a dark greenish-brown streak; however, some uncommon Ti,Nb,Fe-poor varieties in the central intermediate unit are pale brown to brown-yellow with pale brown streaks.

Because they are the most widely distributed of all the Ta-oxide minerals, compositional-structural variations of this group are potentially of the greatest importance. Compositional data for Tanco columbite-group minerals are presented in Appendix D, Table 107. With the exception of one sample (TSE-55: ferrocolumbite), all are manganocolumbites to manganotantalites. Most are titanian; TSE-82 is Ti-richest with 0.95 Ti atoms per unit cell. Most are also stannian; however, Sn contents are generally lower than Ti contents. Some samples are scandian, particularly samples from units (2) and (3); Sc reaches a maximum of 0.29 atoms per unit cell (sample TSE-94).

Figure 60 is a plot of Tanco columbite-group mineral compositions in the columbite quadrilateral; there is strong clustering of samples from different units into different regions of the plot.   Wall-unit columbites show the least amount of compositional variability, and cluster in a region of high Mn/(Mn+Fe) (appx. 0.80 to 0.95) and low Ta/(Ta+Nb) (appx. 0.42 to 0.50).   Columbite-group minerals from the saccharoidal albite unit show a similar, but wider range of Ta/(Ta+Nb) values, and include three samples with Ta/(Ta+Nb) lower than any unit (2)   sample.   Furthermore,   the Mn/(Mn+Fe) ratios of unit (3) samples average 25 atomic % lower than unit 2 samples of similar Ta/(Ta+Nb), and in general are the lowest for columbite-group minerals of the pegmatite.   Upper and lower intermediate unit and lepidolite unit columbite-group minerals have slightly higher Mn/(Mn+Fe) ratios and significantly higher Ta/(Ta+Nb) ratios (to 0.70) than wall-unit samples, and cluster near the high-Mn,   high-Ta ends of their fields as drawn in Figure 60.   Central intermediate unit samples, on the whole, have higher Ta/(Ta+Nb) ratios (0.65-1.00) than all other units, yet Mn/(Mn+Fe) ratios are similar to these units. Samples from the simpsonite paragenesis plot at the high-Ta end of the field for samples from the central intermediate unit.

The strong degree of clustering and the trends in the chemistry of the samples imply that either the columbite-group minerals are primary and reflect primary differences in the geochemistry of the units,   or that if they are largely metasomatic in origin, they are derived from fluids which were themselves quite local in derivation; such fluids were derived from each unit, and not solely from the last unit(s) to crystallize.
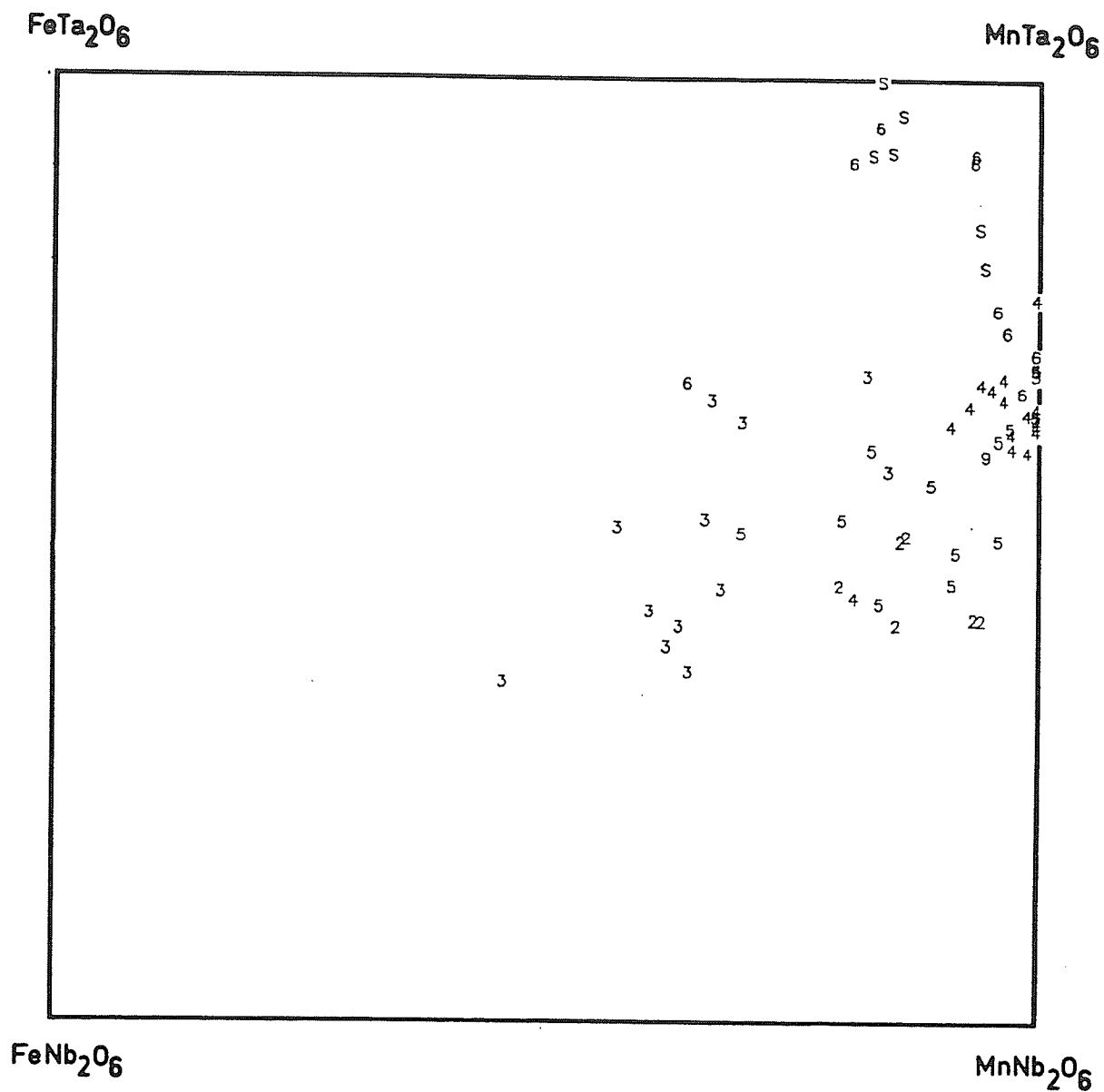
Figure 60: Distribution of Tanco pegmatite columbite-group minerals within the columbite quadrilateral. See Figure 58 for an explanation of the symbols.

On the basis of the expected crystallization sequence of the units, it would seem that earliest-crystallized units, and their possible autometasomatic products have lower Ta/(Ta+Nb) ratios than successively later units, and that, as a gross generalization, Mn/(Mn+Fe) also increased with crystallization. The most notable exceptions to this trend are columbite-group minerals of unit 3, and those of the simpsonite paragenesis.

Because columbite-group minerals are not the only Ta-Nb-Sn-Ti oxide minerals of the pegmatite, and certainly not the only Mn,Fe-minerals of the pegmatite, cation partitioning effects must be taken into consideration before Figure 60 can be fully interpreted. Data given later in this chapter show that although microlites and wodginite-group minerals partition Nb and Ta equally, the columbite-group minerals show a marked preference for Nb over Ta relative to the former two mineral groups. The lower Ta/(Ta+Nb) ratios of some unit(3) samples, as compared to all unit (2) samples most probably is a result of microlite and wodginite co-crystallization with tantalite in unit (3), contrasted with only columbite (plus cassiterite) crystallization in unit (2). Also along this line, the samples which cause the upper and lower intermediate unit stability fields to overlap with the wall unit field have associated microlite; all other samples have much higher Ta/(Ta+Nb) and many, if not most, of these have no associated microlite or wodginite.

Unfortunately, because Fe-Mn partitioning between oxide minerals and Mn-Fe silicates (e.g. tourmalines) and phosphates (e.g. triphylite-lithiophyllite) is not known at all, differences in Mn/(Mn+Fe) between the units cannot be properly interpreted.

Trends in minor versus major element chemistry are shown in Figure 61. Data for Sn are not shown because the Sn contents of columbite-group minerals are erratically variable – they do not vary with pegmatite zonation, nor correlate with other changes in columbite-group mineral chemistry. However, strong correlations exist between Sc plus Ti and some major elements. Sc and Ti both decrease as Ta/(Ta+Nb) increases, dropping sharply over the range Ta/(Ta+Nb)=0.35 to 0.65, and levelling off to near-zero values over Ta/(Ta+Nb)=0.65 to 1.00. Wall unit and saccharoidal albite unit columbite-group minerals are Sc,Ti-richest, followed by those from the upper and lower intermediate units and the lepidolite unit, in turn followed by those from the central intermediate unit, which are Sc-free, and poorest in Ti. Columbite-group minerals from the simpsonite paragenesis are Sc-free and depleted to devoid of Ti. This trend implies that for the columbite-group minerals of the Tanco pegmatite, Ti and Sc are good fractionation indicators, high Sc and Ti contents marking low degrees of fractionation, and low contents marking moderate to high degrees of fractionation. However, as Figure 61 shows, the Sc and Ti contents do not vary linearly with fractionation, thus very low Sc and Ti contents do not necessarily imply extremes in fractionation.

Unit cell dimensions for Tanco columbite-group minerals are given in Table 83. In addition to these data, degrees of order are given, calculated from the values of a and c, as described in Chapter XVI. Figure 62 is a plot of the degree of order of Tanco columbite-group minerals, showing ranges and means for each unit. As can be seen from the plot, Tanco columbite-group minerals range from completely disordered (e.g. TSE-42) to completely ordered (e.g. SMP-12); however, few samples are partially
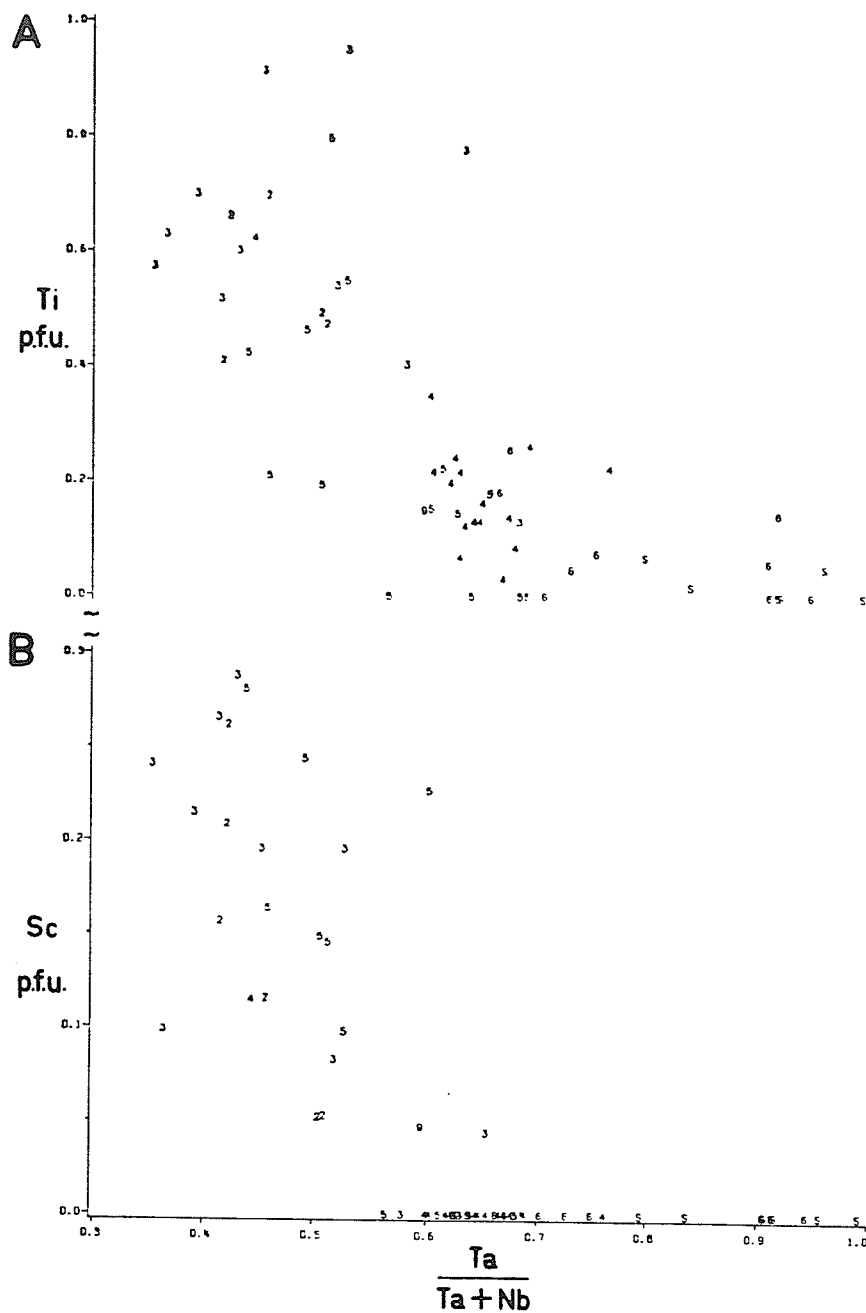
Figure 61: Major element – trace element correlations for Tanco columbite-group minerals. (a) Ti versus Ta/(Ta+Nb), (b) Sc versus Ta/(Ta+Nb). See Figure 58 for an explanation of the symbols.

ordered.   Samples from the wall unit and lower intermediate unit show 10%

or less order.   Most samples from the upper intermediate unit approach

intermediate degrees of order (to 45%), and one sample is fully-ordered.

Samples from the central intermediate unit show much higher degrees of

order (70-95%).   From what is known of the sequence of crystallization of

the units, it is evident that earliest-formed units have columbite-group

minerals with low degrees of order,   and as crystallization advances,

columbite-group minerals of successive units   attain successively higher

degrees of order.

Comparison of Figure 59 with Figure 62 shows that wodginite-group miner-

als of any given unit tend to be more highly ordered than the columbite-

group minerals from the same unit.   Wodginite-group minerals achieve high

($\geq$ 80%) degrees of order by the time of unit (3) crystallization, whereas

columbite-group minerals do not reach the same point until unit (5) crys-

tallization.

The cause of variable degrees of order in columbite-group and wodginite-

group minerals is unknown (Černý & Ercit, 1985).   On the basis of the good

correlation between internal zoning of the pegmatite and the degree of

order of these species, it is tempting to speculate that crystallization

rate plays a significant role. If these oxide minerals are primary in ori-

gin, then the crystallization histories of the different units should pro-

vide the answers.   The low degrees of order of unit (2) and unit (3)

columbite-group and wodginite-group minerals might be a consequence of the

faster rates of crystallization in the outermost regions of the pegmatite,

which, theoretically, should be the fastest-cooling parts of the pegmatite.

The higher degrees of order in oxide minerals from the intermediate units,

Table 83: Unit Cell Dimensions (Å) and Degrees of Order for Columbite-Group Minerals from the Tanco Pegmatite

Sample	a	b	c	V	% Order
		Natural			
G69-30	4.759(1)	5.750(1)	5.159(1)	141.2(1)	0
G69-31	4.758(2)	5.750(2)	5.162(2)	141.2(1)	0
G69-53	14.415(8)	5.754(2)	5.116(2)	424.4(1)	70
G69-55	4.763(1)	5.753(1)	5.157(1)	141.3(1)	5
G69-56	4.761(1)	5.752(1)	5.155(1)	141.2(1)	5
G69-58	14.403(1)	5.759(2)	5.105(2)	423.5(1)	80
G69-60	4.766(1)	5.753(2)	5.153(2)	141.3(1)	10
G69-61	4.762(1)	5.755(1)	5.158(1)	141.4(1)	5
SMP-12	14.410(1)	5.760(1)	5.090(1)	422.5(1)	95
TSE-39	4.745(1)	5.731(1)	5.142(1)	139.8(1)	10
TSE-42	4.763(1)	5.753(1)	5.162(1)	141.4(1)	0
TSE-51	4.764(2)	5.750(2)	5.153(2)	141.1(1)	10
TSE-52	14.298(2)	5.746(1)	5.131(1)	421.6(1)	30
TSE-54	4.750(2)	5.729(2)	5.145(1)	140.0(1)	10
TSE-56	4.758(1)	5.755(2)	5.160(1)	141.3(1)	10
TSE-114	4.746(1)	5.729(1)	5.147(1)	140.0(1)	5
TSE-123	4.759(1)	5.749(1)	5.149(1)	140.9(1)	10
TSE-146	4.758(1)	5.753(1)	5.160(1)	141.3(1)	0
TSE-147	4.762(1)	5.757(1)	5.166(1)	141.6(1)	0
TSE-154	4.741(1)	5.734(1)	5.141(1)	139.8(1)	5
TSE-155	4.758(1)	5.749(1)	5.159(1)	141.1(1)	0
TSE-157	14.316(2)	5.753(1)	5.141(2)	423.4(1)	25
		Heated			
G69-30H	14.405(2)	5.757(1)	5.090(1)	422.2(1)	95
G69-55H	14.418(2)	5.760(2)	5.091(1)	423.0(1)	95
G69-58H	14.430(2)	5.763(2)	5.091(1)	423.4(1)	100
G69-60H	14.430(2)	5.765(1)	5.093(1)	423.8(1)	95
G69-61H	14.439(5)	5.765(2)	5.096(1)	425.2(1)	95
TSE-42H	14.419(2)	5.759(1)	5.092(1)	422.8(1)	95
TSE-51H	14.384(3)	5.751(1)	5.091(1)	421.1(1)	90
TSE-52H	14.393(2)	5.752(1)	5.083(1)	420.8(1)	100
TSE-56H	14.375(1)	5.747(1)	5.090(1)	420.4(1)	85
TSE-154H	14.321(2)	5.731(1)	5.076(1)	416.6(1)	90
TSE-155H	14.392(1)	5.752(1)	5.088(1)	421.2(1)	95
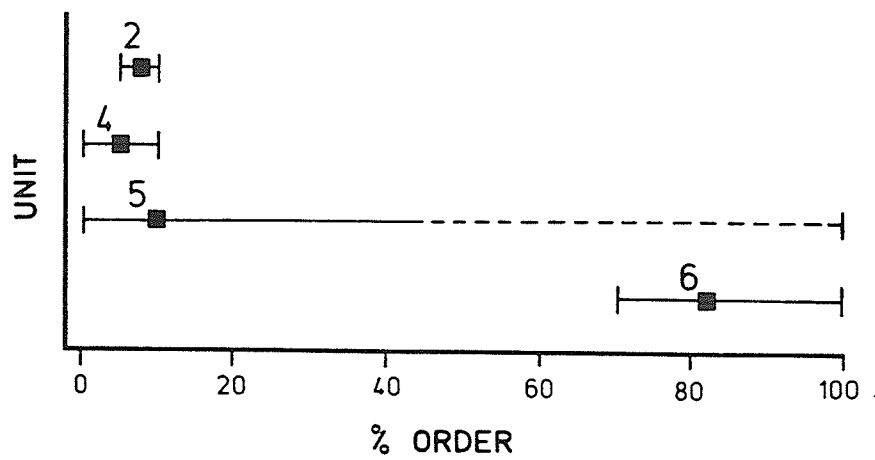
Figure 62: Relationship of the degree of order of columbite-group minerals
to zoning of the Tanco pegmatite.   Squares are means, and bars
are ranges of the degree of order for each unit.

particularly those of units (5) and (6), and also unit (8), might be due to slower rates of crystallization in the central parts of the pegmatite, where much shallower thermal gradients would have existed. Černý et. al. (1986) have suggested that contaminant elements (Ti,Sn,Sc) might play a significant role in order-disorder relationships of columbite-group minerals. Although a weak correlation exists between Ti+Sn+Sc content and the degree of order of columbite-group minerals from the Tanco pegmatite, it remains to be determined whether the high Ti+Sn+Sc contents retarded cation ordering, or are symptomatic of other factors which may control cation ordering.

18.7 PYROCHLORE-GROUP MINERALS AND CESSTIBTANTITE

The physical properties of pyrochlore-group minerals vary significantly between and within units of the Tanco pegmatite. All members belong to the microlite subgroup (Ta≥Nb; Nb+Ta>2Ti) and here on shall be collectively referred to as microlites.

Microlites from the saccharoidal albite unit are typically colourless to pale green in transmitted light, but because of inclusions of dark oxide minerals, they sometimes appear mottled and brownish at low magnification. Crystals are subhedral to euhedral cuboctahedra, and are frequently less than 0.2 mm in diameter. Microlites from the upper and lower intermediate units and the lepidolite unit are slightly to significantly darker than others; some uranmicrolites from the lepidolite unit are black. Microlites from the lepidolite unit are typically slightly larger than those from the saccharoidal albite unit; 1 to 2 mm crystals are not atypical. The crystals are also "cleaner" than those from the saccharoidal albite unit, con-

taining inclusions only in rare cases, suggesting that the microlites of
this unit do not tend to replace other pre-existing oxides. Microlites
from the central intermediate unit have variable properties. They range
from colourless and transparent to green or brown and translucent to pale
orange (cesstibtantite). They are sometimes colour-zoned; uranian microl-
ites from the simpsonite paragenesis have green cores with sharply-defined
oscillatory-zoned green and brown rims. They range in size from approxi-
mately 0.2 to 8 mm; smaller sizes are the norm for the pegmatite. Most are
euhedral; however, less well-developed crystals are not unusual.

Compositional data for the microlites are presented in Appendix D, Table
108. Most species are microlite; cesstibtantite is much rarer and uranmi-
crolite even more so. Microlite exists in a number of varieties: stanni-
an, uranian, antimonian and plumbian. The varieties show strong preferenc-
es for different units (Table 84). Stannian, uranian and antimonian
varieties are typical of the saccharoidal albite unit, whereas common
microlite is very rare in this unit. Uranian microlites are typical of the
upper intermediate and lepidolite units, which are devoid of stannian and
antimonian varieties, and rarely have common varieties. The central inter-
mediate unit has mainly common microlite with lesser amounts of uranian
microlite; antimonian microlite and cesstibtantite are rare.

Figure 63 is a plot of the $\underline{B}$-site constituents of Tanco microlites.
Although the degree of scatter of the data is high, a well-developed neg-
ative correlation exists between Ti content and Ta/(Ta+Nb). Microlites
from the saccharoidal albite unit plot near the top of the trend (high Ti
contents and low Ta/(Ta+Nb) ratios), whereas unit (6) microlites tend to
plot nearer to the base (low Ti contents and high Ta/(Ta+Nb) ratios). Once

Table 84: Mean A-Site Contents of Microlites and Cesstibtantites

Internal Unit	No. Samples	U	Pb	Sb	Cs	Sn	¤
3	32	0.05	0.02	0.06	0.00	0.03	0.23
5	5	0.13	0.02	0	0	0	0.92
6	21	0.02	0.03	0.06	0.03	0	0.35
9	6	0.13	0.07	0	0	0	0.44

Contents on a basis of 2 B-cations.
"0": not detected

again, as with the wodginite-group and columbite-group minerals, a strong correlation exists between internal unit versus $Ti:Ta/(Ta+Nb)$, which indicates that the earliest-formed microlites tend to be Ti- and Nb-richest, and that with fractionation, the trend is toward Ta-enrichment at the expense of Nb and Ti (Figure 63).

Unit cell edges were determined for several Tanco microlites, and are given in Table 85. In general, the cell edges seem to vary only slightly; excluding cesstibtantite, the maximum and minimum values are 10.405 and 10.438 Å. In his study of the compositional-structural systematics of synthetic pyrochlores, Chakoumakos (1984) was able to predict the unit cell edge of pyrochlores to ±0.01 Å. Unfortunately, the results of this study cannot be practically applied here: the cell edge variation for Tanco microlites is only marginally greater than the precision of Chakoumakos' (1984) method. Furthermore, metamictization may affect the unit cell edges of several of the Tanco microlites, and its effects cannot yet be predict-
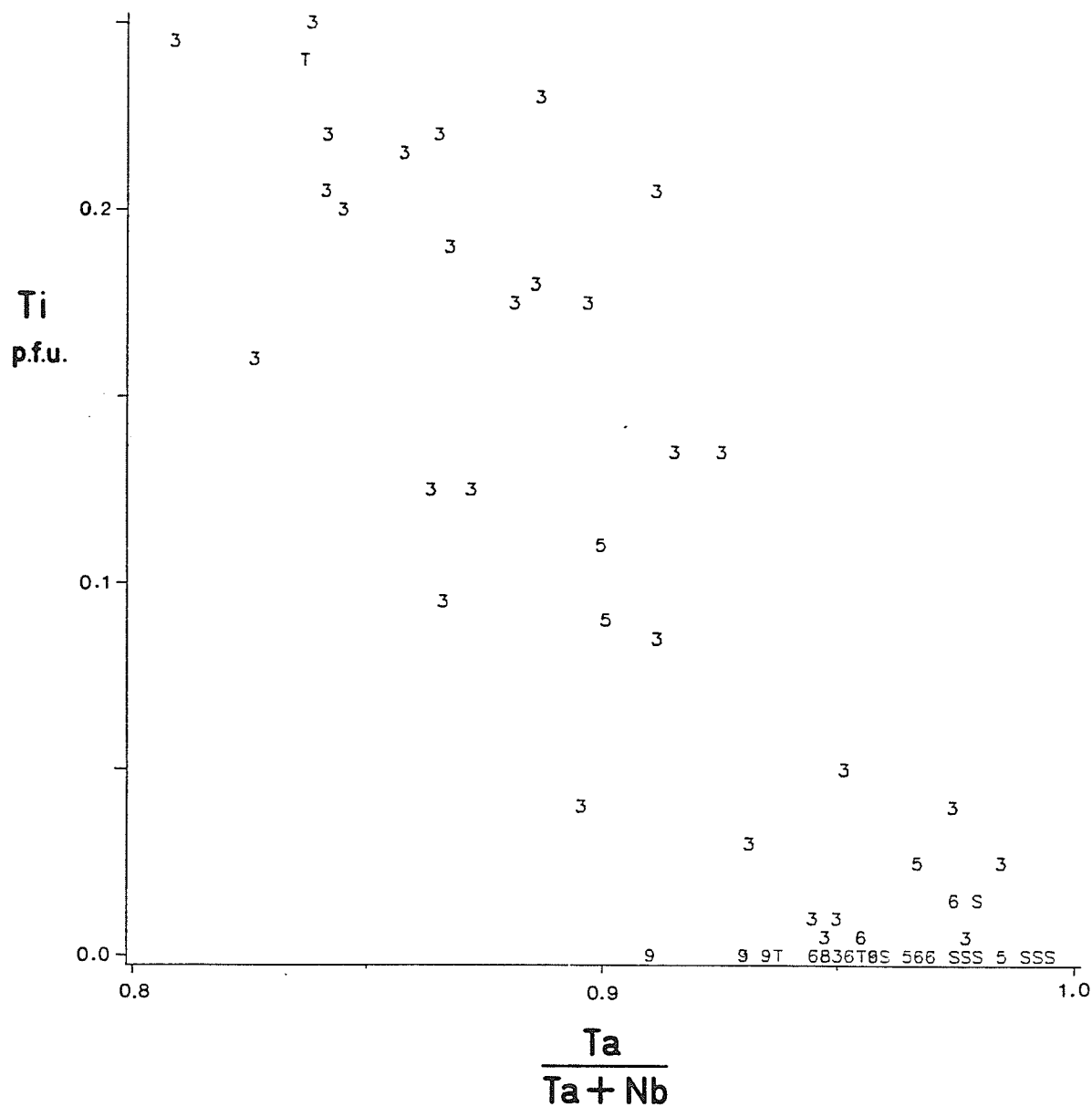
Figure 63: Tanco microlites: variation in B-site major-element chemistry. See Figure 58 for an explanation of the symbols.

ed.   Consequently, the variations in the unit cell edges of the microlites
were not assessed in this study.

Table 85: Unit Cell Dimensions for Microlites and Cesstibtantites
from the Tanco Pegmatite

Sample	a	Sample	a
SMP-4	10.4351(2)	TSE-55	10.402(1)
SMP-6	10.433(2)	TSE-72	10.420(1)
SMP-6*	10.497(1)	TSE-95	10.4144(5)
SMP-51	10.426(4)	TSE-97	10.408(1)
TSE-1f	10.4293(5)	TSE-104	10.420(2)
TSE-5	10.4329(7)	TSE-132	10.4262(4)
TSE-9	10.4170(5)	TSE-134	10.430(2)
TSE-10	10.4185(8)	TSE-137	10.4375(7)
TSE-35	10.4308(4)	TSE-138	10.4199(2)
TSE-48	10.405(1)		

* cesstibtantite

18.8   CASSITERITE

Tanco cassiterites are almost always fine-grained (<1mm), and are usual-
ly euhedral.   Crystals range from being dominantly acicular (saccharoidal
albite unit) to dominantly bipyramidal (lepidolite unit).   The cassiterites
are usually a vitreous dark brown, but some from the saccharoidal albite
unit are a submetallic black.   Thin sections show the brown crystals to be
nearly colourless but with brown rims.   The brown regions do not have sharp
contacts with the colourless ones, and look like oxidation rims.

Electron microprobe analyses of the cassiterites are given in Appendix
D, Table 109.   Although ideally SnO_2, cassiterites from Tanco are usually
tantalian (to 12.4 % Ta_2O_5) and ferroan (to 1.7 % FeO), and rarely niobian

(mean Nb_2O_5 = 0.1 %) or manganoan (mean Mn = 0.3 %). Despite the variability of their chemistry, the cassiterites show no obvious correlations between composition and distribution. Even statistical tests (e.g. discriminant analysis) failed to indicate any correlations.

Figure 64 is a plot of Fe+Mn versus Ta+Nb for the cassiterites. A least-squares fit to the data gives a slope of 0.47(2) which indicates that most Fe+Mn and Ta+Nb enter the cassiterite structure as a tapiolite component, $(Fe,Mn)(Ta,Nb)_2O_6$. Excluding Ti, which is a minor constituent of the cassiterites, nearly all variability in Tanco cassiterites can be ascribed to cassiterite-tapiolite solid solution. The maximum amount of tapiolite component soluble in the cassiterite structure for Tanco samples is 4.9 mol.% .

Despite the chemical variability, the unit cell parameters of the cassiterites are nearly invariant. The range in $\underline{a}$ is only 7σ, and in $\underline{c}$ is only 5σ. This is easy to rationalize: the weighted mean cationic radius for ferrotapiolite is 0.69 Å (Shannon, 1976), identical to the ionic radius of six-coordinated Sn^{4+}; thus ignoring differences in cation order, substitution of even substantial amounts of a tapiolite component into the cassiterite structure should only affect cell parameters slightly.
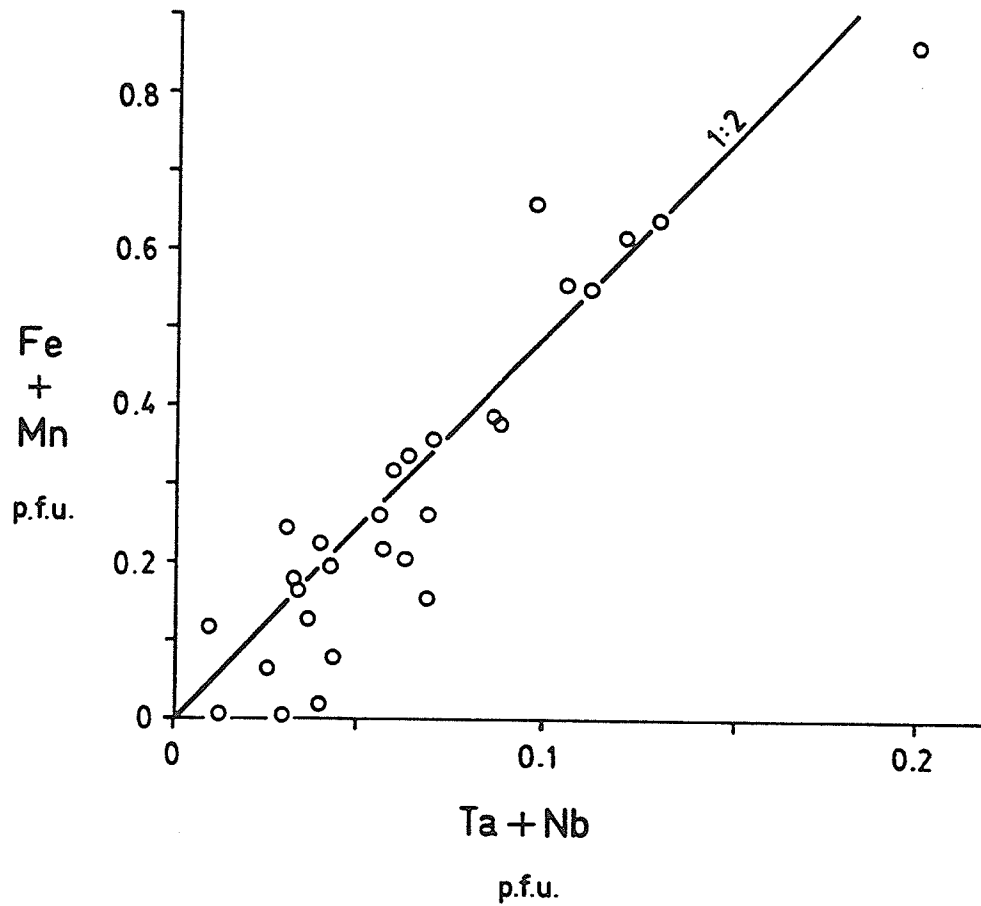
Figure 64: Plot of divalent (Fe^{2+}+Mn) versus pentavalent (Ta+Nb) cations for cassiterites from the Tanco pegmatite. The solid line marks the trend for ideal cassiterite-tapiolite solid solution.

18.9   RUTILE

Tanco pegmatite rutiles always occur as bladed, submetallic crystals of very fine grain size (often ≤ 0.2 mm). Crystals are always euhedral and single, never aggregated. Although persistent in some areas of the saccharoidal albite unit, they are never abundant. In this unit, they occur in intimate association with microlite, wodginite-group minerals, columbite-group minerals and cassiterite. In the upper intermediate unit, rutile occurs in association with microlite and columbite-group minerals, but only in triphylite-lithiophilite nodules. The large (≥ 1 cm) crystals of columbite-group minerals typical of this unit are never found with rutile.

Table 110 of Appendix D gives the chemistry of rutiles from the Tanco pegmatite. A large number of analyses gave apparently cation-excessive sums when an all-Fe^{2+} assumption was used in formula calculation; consequently, all rutile formulae were calculated by normalizing on 2 cations and 4 anions, and adjusting $Fe^{2+}:Fe^{3+}$ accordingly.

The rutiles from units (3) and (5) have similar chemistry. Both are strongly tantalian; niobium is always subordinate to tantalum. Iron is always in greater amounts than manganese. Presuming these impurities to be present as the components $FeTa_2O_6$ (ferrotapiolite) and $FeTaO_4$ (rutile-structure; Turnock, 1966), the Tanco rutiles differ from the cassiterites. They show a higher degree of solid solution with ferrotapiolite (to 13.3 mol.%), and solid solution with a hypothetical Fe^{3+}-bearing component (to 7.3 mol.%); the cassiterites show little evidence of this (Figure 65).

All Tanco rutiles occur as slender (<0.03 mm wide) tiny crystals firmly embedded in a Ta-oxide matrix. Extraction of crystals for X-ray diffraction studies has not been successful.
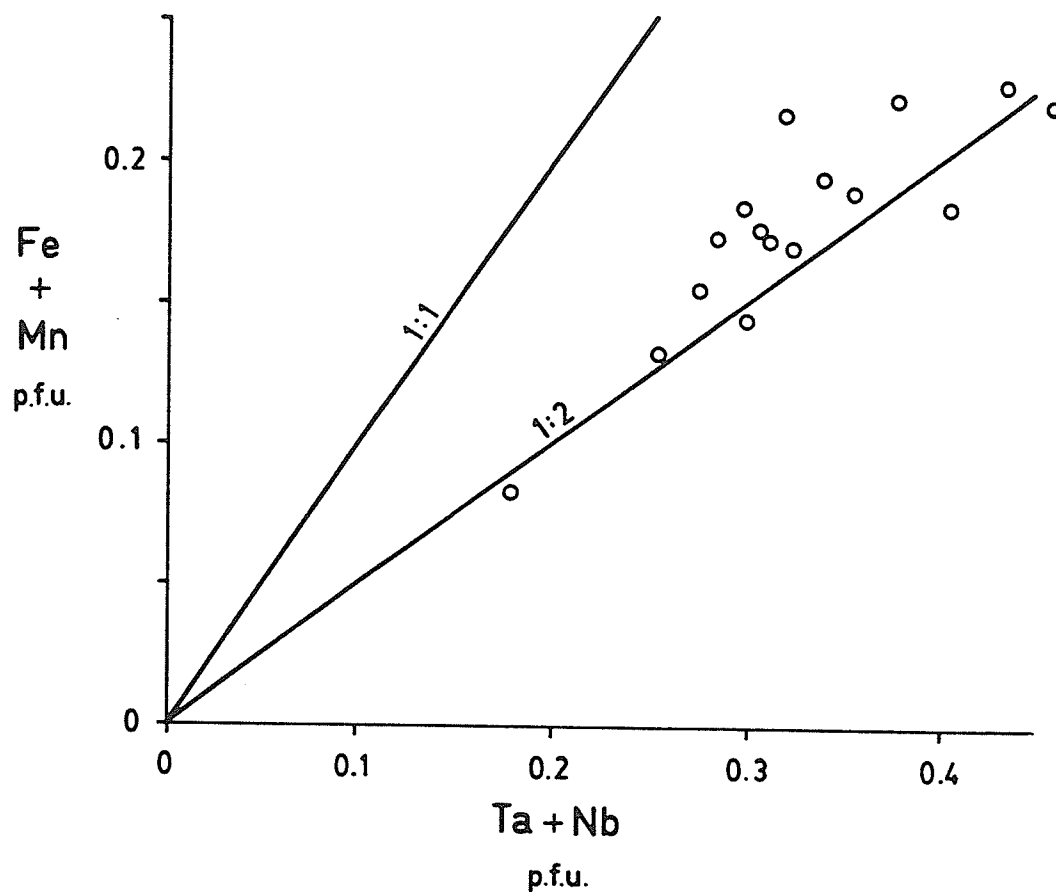
Figure 65: Plot of total (Fe+Mn) versus pentavalent cations (Ta+Nb) for Tanco pegmatite rutiles. Solid lines mark trends for ideal rutile-tapiolite solid solution (slope=0.5) versus ideal rutile-FeNbO$_4$ solid solution (slope=1). Data scatter between the curves, showing that both mechanisms affect the chemistry of Tanco rutiles.

18.10   FERROTAPIOLITE

Ferrotapiolite from the Tanco pegmatite is vitreous black and usually equant. Crystals are rarely euhedral, and most often range from subhedral to anhedral. The red streak of the mineral, its uniaxial optical character and frequent polysynthetic twinning are most useful for its identification.

All the ferrotapiolites are manganoan; Mn is least enriched in samples from the saccharoidal albite unit and most enriched in samples from the simpsonite paragenesis (Appendix D, Table 111). Figure 66 is a plot of ferrotapiolite compositions in the columbite quadrilateral. The data show that Ta/(Ta+Nb) increases with Mn/(Mn+Fe). Figure 67 is a plot of Ti versus Ta/(Ta+Nb) and Mn/(Mn+Fe). The good negative correlation indicates, once again, a consistent geochemical pattern of Ti-depletion with an increase in the ratios Ta/(Ta+Nb) and Mn/(Mn+Fe), and thus with fractionation. In contrast, Sn does not correlate with either Ta/(Ta+Nb) or Mn/(Mn+Fe), nor does it seem to vary with the units.

Because of the small amounts of material, only three sets of unit cell dimensions could be determined for Tanco ferrotapiolites (Table 86). All three samples used in cell refinement were large manganoan ferrotapiolites from the central intermediate unit of the western flank of the pegmatite. The unit cell parameters and diffraction intensities of these samples are typical for fully-ordered manganoan ferrotapiolites (M.A. Wise, pers. comm.).
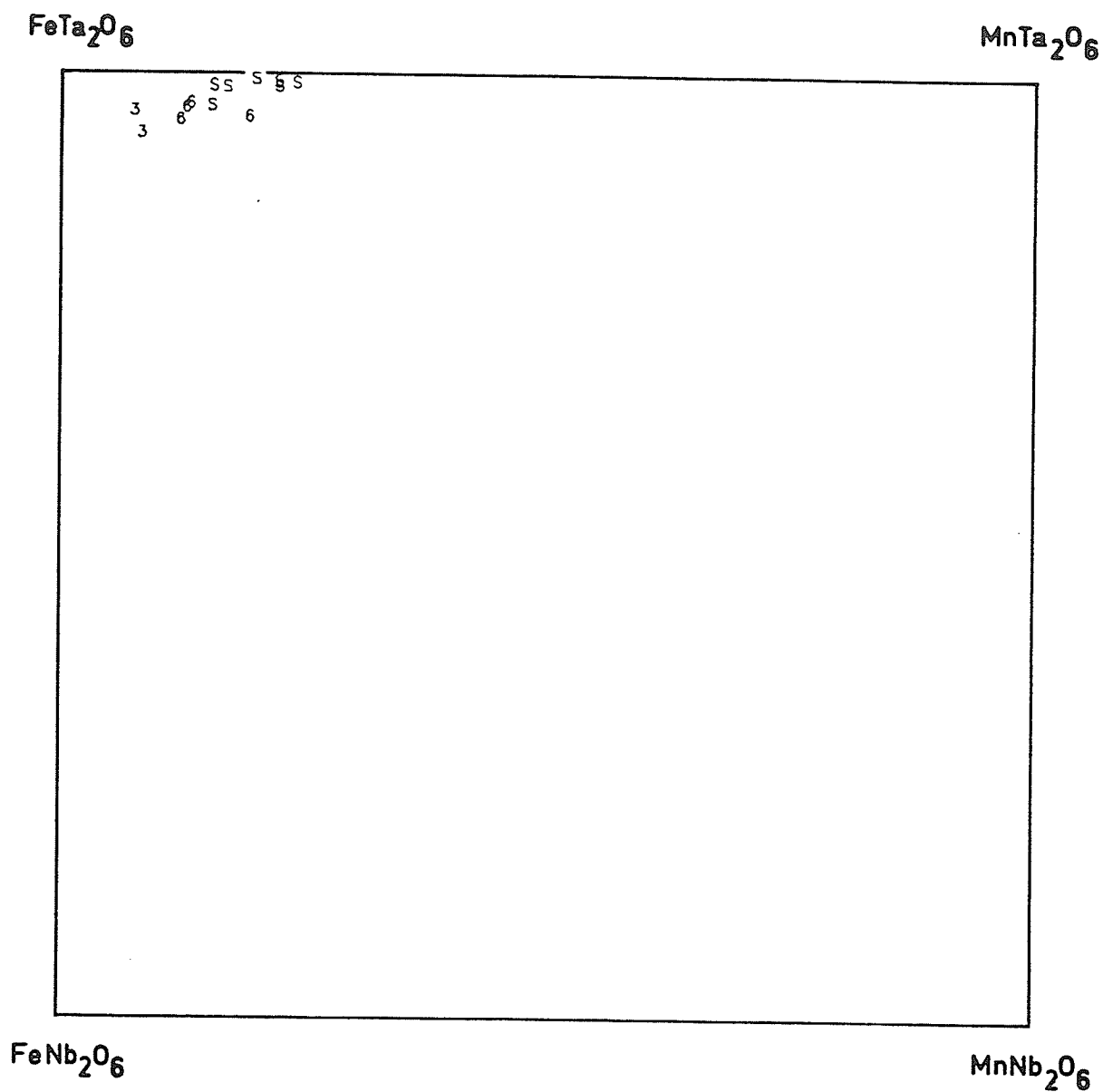
Figure 66: Distribution of Tanco pegmatite ferrotapiolites in the columbite quadrilateral. See Figure 58 for an explanation of the symbols.
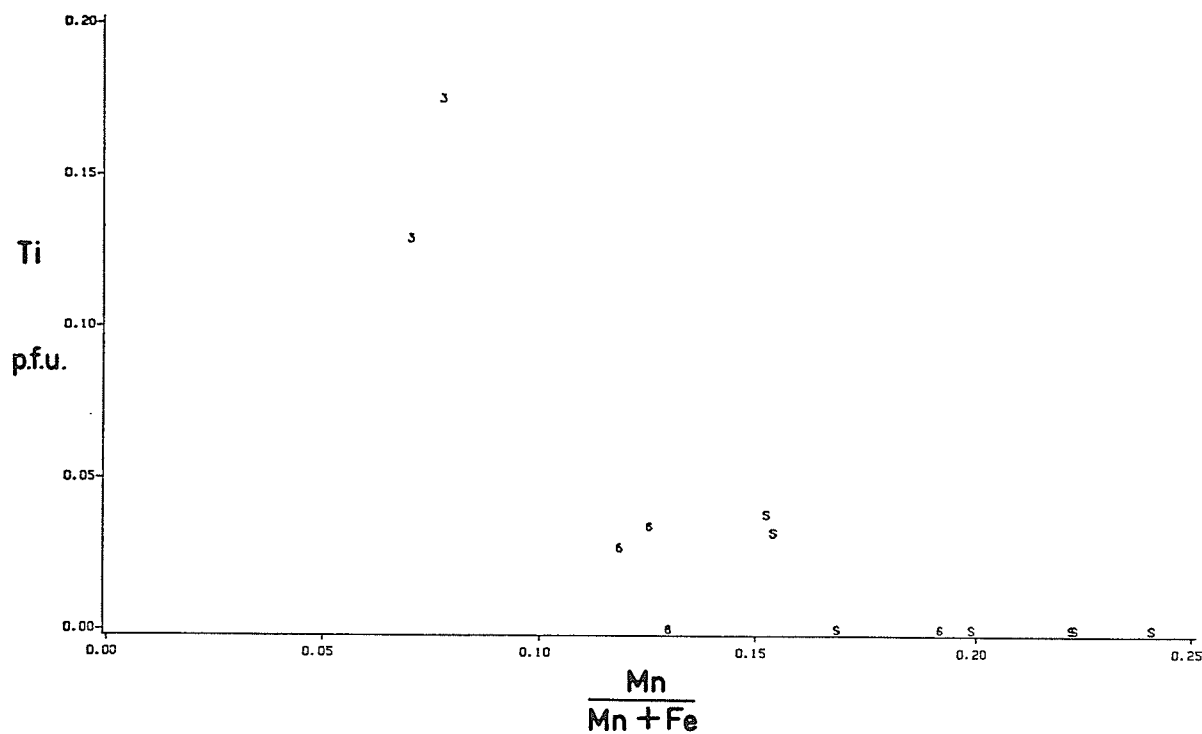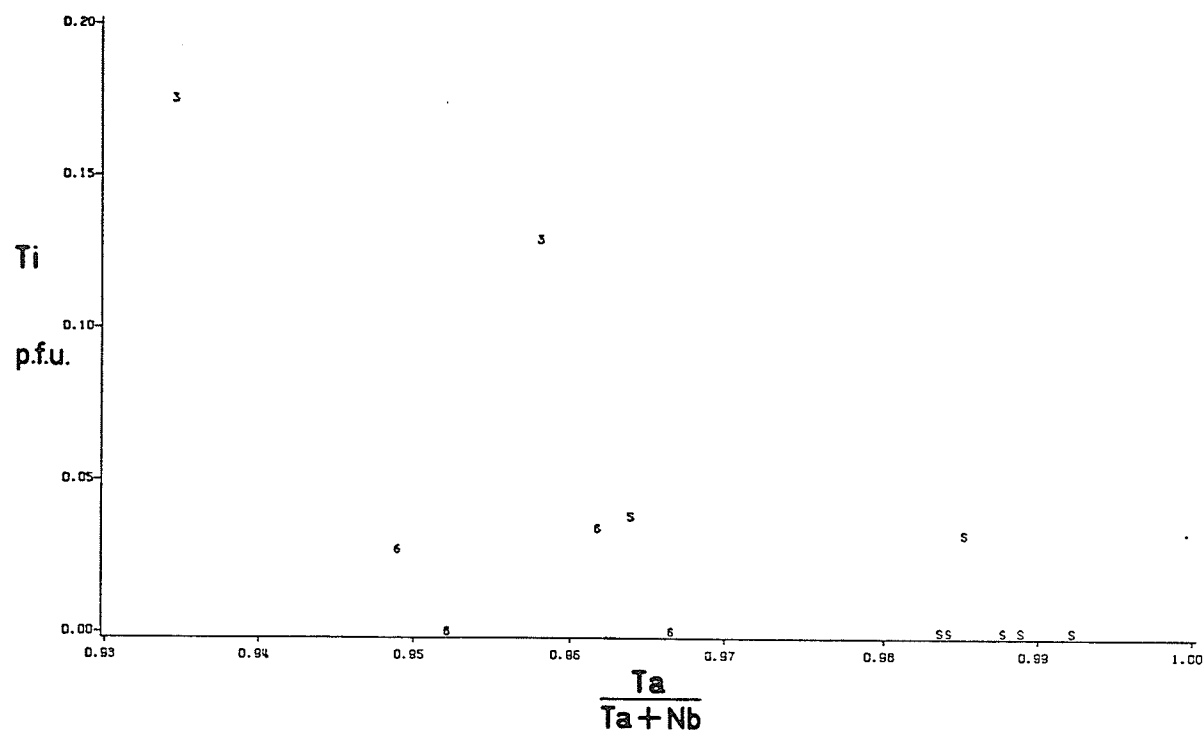
Figure 67: Correlations between Ti and major element chemistry of Tanco pegmatite ferrotapiolites. (a) Ti versus Ta/(Ta+Nb), (b) Ti versus Mn/(Mn+Fe). Numbers refer to units of the pegmatite.

Table 86: Unit Cell Dimensions for Ferrotapiolites
from the Tanco Pegmatite

Sample	a	c	V
SMP-8	4.7610(2)	9.2321(5)	209.26(2)
TSE-25	4.7594(2)	9.2163(8)	208.77(2)
TSE-29	4.7595(2)	9.2195(7)	208.85(2)

18.11   OTHERS

(1) Simpsonite

Simpsonite at Tanco ranges from colourless to pale pink, and is always transparent with a vitreous lustre.   Crystals are typically small, 0.5 mm or less, but can be as large as 8 mm.   They are simple hexagonal prisms plus basal pinacoids with variable aspect ratios, and are typically subhedral.   The strong blue-white fluorescence of simpsonite, described in Chapter VIII was used to locate occurrences of the mineral.   The physical and optical properties and chemistry of Tanco simpsonite were also described in that chapter.

(2) Uraninite

Little data exists for Tanco uraninite because it has been found in only one sample to date.   In this sample, it occurs as tiny opaque cubes, and is associated with scandian manganocolumbite and uranmicrolite.   A chemical analysis of the sample is provided in Appendix D, Table 112.   In addition to the anticipated U and Pb, it also contains minor Ta and Ca.   Because of its small size, no X-ray data were collected on the mineral; however, its morphology and chemistry leave little doubt as to its identity.   The association of the mineral with uranmicrolite strongly suggests that it formed

as a response to a locally high chemical potential for U with respect to Ca (and Ta).

(3) Ilmenite

Ilmenite was first reported by Grice (1970) from mill concentrates of Tanco Ta-ore. Neither the study of Grice (1970), subsequent unpublished work of Černý nor the present study have found the point(s) of origin of this mineral.

Ilmenite samples were taken from mill concentrates, which were themselves mined and processed at the time of this study. The identity of the mineral was confirmed by X-ray powder diffractometry, and it was subsequently chemically analyzed by electron microprobe. The results of microprobe analyses of two separate grains are given in Appendix D, Table 113. Both grains are quite simple in chemistry, containing only Ti, Mn and Fe^{2+}. Neither of the samples were found to contain Ta or Nb at microprobe-detectable levels (0.25 wt.%). The near-ideal mean cation:anion ratio of 2.007:3 indicates that the all-ferrous assumption used for formula calculation is valid.

Although little is known of the chemistry of pegmatitic ilmenites except for Černý et al. (1986) and the partial analyses of Puffer (1975), the complete lack of Ta and Nb and the inability of 15 years of searching for a pegmatitic source of the mineral suggest that ilmenite is non-pegmatitic in origin. Its presence in the concentrates may be due to amphibolite contamination during mining. Although the moderately high Mn contents might be cited as evidence to the contrary, non-pegmatitic ilmenites are sometimes as manganoan as the examples presented here (Rumble, 1976).

18.12   TANCO PEGMATITE OXIDE MINERALS: CONCLUDING REMARKS

Several trends in the geochemistry of individual oxide minerals of the Tanco pegmatite have been outlined in the previous section. Immediately evident, for all cases, is that unit to unit changes in mineral chemistry are smooth, not discontinuous. This suggests that all oxide minerals in the pegmatite formed by a common process; no gaps in the plots of mineral chemistry exist which might be attributed to a change from (primary) crystallization from the melt to (secondary) crystallization from metasomatic fluids. The alternative to this is not attractive: if oxide minerals formed by both processes, then the transition metal geochemical signature of much of the melt was insignificantly different from that of the metasomatic fluid.

Also evident is that several trends in the chemistry of any one oxide mineral are reflected in the trends of the others. This confirms that each such trend shows a strong geochemical influence and is not solely controlled by the crystal-chemistry of the individual mineral species. This point is illustrated in Figure 68, showing the mean $Ta/(Ta+Nb)$ ratio of each mineral group as a function of the unit number. This plot contains much information. First, the absolute trends for microlites and wodginite-group minerals are nearly identical, whereas that for the columbite-group minerals is quite different. This suggests that microlites and wodginites fractionate Ta versus Nb similarly, and that columbites behave much differently by preferring greater proportions of Nb. Secondly, a reasonably smooth increase in $Ta/(Ta+Nb)$ is shown from units (2) through (6) for all minerals, indicating that it is due to broad changes in the geochemistry of the parent medium, not just to differences in competition between species for

these elements. From the data presented in the sections on each mineral, it is also seen that with crystallization, U, Ti and Sc decrease in all pertinent species, and that Sb, Cs, and to an extent Mn/(Mn+Fe) increase in all pertinent species. From these data, the proposed crystallization sequence of the units, (2)-(3)-(4,5,8)-(6) is unchallenged. Data for unit (9) were too few in number to comment on its inferred position in this sequence, except to say that its oxide mineral chemistries are similar to those of units (4)-(6).

A pattern that emerged for all species of wide distribution was one which placed members of the simpsonite paragenesis at the most cation-ordered and most geochemically fractionated end of trends, indicating the paragenesis to be the last group of oxide minerals to crystallize in the pegmatite. This shall be dealt with in more detail in the next section.
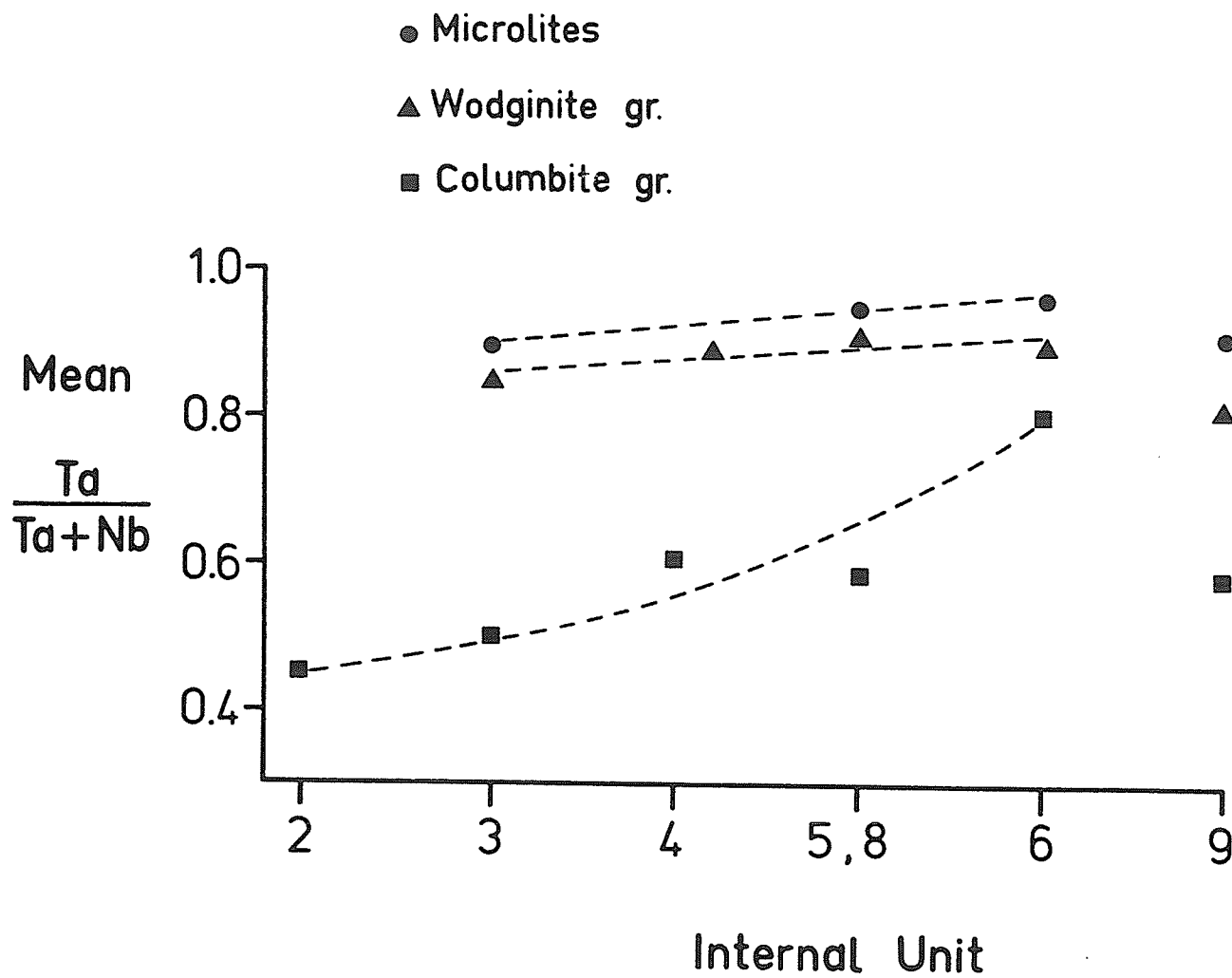
Figure 68: Mean variation of Ta/(Ta+Nb) between units of the Tanco pegma-
tite.

18.13   THE SIMPSONITE PARAGENESIS AT TANCO

18.13.1   Introduction

Simpsonite was first found at Tanco in 1976 by I. Černý as one of a number of oxide mineral species in a saccharoidal albite association of the central intermediate unit of the western flank of the pegmatite. The simpsonite was restricted to a region roughly 1000 m^3 in volume, and has not subsequently been found elsewhere in the pegmatite. Several metre-scale areas in this region were without equal in the mine for their high Ta_2O_5 grades - to 11 wt.%. Associates of the simpsonite are wodginite, tantalowodginite, manganotantalite, ferrotapiolite, microlite and cesstibtantite. Non-oxide mineral associates include albite, quartz, rose and green-coloured muscovite, spodumene, beryl, bismuth and arsenopyrite, approximately in order of decreasing abundance. Most simpsonite-bearing samples were labelled with the prefix "SMP"; all analyses presented in this thesis with this prefix are of minerals from simpsonite-bearing associations.

In all cases, the simpsonite occurs in oxide mineral bands in the saccharoidal albite. The albite bodies, and therefore the bands, are discontinuous compared to the saccharoidal albite unit of the eastern flank of the pegmatite; nonetheless, the similarity is striking.

The saccharoidal albite bodies tend to be curviplanar and convex-upward. Examination of the morphologies of quartz and beryl crystals hosted by the bodies indicates that they taper downward and are most euhedral upward (toward the centre of unit (6)), which implies that the crystallization direction was upward.

One of the most continuous of the layered saccharoidal albite bodies in the central intermediate unit of the western limb of the pegmatite was non-

simpsonite bearing, and was over 3 m in length and up to 2 m thick. However, the simpsonite-bearing saccharoidal albite bodies were often less than 50 cm long and 10 cm thick; one exceptional sample was 20 cm thick. The discontinuity of the bodies and the heterogeneity of their surroundings made geometric interpretations difficult to impossible; however, some simpsonite-bearing saccharoidal albite bodies near the edges of these regions were observed to abut against the more typical coarse-grained K-feldspar, quartz, SQI assemblages of the central intermediate unit. Often a thin (1 to 2 cm) halo of green muscovite separates the saccharoidal albite and the coarser material. The contact between the green muscovite or saccharoidal albite and the K-feldspar-quartz-spodumene assemblage is usually sharp; however, the contact between the green muscovite and saccharoidal albite is more gradational, suggesting a cogenetic origin for the muscovite and albite. The oxide minerals themselves vary within the saccharoidal albite. Simpsonite, some microlite, cesstibtantite and a pale orange-yellow variety of wodginite-tantalowodginite are more concentrated in central bands of the albite; however, a brown wodginite variety and ferrotapiolite are more concentrated toward the uppermost bands, reaching greatest concentration in the green muscovite-rich outermost parts of the albite bodies.

18.13.2 Petrography

Petrographic characteristics of the oxide minerals of the simpsonite bearing associations are remarkably constant.

Simpsonite is always colourless and subhedral to rarely euhedral (Figure 69). Much simpsonite is pristine; however, in several cases, simpsonites collected near the Fe-rich edges of the albite bodies are partially to wholly replaced by tapiolite.

Figure 69: Simpsonite crystals from the Tanco pegmatite. Transmitted, plane-polarized light, 100 X magnification.

The orange-yellow variety of wodginite is the most abundant oxide mineral of the association. This variety forms euhedral, sector-twinned dipyramidal crystals, and ranges from wodginite to tantalowodginite in chemistry. It does not replace other species, but is often rimmed (to slightly replaced) by the brown variety of wodginite (Figure 70). This other variety forms subhedral crystals; only rarely are euhedral crystals found. It is most abundant near the tops of the layered albite bodies, and is almost always in contact with muscovite. Often there is a preferred direction in the growth of the brown rims where they abut against the muscovite.

After wodginite, microlite is the next-most abundant species. Three compositional varieties exist: uranian and common varieties are the most abundant, and an antimonian variety is a distant third. The uranian varieties are anhedral to subhedral, and show strong compositional zoning. The zonation is one of decreasing U,Pb content and $\underline{A}$-site vacancies, and increasing Ta/(Ta+Nb) with progression from the core to the rim. The most uranian of these microlites are translucent green; translucent brown varieties are less uranian, and the least uranian varieties are slightly translucent, but colourless. The antimonian variety is roughly contemporaneous with the uranian one, and may actually represent latest-formed examples of the uranian variety, as evidenced by their trace-to-minor U-contents. These two microlite varieties serve as seed crystals to a later microlite variety, the common microlite with low $\underline{A}$-site vacancies. The contact between the seed and its rimming microlite is sharp. The common variety has anhedral to subhedral crystals, and shows polygonal grain boundaries with other late-forming oxide minerals. Some crystals of this variety enclose what seems to be manganotantalite inclusions, but the typically
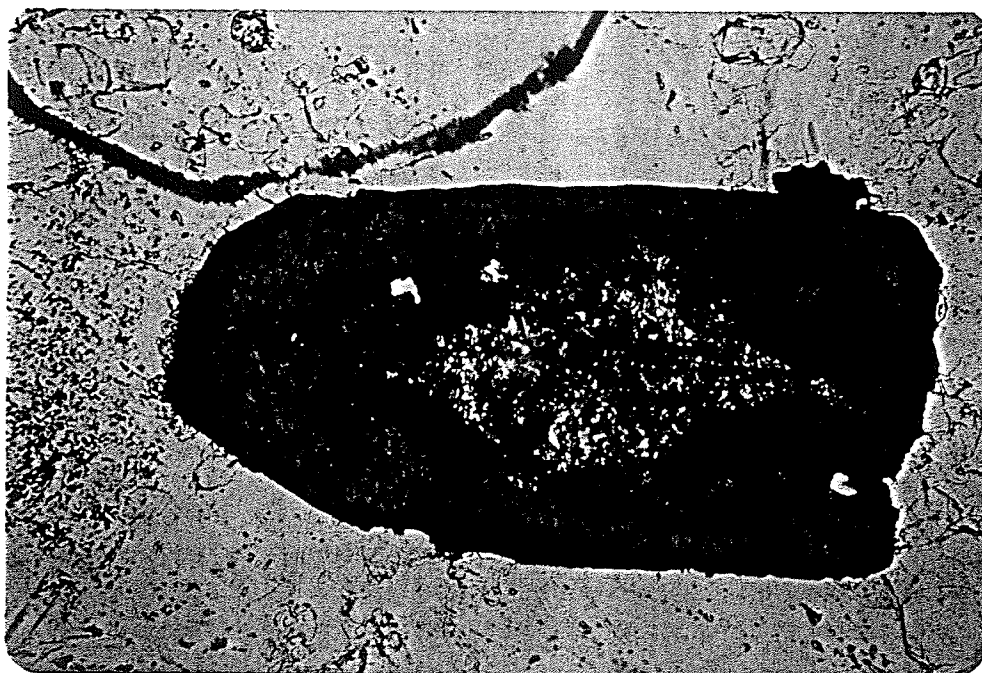
Figure 70: Overgrowths of brown wodginite upon yellow-orange wodginite, simpsonite paragenesis, Tanco pegmatite. Transmitted, plane-polarized light, 100 X magnification.

diffuse boundaries of the "inclusions" and their location along cleavage planes in the microlite suggest that the manganotantalite might be an alteration product of the microlite.

In addition to the microlite varieties, yellow-orange, euhedral cesstibtantite is present. Like the common microlite variety, it rims earlier generations of microlite. A photograph showing cesstibtantite rimming the uranian microlite variety is given in Chapter XIV. Often the cesstibtantite-microlite contacts are sharp, but occasionally gradational contacts are encountered, in which yellow-orange cesstibtantite blebs occur in a antimonian microlite matrix in the contact zone. Whether these blebs represent an exsolution texture or a two-phase co-crystallization is not clear. Cesstibtantite, unlike the common variety of microlite, is found exclusively in the central parts of the albite bodies. This, taken in consideration with the nature of the antimonian microlite - cesstibtantite grain contacts suggests that cesstibtantite is one of the latest of the earlier generation of oxide minerals in the association, not part of the later ferrotapiolite - brown wodginite - common microlite generation.

Unlike other associations, ferrotapiolite is common in simpsonite-bearing associations. It is always transparent red with a strong orange-red to red pleochroism. Crystals are usually subhedral and are often poly-synthetically twinned on (013). As already stated, this ferrotapiolite replaces simpsonite, and is most abundant at the edges of the albite bodies.

Manganotantalite is uncommon to rare in simpsonite-bearing associations. It most frequently occurs as tufts of acicular crystals with a yellow to brown-yellow colour (Figure 71). The rareness of the mineral, and its

infrequency of direct association with other oxide minerals of the albite bodies makes placement of its position in the crystallization sequence of the oxide minerals difficult. As with wodginite, darker coloured rims are often found about lighter cores; however, the contacts between the core and rim regions are always gradational. Manganotantalite may have crystallized with both generations of oxide minerals.

It is concluded that the simpsonite-bearing albite bodies host two generations of oxide minerals which are also somewhat separated spatially. The earlier generation consists of light-coloured minerals poor in chromophoric elements (Fe,Ti), while the later generation is typically dark-coloured and richer in chromophoric elements, and uses the earlier generation as seed crystals. A summary of the crystallization history of the simpsonite paragenesis at Tanco, as outlined in the present section, is given in Figure 72.
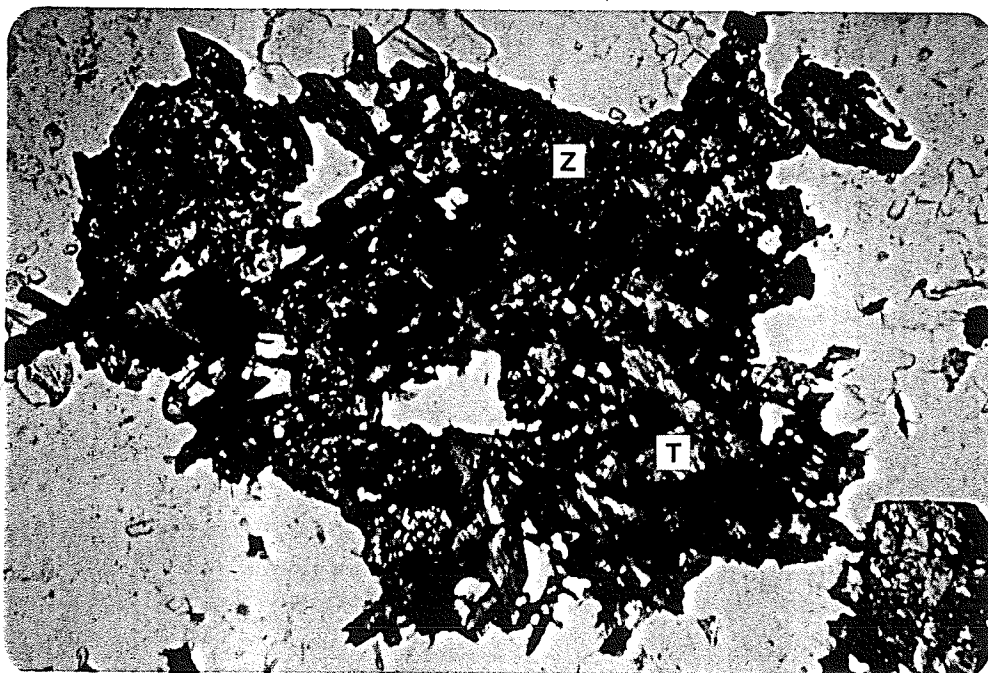
Figure 71: Tufted aggregate of manganotantalite crystals (T) with zircon
(Z), simpsonite paragenesis, Tanco pegmatite. Transmitted,
plane-polarized light, 100 X magnification.

Early   Late

Wodginite gr.

Microlite

Simpsonite

Manganotantalite

Cesstibtantite

Ferrotapiolite
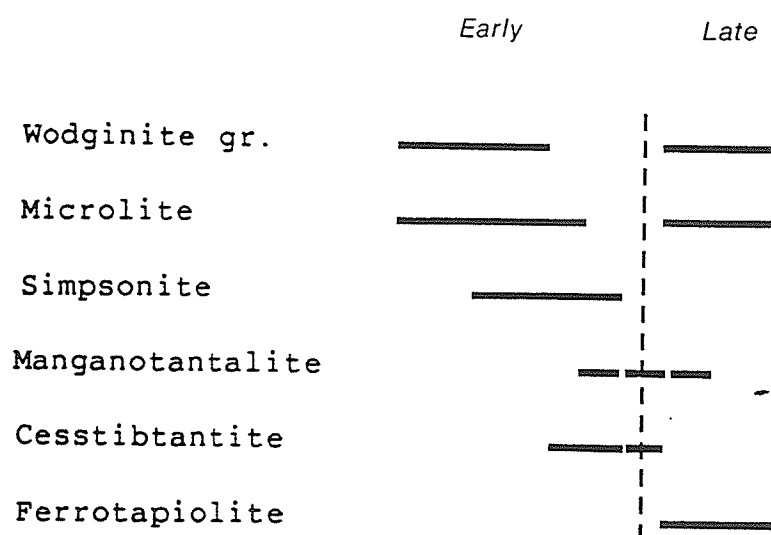
Figure 72: Crystallization history of the simpsonite paragenesis, Tanco pegmatite.

18.13.3 Geochemistry

The chemistry and structural properties of simpsonite paragenesis minerals of the Tanco pegmatite has been outlined in various chapters of Part 3; however, no formal comparison of the properties of these minerals to oxide minerals of the rest of the Tanco pegmatite has yet been presented.

The simpsonite-bearing associations are atypical for their multiphase nature; up to seven Ta-oxide minerals can be found in a single thin section, with few replacement textures evident.   They have atypical mineralogy; (simpsonite), tantalowodginite and cesstibtantite occur nowhere else in the pegmatite. Also noteworthy is the complete absence of cassiterite from the associations.   Furthermore,   the more common oxide minerals,   the wodginite-group minerals, columbite-group minerals, microlites and ferrotapiolites have unusual chemistries which in several ways are distinct from the chemistry of their other occurrences in the pegmatite.   As has been mentioned, the chemistry of these minerals places them at the ends of fractionation trends for the pegmatite.   All species are fully-ordered, an atypical feature for Tanco tantalites, although not necessarily so for the tapiolites and wodginites.

In an attempt to define the differences between the simpsonite paragenesis versus all other oxide mineral associations at Tanco, discriminant analysis was applied,   using the most complete set of mineral properties, namely chemistry, as the variables.   Although some differences in mineral chemistry are easy to discern, other less prominent, but potentially important covariances can easily be missed unless the data are rigorously inspected.   Discriminant analysis has two additional potential benefits. First, if the simpsonite paragenesis represents an extreme in transition

metal fractionation at the Tanco pegmatite, then the discriminant functions separating the simpsonite paragenesis from the rest of Tanco provide information on the direction of fractionation late in the crystallization of the pegmatite. Secondly, if the discriminating powers of these functions are effective, then classification procedures might help in locating other potential occurrences of simpsonite in the pegmatite.

Discriminant analysis involved three steps. To select the chemical variables which would contribute most significantly to discriminating simpsonite paragenesis minerals from other oxide minerals of Tanco, the SAS routine STEPWISE (stepwise discriminant analysis) was used. Variables were selected by backward elimination using a 15% significance level as a criterion for staying. After variable selection, the routine CANDISC (canonical discriminant analysis) was used to construct the canonical variables from linear combinations of the reduced set of chemical variables. Because only two groups were being discriminated between, namely the simpsonite paragenesis minerals versus the rest of Tanco oxide minerals, only one canonical variable exists for each mineral studied. This variable, by nature of the analysis, represents the greatest separation between the two groups in compositional space. Multivariate statistical tests for differences between the two groups (simpsonite- versus non-simpsonite-bearing) were significant beyond the 0.00005 level for all mineral species examined. The final step of the discriminant analysis was a reclassification of the samples by means of the routine DISCRIM. This was done in part as a measure of relative failure or success of the discrimination procedure by observing what proportion of the simpsonite-bearing samples were reclassified otherwise, and in part to find which samples from other regions of the pegmatite

most resembled simpsonite paragenesis samples marked regions of high degrees of fractionation.

(i) Wodginite-group minerals: The linearly independent chemical variables Fe^{2-}, Fe^{3+}, Ti, Nb, and the A-site and B-site vacancies (i.e. substituents for ideal wodginite, $MnSnTa_2O_8$) were used at the start of the stepwise discriminant analysis.   Backward elimination removed none of these variables. Canonical discriminant analysis (Table 87) showed total A-site constituents, Ti and Nb to be generally lower, and B-site Ta to be higher in wodginite-group minerals from the simpsonite paragenesis than the rest of wodginite-group minerals from Tanco.   The histogram of Figure 73 illustrates that both groups show much spread with respect to the canonical variable; however, the group means are well separated.   A summary of the reclassification of samples according to the canonical variable is given in Table 88.   The success of the discrimination is further shown here: on the basis of chemistry alone, 94.1% of all wodginite-group minerals from the simpsonite paragenesis were correctly classified as being associated with simpsonite,   and only 7.6% of all wodginite-group minerals which were not found in association with simpsonite were classified as being associated with it.
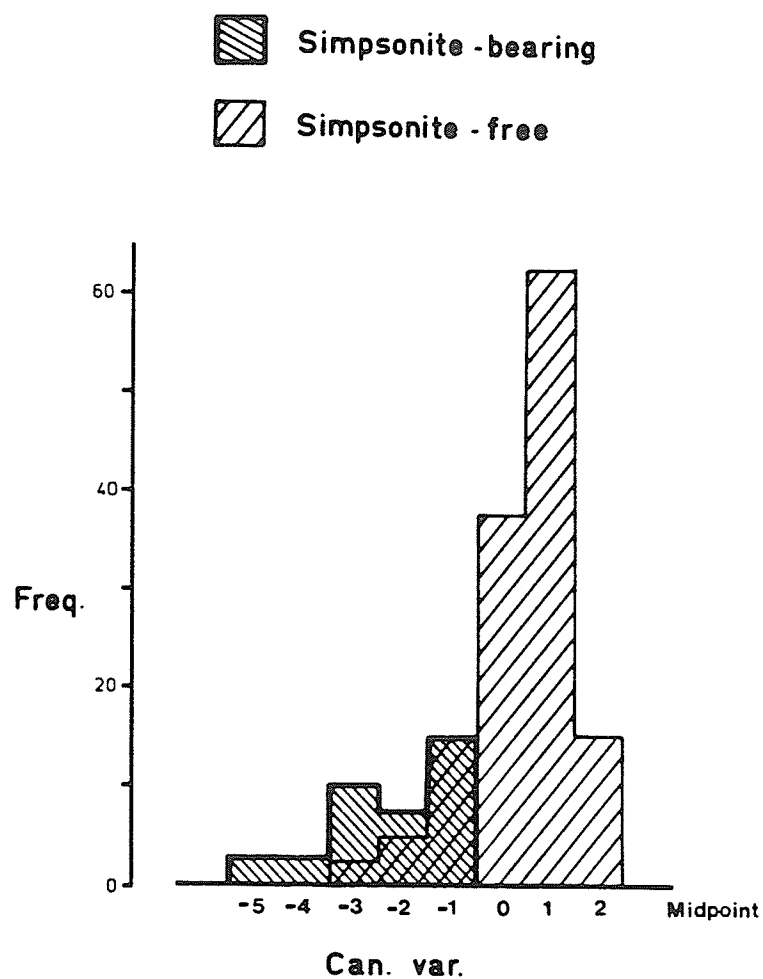
Figure 73: Canonical variable histogram for wodginite-group minerals from simpsonite-bearing versus simpsonite-free associations.

Table 87: Canonical Discriminant Analysis for Wodginite-Group Minerals

---

STANDARDIZED CANONICAL COEFFICIENTS

Fe^{2+}	$¤(A)$	$¤(B)$	Fe^{3+}	Ti	Nb
-0.681	-0.399	1.001	0.590	1.001	0.473

CLASS MEANS

Simpsonite-bearing samples: -2.062
Simpsonite-free samples: 0.535

Table 88: Classification Summary For Tanco Pegmatite Oxide Minerals

---

Association	Wodginite	Microlite	Tantalite	Tapiolite
Simpsonite-bearing	5.9	0.0	0.0	0.0
Simpsonite-free	7.6	16.7	8.6	0.0

The table gives the % of samples from each association which were reclassified otherwise.

(ii) Pyrochlore-group minerals and cesstibtantite: The chemical variables used in the stepwise discriminant analysis were substituents for Na, Ca, and Ta of ideal microlite, $NaCaTa_2O_6(OH,F)$.   Because of the slight amounts of Mn and Fe present, both were summed to make a single variable R2. Similarly, because of only slight amounts of calculated Sn^{4+},   both Sn^{2+} and Sn^{4+} were combined under a single variable Sn.   At the start of the analysis, the model had Pb, U, R2, Cs, Sb, Sn, Ti, Nb and π as variables.   Of these, Cs, U and π did not contribute significantly to the discriminant function, and were removed.

Canonical discriminant analysis (Table 89) showed Cs, Sb, Pb and Ta to be generally higher, and Nb, Ti and R2 to be lower in microlites (plus cesstibtantites) from the simpsonite paragenesis. The distribution of samples with respect to the canonical variable is given in Figure 74.   The group means are well separated, but some overlap occurs.   Table 88 gives a summary of the reclassification of samples.   Although no samples from the simpsonite paragenesis were reclassified, 16.7% of the samples from other locations in the pegmatite were reclassified as belonging to the simpsonite paragenesis.

(iii) Columbite-group minerals: All possible substituents for the manganotantalite end-member were used as variables at the start of the stepwise discriminant analysis.   Backward elimination showed only Nb and Sc to contribute significantly to the discriminant function. Canonical discriminant analysis (Table 90) showed Sc, Nb, Ti, and to an extent, Fe to be generally lower in columbite-group minerals from the simpsonite paragenesis, and showed Ta, and to an extent, Mn to be higher.   Figure 75 shows that the means of both groups are well-separated, and that overlap is minimal. This

Table 89: Canonical Discriminant Analysis for
Microlites and Cesstibtantites

STANDARDIZED CANONICAL COEFFICIENTS

Nb	Ti	Pb	Sb	Sn	R2
1.843	-1.498	-0.335	-0.383	0.860	0.371

CLASS MEANS

Simpsonite-bearing samples: -1.856
Simpsonite-free samples: 0.588

is further emphasized by the classification summary of Table 88: none of the columbite-group minerals from the simpsonite paragenesis were reclassified, and only 8.6% of the other columbite-group minerals were reclassified as belonging instead to the simpsonite paragenesis.

(iv) Ferrotapiolite: Ferrotapiolite is sparsely distributed over the pegmatite, thus only a low degree of confidence can be placed on the results of statistical analysis of this species. Thirteen mineral analyses were used in the discriminant analysis. The set of starting variables was Mn, Fe^{3+}, Nb, Ti and Sn. Backward elimination retained only Nb. Ranking of the data according to Nb content showed Mn, Fe^{3+} and Ta to be generally richer in simpsonite-paragenesis ferrotapiolites, and Fe^{2+}, Ti and Nb to be generally poorer in these samples. Nb discriminates between the groups well, as shown by Figure 76 and Table 88: no samples from either group were reclassified.
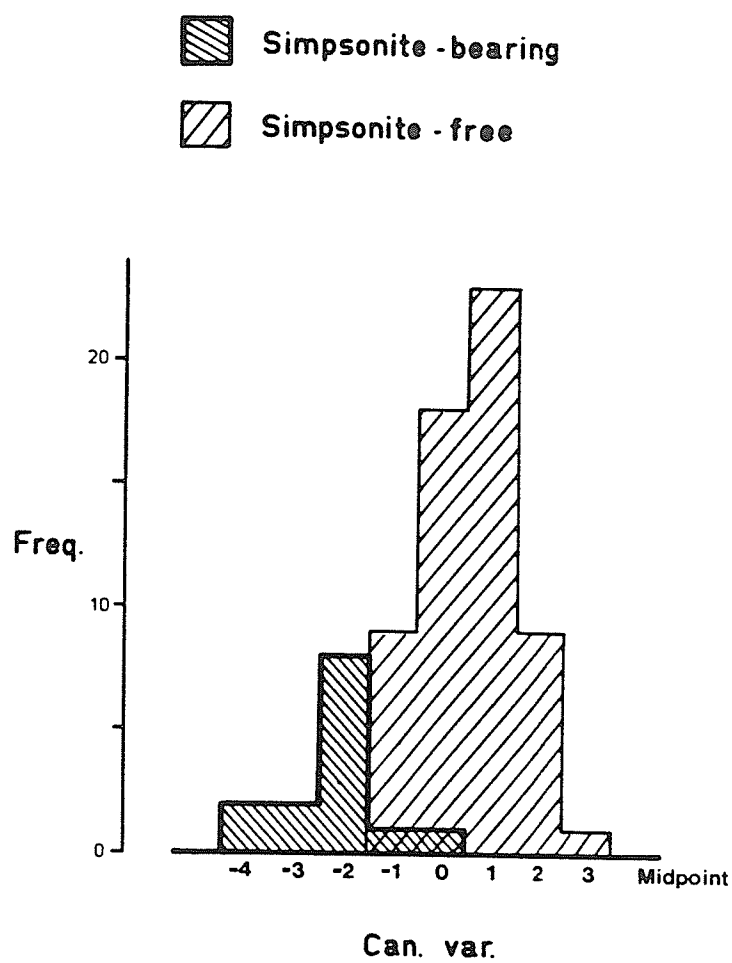
Figure 74: Canonical variable histogram for microlites from simpsonite-bearing versus simpsonite-free associations.

Table 90:   Canonical Discriminant Analysis for
            Columbite-Group Minerals

STANDARDIZED CANONICAL COEFFICIENTS

Nb   Sc

1.563   -0.735

CLASS MEANS

Simpsonite-bearing samples: -2.838
Simpsonite-free samples: 0.147

Table 91 is a list of all simpsonite-free samples which were reclassi-
fied as being simpsonite-bearing. Their locations in the mine are shown in
Figure 77. Several of these samples come from areas immediately adjacent to
the simpsonite-bearing regions of the western flank of the pegmatite. That
samples adjacent to simpsonite-bearing regions should show properties
intermediate to the minerals of the simpsonite paragenesis and simpsonite-
free associations, suggests that the progression from typical oxide mineral
associations to simpsonite-bearing ones was continuous.   Comparison of the
results of the discriminant analyses for all species studied, and consider-
ation of the mineralogy of the paragenesis show that just before and during
the time of formation of the simpsonite paragenesis,   fractionation was
leading to enrichment in Ta (with respect to Nb), Pb, Cs and Sb, to strong
depletion in Ti and Sc, and to an lesser degree, depletion in Mn, Fe and
Sn.

Of the remaining samples reclassified as simpsonite-bearing, the major-
ity come from the central intermediate unit of the eastern flank of the
pegmatite, and belong to the association with muscovitized K-feldspar.
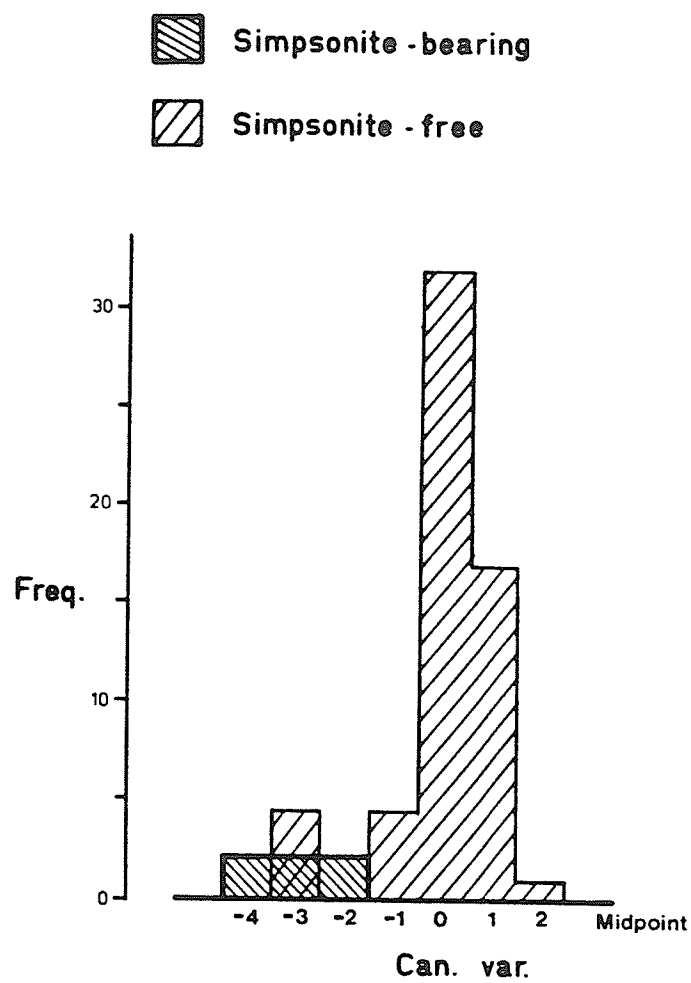
Figure 75: Canonical variable histogram for columbite-group minerals from simpsonite-bearing versus simpsonite-free associations.
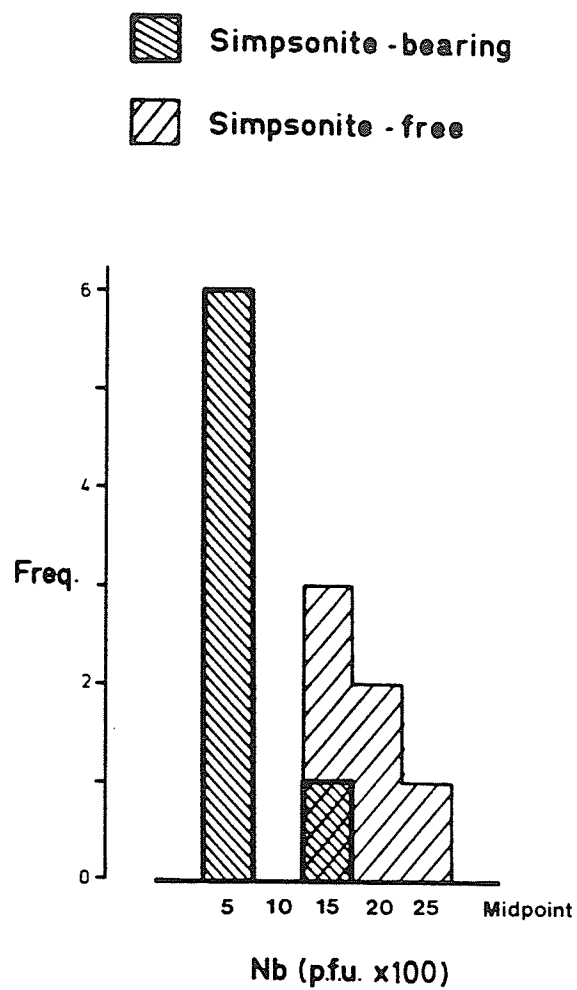
Figure 76: Nb-histogram for ferrotapiolites from simpsonite-bearing versus simpsonite-free associations.

Table 91:   Samples Reclassified as Simpsonite-Bearing

Sample	Oxide Minerals Present	Wd	Mc	Tn	Tp
G69-1	Mc,Wd	–	100	–	–
G69-7	Tn,Wd	0	–	98	–
G69-10	Tn,Wd	0	–	98	–
G69-17	Wd,Mc	0	95	–	–
G69-28	Wd	54	–	–	–
G69-36	Tn,Wd,Mc	1	0	99	–
G69-39	Wd,Mc	0	95	–	–
G69-43	Wd,Mc	0	95	–	–
G69-46	Wd	84	–	–	–
G69-52	Wd,Tn,Tp	60	–	98	0
TRT-15A	Tn,Mc	–	96	2	–
TSE-7	Wd,Tp,Mc	99	–	–	–
TSE-28	Wd,Mc,Tn	100	100	–	–
TSE-30	Wd,Mc	0	95	–	–
TSE-32	Wd,Ct,Mc	0	78	–	–
TSE-35	Mc,Ct	–	95	–	–
TSE-57a	Wd,Tn	100	–	–	–
TSE-63	Wd,Ct	100	–	–	–
TSE-69	Wd	95	–	–	–
TSE-101	Wd,Mc	57	0	–	–
TSE-115	Wd,Tn,Ct	91	–	2	–

Abbreviations: Wd=wodginite-group minerals, Tn=colum-
bite-group minerals, Mc=microlites, Tp=
ferrotapiolite, Ct=cassiterite.

Numbers refer to % probability of reclassification for
analyzed minerals.
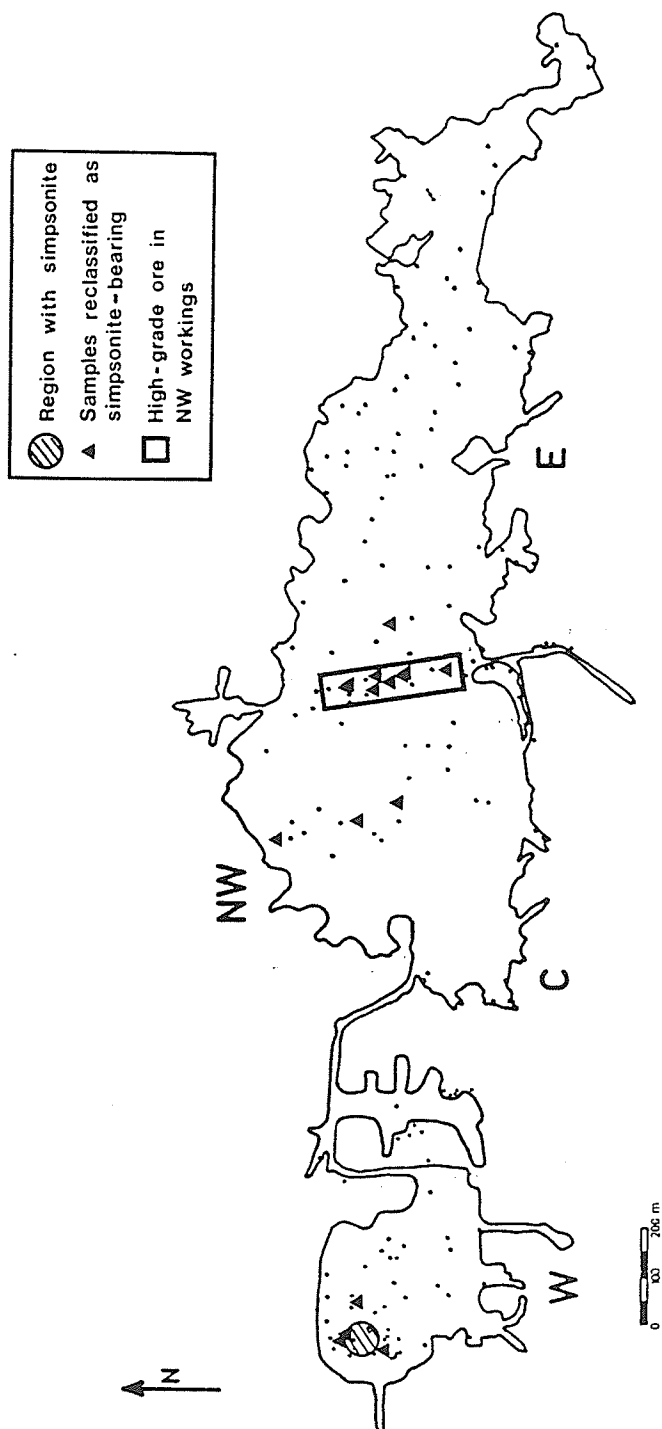
Figure 77: Location of simpsonite-free samples which were classified as simpsonite-bearing.

Several of these samples cluster in an area of very high-grade Ta-ore. One of these has two of its oxide minerals reclassified as belonging to the simpsonite paragenesis (sample G69-52), all others had only one mineral of the association reclassified in this way. These points all strongly indicate the region to be highly fractionated, undoubtedly the most highly fractionated area (with respect to transition metal chemistry) in the eastern flank of the pegmatite. The area was extensively sampled by Grice (1970), who did not find any simpsonite at the location. His samples were re-investigated in the present study, and again, no simpsonite was found. It would seem that although extremes were reached in the geochemical fractionation of transition metal cations in the eastern flank of the pegmatite, fractionation did not progress as far as the western flank, as evidenced by the complete lack of simpsonite and low degrees of depletion of the common transition metal cations (Sn,Mn,Fe) in the most highly fractionated area of the eastern flank.

18.13.4 Simpsonite-Bearing Albite Bodies: Detailed Examination

In an attempt to better define the crystallization sequence of the simpsonite paragenesis at Tanco, and to study the observed banding of the oxide minerals, a detailed sectioning of the largest and most continuous set of bands was done (sample SMP-51). Four 5 cm sections across a 20 cm diameter, mm-scale layered albite body were taken, and analyses of minerals were obtained at an average spacing of 2 mm, $\perp$ to the banding.

In all, analyses of 22 wodginite-group minerals, 13 microlites, 2 cesstibtantites, 6 ferrotapiolites and 3 columbite-group minerals were obtained. Simpsonites were not analyzed because of the difficulty in obtaining quantitative analyses, coupled with the expectation of rather invariable chem-

istry from the results of the crystal-chemical study. The analyses are presented in Appendix D; all have the prefix "SMP-51". Unless otherwise indicated, all mineral analyses were taken at grain cores, except for the brown wodginites, where the analyses were taken half way between the innermost and outermost parts of each grain, because of the lack of a true core in this colour variety.

Mineral distribution within the albite body is uneven. Simpsonite, cesstibtantite and the pale orange-yellow variety of wodginite are most concentrated in lower to central parts of the body, but ferrotapiolite and the brown wodginite variety are most concentrated in the upper parts, and along a thin plane near the base of the body. Microlites are found evenly throughout the body. At the base of the body, a large, medium-grained albite-rich orthogonal pseudomorph (?) is present; the microprobe traverse extended from the top of this pseudomorph through to the top of the albite body.

Figure 78 to Figure 81 illustrate the most important mineral compositional variations across the body. A plot of Fe content of the Fe-Mn oxide minerals is given in Figure 78. In Figure 79, a plot of the Ti contents of all Ti-bearing phases is shown. Figure 80 and Figure 81 are similar plots, but for Nb, and cation site vacancies, respectively. In Figure 80, data for microlites and cesstibtantites are excluded because these minerals show no significant variation in Nb content.

In all four plots, data for orange-yellow versus brown wodginites are separated because of their different chemistries: the earlier orange-yellow variety is significantly Fe, Nb and Ti-poorer than the later brown variety. B-site chemistry of all microlite varieties is practically invar-
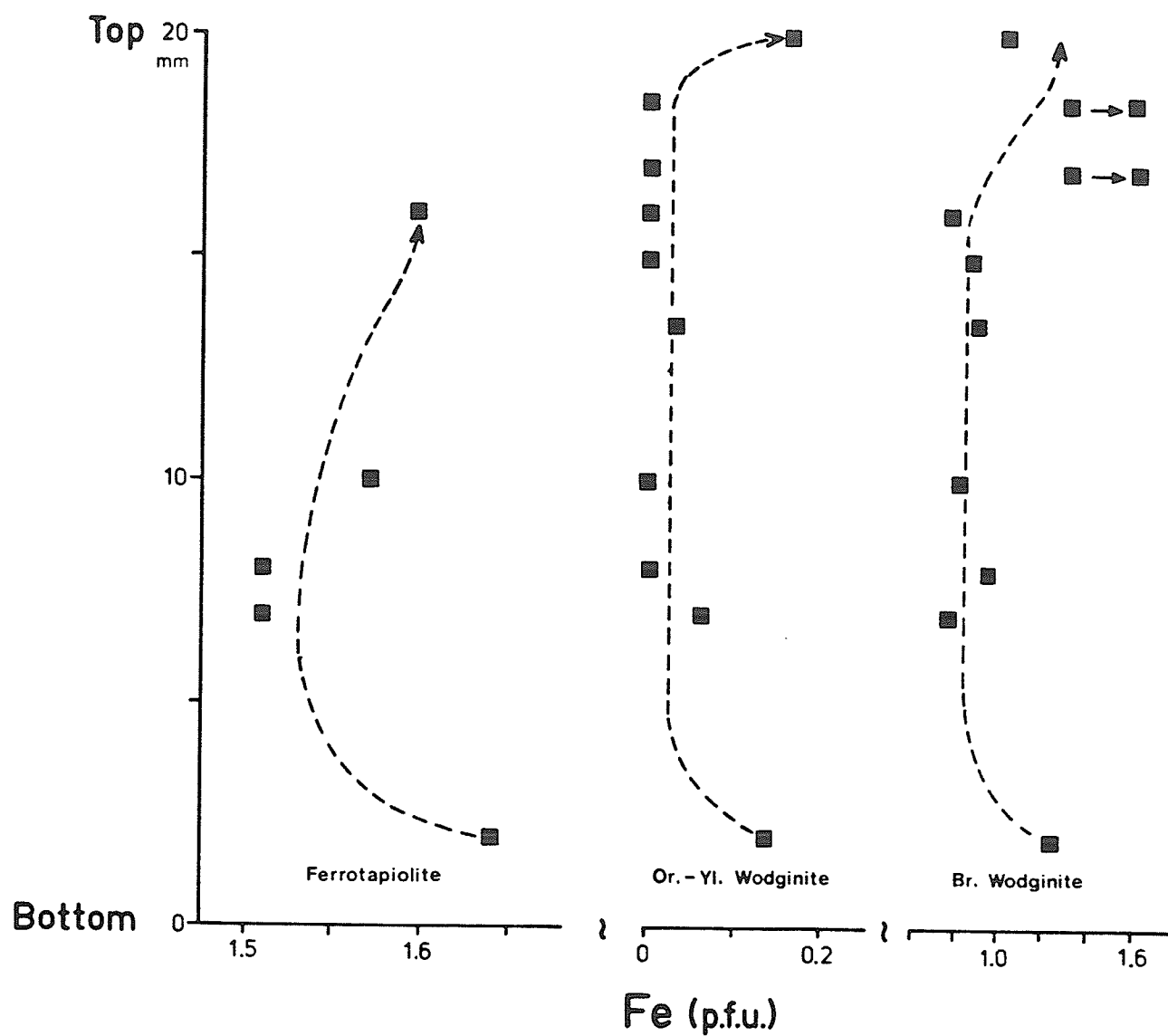
Figure 78: Variation in total Fe content of oxide minerals across the albite body. Horizontal arrows: core→rim zoning.
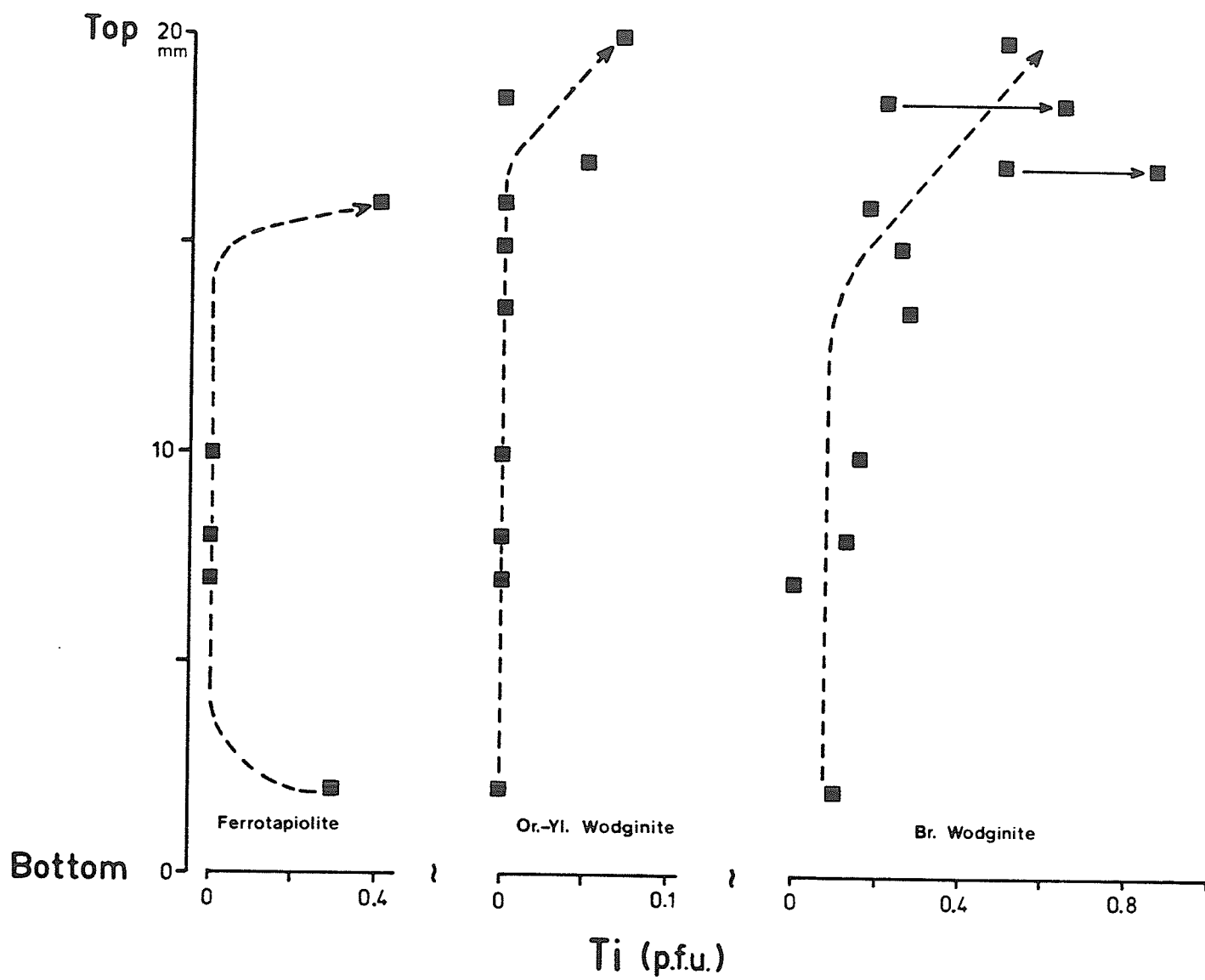
Figure 79: Variation in Ti content of oxide minerals across the albite body.
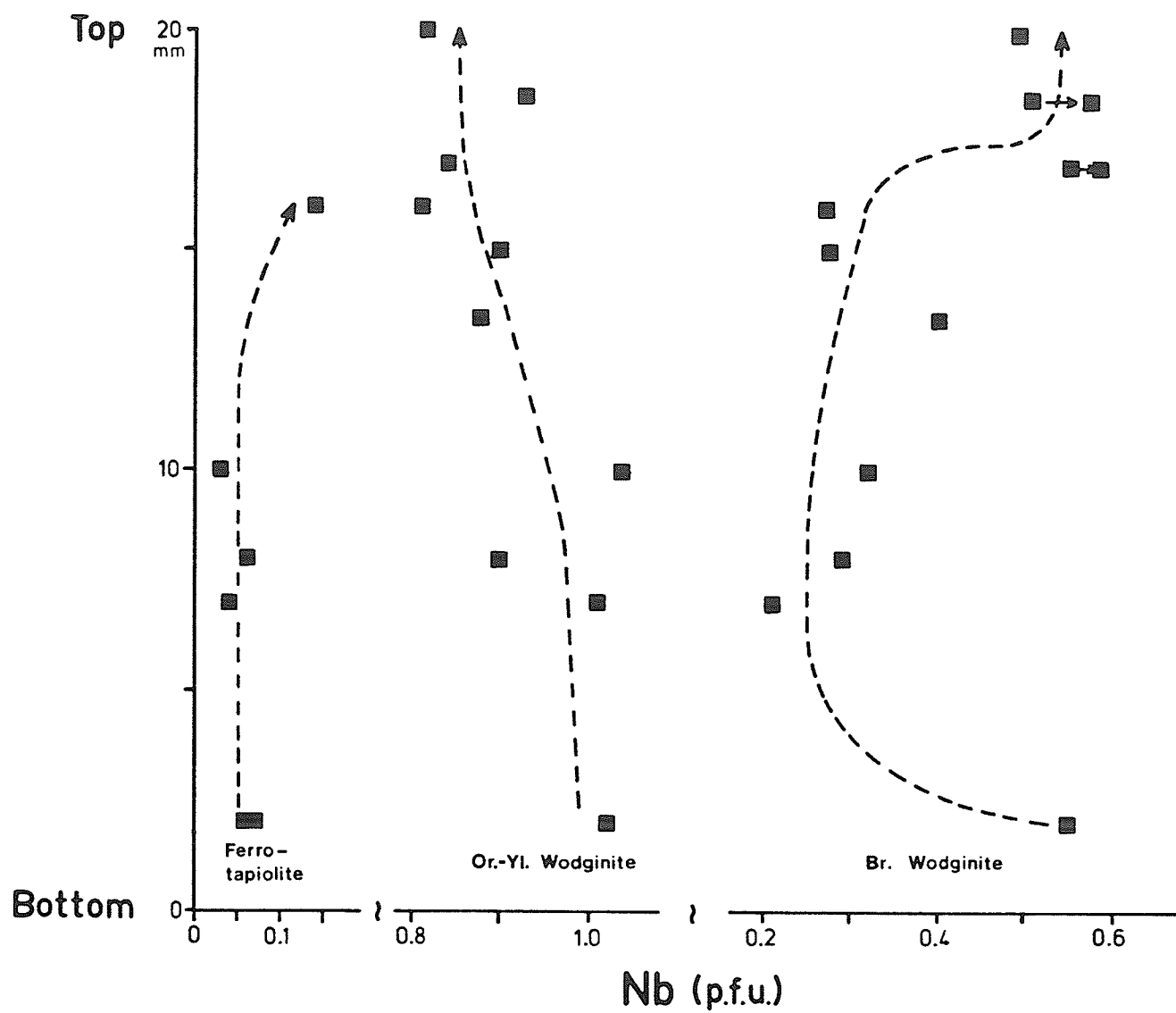
Figure 80: Variation in Nb content of oxide minerals across the albite body.
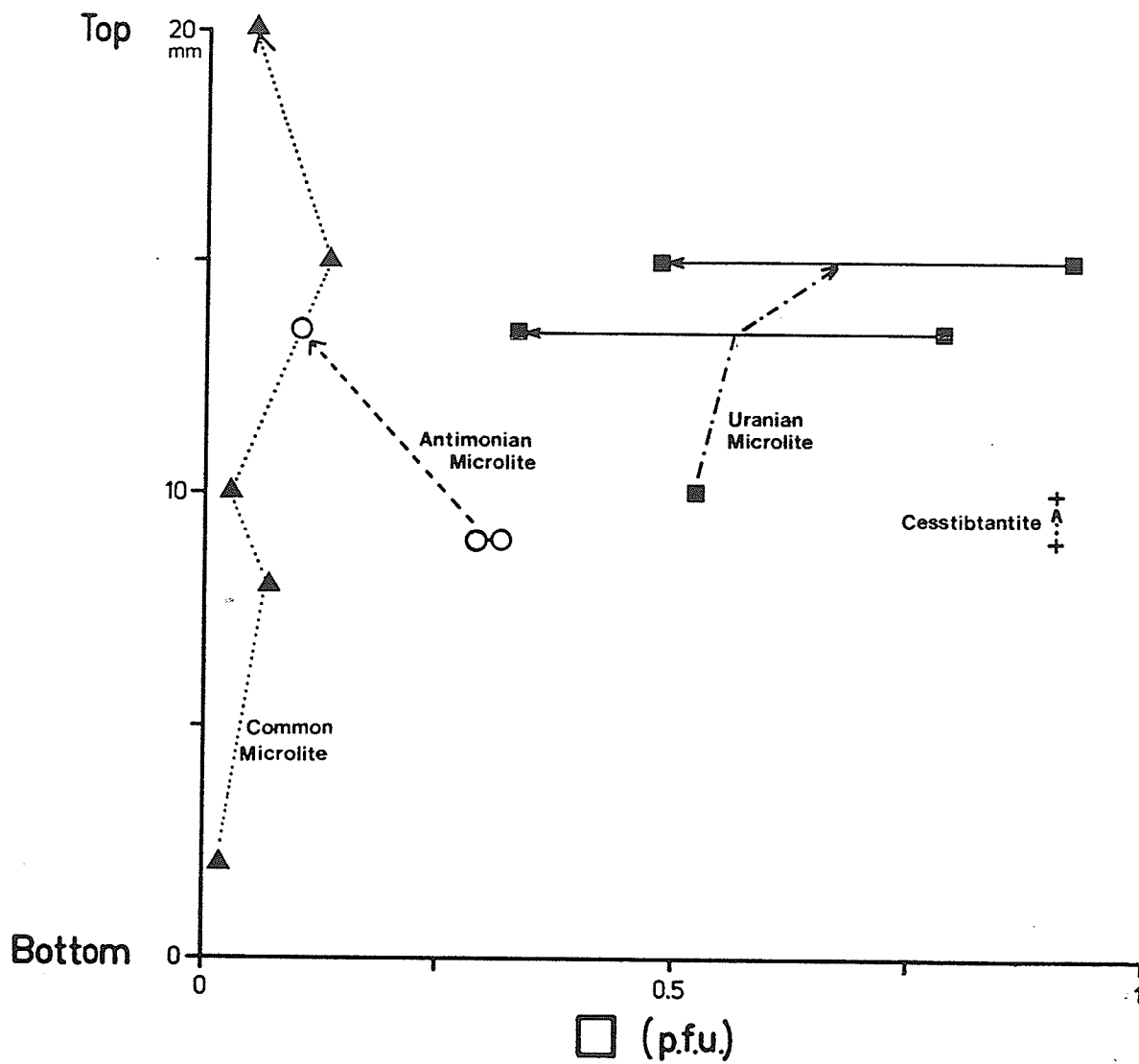
Figure 81: Variation in vacancy content of microlites and cesstibtantites across the albite body.

iant.   Although A-site chemistry between the varieties is quite different,

within each variety, mineral zoning and irregular distribution of the vari-

ety   over the   albite body   make   analysis of   A-site chemical   variability

impossible, except for the common microlites.   In this case, the only use-

ful variable   is A-site   occupancy,   which   is practically   invariant (Fig-

ure 81).   And so, any interpretation of variability of mineral chemistry is

restricted solely to the wodginite-group minerals and ferrotapiolites.

In Figure 78,   a consistent pattern is shown for Fe variation.   For all

species, crystals nearest to the edges of the body are richest in Fe (poor-

est in Mn) than those in the centre of the body.   Furthermore,   samples of

all minerals taken near the centre of   the body show no significant changes

in Fe (or Mn) over approximately 1/2 to 3/4 of the body.   It should also be

noted that the later-forming brown wodginites are always Fe-richer than the

earlier orange-yellow   variety.   The brown   wodginite samples   show strong

colour zoning,   especially obvious in the darker crystals near the edges of

the body.   For the wodginite crystals at 17 and 18½ mm from the base of the

traverse,   core and rim analyses were taken   and are shown in Figure 78 (as

well as Figure 79 to Figure 81).   Both sets   of analyses show that core to

rim variation involves a significant increase in Fe relative to Mn.

The distribution of Ti is the same as that of Fe (Figure 79).   Crystals

at the   edges of the body   are richest in   Ti,   and those from   the central

parts of the body are poorest in Ti (to Ti-free in the case of ferrotapiol-

ites and orange-yellow wodginites).   There is   a slight departure from the

trend for Fe in that the basal edges of   the body are not as Ti-rich as the

upper edges of the body; however, like the Fe distribution, Ti remains con-

stant over the   1/2 to 3/4 of   the body representing the   central sections.

Also parallelling the Fe distribution is the concentration of Ti in the brown wodginite varieties over the orange-yellow ones. Core to rim chemical variations in the brown wodginites involve an increase in Ti, which again parallels the trend for Fe.

A strong departure from the previous two sets of trends is observed for Nb. Although the brown wodginites and the ferrotapiolites from the edges of the albite body are enriched in Nb, as compared to their occurrences in central regions of the body, the trend for the orange-yellow wodginites is just the reverse: the central and basal sections of the albite body have the Nb-richest orange-yellow wodginites, and Nb is seen to decrease reasonably smoothly toward the top edge of the body. Furthermore, all colourless wodginites have Nb contents which are higher than the Nb-richest of the brown wodginites, the reverse of what is observed for Ti and Fe. However, as was observed for Ti and Fe, Nb increases towards the rim in colour-zoned brown wodginites.

The following points summarize the most important conclusions from the study of mineral compositional variation across the albite body.

(1) The early generation of oxide minerals is typified by high Mn/(Mn+Fe) and by low amounts of elements which tend to substitute for Ta, namely Nb, Sn and Ti. The later generation has significantly lower Mn/(Mn+Fe) and higher amounts of quadrivalent cations; however, Ta/(Ta+Nb) is lower than for the early generation.

(2) Despite modal variations, the minerals of the early generation are typified by nearly invariant compositions; the position of the minerals within the albite bodies does not affect mineral composition much. In contrast, the later generation of minerals is constant in composition over a large central region comprising 50-75% of the albite bodies, but shows sharp changes in composition near the edges of the bodies where they are most abundant. This indicates that the mechanisms responsible for oxide mineral formation were similar for both generations of oxide minerals in the central parts of the albite bodies, but dissimilar in edge regions.

(3) The earlier generation of minerals contains most mineral species typical of the simpsonite paragenesis, e.g. simpsonite, Fe-poor wodginite, tantalowodginite and cesstibtantite. By comparison, the later generation is quite ordinary: common microlite instead of uranian or antimonian microlite or cesstibtantite, Fe-enriched wodginite instead of Fe-free wodginite and tantalowodginite.

(4) Wodginite-group minerals and microlites from the earlier generation are richest in cation site vacancies (Figure 81). Not only are the corresponding members of the later generation poorer in site vacancies, their core-to-rim zonation indicates that the number of vacancies diminished during their crystallization.

(5) The significantly higher Ti and Fe (relative to Mn) contents of the later generation of oxide minerals suggests that the melt or fluid from which they crystallized was geochemically more primitive, or less fractionated, than the one which produced the earlier generation. However, data for Nb suggests just the opposite; minerals of the later generation are

Nb-poorer (and Ta-richer) than their earlier-generation counterparts; thus they would seem to have been derived from a more highly fractionated melt or fluid. This is difficult to reconcile unless the system which produced the albite bodies was geochemically open in the latter parts of its crystallization history. If Nb-Ta fractionation were regulated principally by the melt or fluid which produced the albite bodies, and Ti and Fe were provided by an outside source, then the observed trends in mineral chemistry could result. This model demands either (1) that the chemical potential of Ta within the system that produced the albite bodies was much greater than that of the external system which supplied Ti and Fe, or (2) that its Ta:Nb signature was similar to the system which produced the albite bodies. It is important to note that mineral zoning within the later generation indicates that $\mu(Ti)$, $\mu(FeMn_{-1})$ and $\mu(NbTa_{-1})$ all increased during the crystallization of this generation. If this zoning is an indication of increasing openness of the system which produced the albite bodies, then the external source of transition-metal cations must have been richer in Nb relative to Ta than the source which produced the albite bodies. It is concluded that the second scenario is the better one, and that the external source of cations was geochemically more primitive, as regards all transition metal cations, than the source of the albite bodies.

(6) When the systems which produced the albite bodies interacted with external systems, $\mu(Ta)$ must still have been relatively high, yet $\mu(NbTa_{-1})$, $\mu(Ti)$, $\mu(FeMn_{-1})$ were quite low. This is proven by the immediate and sharp increase in Ti and Fe concentrations in late generation minerals as contrasted with the initially lower concentrations of Nb in these minerals. That $\mu(Ta)$ itself was very high is further supported, but not proven by the typically very high grade of simpsonite-bearing Ta-ore.

(7) The association of late-generation oxide minerals with green muscovite, within the albite bodies, implies that the external supply of transition metal cations must have been more potassic, and therefore more acidic than the system which produced the albite bodies. As was described earlier, the albite bodies often have variably extensive muscovitic rims. It is probable that the muscovite veinlets within the albite bodies are related, if not identical to the rim material. Because of the lack of an appreciable muscovite rim on the studied albite body (the sample was collected some 6 years before the present study began, and may have had a rim at one time), no attempt could be made to test the relationship through oxide mineral chemistry. Whether the rims represent (1) reaction rims about the albite body, (2) an immiscible liquid within the sodic fluid which produced the albite bodies, or (3) a zone of hydrolysis which may have preceded a once-expanding Na-metasomatic front, behind which the albite bodies crystallized, is not known and cannot be answered at the present. The association of muscovitic rims with saccharoidal albite bodies is not unique to simpsonite-bearing bodies; the question presented here is one which holds for all of the Tanco pegmatite albite bodies, and the answer can only be found with more detailed work on the distribution and chemistry of all mineral species of the albite bodies.

Chapter XIX

BRAZILIAN PEGMATITES

Simpsonite occurs in two locations in Brazil: the Alto do Giz and Onça pegmatites. Both pegmatites are located in the Brazilian Precambrian Shield, and are two of many Be,Ta,Li-bearing pegmatites in a 3750 km_2 belt centred about the Paraiba - Rio Grande do Norte border in the vicinity of Equador (De Almeida et al., 1944). Very little has been published on the geology of this region; available information is given by De Almeida (1944) and Pough (1945).

19.1 ALTO DO GIZ PEGMATITE

19.1.1 Location and Geology

The Alto do Giz is located 2 km S of the main road connecting the towns of Equador and Parelhas, in the state of Rio Grande do Norte, Brazil. The pegmatite is hosted by a micaceous quartzite overlying an inferred granitic batholitic source, and has a vertical attitude (Pough, 1945). Although heavily weathered, the pegmatite is well-exposed, located at the crest of a ridge. Published photographs and descriptions indicate pegmatite zoning to be horizontally symmetric; the vertical zonation is not well documented. There is a wall unit of quartz, mica and kaolinized feldspars. Progression toward the centre first shows an intermediate unit(s) consisting mainly of coarse-grained quartz, feldspar and mica, followed by a quartz core. Beryl

- 342 -

and Ta-oxide minerals are from the intermediate zone, and tend to be concentrated in the innermost parts of this zone. A photograph presented by Pough (1945) indicates that large spodumene + quartz pseudomorphs after petalite were present in the intermediate zone. This, plus the list of accessory minerals given above, indicates the pegmatite to belong to the petalite subtype of complex-type, rare-element granitic pegmatites of orogenic association (Černý, 1986).

19.1.2 Oxide Mineralogy

Manganotantalite is the dominant Ta-oxide mineral of the Alto do Giz pegmatite. Crystals are typically blocky, euhedral to subhedral, opaque and black. Unit cell parameters were determined for a blocky black crystal: a=14.290(1), b=5.7416(3), c=5.1476(4) Å. The cell parameters indicate the Mn/(Mn+Fe) ratio to be 0.9 and the degree of order to be 14%.

Microlite is the next most-abundant oxide mineral of the pegmatite. Pough (1945) does not describe the properties of this microlite, and because only microlites associated with simpsonite were obtained for the present study, nothing is known of the chemistry or physical properties of the average microlite of the pegmatite.

Ferrotapiolite is a frequent associate of simpsonite, but occurs as isolated crystals elsewhere in the pegmatite. Pough (1945) did not recognize ferrotapiolite at the Alto do Giz pegmatite, so little is known of its distribution. A single black ferrotapiolite crystal from a simpsonite-free assemblage was obtained late in the present study. Its unit cell parameters are: a=4.7561(1), c=9.2175(3), which indicate it to be fully-ordered, or nearly so, and to have a low Mn-content: Mn/(Mn+Fe)=0.1 (M. Wise, pers. comm.).

19.1.2.1 Simpsonite Paragenesis

The occurrence of the simpsonite paragenesis at the Alto do Giz pegmatite is one of the most mineralogically diverse, second only to the Leshaia, Kola Peninsula occurrence. Ten mineral species are known (Table 92).

Manganotantalite and ferrotapiolite are the only oxide minerals studied which are found both as members and non-members of the paragenesis. As members, they have high $Ta/(Ta+Nb)$ and $Mn/(Mn+Fe)$ ratios (Table 92). The manganotantalite varieties are comparable to other manganotantalites of the pegmatite in terms of $Mn/(Mn+Fe)$, but have distinctly higher degrees of order (100%). Two varieties exist: an early, red variety, and a later, yellow one. The red variety shows lower $Ta/(Ta+Nb)$ and higher $Mn/(Mn+Fe)$ than the later variety, which indicates that during crystallization of the paragenesis, a reversal in Fe-Mn fractionation occurred. The ferrotapiolite shows degrees of order comparable to the ferrotapiolite from outside the simpsonite paragenesis, but has $Mn/(Mn+Fe)$ ratios (Table 92) approximately six times higher than the one from outside the paragenesis.

Simpsonite was a very abundant member of this occurrence of the paragenesis; Pough (1945) reports that more than 300 kg of the mineral were mined during 1943. On the basis of the production during 1943 alone, the Alto do Giz is the world's largest deposit of simpsonite. Simpsonite occurs as sharp, subhedral crystals to several cm in diameter; its other physical properties are described in Part 3.

Microlite occurs as green crystals which are usually euhedral and octahedral. As a member of the simpsonite paragenesis, it is less abundant than simpsonite or manganotantalite. It occurs as the common variety; its chemistry is quite simple compared to other members of the microlite sub-

group that occur at Alto do Giz. Some features of its geochemistry are given in Table 92.

Simpsonite, manganotantalite, microlite and ferrotapiolite mark one appoximately coeval generation of oxide minerals in the Alto do Giz occurrence of the simpsonite paragenesis. All other members occur as late-stage replacement minerals of the simpsonite and microlite of the paragenesis. Natrotantite, alumotantite and stibiotantalite occur as fine-grained replacements of simpsonite, while parabariomicrolite and plumbian stibiomicrolite occur as similarly-textured replacements of the microlite of the paragenesis. Tantalowodginite occurs as inclusions within alumotantite crystals, hence is assumed to be roughly coeval, but slightly earlier than the alumotantite. The relationship between the rest of the late-stage minerals is difficult to assess; few occur in contact. However, on the basis of the higher water content of parabariomicrolite as compared to stibiomicrolite (Chapters XIII and XV), parabariomicrolite is suspected to be later than stibiomicrolite, which is assumed to be roughly coeval with alumotantite, tantalowodginite, natrotantite and stibiotantalite. Figure 82 summarizes the crystallization history of the Alto do Giz occurrence of the simpsonite paragenesis.

A summary of the geochemistry of the members of the simpsonite paragenesis is given in Table 92. The following features typify this occurrence: (1) consistently extremely high Ta/(Ta+Nb), (2) variable but high Mn/(Mn+Fe), (3) undetectable to ultratrace Ti, and (4) low Sn. The values of Ta/(Ta+Nb), Ti and Sn are too extreme to be taken as representative of the whole pegmatite, and by analogy to the background study done for the Tanco occurrence of the simpsonite paragenesis, these variables indicate

that the simpsonite paragenesis at the Alto do Giz pegmatite marks one of, if not the most fractionated part of the pegmatite, in terms of transition-metal cation chemistry.

Although the conclusion is weak due to a lack of data, the degree of order of oxide minerals from the Alto do Giz pegmatite seems to have been following a path similar to that of Tanco pegmatite oxide minerals. Samples from outside the simpsonite paragenesis show low degrees of order, while those from within the paragenesis are fully-ordered.

The values of Ta/(Ta+Nb) are too extreme to be put to any use in inferring crystallization sequences within the paragenesis. However, the crystallization of the Fe-enriched (with respect to Mn) yellow tantalite variety coincides with tapiolite crystallization, which indicates that a late reversal in Fe-Mn fractionation occurred, again similar to the Tanco occurrence of the simpsonite paragenesis.

Table 92: Simpsonite Paragenesis at Alto do Giz:
Geochemistry Summary

Mineral	Ta/(Ta+Nb)	Mn/(Mn+Fe)	Ti*	Sn*
Manganotantalite (red)	0.888	0.973	0.000	0.000
Microlite	0.967	---	0.000	0.000
Simpsonite	0.987	---	0.002	0.004
Ferrotapiolite	0.997	0.336	0.000	0.000
Manganotantalite (yellow)	0.994	0.884	0.000	0.000
Stibiotantalite	0.943	---	0.000	0.000
Tantalowodginite	0.988	1.000	0.000	0.093
Alumotantite	1.000	---	0.000	0.015
Natrotantite	0.985	---	0.000	0.000
Stibiomicrolite	0.999	---	0.000	0.000
Parabariomicrolite	0.970	---	0.000	0.000

* per 24(O)

Early   *Late*

Manganotantalite   *red*   *yl.*

Microlite

Simpsonite

Ferrotapiolite

Tantalowodginite

Stibiotantalite

Stibiomicrolite

Alumotantite

Natrotantite

Parabariomicrolite
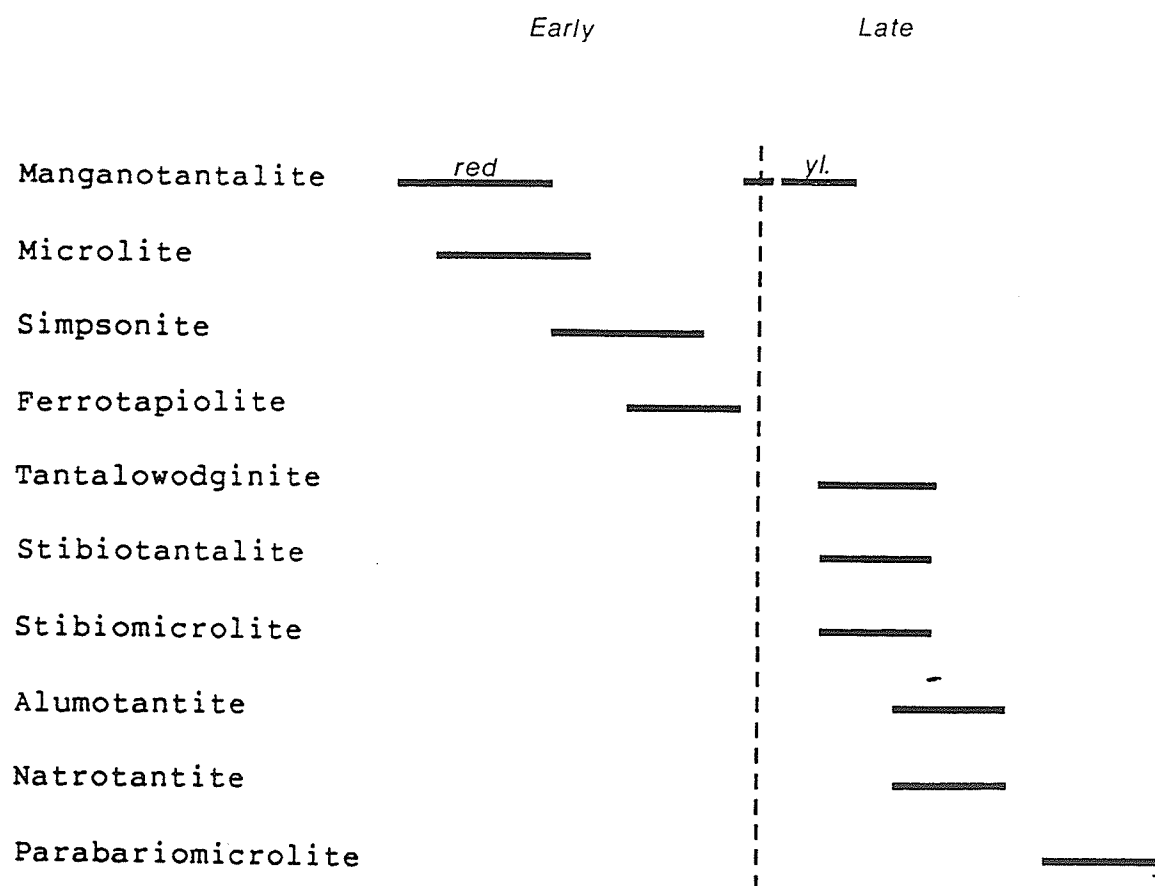
Figure 82: Crystallization history of the simpsonite paragenesis, Alto do Giz pegmatite.

19.2   ONÇA PEGMATITE

19.2.1   Location and Geology

The Onça pegmatite is located 25 km NE of the Alto do Giz. Much less is known of this pegmatite than the Alto do Giz pegmatite; the only account of its geologic setting and internal zoning is in De Almeida et al. (1944).

Like several other complex pegmatites in this region, the Onça pegmatite is hosted by metasedimentary rocks and is vertical in attitude. De Almeida et al. (1944) describe two of its internal units.   The quartz unit forms a true core in horizontal section. An internal unit about the quartz core was the host of the economic mineralization (beryl and tantalite), and consisted mainly of coarse-grained (K-)feldspar and quartz. Not enough of the pegmatite's mineralogy is known to fully classify it, but according to its complex zonation and the presence of beryl and tantalite, it belongs either to the spodumene or petalite subtypes of complex-type, rare-element granitic pegmatites of orogenic association.

19.2.2   Oxide Mineralogy

According to De Almeida et al. (1944), the Onça pegmatite was one of the largest beryl- and tantalite-bearing pegmatites in the region. Despite the impressive size, the pegmatite and its oxide mineralogy are poorly documented.   No chemical analyses for the most abundant oxide minerals have been published, but De Almeida et al. (1944) claim that tantalite, not columbite, is the most abundant oxide mineral of the pegmatite.   Cassiterite is conspicuously absent; most pegmatites in the field are cassiterite-bearing to cassiterite-rich.

Pough (1945) added tapiolite, microlite and simpsonite to the list of oxide minerals from the pegmatite. The tapiolite and microlite are not described as being associated with the simpsonite, and were not found as its associates in the present study.

19.2.2.1   Simpsonite Paragenesis

The only member of the simpsonite paragenesis found from the Onça pegmatite to date is simpsonite. This most probably reflects the lack of scientific interest in the simpsonite paragenesis at the time samples could be collected (1940-1950), not the true mineralogic diversity of the paragenesis at Onça.

Unlike the Alto do Giz occurrence, the simpsonite at the Onça pegmatite is often found embedded in its original matrix. The matrix mineral is a white mica. This is atypical for simpsonite occurrences; minerals of the paragenesis are usually associated with saccharoidal albite bodies.

A single chemical analysis was obtained for simpsonite from the Onça pegmatite (Chapter VIII). The analysis is typical for a simpsonite. The Ta/(Ta+Nb) ratio of 0.993 is within the range shown by simpsonites from the Alto do Giz pegmatite; it would seem that high degrees of transition-metal cation fractionation were also attained by the Onça pegmatite.

Chapter XX

THE BIKITA PEGMATITE

20.1 LOCATION AND GEOLOGY

The Bikita pegmatite is located in the Victoria Schist Belt, approximately 60 km ENE of Fort Victoria, SE Zimbabwe. The Belt is part of the Archean Bulawayan System, which consists of greenstone belts of dominantly basic metavolcanic rocks and pelitic metasedimentary rocks, bordered by granodioritic intrusions. The most recent accounts of the geology of the region are given by Tyndale-Biscoe (1951) and Cooper (1964).

Metamorphism in the region of the pegmatite attained amphibolite grade. Little is known of the tectonic history of the area, thus of the relative timing of metamorphism and intrusive events.

The Bikita pegmatite has the shape of an irregular sheet, has a variable, but generally shallow dip (15-45°) and is amphibolite-hosted. The maximum dimensions of the pegmatite are length 1600 m, thickness 70 m. On the basis of its accessory mineralogy (petalite, beryl, lepidolite, tantalite), the pegmatite classifies as the petalite subtype of the complex type of rare-element granitic pegmatites of orogenic association (Černý, 1986).

Several attempts have been made at describing the internal zoning of the pegmatite (Tyndale-Biscoe, 1951; Symons, 1961; Cooper, 1964; Heinrich, 1976; Norton, 1983). The most recent attempt (Norton, 1983) simplifies the picture considerably by assigning only six internal units to the pegmatite. These are as follows (names are assigned by the present author; unit num-

bers are those of Norton, 1983). The border unit (1) consists of fine-grained albite, quartz and muscovite. The wall unit (2) consists of coarser-grained muscovite and quartz, with albite. The outer intermediate unit (4) lies inward of these units, and consists of perthite, quartz and muscovite. The petalite unit (5) lies inward of unit (4) and consists of perthite, albite, quartz, muscovite, petalite and SQI, and pollucite. The central intermediate unit (7) is the innermost of the intermediate units, and consists mainly of coarse-grained perthite plus quartz. The lepidolite unit (8-9), is a replacement unit, and consists of lepidolite and quartz. Norton's (1983) assignment of the units differs most prominently from earlier ones in considering the pollucite-rich areas as part of the petalite unit (5), and in assigning the footwall albites to the wall unit (which seems a bit unusual - Norton (1983) usually classifies these bodies as a sodic occurrence of his feldspar unit (3)).

The pegmatite is one of the Li-richest and largest of complexly-zoned pegmatites. Norton (1983) claims that Gallagher (1962) estimated the overall Li_2O content to be 1.5 wt%. Although rich in Li like Tanco, Bikita has much lower Ta_2O_5 contents, but shows similar degrees of Nb-Ta fractionation. Except for the Zr-Hf signature of a hafnon determined by the author (Hf/(Hf+Zr)=0.53), other geochemical data for the pegmatite are unavailable, thus other extremes in geochemical fractionation are unknown.

The Bikita pegmatite has been worked over a large period of time, from 1909 to the present. Several claim groups have existed for different parts of the pegmatite, consequently several names exist for the different workings of the pegmatite. These include the Mdara mine, the Nigel tin mine, the Al Hayat mine, and the Bikita mine. At the time of discovery of simp-

sonite at Bikita, all four names represented geographically separate workings. With the purchase of the Al Hayat claims by Bikita Minerals Ltd. in the late 1950's, the "Bikita mine" came to represent both the Al Hayat and Bikita mine workings (Symons, 1961).

20.2   OXIDE MINERALOGY

Except for the work of Macgregor (1946), little is known of the oxide mineralogy of the Bikita pegmatite.

The most abundant oxide minerals of the pegmatite are tantalite and cassiterite, which are dominantly associated with saccharoidal albites of the pegmatite (Tyndale-Biscoe, 1951). The tantalite is typically black, and averages 5.3:1 $Ta_2O_5:Nb_2O_5$ (Macgregor, 1946). Little else is known of the tantalite or the cassiterite, and attempts by the author and Dr. P. Černý to obtain more material have been unsuccessful.

A grey microlite variety is an abundant mineral phase in the Al Hayat claims. Only a semi-quantitative chemical analysis exists for this mineral (Macgregor, 1946), which does not distinguish Ta from Nb.

20.2.1   Simpsonite Paragenesis

Simpsonite was discovered at the Mdara mine workings of the Bikita pegmatite by Macgregor (1946). The occurrence of the mineral is quite similar to the Tanco one. Simpsonite was found in a 0.3 to 0.6 m band in a layered saccharoidal albite body, just below a quartz body in a central region of the pegmatite. The uppermost parts of the band, near the albite-quartz contact, are quite muscovite-rich; Macgregor (1946) describes this area as greisenized and sericitized. Simpsonite was found nowhere else outside of the band; stratigraphically lower sections of the host saccharoidal albite body contain only tantalite and cassiterite as oxide minerals.

In his 1946 study, Macgregor found simpsonite and what is now known as alumotantite as the sole members of the simpsonite paragenesis. In the present study, manganoan ferrotapiolite and manganotantalite have been added to the list of members of the paragenesis. Cassiterite, which is present in immediately adjacent parts of the pegmatite, is noticeably absent from the paragenesis. In addition to the members of the simpsonite paragenesis, zirconian hafnon has been found, a chemical analysis for which is given in Table 93. This is the second known occurrence of a hafnon, and it indicates that extremely high degrees of Zr-Hf fractionation were attained by the time of formation of the simpsonite paragenesis at Bikita.

Table 93: Electron Microprobe Analysis of Hafnon,
Bikita Pegmatite

HfO_2	49.1
ZrO_2	25.1
SiO_2	27.1
	101.3

Cations per 4(O)

Hf^{4+}	0.53
Zr^{4+}	0.46
Si^{4+}	1.02
	2.01

Simpsonite was the first mineral of the simpsonite paragenesis to form at Bikita. All other members of the paragenesis occur as overgrowths and partial replacements of the simpsonite: fine-grained crystals about the edges and along fractures in the much larger simpsonite crystals (to 5 mm

in diameter). As described in Part 3, alumotantite also occurs as a pervasive alteration of parts of the simpsonite crystals. A summary of the crystallization history of the simpsonite paragenesis at Bikita is given in Figure 83.

The late changes in oxide mineralogy were also accompanied by a change in the silicate mineralogy. The dominant matrix mineral to oxide minerals of the simpsonite paragenesis is albite; however, the later oxide minerals (ferrotapiolite, alumotantite and manganotantalite) are hosted by muscovite, indicating a similarly late shift in melt/fluid chemistry from albitic to potassic, and therefore more acidic.

As with most occurrences of the simpsonite paragenesis, so little is known of the oxide mineral chemistry of the host pegmatite, that a purely factual discussion of the geochemical setting of the simpsonite paragenesis at Bikita is impossible. However, on the basis of the extremely high Ta/(Ta+Nb) and Mn/(Mn+Fe) ratios, the absence of Ti in members of the paragenesis (Table 94) and the chemistry of the associated hafnon, it is safe to speculate that the simpsonite paragenesis represents a most-highly fractionated assemblage of oxide minerals at Bikita. It is difficult to determine fractionation trends within the paragenesis because of the chemical dissimilarity of the species which crystallize with simpsonite versus those which crystallized after it. The only elements common to all species are Ta, Nb and Sn; Sn remains constant for all species, and Ta/(Ta+Nb) is so extremely high that no significant variations in the ratio could be detected.

Table 94: Simpsonite Paragenesis at Bikita:
          Geochemistry Summary

Mineral	Ta/(Ta+Nb)	Mn/(Mn+Fe)	Ti*	Sn*
Simpsonite	1.000	---	0.001	0.110
Alumotantite	1.000	---	0.000	0.010
Manganotantalite	0.995	0.895	0.000	0.090
Ferrotapiolite	0.996	0.329	0.000	0.130

* per 24(O)

Early   Late

Simpsonite

Manganotantalite

Ferrotapiolite

Alumotantite
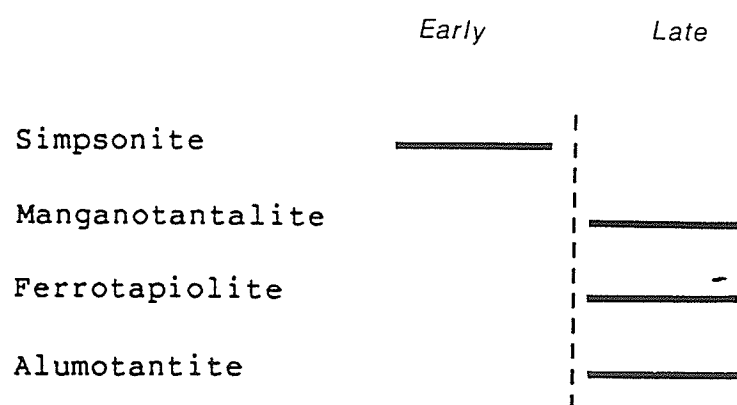
Figure 83: Crystallization history of the simpsonite paragenesis, Bikita pegmatite.

Chapter XXI

THE BENSON NO. 3 PEGMATITE

21.1 LOCATION AND GEOLOGY

The Benson mine pegmatites are located at Mtoko in NE Zimbabwe. In all, some forty pegmatites occur in the region known as the Benson mine (von Knorring & Hornung, 1963). The pegmatite which hosts the simpsonite in this region is known as the Benson no. 3.

The only accounts of the regional geology are given in von Knorring & Hornung (1962,1963) and Hornung & von Knorring (1962). The country rocks to the pegmatite are basic metavolcanic rocks of the Bulawayan System, which have been metamorphosed to amphibolite grade. The Benson no. 3 pegmatite is dyke-like, with a vertical dip, and has maximum dimensions of 300 m long by 11 m wide by 13 m thick.

The pegmatite is symmetrically zoned; von Knorring & Hornung (1963) assign four internal units: (1) a wall unit of quartz, albite and muscovite, (2) an intermediate unit of quartz, lepidolite and albite, (3) a late-stage unit of cleavelandite plus lithium mica, and (4) a quartz core.

von Knorring & Hornung (1963) have outlined the distribution of accessory minerals in the pegmatite, a compilation of which is given in Table 95. On the basis of the regional geology, the accessory mineralogy, and published Ta/(Ta+Nb) ratios (von Knorring & Hornung, 1963), the pegmatite classifies as either the petalite or spodumene subtypes of complex-type, rare-element granitic pegmatites of orogenic association (Černý, 1986).

Table 95: Accessory Mineral Distribution

Unit	Accessory Minerals
Wall	spessartine, cassiterite
Intermediate	tantalite, beryl, spodumene
Late Stage	lepidolite, microlite, manganotantalite, topaz, simpsonite, stibiotantalite

21.2   OXIDE MINERALOGY

The oxide mineralogy of the Benson no. 3 pegmatite has been comparatively well-documented by von Knorring & Hornung (1963). Cassiterite is limited to the wall unit, while tantalite, microlite simpsonite and stibiotantalite are found in the intermediate and late-stage units (Table 95). However, individual assemblages are not reported by von Knorring & Hornung (1963), and naught is known of the mineralogy or structures shown by the rocks hosting these minerals, except for members of the simpsonite paragenesis.

21.2.1   Simpsonite Paragenesis

Simpsonite and its associates were found in "bands" of fine-grained "massive" (?) colourless mica of the late-stage unit, associated with spodumene, quartz, topaz and albite (von Knorring & Hornung, 1963). The members of the paragenesis at the Benson pegmatite are simpsonite, stibiotantalite and microlite, which although simple by standards set by occurrences of the paragenesis in many other pegmatites, is still the most diverse

oxide mineral assemblage of the pegmatite. Although attempts were made to obtain simpsonite samples from the Benson no. 3 pegmatite, all were unsuccessful; consequently, the accounts to follow are derived wholly from von Knorring & Hornung (1963).

A summary of the crystallization history is given in Figure 84.

Simpsonite was the first member of the paragenesis to form. It is anhedral and ranges in diameter from "minute" to 10 mm. It is usually found on its own, but a few cases of simpsonite inclusions in stibiotantalite indicate it to have formed slightly before the stibiotantalite. Note that the textural relationship here is one of overgrowth, and not replacement.

Microlite was the last oxide mineral to form, and it did so later than the simpsonite plus stibiotantalite; it occurs as replacements of the stibiotantalite only. No analysis of the microlite was obtained by von Knorring & Hornung (1963), consequently it is not known whether the microlite is a common or antimonian variety. Its unit cell edge of 10.42 Å precludes the presence of substantial Cs in the structure, so it is not a cesstibtantite.

Chemical analyses of the simpsonite and stibiotantalite were done by von Knorring & Hornung (1963), and have been presented in earlier chapters of this thesis. Important features of the chemistry of these minerals, from a geochemical point of view, are given in Table 96. The Ta/(Ta+Nb) ratios indicate the Benson no. 3 pegmatite to be amongst the most highly fractionated pegmatites in the Benson mine region, and show the members of the simpsonite paragenesis to be the most highly fractionated assemblage of the Benson no. 3 pegmatite (von Knorring & Hornung, 1963).

Table 96: Simpsonite Paragenesis at Benson no.3:
          Geochemistry Summary

Mineral	Ta/(Ta+Nb)	Ti*	Sn*
Simpsonite	0.952	0.00	0.11
Stibiotantalite	0.950	0.00	0.00

* per 24(O)

Early   Late

Simpsonite   ———————— |
                                  |
Stibiotantalite   ———————— | ⟶
                                  |
Microlite | ————————
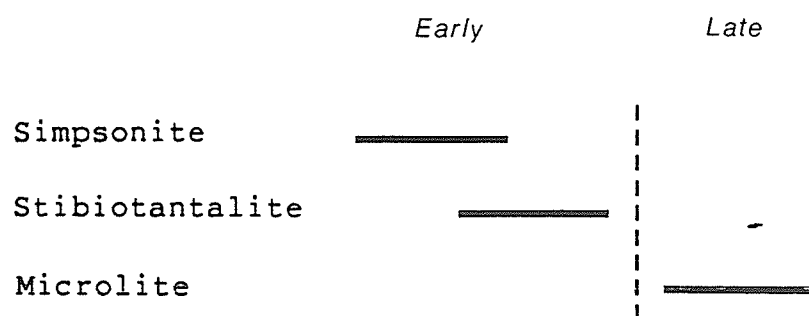
Figure 84: Crystallization history of the simpsonite paragenesis, Benson no. 3 pegmatite.

Chapter XXII

THE LESHAIA PEGMATITE

22.1   LOCATION AND GEOLOGY

Simpsonite was found in a granitic pegmatite in the vicinity of Leshaia, Kola Peninsula, USSR by Sosedko & Denisov (1957). Despite several publications on the pegmatite (Sosedko & Denisov, 1957 and several of Voloshin et al., 1981-), the regional geology of the area is not documented, nor are the geology and internal structure of the pegmatite.

The overall mineralogy of the pegmatite, and the silicate mineralogy near the simpsonite occurrence have been described by Sosedko & Denisov (1957) and Voloshin et al. (1981). The list includes muscovite, Cs-beryl, spodumene, montebrasite, pollucite, petalite, eucryptite and tourmaline, which indicate the pegmatite to belong to the petalite subtype of complex-type, rare-element granitic pegmatites of orogenic association (Černý, 1986).

No work has been done on the oxide mineralogy of the pegmatite outside of investigations of the simpsonite paragenesis.

22.2   SIMPSONITE PARAGENESIS

Incomplete references to the host pegmatites of several new minerals from granitic pegmatites of the Kola Peninsula in recent years confuses the issue; nevertheless, a conservative list of all oxide mineral species which are undisputedly associated with the simpsonite from the Leshaia pegmatite

are given in Table 97. The list is impressive: 11 individual species are known to be members of this occurrence of the simpsonite paragenesis, making it the most diverse occurrence of the paragenesis.

As with several other simpsonite occurrences, the simpsonite in the Leshaia pegmatite is associated with albitic bodies. Simpsonite, cassiterite, manganotantalite, wodginite, microlite and tapiolite all crystallized during the time of formation of the albite bodies. Simpsonite was the first of these to crystallize, with all other species forming slightly after the simpsonite (Voloshin, 1983). Members of this early generation of mineralization, particularly the microlite and simpsonite, were in turn replaced by alumotantite, natrotantite, cesstibtantite, stibiotantalite and sosedkoite. This later generation of Ta-oxide minerals is ascribed by Voloshin et al. (1981) to a potassic (metasomatic) event. The crystallization sequence is summarized in Figure 85.

A summary of important aspects of the geochemistry of the oxide minerals is given in Table 97. This occurrence of the simpsonite paragenesis is typical for its high Ta/(Ta+Nb), moderately high Mn/(Mn+Fe), and low Ti-contents. Sn distribution is erratic, but the presence of wodginite (as opposed to tantalowodginite) and cassiterite indicate higher-than-average μ(Sn) for an occurrence of the simpsonite paragenesis.

Because of the diversity of species, it is difficult to make comparisons between the geochemistry of both generations of oxide minerals. The mean Ta/(Ta+Nb) ratio for the early generation is 0.934, and for the later generation it is 0.946; Ta/(Ta+Nb) does not seem to have varied significantly during the crystallization of the paragenesis. This is the Ti-richest occurrence of the simpsonite paragenesis. All Ti is concentrated in the

manganotantalite and tapiolite of the earlier generation; the late genera-
tion is free of Ti. Fe^{2+}-Mn oxide minerals are similarly restricted to the
early generation of mineralization; except for sosedkoite, which contains
Fe^{3+}, no late generation minerals contain iron or manganese. In general,
late generation minerals have rather atypical A-cation chemistries (Al^{3+},
Sb^{3+}, Na>>Ca) for Ta-oxide minerals. Alternately, the early generation
minerals, except for simpsonite, are rather unexceptional Ta-oxide minerals
in terms of their A-site chemistries.

Table 97: Simpsonite Paragenesis at Leshaia:
Geochemistry Summary

Mineral	Ta/(Ta+Nb)	Mn/(Mn+Fe)	Ti*	Sn*
Simpsonite**	0.955	---	0.000	0.110
Manganotantalite	0.793	0.791	0.131	0.058
Wodginite	0.902	1.000	0.000	2.352
Ferrotapiolite**	0.966	0.160	0.080	0.000
Cassiterite	1.000	0.769	0.000	11.54
Microlite**	0.985	---	0.000	0.000
Stibiotantalite	0.905	---	0.000	0.000
Alumotantite	0.983	---	0.000	0.000
Cesstibtantite	0.938	---	0.000	0.000
Natrotantite**	0.952	---	0.000	0.000
Sosedkoite**	0.953	---	0.000	0.000

* per 24(O)
** from Voloshin (1983)
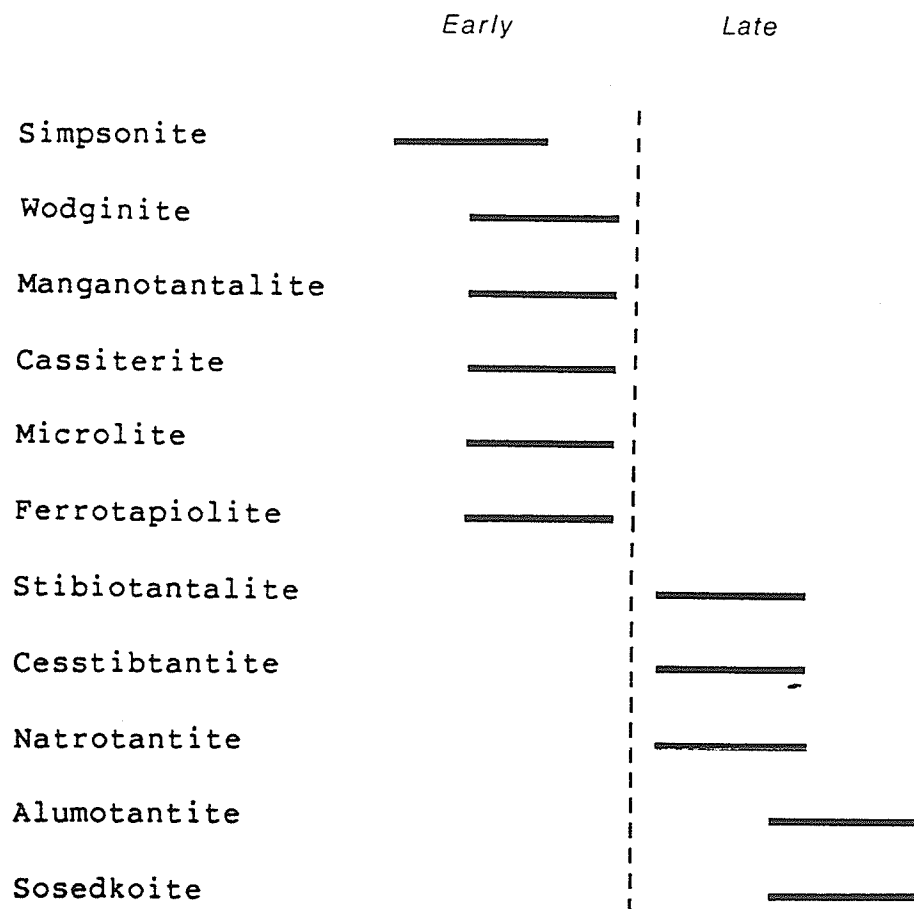
Figure 85: Crystallization history of the simpsonite paragenesis, Leshaia.

Chapter XXIII

TABBA TABBA

23.1 LOCATION AND GEOLOGY

The Tabba Tabba pegmatites are about 50 km SE of Port Hedland, W.A., Australia. The geology of the area is not well-documented; the most recent accounts are Ellis (1950) and Blockley (1980).

The Tabba Tabba deposits are located in a "tongue" of meta- basalts, gabbros, basic tuffs and pelitic sedimentary rocks which have been metamorphosed to amphibolite facies conditions (Blockley, 1980). This tongue is located between two masses of granitic rocks. A younger, syntectonic granitic intrusion which cross-cuts the rocks of the tongue and the older granites is proposed by Blockley (1980) to be the source of the pegmatites, although this connection has not been proven geochemically.

Two groups of granitic pegmatites are present at the locality; both are heavily weathered. The southern-most group consists of two interpenetrating dykes of shallow dip (25-35°) which form a V-structure. These pegmatites hosted most of the cassiterite which was mined in the area. The second occurrence of granitic pegmatites at the locality is of a single, large pegmatite to the immediate north of the V-shaped group. This pegmatite, known as MC116, hosts the simpsonite, and is the main source of Ta-oxide minerals in the area.

Pegmatite MC116 has maximum dimensions of length 600 m, thickness 55 m, and has a shallow dip. The country rocks to the dyke are sheared, basic

metavolcanic rocks. Only the zoning of the intermediate units of the pegmatite has been published (Ellis, 1950). The units are (1) a microcline-perthite plus quartz unit, which comprises most of the pegmatite, (2) a (later) saccharoidal albite unit consisting of fine-grained albite, quartz and muscovite, with accessory amounts of Ta-oxide minerals, cassiterite, beryl and lepidolite, and (3) a quartz unit, expressed as several tabular bodies.

23.2   OXIDE MINERALOGY

The oxide minerals of MC 116 are confined to the saccharoidal albite unit, particularly those parts of the unit below occurrences of the quartz unit. Ellis (1950) has documented the rhythmic layering of this unit. The oxide minerals are tantalite, microlite (Ellis, 1950), simpsonite (Bowley, 1939) and wodginite (Pryce, 1970). No chemical analyses of individual oxide minerals have been done outside of members of the simpsonite paragenesis; however, Ellis (1950) gives analyses for batches of oxide mineral concentrates (Table 98), which show that $Ta/(Ta+Nb)$ is high over much of the pegmatite.

Table 98: Ta_2O_5 and Nb_2O_5 Contents of Oxide Mineral
Concentrates at Tabba Tabba

Workings	Ta_2O_5*	Nb_2O_5*	$Ta/(Ta+Nb)$
North	57.7	2.8	0.92
Central	64.9	2.1	0.95
South	68.8	4.1	0.91

* wt.%
All data from Ellis (1950).

23.2.1 Simpsonite Paragenesis

Tabba Tabba is the type locality for simpsonite (Bowley, 1939). Ellis (1950) describes the simpsonite occurrence. Simpsonite is confined to a 5-8 cm thick by 1 m long band in the central workings of the saccharoidal albite unit, located at a surface exposure of the saccharoidal albite unit - quartz unit contact. The simpsonite-bearing region seems to be more weathered than stratigraphically lower sections of the saccharoidal albite unit, perhaps reflective of the higher proportions of muscovite at the contact (Ellis, 1950).

The mineralogy of the Tabba Tabba occurrence of the simpsonite paragenesis is simple: simpsonite, wodginite and microlite. The simpsonite forms subhedral to euhedral cm-scale crystals. Microlite replaces the simpsonite, and is associated with muscovite veinlets, which mark a late shift in fluid/melt chemistry from sodic to potassic. Wodginite is also partially replaced by the microlite. The crystallization history of the paragenesis is summarized in Figure 86.

The data given in Table 98 show that oxide minerals in the region of the simpsonite occurrence (central workings) have slightly higher $Ta/(Ta+Nb)$ ratios than those from adjacent workings to the north and south. A summary of the geochemistry of the Tabba Tabba occurrence of the simpsonite paragenesis is given in Table 99. On the basis of uniformly high $Ta/(Ta+Nb)$ and $Mn/(Mn+Fe)$ ratios, and low Ti contents, it is inferred that the paragenesis is a late crystallization product, and represents a high degree of transition-metal cation fractionation. Like the Bikita pegmatite samples, the Sn-contents of all members of the simpsonite paragenesis at Tabba Tabba are high; $\mu(Sn)$ was even high enough to initiate cassiterite crystallization.

Table 99:   Simpsonite Paragenesis at Tabba Tabba:
                Geochemistry Summary

Mineral	Ta/(Ta+Nb)	Mn/(Mn+Fe)	Ti*	Sn*
Simpsonite	0.909	---	0.005	0.21
Wodginite	0.963	0.992	0.000	1.80
Microlite	0.972	---	0.000	0.28

* per 24(O)

```
                          Early           Late

        Simpsonite      ══════════  |
                                    |
        Wodginite       ══════════  |
                                    |
        Microlite                   |  ══════════
                                    |
```
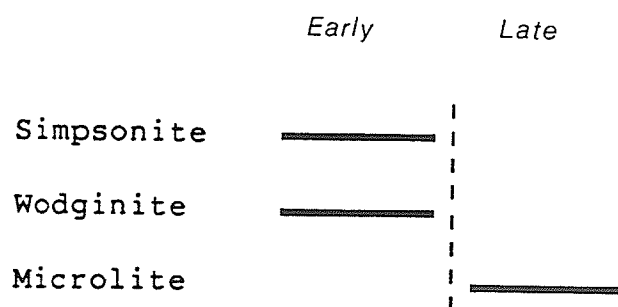
Figure 86: Crystallization history of the simpsonite paragenesis, Tabba Tabba.

Chapter XXIV

LAKE KIVU

24.1   LOCATION AND GEOLOGY

Simpsonite and other oxide minerals were found by Safiannikoff & von Wambeke (1961) as pebbles in an alluvial deposit at Mumba, near Lake Kivu in Zaire.   The mineralogy of these pebbles clearly indicates the original host rock to have been a rare-element granitic pegmatite, most probably belonging to either the spodumene or petalite subtypes of complex-type, rare-element granitic pegmatites of orogenic association (Černý, 1986). Unfortunately, the source of the pebbles has never been located, so nothing is known of the geologic setting or internal zoning of the parental pegmatite.

24.2   SIMPSONITE PARAGENESIS

It is unfortunate that the simpsonite-bearing samples at Lake Kivu were not found in situ; the paragenesis here has an atypical geochemistry and a very diverse mineralogy.   To date, investigations of only one pebble have shown simpsonite, cassiterite, manganocolumbite, rankamaite, plumbomicrolite, microlite and parabariomicrolite to be present.

Simpsonite, manganocolumbite and cassiterite were the first minerals of this occurrence of the paragenesis to form.   Rounded relicts of partially-replaced simpsonite and manganocolumbite, as opposed to sharp, euhedral cassiterite crystals, all in a rankamaite matrix indicate that the replace-

ment event marked by rankamaite formation was highly selective; only the Ta,Nb-oxides were replaced. As discussed earlier (Part 3), the pervasiveness of this replacement event is marked by selective cation leaching of the relict manganocolumbite, in which the lowest-charged cations (Mn^{2+}, Fe^{2+}) are significantly depleted.

Plumbomicrolite is of uncertain origin. Safiannikoff & van Wambeke (1961) indicate it to have crystallized after simpsonite; however, the sample examined in the present study has plumbomicrolite and microlite inclusions in simpsonite; thus it would seem here that plumbomicrolite precedes simpsonite in the crystallization sequence. It is assumed that plumbomicrolite and microlite formed at about the same time as simpsonite, but over a wider period of time.

Parabariomicrolite occurs as a replacement of the microlite, and by analogy with the Alto do Giz occurrence, is assumed to have been one of the last oxide minerals to form, perhaps during the rankamaite-forming event. Figure 87 summarizes the inferred crystallization sequence.

Some aspects of the geochemistry of the Lake Kivu occurrence of the simpsonite paragenesis are outlined in Table 100. The following features are typical of the occurrence:

(1) Moderate to high Ta/(Ta+Nb). This occurrence shows the lowest degrees of Nb-Ta fractionation of all known occurrences of the simpsonite paragenesis. Furthermore, the range in Ta/(Ta+Nb) is large; the low end is marked by manganocolumbite with a value of 0.343, and the high end by parabariomicrolite with a value of 0.826. The ratio does not seem to increase with crystallization; however, the mineralogical diversity of the occurrence may mask the subleties of any such increase.

(2) High Mn/(Mn+Fe). The only Fe-Mn mineral, manganocolumbite, has Mn/(Mn+Fe)=0.857. Ferrotapiolite is conspicuously absent.

(3) Undetectable Ti.

(4) High Sn contents (earliest-formed oxide minerals).

Table 100: Simpsonite Paragenesis at Lake Kivu:
Geochemistry Summary

Mineral	Ta/(Ta+Nb)	Mn/(Mn+Fe)	Ti*	Sn*
Simpsonite	0.817	---	0.000	0.090
Manganocolumbite	0.343	0.857	0.000	0.086
Cassiterite	0.913	---	0.000	11.40
Microlite	0.805	---	0.000	0.000
Plumbomicrolite	0.670	---	0.000	0.070
Parabariomicrolite	0.826	--- .	0.000	0.000
Rankamaite	0.678	---	0.000	0.000

* per 24(O)
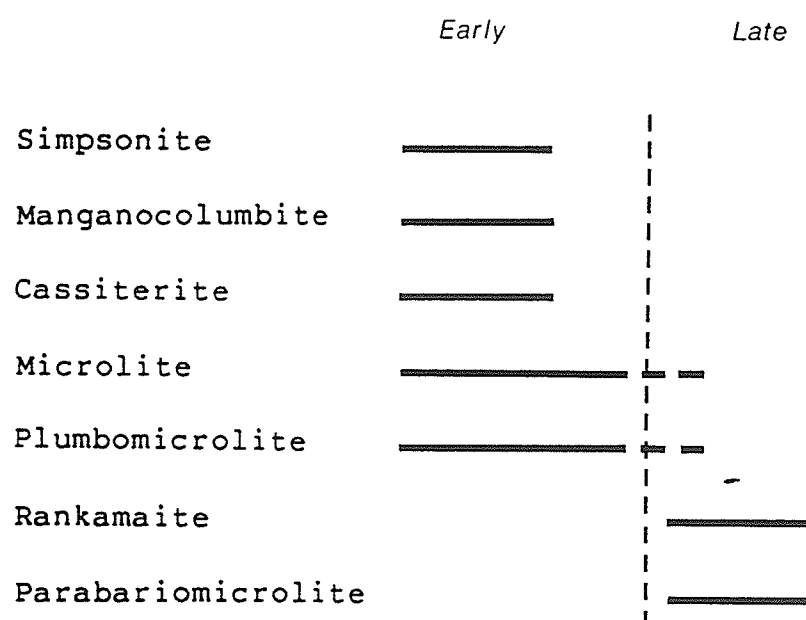
Figure 87: Crystallization history of the simpsonite paragenesis, Lake Kivu.

Chapter XXV

THE MANONO PEGMATITE

25.1   LOCATION AND GEOLOGY

The Manono pegmatite is located 500 km E of the Lualaba Valley, Zaire, and is enclosed by schists of the Kilabara System (Thoreau, 1950).   The pegmatite consists of a network of dyke-like intrusions which range up to 14 km in length and 700 m in width.

The pegmatite is zoned; Thoreau (1950) describes three units consisting of: (1) K-feldspar unit – K-feldspar,   quartz and minor muscovite,   (2) albite unit – albite, quartz and muscovite, and (3) spodumene unit – spodumene, albite and muscovite. Most accessory minerals are described as being associated with the albite unit;   these are beryl, tourmaline,   oxide-minerals, apatite, zircon and garnet.   Černý (1986) classifies this pegmatite as belonging to the spodumene subtype of complex-type rare-element granitic pegmatites.

25.2   SIMPSONITE PARAGENESIS

Little has been published on the oxide mineralogy of the Manono pegmatite, outside of Thoreau's (1950) enumeration of the oxide mineral species and Mélon's (1950) analyses of thoreaulite.   The list of oxide mineral species is cassiterite, columbite-group minerals, thoreaulite and simpsonite.

Simpsonite was found as an isolated crystal in a banded "nodule" of undescribed mineralogy (Sarp & Duferne, 1983). A partial chemical analysis of the simpsonite was published by Sarp & Duferne (1983), but in the absence of a Nb determination, little use can be made of the analysis. Attempts by the present author to obtain material were unsuccessful.

Chapter XXVI

DISCUSSION: THE ORIGIN OF THE SIMPSONITE PARAGENESIS

26.1 SUMMARY OF OCCURRENCE

Despite the wide geographical separation between localities, it is remarkable just how similar the various occurrences of the simpsonite paragenesis are.

Where data on the regional geology of the pegmatites hosting the simpsonite are available, it is seen that the country rocks are of Precambrian age, that these rocks typically lie in greenstone belts, and that metabasalts and metasedimentary rocks are the typical country rocks.

All occurrences of the simpsonite paragenesis are restricted to the same class and type of granitic pegmatite: the complex type of rare-element granitic pegmatites of orogenic association. At the level of subtype, the similarities still persist; regarding the pegmatites which could be unambiguously classified at this level of examination, all but one, Manono, belong to the petalite subtype, which limits their conditions of formation to relatively low pressure (<3.5 kbar) environments, and the range of primary crystallization to 350-650°C (London, 1984; Černý, 1986). Manono belongs to the spodumene subtype of the same type of pegmatite as the others (complex), which implies conditions of formation at slightly higher pressures than the petalite subtype (3<P<4 kbar).

Where the internal zoning of the host pegmatite is well-enough defined, the simpsonite paragenesis is observed to occur in some of the latest units

to crystallize. A preference seems to be shown for saccharoidal albite bodies of rather limited size, which tend to be located near or at the contacts of the intermediate unit to which the bodies belong, and the quartz unit of the pegmatite.

The only restriction in defining an occurrence of the simpsonite paragenesis is the presence of simpsonite. It is again remarkable just how similar the mineralogy of the various deposits are, working under this rather loose definition of the paragenesis (Table 101). Simpsonite is an index mineral, the presence of which implies rather specific conditions at the time of formation of the mineral. A comparison of the two most mineralogically diverse occurrences of the paragenesis, namely Alto do Giz and Leshaia, shows that seven species are common to both occurrences, and that there are two sets of analogous species (wodginite and cesstibtantite at Leshaia occupy the same niche as tantalowodginite and stibiomicrolite, respectively, at Alto do Giz). This leaves only two species at Leshaia (cassiterite and sosedkoite) and one species at Alto do Giz (parabariomicrolite) for which no analogue exists at the other deposit.

Strong similarities exist between the occurrences even at the level of mineral chemistry. Table 102 gives mean unweighted (i.e. not weighted by abundance of each mineral phase) Ta/(Ta+Nb) ratios for each occurrence, and Ta/(Ta+Nb) ratios for the simpsonite of each occurrence. Eight out of nine of the occurrences have only marginally different mean ratios: 0.94 < Ta/(Ta+Nb) < 1.00. The Kivu occurrence is the exception with Ta/(Ta+Nb) = 0.722, but serves to show that the simpsonite paragenesis can form at relatively moderate Ta/(Ta+Nb). Extreme Ta fractionation is not necessary for the formation of the paragenesis, but extremity tends to be the rule, rather than the exception.

Table 101: Mineralogy of the Simpsonite Paragenesis

Mineral Species	Tanco	Alto do Giz	Onça	Bik-ita	Ben-son	Lesha-ia	Tabba	Kivu	Mano-no
Alumotantite		x		x		x			
Cassiterite						x		x	x
Cesstibtantite	x					x			
Ferrotapiolite	x	x		x		x			
Manganocolumbite								x	
Manganotantalite	x	x		x		x			
Microlite	x	x		x	x	x	x	x	
Natrotantite		x				x			
Parabariomicrolite		x						x	
Plumbomicrolite								x	
Rankamaite								x	
Simpsonite	x	x	x	x	x	x	x	x	x
Sosedkoite						x			
Stibiomicrolite		x							
Stibiotantalite		x			x	x			
Tantalowodginite	x	x							
Wodginite	x					x	x		
No. of species	7	10	1	5	3	11	3	7	2

Other similarities in the geochemistry of the occurrences are (1) impoverishment in Ti, (2) enrichment in large, low-valence cations (e.g. Pb, Cs, Ba), particularly in late-stage replacement minerals, (3) a frequent genetic association of early-stage members of the paragenesis with sodic matrix mineral assemblages, and of late-stage (replacement) members with potassic assemblages, and (4) occasional reversals in Fe-Mn fractionation, marked by changes in tantalite chemistry and first appearances of ferrotapiolite.

It is concluded that the processes leading to the formation, and perhaps ultimately affecting the development of the simpsonite paragenesis at each of its occurrences are extremely similar. Despite all of its diversity,

Table 102: Mean Ta/(Ta÷Nb) Ratios for Occurrences
of the Simpsonite Paragenesis

Locality	Ta/(Ta+Nb)	
	Mean*	Simpsonite
Tanco	0.948	0.980
Alto do Giz	0.974	0.987
Onça	0.993**	0.993
Bikita	0.998	1.000
Benson	0.951	0.952
Leshaia	0.939	0.955
Tabba Tabba	0.948	0.909
Kivu	0.722	0.817
Manono	---	---

* mean for all species of the parage-
  nesis (not weighted by abundance).
** based on a single analysis

the simpsonite paragenesis is a rather predictable phenomenon; several
aspects of the regional geology, as well as the type of host pegmatite, the
relative time of formation of the paragenesis with respect to the crystal-
lization of the host pegmatite, crystallization sequences within the para-
genesis, the matrix mineralogy, and the bulk geochemical signature of the
paragenesis can all be predicted with considerable confidence. The most
significant difference between the occurrences of the simpsonite paragene-
sis seems to be the extent to which the processes responsible for the for-
mation of each occurrence operated, thereby determining the diversity of
mineralization.

26.2   FORMATION OF THE SIMPSONITE PARAGENESIS

Only one deposit, namely the Tanco pegmatite, has been well-enough stud-ied in terms of both its geology and oxide mineralogy to provide considera-ble evidence on the conditions necessary for the formation of the simpso-nite paragenesis.   All conclusions derived from the other occurrences are based mainly on inference and comparison to the Tanco occurrence.

From the study of the oxide mineralogy of the Tanco pegmatite, it was shown that the original melt or fluids in the vicinity of the simpsonite occurrences had the highest concentrations of Ta for the whole pegmatite. As will be shown later, this is probably not a coincidence; increasing tan-talum activity during the crystallization of the paragenesis may have played a significant role in determining crystallization sequences.   How-ever, it must be noted that high overall abundance of Ta in the host pegma-tite is not a prerequisite to the development of the simpsonite paragene-sis; the Bikita pegmatite contains only negligible quantities of Ta-oxide minerals, yet hosts an occurrence of the simpsonite paragenesis.   Further-more, on the basis of the highly localized nature of the occurrences and generally small quantities of simpsonite in its host pegmatites, it is con-cluded that Ta concentrations sufficient for simpsonite formation can only be attained on a highly local scale.   It is the efficiency of tantalum accumulation during the internal evolution of the pegmatite, rather than the initial quantitative accumulation of Ta in the pegmatitic melt which is responsible for these concentrations.

In the case of the Tanco pegmatite,   it was shown that the simpsonite paragenesis was typified by much higher Ta/(Ta+Nb) and lower Ti than any other oxide mineral assemblage at the pegmatite.   The geochemistry of the

Kivu occurrence shows that extremely high Ta/(Ta+Nb) (i.e. differences in the crystal chemistry of Ta and Nb) is not a factor which controls the formation of the paragenesis. Instead, both high Ta/(Ta+Nb) and low Ti contents are symptomatic of high degrees of transition-metal cation fractionation which are necessary for the high local accumulations of Ta.

Locally high μ(Ta) during crystallization cannot be the sole criterion responsible for the formation of the simpsonite paragenesis. The Harding pegmatite, which belongs to the spodumene subtype of the same type of granitic pegmatite as the simpsonite-bearing ones, contains large, microlite-rich regions which imply local Ta concentrations of the parental melt or fluids in excess of those observed for the simpsonite paragenesis at Tanco (L. Cook, pers. comm.), yet the Harding pegmatite does not host simpsonite. Rather obviously, μ(Na,Ca) and probably μ(F) must have been relatively high in these regions, producing a stable environment for microlite formation. Evidently, a high chemical potential of Ta relative to the potentials of other alkali and transition-metal cations is required for the formation of the simpsonite paragenesis.

26.3   EVOLUTION OF THE SIMPSONITE PARAGENESIS

The division drawn here between the formation and evolution of the simpsonite paragenesis is a bit artificial; it is probable that the factors responsible for the formation of the paragenesis also guide the mineralogical and geochemical evolution of the paragenesis. Alternately, several events which did not take place until the time of formation of the paragenesis, may also have affected the evolution of the paragenesis, and merit discussion here. As will be shown, both increasing μ(Ta) and melt/fluid

acidity can be called on to explain the changes in mineralogy and geochemistry observed during the crystallization of the paragenesis.

1. <u>Increasing μ(Ta)</u>. It was shown that relatively high μ(Ta) was necessary for the formation of the simpsonite paragenesis. It is important to consider whether or not μ(Ta) showed further changes during crystallization of the paragenesis, and if so, how this behaviour affected the crystallization history of the paragenesis.

Figure 88 is an attempt to address this question. The ordinate variable is the number of <u>A</u>-cations, and the abscissa variable is the number of <u>B</u>-cations per mineral species, on a basis of 24(O). Ta and Nb are designated as <u>B</u>-cations, and all other cations are designated as <u>A</u>-cations. Mineral species were divided into two groups: those species which tend to crystallize at the same time as simpsonite, and those which tend to crystallize after simpsonite. The minerals which crystallize about the same time as simpsonite cluster near the end of the plot with low <u>B</u>-cation:<u>A</u>-cation ratios; later-formed minerals cluster near the end with high <u>B</u>-cation:<u>A</u>-cation ratios. The last species to crystallize (e.g. rankamaite-sosedkoite and parabariomicrolite) tend to plot at the <u>B</u>-cation-richest end of this latter field. It is obvious that crystallization resulted in increasingly <u>B</u>-cation-enriched and <u>A</u>-cation-impoverished mineral species. It is inferred that this was a response to progressively increasing μ(Ta) relative to μ(<u>A</u>).

The inferred increase in μ(Ta)/μ(<u>A</u>) is also accompanied by a change in <u>A</u>-cation chemistry. Earliest-formed species tend to have smaller and more highly-charged <u>A</u>-cations (Mn,Fe^{2+},Al, Sn^{4+},Ca,Na) than later species, which instead host major amounts of large, low-valence cations (Na,Pb,Cs,Ba). It

is proposed that as $\mu(Ta)$ increased, and the chemical potentials of the compatible elements Mn,Fe,Ca and Na decreased to such low levels that "typical" Ta-oxide minerals could no longer form, Ta began to combine with elements which are more strongly partitioned into silicate phases (e.g. Al). As the chemical potentials of these elements also became infinitesimally low, Ta was forced to form oxide minerals with the minor amounts of incompatible elements in these latest batches of melt/fluid. The model explains several important properties of the paragenesis: (1) why simpsonite is one of the first species to form, (2) why simpsonite is one of the most abundant phases of the paragenesis, and (3) why replacement phases are rich in LIL's and poor in Mn,Fe,Sn and other highly-charged transition-metal cations.

2. <u>Increasing acidity</u>. In four of the eight occurrences of the simpsonite paragenesis (which perhaps not so coincidentally are among the best-documented occurrences), a change in matrix mineralogy was noted, indicative of a late increase in melt or fluid acidity. Accompanying this change in acidity is a change in the types of species which crystallized. To what extent can the changes in oxide mineralogy be related to melt/fluid acidity?

Igneous melts contain a variety of polyanions at various stages during their crystallization. As igneous melts cool and crystallize, or differentiate, the acidity and degree of polymerization of silicate polyanions in the melt increases. Silicate mineral species which crystallize from the melt reflect these changes. The first silicate minerals to crystallize host the most basic, and least-polymerized silicate structure modules (e.g. isolated $[SiO_4]^{4-}$ tetrahedra in olivine); the last minerals to crystallize

At   Alumotantite
Cs   Cesstibtantite
Mc   Microlite
Nt   Natrotantite
Pb   Plumbomicrolite
Pm   Parabariomicrolite
Rk   Rankamaite
Sb   Stibiotantalite
Sm   Stibiomicrolite
Sp   Simpsonite
So   Sosedkoite
Tn   Manganotantalite
Tp   Ferrotapiolite
Tw   Tantalowodginite
Wd   Wodginite
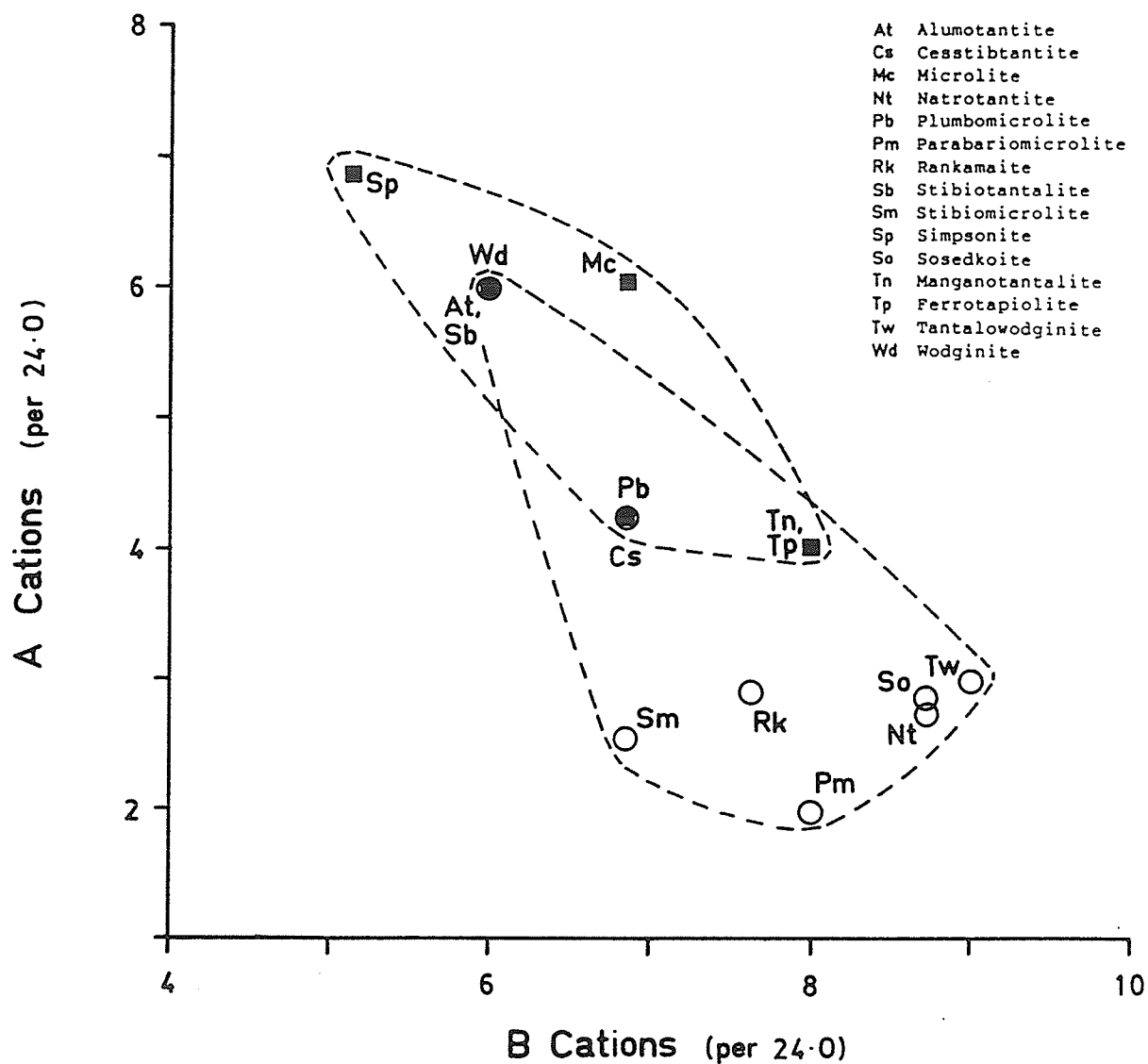
Figure 88:   Normalized cation proportions in Ta-oxide minerals of the simp-
sonite paragenesis.   Squares denote minerals which tend to
crystallize at the same time as simpsonite.   Circles denote
minerals which tend to crystallize after simpsonite.

often host the most acidic, and most highly-polymerized silicate structure modules (e.g. $[Si_4O_{10}]^{4-}$ sheets of the micas).

Tantalum, like silicon, is a highly-charged cation and forms relatively strong bonds with oxygen. Although it is more highly charged than Si, its preference for octahedral coordination results in a Pauling bond strength marginally lower than Si (by 1/6 v.u.). With a bond strength close to, but less than 1 v.u., $[TaO_6]^{7-}$ octahedra can polymerize to form rather strongly-bonded structure modules, like silicate anions. It is reasonable to assume that if such modules exist in the melt or fluid from which tantalum oxide minerals form, then, like silicates, variations in melt/fluid acidity could affect the degree of polymerization and basicity of the "tantalate" structure modules from which tantalum oxide minerals form by condensation of these modules.

As Brown (1981) and Hawthorne (1985) have shown, crystal structure analyses provide data from which the Lewis basicity and polymerization of structure modules can be calculated. Brown (1981) defines the Lewis acid strength of a cation as its valence divided by its average coordination number, which is the average bond valence of a characteristic bond formed by the cation. The characteristic valence of a bond formed by an anion could analogously be termed the Lewis base strength of the anion.

The Lewis basicity of a single $[TaO_6]^{7-}$ polyhedron should serve as a pertinent example of the calculation. The strength of a Ta-O bond is 5/6 v.u., which multiplied over six bonds of the octahedron means that the charge at Ta is satisfied. However, each O atom requires 2 v.u. of charge, but receives only 5/6 v.u. from the Ta atom. This leaves each O with 7/6 v.u. to form additional bonds; the resulting Lewis base strength of the

oxygen atoms will be 7/6 divided by the number of additional bonds formed by each oxygen. If it is assumed that the O atoms are [4]-coordinated, then during crystallization, 3 additional bonds must be formed at each O atom, resulting in a Lewis base strength of 0.39 v.u. . Obviously, the calculation is highly dependent upon anion coordination, further emphasizing that a reasonably precise knowledge of the structure of a mineral is necessary before such calculations can be done.

Lewis basicities and degrees of polymerization of the structure modules for the minerals of the simpsonite paragenesis are given in Table 103. The entries in Table 103 are arranged in order of decreasing basicity, which also corresponds well with increasing polymerization of the structure modules. Decreasing basicity marks progression from finite cluster structures (e.g. simpsonite) to sheet structures (e.g. stibiotantalite) to framework structures (e.g. microlite). A comparison of Table 103 to the crystallization histories outlined in preceding chapters of this Part shows that earliest-crystallized minerals of the simpsonite paragenesis host the least polymerized and most basic structure modules (e.g. simpsonite), and that latest-formed species host the most polymerized and least basic modules (e.g. rankamaite).

The data presented here suggest that melt or fluid basicity played a significant role in the evolution of the paragenesis. A model of increasing acidity of the parental melt/fluid accounts for (1) replacement of simpsonite by alumotantite, (2) increasing Ta content at the B-site of wodginite-group minerals with fractionation, and (3) predominance of microlite subgroup minerals and structurally similar minerals (natrotantite, parabariomicrolite) in the latest crystallization products of the

Table 103: Lewis Basicities of B-O Structure Modules
of Simpsonite Paragenesis Minerals

Mineral	Module	Polymer Class	Basicity
Simpsonite	$[Ta_3O_{13}]^{11-}$	FC	0.55
Stibiotantalite	$[TaO_4]^{3-}$	S	0.50
Alumotantite	$[TaO_4]^{3-}$	S	0.50
Manganocolumbite-Manganotantalite	$[TaO_3]^{-}$	S	0.50
Wodginite	$[SnTa_2O_8]^{2-}$	FW	0.45
Tantalowodginite	$[Ta_3O_8]^{-}$	FW	0.33
Ferrotapiolite	$[TaO_3]^{-}$	FW	0.33
Natrotantite	$[Ta_4O_{11}]^{2-}$	FW	0.29
Microlite, Plumbomicrolite, Stibiomicrolite, Cesstibtantite, Parabariomicrolite	$[TaO_3]^{-}$	FW	0.17
Rankamaite-Soseckoite	?	FW	~0.2*

FC: finite cluster, S: sheet, FW: framework
* by analogy with the tetragonal tungsten bronzes

paragenesis, on the basis of calculated Lewis basicities of the various Ta-O structure modules.

In summary, both models of increasing μ(Ta) and increasing melt/fluid acidity adequately explain crystallization sequences of the simpsonite paragenesis. Both could operate complementarily, in which case they highlight different aspects of the same geochemical event. To which extent one of the two models could be an artifact of the other is not known - it is easy to conceive a situation where increasing melt/fluid acidity results in increased μ(Ta); alternatively, if an increase in μ(Ta), coupled with a decrease in temperature should lead to more polymerized Ta-oxide minerals, then the Ta-O structure modules of the minerals would necessarily become less basic with crystallization. Along this line, it is important to note that the model of increasing melt/fluid acidity does not explain the formation of the simpsonite paragenesis; taking Tanco as an example, the mean basicity of simpsonite-paragenesis minerals is indistinguishable from that of simpsonite-free parageneses (involving wodginite, microlite and tantalite). Without more work on the non-oxide associates of simpsonite, the ambiguities surrounding the evolution of the simpsonite paragenesis cannot be resolved.

REFERENCES

Andersen, C.A. & Wittry, D.B. (1968): An evaluation of absorption correction functions for electron probe microanalysis. _Journal of Physics D1_, 529-540.

Andersson, S. (1967): Phase analysis studies on the $NaNbO_3-Nb_2O_5$, and $NaNbO_3-Nb_2O_5-H_2O$ systems. _Acta Chemica Scandinavica 21_, 1777-1782.

Appleman, D.E. & Evans, H.T. (1973): Job 9214: Indexing and least-squares refinement of powder diffraction data. U.S. National Technical Information Service, _PB 216 188_.

Bambynek, W., Craseman, B., Fink, R.W., Freund, H.-U. et al. (1972): X-ray fluorescence yields, Auger, and Coster-Kronig transition probabilities. _Reviews of Modern Physics 144_, 716-813.

Bernotat-Wulf, H. & Hoffmann, W. (1982): The crystal structures of lead niobates of the pyrochlore type. _Zeitschrift für Kristallographie 158_, 101-117 (in German).

Beyerlein, R.A., Horowitz, H.S., Longo, J.M. & Leonowicz, M.E. (1984): Neutron diffraction investigation of ordered oxygen vacancies in the defect pyrochlores, $Pb_2Ru_2O_6._5$ and $PbTlNb_2O_6._5$. _Journal of Solid State Chemistry 51_, 253-265.

Beus, A.A., Berengilova, V.V., Grabovskaya, L.I., and others (1968): _Geochemical Exploration for Endogenic Deposits of Rare Elements_. Nedra, Moscow; English translation: Geological Survey of Canada, Library, Ottawa.

Birchall, T. & Sleight, A.W. (1975): Nonstoichiometric phases in the Sn-Nb-O and Sn-Ta-O systems having pyrochlore-related structures. _Journal of Solid State Chemistry 13_, 118-130.

Bishop, H.E. (1974): The prospects for an improved absorption correction in electron probe microanalysis. _Journal of Physics D7_, 2009-2020.

Blasse, G. (1964): Qualitative approach to the structural differences between some mixed metal oxides containing Sb^{5+}, Nb^{5+} and Ta^{5+}. _Journal of Inorganic and Nuclear Chemistry 26_, 1191-1199.

Blockley, J.G. (1980): The tin deposits of Western Australia with special reference to the associated granites. _Geological Survey of Western Australia, Mineral Resources Bulletin 12_, 184 p.

Borisov, S.V. & Belov, N.V. (1962): Crystal structure of simpsonite $Al_4Ta_3O_{13}(F,OH)$. Doklady Akademii Nauk SSSR 147, 683-686 (in Russian).

Bourguignon, P. & Melon, J. (1965): Wodginite du Rwanda. Annales de la Société géologique de Belgique 88, 291-300.

Bowley, H. (1939): Simpsonite (sp. nov.) from Tabba Tabba, Western Australia. Journal of the Royal Society of Western Australia 25, 89-92.

Brisbin, W.C. (1986): Mechanics of pegmatite intrusion. American Mineralogist 71, 644-651.

Brown, I.D. (1981): The bond-valence method: an empirical approach to chemical structure and bonding. In Structure and Bonding in Crystals, Volume II, Academic Press, New York.

_____ & Shannon, R.D. (1973): Empirical bond-strength - bond-length curves for oxides. Acta Crystallographica A29, 266-282.

Burhop, E.H.S. (1955): Le rendement de fluorescence. Journal de Physique et le Radium 16, 625-629.

Burke, E.A.J., Kieft, C., Felius, R.O. & Adusumilli, S.M. (1970): Wodginite from Northeastern Brazil. Geologie en Mijnbouw 49, 235-240.

Byström, A., Hök, B. & Mason, B. (1941): Crystal structure of zinc metantimonate and similar compounds. Arkiv för Kemi, Mineralogi och Geologi 15b, 1-8.

Černý, P. (1982): The Tanco pegmatite at Bernic Lake, southeastern Manitoba. In Granitic Pegmatites in Science and Industry, Mineralogical Association of Canada Short Course Handbook 8, 527-543.

_____ (1986): Classification of granitic pegmatites. Colorado Pegmatite Symposium, Abstracts and Field Guide, Friends of Mineralogy, Denver.

_____ & Ercit, T.S. (1985): Some recent advances in the mineralogy and geochemistry of Nb and Ta in rare-element granitic pegmatites. Bulletin de Minéralogie 108, 499-532.

_____, Goad, B.E., Hawthorne, F.C. & Chapman, R. (1986): Fractionation trends of the Nb- and Ta-bearing oxide minerals in the Greer Lake pegmatitic granite and its pegmatite aureole, southeastern Manitoba. American Mineralogist 71, 501-517.

_____ & Harris, D.C. (1973): Tapiolite, stibiotantalite, and antimonian microlite from the Odd West pegmatite, southeastern Manitoba. Canadian Mineralogist 12, 76-78.

_____, Hawthorne, F.C., LaFlamme, J.H.G. & Hinthorne, J.R. (1979): Stibiobetafite, a new member of the pyrochlore group from Věžná, Czechoslovakia. Canadian Mineralogist 17, 583-588.

_____, Meintzer, R.E. & Anderson, A.J. (1985): Extreme fractionation in rare-element granitic pegmatites: selected examples of data and mechanisms. Canadian Mineralogist 23, 381-421.

_____, Trueman, D.L., Ziehlke, D.V., Goad, B.E. & Paul, B.J. (1981): The Cat Lake - Winnipeg River and the Wekusko Lake Pegmatite Fields, Manitoba. Economic Geology Report ER80-1, Manitoba Department of Energy & Mines, Winnipeg.

_____ & Turnock, A.C. (1971): Niobium-tantalum minerals from granitic pegmatites at Greer Lake, Southeastern Manitoba. Canadian Mineralogist 10, 755-772.

Chakoumakos, B.C. (1984): Systematics of the pyrochlore structure type, ideal $A_2B_2X_6Y$. Journal of Solid State Chemistry 53, 120-129.

Chaminade, J.P., Pouchard, M. & Hagenmuller, P. (1972): Tantalates et oxy-fluorotantalates de sodium. Revue de Chimie Minérale 9, 381-402.

Chen, M.H., Craseman, B. & Mark, H. (1980): Relativistic K-shell auger rates, level widths and fluorescence yields. Physical Review A21, 436-441.

Clark, A.M. & Fejer, E.E. (1978): Tapiolite, its chemistry and cell dimensions. Mineralogical Magazine 42, 477-480.

Colby, J.W. (1968): Quantitative microprobe analysis of thin insulating films. Advances in X-ray Analysis 11, 287-305.

_____ (1980): MAGIC V - a computer program for quantitative electron-excited energy dispersive analysis. In QUANTEX-Ray Instruction Manual, Kevex Corporation, Foster City.

Cooper, D.G. (1964): The geology of the Bikita pegmatite. In The Geology of Some Ore Deposits of Southern Africa, v. II, 441-461.

Crouse, R.A. & Černý, P. (1972): The Tanco pegmatite at Bernic Lake, Manitoba. I. Geology and paragenesis. Canadian Mineralogist 11, 591-608.

_____, Černý, P., Trueman, D.L. & Burt, R.O. (1979): The Tanco pegmatite, southeastern Manitoba. Canadian Institute of Mining and Metallurgy Bulletin, No. 2, 1-10.

Cromer, D.T. & Liberman, D. (1970): Relativistic calculation of anomalous scattering factors for X-rays. Journal of Chemical Physics 53, 1891-1898.

_____ & Mann, J. (1967): X-ray scattering factors computed from numerical Hartree-Fock wave functions. Acta Crystallographica A24, 321-324.

Cummings, J.P. & Simonsen (1970): The crystal structure of calcium niobate ($CaNb_2O_6$). *American Mineralogist 55*, 90-97.

Darlington, E.H. (1975): Backscattering of 10-100 keV electrons from thick targets. *Journal of Physics D8*, 85-93.

Darriet, B., Rat, M., Galy, J. & Hagenmuller, P. (1971): Sur quelques nouveaux pyrochlores des systémes MTO_3-WO_3 et MTO_3-TeO_3 (M = K,Rb,Cs,Tl ; T = Nb,Ta). *Materials Research Bulletin 6*, 1305-1316.

De Almeida, S.C., Johnston, W.D., Leonardos, O.H. & Scorza, E.P. (1944): The beryl-tantalite-cassiterite pegmatites of Paraiba and Rio Grande do Norte, northeastern Brazil. *Economic Geology 39*, 206-223.

Dent-Glasser, L.S., Glasser, F.P. & Taylor, H.F.W. (1962): Topotactic reactions in inorganic oxy-compounds. *Quarterly Reviews, Chemical Society of London 16*, 343-360.

Donnay, G. & Allmann, R. (1970): How to recognise O^{2-}, OH^-, and H_2O in crystal structures determined by X-rays. *American Mineralogist 55*, 1003-1015.

Dunham, A.C. & Wilkinson, F.C.F. (1978): Accuracy, precision and detection limits of energy-dispersive electron-microprobe analyses of silicates. *X-Ray Spectrometry 7*, 50-56.

Dunn, P.J., Gaines, R.V., Wolfe, C.W. & do Prado Barbosa, C. (1978): Epitaxial wodginite and cassiterite from Lavra Jabuti, Baixio, Galilea, Minas Gerais, Brazil. *Mineralogical Record 9*, 14-18.

Eid, A.S. & von Knorring, O. (1976): Geochemical aspects of the tantalum mineral microlite from some African pegmatites. In *Research Institute of African Geology, University of Leeds, Annual Report 20*, 56-58.

Ellis, H.A. (1950): Some economic aspects of the principal tantalum-bearing deposits of the Pilbara goldfield. *Western Australia Geological Survey Bulletin 104*.

English, A.D. & Sleight, A.W. (1980): ^{205}Tl and ^{19}F NMR study of ionic motion and structure in a series of thallium pyrochlore ionic conductors. *Materials Research Bulletin 15*, 1727-1735.

Ercit, T.S., Černý, P. & Hawthorne, F.C. (1985): Normal and inverse pyrochlore group minerals. *Geological Association of Canada, Program with Abstracts 10*, A17.

Evans, H.T. (1960): Crystal structure refinement and vanadium bonding in the metavanadates KVO_3, NH_4VO_3 and $KVO_3 \cdot H_2O$. *Zeitschrift für Kristallographie 114*, 257-277.

Ewing, R.C. (1975): Alteration of metamict, rare-earth, $A_2B_2O_6$-type Nb-Ta-Ti oxides. *Geochimica et Cosmochimica Acta 39*, 521-530.

Felten, E.J. (1967): Composition dependent order-disorder phenomena in $CoNb_{2-x}Ta_xO_6$ and $NiNb_{2-x}Ta_xO_6$. Materials Research Bulletin 2, 13-24.

Ferguson, R.B. (1974): A cation-anion distance-dependent method for evaluating valence-bond distributions in ionic structures and results for some olivines and pyroxenes. Acta Crystallographica B30, 2527-2539.

_____, Hawthorne, F.C. & Grice, J.D. (1976): The crystal structures of tantalite, ixiolite and wodginite from Bernic Lake, Manitoba II. Wodginite. Canadian Mineralogist 14, 550-560.

Finger, L.W. (1969): RFINE. A Fortran IV computer program for structure factor calculation and least-squares refinement of crystal structures. Geophysical Laboratory, Carnegie Institute of Washington (unpubl.).

Flörke, O.W., Gebert, W. & Wedepohl, K.H. (1974): Tantalum. In Handbook of Geochemistry 73, Springer-Verlag, Berlin.

Foord, E.E. (1976): Mineralogy and Petrogenesis of Layered Pegmatite-Aplite Dikes in the Mesa Grande District, San Diego County, California. Ph.D. thesis, Stanford University, Stanford.

Foord, E.E. (1982): Minerals of tin, titanium, niobium and tantalum in granitic pegmatites. In Granitic Pegmatites in Sciences and Industry, Mineralogical Association of Canada, Short Course Handbook 8, 187-238.

Fourquet, J.L., Jacoboni, C. & de Pape, R. (1973): Les pyrochlores $A^1B_2O_6$: Mise en évidence de l'occupation par le cation A^1 de nouvelles positions cristallographiques dans le groupe d'espace Fd3m. Materials Research Bulletin 8, 393-404.

Gallagher, M.J. (1962): Mineralogy of the Bikita pegmatites, Southern Rhodesia, with special reference to beryl deposits in Bikita Main pegmatite. Great Britain Geological Survey, Atomic Energy Division, Report 242.

Gatehouse, B.M., Negas, T. & Roth, R.S. (1976): The crystal structure of $M-LiTa_3O_8$ and its relationship to the mineral wodginite. Journal of Solid State Chemistry 18, 1-7.

Giese, R.F. (1975): Electrostatic energy of columbite/ixiolite. Nature 256, 31-32.

Gondrand, M., Collomb, A., Joubert, J.C. & Shannon R.D. (1974): Synthesis of new high-pressure columbite phases containing pentavalent vanadium. Journal of Solid State Chemistry 11, 1-9.

Gorzhevskaya, S.A. & Sidorenko, G.A. (1974): Crystallochemical characteristics of minerals from the columbite-ixiolite-wodginite series. In Konstitutsiya i Svoystva Mineralov 8. Naukova Dumka, Kiev, 30-36 (in Russian).

Graham, J. & Thornber, M.R. (1974a): The crystal chemistry of complex niobium and tantalum oxides. I. Structural classification of MO_2 phases. American Mineralogist 59, 1026-1039.

_____ & Thornber, M.R. (1974b): The crystal chemistry of complex niobium and tantalum oxides. II. Composition and structure of wodginite. American Mineralogist 59, 1040-1044.

Green, M. & Cosslett, V.E. (1961): The efficiency of production of characteristic X-radiation in thick targets of a pure element. Proceedings of the Physics Society of London 78, 1206-1214.

Grice, J.D. (1970): The Nature and Distribution of the Tantalum Minerals in the Tanco Mine Pegmatite at Bernic Lake, Manitoba. M.Sc. thesis, University of Manitoba, Winnipeg.

_____ (1973): Crystal Structures of the Tantalum Oxide Minerals Tantalite and Wodginite, and of Millerite NiS. Ph.D. thesis, University of Manitoba, Winnipeg.

_____, Černý, P. & Ferguson, R.B. (1972): The Tanco pegmatite at Bernic Lake, Manitoba. II. Wodginite, tantalite, pseudo-ixiolite and related minerals. Canadian Mineralogist 11, 609-642.

_____, Ferguson, R.B. & Hawthorne, F.C. (1976): The crystal structures of tantalite, ixiolite and wodginite from Bernic Lake, Manitoba. I. Tantalite and ixiolite. Canadian Mineralogist 14, 540-549.

Grins, J., Nygren, M. & Wallin, T. (1980): Studies on composition, structure and ionic conductivity of the pyrochlore type system $K_{1+x}Ta_{1+x}W_{1-x}O_6 \cdot nH_2O$, $0 \leq x \leq 1$. Materials Research Bulletin 15, 53-61.

Groult, D., Pannetier, J. & Raveau, B. (1982): Neutron diffraction study of the defect pyrochlores $TaWO_{5.5}$ $HTaWO_6$, $H_2Ta_2O_6$, and $HTaWO_6 \cdot H_2O$. Journal of Solid State Chemistry 41, 277-285.

Guimarães, C.P. (1944): Calogerasite, a new mineral of the tantalate family. Mineração e Metalurgia 8, 135-136 (in Portuguese).

Hawthorne, F.C. (1985): Towards a structural classification of minerals: $^{VI}M\ ^{IV}T_2\phi_n$ minerals. American Mineralogist 70, 455-473.

Heinrich, E.W. (1976): A comparison of three major lithium pegmatites: Varuträsk, Bikita, and Bernic Lake. In Lithium Resources and Requirements by the Year 2000, United States Geological Survey Professional Paper 1005, 50-54.

Hildreth, W. (1979): The Bishop Tuff: evidence for the origin of compositional zonation in silicic magma chambers. Geological Society of America, Special Paper 180, 43-75.

Hogarth, D.D. (1977): Classification and nomenclature of the pyrochlore group. American Mineralogist 62, 403-410.

Hornung, G. & von Knorring, O. (1962): The pegmatites of the north Mtoko region, Southern Rhodesia. Transactions of the Geological Society of South Africa 65, 176.

Jahnberg, L. (1970): Crystal structures of $Na_2Nb_4O_{11}$ and $CaTa_4O_{11}$. Journal of Solid State Chemistry 1, 454-462.

Jahnberg, L. (1971): Hexa- and Hepta-coordination in niobium and tantalum oxides and oxide fluorides and structurally related compounds. Chemical Communications of the University of Stockholm 13.

Jahns, R.H. & Tuttle, O.F. (1963): Layered pegmatite-aplite intrusives. Mineralogical Society of America, Special Paper 1, 78-92.

Jeanne, G., Desjardin, G. & Raveau, B. (1974): Synthèse et évolution structurale de nouveaux pyrochlores au bismuth. Materials Research Bulletin 9, 1321-1332.

Joyce, B.D. (1960): Mixed Oxides of Uranium and a Study of the Pyrochlore Structure. Ph.D. thesis, University of London, London.

Kerr, P.F. & Holmes, R.J. (1945): X-ray study of the tantalum mineral simpsonite. Bulletin of the Geological Society of America 56, 479-504.

Khattak, C.P. & Cox, D.E. (1977): Profile analysis of X-ray powder diffractometer data: structural refinement of $La_{0.75}Sr_{0.25}CrO_3$. Journal of Applied Crystallography 10, 405-411.

Khodyreva, A.I. & Kashaev, A.A. (1973): Wodginite from pegmatites in eastern Sayan. In Voprosy Mineralogii i Geokhimii Mestorozhdeniy Vostochnoy Sibiri. Izdatelstvo Sibirskogo Otdeleniya Akademii Nauk SSSR, Irkutsk, 39-42 (in Russian).

Khvostova, V.A., Lebedeva, S.I. & Maksimova, N.V. (1982): Stanniferous tantalum niobates and their typomorphic features. I. Ixiolite as a parent of structures of the columbite-tantalite and wodginite series. Izvestia Akademii Nauk SSSR, Serii Geol. no. 7, 70-81 (in Russian).

—————————, Pavlova, V.N., Aleksandrov, V.B. & Maksimova, N.V. (1966): First find of wodginite in the USSR. Doklady Akademii Nauk SSSR 167, 1135-1138 (in Russian).

King, B.W., Shultz, S.S., Durbin, E.A. & Duckworth, W.H. (1956): U.S. Atomic Energy Commission Report BMI-1106.

von Knorring, O. & Fadipe, A. (1981): On the mineralogy and geochemistry of niobium and tantalum in some granite pegmatites and alkali granites of Africa. Bulletin de Minéralogie 104, 496-507.

————————— & Hornung, G. (1962): On the lithium amphibole holmquistite, from Benson pegmatite mine, Mtoko, Southern Rhodesia. Mineralogical Magazine 32, 731-735.

_____ & Hornung, G. (1963): Simpsonite and stibiotantalite from Benson pegmatite mine, Mtoko, Southern Rhodesia. <u>Mineralogical Magazine 33</u>, 458-466.

_____, Sahama, Th.G. & Lehtinen, M. (1969): Wodginite from Karibib, South West Africa. <u>Indian Mineralogist 10</u>, 105-108.

_____, Sahama, Th.G. & Lehtinen, M. (1969): Ferroan wodginite from Ankole, south-west Uganda. <u>Bulletin of the Geological Society of Finland 41</u>, 65-69.

_____, Vorma, A. & Nixon, P.H. (1969): Rankamaite, a new tantalum mineral from Kivu, Congo. <u>Bulletin of the Geological Society of Finland 41</u>, 47-56.

Komkov, A.I. (1970): Relationship between the X-ray constants of columbites and composition. <u>Doklady Akademii Nauk SSSR 195</u>, 434-436 (in Russian).

_____ & Dubik, O.Yu. (1983): Chemical composition of wodginites and possible conditions of their formation in nature. In <u>Problemy Kristallokhimii i Genezisa Mineralov</u>, Sidorenko, A.V. & Rundkvist, D.V., editors. Izdatel'stvo Nauka, Leningrad, 124-129 (in Russian).

Kornetova, V.A., Sidorenko, G.A., Kazakova, M.E., Troneva, N.V. & Boyarskaya, R.V. (1978): Iron-rich wodginite. <u>Trudy Mineralogicheskogo Museya Akademii Nauk SSSR 27</u>, 75-85 (in Russian).

Lahti, S.I. (1981): On the granitic pegmatites of the Eräjärvi area in Orivesi, southern Finland. <u>Bulletin of the Geological Survey of Finland 314</u>.

_____ (1982): A new pseudo-orthorhombic wodginite variety from the Eräjärvi pegmatite area. <u>Geologi 34</u>, No. 1, 6-7 (in Finnish).

_____, Johanson, B. & Virkkunen, M. (1983): Contributions to the chemistry of tapiolite - Manganotapiolite, a new mineral. <u>Bulletin of the Geological Society of Finland 55</u>, 101-109.

Le Maitre, R.W. (1982): <u>Numerical Petrology</u>. Elsevier, New York.

London, D. (1984): Experimental phase equilibria in the system $LiAlSiO_4$-SiO_2-H_2O: a petrogenetic grid for lithium-rich pegmatites. <u>American Mineralogist 69</u>, 995-1004.

London, D. (1986): Magmatic-hydrothermal transition in the Tanco rare-element pegmatite: Evidence from fluid inclusions and phase-equilibrium experiments. <u>American Mineralogist 71</u>, 376-395.

Love, G., Cox, M.G. & Scott, V.D. (1978): Evaluation of a new correction procedure for quantitative electron probe microanalysis. <u>Journal of Physics D11</u>, 1369-1376.

         & Scott, V.D. (1980): A critical appraisal of some recent
correction procedures for quantitative electron-probe microanalysis.
Journal of Physics D13, 995-1004.

Lugovskoy, G.P. & Surkov, B.K. (1976): Wodginite from Siberian pegmatites.
In Novoe v Mineralogicheskikh Issledovaniyakh. Vsesoyuznyi Nauchno-
Issledovatel'skyi Institut Mineral'nogo Syr'ya, Moskovskoe Otdelenie
Vsesoyuznogo Mineralogicheskogo Obshchestva, Moscow, 46-47 (abstract,
in Russian).

Luna, J. (1965): Wodginite and columbite-tantalite from a pegmatite at
Krasonice. Acta Universitatis Carolinae - Geologica, No. 3, 157-162
(in Czech).

Lundberg, M. (1971): On the crystal structures of some groups of niobium
oxide compounds. Chemical Communications of the University of Stock-
holm 12.

Macgregor, A.M. (1946): Simpsonite and other tantalates from Bikita, South-
ern Rhodesia. Mineralogical Magazine 26, 157-165.

Maksimova, N.V. & Khvostova, V.A. (1970): Mineralogy and crystal chemistry
of some tantaloniobates. Doklady Akademii Nauk SSSR 193, 167-170 (in
Russian).

Matias, V.V. (1961): Olovotantalite, a new variety of tantalite. Geol.
Mestorozhdeniy Redkikh Elementov 9, 30-41 (in Russian).

McGuire, N.K. & O'Keeffe (1984): Bond lengths in alkali metal oxides.
Journal of Solid State Chemistry 54,49-53.

Mélon, J. & Toussaint, J. (1950): La thoreaulite de Kubitaka (Punia, Manie-
ma, Congo Belge) et la cristallographie de la thoreaulite. Annales
de la Société géologique de Belgique 74, 25-32.

Newton, R.C. & Wood, B.J. (1980): Volume behavior of silicate solid solu-
tions. American Mineralogist 65, 733-745.

Nickel, E.H. & Robinson, B.W. (1986): Kimrobinsonite, a new tantalum min-
eral from Western Australia, and its association with cesstibtantite.
In press.

          , Rowland, J.F. & McAdam, R.C. (1963a): Ixiolite - A columbite
substructure. American Mineralogist 48, 961-979.

          , Rowland, J.F. & McAdam, R.C. (1963b): Wodginite -- a new
tin-manganese tantalate from Wodgina, Australia and Bernic Lake, Man-
itoba. Canadian Mineralogist 7, 390-402.

North, A.C.T., Phillips, D.C. & Mathews, F.S. (1968): A semi-empirical
method of absorption correction. Acta Crystallographica A24,
351-359.

Norton, J.J. (1983): Sequence of mineral assemblages in differentiated granitic pegmatites. _Economic Geology 78_, 854-874.

Nyman, H., Andersson, S., Hyde, B.G. & O'Keefe, M. (1978): The pyrochlore structure and its relatives. _Journal of Solid State Chemistry 26_, 123-131.

Parker, R.L. & Fleischer, M. (1968): Geochemistry of niobium and tantalum. _U.S. Geological Survey Professional Paper 612_.

Parobek, L. & Brown, J.D. (1978): The atomic number and absorption corrections in electron microprobe analysis at low electron energies. _X-Ray Spectrometry 7_, 26-30.

Pauling, L. (1929): The principles determining the structure of complex ionic crystals. _Journal of the American Chemical Society 51_, 1010-1026.

Pauling, L. (1960): _The Nature of the Chemical Bond_. Cornell University Press, Ithica, N.Y.

Phillips, J.C. (1970): Ionicity of the chemical bond in crystals. _Reviews of Modern Physics 42_, 318-356.

Piffard, Y., Dion, M. & Tournoux, M. (1978): Structure cristalline du pyrochlore, $K_{.51}Sb_{.67}Sb_2O_{6.26}$. _Acta Crystallographica B34_, 366-368.

Polyakov, V.O. & Cherepivskaya, G.E. (1981): Ixiolite from the Ilmen Mountains. _Mineralogicheskii Zhurnal 1_, 67-75 (in Russian).

Pough, F.H. (1945): Simpsonite and the northern Brazilian pegmatite region. _Bulletin of the Geological Society of America 56_, 505-514.

Pryce, M.W. (1970): Identification of Western Australian columbite-tantalite, ixiolite and wodginite. _Journal of the Royal Society of Western Australia 53_, 65-68.

Puffer, J.H. (1975): Some North American iron-titanium oxide-bearing pegmatites. _American Journal of Science 275_, 708-730.

Pyatenko, Yu.A. (1973): Unified approach to analysis of the local balance of valences in inorganic structures. _Soviet Physics - Crystallography 17_, 677-682.

Quensel, P. (1945): Minerals of the Varuträsk pegmatite. XXXV. Stibiomicrolite. _Geologiska Föreningens i Stockholm Förhandlingar 67_, 15-27.

Reed, S.J.B. (1965): Characteristic fluorescence corrections in electron-probe microanalysis. _British Journal of Applied Physics 16_, 913-926.

Reisman, A. (1962): Compound repetition in oxide systems. Solid phases in the system $Li_2O-Ta_2O_5$ and $Na_2O-Ta_2O_5$. _Journal of Physical Chemistry 66_, 15-21.

Roth, R.S. & Waring, J.L. (1964): Ixiolite and other polymorphic types of FeNbO$_4$. <u>American Mineralogist 49</u>, 242-246.

Rucklidge, J. & Gasparrini, E. (1969): Electron microprobe analytical data reduction (EMPADR VII). <u>Department of Geology, University of Toronto</u>.

Rumble, D. (1976): Oxide minerals in metamorphic rocks. In <u>Oxide Minerals</u>, Mineralogical Society of America Short Course Notes <u>3</u>, R1-R24.

Ruste, J. & Zeller, C. (1977): Correction d'absorption en micro-analyse. <u>Comptes Rendus de la Academie des Sciences de Paris B284</u>, 507-510.

Safiannikoff, A. & van Wambeke, L. (1961): Sur une terme plombifère du groupe pyrochlore-microlite. <u>Bulletin de la Société Française de Minéralogie et Cristallographie 84</u>, 382-384.

Sahama, Th.G. (1980): Minerals of the tantalite-niobite series from Mozambique. <u>Bulletin de Minéralogie 103</u>, 190-197.

Santoro, A., Roth, R.S. & Minor, D. (1977): Neutron powder diffraction study of the intermediate-temperature form of lithium tantalate. <u>Acta Crystallographica B33</u>, 3945-3947.

Sarp, H. & Deferne, J. (1983): Présence de simpsonite, un oxyde de tantale et d'aluminum, dans un nodule provenant de la mine de Manono (Shaba, Zaire). <u>Archives des Sciences 36</u>, 341-343.

Schrewelius, N. (1943): <u>A Study of Antimonates, Hydroxyantimonates and Fluorantimonates</u>. Ph.D. thesis, University of Stockholm, Stockholm (in Swedish).

Schröcke, H. (1966): Solid equilibria within the columbite-tapiolite group, and of the columbite-tapiolite group with YTi(Nb,Ta)O$_6$, euxenite, and FeNbO$_4$. <u>Neues Jahrbuch für Mineralogie, Abhandlungen 106</u>, 1-54 (in German).

Shannon, R.D. (1976): Revised effective ionic radii and systematic studies of interatomic distances in halides and chalcogenides. <u>Acta Crystallographica A32</u>, 751-767.

Sidorenko, G.S., Solntseva, L.S. & Gorzhevskaya, S.A. (1974): Minerals with the wodginite structure and their synthetic analogues. <u>Doklady Akademii Nauk SSSR 216</u>, 172-175 (in Russian).

Sleight, A.W. & Jones, G.A. (1975): Ferroelastic transitions in β-BiNbO$_4$ and β-BiTaO$_4$. <u>Acta Crystallographica B31</u>, 2748-2749.

Sosedko, A.F. & Denisov, A.P. (1958): The first discovery of simpsonite in the USSR. <u>Doklady Akademii Nauk SSSR 118</u>, 189-192 (in Russian).

Springer, G. (1976): Iterative procedures in electron probe analysis corrections. <u>X-Ray Spectrometry 5</u>, 88-91.

Stewart, D.J., Knop, O., Ayasse, C. & Woodhams, F.W.D. (1972): Pyrochlores. VII. The oxides of antimony: an X-ray and Mössbauer study. Canadian Journal of Chemistry 50, 690-700.

Stone, M. (1969): Nature and origin of banding in the granitic sheets, Tremearne, Porthleven, Cornwall. Geological Magazine, 106, 142-158.

Sturdivant, J.H. (1930): The crystal structure of columbite. Zeitschrift für Kristallographie 75, 88-108 (in German).

Subramanian, M.A., Aravamudan, G. & Subba Rao, G.V. (1983): Oxide pyrochlores -- A review. Progress in Solid State Chemistry 15, 55-143.

Sugitani, Y., Suzuki, Y. & Nagashima, K. (1985): Polymorphism of samarskite and its relationship to other structurally related Nb-Ta oxides with the a-PbO$_2$ structure. American Mineralogist 70, 856-866.

Symons, R. (1961): Operation at Bikita Minerals (Private), Ltd., Southern Rhodesia. Institute of Mining and Metallurgy Bulletin 661, 129-172.

Taylor, B.E. & Friedrichsen, H. (1983): Light stable isotope systematics of granitic pegmatites from North America and Norway. Isotope Geoscience 1, 127-167.

Taylor, L.E.R. (1939): X-ray studies of simpsonite. Journal of the Royal Society of Western Australia 25, 93-97.

Thomas, A.V. & Spooner, E.T.C. (1985): Occurrence, petrology and fluid intrusion characteristics of tantalum mineralization in the Tanco granitic pegmatite, S.E. Manitoba. In Granite-Related Mineral Deposits - Geology, Petrogenesis and Tectonic Setting, Canadian Institute of Mining, 274-277.

Thoreau, J. (1950): La pegmatite stannifère de Manono (Katanga). Comptes Rendus des Travaux du Congrès Scientifique, Elisabethville 1950, 1-33.

Turnock, A.C. (1966): Synthetic wodginite, tapiolite and tantalite. Canadian Mineralogist 8, 461-470.

Tyndale-Biscoe, R. (1951): The geology of the Bikita tin-field, Southern Rhodesia. Transactions of the Geological Society of South Africa 54, 11-25.

Van Wambeke, L. (1970): The alteration processes of the complex titano-niobo-tantalates and their consequences. Neues Jahrbuch für Mineralogie, Abhandlungen 112, 117-149.

van der Veen, A.H. (1963): A study of pyrochlore. Nederlands Geologisch Mijnbouwkundig Genootschap Verhandelingen, Geolische Serie 22, 188 p.

Voloshin, A.V. (1983): Evolutionary and reactionary series of tantalum oxide minerals. In Novye Idei v Geneticheskoy Mineralogii. Nauka, Leningrad, 21-26 (in Russian).

_____, Men'shikov, Yu.P. & Pakhomovskii, Ya.A. (1981): Alumotantite and natrotantite, new tantalum minerals. Zapiski Vsesoyuznogo Mineralogicheskogo Obshchestva 110, 338-345 (in Russian).

_____, Men'shikov, Yu.P. & Pakhomovskii, Ya.A. (1982): Sosedkoite $(K,Na)_5Al_2(Ta,Nb,Sb)_{22}O_{60}$ - A new mineral from granitic pegmatites. Doklady Akademii Nauk SSSR 264, 442-445 (in Russian).

_____, Men'shikov, Yu.P., Pakhomovskii, Ya.A. & Polezhaeva, L.I. (1981): Cesstibtantite, $(Cs,Na)SbTa_4O_{12}$ - a new mineral from granitic pegmatites. Zapiski Vsesoyuznogo Mineralogicheskogo Obshchestva 110, 345-351 (in Russian).

_____ & Pakhomovskii, Ya.A. (1983a): Aluminum-tantalum mineral phases in rare-metal pegmatites. Zapiski Vsesoyuznogo Mineralogicheskogo Obshchestva 117, 67-76 (in Russian).

_____ & Pakhomovskii, Ya.A. (1983b): Rhythmically-banded structures of microlite-muscovite in rare-metal pegmatites. Zapiski Vsesoyuznogo Mineralogicheskogo Obshchestva 117, 520-526 (in Russian).

_____, Pakhomovskii, Ya.A., Stepanov, V.I. & Tyusheva, F.H. (1983): Natrobistantite, $(Na,Cs)Bi(Ta,Nb,Sb)_4O_{12}$ - a new mineral from granitic pegmatites. Mineralogicheskii Zhurnal 5, 82-86 (in Russian).

Vorma, A. & Siivola, J. (1967): Sukulaite - $Ta_2Sn_2O_7$ - and wodginite as inclusions in cassiterite in the granite pegmatite in Sukula, Tammela in SW Finland. Comptes Rendus de la Société géologique de Finlande 39, 173-187.

Waburg, M. & Müller-Buschbaum, H. (1984): $ZnTa_2O_6$, a new member of the tri-α-PbO_2 Type (with supplemental data for $ZnNb_2O_6$). Zeitschrift für Anorganische allgemeine Chemie 508, 55-60 (in German).

Wang, Y., Li, J., Lu, J. & Fan, W. (1982): Geochemical mechanism of Nb,Ta-mineralization during the late stage of granite crystallization. Geochemistry Bejing 1, 175-185.

Ware, N.G. & Reed, S.J.B. (1973): Background corrections for quantitative electron microprobe analysis using a lithium drifted silicon X-ray detector. Journal of Physics E6, 286-288.

Weitzel, H. (1976): Crystal structure refinement of wolframite and columbite. Zeitschrift für Kristallographie 144, 238-258 (in German).

_____ & Klein, S. (1974): Magnetic structure of the trirutile $FeTa_2O_6$. Acta Crystallographica A30, 380-384 (in German).

Whiston, C.D. & Smith, A.J. (1965): Double oxides containing niobium or tantalum. I. Systems including alkali metals. Acta Crystallographica 19, 169-173.

Wichmann, R. & Müller-Buschbaum, H. (1983): Synthesis and investigation of $NiNb_2O_6$ - Single crystals with the columbite- and rutile-structure. <u>Zeitschrift für Anorganische allgemeine Chemie 503</u>, 101-105 (in German).

Wiles, D.B. & Young, R.A. (1981): A new computer program for Rietveld analysis of X-ray powder diffraction patterns. <u>Journal of Applied Crystallography 14</u>, 149-151.

Wise, M.A., Turnock, A.C. & P. Černý (1985): Improved unit cell dimensions for ordered columbite-tantalite end members. <u>Neues Jahrbuch für Mineralogie, Monatshefte</u>, 372-378.

Yagi, K. & Roth, R.S. (1978): Electron-microscope study of crystal structures of mixed oxides in the systems $Rb_2O-Ta_2O_5$, $Rb_2O-Nb_2O_5$ and $K_2O-Ta_2O_5$ with composition ratios near 1:3. I. Stacking characteristics of MO_6 layers. <u>Acta Crystallographica A34</u>, 765-773.

Zachariasen, W.H. (1963): The crystal structure of monoclinic metaboric acid. <u>Acta Crystallographica 16</u>, 385-389.

Zachariasen, W.H. (1978): Bond lengths in oxygen and halogen compounds of d and f elements. <u>Journal of the Less-Common Metals 62</u>, 1-7.

Zelt, G.A.D. (1975): Data for some African columbite-tantalite specimens. <u>Bulletin of the Geological Society of Finland 47</u>, 117-125.

Zhang, R.-B., Tian, H.-X., Peng, Z.-H., Ma, Z.-S. and others (1980): A new mineral - ashanite $(Nb,Ta,U,Fe,Mn)_4O_8$. <u>Kexue Tongbao, 25</u>, 510-514.

The program EMPADR VII (Electron MicroProbe Data Reduction) was written by Rucklidge & Gasparini (1969) for the reduction and ZAF correction of microprobe data collected with wavelength-dispersive spectrometers. The many important advances made in the 1970's in modelling interactions between electron beams and materials, particularly with respect to X-ray generation and emission, were not incorporated into the original program. Because of the initial dependence of this thesis upon microprobe data collected with such spectrometers, and because of the failure of the Rucklidge & Gasparrini version of the program to properly reduce data for minerals such as simpsonite, changes were made to the program to improve its ZAF correction routines and to optimize its operation.

ZAF correction involves the standard formula:

$$W_1 = W_0 \cdot \frac{I_1}{I_0} \cdot \frac{R_0 S_1}{R_1 S_0} \cdot \frac{f(\chi)_0}{f(\chi)_1} \cdot \frac{1+\gamma_0}{1+\gamma_1} \tag{1}$$

where $\underline{W}$ is the element concentration (wt. %).

$\underline{I}$ is the count rate (after dead time and background correction).

$\underline{R}$ is the electron backscatter factor.

$\underline{S}^{-1}$ is the electron stopping power factor.

$\underline{f}(\chi)$ is the X-ray transmission factor.

$\underline{\gamma}$ is the characteristic fluorescence factor.

The subscripts "0" and "1" refer to the standard and sample respectively. The ratio $(R_0S_1)/(R_1S_0)$ is called the atomic number correction, because of the strong dependence of $\underline{R}$ and $\underline{S}$ upon atomic number. This is the "Z" part of the "ZAF" correction. The ratio $f(\chi)_0/f(\chi)_1$ is called the absorption correction (the "A" part of "ZAF"). The ratio $(1+\gamma_0)/(1+\gamma_1)$ is the fluorescence correction (the "F" part of "ZAF"). Several significant changes have been made to the atomic number and absorption corrections, whereas changes to the fluorescence correction have been more cosmetic in nature (simplifications to the calculation of the correction have been made which do not significantly alter the results).

Changes to the atomic number and absorption corrections follow the approach of Love & Scott (1978). Of four new approaches to atomic number and absorption correction of electron microprobe data developed in the late 1960's and the 1970's (Andersen & Wittry, 1968; Ruste & Zeller, 1977; Parobek & Brown, 1978; Love & Scott, 1978), that of Love & Scott (1978) is superior for light element analysis and slightly superior for heavier element analysis (Love & Scott, 1980).

BACKSCATTER FACTOR

$\underline{R}$ is calculated from the following equation:

$$R = 1 - \eta_0 \cdot [I(U) + \eta_0 \cdot G(U)] \tag{2}$$

$\underline{U}$ is the overvoltage, and is defined as

$$U = E_0/E_C \tag{3}$$

where E_0 is the operating potential and E_c is the critical excitation potential of the line used in analysis. I and G are functions of the overvoltage:

$$I(U) = A \ln U + B(\ln U)^2 + C(\ln U)^3 + D(\ln U)^4 \qquad (4)$$

$$G(U) = U^{-1}[E \ln U + F(\ln U)^2 + G(\ln U)^3 + H(\ln U)^4] \qquad (5)$$

From least-squares regression analysis, the constants A through H of (4) and (5) were determined by Love & Scott (1978):

$$
\begin{array}{ll}
A = 0.33148 & E = 2.87898 \\
B = 0.05596 & F = -1.51307 \\
C = -0.06339 & G = 0.81312 \\
D = 0.00947 & H = -0.08241
\end{array}
$$

η_0, the total backscatter coefficient of the specimen, is obtained through a series of steps. Love & Scott (1978) determine initial backscatter coefficients of each element of the specimen ($\eta(E_0)$) at the operating potential of analysis (E_0) by extrapolating from an expression they give for operation at $E_0=20$ kV:

$$\eta_{20} = (-52.3791 + 150.48371 \cdot Z - 1.67373 \cdot Z^2 + + .00716 \cdot Z^3) \times 10^4 \qquad (6)$$

Extrapolation is carried out via the following equation:

$$\eta(E_0) = \eta_{20} \cdot [1 + G(Z)/\eta_{20} \cdot \ln(E_0/20)] \qquad (7)$$

Love & Scott (1978) express $G(Z)/\eta_{20}$ as a polynomial of atomic number (Z):

$$G(Z)/\eta_{20} = (-1112.8 + 30.289 \cdot Z - 0.15498 \cdot Z^2) \times 10^4 \qquad (8)$$

In the case of non-normal beam incidence, $\eta(E_0)$ is transformed to $\eta(\beta)$, where β is the incidence angle:

$$\eta(\beta) = 0.891 \cdot [\eta(E_0)/0.891]^{\sin \beta} \qquad (9)$$

(Darlington, 1975). From this $\underline{\eta}_0$ is calculated:

$$\eta_0 = \overset{m}{\Sigma} C_i \cdot \eta(\beta)_i \qquad (10)$$

i.e. by summation over all $\underline{m}$ elements of the specimen, where $\underline{C}$ is the weight proportion of element "i".

STOPPING POWER FACTOR

$\underline{S}^{-1}$ has the Bethe expression as its basis, as does the stopping power expression of conventional ZAF routines; however, the Love & Scott (1978) expression for S^{-1} results from a more rigorous treatment of the Bethe expression than the conventional approach (Green & Cosslett, 1961). Love & Scott (1978) give

$$S^{-1} = \{1 + 16.05 \cdot (J_0/Ec)^{0.5} ([U_0^{0.5}-1]/[U_0-1])^{1.07}\} / \overset{m}{\Sigma} (C_i Z_i/A_i) \qquad (11)$$

where $\underline{J}_0$ is the mean ionization potential of the specimen, and $\underline{A}$ is the atomic weight of element "i"; $\underline{C}$ and $\underline{Z}$ are as defined before. $\underline{J}_0$ is calculated from the individual ionization potentials for the constituent elements of the specimen ($\underline{J}$):

$$\ln(J_0) = \overset{m}{\Sigma} [(C_i Z_i/A_i) \cdot \ln J] / \overset{m}{\Sigma} (C_i Z_i/A_i) \qquad (12)$$

For each element "i",

$$J_i = 0.0135 \cdot Z_i \qquad (13)$$

X-RAY TRANSMISSION FACTOR

The method of Love & Scott (1978) uses an expression for $f(\chi)$ after Bishop (1974):

$$f(\chi) = \frac{1-\exp(-2\chi \cdot \bar{\rho z})}{2\chi \cdot \rho z} \qquad (14)$$

where χ is defined as follows:

$$\chi = (\mu/\rho)_0 \cosec \psi \qquad (15)$$

ψ is the take-off angle (angle between the detector and the surface of the specimen). If $\beta \neq 90°$, the effective take-off angle (ψ') is used in (15) instead, where

$$\psi' = \cosec^{-1}\{\cosec \psi \cdot (1 - 0.5 \cdot \cos^2 \beta)\} \qquad (16)$$

(Reed, 1975). $(\mu/\rho)_0$ is the mass absorption coefficient of the specimen and is calculated from:

$$(\mu/\rho)_0 = \overset{m}{\Sigma} C (\mu/\rho) \qquad (17)$$

where C is as defined before, and (μ/ρ) is the mass absorption coefficient of element "i" of the specimen.

$\bar{\rho z}$ is the mean mass depth of X-ray generation. Through Monte-Carlo methods, Love & Scott have obtained an expression for $\bar{\rho z}$:

$$\bar{\rho z} = \rho s(m) \cdot \frac{(0.49269 - 1.09870 \cdot \eta_0 + 0.78557 \cdot \eta_0^2) \cdot \ln U}{(0.70256 - 1.09865 \cdot \eta_0 + 1.00460 \cdot \eta_0^2) + \ln U} \qquad (18)$$

where $\underline{\eta}_0$ is calculated from (10). $\underline{\rho s}(m)$ is the maximum path length of an electron in the specimen, and is calculated from:

$$\rho s(m) = (0.787 \times 10^{-5} \cdot J_0^{0.5} \cdot E_0^{1.5} + 0.735 \times 10^{-6} \cdot E_0^2) / \overset{m}{\Sigma}(C_i Z_i / A_i) \quad (19)$$

where $\underline{J}_0$ is calculated from (12), and $\underline{E}_0$, $\underline{C}$, $\underline{Z}$ and $\underline{A}$ are as defined earlier.

FLUORESCENCE CORRECTION

The characteristic fluorescence correction of the program EMPADR is that of Reed (1965) where:

$$\gamma = 0.5 \cdot P(ij) \cdot C_B \cdot a_A \cdot \omega_B \cdot \left\{\frac{U-1}{U-1}\right\}^{1.67} \cdot \left\{\frac{\mu B_A}{\mu B_0}\right\} \cdot \left\{\frac{\ln(1+x)}{x} + \frac{\ln(1+y)}{y}\right\} \cdot \left\{\frac{A_A}{A_B}\right\} \quad (20)$$

The sub- and superscripts "A" and "B" refer to the characteristic line of the analyzed element and the enhancing element respectively. In order to obtain the characteristic fluorescence correction, γ must be summed for all lines of all elements $\underline{B}$ which enhance the intensity of the analyzed line of element $\underline{A}$. In practice this is done only for Kα, Kβ, Lα and Lβ lines; other L lines and all other M lines are ignored in the calculation, as their effect is considered negligible (Rucklidge & Gasparrini, 1969).

The various terms of equation (20) are defined below:

$\underline{C}$ and $\underline{A}$ are as defined earlier.

$\underline{P}(ij)$ is a constant which has a value of 1.0 for K-K and L-L fluorescence, 4.0 for L-K fluorescence and 0.25 for K-L fluorescence.

$\underline{a}_A$ is the absorption jump factor. The original expression for $\underline{a}$ has been replaced by an analytic expression (Colby, 1968):

$$a_A = \alpha - \beta \cdot Z \tag{21}$$

where

$\alpha = 0.954$, $\beta = 2.77 \times 10^{-3}$ for K-line radiation of element A

$\alpha = 0.996$, $\beta = 4.98 \times 10^{-3}$ for L-line radiation of element A

$\underline{\omega}_B$ is the fluorescence yield of element B. The original look-up table of $\underline{\omega}$'s in EMPADR has been replaced by the the semi-empirical expression of Burhop (1955):

$$\omega_B = \frac{x^4}{(1+x^4)} \tag{22}$$

where

$$x = A + B \cdot Z + C \cdot Z^3 \tag{23}$$

Burhop's expression has been found to be the most suitable empirical expression for estimating fluorescence yields (Bambynek et al., 1972). Bambynek et al. (1972) provide values for the constants of (22) based on fair- to good-quality experimental data; however, I decided to derive my own constants for the expression by fitting (22) to the calculated $\underline{\omega}$'s of Chen (1980) using the SAS routine NLIN (Non LINear least squares regression):

$A = 1.789 \times 10^{-2}$ $B = 3.308 \times 10^{-2}$ $C = -8.369 \times 10^{-7}$

For L-shells, (22) was fitted to weighted (σ^{-2}), mean experimental yields of Bambynek et al. (1972), using the same NLIN routine used for K-shell data:

$$A = -1.80 \times 10^{-1} \qquad B = 1.42 \times 10^{-2} \qquad C = -1.61 \times 10^{-7}$$

U, in equation (20) is the overvoltage.

μB_A is the mass absorption coefficient of element A for B radiation, and μB_0 is the mass absorption coefficient of the specimen for B radiation (see equation 17).

x and y are X-ray and electron absorption parameters respectively, where:

$$x = (\mu_A/\mu_B) \operatorname{cosec} \psi \qquad (24)$$

$$y = \sigma/\mu_B \qquad (25)$$

All terms in the expression for x are as defined before. σ is the electron mass absorption coefficient. I have replaced the original lookup tables for σ with the following empirical expression, derived by polynomial regression of the data of the lookup table:

$$\sigma = 26200 - 2522 \cdot E_0 + 106.2 \cdot E_0^2 - 2.156 \cdot E_0^3 + 1.716 \times 10^{-2} \cdot E_0^4 \qquad (26)$$

OTHER CHANGES

For both the unrevised and revised versions of the program, it was found that in several circumstances, calculations were converging too slowly or not converging at all. To remedy the situation, the simple iteration routine originally used was replaced with the Newton-Raphson algorithm (otherwise known as the "Wegstein" method: Springer, 1976). With this routine, convergence problems have disappeared; most runs now converge in 3 cycles of iteration, all in less than 5.

Appendix B

QUANTITATIVE ED ANALYSIS OF TA-NB-SN-TI OXIDE MINERALS

Energy-dispersive (ED) electron microprobe analyses presented in this thesis were done with a Kevex Micro-X 7000 spectrometer and Kevex software. Despite the relative ease of success of K-line analysis with this software, L-line and M-line analysis, and especially mixed-line (e.g. K and L) analysis is still a non-trivial procedure. The problem is further complicated by numerous errors in the Version 3.2K software used with the Micro-X 7000 system. This appendix describes the problems involved in quantitative ED analysis of REE-free Ta-Nb-Sn-Ti oxide minerals with Kevex software.

B.1   BACKGROUND REMOVAL

Background models are calculated with the semi-empirical method of Ware and Reed (1973), which uses the expression:

$$I = F(E) + k \cdot F\{E, \chi, x\} \tag{1}$$

where I is the intensity of the continuous spectrum,

   $F(E)$ is an empirical energy-dependent correction factor, and

   k is an instrumental constant.

The remaining part is an abbreviation for:

$$\{(E_0 - E)/E\} \cdot f(\chi) \cdot \exp\{-\Sigma \mu(i) \cdot p(i) \cdot x(i)\} \tag{2}$$

$\underline{E}_0$ is the operating potential. $\underline{f}(\chi)$ is the X-ray transmission factor for the target, and is strongly composition-dependent (see Appendix A). The summation accounts for absorption at sources other than the sample: absorption at the Be window, the gold layer and the Si dead layer of the detector all contribute to this. Kevex software allows user intervention in background calculation: all terms except $\underline{F}(E)$ and $\underline{k}$ can be directly or indirectly altered.

It was found that indiscriminate use of the routine used in background modelling (BKA), as advocated by Kevex, gave poor results. In particular, calculated models fit the observed background very poorly at both low and high energy ends of the spectrum. Much of the error was due to incorrect estimation of the sample composition used in the background calculation (pers. comm. G. Pringle, Geological Survey of Canada). Although reasonable estimates were determined by the software for the concentrations of detected elements ($\underline{Z}=11{\rightarrow}92$), the calculation of oxygen (by stoichiometry) from these concentrations was in error. By suppressing the command for oxygen calculation (SETOX), and supplying an expected estimate of the wt.% oxygen, the BKA routine was found to consistently give very good background models for all oxide minerals analyzed. Although the shape of the background profile was excellent when using this procedure, the entire model often appeared to be linearly displaced by a few channels when the true value of the thickness of the Be-window ($\underline{x}$(Be)) of the detector was used in equation (1). The degree of shift was found to be only composition-dependent, and by trial and error, effective best values for $\underline{x}$(Be) were determined for each mineral species analyzed. For some solid-solution series, $\underline{x}$(Be) was found to vary slightly across the series; values of $\underline{x}$(Be) were determined

for end-members of the series, and were estimated for intermediate members according to peak height ratios of the elements involved in the solid solution. Ideal values of the wt.% oxygen and x(Be) for different mineral species are given in Table 104.

Table 104: Parameters Used in Modelling Backgrounds of ED Spectra of Selected Ta-Nb-Sn-Ti Oxide Minerals

Mineral	$\bar{Z}$	x(Be)	Wt.% O
Columbite	29	22.5	28
Tantalite	55	21.5	19
Wodginites	53	21.5	20
Microlites	51	21.5	21.5
Tapiolite	56	21.5	19
Cassiterite	41	22.5	21
Tantalian Rutile	32	23.0	32

By supplying appropriate values of the wt.% oxygen and x(Be) to equation (1), consistently high-quality background models were generated by BKA over the region 1.5→10 keV. However, misfit in the region <1.5 keV was still observed; this was due to shortcomings in the theory rather than in practice; consequently, good background models for this region could not be calculated with equation (1). The model calculated with equation (1) had to be improved empirically in this region by fitting a quadratic function to the observed background in the range 0.85→1.5 keV. This was made possible by the fact that the oxide minerals analyzed had no Mg ($\underline{E}$=1.254 keV) and Al ($\underline{E}$=1.487 keV), thus the background model in this range needed to be precise only near the region of the Na $K\alpha$ peak ($\underline{E}$=1.041 keV), which is not difficult to achieve.

To simplify and speed analysis, two command lists ("ATO"'s in Kevex terminology) were written to carry out the above-described procedures. These were named BACK and NABACK, and were used to calculate the backgrounds for Na-free, and Na-bearing samples respectively (although NABACK is now suitable for both purposes). Both command lists prompt the user for the appropriate data needed for background calculation, remove escape peaks and calculate the background model for later subtraction.

ANALYSIS

After background removal, spectra were stored on disk for later retrieval in analysis. Batches of up to 30 samples per session could be analyzed fully automatically with Kevex software after background removal. Never more than one day's collection of data was analyzed at a time, so that software calibration could be kept at an optimum.

Hardware energy drift never exceeded ± 1 eV over the $2\frac{1}{2}$ year period of analysis; consequently, all drift correction could be done with the software provided by Kevex. Most drift was in the gain of the pulse processor; the zero-setting drifted very little over the entire time. Consequently, the ± 1 eV shift described above pertained almost exclusively to gain, and refers to shifts observed for the Fe $K\alpha$ peak of fayalite. Drift at the low-energy end of the spectrum was necessarily much less than this amount; drift in the $E < 2$ keV region was virtually undetectable.

Drift correction with the software involved semi-automatic peak centroid and shape calibration. The software was calibrated once per analytical session by making measurements on a composite of standard fayalite spectra collected during each session. The Kevex software routine INI(tialize) was

used for calibration; the alternate routine PUR(ge) was found to be ineffectual.

Quantitative ZAF analysis of Ta-Nb-Ti-Sn oxide minerals was initially difficult for a number of reasons:

1. Peak overlaps were numerous. Some important overlaps were:

   (1) Ta Mδ+Ta Mη with Nb La,β with Pb Ma,β with Bi Ma,β

   (2) K Ka,β with Sb La,β

   (3) Ca Ka,β with Sb La,β

   (4) Sb Lγ,Lβ_5 with Cs Lalpha

   (5) U Mβ with Sn La

   (6) Sn Lβ with Ca Ka

   (7) Sn Lγ with Sc Ka,β with Ti Ka

   (8) Mn Kβ with Fe Ka

2. The software deconvolution routine frequently failed for cases of moderate to extreme peak overlap.

3. Minor L-, and M-lines (e.g. Lγ and Mη) were not recognized by the deconvolution routine, thus further contributing to its failure.

4. Intra-shell line intensity ratios used by the peak synthesis and deconvolution routines were always in error for L-, and M-lines.

5. Non-idealities in peak shapes contributed to errors in peak synthesis and deconvolution; e.g. (1) skew toward the low-energy side of each peak due to incomplete charge collection and (2) a slight Lorentzian component of each peak were not recognized by the software, resulting in constant underestimation of tail intensities, and consequently, in overestimation of intensities of other peaks overlapping with these tails.

Eventually it was concluded that all overlap problems had to be resolved semi-manually. Peak overlap was resolved by stripping techniques using library spectra of individual elements which were themselves stripped from spectra of standards free of overlap problems. The standards from which these spectra came were chosen so as to have matrices as similar as possible to samples, thus minimizing spectral mismatch between the library and sample spectra. In acquiring the spectra parental to the library spectra, the main line of the element of interest was acquired to 1-2% counting precision, the actual value depending upon collection time constraints.

The stripping technique used depended upon the degree and type of overlap involved. Minor overlaps, or overlaps of lesser lines on a line intended for analysis were corrected by one-step stripping of the lesser line or a part of the energy distribution of the offending line. In this case, normalization was done by scaling on parts of the library spectrum corresponding to segments of the sample spectrum which were free of overlap.

In cases of major line overlaps, segments free of overlap were often too small (or non-existent) for use in normalization. Stripping necessarily involved an iterative approach. For the special case in which two or more lines intended for analysis were extremely close, only parts of the full Gaussian distribution (12 channels or more) per peak were used for analysis, after extraneous energy was stripped from each analytical region. This approach has been tested extensively by Dr. G. Pringle (pers. comm.) and has been found to give good quantitative results for analytical problems as difficult as REE elements in minerals such as euxenite.

All stripping techniques involve sets of two library spectra. The first of the two consists of all detected lines of a given element. The second spectrum consists of a copy of the first spectrum, but with all energy to be used in the analysis stripped away (Figure 89). Initially, the first spectrum is scaled to the sample spectrum, often by total count normalization in the analysis region (ROI) of the element. The second library spectrum is then scaled to the first spectrum, bringing it now to the same absolute scale as the sample spectrum. The second library spectrum is then subtracted from the sample spectrum, which removes all undesirable energy associated with this element (i.e. that not intended for analysis) from the sample spectrum.

In iterative stripping, the region used in normalizing library spectra coincided with the analysis region. For the iterative approach to work, different analysis regions cannot overlap, and for practical purposes only, they must be separated by at least one channel (software limitations). Analysis regions were most often centred about peak centroids, but in cases of significant line overlaps, they were shifted slightly away from the region of overlap, which improved the success of deconvolution, but lowered the precision of analysis.

Because of hardware drift, and the inability of software routines to adjust library spectra to compensate for such drift, library spectra had to be re-acquired once every month to once per session (which could be as frequent as once per day), depending upon the seriousness of the overlap problem and the rate of drift.

Once all overlap problems were eliminated, the sample spectra could be analyzed. Care was taken to analyze the same relative spectral regions of samples and standards.
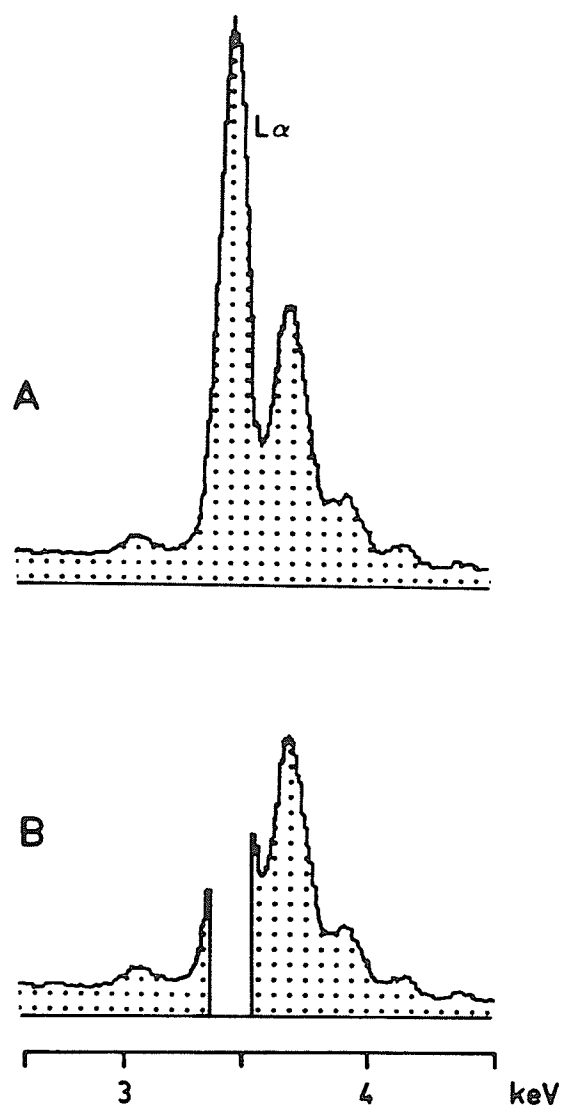
Figure 90: Typical library spectra used in energy stripping. The example here is for Sn. (a) Spectrum 1: all lines of the element in the spectrometer energy range (1-10 keV). (b) Spectrum 2: copy of spectrum 1, but with the analysis region for Sn Lα (3.34-3.52 keV) removed.

Using the above techniques, all line overlaps encountered in the Ta-Nb-Sn-Ti oxide minerals studied here could be dealt with. To generalize, non-iterative stripping was used to sort out Ta-Nb, Ti-Sn, Sc-Ti, Mn-Fe overlap, but iterative methods were necessary for resolving, for example, Pb-Bi-Nb overlap and U-Sn-Ca-Sb overlap.

Although the analytical procedures described above are tedious and awkward, ATO's could be written to perform all such tasks fully automatically, thus putting simplicity back into ED analysis, once the method of analysis was determined. Consequently, quantitative analysis of Ta-Nb-Sn-Ti oxide minerals at the University of Manitoba is now a rapid and simple task.

BEAM CURRENT DRIFT

Because of the imprecision of the sample current meter supplied with the MAC 5, relative beam current drift less than $\pm2\%$ can go by undetected; consequently, this ammeter was only used for coarse adjustment of the sample current.

Relative variations in sample current were precisely determined by monitoring intensity changes of selected lines of standard spectra ("reference spectra"). Synthetic fayalite (Fe_2SiO_4) and sphalerite (ZnS) were used as reference spectra because (1) they have peaks distributed at low and high ends of the ED spectrum, necessary for discerning between zero and gain drift of the pulse processor, (2) they are comprised only of $\underline{K}$-lines, which made for rapid and simple analysis, and (3) they could also be used in software calibration. Because of similar absolute peak intensities of Si $K\alpha$ and Fe $K\alpha$ in fayalite, as compared to very dissimilar absolute intensities of S $K\alpha$ and Zn $K\alpha$ in sphalerite, and because of the poor polishing

properties of sphalerite, use of sphalerite as a reference standard was eventually discontinued.

One reference spectrum, designated the "prime reference spectrum" (a composite of reference spectra of one type acquired during the collection of all standard spectra to be used in analysis) was arbitrarily assigned a current of 5 nA. Currents were assigned to samples (and standards) by comparing the line intensities in reference spectra acquired at the same time as the sample spectra to the intensities of the same lines in the prime reference spectrum. Line intensity varies linearly with beam current, thus the calculated sample currents were simple 1:1 linear extrapolations of the prime reference current.

Using this method, both inter-, and intrasession current drift could be handled. To simplify drift correction, a FORTRAN program, REF, was written by the author to carry out the calculations. Current calculations were done prior to background removal and sample analysis, and currents were stored with sample spectra as part of the normal functions of the ATO's BACK and NABACK, described earlier in this appendix.

Because intersession drift could be compensated for, it was found that standard spectra could be stored, and used to analyze sample spectra collected at later dates. However, because of long-term voltage drift, such standard spectral datasets had to be updated approximately once every two months. To test the validity of this method, spectra of the manganotantalite standard were collected over the $2\frac{1}{2}$ year period of the study. The spectra were analyzed against similar spectra from this standard which were used in mineral analysis. All spectra were acquired at least two weeks after the spectrum against which they were analyzed.

The analyses and their mean are given in Table 105. Two points deserve mention. First, the measured standard deviations for the mean are only slightly larger than the 1σ estimates from count statistics alone. Secondly, the mean falls well within 1σ of the ideal composition for all constituents. It is concluded that (1) inter-session current drift was adequately compensated for, (2) standards can be stored for later use in analysis when the method of operation described above is used, (3) the 1σ estimates based on count statistics give slight underestimates of the true standard error.

Table 105: Repeated Analyses of the Manganotantalite Standard

	1	2	3	4	5	6	7	8	9
MnO	14.2	14.4	14.3	14.7	14.6	14.7	14.7	14.6	14.5
Nb_2O_5	8.0	8.1	8.1	8.2	8.5	8.5	8.4	8.4	8.5
Ta_2O_5	76.9	77.1	78.0	77.6	77.3	77.0	76.7	76.8	76.2
	99.1	99.6	100.4	100.4	100.3	100.0	99.8	99.9	99.3

Oxide	Ideal Conc.	Mean Conc.	σ (meas)	σ (est)
MnO	14.6	14.5	.2	.1
Nb_2O_5	8.1	8.3	.2	.1
Ta_2O_5	77.3	77.1	.5	.4
	100.0	99.9	.5	.4

Appendix C

CHEMICAL ANALYSES OF WODGINITE-GROUP MINERALS (LESS TANCO)

Abbreviations Used in Appendices C and D

(c): centre of grain
(r): rim of grain
(e): edge of grain (not necessarily the
     true rim of the grain)
(i): between edge or rim and core
(d): dark
(l): light

Numbers in parentheses refer to different
grains or to different spots on crystal
clusters.

	A-3	A-17 (r)	A-17 (c)	A-26	A-28	A-29 (1)	A-29 (2c)	A-29 (2e)	A-30	GB-1	GB-2	GB-3	GB-4	H2-1	KO-2	KZ-1 (d)	KZ-1 (1)	KZ-1 (1)	L-10	L-15
MnO	10.7	4.7	5.4	4.3	9.4	10.5	10.5	10.4	10.9	6.0	6.4	8.1	6.2	8.0	9.9	6.6	7.1	7.0	5.8	5.0
FeO	0.0	6.3	5.4	6.5	1.1	0.0	0.0	0.0	0.0	4.8	4.5	2.5	4.7	3.1	0.0	4.7	0.0	0.0	5.0	0.0
Fe_2O_3	1.1	1.5	1.7	1.4	0.7	0.4	0.3	0.5	0.3	2.0	1.8	2.9	1.8	1.0	0.0	1.3	0.0	0.0	2.0	0.0
TiO_2	0.2	3.3	2.2	0.9	0.2	0.0	0.0	0.0	0.2	1.3	0.7	0.4	1.4	4.0	0.0	4.3	0.0	0.0	0.4	0.0
SnO_2	15.8	10.4	11.0	14.5	18.3	15.5	15.2	15.7	19.2	12.4	14.6	9.9	13.2	11.3	17.8	10.0	7.7	7.8	13.8	0.7
Nb_2O_5	6.6	8.0	7.5	10.9	5.8	3.6	3.5	3.7	4.2	6.2	6.3	5.7	5.6	6.3	4.3	10.3	10.4	11.1	9.1	0.7
Ta_2O_5	64.6	64.8	66.9	61.1	62.9	68.0	69.2	69.0	64.9	65.9	64.5	69.7	66.5	66.7	66.3	62.6	73.7	73.7	62.2	92.2
	99.1	99.0	100.1	99.7	98.5	98.0	98.7	99.2	99.6	98.5	98.8	99.1	99.4	100.4	98.4	99.7	99.0	99.5	98.3	98.5

Cations per 32(O)

	A-3	A-17 (r)	A-17 (c)	A-26	A-28	A-29 (1)	A-29 (2c)	A-29 (2e)	A-30	GB-1	GB-2	GB-3	GB-4	H2-1	KO-2	KZ-1 (d)	KZ-1 (1)	KZ-1 (1)	L-10	L-15
Mn^{2+}	3.89	1.66	1.89	1.52	3.45	3.95	3.93	3.86	4.00	2.18	2.33	2.95	2.24	2.78	3.71	2.24	2.61	2.52	2.09	1.98
Fe^{2+}	0.0	2.19	1.89	2.26	0.39	0.0	0.0	0.0	0.0	1.71	1.61	0.88	1.66	1.06	0.0	1.59	0.0	0.0	1.77	0.0
ΣA	3.89	3.84	3.78	3.78	3.84	3.95	3.93	3.86	4.00	3.89	3.94	3.84	3.90	3.84	3.71	3.83	2.61	2.52	3.86	1.98
Sn^{4+}	2.71	1.71	1.81	2.38	3.16	2.75	2.67	2.74	3.31	2.11	2.48	1.70	2.24	1.85	3.14	1.60	1.33	1.33	2.33	0.12
Ti^{4+}	0.06	1.03	0.69	0.29	0.06	0.0	0.0	0.0	0.05	0.41	0.23	0.12	0.44	1.24	0.0	1.29	0.0	0.0	0.12	0.0
Fe^{3+}	0.36	0.48	0.52	0.44	0.23	0.12	0.11	0.17	0.09	0.63	0.58	0.93	0.56	0.30	0.0	0.39	0.0	0.0	0.63	0.0
Ta(B)	0.81	0.79	0.97	0.89	0.54	0.95	1.02	0.96	0.45	0.85	0.71	1.26	0.76	0.62	0.81	0.72	2.69	2.73	0.92	3.91
ΣB	3.94	4.00	4.00	4.00	4.00	3.82	3.81	3.87	3.91	4.00	4.00	4.00	4.00	4.00	3.94	4.00	4.02	4.06	4.00	4.03
Ta(C)	6.72	6.51	6.59	5.97	6.87	7.27	7.30	7.27	7.19	6.80	6.79	6.89	6.92	6.83	7.14	6.13	5.96	5.85	6.25	7.85
Nb^{5+}	1.28	1.49	1.41	2.03	1.13	0.73	0.70	0.73	0.81	1.20	1.21	1.11	1.08	1.17	0.86	1.87	2.04	2.15	1.75	0.15
$\Sigma Cat.$	15.84	15.84	15.78	15.78	15.84	15.77	15.74	15.73	15.91	15.89	15.94	15.84	15.90	15.84	15.65	15.83	14.63	14.58	15.86	14.01

	LJ-1 (c)	LJ-1 (r)	LJ-2 (c)	LJ-2 (r)	MC-1 (d)	MC-1 (1)	MT-1	OW-102 (d)	OW-102 (d)	OW-102A (1)	OW-102A (d)	SK-1 (1)	SK-1 (2)	SQ-1 (c)	SQ-1 (r)	TT-1	VII-1 (1)	VII-1 (2)	WD-1
MnO	7.4	7.8	7.5	7.1	8.3	10.9	5.8	5.7	6.0	10.3	9.2	2.8	2.8	10.6	11.0	10.0	10.9	11.0	10.6
FeO	3.5	2.9	3.3	3.5	2.9	0.0	5.3	4.8	4.8	0.0	1.2	9.5	9.1	0.0	0.8	0.0	0.0	0.0	0.0
Fe_2O_3	1.5	1.7	1.7	1.5	1.6	0.0	2.0	1.7	2.0	0.9	1.5	1.8	1.9	1.0	0.9	0.1	0.4	0.0	0.3
TiO_2	0.0	0.0	0.0	0.0	1.2	0.0	1.8	0.4	0.2	0.0	0.2	4.8	3.9	0.5	0.0	0.0	0.0	0.0	0.0
SnO_2	16.9	15.6	15.3	15.6	15.3	14.5	12.4	13.6	14.0	16.0	14.9	10.1	10.1	16.4	15.2	13.3	16.1	15.4	17.1
Nb_2O_5	6.0	6.1	6.9	7.2	5.9	4.4	6.4	8.6	8.2	3.1	6.4	15.1	14.5	3.7	4.4	1.7	6.1	5.7	6.9
Ta_2O_5	64.2	65.4	65.0	64.2	64.0	68.9	65.2	62.6	62.5	69.1	65.5	56.1	56.4	66.0	66.1	73.3	65.5	65.8	64.2
	99.3	99.6	99.6	99.2	99.3	98.8	98.9	97.4	97.7	99.4	98.9	100.2	98.7	98.2	98.6	98.4	99.0	98.9	99.1

Cations per 32(O)

	LJ-1 (c)	LJ-1 (r)	LJ-2 (c)	LJ-2 (r)	MC-1 (d)	MC-1 (1)	MT-1	OW-102 (d)	OW-102 (d)	OW-102A (1)	OW-102A (d)	SK-1 (1)	SK-1 (2)	SQ-1 (c)	SQ-1 (r)	TT-1	VII-1 (1)	VII-1 (2)	WD-1
Mn^{2+}	2.67	2.83	2.69	2.57	2.97	4.08	2.08	2.06	2.17	3.83	3.34	0.93	0.93	3.93	4.05	3.82	3.99	4.05	3.85
Fe^{2+}	1.24	1.05	1.17	1.25	1.03	0.0	1.87	1.74	1.71	0.0	0.44	3.08	3.01	0.0	0.0	0.0	0.0	0.0	0.0
ΣA	3.91	3.88	3.86	3.82	4.00	4.08	3.95	3.79	3.89	3.83	3.78	4.00	3.94	3.93	4.05	3.82	3.99	4.05	3.85
Sn^{4+}	2.88	2.65	2.60	2.66	2.58	2.55	2.09	2.33	2.40	2.80	2.56	1.55	1.60	2.86	2.64	2.40	2.78	2.66	2.94
Ti^{4+}	0.0	0.0	0.0	0.0	0.39	0.0	0.56	0.13	0.07	0.0	0.05	1.39	1.15	0.16	0.30	0.0	0.0	0.0	0.0
Fe^{3+}	0.47	0.56	0.55	0.49	0.52	0.0	0.62	0.57	0.65	0.28	0.48	0.53	0.57	0.33	0.28	0.03	0.12	0.29	0.10
Ta(B)	0.64	0.79	0.84	0.85	0.51	1.13	0.73	0.98	0.88	0.85	0.91	0.53	0.69	0.62	0.66	1.33	0.91	0.88	0.85
ΣB	4.00	4.00	4.00	4.00	4.00	3.68	4.00	4.00	4.00	3.94	4.00	4.00	4.00	3.97	3.88	3.77	3.81	3.83	3.89
Ta(C)	6.84	6.82	6.68	6.61	6.87	7.12	6.77	6.33	6.42	7.38	6.76	5.36	5.40	7.26	7.14	7.66	6.80	6.88	6.67
Nb^{5+}	1.16	1.18	1.32	1.39	1.13	0.88	1.23	1.67	1.58	0.62	1.24	2.64	2.60	0.74	0.86	0.34	1.20	1.12	1.33
ΣCat.	15.91	15.88	15.86	15.82	16.00	15.76	15.95	15.79	15.09	15.77	15.78	16.00	15.94	15.89	15.93	15.58	15.80	15.88	15.74

Appendix D

CHEMICAL ANALYSES OF OXIDE MINERALS FROM THE TANCO PEGMATITE

Table 106: Analyses of Wodginite-Group Minerals

	A-25 (1)	A-25 (2)	A-25 (3)	G69-7	G69-10	G69-11	G69-14 (d)	G69-14 (1)	G69-17	G69-20	G69-22 (r)	G69-22 (c)	G69-23 (r)	G69-23 (c)	G69-28 (r)	G69-28 (c)	G69-29B-III	G69-32	G69-35	G69-36	G69-39	G69-42 (e)	G69-42 (c)	G69-43A	G69-46A
MnO	10.3	9.0	9.6	9.8	10.4	9.4	10.6	11.2	10.9	10.5	10.2	10.6	10.1	10.8	9.9	10.3	8.5	11.2	8.2	10.3	8.9	10.4	10.2	8.9	9.0
FeO	1.4	3.1	2.5	0.7	0.0	1.4	0.4	0.0	0.0	0.0	0.8	0.2	0.4	0.0	0.6	0.1	2.3	0.0	2.8	0.1	1.7	0.4	0.3	1.4	1.7
Fe$_2$O$_3$	1.0	0.1	0.5	1.6	1.7	1.2	1.2	0.2	1.1	1.5	1.1	1.4	1.6	0.9	1.2	0.6	1.4	0.4	1.1	1.6	1.8	1.1	1.0	2.4	1.3
TiO$_2$	5.5	9.2	8.0	2.4	0.3	2.2	3.3	2.3	1.8	0.3	2.6	2.8	1.3	2.9	0.5	0.9	0.8	2.3	1.4	0.5	2.2	2.1	2.8	0.4	0.7
SnO$_2$	10.3	7.4	8.1	10.2	13.0	13.5	12.1	9.3	11.7	13.8	13.4	11.6	13.1	11.5	16.1	17.4	15.7	11.4	16.1	13.9	10.9	13.8	12.2	11.4	16.1
Nb$_2$O$_5$	8.4	11.1	11.1	6.1	2.4	4.6	6.6	3.2	3.1	2.0	5.7	4.8	2.9	4.4	3.5	4.1	5.7	4.4	4.3	3.4	3.5	4.9	5.4	2.3	3.5
Ta$_2$O$_5$	64.0	59.9	60.3	69.1	70.6	66.3	65.0	72.6	70.3	71.5	65.6	67.8	69.0	68.1	67.3	64.7	63.3	70.4	66.2	70.9	68.8	67.3	67.0	71.5	66.9
	100.9	99.7	100.3	99.9	98.5	98.6	99.1	98.8	98.8	99.5	99.4	99.2	98.3	98.6	99.1	98.2	97.7	100.1	100.1	100.7	98.0	99.9	99.0	98.4	99.2

Cations per 32(0)

	A-25 (1)	A-25 (2)	A-25 (3)	G69-7	G69-10	G69-11	G69-14 (d)	G69-14 (1)	G69-17	G69-20	G69-22 (r)	G69-22 (c)	G69-23 (r)	G69-23 (c)	G69-28 (r)	G69-28 (c)	G69-29B-III	G69-32	G69-35	G69-36	G69-39	G69-42 (e)	G69-42 (c)	G69-43A	G69-46A
Mn^{2+}	3.45	2.93	3.15	3.49	3.91	3.40	3.74	4.12	4.00	3.89	3.62	3.80	3.73	3.92	3.65	3.81	3.13	4.01	2.94	3.75	3.27	3.71	3.66	3.33	3.31
Fe^{2+}	0.48	0.99	0.79	0.25	0.0	0.50	0.14	0.0	0.0	0.0	0.27	0.06	0.14	0.0	0.22	0.05	0.82	0.0	1.00	0.03	0.62	0.13	0.12	0.53	0.62
ΣA	3.93	3.91	3.94	3.74	3.91	3.90	3.88	4.12	4.00	3.89	3.89	3.87	3.87	3.92	3.87	3.86	3.94	4.01	3.94	3.78	3.90	3.84	3.79	3.86	3.93
Sn^{4+}	1.63	1.14	1.28	1.70	2.30	2.30	2.01	1.61	2.03	2.41	2.24	1.95	2.28	1.96	2.80	3.03	2.71	1.94	2.73	2.38	1.88	2.32	2.06	2.01	2.78
Ti^{4+}	1.64	2.66	2.32	0.75	0.11	0.71	1.02	0.75	0.57	0.10	0.82	0.88	0.42	0.92	0.15	0.28	0.25	0.74	0.46	0.16	0.71	0.65	0.90	0.13	0.21
Fe^{3+}	0.29	0.02	0.14	0.51	0.57	0.40	0.36	0.05	0.35	0.49	0.36	0.45	0.52	0.29	0.39	0.21	0.46	0.13	0.34	0.51	0.60	0.35	0.30	0.79	0.43
Ta(B)	0.44	0.19	0.26	1.04	0.97	0.60	0.61	1.23	0.91	0.93	0.57	0.72	0.78	0.76	0.66	0.48	0.58	0.98	0.47	0.95	0.81	0.67	0.73	1.07	0.57
ΣB	4.00	4.00	4.00	4.00	3.94	4.00	4.00	3.65	3.86	3.94	4.00	4.00	4.00	3.93	4.00	4.00	4.00	3.78	4.00	4.00	4.00	4.00	4.00	4.00	4.00
Ta(C)	6.48	6.07	6.06	6.84	7.52	7.11	6.75	7.37	7.39	7.60	6.91	7.07	7.42	7.15	7.31	7.19	6.88	7.15	7.17	7.33	7.31	7.06	6.97	7.53	7.31
Nb^{5+}	1.52	1.93	1.94	1.16	0.48	0.89	1.25	0.63	0.61	0.40	1.09	0.93	0.58	0.85	0.69	0.81	1.12	0.85	0.83	0.67	0.69	0.94	1.03	0.47	0.69
ΣCat.	15.93	15.91	15.94	15.74	15.86	15.90	15.88	15.77	15.86	15.83	15.89	15.87	15.87	15.84	15.87	15.86	15.94	15.79	15.94	15.78	15.90	15.84	15.79	15.86	15.93

Table 106 (cont.)

	G69-52	SMP-6 (1)	SMP-6 (2)	SMP-6A	SMP-12A (1)	SMP-12A (2)	SMP-40 (1d)	SMP-40 (2d)	SMP-40 (3d)	SMP-40 (31)	SMP-51A-3	SMP-51A-4	SMP-51B-1E	SMP-51B-1F	SMP-51B-3A	SMP-51B-3B	SMP-51B-5B	SMP-51B-5C	SMP-51C-2A	SMP-51C-2B	SMP-51C-4A	SMP-51C-4D	SMP-51D-1A	SMP-51D-1C	SMP-51D-2A
MnO	8.7	10.2	10.0	10.2	9.4	10.0	8.7	6.7	6.8	8.7	8.2	9.0	9.8	6.9	7.0	10.4	9.9	7.3	7.0	9.7	8.3	10.1	9.6	8.8	8.3
FeO	1.5	0.0	0.0	0.1	0.0	0.0	1.5	1.6	1.2	0.0	2.2	0.2	0.0	1.6	1.7	0.0	0.0	1.3	1.5	0.0	1.2	0.0	0.5	1.6	2.4
Fe$_2$O$_3$	1.4	0.0	0.0	0.1	0.0	0.0	1.2	0.5	0.8	0.0	1.3	0.2	0.0	0.6	0.9	0.0	0.2	0.8	0.8	0.0	1.3	0.1	0.5	1.3	1.3
TiO$_2$	0.0	0.0	0.0	0.1	0.0	0.0	1.5	0.5	0.5	0.0	0.3	0.0	0.0	0.5	0.4	0.0	0.0	0.0	0.7	0.0	0.8	0.0	0.2	1.5	0.6
SnO$_2$	15.9	14.1	14.2	14.2	14.1	14.2	13.0	10.2	7.9	12.8	15.7	15.8	16.1	10.6	10.8	15.6	14.5	11.4	9.2	15.6	11.3	15.3	15.4	13.2	15.9
Nb$_2$O$_3$	2.5	4.6	4.9	4.6	5.0	5.6	2.5	2.2	1.8	4.1	2.8	5.1	5.3	1.6	1.4	4.5	5.1	1.0	1.3	4.5	2.0	4.5	4.3	2.5	2.6
Ta$_2$O$_5$	67.4	70.2	69.3	69.2	70.4	69.4	70.0	76.2	79.2	71.8	68.2	68.0	68.2	77.3	76.4	68.0	68.9	75.8	78.1	70.2	74.2	69.4	69.3	70.4	68.8
	97.5	99.2	98.5	98.4	99.0	99.2	98.3	97.8	98.2	97.5	98.7	98.3	99.4	99.1	98.6	98.5	98.5	97.7	98.7	100.0	99.2	99.3	99.2	99.3	99.9
Cations per 32(O)																									
Mn^{2+}	3.30	3.78	3.74	3.82	3.50	3.71	3.22	2.57	2.61	3.31	3.05	3.37	3.62	2.62	2.69	3.88	3.68	2.83	2.67	3.56	3.11	3.75	3.54	3.25	3.03
Fe^{2+}	0.57	0.0	0.0	0.0	0.0	0.0	0.55	0.59	0.46	0.0	0.81	0.08	0.0	0.61	0.65	0.0	0.0	0.49	0.56	0.0	0.46	0.0	0.00	0.58	0.87
ΣA	3.88	3.78	3.74	3.82	3.50	3.71	3.77	3.16	3.07	3.31	3.86	3.45	3.62	3.23	3.33	3.88	3.68	3.32	3.23	3.56	3.57	3.75	3.54	3.83	3.90
Sn^{4+}	2.84	2.47	2.50	2.49	2.48	2.47	2.28	1.84	1.44	2.31	2.76	2.78	2.80	1.90	1.94	2.74	2.55	2.08	1.64	2.71	2.00	2.67	2.68	2.28	2.75
Ti^{4+}	0.0	0.0	0.0	0.04	0.0	0.0	0.48	0.15	0.15	0.0	0.10	0.0	0.0	0.15	0.12	0.0	0.0	0.25	0.25	0.0	0.27	0.0	0.07	0.50	0.21
Fe^{3+}	0.46	0.0	0.0	0.05	0.0	0.0	0.39	0.16	0.28	0.0	0.44	0.06	0.0	0.21	0.30	0.0	0.06	0.28	0.28	0.0	0.44	0.03	0.16	0.44	0.43
Ta(B)	0.70	1.31	1.30	1.21	1.42	1.34	0.85	1.84	2.13	1.63	0.71	1.16	1.11	1.75	1.63	1.06	1.26	1.64	1.83	1.21	1.30	1.15	1.08	0.79	0.62
ΣB	4.00	3.78	3.80	3.80	3.90	3.81	4.00	4.00	4.00	3.94	4.00	4.00	3.91	4.00	4.00	3.80	3.86	4.00	4.00	3.92	4.00	3.85	4.00	4.00	4.00
Ta(C)	7.49	7.08	7.01	7.08	7.00	6.90	7.51	7.54	7.64	7.17	7.45	6.99	6.96	7.68	7.71	7.10	6.99	7.79	7.73	7.10	7.60	7.12	7.16	7.52	7.49
Nb^{5+}	0.51	0.92	0.99	0.92	1.00	1.10	0.49	0.46	0.36	0.83	0.55	1.01	1.04	0.32	0.29	0.90	1.01	0.21	0.27	0.90	0.40	0.88	0.84	0.48	0.51
ΣCat.	15.88	15.56	15.55	15.62	15.39	15.52	15.77	15.16	15.07	15.25	15.86	15.45	15.53	15.23	15.33	15.67	15.54	15.32	15.23	15.48	15.57	15.60	15.54	15.83	15.90

Table 106 (cont.)

	SMP-51D-2B	SMP-51D-2D	SMP-51D-3A	SMP-51D-3B	SMP-51D-3C	SMP-51D-4C	SMP-51D-4D	TL-45	TSE-7	TSE-16(c)	TSE-16(i)	TSE-16(r)	TSE-17	TSE-26	TSE-28	TSE-30	TSE-32	TSE-36	TSE-37	TSE-40(l)	TSE-40(d)	TSE-41	TSE-45(r)	TSE-45(c)	TSE-48
MnO	7.6	10.1	8.9	7.6	9.9	9.5	8.9	10.1	10.3	9.7	9.9	8.9	10.3	10.8	9.4	10.0	11.1	10.4	11.1	11.0	9.0	11.7	9.8	10.2	10.2
FeO	3.3	0.0	1.9	3.4	0.1	0.0	0.9	0.5	0.0	0.5	0.9	2.4	0.7	0.0	0.0	1.0	0.8	1.2	0.2	0.7	1.8	0.0	0.6	0.5	0.6
Fe₂O₃	1.2	0.0	1.4	1.3	0.2	0.0	1.4	1.2	0.0	1.3	1.0	1.0	0.9	0.5	0.0	1.3	0.8	0.9	0.9	0.7	1.7	0.3	0.8	0.8	1.3
TiO₂	2.0	0.0	1.5	2.7	0.2	0.0	0.5	2.1	0.0	2.1	3.6	5.5	3.4	0.5	0.0	3.7	2.8	5.6	2.8	0.9	1.0	4.2	3.6	3.0	2.1
SnO₂	14.3	16.0	14.3	12.7	15.3	16.5	12.6	13.2	16.6	11.7	11.7	8.8	12.5	13.6	13.2	10.8	12.0	10.7	13.1	13.4	14.2	12.3	10.6	12.9	12.9
Nb₂O₅	2.9	4.7	2.8	3.0	4.3	4.1	1.4	4.5	4.1	4.7	4.6	11.1	6.1	5.2	5.5	6.3	6.0	8.1	6.0	2.9	3.9	8.2	5.6	5.8	3.8
Ta₂O₅	67.8	68.4	68.9	69.3	69.8	69.4	74.5	67.1	67.3	67.1	66.5	60.4	66.4	69.5	70.5	65.8	65.5	62.6	65.0	69.6	68.0	61.9	67.5	64.9	68.3
	98.9	99.2	99.8	99.9	99.6	99.5	100.2	98.7	98.3	97.2	98.2	98.1	100.3	100.0	98.6	98.9	98.1	99.4	98.2	98.5	99.7	98.6	98.5	98.1	99.2
Cations per 32(O)																									
Mn²⁺	2.76	3.74	3.24	2.72	3.66	3.53	3.31	3.66	3.87	3.59	3.56	3.02	3.59	3.94	3.50	3.54	3.98	3.56	3.98	4.10	3.28	4.07	3.51	3.68	3.68
Fe²⁺	1.17	0.0	0.68	1.20	0.0	0.0	0.34	0.19	0.0	0.20	0.31	0.82	0.25	0.0	0.0	0.34	0.0	0.40	0.0		0.65	0.0	0.20	0.16	0.20
ΣA	3.93	3.74	3.92	3.92	3.66	3.53	3.64	3.85	3.87	3.79	3.87	3.84	3.84	3.94	3.50	3.88	3.98	3.96	3.98	4.10	3.93	4.07	3.71	3.84	3.88
Sn⁴⁺	2.45	2.80	2.45	2.15	2.67	2.88	2.21	2.25	2.93	2.02	1.98	1.41	2.05	2.34	2.32	1.80	2.03	1.71	2.23	2.35	2.43	2.01	1.79	2.19	2.21
Ti⁴⁺	0.64	0.0	0.50	0.85	0.05	0.0	0.17	0.69	0.0	0.70	1.14	1.67	1.07	0.17	0.0	1.17	0.90	1.68	0.89	0.28	0.33	1.30	1.15	0.95	0.69
Fe³⁺	0.39	0.0	0.45	0.42	0.03	0.0	0.45	0.38	0.0	0.43	0.31	0.30	0.28	0.13	0.0	0.39	0.27	0.26	0.08	0.25	0.55	0.10	0.24	0.27	0.43
Ta(B)	0.52	1.07	0.60	0.58	1.14	1.09	1.17	0.68	0.91	0.85	0.56	0.62	0.60	1.15	1.55	0.64	0.71	0.34	0.67	0.91	0.69	0.47	0.82	0.59	0.68
ΣB	4.00	3.86	4.00	4.00	3.89	3.96	4.00	4.00	3.84	4.00	4.00	4.00	4.00	3.78	3.86	4.00	3.90	4.00	3.86	3.78	4.00	3.87	4.00	4.00	4.00
Ta(C)	7.43	7.07	7.45	7.42	7.16	7.19	7.73	7.14	7.18	7.08	7.11	5.98	6.86	6.99	6.90	6.81	6.85	6.52	6.85	7.42	7.23	6.47	6.94	6.89	7.27
Nb⁵⁺	0.57	0.93	0.55	0.58	0.84	0.81	0.27	0.86	0.82	0.92	0.89	2.02	1.14	1.01	1.10	1.19	1.15	1.48	1.15	0.58	0.77	1.53	1.06	1.11	0.73
ΣCat.	15.93	15.60	15.92	15.92	15.55	15.49	15.64	15.85	15.71	15.79	15.87	15.84	15.84	15.71	15.36	15.88	15.88	15.96	15.84	15.89	15.93	15.94	15.71	15.84	15.88

430

Table 106 (cont.)

	TSE-55	TSE-57A	TSE-57B	TSE-63 (1)	TSE-63 (2)	TSE-63 (3)	TSE-65 (1)	TSE-65 (2)	TSE-65 (3)	TSE-66 (1)	TSE-66 (2)	TSE-69	TSE-73 (c)	TSE-73 (r)	TSE-76 (1)	TSE-76 (2)	TSE-76 (3)	TSE-77	TSE-78	TSE-79	TSE-80 (r)	TSE-80 (c)	TSE-82	TSE-86 (r)	TSE-86 (c)
MnO	10.0	8.5	11.0	9.2	10.0	7.9	7.3	8.5	7.4	10.9	11.3	11.3	10.7	10.9	4.9	4.4	7.0	10.7	10.4	8.4	10.6	11.3	3.4	10.2	10.0
FeO	1.3	0.0	0.0	2.2	1.5	0.6	3.6	2.4	3.5	0.0	0.0	0.0	0.0	0.0	0.2	0.0	3.3	0.0	0.2	2.0	0.1	0.0	9.6	0.8	0.5
Fe$_2$O$_3$	1.0	0.1	0.1	0.8	0.8	1.0	1.6	1.4	1.6	0.6	0.4	0.0	1.0	0.7	0.0	0.0	2.2	0.8	1.0	1.7	0.9	0.6	0.6	0.6	1.0
TiO$_2$	4.7	0.0	0.3	6.2	6.7	1.1	0.6	1.8	0.3	2.5	1.6	0.6	2.4	3.0	0.0	0.0	0.2	3.7	3.0	2.6	3.5	3.8	10.4	7.5	5.0
SnO$_2$	10.9	10.3	15.3	8.7	8.6	7.9	15.9	13.8	16.2	13.8	15.5	18.0	9.2	8.9	3.4	5.9	11.6	11.5	11.7	9.5	11.6	10.2	5.7	5.8	7.8
Nb$_2$O$_5$	8.2	2.8	4.0	9.1	8.0	2.3	4.2	5.9	3.3	6.0	5.1	6.3	3.7	4.2	4.8	5.6	5.6	6.7	5.4	3.5	6.5	7.2	16.7	5.6	4.3
Ta$_2$O$_5$	63.8	77.3	68.1	63.5	62.6	77.7	65.9	65.5	66.8	64.5	63.9	62.7	71.9	71.4	85.0	81.8	68.9	65.0	68.0	70.5	65.1	65.7	53.2	67.2	68.6
	99.9	99.0	98.9	99.8	98.2	98.4	99.0	99.4	99.1	98.3	97.9	98.8	98.8	99.1	98.4	97.7	98.8	98.5	99.7	98.1	98.3	98.6	99.7	97.6	97.2

Cations per 32(O)

	TSE-55	TSE-57A	TSE-57B	TSE-63 (1)	TSE-63 (2)	TSE-63 (3)	TSE-65 (1)	TSE-65 (2)	TSE-65 (3)	TSE-66 (1)	TSE-66 (2)	TSE-69	TSE-73 (c)	TSE-73 (r)	TSE-76 (1)	TSE-76 (2)	TSE-76 (3)	TSE-77	TSE-78	TSE-79	TSE-80 (r)	TSE-80 (c)	TSE-82	TSE-86 (r)	TSE-86 (c)
Mn^{2+}	3.44	3.24	4.10	3.12	3.44	3.00	2.68	3.05	2.72	3.93	4.15	4.10	3.89	3.93	1.89	1.69	2.58	3.79	3.69	3.08	3.78	3.98	1.07	3.55	3.61
Fe^{2+}	0.45	0.0	0.0	0.75	0.52	0.21	1.28	0.85	1.26	0.0	0.0	0.0	0.0	0.0	0.09	0.0	1.18	0.01	0.08	0.72	0.03	0.0	2.96	0.26	0.17
ΣA	3.90	3.24	4.10	3.86	3.96	3.21	3.97	3.90	3.98	3.93	4.15	4.10	3.89	3.93	1.98	1.69	3.76	3.80	3.77	3.80	3.81	3.98	4.03	3.81	3.79
Sn^{4+}	1.75	1.85	2.68	1.38	1.38	1.42	2.74	2.33	2.81	2.34	2.67	3.07	1.58	1.52	0.62	1.06	2.01	1.92	1.95	1.63	1.95	1.69	0.84	0.95	1.32
Ti^{4+}	1.42	0.0	0.10	1.84	2.03	0.35	0.18	0.58	0.10	0.79	0.51	0.19	0.77	0.95	0.0	0.0	0.08	1.17	0.95	0.84	1.12	1.18	2.87	2.32	1.59
Fe^{3+}	0.31	0.03	0.02	0.25	0.25	0.32	0.51	0.45	0.53	0.20	0.13	0.0	0.33	0.24		0.0	0.72	0.25	0.32	0.56	0.28	0.18	0.18	0.18	0.33
Ta(B)	0.52	2.01	0.92	0.52	0.34	1.91	0.57	0.64	0.56	0.60	0.51	0.55	1.16	1.10	3.51	3.28	1.20	0.66	0.78	0.97	0.66	0.81	0.11	0.55	0.76
ΣB	4.00	3.89	3.72	4.00	4.00	4.00	4.00	4.00	4.00	3.93	3.83	3.81	3.84	3.82	4.13	4.34	4.00	4.00	4.00	4.00	4.00	3.85	4.00	4.00	4.00
Ta(C)	6.50	7.43	7.20	6.36	6.55	7.54	7.17	6.88	7.35	6.85	7.00	6.77	7.27	7.20	7.01	6.84	6.91	6.73	6.98	7.32	6.77	6.65	5.22	6.95	7.18
Nb^{5+}	1.50	0.57	0.80	1.64	1.45	0.46	0.83	1.12	0.65	1.15	1.00	1.23	0.73	0.80	0.99	1.16	1.09	1.27	1.02	0.68	1.23	1.35	2.78	1.05	0.82
ΣCat.	15.90	15.12	15.82	15.86	15.96	15.21	15.97	15.90	15.98	15.86	15.98	15.91	15.74	15.75	14.11	14.02	15.76	15.80	15.77	15.80	15.81	15.83	16.03	15.81	15.79

Table 106 (cont.)

	TSE-88	TSE-89	TSE-90 (1)	TSE-90 (2)	TSE-91 (1)	TSE-91 (2)	TSE-92 (r)	TSE-92 (i)	TSE-92 (c)	TSE-94	TSE-95	TSE-96	TSE-97	TSE-99 (r)	TSE-99 (c)	TSE-100 (1)	TSE-100 (2)	TSE-101	TSE-103 (c)	TSE-103 (r)	TSE-104	TSE-105	TSE-106 (1)	TSE-106 (2)	TSE-107
MnO	8.9	11.5	11.2	8.4	10.8	10.9	10.0	10.4	10.5	4.5	7.7	10.2	10.1	6.1	10.0	10.3	10.5	11.0	9.9	10.2	10.4	10.7	10.5	10.8	6.2
FeO	2.4	0.0	0.3	3.0	0.0	0.0	0.7	0.0	0.0	7.7	3.4	0.7	0.2	5.3	1.1	0.7	0.6	0.0	0.9	0.7	0.9	0.0	0.0	0.0	5.2
Fe_2O_3	0.9	0.0	0.6	0.9	0.0	0.0	0.9	0.8	0.8	0.7	1.2	0.9	1.2	0.9	0.3	1.1	0.9	0.0	1.2	1.1	0.5	0.8	1.2	0.6	2.1
TiO_2	4.8	0.8	7.3	4.6	0.4	0.3	2.6	2.3	2.9	9.2	2.2	4.1	3.0	4.9	6.2	3.5	4.0	0.3	3.0	3.6	6.4	0.8	1.3	3.4	3.4
SnO_2	11.4	14.5	7.4	12.1	15.8	15.4	13.0	12.3	11.0	5.5	14.4	10.7	10.2	10.7	9.4	11.8	11.4	17.4	12.1	11.2	9.2	13.5	13.4	10.7	9.5
Nb_2O_5	8.1	8.0	8.9	7.7	2.2	1.7	6.0	4.3	5.0	9.6	5.7	5.9	4.4	8.9	9.5	7.1	7.8	1.5	4.8	6.3	7.2	3.1	3.7	3.8	6.7
Ta_2O_5	62.7	64.2	63.7	61.7	70.1	69.9	65.4	68.0	68.4	61.7	64.7	67.4	69.2	62.4	62.5	64.7	65.1	68.7	67.1	65.3	65.0	69.6	69.0	68.4	66.0
	99.2	99.0	99.3	98.4	99.3	98.1	98.6	98.0	98.6	98.9	99.2	99.7	98.4	99.3	99.1	99.2	100.2	98.9	98.9	98.5	99.7	98.4	99.2	97.7	99.2

Cations per 32(O)

	TSE-88	TSE-89	TSE-90 (1)	TSE-90 (2)	TSE-91 (1)	TSE-91 (2)	TSE-92 (r)	TSE-92 (i)	TSE-92 (c)	TSE-94	TSE-95	TSE-96	TSE-97	TSE-99 (r)	TSE-99 (c)	TSE-100 (1)	TSE-100 (2)	TSE-101	TSE-103 (c)	TSE-103 (r)	TSE-104	TSE-105	TSE-106 (1)	TSE-106 (2)	TSE-107
Mn^{2+}	3.08	4.15	3.76	2.94	4.04	4.13	3.57	3.81	3.81	1.49	2.74	3.57	3.67	2.09	3.41	3.63	3.63	4.14	3.55	3.60	3.55	3.98	3.85	3.96	2.18
Fe^{2+}	0.83	0.0	0.09	1.03	0.0	0.0	0.25	0.0	0.0	2.50	1.19	0.23	0.09	1.80	0.38	0.23	0.19	0.0	0.31	0.26	0.31	0.0	0.0	0.0	1.81
ΣA	3.92	4.15	3.86	3.97	4.04	4.13	3.82	3.81	3.81	3.99	3.93	3.80	3.75	3.89	3.79	3.86	3.82	4.14	3.86	3.87	3.87	3.98	3.85	3.96	3.99
Sn^{4+}	1.84	2.46	1.18	1.98	2.78	2.76	2.20	2.12	1.87	0.85	2.43	1.77	1.74	1.73	1.50	1.96	1.86	3.07	2.04	1.88	1.47	2.36	2.31	1.84	1.57
Ti^{4+}	1.45	0.25	2.18	1.42	0.13	0.08	0.83	0.75	0.93	2.70	0.68	1.27	0.97	1.50	1.87	1.09	1.22	0.11	0.94	1.13	1.93	0.27	0.43	1.09	1.07
Fe^{3+}	0.27	0.0	0.18	0.27	0.0	0.0	0.30	0.25	0.25	0.22	0.38	0.28	0.39	0.27	0.10	0.33	0.28	0.0	0.37	0.36	0.16	0.27	0.40	0.19	0.66
Ta(B)	0.44	0.97	0.47	0.32	0.86	0.87	0.67	0.84	0.89	0.23	0.51	0.68	0.89	0.50	0.53	0.62	0.64	0.60	0.65	0.63	0.43	0.94	0.82	0.76	0.69
ΣB	4.00	3.68	4.00	4.00	3.77	3.72	4.00	3.95	3.93	4.00	4.00	4.00	4.00	4.00	4.00	4.00	4.00	3.78	4.00	4.00	4.00	3.84	3.97	3.87	4.00
Ta(C)	6.50	6.46	6.41	6.58	7.55	7.65	6.85	7.16	7.04	6.31	6.91	6.90	7.15	6.37	6.28	6.67	6.57	7.70	7.08	6.80	6.68	7.39	7.28	7.26	6.75
Nb^{5+}	1.50	1.54	1.59	1.42	0.45	0.35	1.15	0.84	0.96	1.69	1.09	1.10	0.85	1.63	1.72	1.33	1.43	0.30	0.92	1.20	1.32	0.61	0.72	0.74	1.25
ΣCat.	15.92	15.83	15.86	15.97	15.81	15.85	15.82	15.76	15.74	15.99	15.93	15.80	15.75	15.89	15.79	15.86	15.82	15.92	15.86	15.87	15.87	15.82	15.82	15.84	15.99

Table 106 (cont.)

	TSE-108	TSE-109 (1)	TSE-109 (2)	TSE-112	TSE-113	TSE-115	TSE-116 (r)	TSE-116 (c)	TSE-117 (1)	TSE-117 (2)	TSE-119 (c)	TSE-119 (r)	TSE-120	TSE-121 (e)	TSE-121 (c)	TSE-122 (c)	TSE-122 (r)	TSE-122 (r)	TSE-126 (r)	TSE-126 (c)	TSE-129	TSE-130	TSE-131	TSE-132 (1)	TSE-132 (2)
MnO	10.1	10.2	10.3	4.9	10.9	10.8	8.8	10.1	4.4	9.8	9.3	10.3	11.3	10.3	7.9	9.4	9.3	9.0	10.0	10.2	11.4	8.5	10.3	9.9	10.2
FeO	0.5	0.8	0.7	6.8	0.2	0.0	2.4	0.6	7.0	1.1	1.5	0.2	0.0	0.4	3.5	2.7	2.5	2.6	1.3	1.6	0.0	2.6	0.6	0.4	1.1
Fe$_2$O$_3$	1.0	1.0	0.4	1.7	0.6	0.1	0.9	0.9	1.5	1.1	1.1	1.0	0.6	1.1	1.1	0.3	0.7	1.0	1.1	0.6	0.2	0.8	0.9	1.2	0.9
TiO$_2$	3.2	4.4	7.1	5.2	5.2	0.5	4.8	3.3	4.6	3.3	3.5	4.6	3.7	3.6	4.3	10.1	8.0	5.8	4.6	7.7	1.1	4.5	5.4	2.0	6.1
SnO$_2$	11.9	10.2	7.0	7.5	10.7	16.6	10.5	12.1	9.3	12.3	11.2	8.3	11.1	10.8	11.5	5.0	6.8	9.6	10.6	7.9	13.5	11.3	7.9	12.3	7.9
Nb$_2$O$_5$	5.6	6.5	7.1	9.4	6.7	2.7	8.4	6.2	8.6	7.0	5.8	5.9	6.8	6.3	6.7	10.3	9.3	9.1	7.9	9.5	9.7	8.5	6.5	3.8	7.8
Ta$_2$O$_5$	65.2	66.2	66.6	65.1	63.7	68.1	61.8	65.4	63.7	64.1	65.9	68.2	67.0	65.7	64.2	61.2	61.8	61.6	62.6	61.1	63.1	61.6	67.3	69.3	66.1
	97.6	99.2	99.3	100.6	98.0	98.8	97.7	98.6	99.1	98.8	98.3	98.3	100.5	98.3	99.1	98.9	98.4	98.8	98.0	98.6	99.0	97.7	98.9	99.0	100.0
												Cations per 32(O)													
Mn^{2+}	3.65	3.56	3.53	1.64	3.81	4.02	3.06	3.60	1.53	3.47	3.32	3.65	3.93	3.68	2.76	3.06	3.12	3.06	3.49	3.42	4.07	2.98	3.58	3.62	3.46
Fe^{3+}	0.19	0.26	0.25	2.25	0.08	0.0	0.83	0.22	2.38	0.40	0.52	0.06	0.0	0.14	1.20	0.86	0.82	0.89	0.44	0.54	0.0	0.88	0.19	0.16	0.35
ΣA	3.85	3.83	3.78	3.89	3.89	4.02	3.90	3.82	3.91	3.87	3.84	3.71	3.93	3.82	3.96	3.92	3.95	3.95	3.93	3.96	4.07	3.87	3.78	3.78	3.81
Sn^{4+}	2.02	1.68	1.13	1.19	1.76	2.92	1.73	2.02	1.51	2.05	1.88	1.38	1.82	1.82	1.88	0.76	1.08	1.54	1.75	1.25	2.26	1.86	1.29	2.11	1.26
Ti^{4+}	1.03	1.35	2.16	1.55	1.61	0.17	1.49	1.03	1.40	1.02	1.12	1.43	1.15	1.12	1.34	2.93	2.40	1.77	1.42	2.30	0.34	1.39	1.68	0.65	1.85
Fe^{3+}	0.32	0.31	0.13	0.52	0.20	0.02	0.29	0.29	0.45	0.34	0.34	0.30	0.18	0.35	0.35	0.08	0.21	0.30	0.34	0.19	0.06	0.24	0.29	0.40	0.26
Ta (B)	0.63	0.66	0.58	0.74	0.42	0.71	0.49	0.65	0.63	0.59	0.66	0.88	0.74	0.71	0.43	0.23	0.32	0.40	0.49	0.27	1.06	0.51	0.74	0.84	0.64
ΣB	4.00	4.00	4.00	4.00	4.00	3.82	4.00	4.00	4.00	4.00	4.00	4.00	3.90	4.00	4.00	4.00	4.00	4.00	4.00	4.00	3.72	4.00	4.00	4.00	4.00
Ta (C)	6.93	6.78	6.72	6.31	6.74	7.46	6.43	6.82	6.41	6.68	6.89	6.89	6.73	6.80	6.75	6.20	6.34	6.34	6.53	6.30	6.16	6.41	6.79	7.27	6.58
Nb^{5+}	1.07	1.22	1.28	1.69	1.26	0.54	1.57	1.18	1.59	1.32	1.11	1.11	1.27	1.20	1.25	1.80	1.66	1.66	1.47	1.70	1.84	1.59	1.21	0.73	1.42
ΣCat.	15.85	15.83	15.78	15.89	15.89	15.84	15.90	15.82	15.91	15.87	15.84	15.71	15.82	15.82	15.96	15.92	15.95	15.95	15.93	15.96	15.79	15.87	15.78	15.78	15.81

Table 106 (cont.)

	TSE-133 (1)	TSE-133 (2)	TSE-134 (1)	TSE-134 (2)	TSE-135 (1)	TSE-135 (2)	TSE-136 (1)	TSE-136 (2)	TSE-137 (1)	TSE-137 (2)	TSE-138	TSE-139	TSE-141 (r)	TSE-141 (c)	TSE-163
MnO	8.7	10.3	9.9	10.3	6.1	10.0	4.1	10.3	10.9	10.6	10.1	10.8	10.8	11.0	9.7
FeO	2.3	0.0	0.8	0.8	5.5	1.0	7.4	0.2	0.0	0.0	0.6	0.1	0.0	0.0	1.1
Fe_2O_3	0.6	0.9	0.7	0.8	1.2	1.1	1.0	0.7	0.7	0.8	1.0	0.8	0.5	0.5	0.9
TiO_2	4.6	4.4	3.7	5.0	4.5	3.0	6.5	3.6	2.4	2.3	1.3	3.6	1.8	3.1	2.9
SnO_2	11.9	8.2	11.9	10.1	11.1	12.9	7.3	11.3	13.7	13.8	15.9	12.0	13.6	11.1	13.6
Nb_2O_5	8.1	6.4	5.8	7.7	7.2	6.0	9.6	6.3	5.3	5.2	3.8	7.3	4.2	5.1	6.0
Ta_2O_5	61.3	67.8	67.4	65.2	64.1	66.0	63.3	66.0	66.6	66.4	66.5	64.5	67.6	67.5	63.5
	97.4	97.9	100.2	99.8	99.7	100.0	99.2	98.5	99.6	99.1	99.2	99.2	98.6	98.3	97.7

Cations per 32(O)

	TSE-133 (1)	TSE-133 (2)	TSE-134 (1)	TSE-134 (2)	TSE-135 (1)	TSE-135 (2)	TSE-136 (1)	TSE-136 (2)	TSE-137 (1)	TSE-137 (2)	TSE-138	TSE-139	TSE-141 (r)	TSE-141 (c)	TSE-163
Mn^{2+}	3.05	3.67	3.48	3.55	2.09	3.53	1.39	3.68	3.89	3.82	3.67	3.79	3.95	3.96	3.51
Fe^{2+}	0.81	0.0	0.29	0.27	1.87	0.35	2.48	0.07	0.0	0.0	0.23	0.03	0.0	0.0	0.38
ΣA	3.87	3.67	3.77	3.82	3.96	3.87	3.86	3.75	3.89	3.82	3.90	3.82	3.95	3.96	3.89
Sn^{4+}	1.97	1.37	1.97	1.64	1.81	2.15	1.16	1.89	2.30	2.34	2.72	1.99	2.35	1.88	2.31
Ti^{4+}	1.42	1.38	1.14	1.52	1.39	0.93	1.95	1.14	0.77	0.72	0.42	1.12	0.58	1.01	0.92
Fe^{3+}	0.17	0.27	0.21	0.23	0.36	0.33	0.31	0.23	0.22	0.24	0.33	0.26	0.17	0.15	0.27
$Ta(B)$	0.44	0.97	0.68	0.60	0.44	0.59	0.58	0.73	0.65	0.68	0.53	0.63	0.77	0.81	0.49
ΣB	4.00	3.99	4.00	4.00	4.00	4.00	4.00	4.00	3.95	3.98	4.00	4.00	3.87	3.85	4.00
$Ta(C)$	6.48	6.79	6.92	6.60	6.67	6.87	6.27	6.80	6.99	7.00	7.26	6.63	7.17	7.01	6.84
Nb^{5+}	1.52	1.21	1.08	1.40	1.33	1.13	1.73	1.20	1.01	1.00	0.74	1.37	0.83	0.99	1.16
$\Sigma Cat.$	15.87	15.66	15.77	15.82	15.96	15.87	15.86	15.75	15.84	15.80	15.90	15.82	15.82	15.82	15.89

Table 107: Analyses of Columbite-Group Minerals

	A-25	G69-7-III	G69-8-I	G69-10	G69-29B	G69-30 (c)	G69-30 (r)	G69-31 (r)	G69-31 (c)	G69-36	G69-52-III	G69-53	G69-55 (e)	G69-55 (c)	G69-56 (r)	G69-56 (i)	G69-56 (c)	G69-59	G69-61 (r)	G69-61 (i)	G69-61 (c)	SMP-6	SMP-6A	SMP-51B-1D	SMP-51B-1H
MnO	10.6	13.2	15.0	11.7	16.1	14.7	15.3	15.6	15.1	11.9	13.4	14.7	15.6	15.7	15.6	12.2	13.4	13.1	15.5	15.3	15.8	12.0	13.5	11.6	11.0
FeO	6.1	0.9	0.2	2.8	0.0	1.4	0.4	0.4	0.1	2.3	0.9	0.7	0.0	0.0	0.0	0.0	0.0	3.0	0.1	0.0	0.0	2.0	0.8	2.2	1.9
CaO	0.0	0.0	0.0	0.0	0.0	0.0	0.0	0.0	0.0	0.0	0.0	0.0	0.0	0.0	0.0	0.0	0.0	0.0	0.0	0.0	0.0	0.0	0.0	0.0	0.0
Sc_2O_3	1.2	0.6	0.0	0.0	0.0	0.0	0.0	0.0	0.0	0.0	0.0	0.0	0.0	0.0	0.0	0.0	0.0	0.5	0.0	0.0	0.0	0.0	0.0	0.0	0.0
TiO_2	2.6	0.6	0.8	0.2	0.0	1.0	0.9	1.0	1.6	0.0	0.0	0.1	0.3	0.6	1.1	1.0	1.1	3.1	0.6	0.6	0.6	0.2	0.1	0.0	0.0
SnO_2	0.5	0.5	0.7	0.3	0.0	0.0	1.1	0.2	0.8	0.0	0.5	0.4	0.9	0.6	0.6	14.0	7.9	0.7	0.1	0.6	0.8	0.5	0.2	0.4	1.0
Nb_2O_5	37.2	4.5	19.5	5.0	21.4	21.7	22.1	23.6	23.2	3.0	4.9	19.5	22.2	21.3	22.0	11.5	16.3	34.4	20.9	20.4	21.6	2.3	8.9	0.4	4.5
Ta_2O_5	43.4	79.1	63.4	79.4	62.6	60.6	59.6	59.4	57.8	83.7	79.6	64.5	61.9	63.0	60.2	60.8	59.9	45.5	61.5	61.5	61.5	83.1	75.7	85.4	81.9
	101.6	98.9	99.6	99.5	100.1	99.4	99.4	100.2	98.6	101.0	99.4	100.0	100.8	101.3	99.5	99.4	98.6	100.3	98.7	98.3	100.3	100.1	99.2	99.6	100.3

Cations per 24(O)

	A-25	G69-7-III	G69-8-I	G69-10	G69-29B	G69-30 (c)	G69-30 (r)	G69-31 (r)	G69-31 (c)	G69-36	G69-52-III	G69-53	G69-55 (e)	G69-55 (c)	G69-56 (r)	G69-56 (i)	G69-56 (c)	G69-59	G69-61 (r)	G69-61 (i)	G69-61 (c)	SMP-6	SMP-6A	SMP-51B-1D	SMP-51B-1H
Mn^{2+}	2.36	3.72	3.83	3.29	4.07	3.71	3.83	3.86	3.77	3.35	3.76	3.76	3.89	3.91	3.91	3.21	3.46	2.98	3.97	3.93	3.97	3.41	3.71	3.36	3.08
Fe^{2+}	1.35	0.25	0.06	0.76	0.0	0.35	0.10	0.10	0.03	0.65	0.26	0.18	0.0	0.0	0.0	0.0	0.0	0.67	0.04	0.0	0.0	0.55	0.23	0.64	0.54
Ca^{2+}	0.0	0.0	0.0	0.0	0.0	0.0	0.0	0.0	0.0	0.0	0.0	0.0	0.0	0.0	0.0	0.0	0.0	0.0	0.0	0.0	0.0	0.0	0.0	0.0	0.0
Sc^{3+}	0.27	0.14	0.0	0.0	0.0	0.0	0.0	0.0	0.0	0.0	0.0	0.0	0.0	0.0	0.0	0.0	0.0	0.11	0.0	0.0	0.0	0.0	0.0	0.0	0.0
Ti^{4+}	0.52	0.08	0.18	0.06	0.0	0.22	0.20	0.22	0.35	0.0	0.0	0.03	0.07	0.13	0.24	0.22	0.26	0.62	0.13	0.13	0.12	0.05	0.02	0.0	0.0
Sn^{4+}	0.05	0.0	0.09	0.04	0.0	0.0	0.13	0.03	0.10	0.0	0.06	0.05	0.07	0.07	0.07	1.73	0.96	0.08	0.01	0.07	0.10	0.07	0.03	0.0	0.14
Nb^{5+}	4.41	0.68	2.65	0.75	2.89	2.91	2.97	3.11	3.09	0.45	0.74	2.66	2.95	2.83	2.94	1.61	2.25	4.18	2.85	2.80	2.89	0.35	1.31	0.06	0.67
Ta^{5+}	3.10	7.16	5.19	7.15	5.08	4.89	4.80	4.72	4.63	7.55	7.20	5.30	4.96	5.04	4.84	5.14	4.98	3.32	5.04	5.07	4.95	7.57	6.68	7.94	7.37
	12.04	12.03	11.99	12.05	12.04	12.08	12.02	12.03	11.97	12.00	12.03	11.98	11.97	11.99	12.01	11.92	11.92	11.98	12.03	12.00	12.02	12.00	11.98	12.00	11.80

Table 107 (cont.)

	SMP-51B-11	TRT-15A	TRT-15N	TRT-42	TRT-43	TRT-51	TRT-52(1)	TRT-52(2)	TRT-53(1)	TRT-53(2)	TSE-26(r)	TSE-26(c)	TSE-36	TSE-42(e)	TSE-42(c)	TSE-42(i)	TSE-49(c)	TSE-49(e)	TSE-52	TSE-55	TSE-57B	TSE-71	TSE-76	TSE-77	TSE-82
MnO	10.7	15.5	15.1	13.5	13.6	15.3	12.3	14.1	12.5	10.4	14.8	14.7	15.8	14.1	14.8	14.7	13.8	13.5	14.3	7.7	14.2	15.2	14.3	9.6	10.2
FeO	2.2	0.0	0.0	1.2	2.6	0.6	2.5	1.7	3.1	4.5	0.5	0.6	0.0	0.8	1.1	0.5	2.2	2.1	1.4	9.3	0.5	0.8	0.8	5.4	5.2
CaO	0.0	0.0	0.0	0.0	0.0	0.0	0.3	0.4	0.0	0.0	0.0	0.0	0.0	0.0	0.0	0.0	0.0	0.0	0.2	0.0	0.8	0.0	0.0	0.0	0.0
Sc$_2$O$_3$	0.0	0.0	0.0	1.0	1.2	0.6	0.9	0.0	0.4	0.6	0.2	0.3	0.0	0.6	0.7	0.4	0.2	0.2	0.7	1.1	0.0	0.2	0.0	0.0	0.8
TiO$_2$	0.0	0.0	0.0	2.2	2.1	0.9	0.7	0.0	2.6	3.8	0.2	0.0	0.0	0.0	0.0	0.0	2.4	2.2	1.0	3.0	0.0	0.7	0.3	1.1	4.6
SnO$_2$	1.3	0.0	1.2	0.3	0.0	0.0	0.9	0.0	0.7	1.2	0.3	0.0	0.3	2.0	0.3	3.3	1.1	1.1	1.0	0.5	0.2	0.4	0.0	0.7	1.8
Nb$_2$O$_5$	4.6	18.2	18.2	30.8	35.3	30.0	23.7	26.5	28.2	28.5	15.7	14.2	17.1	18.6	20.4	18.0	29.8	29.3	33.6	41.5	19.9	24.2	11.4	18.7	27.0
Ta$_2$O$_5$	80.4	66.5	64.6	49.5	45.6	50.9	59.3	56.9	52.1	49.7	69.6	71.0	67.2	62.9	62.2	62.5	50.3	50.5	47.3	37.6	62.7	59.2	73.4	63.5	49.9
	99.2	100.2	99.1	98.5	100.4	98.3	100.6	99.6	99.6	98.7	101.2	100.9	100.3	99.0	99.5	99.3	99.8	99.0	98.5	100.6	99.0	100.7	100.1	98.9	99.4
Cations per 24(O)																									
Mn^{2+}	3.04	3.99	3.92	3.20	3.10	3.70	3.02	3.48	2.97	2.46	3.83	3.84	4.08	3.64	3.75	3.79	3.26	3.22	3.39	1.68	3.62	3.73	3.82	2.46	2.39
Fe^{2+}	0.62	0.0	0.0	0.28	0.58	0.14	0.61	0.41	0.73	1.05	0.12	0.16	0.0	0.22	0.27	0.13	0.52	0.49	0.32	2.01	0.12	0.20	0.21	1.36	1.21
Ca^{2+}	0.0	0.0	0.0	0.0	0.0	0.0	0.09	0.12	0.0	0.0	0.0	0.0	0.0	0.0	0.0	0.0	0.0	0.0	0.05	0.0	0.25	0.0	0.0	0.0	0.0
Sc^{3+}	0.0	0.0	0.0	0.24	0.28	0.15	0.23	0.0	0.10	0.15	0.05	0.07	0.0	0.14	0.16	0.08	0.05	0.05	0.16	0.24	0.0	0.05	0.0	0.0	0.20
Ti^{4+}	0.0	0.0	0.0	0.46	0.42	0.19	0.15	0.0	0.55	0.80	0.04	0.0	0.0	0.0	0.0	0.0	0.49	0.47	0.21	0.57	0.18	0.15	0.07	0.26	0.95
Sn^{4+}	0.18	0.0	0.15	0.03	0.0	0.0	0.10	0.0	0.08	0.13	0.05	0.0	0.03	0.24	0.03	0.40	0.12	0.13	0.0	0.05	0.02	0.05	0.0	0.09	0.20
Nb^{5+}	0.69	2.50	2.52	3.90	4.29	3.87	3.10	3.49	3.58	3.59	2.17	1.99	2.36	2.55	2.76	2.47	3.75	3.74	4.24	4.84	2.71	3.18	1.62	2.56	3.37
Ta^{5+}	7.31	5.50	5.39	3.77	3.33	3.95	4.67	4.51	3.98	3.77	5.78	5.96	5.58	5.20	5.07	5.17	3.81	3.87	3.59	2.64	5.13	4.67	6.31	5.24	3.75
	11.83	12.00	11.98	11.89	12.01	12.00	11.97	12.01	11.99	11.95	11.99	12.01	12.06	11.99	12.05	12.05	12.01	11.96	11.96	12.04	12.03	12.01	12.04	11.96	12.07

Table 107 (cont.)

	TSE-83 (c)	TSE-83 (r)	TSE-84	TSE-89	TSE-94	TSE-98	TSE-107	TSE-112	TSE-114	TSE-115	TSE-123 (c)	TSE-123 (r)	TSE-130	TSE-131	TSE-137
MnO	14.5	14.9	10.9	10.6	10.0	13.8	8.7	10.0	12.6	12.6	14.9	14.8	10.2	10.6	13.0
FeO	0.8	1.0	6.0	5.3	6.6	2.3	6.6	6.1	3.2	2.7	0.6	0.4	4.9	4.6	2.3
CaO	0.0	0.0	0.0	0.2	0.0	0.7	0.0	0.0	0.0	0.0	0.0	0.2	0.0	0.0	0.0
Sc_2O_3	0.9	1.1	0.4	0.2	1.3	0.7	0.3	1.0	0.5	0.6	0.0	0.6	0.8	0.0	0.0
TiO_2	3.2	3.3	3.3	0.8	3.0	2.0	2.5	3.6	3.4	0.6	1.0	0.0	4.5	3.6	1.8
SnO_2	0.4	0.0	0.9	0.2	0.5	0.9	0.8	0.7	1.2	0.3	0.0	0.0	1.3	1.3	0.7
Nb_2O_5	35.1	36.2	41.5	20.3	35.7	37.0	28.5	38.7	32.9	18.4	22.6	21.7	32.3	20.7	24.6
Ta_2O_5	42.3	43.8	39.5	63.5	44.6	43.6	51.0	41.3	45.9	65.0	58.9	60.1	44.3	58.8	56.1
	97.2	100.4	102.6	100.8	101.6	100.3	98.5	101.3	99.6	99.4	97.9	97.8	98.3	99.5	98.5

Cations per 24(O)

	TSE-83 (c)	TSE-83 (r)	TSE-84	TSE-89	TSE-94	TSE-98	TSE-107	TSE-112	TSE-114	TSE-115	TSE-123 (c)	TSE-123 (r)	TSE-130	TSE-131	TSE-137
Mn^{2+}	3.36	3.35	2.35	2.65	2.24	3.13	2.09	2.21	2.89	3.24	3.77	3.78	2.35	2.60	3.20
Fe^{2+}	0.19	0.22	1.29	1.31	1.45	0.52	1.56	1.33	0.72	0.67	0.15	0.10	1.11	1.11	0.57
Ca^{2+}	0.0	0.0	0.0	0.0	0.0	0.0	0.0	0.0	0.0	0.0	0.0	0.07	0.0	0.0	0.0
Sc^{3+}	0.21	0.26	0.10	0.04	0.29	0.16	0.08	0.21	0.12	0.0	0.0	0.0	0.20	0.0	0.0
Ti^{4+}	0.66	0.66	0.63	0.18	0.60	0.41	0.54	0.70	0.70	0.13	0.22	0.14	0.91	0.78	0.40
Sn^{4+}	0.04	0.0	0.09	0.02	0.05	0.09	0.09	0.07	0.13	0.03	0.0	0.0	0.14	0.15	0.09
Nb^{5+}	4.34	4.33	4.78	2.72	4.24	4.48	3.66	4.53	4.04	2.53	3.05	2.97	3.97	2.73	3.25
Ta^{5+}	3.15	3.15	2.74	5.11	3.19	3.17	3.93	2.91	3.39	5.38	4.80	4.94	3.28	4.65	4.45
	11.96	11.98	11.97	12.03	12.06	11.95	11.95	11.96	11.98	11.98	12.00	12.00	11.96	12.01	11.96

Table 108: Analyses of Microlite-Subgroup Minerals

	A-14	A-25	G69-1-II	G69-8-I	G69-17	G69-29B-I	G69-36	G69-39	G69-43A-III	SMP-4	SMP-6	SMP-51A-5	SMP-51B-1B	SMP-51B-1C	SMP-51B-3C	SMP-51B-2B	SMP-51B-2C	SMP-51C-1A	SMP-51C-1B	SMP-51C-1C	SMP-51C-4B	SMP-51C-4C	SMP-51C-4E	SMP-51D-1B	TL-45
Na2O	0.4	4.1	5.4	1.6	4.9	1.9	5.3	5.0	5.3	5.2	3.6	5.4	2.7	5.3	5.2	3.9	4.1	4.9	1.9	4.1	3.7	1.6	5.2	5.4	4.7
CaO	4.6	14.6	9.8	6.5	9.3	7.2	9.2	8.7	9.8	9.2	7.6	10.1	8.5	10.3	10.3	8.3	8.3	10.1	5.9	7.6	10.1	9.0	9.8	10.2	10.5
MnO	0.2	0.0	0.0	0.3	0.0	0.8	0.0	0.0	0.0	0.0	0.0	0.0	0.0	0.0	0.0	0.0	0.0	0.0	0.2	0.0	0.0	0.0	0.0	0.0	0.0
FeO	0.0	0.0	0.0	0.0	0.0	1.1	0.6	0.0	0.0	0.0	0.0	0.0	0.5	0.0	0.0	0.0	0.0	0.0	0.0	0.0	0.0	0.0	0.0	0.0	0.0
SnO	0.5	1.2	0.0	0.7	0.0	0.0	0.0	0.0	0.0	0.0	0.8	0.0	0.0	0.0	0.0	0.0	0.0	0.0	0.0	0.0	0.0	0.0	0.0	0.0	0.7
PbO	3.8	0.0	0.0	0.0	0.0	1.0	0.0	0.0	0.0	0.5	0.0	0.0	0.9	0.0	0.0	0.0	0.0	0.0	2.9	1.3	0.5	0.7	0.6	0.0	0.0
Sb2O3	0.0	0.0	0.0	1.7	0.0	0.0	0.0	0.0	0.0	0.0	0.5	0.0	0.0	0.0	0.0	0.0	0.0	0.0	0.0	0.0	0.0	0.0	0.0	0.0	0.5
UO2	6.6	0.2	0.0	0.0	0.0	7.3	0.0	0.0	0.0	0.0	3.2	0.0	3.6	0.0	0.0	3.3	3.1	0.0	3.5	1.3	1.3	2.4	0.0	0.0	0.0
TiO2	0.0	3.9	0.0	0.0	0.0	0.0	0.0	0.0	0.0	0.0	0.0	0.0	0.0	0.0	0.0	0.5	0.6	0.0	0.0	0.3	0.0	0.0	0.0	0.0	0.0
SnO2	0.0	0.7	0.0	0.0	0.0	0.0	0.0	0.0	0.0	0.0	0.0	0.0	0.0	0.0	0.0	0.0	0.0	0.0	0.0	0.0	0.0	0.0	0.0	0.0	0.0
Nb2O5	3.0	7.6	1.5	2.3	2.2	1.3	2.4	2.1	2.1	2.0	1.1	0.2	0.9	0.2	0.2	0.5	0.4	0.2	1.1	1.0	1.2	1.1	0.9	1.2	2.1
Ta2O5	72.8	64.1	78.6	78.8	80.2	71.2	80.1	80.0	79.1	81.0	81.5	80.4	78.6	81.2	81.9	79.3	79.5	81.8	79.8	80.4	80.2	81.1	81.1	80.9	77.3
	92.0	96.3	95.2	92.0	96.6	91.9	97.8	95.8	96.4	97.9	98.5	96.0	95.7	97.0	97.7	95.8	96.0	97.0	95.4	95.9	96.9	96.0	97.6	97.7	95.8
Ions per 2 B-Cations																									
Na+	0.08	0.66	0.94	0.28	0.83	0.38	0.90	0.85	0.92	0.88	0.62	0.95	0.48	0.93	0.90	0.70	0.73	0.86	0.33	0.70	0.64	0.28	0.90	0.94	0.82
Ca2+	0.47	1.30	0.95	0.62	0.88	0.77	0.86	0.82	0.94	0.86	0.72	0.98	0.84	0.99	0.99	0.82	0.82	0.97	0.57	0.72	0.96	0.85	0.93	0.97	1.03
Mn2+	0.02	0.0	0.0	0.02	0.0	0.07	0.0	0.0	0.0	0.0	0.0	0.0	0.0	0.0	0.0	0.0	0.0	0.0	0.02	0.0	0.0	0.0	0.0	0.0	0.0
Fe2+	0.0	0.04	0.0	0.0	0.0	0.09	0.03	0.0	0.0	0.0	0.0	0.0	0.03	0.0	0.0	0.0	0.0	0.0	0.0	0.0	0.0	0.0	0.0	0.0	0.0
Sn2+	0.02	0.0	0.0	0.02	0.0	0.0	0.0	0.0	0.0	0.0	0.02	0.0	0.0	0.0	0.0	0.0	0.0	0.0	0.0	0.0	0.0	0.0	0.0	0.0	0.03
Pb2+	0.10	0.0	0.0	0.0	0.0	0.03	0.0	0.0	0.0	0.01	0.02	0.0	0.02	0.0	0.0	0.0	0.0	0.0	0.07	0.03	0.01	0.02	0.02	0.0	0.0
Sb3+	0.0	0.0	0.0	0.0	0.0	0.0	0.0	0.0	0.0	0.0	0.0	0.0	0.0	0.0	0.0	0.0	0.0	0.0	0.0	0.0	0.0	0.0	0.0	0.0	0.02
U4+	0.14	0.00	0.0	0.03	0.0	0.16	0.0	0.0	0.0	0.0	0.06	0.0	0.07	0.0	0.0	0.12	0.12	0.0	0.07	0.02	0.03	0.05	0.0	0.0	0.0
ΣA	0.83	2.00	1.89	0.98	1.71	1.50	1.79	1.67	1.85	1.75	1.44	1.93	1.45	1.92	1.88	1.65	1.67	1.83	1.06	1.48	1.64	1.20	1.85	1.90	1.90
Ti4+	0.0	0.24	0.0	0.0	0.0	0.0	0.0	0.0	0.0	0.0	0.0	0.0	0.0	0.0	0.0	0.0	0.0	0.0	0.0	0.02	0.0	0.0	0.0	0.0	0.0
Sn4+	0.0	0.02	0.0	0.0	0.0	0.0	0.0	0.0	0.0	0.0	0.0	0.0	0.0	0.0	0.0	0.0	0.0	0.0	0.0	0.0	0.0	0.0	0.0	0.0	0.0
Nb5+	0.13	0.28	0.06	0.09	0.09	0.06	0.10	0.08	0.08	0.08	0.05	0.01	0.04	0.01	0.01	0.02	0.02	0.01	0.04	0.04	0.05	0.04	0.04	0.05	0.09
Ta5+	1.87	1.45	1.94	1.91	1.91	1.94	1.90	1.92	1.92	1.92	1.95	1.99	1.96	1.99	1.99	1.98	1.98	1.99	1.96	1.94	1.95	1.96	1.96	1.95	1.91
O(eff)	5.92	6.54	6.42	5.87	6.29	6.48	6.34	6.25	6.40	6.31	6.20	6.46	6.28	6.46	6.44	6.37	6.38	6.40	5.96	6.14	6.35	6.11	6.41	6.43	6.49

Table 108 (cont.)

	TRT-15A (1)	TRT-15A (2)	TRT-15N	TRT-42	TSE-28	TSE-30	TSE-32	TSE-35	TSE-36	TSE-45	TSE-48	TSE-52	TSE-55	TSE-71 (r)	TSE-71 (i)	TSE-71 (c)	TSE-78	TSE-82	TSE-84	TSE-85	TSE-88	TSE-89	TSE-94	TSE-95	TSE-97
Na_2O	1.1	1.9	4.9	0.0	5.2	5.1	5.0	5.4	4.3	5.2	4.0	0.5	4.1	2.4	4.1	3.5	4.7	5.0	4.4	4.3	1.3	0.8	5.0	4.9	4.5
CaO	7.5	6.1	9.1	3.5	10.3	10.7	10.4	10.6	10.1	9.8	14.4	3.9	13.0	6.2	6.6	6.6	11.8	13.6	10.4	13.9	7.5	8.6	11.4	11.3	13.6
MnO	0.3	0.4	0.0	0.0	0.0	0.0	0.0	0.0	0.0	0.0	0.0	1.0	0.0	0.4	0.2	0.4	0.0	0.0	0.0	0.0	0.3	0.5	0.0	0.0	0.0
FeO	0.0	0.0	0.0	0.0	0.0	0.0	0.0	0.0	0.4	0.0	0.0	0.0	0.0	0.0	0.0	0.0	0.0	0.0	0.0	0.0	1.2	2.0	0.4	0.0	0.0
SnO	0.0	0.0	0.0	0.0	0.0	0.0	0.0	0.0	0.0	0.0	0.3	0.0	1.5	0.0	0.0	0.0	0.3	0.0	0.4	0.9	0.0	0.0	0.0	0.0	0.0
PbO	0.8	1.1	0.0	0.0	0.0	0.0	0.0	0.0	0.0	0.0	0.0	0.9	0.0	2.9	3.3	2.6	0.0	0.0	0.0	0.0	2.5	2.8	0.0	0.0	0.0
Sb_2O_3	0.0	0.0	0.0	0.0	0.0	0.0	0.0	0.0	0.3	0.0	0.0	0.0	3.8	0.0	0.0	0.0	4.3	0.0	2.3	1.6	0.0	0.0	4.1	4.8	1.9
UO_2	3.5	4.6	0.4	10.8	0.2	0.0	0.1	0.0	0.0	0.0	0.0	13.7	0.0	6.1	6.6	5.9	0.0	0.0	0.0	0.0	10.5	8.7	0.0	0.0	0.0
TiO_2	0.0	0.0	0.0	1.6	0.0	0.0	0.0	0.0	0.0	0.0	3.2	1.3	4.0	0.0	0.0	0.0	3.4	3.4	0.6	3.3	1.7	2.3	2.8	3.5	3.7
SnO_2	0.0	0.0	0.0	0.0	0.0	0.0	0.0	0.0	0.0	0.0	2.9	0.0	0.5	0.0	0.0	0.0	2.0	2.8	0.0	1.3	0.0	0.0	1.4	1.2	1.6
Nb_2O_5	1.7	0.7	1.6	4.7	1.5	2.0	2.2	2.0	2.1	2.6	3.9	4.3	8.8	3.0	3.2	3.0	6.1	6.3	5.2	7.3	5.8	7.8	5.6	7.2	5.1
Ta_2O_5	76.1	76.3	78.7	69.0	78.8	78.0	77.5	77.7	78.4	79.1	66.2	65.6	62.3	71.6	70.7	71.6	64.3	63.6	74.0	66.0	60.5	61.0	68.9	63.6	67.2
Σ	91.0	91.1	94.7	89.6	96.1	95.9	95.2	95.7	95.5	96.6	95.0	91.2	98.0	92.5	94.8	93.7	96.9	94.7	97.3	98.4	91.4	94.7	99.7	96.6	97.7
Ions per 2 B-Cations																									
Na^+	0.20	0.35	0.85	0.0	0.92	0.90	0.88	0.95	0.75	0.88	0.66	0.09	0.65	0.44	0.77	0.64	0.77	0.81	0.74	0.68	0.25	0.15	0.82	0.81	0.73
Ca^{2+}	0.75	0.62	0.87	0.34	1.00	1.03	1.01	1.03	0.97	0.92	1.32	0.40	1.16	0.63	0.68	0.68	1.07	1.23	0.97	1.23	0.79	0.85	1.03	1.03	1.22
Mn^{2+}	0.02	0.03	0.0	0.0	0.0	0.0	0.0	0.0	0.0	0.0	0.0	0.09	0.0	0.03	0.02	0.03	0.0	0.0	0.0	0.0	0.02	0.04	0.0	0.0	0.0
Fe^{2+}	0.0	0.0	0.0	0.0	0.0	0.0	0.0	0.0	0.01	0.0	0.0	0.0	0.06	0.0	0.0	0.0	0.0	0.0	0.0	0.0	0.10	0.15	0.02	0.0	0.0
Sn^{2+}	0.0	0.0	0.0	0.0	0.0	0.0	0.0	0.0	0.0	0.0	0.01	0.0	0.06	0.0	0.0	0.0	0.01	0.0	0.02	0.03	0.0	0.0	0.0	0.0	0.0
Pb^{2+}	0.02	0.03	0.0	0.0	0.0	0.0	0.0	0.0	0.0	0.0	0.0	0.02	0.0	0.07	0.09	0.07	0.0	0.0	0.0	0.0	0.06	0.07	0.0	0.0	0.0
Sb^{3+}	0.0	0.0	0.0	0.0	0.0	0.0	0.0	0.0	0.01	0.0	0.0	0.0	0.13	0.0	0.0	0.0	0.15	0.0	0.08	0.05	0.0	0.0	0.14	0.17	0.07
U^{4+}	0.07	0.10	0.0	0.22	0.00	0.0	0.0	0.0	0.0	0.0	0.0	0.29	0.0	0.13	0.14	0.13	0.0	0.0	0.0	0.0	0.23	0.18	0.0	0.0	0.0
ΣA	1.06	1.13	1.72	0.56	1.92	1.94	1.89	1.98	1.74	1.81	2.00	0.89	2.00	1.31	1.70	1.55	2.00	2.04	1.81	2.00	1.47	1.44	2.00	2.00	2.01
Ti^{4+}	0.0	0.0	0.03	0.11	0.0	0.0	0.01	0.0	0.0	0.0	0.21	0.09	0.25	0.0	0.0	0.0	0.22	0.21	0.04	0.20	0.13	0.16	0.18	0.22	0.23
Sn^{4+}	0.0	0.0	0.0	0.0	0.0	0.0	0.0	0.0	0.0	0.0	0.10	0.0	0.02	0.0	0.0	0.0	0.07	0.09	0.0	0.04	0.0	0.0	0.05	0.04	0.05
Nb^{5+}	0.07	0.03	0.06	0.19	0.06	0.08	0.09	0.08	0.08	0.10	0.15	0.19	0.33	0.13	0.14	0.13	0.23	0.24	0.20	0.27	0.26	0.32	0.21	0.27	0.19
Ta^{5+}	1.93	1.97	1.91	1.70	1.94	1.92	1.90	1.92	1.92	1.90	1.54	1.72	1.41	1.87	1.86	1.87	1.48	1.45	1.75	1.48	1.62	1.52	1.57	1.46	1.52
O(eff)	6.04	6.05	6.28	5.72	6.47	6.48	6.44	6.50	6.37	6.37	6.51	6.09	6.61	6.23	6.46	6.35	6.54	6.48	6.46	6.56	6.51	6.46	6.55	6.55	6.54

Table 108 (cont.)

	TSE-100	TSE-101 (1)	TSE-101 (2)	TSE-103	TSE-104 (1)	TSE-104 (2)	TSE-105	TSE-106 (c)	TSE-106 (r)	TSE-107	TSE-108	TSE-109	TSE-110 (1)	TSE-110 (2)	TSE-113	TSE-120	TSE-129	TSE-130	TSE-132	TSE-134	TSE-136	TSE-137	TSE-138	TSE-139 (1)	TSE-139 (2)
Na_2O	4.6	1.0	2.0	0.7	4.3	0.9	4.3	3.8	4.9	2.8	1.9	5.3	1.6	0.8	3.7	2.1	1.9	4.5	5.5	3.4	5.0	2.1	5.2	5.1	1.8
CaO	13.5	5.7	7.9	4.4	9.0	8.3	12.4	12.6	12.6	9.3	8.7	10.6	7.9	5.1	11.0	7.7	8.8	8.9	11.1	9.9	10.2	8.5	10.5	10.1	7.1
MnO	0.0	0.6	0.4	0.6	0.0	0.3	0.0	0.0	0.0	0.2	0.6	0.0	2.0	0.3	0.0	0.3	0.4	0.0	0.0	0.4	0.0	0.3	0.0	0.0	0.6
FeO	0.0	0.4	0.9	0.7	0.0	2.0	0.0	0.0	0.0	1.4	1.5	0.0	0.3	0.0	0.0	0.7	0.6	0.0	0.0	0.2	0.0	1.1	0.0	0.0	1.3
SnO	0.0	0.0	0.0	0.0	0.0	0.0	0.8	0.9	0.0	0.0	0.0	0.0	0.0	0.0	0.0	0.0	0.0	1.0	0.2	0.0	0.2	0.0	0.0	0.0	0.0
PbO	0.0	1.2	0.0	3.4	0.0	0.9	0.0	0.0	0.0	0.3	1.1	0.0	2.1	5.5	3.1	1.9	1.2	0.0	0.0	0.6	0.0	0.8	0.0	0.0	0.2
Sb_2O_3	2.0	0.0	0.0	0.0	5.3	0.0	2.0	3.7	1.5	0.0	0.0	0.0	0.0	0.0	0.0	0.0	0.0	6.5	0.3	0.0	0.2	0.0	0.0	0.0	0.0
UO_2	0.0	8.6	6.2	11.7	0.0	3.9	0.0	0.0	0.0	1.0	5.8	0.0	8.4	8.0	6.9	4.4	4.5	0.0	0.0	2.4	0.0	2.8	0.0	0.0	1.6
TiO_2	2.8	1.4	0.4	3.1	1.9	1.3	2.1	2.7	2.1	0.7	0.0	0.2	0.0	0.0	0.0	0.1	0.1	2.8	0.4	0.0	0.6	0.1	0.0	0.2	0.0
SnO_2	2.2	0.0	0.0	0.0	0.0	0.0	0.7	1.9	1.7	0.0	0.0	0.0	0.0	0.0	3.9	0.0	0.0	0.0	0.0	0.0	0.0	0.0	0.0	0.0	0.0
Nb_2O_5	5.3	6.2	0.7	7.2	6.0	4.1	3.9	4.6	3.5	2.4	2.2	2.5	2.8	4.2	7.2	2.6	1.0	6.0	3.4	3.4	1.3	2.5	2.7	1.2	2.7
Ta_2O_5	67.1	67.5	75.4	63.5	67.8	69.6	70.8	66.1	71.2	74.8	70.9	79.3	67.4	70.9	62.2	74.4	73.1	64.3	77.0	75.1	79.6	74.4	78.5	80.1	78.3
Total	97.5	92.7	94.8	95.5	95.1	91.2	97.2	96.2	97.6	93.0	92.7	97.9	92.5	94.8	98.0	94.4	91.5	94.0	97.9	95.3	96.9	92.5	96.9	96.7	93.6

Ions per 2 B-Cations

	TSE-100	TSE-101 (1)	TSE-101 (2)	TSE-103	TSE-104 (1)	TSE-104 (2)	TSE-105	TSE-106 (c)	TSE-106 (r)	TSE-107	TSE-108	TSE-109	TSE-110 (1)	TSE-110 (2)	TSE-113	TSE-120	TSE-129	TSE-130	TSE-132	TSE-134	TSE-136	TSE-137	TSE-138	TSE-139 (1)	TSE-139 (2)
Na^+	0.76	0.17	0.37	0.12	0.74	0.16	0.73	0.65	0.82	0.50	0.36	0.89	0.31	0.14	0.62	0.39	0.36	0.78	0.93	0.60	0.85	0.38	0.89	0.88	0.31
Ca^{2+}	1.22	0.55	0.81	0.41	0.85	0.82	1.16	1.18	1.16	0.91	0.92	0.99	0.87	0.52	1.02	0.77	0.93	0.86	1.04	0.97	0.97	0.85	1.00	0.96	0.68
Mn^{2+}	0.0	0.05	0.03	0.05	0.0	0.02	0.0	0.0	0.0	0.01	0.05	0.0	0.17	0.02	0.0	0.03	0.04	0.0	0.0	0.03	0.0	0.02	0.0	0.0	0.04
Fe^{2+}	0.0	0.03	0.07	0.05	0.0	0.15	0.03	0.04	0.0	0.11	0.12	0.0	0.02	0.0	0.0	0.06	0.05	0.04	0.01	0.01	0.0	0.09	0.0	0.0	0.10
Sn^{2+}	0.0	0.0	0.0	0.0	0.0	0.0	0.0	0.0	0.0	0.0	0.0	0.0	0.0	0.0	0.12	0.0	0.0	0.0	0.0	0.0	0.01	0.0	0.0	0.0	0.0
Pb^{2+}	0.0	0.03	0.03	0.08	0.0	0.02	0.0	0.0	0.0	0.01	0.03	0.0	0.06	0.14	0.0	0.05	0.03	0.0	0.0	0.01	0.0	0.02	0.0	0.0	0.0
Sb^{3+}	0.07	0.0	0.0	0.0	0.19	0.0	0.07	0.13	0.05	0.0	0.0	0.0	0.0	0.0	0.0	0.0	0.0	0.24	0.01	0.0	0.01	0.0	0.0	0.0	0.0
U^{4+}	0.0	0.17	0.13	0.23	0.0	0.08	0.0	0.0	0.0	0.02	0.13	0.0	0.19	0.17	0.25	0.09	0.10	0.0	0.0	0.05	0.0	0.06	0.0	0.0	0.03
ΣA	2.06	1.00	1.44	0.94	1.82	1.26	2.00	2.00	2.03	1.56	1.61	1.89	1.63	0.99	2.00	1.38	1.49	1.92	1.99	1.68	1.83	1.42	1.89	1.85	1.17
Ti^{4+}	0.18	0.10	0.03	0.21	0.13	0.09	0.14	0.18	0.14	0.05	0.0	0.01	0.0	0.0	0.25	0.01	0.01	0.19	0.03	0.0	0.04	0.0	0.0	0.01	0.0
Sn^{4+}	0.07	0.0	0.0	0.0	0.0	0.0	0.03	0.07	0.06	0.0	0.0	0.0	0.0	0.0	0.00	0.0	0.0	0.0	0.0	0.0	0.0	0.0	0.0	0.0	0.0
Nb^{5+}	0.20	0.25	0.03	0.29	0.24	0.17	0.16	0.18	0.14	0.10	0.10	0.10	0.13	0.18	0.28	0.11	0.04	0.24	0.14	0.14	0.05	0.11	0.11	0.05	0.11
Ta^{5+}	1.54	1.65	1.95	1.51	1.63	1.74	1.68	1.57	1.67	1.85	1.90	1.89	1.87	1.82	1.46	1.88	1.95	1.57	1.84	1.86	1.91	1.89	1.89	1.94	1.89
$O(eff)$	6.58	6.04	6.37	6.00	6.48	6.22	6.59	6.62	6.55	6.31	6.56	6.43	6.66	6.09	6.68	6.27	6.41	6.55	6.52	6.42	6.39	6.28	6.45	6.40	6.04

Table 109: Cassiterite Analyses

	G69-8-1	G69-29B-1	G69-32	G69-35	G69-59	TSE-35	TSE-37	TSE-41	TSE-46	TSE-49	TSE-55	TSE-56	TSE-63	TSE-71	TSE-83	TSE-85	TSE-88	TSE-89	TSE-90	TSE-96
MnO	1.2	0.5	0.4	0.4	0.4	0.1	0.0	0.4	0.8	0.0	0.0	0.4	0.0	0.3	0.3	0.3	1.0	0.3	0.8	0.0
FeO	0.2	0.0	0.3	0.4	1.7	0.0	0.0	0.0	0.8	0.5	0.6	0.4	0.0	0.2	1.3	0.0	0.4	0.3	0.1	0.4
TiO$_2$	0.0	0.0	0.0	0.0	1.6	0.0	0.0	0.0	0.0	0.0	0.5	0.0	0.0	0.0	0.4	0.0	0.0	0.3	0.0	0.4
SnO$_2$	89.3	98.1	95.5	95.5	82.9	97.5	100.2	94.3	91.6	97.5	95.7	93.7	98.1	98.1	90.6	99.0	91.1	98.7	93.3	96.2
Nb$_2$O$_5$	0.0	0.0	0.0	0.0	1.4	0.0	0.1	0.0	0.5	0.3	0.3	0.0	0.0	0.0	0.6	0.0	0.0	0.0	0.0	0.2
Ta$_2$O$_5$	8.9	3.4	4.4	4.7	12.4	3.0	1.0	5.1	6.5	2.5	3.7	5.0	2.2	2.6	8.7	2.8	8.3	2.4	6.4	2.4
	99.7	101.9	100.7	101.0	100.3	100.6	101.2	99.8	100.0	100.9	100.8	99.6	100.3	101.2	101.8	102.1	100.7	102.1	100.6	99.6

Cations per 4(O)

	G69-8-1	G69-29B-1	G69-32	G69-35	G69-59	TSE-35	TSE-37	TSE-41	TSE-46	TSE-49	TSE-55	TSE-56	TSE-63	TSE-71	TSE-83	TSE-85	TSE-88	TSE-89	TSE-90	TSE-96
Sn^{4+}	1.814	1.934	1.908	1.903	1.647	1.947	1.981	1.905	1.843	1.937	1.898	1.895	1.963	1.946	1.791	1.947	1.830	1.935	1.870	1.929
Ti^{4+}	0.0	0.0	0.0	0.0	0.059	0.0	0.0	0.0	0.0	0.0	0.019	0.0	0.0	0.0	0.013	0.0	0.0	0.012	0.0	0.016
Mn^{2+}	0.054	0.020	0.018	0.017	0.015	0.003	0.0	0.016	0.034	0.0	0.0	0.017	0.0	0.012	0.011	0.012	0.041	0.015	0.033	0.0
Fe^{2+}	0.010	0.0	0.014	0.017	0.072	0.0	0.0	0.0	0.033	0.023	0.026	0.019	0.0	0.007	0.055	0.0	0.016	0.011	0.006	0.018
Nb^{5+}	0.0	0.0	0.0	0.0	0.032	0.0	0.002	0.0	0.011	0.007	0.006	0.0	0.0	0.0	0.013	0.0	0.0	0.0	0.0	0.004
Ta^{5+}	0.123	0.045	0.061	0.064	0.168	0.041	0.013	0.070	0.089	0.034	0.051	0.070	0.030	0.035	0.117	0.038	0.113	0.033	0.088	0.033
	2.001	1.999	2.001	2.001	1.994	1.991	1.996	1.991	2.008	2.001	1.999	2.000	1.993	2.001	2.001	1.997	2.000	2.004	1.997	2.000

Table 109 (cont.)

	TSE-98	TSE-106	TSE-114	TSE-116	TSE-120	TSE-132	TSE-134	TSE-136	TSE-137
MnO	0.0	0.0	0.0	0.2	0.7	0.0	0.9	0.5	0.2
FeO	0.4	0.6	0.6	0.0	0.3	0.3	0.4	0.0	0.0
TiO_2	0.3	0.4	0.8	0.0	0.0	1.0	0.0	0.0	0.0
SnO_2	97.7	94.2	93.8	97.4	94.3	98.9	92.7	95.5	98.6
Nb_2O_5	0.2	0.0	0.0	0.0	0.0	0.0	0.4	0.0	0.0
Ta_2O_5	2.1	4.2	5.0	3.3	6.4	0.8	7.2	4.6	1.9
	100.7	99.4	100.2	100.9	101.6	101.0	101.5	100.5	100.7

Cations per 4(o)

Sn^{4+}	1.940	1.900	1.873	1.940	1.873	1.945	1.840	1.911	1.965
Ti^{4+}	0.010	0.016	0.030	0.0	0.0	0.035	0.0	0.0	0.0
Mn^{2+}	0.0	0.0	0.0	0.009	0.028	0.0	0.040	0.021	0.007
Fe^{2+}	0.016	0.023	0.026	0.0	0.011	0.013	0.016	0.0	0.0
Nb^{5+}	0.005	0.0	0.0	0.0	0.0	0.0	0.008	0.0	0.0
Ta^{5+}	0.029	0.058	0.068	0.045	0.086	0.011	0.098	0.063	0.026
	2.000	1.997	1.996	1.993	1.998	2.004	2.001	1.995	1.997

Table 110: Rutile Analyses

	TRT-10 (1)	TRT-10 (2)	TRT-43	TSE-55	TSE-78	TSE-82	TSE-85	TSE-95	TSE-96	TSE-97	TSE-104	TSE-105	TSE-112	TSE-126	TSE-130	TSE-132
MnO	0.0	0.5	0.0	0.0	0.2	0.0	0.0	0.0	0.0	0.0	0.0	0.0	0.0	0.0	0.3	0.0
FeO	7.1	5.6	3.4	3.5	5.1	5.4	5.0	4.4	5.5	4.0	4.7	5.5	5.9	3.7	4.2	7.0
Fe_2O_3	0.0	0.0	0.0	5.0	2.0	0.0	1.5	0.6	2.7	2.7	2.1	0.8	0.9	3.4	1.4	0.7
Sc_2O_3	0.0	0.4	0.0	0.2	0.0	0.0	0.0	0.0	0.0	0.3	0.0	0.0	0.0	0.6	0.0	0.0
TiO_2	47.3	52.2	75.8	59.0	59.5	62.8	61.3	64.0	54.5	63.5	61.3	59.8	57.1	61.1	65.0	49.2
SnO_2	0.7	0.7	0.0	1.0	1.8	0.7	0.9	4.4	1.2	1.2	1.2	1.1	1.0	1.0	0.7	1.3
Nb_2O_5	2.7	3.3	2.4	3.6	5.9	3.8	6.9	3.5	5.8	4.3	5.9	3.4	3.3	6.4	2.7	3.5
Ta_2O_5	41.1	38.1	17.9	29.9	28.4	27.3	23.6	23.4	31.5	25.8	25.0	30.3	33.3	23.6	27.1	39.2
	98.9	100.8	99.5	102.3	102.8	100.1	99.2	100.3	101.2	101.7	100.2	100.9	101.5	99.8	101.4	100.9

Cations per 4(O)

	TRT-10 (1)	TRT-10 (2)	TRT-43	TSE-55	TSE-78	TSE-82	TSE-85	TSE-95	TSE-96	TSE-97	TSE-104	TSE-105	TSE-112	TSE-126	TSE-130	TSE-132
Ti^{4+}	1.310	1.373	1.731	1.445	1.449	1.543	1.504	1.553	1.383	1.520	1.497	1.490	1.444	1.486	1.562	1.318
Sn^{4+}	0.010	0.010	0.0	0.014	0.023	0.010	0.012	0.057	0.016	0.015	0.016	0.014	0.013	0.012	0.009	0.018
Mn^{2+}	0.0	0.015	0.0	0.0	0.005	0.0	0.0	0.0	0.0	0.0	0.0	0.0	0.0	0.0	0.007	0.0
Fe^{2+}	0.219	0.164	0.086	0.095	0.139	0.147	0.138	0.120	0.155	0.106	0.128	0.152	0.166	0.100	0.113	0.209
Fe^{3+}	0.0	0.0	0.0	0.122	0.049	0.0	0.036	0.015	0.068	0.064	0.052	0.020	0.022	0.083	0.034	0.019
Sc^{3+}	0.0	0.012	0.0	0.006	0.0	0.0	0.0	0.0	0.0	0.009	0.0	0.0	0.0	0.017	0.0	0.0
Nb^{5+}	0.045	0.052	0.033	0.053	0.086	0.057	0.102	0.050	0.089	0.062	0.086	0.051	0.050	0.093	0.039	0.057
Ta^{5+}	0.412	0.363	0.148	0.265	0.251	0.243	0.209	0.205	0.289	0.223	0.221	0.273	0.305	0.208	0.236	0.379
	1.995	1.989	1.998	2.000	2.000	1.999	2.000	2.000	2.000	2.000	2.000	2.000	2.000	2.000	2.000	2.000

Table 111:   Ferrotapiolite Analyses

	G69-52	SMP-6	SMP-51A-(r)	SMP-51A-(c)	SMP-51B-1A	SMP-51B-3D	SMP-51B-5A	SMP-51D-4A	TSE-25 (1)	TSE-25 (2)	TSE-116	TSE-117	TSE-139
MnO	2.7	3.2	2.1	2.3	2.8	3.0	3.0	2.2	1.7	1.8	1.0	1.1	1.7
FeO	11.0	10.3	11.5	11.3	11.1	10.6	10.6	11.4	11.6	12.0	12.7	12.6	12.5
Fe$_2$O$_3$	0.8	0.0	0.0	0.0	0.2	0.0	0.0	0.9	0.9	0.4	0.1	0.5	0.0
TiO$_2$	0.0	0.0	0.3	0.0	0.0	0.0	0.0	0.3	0.3	0.0	1.0	1.4	0.2
SnO$_2$	0.4	0.6	0.5	0.8	0.6	0.8	1.2	0.7	1.0	0.5	1.1	0.8	0.4
Nb$_2$O$_5$	2.5	0.6	0.8	0.8	0.4	0.8	0.6	1.9	1.9	1.7	2.1	3.4	2.7
Ta$_2$O$_5$	82.6	85.3	84.6	82.8	85.4	84.8	84.1	83.0	81.5	83.3	80.7	79.9	83.5
	100.0	100.2	99.7	98.1	100.4	100.1	99.4	100.4	98.9	99.8	98.7	99.7	101.0

Cations per 12(O)

	G69-52	SMP-6	SMP-51A-(r)	SMP-51A-(c)	SMP-51B-1A	SMP-51B-3D	SMP-51B-5A	SMP-51D-4A	TSE-25 (1)	TSE-25 (2)	TSE-116	TSE-117	TSE-139
Mn^{2+}	0.39	0.47	0.30	0.33	0.40	0.43	0.43	0.31	0.25	0.26	0.14	0.15	0.23
Fe^{2+}	1.54	1.47	1.64	1.64	1.57	1.51	1.51	1.59	1.64	1.70	1.79	1.73	1.73
Fe^{3+}	0.10	0.0	0.0	0.0	0.03	0.0	0.0	0.11	0.11	0.05	0.01	0.07	0.0
Ti^{4+}	0.0	0.0	0.03	0.0	0.0	0.0	0.0	0.04	0.03	0.0	0.13	0.18	0.03
Sn^{4+}	0.02	0.04	0.04	0.06	0.04	0.06	0.08	0.05	0.07	0.03	0.07	0.05	0.02
Nb^{5+}	0.19	0.05	0.06	0.06	0.03	0.06	0.04	0.14	0.15	0.13	0.16	0.25	0.20
Ta^{5+}	3.76	3.94	3.91	3.90	3.94	3.92	3.91	3.76	3.75	3.83	3.70	3.58	3.77
	6.00	5.97	5.97	5.99	6.00	5.98	5.98	6.00	6.00	6.00	6.00	6.00	5.99

Table 113: Ilmenite Analyses

	PC-3-1	PC-3-2
MnO	3.3	2.0
FeO	44.6	45.7
TiO_2	52.3	51.9
	100.3	99.6

Cations per 3(O)

	PC-3-1	PC-3-2
Mn^{2+}	0.071	0.042
Fe^{2+}	0.942	0.973
Ti^{4+}	0.994	0.993
	2.007	2.008

Table 112: Uraninite Analyses

	TRT-42
UO_2	79.8
PbO	15.4
CaO	1.6
Ta_2O_5	2.1
	98.9

Cations per 2(O)

	TRT-42
U^{4+}	0.83
Pb^{2+}	0.19
Ca^{2+}	0.08
Ta^{5+}	0.03
	1.13

Appendix E

SAMPLING INFORMATION FOR TANCO PEGMATITE OXIDE MINERALS

No.	Zone	Loca-tion	Oxide Minerals	Asso-ciation	Probe	X-Ray	Notes
SMP-1 to -52	6	W	Wd,Mc,Tp,Sp, Tn,Cs	Ab	x	x	
TSE-1	6	W	Wd,Mc,(Sm,Tp)	Ab,Mu	x	c	below Sm parag.
-2	6	W	Wd,Mc	Ab			
-3	6	W	Mc,Tn	Ab		x	
-5	6	W	Mc,Wd,(Tp)	Ab		c	(SQI)
-6	6	W	Wd,Tn	Ab			
-7	6	W	Wd,(Tp,Mc)	Ab	x	c	
-8	6	W	Wd,Mc	Ab			
-9	6	W	Mc,(Tp)	Ab		c	(Zr)
TSE-10	6	W	Mc,(Tn)	Ab		c	
-11	6	W	Wd,Mc	Ab			
-12	6	W	Wd,Mc	Ab			
-13	6	W	Tp,Wd	Ab			(Zr)
-14	6	W	Wd	Ab			
-15	6	W	Wd	Ab			
-16	6	W	Wd,Mc	Ab	x	c	(Zr)
-17	6	W	Wd	Ab	x		
-18	6	W	Mc,(Tn)	Ab			
-19	4	W	Tn	Ab			
TSE-20	6	W		Ab			
-21	6	W	Mc,Ct	Ab			
-22	6	W		Ab			
-23	6	W		Ab			
-24	4	W	Ct,Tn	Ab		x	
-25	6	W	Tp	Ab		c	
-26	6	W	Wd,Tn	Ab	x		
-27	6	W		Ab			
-28	6	W	Wd,Mc,(Tn)	Ab	x	c	(SQI)
-29	6	W	Tp	Ab		c	
TSE-30	6	W	Wd,(Mc)	Ab	x	c	near 6/4
-31	6	W	Wd	Ab		c	
-32	6	W	Wd,Ct,(Mc)	Ab	x	c	
-33	6	W		Ab			
-34	6	W		Lp			
-35	9	W	Mc,(Ct)	Lp	x	c	
-36	6	W	Tn,Wd,(Mc)	Ab	x	c	
-37	6	W	Ct,Wd,(Tn)	Ab	x	c	near 4/6
-38	4	W	Ct,Mc	Ab			
-39	4	W	Ct,Tn	Ab	x	c	
TSE-40	5	W	Wd	Ab	x	c	
-41	4	W	Ct,(Wd)	Kf	x	c	
-42	4	W	Tn	Ab	x	c	
-43	4?	W	Tn	Kf			
-44	4	W	Tn,Ct	Kf		c	(Zr,Am)
-45	8	W	Wd,(Ct,Mc)	Ab	x	c	(Am)
-46	9	C	Ct	Lp	x	c	
-47	9	C	Ct,Tn	Lp			
-48	3	E	Wd,Mc,(Ct)	Ab	x	c	
-49	2	E	Ct,(Tn)	Kf	x	c	

No.	Zone	Loca-tion	Oxide Minerals	Asso-ciation	Probe	X-Ray	Notes
TSE-50	5	C	Wd	Ab		x	
-51	5	C	Tn	Ab		c	(Am)
-52	5	W	Tn,Mc	Ab	x	c	
-53	5	W	Ct	Lp			
-54	2	E	Ct,(Tn)	Kf		c	
-55	3	E	Wd,Mc,Ct,(Ru,Tn)	Ab	x	c	(Be)
-56	5	C	Tn,(Ct)	Ab	x	c	(Am)
-57A	6	W	Wd,Tn	Ab	x		
-57B	4	NW	Wd,Tn	Mu	x		
-58	9	C	Mc	Lp			
-59	6	NW		Ab			
TSE-60	6	NW	Wd	Mu			
-61	4	NW		Kf			
-62	4	NW		Kf			
-63	6	NW	Wd,Ct	Lp	x		
-64	6	NW		Mu			near 6/4
-65	6	NW	Wd	Mu	x	c	near 6/4
-66	6	NW	Wd	Mu	x		near 6/4
-67	6	NW		Mu			
-68	6	NW		Mu			
-69	6	NW	Wd	Mu	x		near 6/4
TSE-70	9	C		Lp			at 9/5
-71	9	C	Ct,Tn,Mc	Lp	x		near 9/6
-72	3	E	Mc,Ct	Ab	x	c	at 7/3, (Be)
-73	3	E	Wd	Ab	x		1 m from 7/3
-74	3	E	Wd,(Mc)	Ab			at 7/3,(Be)
-75	6	W		Ab			
-76	6	W	Wd,Tn	Ab	x	c	
-77	6	W	Wd,Tn	Ab	x	c	near 6/4
-78	3	E	Mc,Wd,(Ru)	Ab	x		
-79	3	E	Wd	Ab	x		1 m from 7/3
TSE-80	3	E	Wd	Ab	x		
-81	3	E		Ab			
-82	3	E	Mc,(Tn,Ru)	Ab	x	x	near base of 3
-83	2	E	Ct,Tn,Ru	Ab	x	x	near 3/2, (Tu)
-84	3	E	Ct,Wd,(Mc)	Ab	x		3 m below 7/3
-85	3	E	Mc,Ct,(Ru,Wd)	Ab	x		
-86	3	E	Wd	Ab	x		
-87	3	E		Ab			
-88	3	E	Mc,Ct,(Wd)	Ab	x		7 m below 7/3
-89	3	E	Wd,Tn,Mc,Ct,Ru	Ab	x		7 m below 7/3
TSE-90	3	E	Ct,Wd	Ab	x	c	(Zr)
-91	6	E	Ct,Wd	Lp	x		at 6/3, (Be)
-92	3	NW	Wd	Ab	x		
-93	3	E		Ab			2 m above 3/2
-94	3	E	Wd,Mc,Tn	Ab	x		near 3/2
-95	3	E	Mc,(Wd,Ru,Ct)	Ab	x	c	near 3/2
-96	3	E	Mc,Wd,Ct,(Ru)	Ab	x		mid-lower 3
-97	3	E	Wd,Mc,(Ru)	Ab	x	c	mid-lower 3, (Be)
-98	2	E	Ct,Tn	Ab	x		near 3/2, (Tn)
-99	3	E	Wd	Ab	x		7 m below 7/3
TSE-100	3	E	Wd,Mc,(Ct)	Mu	x	c	
-101	3	E	Wd,Mc	Ab	x		near 4/3
-102	3	E		Ab			
-103	3	E	Wd	Ab	x		
-104	3	E	Wd,Ct,Mc,Ru	Ab	x	c	
-105	3	E	Mc,Ru,Wd	Ab	x		at 7/3
-106	3	E	Wd,Mc,Ct	Ab	x		
-107	3	E	Wd,(Mc,Ct,Tn)	Ab	x	c	1m below 7/3
-108	3	E	Wd,Mc	Ab	x		at 7/3
-109	3	E	Wd,(Mc)	Ab	x	c	at 7/3
TSE-110	9	C	Wd,Mc	Lp	x		near 9/5
-111	6	C	Ct	Ab			at 9/6
-112	3	E	Mc,Wd,Tn,Ru	Ab	x		near 3/4
-113	3	E	Mc,Wd	Ab	x		1m below 7/3
-114	2	E	Tn,Ct	Ab	x	c	
-115	3	E	Wd,Tn,(Ct)	Ab	x		near 3/2
-116	3	E	Wd,Tn,Ct,Tp,Mc	Ab	x		
-117	3	E	Wd,Tp	Ab	x		near 3/2
-118	3	E		Ab			at 3/2
-119	3	E	Wd	Ab	x		near 3/2

No.	Zone	Location	Oxide Minerals	Association	Probe	X-Ray	Notes
TSE-120	3	E	Mc,Ct,Wd	Ab	x		
-121	3	E	Wd	Ab	x		
-122	3	E	Wd	Ab	x	c	at 4/3, (Ap,Be)
-123	5	C	Tn	Ab	x	c	
-124	6	W		Ab			
-125	6	W	Wd,(Tp?)	Ab			
-126	3	E	Wd,Mc,Ru	Ab	x	c	
-127	9	NW		Lp			
-128	4	NW		Ab			
-129	3	E	Wd,Mc	Ab	x		5 m above 3/2
TSE-130	3	E	Wd,Mc,Ct,Tn,Ru	Ab	x	c	
-131	3	E	Wd,Mc,Tn,(Ct)	Ab	x		at 7/3
-132	3	E	Wd,Mc,(Ct,Ru)	Ab	x	c	
-133	3	E	Wd	Ab	x		
-134	3	E	Wd,Mc,Ct	Ab	x	c	at 3/4, (Su)
-135	3	E	Wd	Ab	x		
-136	3	E	Wd,Mc,Ct	Ab	x	c	
-137	3	E	Wd,Ct,Tn,(Mc)	Ab	x	c	
-138	6	NW	Wd,Mc	Ab	x	c	
-139	6	NW	Wd,Tp,(Mc)	Ab	x		near 6/4
TSE-140	6	NW		Ab			
-141	6	NW	Wd	Mu	x		
-142	6	NW		Mu		x	at 7/6
-143	6	NW	Wd	Ab	x		
-144	9	C		Lp			
-145	6	C		Mu			
-146	5	C	Tn	Ab		c	near 5/4, (Am)
-147	5	C	Tn	Kf		c	(SQI)
-148	5	C	Tn	Kf		x	(SQI)
-149	5	C	Tn,Wd	Kf		x	
TSE -150	5	C	Tn	Kf		x	
-151	5	C	Tn,Wd	Kf		x	
-152	5	C	Tn	Kf			
-153	5	C	Tn	Kf		x	
-154	5	C	Tn,Ct	Kf		c	(Rh)
-155	5	C	Tn	Kf		c	
-156	5	C	Tn	Kf		c	
-157	5	C	Tn,Mc	Kf		c	
-158	5	C	Tn	Kf		x	
G69-1	6	NW	Wd,(Mc)	Mu	x		(Be)
-2	6	NW	Wd	Mu	x	c	
-7	6	NW	Wd,Tn	Ab	x		
-8	6	NW	Tn,Wd,Ct,Mc	Lp	x		
G69-10	6	NW	Wd,Tn,Ct	Mu	x		(SQI)
-11	6	NW	Wd,(Mc)	Mu	x		near 4/6
-13	6	NW	Wd,(Tn)	Mu	x	c	
-14	6	NW	Wd,Ct	Mu	x	c	
-17	6	NW	Wd,(Mc)	Mu	x	c	
G69-20	6	NW	Wd	Mu	x	c	
-22	6	NW	Wd	Mu	x		
-23	6	NW	Wd	Mu	x	c	
-28	5	NW	Wd	Mu	x		
-29	5	NW	Wd,(Tn,Mc,Cs)	Ab	x		
G69-30	4	NW	Tn,(Mc)	Kf	x	c	(Ap)
-31	4	NW	Tn,(Mc)	Kf	x	c	
-32	5	NW	Ct,Wd,Tn	Ab	x		
-35	6	NW	Ct,Wd	Mu	x		
-36	6	NW	Wd,Tn,(Mc)	Mu	x		
-39	6	NW	Wd,Mc	Mu	x	c	near 4/6
G69-42	6	NW	Wd	Mu	x	c	(Be)
-43	6	NW	Wd,Mc	Ab	x		
-46	6	NW	Wd	Mu	x	c	
G69-52	6	NW	Wd,Tn,Tp,(Mc)	Mu	x		
-53	4	NW	Tn	Ab	x	c	
-55	4	NW	Tn	Kf	x	c	
-56	4	NW	Tn	Kf	x	c	
-58	4	NW	Tn	Kf	x	c	
-59	4?	NW	Tn,Ct	Kf	x		
G69-60	4	NW	Tn	Kf	x	c	
-61	4	NW	Tn	Kf	x	c	

No.	Zone	Loca-tion	Oxide Minerals	Asso-ciation	Probe	X-Ray	Notes
TRT-series	5-4	C?	Tn,Ct,Mc,(Ru,Ur)	Kf	x	c	
A-25	3	E	Wd,Mc,Tn	Ab	x	c	(Be)

ABBREVIATIONS

Zones: W=west, C=central, NW=northwest, E=east.

Minerals: Cs=cesstibtantite, Ct=cassiterite, Mc=microlite subgroup, Ru=rutile, Sm=simpsonite, Tn=columbite group, Tp=ferrotapiolite, Wd=wodginite-group, Ur=uraninite.

Associations: Ab=saccharoidal albite plus quartz ± muscovite, tourmaline, beryl, apatite.
Mu=K-feldspar partially hydrolized to muscovite ± quartz, albite.
Lp=K-feldspar partially hydrolized to lepidolite-lithian muscovite ± quartz,albite.
Kf=Coarse-grained quartz, k-feldspar with lesser amounts of saccharoidal albite or cleavelandite ± muscovite, beryl, apatite, amblygonite and SQI (zones 4 & 5).

Probe: denotes whether or not sample was studied by electron microprobe.

X-ray: denotes whether or not sample was studied by XRD methods (x) and whether or not unit-cell dimensions were obtained (c).

Notes: 1. Abbreviations in parentheses are notable accessory minerals - Am=amblygonite, Ap=apatite, Be=beryl, Qz=quartz, Rh=rhodochrosite, SQI=spodumene-quartz pseudomorphs after petalite, Su= undesignated sulphide minerals, Tu=tourmaline, Zr=zircon.
2. Numbers separated by slashes represent zone contacts.

Appendix F

BOND VALENCES

F.1 INTRODUCTION

Pauling (1929) introduced the idea of empirical bond strength with his electrostatic valence rule:

> In a stable coordination structure the electric charge of each anion tends to compensate the strength of the electrostatic valence bonds reaching to it from the cations at the centres of the polyhedra of which it forms a corner.

For a cation of valence Z surrounded by n coordinating anions, the Pauling strength (s) of a single cation-anion bond is given by:

$$s = Z/n \tag{1}$$

Pauling did not consider bond length – bond strength interdependency in his model, and it was not until Evans (1960) and Zachariasen (1963) that models relating bond length and bond strength came into being. In the last 15 years, several formulations have been proposed: Donnay & Allmann (1970), Pyatenko (1972), Brown & Shannon (1973), Ferguson (1974), Zachariasen (1978). Of these, the most widely used expression is that of Brown & Shannon (1973) where:

$$s = (R/R_0)^{-N} \tag{2}$$

$\underline{s}$ is the bond strength (formally referred to as the "bond valence") and $\underline{R}$, the bond length. $\underline{R}_0$ (the length of a bond of unit strength) and $\underline{N}$ are constants which are derived by fitting data from well-refined structures to the above relationship. Tables (e.g. Brown, 1981) now exist with values of $\underline{R}_0$ and $\underline{N}$ for almost any cation of any valence coordinated by any common anion (O, F, Cl, I, S, N, C).

TANTALUM-OXYGEN AND NIOBIUM-OXYGEN BONDS

Because of the lack of precise structural data available for tantalum oxides up to the mid-1970's, constants for equation (2) for Ta-O bonds are not available. Considerably more precise structural data is available today, largely due to growing interest in the chemistry of Ta in the late 1970's. Consequently, I decided to derive constants for equation (2) for both tantalum-oxygen and niobium-oxygen bonds.

The approach taken was that of Brown & Shannon (1973). Precise structural data ($\sigma\underline{R}\leq.02$ Å) for 13 tantalum oxide compounds and 13 niobium oxide compounds involving 19, and 25 independent coordination polyhedra respectively were used for the calculations. Of these, 16 Ta polyhedra were 6-coordinate and 3 were 7-coordinate; 24 Nb polyhedra were 6-coordinate and 1 was 5-coordinate. A wide variety of compositions was sampled, and care was taken to not over-represent any particular structure type.

In order to minimize correlation between $\underline{R}_0$ and $\underline{N}$, equation (2) was recast as:

$$s=s_0(R/R_0)^{-N} \tag{3}$$

where s_0 is the Pauling bond strength for a cation in its most frequent coordination ($s_0=5/6$ for Ta, Nb oxides).

The quantity,

$$\Delta^2 = \overset{m}{\Sigma} w_j \, (Z_j - p_j)^2 \tag{4}$$

was minimized, where Z and n are as defined above, m is the number of polyhedra used in the calculation, p is the bond valence sum to the central cation of a polyhedron (i.e. $p=\Sigma s$) and w is a weight calculated from the estimated standard deviation of the observed bond valence sums. Specifically, $w=\sigma(p)^{-2}$, where $\sigma(p)$ is the standard deviation in the bond valence sum to the cation and is estimated by:

$$\sigma(p)^2 = \Sigma(\delta s_i / \delta R_i)^2 \sigma(R_i)^2 \tag{5}$$

All calculations were done with a computer program written by the author using the SAS routine NLIN. Starting values for R_0 and N were published constants for Nb-O bonds (Brown, 1981). Refinement converged on the following values:

Ta-O bonds: $R_0=1.983(1)$, $N=6.4(3)$

Nb-O bonds: $R_0=1.988(3)$, $N=4.4(4)$

(constants for equation (3)). This translated to the following set of constants for the simpler equation (2):

Ta-O bonds: $R_0=1.927$, $N=6.4$

Nb-O bonds: $R_0=1.907$, $N=4.4$

The result for Nb-O bonds is in excellent agreement with the result of Brown (1981), where $R_0 = 1.907$, $N = 5$.

Bond valence sums for the cations used in the calculations are given in Table 114 (Ta oxides) and Table 115 (Nb oxides). Only one polyhedron (the Ta(3) polyhedron of $Cu_5Ta_{11}O_{30}$) had to be removed from the refinement because of a grossly deviant bond valence sum ($\underline{z} - \underline{p} > .3$), indicative of either problems with the refinement of its structure, or of factors affecting its bond lengths which cannot be accounted for with such a bond valence model (e.g. McGuire & O'Keefe, 1984).

Bond valence - bond length curves for Ta-O and Nb-O bonds are given in Figure 90. The two curves cross near 5/6 v.u., the Pauling bond strength for octahedrally coordinated Ta and Nb (at 5/6 v.u. $\underline{R}$(Ta-O)=1.983 Å and $\underline{R}$(Nb-O)=1.988 Å). This indicates that in undistorted octahedra, Ta and Nb have about the same effective ionic radius ($\underline{r}$), as confirmed by the investigations of Shannon (1976): he gives $\underline{r}$(Nb)=$\underline{r}$(Ta)=0.64 Å.

The different slopes and degrees of curvature of the bond valence curves reflect differences in the covalency of Ta-O versus Nb-O bonds: short Ta-O bonds (< 1.98 Å) are less covalent than short Nb-O bonds, whereas long Ta-O bonds are somewhat more covalent than long Nb-O bonds. It can also be seen from Figure 90 that niobium can form shorter bonds than tantalum (compare the curves at $\underline{s}$=1.3 v.u., for example).

Table 114: Calibration Dataset for Ta-O Bond Valence Curve

Compound	Number of Polyhedra	Reference
$FeTa_2O_6$	1	AC 130
$MnTa_2O_6$	1	ZK 144
$CuTa_2O_6$	1	JSSC 24
$H_2Ta_2O_6$	1	JSSC 41
$M-LiTa_3O_8$	2	AC B33
$CeTaO_4$	1	JSSC 35
$NdTaO_4$	1	JSSC 35
$LaTaO_4$	1	JSSC 36
$Sr_2Ta_2O_7$	2	AC B32
$CaTa_4O_{11}$	2	AC B31
$Ba_3SrTa_2O_9$	1	AC C39
$Cu_5Ta_{11}O_{30}$	2	JSSC 41
KTa_5O_{13}	3	JSSC 24

AC: Acta Crystallographica, AMIN: American Mine-
ralogist, CSC: Crystal Structure Communications,
JSSC: Journal of Solid State Chemistry, MRB:
Materials Research Bulletin, ZAAC: Zeitschrift
fur Anorganische allgemeine Chemie, ZF: Zeits-
chrift fur Kristallographie.

Table 115: Calibration Dataset for Nb-O Bond Valence Curve

Compound	Number of Polyhedra	Reference
$CaNb_2O_6$	1	AMIN 55
$NiNb_2O_6$	1	ZAAC 503
$CoNb_2O_6$	1	ZC 144
$FeNb_2O_6$	1	ZC 144
$MnNb_2O_6$	1	ZC 144
$NaNbO_3$	1	AC B25
$CeNbO_4$	1	JSSC 35
$InNbO_4$	1	MRB 15
$LiNb_3O_8$	3	CSC 1
$Ca_2Nb_2O_7$	4	ACB 36
$Te_3Nb_2O_{11}$	1	JSSC 27
$Cs_2Nb_4O_{11}$	7	ACB 37
$Pr_3NbO_4Cl_6$	1	MRB 18
$Ba_4Nb_3LiO_{12}$	1	JSSC 9
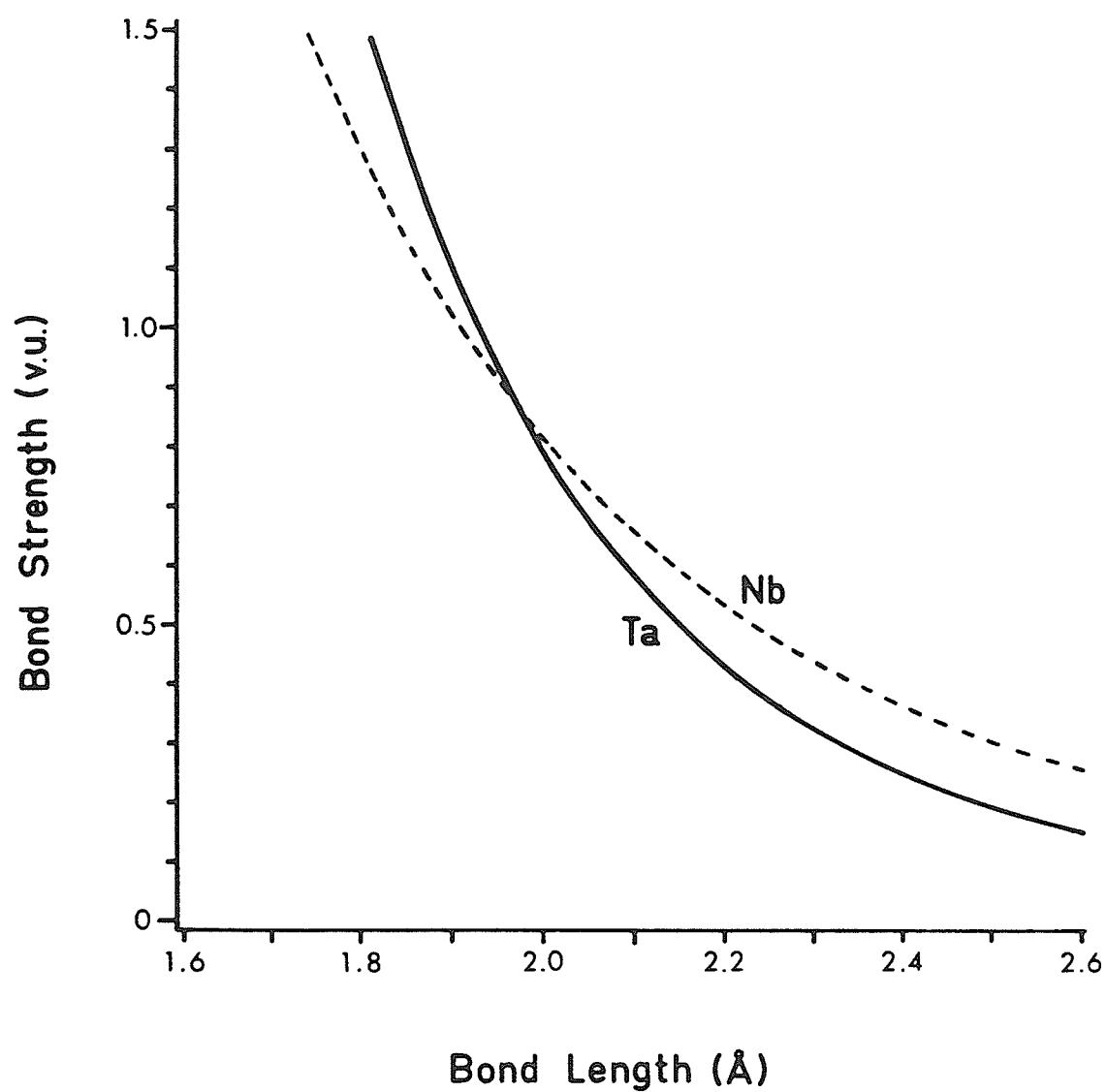
<u>Figure 91</u>: Bond valence – bond length curves for Ta–O (solid rule) and
Nb–O (broken rule) bonds.

Appendix G

STRUCTURE FACTOR TABLES

OBSERVED AND CALCULATED STRUCTURE FACTORS FOR SIMPSONITE -- LS 03 (FINAL)

H	K	L	FO	FC	H	K	L	FO	FC	H	K	L	FO	FC	H	K	L	FO	FC	H	K	L	FO	FC
0	0	-6	72	72	-4	4	-5	56	56	-1	3	-4	88	97	-2	6	-4	56	58	-7	4	-3	25	27
-1	1	-6	22	21	-3	4	-5	78	76	0	3	-4	35	34	-1	6	-4	33	34	-6	4	-3	55	59
0	1	-6	22	21	-2	4	-5	7	5	1	3	-4	77	77	0	6	-4	76	75	-5	4	-3	79	80
1	1	-6	46	44	-1	4	-5	23	22	2	3	-4	28	27	1	6	-4	22	22	-4	4	-3	68	70
-3	2	-6	68	67	0	4	-5	54	51	3	3	-4	29	29	-7	7	-4	31	30	-3	4	-3	106	103
-2	2	-6	40	38	1	4	-5	37	38	-7	4	-4	23	23	-6	7	-4	16	16	-2	4	-3	9	8
-1	2	-6	36	36	2	4	-5	33	31	-6	4	-4	50	53	-5	7	-4	50	50	-1	4	-3	34	36
0	2	-6	33	32	-6	5	-5	20	20	-5	4	-4	55	58	-4	7	-4	65	65	0	4	-3	71	69
1	2	-6	26	23	-5	5	-5	20	17	-4	4	-4	48	47	-3	7	-4	27	25	1	4	-3	57	60
-3	3	-6	24	22	-4	5	-5	36	38	-3	4	-4	77	79	-2	7	-4	49	48	2	4	-3	52	52
-2	3	-6	20	20	-3	5	-5	34	31	-2	4	-4	6	5	-1	7	-4	26	27	3	4	-3	85	83
-1	3	-6	72	72	-2	5	-5	67	68	-1	4	-4	38	31	0	7	-4	28	26	4	4	-3	9	9
0	3	-6	22	24	-1	5	-5	50	50	0	4	-4	51	53	-5	8	-4	26	27	-9	5	-3	19	20
0	0	-5	67	71	0	5	-5	21	23	1	4	-4	85	87	-4	8	-4	5	5	-8	5	-3	74	73
-1	1	-5	42	40	1	5	-5	18	19	2	4	-4	51	52	-3	8	-4	58	57	-7	5	-3	50	52
0	1	-5	39	38	-5	6	-5	15	15	3	4	-4	58	58	0	0	-3	108	120	-6	5	-3	28	30
1	1	-5	61	60	-4	6	-5	34	36	4	4	-4	11	8	-1	1	-3	46	47	-5	5	-3	28	29
-3	2	-5	69	73	-3	6	-5	23	21	-8	5	-4	60	60	0	1	-3	47	47	-4	5	-3	54	60
-2	2	-5	51	50	-2	6	-5	41	41	-7	5	-4	45	45	1	1	-3	107	99	-3	5	-3	36	35
-1	2	-5	61	61	-1	6	-5	22	23	-6	5	-4	31	31	-3	2	-3	59	63	-2	5	-3	107	107
0	2	-5	52	51	0	0	-4	140	155	-5	5	-4	29	30	-2	2	-3	93	88	-1	5	-3	76	77
1	2	-5	29	29	-1	1	-4	29	30	-4	5	-4	80	88	-1	2	-3	105	103	0	5	-3	28	28
2	2	-5	6	1	0	1	-4	31	31	-3	5	-4	26	30	0	2	-3	91	89	1	5	-3	30	29
-5	3	-5	69	66	1	1	-4	60	61	-2	5	-4	68	68	1	2	-3	56	58	2	5	-3	70	66
-4	3	-5	25	26	-3	2	-4	96	104	-1	5	-4	48	48	2	2	-3	16	11	3	5	-3	9	15
-3	3	-5	28	27	-2	2	-4	48	49	0	5	-4	31	30	-5	3	-3	109	107	4	5	-3	58	55
-2	3	-5	31	31	-1	2	-4	72	71	1	5	-4	27	27	-4	3	-3	34	32	-9	6	-3	20	20
-1	3	-5	51	54	0	2	-4	58	59	2	5	-4	45	47	-3	3	-3	44	47	-8	6	-3	46	44
0	3	-5	27	25	1	2	-4	27	25	3	5	-4	32	29	-2	3	-3	54	52	-7	6	-3	37	40
1	3	-5	81	78	2	2	-4	6	6	-7	6	-4	23	20	-1	3	-3	98	114	-6	6	-3	95	94
2	3	-5	31	33	-5	3	-4	76	78	-6	6	-4	69	69	0	3	-3	44	43	-5	6	-3	31	29
3	3	-5	24	24	-4	3	-4	32	34	-5	6	-4	27	27	1	3	-3	105	102	-4	6	-3	49	51
-6	4	-5	27	28	-3	3	-4	31	30	-4	6	-4	51	51	2	3	-3	37	38	-3	6	-3	35	33
-5	4	-5	50	48	-2	3	-4	34	36	-3	6	-4	30	32	3	3	-3	35	38	-2	6	-3	28	29

OBSERVED AND CALCULATED STRUCTURE FACTORS FOR SIMPSONITE -- LS 03 (FINAL)

H	K	L	FO	FC	H	K	L	FO	FC	H	K	L	FO	FC	H	K	L	FO	FC	H	K	L	FO	FC
-1	6	-3	26	24	1	2	-2	48	48	2	5	-2	66	66	-3	8	-2	71	72	-5	4	-1	92	91
0	6	-3	101	99	2	2	-2	5	4	3	5	-2	52	49	-2	8	-2	44	43	-4	4	-1	101	101
1	6	-3	35	35	-5	3	-2	100	100	4	5	-2	72	71	-1	8	-2	59	56	-3	4	-1	166	145
2	6	-3	34	36	-4	3	-2	42	45	-9	6	-2	21	24	0	8	-2	45	44	-2	4	-1	13	14
3	6	-3	22	22	-3	3	-2	49	50	-8	6	-2	42	44	1	8	-2	22	22	-1	4	-1	44	46
-8	7	-3	42	42	-2	3	-2	40	44	-7	6	-2	33	32	-8	9	-2	21	21	0	4	-1	108	97
-7	7	-3	7	13	-1	3	-2	168	188	-6	6	-2	97	99	-7	9	-2	60	62	1	4	-1	65	69
-6	7	-3	37	35	0	3	-2	47	50	-5	6	-2	30	32	-6	9	-2	28	27	2	4	-1	61	60
-5	7	-3	69	70	1	3	-2	109	105	-4	6	-2	64	65	-5	9	-2	73	73	3	4	-1	102	103
-4	7	-3	87	86	2	3	-2	36	35	-3	6	-2	39	41	-4	9	-2	27	29	4	4	-1	9	7
-3	7	-3	21	23	3	3	-2	39	36	-2	6	-2	86	94	-3	9	-2	26	23	-9	5	-1	20	23
-2	7	-3	48	50	-7	4	-2	37	38	-1	6	-2	42	44	-2	9	-2	33	31	-8	5	-1	91	93
-1	7	-3	40	37	-6	4	-2	90	97	0	6	-2	94	93	-1	9	-2	67	63	-7	5	-1	58	61
0	7	-3	30	29	-5	4	-2	66	69	1	6	-2	24	23	0	0	-1	134	152	-6	5	-1	31	34
1	7	-3	45	45	-4	4	-2	67	68	2	6	-2	51	49	-1	1	-1	96	84	-5	5	-1	35	34
-7	8	-3	40	42	-3	4	-2	111	105	3	6	-2	26	25	0	1	-1	97	84	-4	5	-1	63	69
-6	8	-3	36	36	-2	4	-2	13	10	-9	7	-2	31	31	1	1	-1	159	135	-3	5	-1	60	56
-5	8	-3	30	29	-1	4	-2	46	45	-8	7	-2	52	54	-3	2	-1	146	174	-2	5	-1	142	134
-4	8	-3	11	6	0	4	-2	68	70	-7	7	-2	50	49	-2	2	-1	122	112	-1	5	-1	98	98
-3	8	-3	74	74	1	4	-2	71	76	-6	7	-2	27	30	-1	2	-1	161	132	0	5	-1	34	35
-2	8	-3	46	46	2	4	-2	66	65	-5	7	-2	59	53	0	2	-1	128	109	1	5	-1	31	31
-1	8	-3	46	46	3	4	-2	85	86	-4	7	-2	81	80	1	2	-1	69	66	2	5	-1	86	83
-6	9	-3	23	24	4	4	-2	12	10	-3	7	-2	33	35	2	2	-1	8	6	3	5	-1	48	38
-5	9	-3	58	58	-9	5	-2	27	25	-2	7	-2	62	64	-5	3	-1	132	127	4	5	-1	69	70
-4	9	-3	19	19	-8	5	-2	69	74	-1	7	-2	30	33	-4	3	-1	42	43	5	5	-1	51	58
-3	9	-3	20	19	-7	5	-2	63	66	0	7	-2	54	52	-3	3	-1	56	56	-10	6	-1	48	41
0	0	-2	121	138	-6	5	-2	45	45	1	7	-2	64	63	-2	3	-1	71	65	-9	6	-1	20	25
-1	1	-2	50	50	-5	5	-2	37	39	2	7	-2	62	61	-1	3	-1	70	65	-8	6	-1	57	60
0	1	-2	47	46	-4	5	-2	68	77	-9	8	-2	59	61	0	3	-1	59	53	-7	6	-1	42	45
1	1	-2	111	103	-3	5	-2	36	37	-8	8	-2	41	43	1	3	-1	161	146	-6	6	-1	121	118
-3	2	-2	158	180	-2	5	-2	108	105	-7	8	-2	58	60	2	3	-1	57	57	-5	6	-1	35	33
-2	2	-2	90	87	-1	5	-2	75	76	-6	8	-2	50	52	3	3	-1	40	44	-4	6	-1	59	60
-1	2	-2	91	85	0	5	-2	37	36	-5	8	-2	52	53	-7	4	-1	28	30	-3	6	-1	44	42
0	2	-2	78	73	1	5	-2	32	33	-4	8	-2	14	14	-6	4	-1	29	34	-2	6	-1	70	79

OBSERVED AND CALCULATED STRUCTURE FACTORS FOR SIMPSONITE -- LS #3 (FINAL)

H	K	L	FO	FC	H	K	L	FO	FC	H	K	L	FO	FC	H	K	L	FO	FC	H	K	L	FO	FC
-1	6	-1	35	35	-5	9	-1	67	67	-1	4	0	51	50	3	6	0	28	28	-2	9	0	42	38
0	6	-1	118	114	-4	9	-1	22	21	0	4	0	83	81	4	6	0	41	42	-1	9	0	70	64
1	6	-1	41	40	-3	9	-1	23	20	1	4	0	142	156	-10	7	0	62	65	0	9	0	20	19
2	6	-1	46	48	-2	9	-1	22	21	2	4	0	77	79	-9	7	0	36	38	-7	10	0	16	13
3	6	-1	30	30	-1	9	-1	80	75	3	4	0	86	88	-8	7	0	55	58	-6	10	0	42	40
4	6	-1	50	49	-7	10	-1	23	25	4	4	0	13	11	-7	7	0	38	39	-5	10	0	49	47
-10	7	-1	56	59	-6	10	-1	53	53	-9	5	0	32	31	-6	7	0	25	27	-4	10	0	49	47
-9	7	-1	20	21	-5	10	-1	57	54	-8	5	0	80	84	-5	7	0	68	67	-3	10	0	71	64
-8	7	-1	51	55	-4	10	-1	42	41	-7	5	0	69	71	-4	7	0	91	89	0	0	1	156	151
-7	7	-1	39	37	-3	10	-1	61	56	-6	5	0	46	48	-3	7	0	37	36	-1	1	1	95	84
-6	7	-1	40	40	-1	1	0	60	53	-5	5	0	47	50	-2	7	0	74	72	0	1	1	98	85
-5	7	-1	81	81	0	1	0	62	52	-4	5	0	147	156	-1	7	0	35	35	1	1	1	159	132
-4	7	-1	100	98	1	1	0	140	112	-3	5	0	45	47	0	7	0	39	40	-3	2	1	77	66
-3	7	-1	33	36	-3	2	0	140	155	-2	5	0	119	111	1	7	0	67	65	-2	2	1	128	108
-2	7	-1	65	65	-2	2	0	104	92	-1	5	0	83	79	2	7	0	72	73	-1	2	1	176	136
-1	7	-1	45	42	-1	2	0	136	111	0	5	0	50	48	3	7	0	13	15	0	2	1	129	112
0	7	-1	20	9	0	2	0	106	91	1	5	0	41	39	-9	8	0	62	66	1	2	1	73	67
1	7	-1	52	51	1	2	0	58	52	2	5	0	65	69	-8	8	0	44	44	2	2	1	18	13
2	7	-1	77	76	2	2	0	6	3	3	5	0	39	40	-7	8	0	65	66	-5	3	1	151	132
3	7	-1	26	24	-5	3	0	119	114	4	5	0	74	76	-6	8	0	53	54	-4	3	1	48	44
-9	8	-1	67	70	-4	3	0	50	51	5	5	0	45	48	-5	8	0	39	40	-3	3	1	55	56
-8	8	-1	43	45	-3	3	0	59	55	-10	6	0	45	46	-4	8	0	13	12	-2	3	1	66	65
-7	8	-1	53	55	-2	3	0	57	54	-9	6	0	50	45	-3	8	0	90	84	-1	3	1	153	174
-6	8	-1	41	42	-1	3	0	130	155	-8	6	0	48	53	-2	8	0	55	51	0	3	1	59	54
-5	8	-1	17	11	0	3	0	59	57	-7	6	0	34	32	-1	8	0	61	57	1	3	1	157	145
-4	8	-1	12	6	1	3	0	138	129	-6	6	0	101	104	0	8	0	45	45	2	3	1	60	58
-3	8	-1	96	95	2	3	0	47	44	-5	6	0	39	40	1	8	0	25	26	3	3	1	43	44
-2	8	-1	63	60	3	3	0	43	41	-4	6	0	81	77	-9	9	0	18	19	-7	4	1	34	35
-1	8	-1	51	50	-7	4	0	35	36	-3	6	0	41	43	-8	9	0	25	25	-6	4	1	75	79
0	8	-1	44	43	-6	4	0	73	81	-2	6	0	76	81	-7	9	0	71	71	-5	4	1	99	98
1	8	-1	39	35	-5	4	0	79	80	-1	6	0	47	49	-6	9	0	28	28	-4	4	1	104	99
-8	9	-1	36	37	-4	4	0	83	79	0	6	0	107	103	-5	9	0	76	76	-3	4	1	168	146
-7	9	-1	76	76	-3	4	0	147	128	1	6	0	28	26	-4	9	0	34	32	-2	4	1	8	6
-6	9	-1	26	26	-2	4	0	7	3	2	6	0	54	53	-3	9	0	52	48	-1	4	1	43	43

OBSERVED AND CALCULATED STRUCTURE FACTORS FOR SIMPSONITE -- LS 83 (FINAL)

H	K	L	FO	FC	H	K	L	FO	FC	H	K	L	FO	FC	H	K	L	FO	FC	H	K	L	FO	FC
0	4	1	104	99	-10	7	1	54	57	-6	10	1	51	49	4	4	2	15	13	-3	7	2	36	37
1	4	1	65	69	-9	7	1	21	21	-5	10	1	55	51	-9	5	2	28	27	-2	7	2	65	65
2	4	1	62	59	-8	7	1	48	49	-4	10	1	44	42	-8	5	2	72	74	-1	7	2	30	33
3	4	1	98	97	-7	7	1	9	14	-3	10	1	63	59	-7	5	2	64	64	0	7	2	48	50
4	4	1	10	7	-6	7	1	41	39	0	0	2	129	139	-6	5	2	44	44	1	7	2	60	60
-9	5	1	20	23	-5	7	1	87	85	-1	1	2	46	47	-5	5	2	35	37	2	7	2	59	60
-8	5	1	94	94	-4	7	1	188	182	0	1	2	49	49	-4	5	2	64	77	-9	8	2	60	63
-7	5	1	63	65	-3	7	1	30	30	1	1	2	92	86	-3	5	2	36	37	-8	8	2	42	44
-6	5	1	33	35	-2	7	1	62	61	-3	2	2	168	188	-2	5	2	101	99	-7	8	2	64	62
-5	5	1	34	33	-1	7	1	47	44	-2	2	2	77	74	-1	5	2	70	67	-6	8	2	51	50
-4	5	1	67	68	0	7	1	37	37	-1	2	2	106	102	0	5	2	38	38	-5	8	2	52	50
-3	5	1	58	55	1	7	1	54	55	0	2	2	91	87	1	5	2	33	33	-4	8	2	12	11
-2	5	1	131	128	2	7	1	75	76	1	2	2	44	41	2	5	2	59	60	-3	8	2	73	71
-1	5	1	93	93	3	7	1	24	23	2	2	2	10	10	3	5	2	52	52	-2	8	2	44	44
0	5	1	34	37	-9	8	1	73	73	-5	3	2	106	106	4	5	2	71	73	-1	8	2	53	54
1	5	1	31	33	-8	8	1	42	43	-4	3	2	44	48	-9	6	2	24	24	0	8	2	41	42
2	5	1	81	80	-7	8	1	50	51	-3	3	2	50	46	-8	6	2	42	43	1	8	2	21	22
4	5	1	65	66	-6	8	1	47	46	-2	3	2	48	49	-7	6	2	33	30	-8	9	2	21	20
5	5	1	54	55	-5	8	1	39	38	-1	3	2	171	180	-6	6	2	91	93	-7	9	2	62	62
-10	6	1	39	42	-4	8	1	9	6	0	3	2	58	51	-5	6	2	33	33	-6	9	2	27	26
-9	6	1	19	23	-3	8	1	100	94	1	3	2	109	103	-4	6	2	63	65	-5	9	2	74	71
-8	6	1	58	59	-2	8	1	64	60	2	3	2	37	36	-3	6	2	34	40	-4	9	2	27	27
-7	6	1	40	44	-1	8	1	56	55	3	3	2	41	39	-2	6	2	86	98	-3	9	2	25	23
-6	6	1	116	114	0	8	1	45	43	-7	4	2	34	35	-1	6	2	44	47	-2	9	2	32	31
-5	6	1	30	31	1	8	1	37	36	-6	4	2	89	93	0	6	2	94	99	-1	9	2	64	61
-4	6	1	60	62	-8	9	1	37	36	-5	4	2	75	77	1	6	2	28	28	0	0	3	114	119
-3	6	1	45	41	-7	9	1	77	76	-4	4	2	71	67	2	6	2	51	50	-1	1	3	47	47
-2	6	1	35	31	-6	9	1	31	30	-3	4	2	117	107	3	6	2	28	27	0	1	3	46	46
-1	6	1	33	32	-5	9	1	72	69	-2	4	2	6	3	-9	7	2	30	31	1	1	3	109	102
0	6	1	117	120	-4	9	1	24	21	-1	4	2	48	44	-8	7	2	54	56	-3	2	3	105	113
1	6	1	40	40	-3	9	1	25	22	0	4	2	67	70	-7	7	2	52	51	-2	2	3	90	89
2	6	1	42	43	-2	9	1	21	21	1	4	2	69	77	-6	7	2	23	24	-1	2	3	99	100
3	6	1	26	26	-1	9	1	73	69	2	4	2	65	66	-5	7	2	68	65	0	2	3	91	90
4	6	1	53	52	-7	10	1	24	25	3	4	2	81	81	-4	7	2	85	86	1	2	3	54	54

OBSERVED AND CALCULATED STRUCTURE FACTORS FOR SIMPSONITE -- LS 03 (FINAL)

H	K	L	FO	FC	H	K	L	FO	FC	H	K	L	FO	FC	H	K	L	FO	FC	H	K	L	FO	FC
2	2	3	15	8	3	5	3	38	29	-4	9	3	21	19	-7	5	4	48	49	1	1	5	63	61
-5	3	3	109	107	4	5	3	57	58	-3	9	3	22	18	-6	5	4	36	33	-3	2	5	56	54
-4	3	3	37	34	-9	6	3	19	21	0	0	4	141	155	-5	5	4	30	31	-2	2	5	54	51
-3	3	3	43	45	-8	6	3	46	45	-1	1	4	30	32	-4	5	4	81	87	-1	2	5	60	61
-2	3	3	56	56	-7	6	3	37	40	0	1	4	30	29	-3	5	4	26	29	0	2	5	51	49
-1	3	3	60	63	-6	6	3	99	98	1	1	4	71	72	-2	5	4	75	76	1	2	5	31	31
0	3	3	45	44	-5	6	3	28	30	-3	2	4	91	97	-1	5	4	57	58	2	2	5	9	5
1	3	3	107	104	-4	6	3	53	51	-2	2	4	59	59	0	5	4	30	29	-5	3	5	72	66
2	3	3	36	35	-3	6	3	38	36	-1	2	4	62	59	1	5	4	27	26	-4	3	5	24	22
3	3	3	32	36	-2	6	3	57	58	0	2	4	49	47	2	5	4	47	51	-3	3	5	27	27
-7	4	3	22	22	-1	6	3	31	28	1	2	4	35	35	3	5	4	27	27	-2	3	5	30	28
-6	4	3	29	31	0	6	3	88	94	2	2	4	7	5	-7	6	4	27	26	-1	3	5	72	72
-5	4	3	77	76	1	6	3	35	36	-5	3	4	71	69	-6	6	4	76	76	0	3	5	28	27
-4	4	3	70	71	2	6	3	34	37	-4	3	4	32	31	-5	6	4	25	27	1	3	5	78	76
-3	4	3	101	102	3	6	3	24	24	-3	3	4	34	35	-4	6	4	51	51	2	3	5	33	33
-2	4	3	11	11	-8	7	3	45	46	-2	3	4	26	27	-3	6	4	28	30	3	3	5	23	23
-1	4	3	33	36	-7	7	3	31	28	-1	3	4	96	104	-2	6	4	51	53	-6	4	5	44	40
0	4	3	71	69	-6	7	3	34	35	0	3	4	29	33	-1	6	4	31	31	-5	4	5	52	50
1	4	3	56	60	-5	7	3	64	67	1	3	4	79	80	0	6	4	68	68	-4	4	5	55	53
2	4	3	49	51	-4	7	3	82	84	2	3	4	29	28	1	6	4	17	16	-3	4	5	81	79
3	4	3	82	86	-3	7	3	25	27	3	3	4	30	29	-7	7	4	26	27	-1	4	5	24	25
4	4	3	9	7	-2	7	3	50	52	-7	4	4	25	26	-6	7	4	20	22	0	4	5	56	55
-9	5	3	19	20	-1	7	3	40	38	-6	4	4	57	58	-5	7	4	46	44	1	4	5	37	38
-8	5	3	73	73	0	7	3	16	18	-5	4	4	50	49	-4	7	4	59	58	2	4	5	35	34
-7	5	3	48	49	1	7	3	41	41	-4	4	4	53	52	-3	7	4	23	24	-6	5	5	24	22
-6	5	3	24	27	-7	8	3	46	45	-3	4	4	76	77	-2	7	4	45	46	-5	5	5	24	21
-5	5	3	28	28	-6	8	3	37	34	-2	4	4	15	5	-1	7	4	19	22	-4	5	5	37	37
-4	5	3	55	60	-5	8	3	16	10	-1	4	4	34	32	0	7	4	28	30	-3	5	5	32	31
-3	5	3	38	37	-4	8	3	11	8	0	4	4	47	49	-5	8	4	31	30	-2	5	5	66	66
-2	5	3	111	109	-3	8	3	72	74	1	4	4	82	87	-4	8	4	13	9	-1	5	5	49	49
-1	5	3	82	80	-2	8	3	44	45	2	4	4	49	52	-3	8	4	61	60	0	5	5	18	19
0	5	3	28	29	-1	8	3	40	43	3	4	4	63	64	0	0	5	69	70	1	5	5	14	15
1	5	3	29	29	-6	9	3	23	22	4	4	4	11	5	-1	1	5	39	38	-5	6	5	19	18
2	5	3	67	69	-5	9	3	57	56	-8	5	4	56	57	0	1	5	40	41	-4	6	5	31	33

OBSERVED AND CALCULATED STRUCTURE FACTORS FOR SIMPSONITE -- LS #3 (FINAL)

H	K	L	FO	FC		H	K	L	FO	FC		H	K	L	FO	FC		H	K	L	FO	FC		H	K	L	FO	FC
-3	6	5	25	22		-1	1	6	23	21		-3	2	6	76	72		0	2	6	40	39		-2	3	6	24	24
-2	6	5	27	28		0	1	6	23	21		-2	2	6	35	32		1	2	6	23	18		-1	3	6	71	67
-1	6	5	20	19		1	1	6	39	35		-1	2	6	46	44		-3	3	6	27	21		0	3	6	24	23
0	0	6	73	73																											

Observed and Calculated Structure Factors for ALUMOTANTITE

H	K	L	PO	PC	H	K	L	PO	PC	H	K	L	PO	PC	H	K	L	PO	PC
0	0	2	210	228	1	1	8	55	59	1	10	3*	6	1	2	5	2*	5	6
0	0	8	161	177	1	1	5	129	128	1	10	8*	6	3	2	5	3*	5	2
0	0	6	155	155	1	1	6	88	82	1	10	5*	5	2	2	5	8*	7	3
0	2	0	93	107	1	1	7	90	89	1	11	0	103	95	2	5	5*	8	1
0	2	1	173	187	1	2	1*	5	0	1	11	1	147	188	2	5	6*	6	1
0	2	2	99	99	1	2	2*	5	1	1	11	2	89	90	2	6	0	168	170
0	2	3	141	189	1	2	3*	6	3	1	11	3	131	127	2	6	1	12	6
0	2	8	63	65	1	2	8*	6	2	1	11	8	78	75	2	6	2	152	156
0	2	5	108	109	1	2	5*	6	3	1	11	5	101	96	2	6	3	14	3
0	2	6	51	51	1	2	6*	5	3	1	12	1	25	25	2	6	8	128	128
0	2	7	75	71	1	2	7*	6	0	1	12	2*	9	8	2	6	5*	11	6
0	4	0	113	111	1	3	0	247	258	1	12	3*	2	1	2	6	6	96	91
0	8	1	197	208	1	3	1	25	28	1	12	8*	6	8	2	7	1*	5	3
0	4	2	96	105	1	3	2	208	226	1	12	5	15	18	2	7	2*	2	8
0	8	3	219	282	1	3	3	26	24	1	13	0	50	86	2	7	3*	6	2
0	8	8	78	77	1	3	8	167	170	1	13	1	114	118	2	7	4*	7	3
0	8	5	123	122	1	3	5	13	11	1	13	2	39	81	2	7	5*	7	3
0	8	6	53	53	1	3	6	117	117	1	13	3	101	99	2	7	6*	5	1
0	8	7	30	88	1	3	7*	7	8	1	13	8	37	35	2	8	0	82	83
0	6	0	180	198	1	4	1	72	68	1	14	1*	6	8	2	8	1	137	142
0	6	1	11	7	1	8	2*	8	3	1	14	2*	6	2	2	8	2	135	131
0	6	2	156	175	1	8	3*	8	3	1	18	3*	6	2	2	8	3	127	128
0	6	3	13	7	1	8	8*	6	2	1	18	8*	6	1	2	8	4	103	100
0	6	4	139	132	1	8	5	23	21	1	15	0	138	137	2	8	5	96	94
0	6	5*	6	1	1	8	6*	6	0	1	15	1	17	19	2	8	6	52	49
0	6	6	135	101	1	5	0	132	131	1	15	2	131	126	2	9	1*	6	8
0	8	0	196	189	1	5	1	149	157	1	15	3	18	15	2	9	2*	8	3
0	8	1	152	168	1	5	2	113	122	1	15	1*	6	5	2	9	3*	6	0
0	8	2	98	101	1	5	3	114	123	1	16	2	16	16	2	9	4*	4	8
0	8	3	135	131	1	5	8	94	94	2	0	0	205	187	2	9	5*	8	3
0	8	8	37	86	1	5	5	99	97	2	0	2	262	268	2	10	0	75	73
0	8	5	111	105	1	5	6	66	68	2	0	8	190	189	2	10	1	122	125
0	8	6	35	88	1	6	1*	3	8	2	0	6	102	108	2	10	2	72	74
0	10	0	97	89	1	6	2*	7	3	2	1	1*	5	7	2	10	3	104	107
0	10	1	147	132	1	6	3*	5	8	2	1	2*	6	6	2	10	4	62	56
0	10	2	77	74	1	6	4*	8	0	2	1	3*	5	2	2	10	5	90	86
0	10	3	132	119	1	6	5*	6	1	2	1	8*	1	5	2	11	1*	6	3
0	10	8	65	65	1	6	6*	6	2	2	1	5*	6	3	2	11	2*	5	2
0	10	5	97	92	1	7	0	117	120	2	1	6*	5	2	2	11	3*	6	1
0	12	0	158	188	1	7	1	171	185	2	2	0	106	94	2	11	4*	8	1
0	12	1	26	20	1	7	2	95	103	2	2	1	183	168	2	11	5*	6	1
0	12	2	151	188	1	7	3	154	151	2	2	2	88	80	2	12	0	143	149
0	12	3	54	54	1	7	8	87	81	2	2	3	130	131	2	12	1	43	44
0	12	8	131	121	1	7	5	119	114	2	2	8	68	67	2	12	2	130	131
0	12	5	13	11	1	7	6	62	59	2	2	5	96	97	2	12	3*	9	6
0	14	0	77	71	1	8	1*	5	5	2	2	6	53	47	2	12	4	111	110
0	14	1	117	110	1	8	2	32	33	2	3	1*	7	9	2	13	1*	4	8
0	14	2	59	64	1	8	3*	6	0	2	3	2*	5	6	2	13	2*	6	3
0	14	3	107	102	1	8	8	26	24	2	3	3*	3	2	2	13	3*	8	1
0	18	8	50	53	1	8	5*	6	1	2	3	8*	1	2	2	13	4*	2	2
0	16	0	15	12	1	8	6*	6	2	2	3	5*	6	1	2	14	0	60	62
0	16	1	117	114	1	9	0	144	153	2	3	6*	6	2	2	14	1	102	105
0	16	2	38	80	1	9	1	27	29	2	8	0	115	105	2	14	2	58	61
1	0	2	72	68	1	9	2	147	147	2	8	1	237	240	2	18	3	89	89
1	0	4	31	34	1	9	3	21	20	2	8	2	87	88	2	15	1*	7	1
1	0	6*	2	3	1	9	4	121	118	2	4	3	127	136	2	15	2*	6	2
1	1	0	95	81	1	9	5	20	17	2	4	4	70	69	2	16	0	47	48
1	1	1	252	237	1	9	6	91	88	2	8	5	140	142	2	16	1	98	102
1	1	2	86	84	1	10	1*	6	1	2	8	6	53	52	3	0	2	35	33
1	1	3	155	176	1	10	2*	7	1	2	5	1*	9	8	3	0	8	25	24

Observed and Calculated Structure Factors for ALUMOTANTITE

H	K	L	FO	FC	H	K	L	FO	FC	H	K	L	FO	FC	H	K	L	FO	FC
3	0	6*	6	1	3	9	1	20	18	4	5	1*	8	8	5	3	2	131	130
3	1	0	90	81	3	9	2	115	119	4	5	2*	10	7	5	3	3	19	17
3	1	1	180	169	3	9	3	26	24	4	5	3*	6	3	5	3	4	110	112
3	1	2	61	56	3	9	4	100	103	4	5	4*	8	3	5	4	1	18	15
3	1	3	158	153	3	9	5	12	13	4	5	5*	7	3	5	4	2*	6	1
3	1	4	88	51	3	10	1*	5	1	4	6	0	131	131	5	4	3*	4	1
3	1	5	103	110	3	10	2*	6	1	4	6	1	13	3	5	4	4*	5	1
3	1	6	85	82	3	10	3*	6	1	4	6	2	120	122	5	5	0	68	67
3	2	1*	5	0	3	10	4*	6	2	4	6	3*	7	8	5	5	1	95	94
3	2	2*	6	0	3	11	0	78	86	4	6	4	101	101	5	5	2	73	73
3	2	3*	6	2	3	11	1	115	125	4	6	5*	6	1	5	5	3	76	73
3	2	4*	6	1	3	11	2	72	77	4	7	1*	5	4	5	5	4	61	64
3	2	5*	6	0	3	11	3	100	104	4	7	2*	5	5	5	6	1*	6	1
3	2	6*	6	2	3	11	4	62	60	4	7	3*	2	2	5	6	2*	4	0
3	3	0	210	205	3	12	1	17	18	4	7	4*	11	5	5	6	3*	5	0
3	3	1	27	24	3	12	2*	3	8	4	7	5*	6	6	5	6	4*	4	0
3	3	2	174	177	3	12	3*	7	1	4	8	0	114	116	5	7	0	71	74
3	3	3	17	9	3	12	4*	6	3	4	8	1	107	114	5	7	1	107	113
3	3	4	135	136	3	13	0	32	34	4	8	2	73	76	5	7	2	56	57
3	3	5	15	15	3	13	1	89	97	4	8	3	94	96	5	7	3	95	91
3	3	6	104	108	3	13	2	36	39	4	8	4	65	64	5	8	1*	3	2
3	4	1	38	35	3	13	3	88	94	4	9	1*	6	5	5	8	2	13	13
3	4	2*	6	2	3	14	1*	6	3	4	9	2*	3	5	5	8	3*	3	0
3	4	3*	6	1	3	14	2*	6	1	4	9	3*	3	1	5	9	0	89	92
3	4	4*	6	1	3	15	0	107	115	4	9	4*	1	5	5	9	1	20	20
3	4	5	14	15	3	15	1	13	14	4	10	0	61	63	5	9	2	97	100
3	4	6*	6	0	4	0	0	216	215	4	10	1	92	99	5	9	3	12	7
3	5	0	115	115	4	0	2	159	156	4	10	2	52	55	5	10	1*	7	0
3	5	1	120	120	4	0	4	124	128	4	10	3	91	90	5	10	2*	6	1
3	5	2	95	95	4	1	1*	5	7	4	10	4	48	47	5	11	0	57	58
3	5	3	113	113	4	1	2*	9	7	4	11	1*	10	5	5	11	1	85	90
3	5	4	72	74	4	1	3*	6	1	4	11	2*	2	4	6	0	0	107	110
3	5	5	79	78	4	1	4*	7	6	4	11	3*	6	1	6	0	2	125	122
3	5	6	51	61	4	1	5*	5	7	4	12	0	101	111	6	1	1*	6	6
3	6	1*	4	2	4	2	0	70	66	4	12	1	17	16	6	1	2*	9	5
3	6	2*	5	1	4	2	1	121	118	4	12	2	105	111	6	1	3*	4	2
3	6	3*	6	2	4	2	2	66	63	4	13	1*	6	6	6	2	0	50	48
3	6	4*	6	0	4	2	3	103	102	4	13	2*	6	8	6	2	1	84	82
3	6	5*	6	0	4	2	4	52	51	5	0	2	18	16	6	2	2	47	44
3	7	0	84	86	4	2	5	83	82	5	0	8	16	13	6	2	3	79	75
3	7	1	146	146	4	3	1*	9	9	5	1	0	42	40	6	3	1	12	7
3	7	2	89	91	4	3	2*	8	7	5	1	1	121	126	6	3	2*	6	6
3	7	3	128	133	4	3	3*	6	2	5	1	2	54	52	6	3	3*	6	2
3	7	4	69	69	4	3	4*	7	2	5	1	3	103	99	6	4	0	54	51
3	7	5	98	101	4	3	5*	6	2	5	1	4	43	40	6	4	1	113	111
3	8	1*	6	3	4	4	0	73	71	5	2	1*	5	0	6	4	2	46	47
3	8	2	22	22	4	4	1	144	141	5	2	2*	3	0	6	5	1*	6	7
3	8	3*	7	0	4	4	2	71	69	5	2	3*	5	0	6	5	2*	1	6
3	8	4	17	19	4	4	3	155	155	5	2	4*	6	1	6	6	0	94	93
3	8	5*	6	2	4	4	4	56	56	5	3	0	130	129	6	6	1*	8	2
3	9	0	136	140	4	4	5	91	93	5	3	1	12	8	6	6	2	90	88

OBSERVED AND CALCULATED STRUCTURE FACTORS FOR   DISORDERED WODGINITE. Alabama

H	K	L	FO	FC	H	K	L	FO	FC	H	K	L	FO	FC	H	K	L	FO	FC	H	K	L	FO	FC
2	0	0	142	131	7	5	0	17	15	2	12	0	50	51	-3	3	1	28	12	0	6	1	25	20
4	0	0	491	474	9	5	0	22	22	4	12	0	249	246	-1	3	1	37	14	2	6	1	43	28
6	0	0	73	88	11	5	0	13	8	6	12	0	44	43	1	3	1	39	15	4	6	1	19	4
8	0	0	382	408	0	6	0	91	95	8	12	0	160	156	3	3	1	25	16	6	6	1	17	7
10	0	0	52	51	2	6	0	524	538	7	13	0	15	4	5	3	1	16	7	8	6	1	24	24
12	0	0	161	169	4	6	0	83	92	2	14	0	89	77	7	3	1	21	13	10	6	1	15	20
1	1	0	46	28	6	6	0	363	364	6	14	0	69	60	-12	4	1	165	152	-11	7	1	14	14
3	1	0	34	31	8	6	0	52	54	1	15	0	18	16	-10	4	1	19	22	-9	7	1	15	20
5	1	0	22	10	10	6	0	226	221	0	16	0	80	77	-8	4	1	257	258	-7	7	1	26	30
11	1	0	15	17	12	6	0	37	34	-13	1	1	17	14	-6	4	1	123	121	-5	7	1	38	32
0	2	0	64	59	1	7	0	15	11	-9	1	1	23	28	-4	4	1	506	496	-3	7	1	43	42
2	2	0	416	371	0	8	0	294	280	-7	1	1	30	28	-2	4	1	74	44	-1	7	1	40	46
4	2	0	49	49	2	8	0	19	21	-5	1	1	44	41	0	4	1	509	461	1	7	1	39	36
6	2	0	200	199	4	8	0	114	109	-3	1	1	46	43	2	4	1	230	207	3	7	1	39	37
8	2	0	26	25	6	8	0	14	15	-1	1	1	59	56	4	4	1	445	489	5	7	1	31	34
10	2	0	133	140	8	8	0	142	135	1	1	1	53	57	6	4	1	30	12	7	7	1	23	28
12	2	0	19	20	10	8	0	17	9	3	1	1	36	41	8	4	1	245	243	9	7	1	15	19
1	3	0	68	60	1	9	0	33	37	5	1	1	35	40	10	4	1	58	56	11	7	1	19	17
3	3	0	49	46	3	9	0	30	30	7	1	1	21	25	12	4	1	153	138	-10	8	1	47	41
5	3	0	42	43	5	9	0	16	17	9	1	1	22	27	-11	5	1	20	17	-8	8	1	225	222
7	3	0	28	32	7	9	0	21	20	11	1	1	16	14	-7	5	1	19	23	-6	8	1	52	54
9	3	0	22	24	9	9	0	20	18	-12	2	1	23	24	-5	5	1	27	26	-4	8	1	329	332
11	3	0	18	17	0	10	0	49	52	-10	2	1	216	221	-3	5	1	40	42	-2	8	1	93	98
13	3	0	12	15	2	10	0	184	187	-8	2	1	78	82	-1	5	1	25	29	0	8	1	381	393
0	4	0	340	330	4	10	0	45	49	-6	2	1	412	414	1	5	1	30	25	2	8	1	64	64
2	4	0	61	69	6	10	0	155	159	-4	2	1	76	68	3	5	1	25	28	4	8	1	316	319
4	4	0	310	299	8	10	0	35	36	0	2	1	138	120	5	5	1	20	18	6	8	1	67	66
6	4	0	52	53	10	10	0	82	77	2	2	1	575	577	7	5	1	27	31	8	8	1	191	214
8	4	0	162	169	1	11	0	23	29	4	2	1	108	107	-12	6	1	19	18	10	8	1	28	34
10	4	0	25	30	3	11	0	24	26	6	2	1	420	404	-10	6	1	15	15	-9	9	1	18	14
12	4	0	92	89	5	11	0	12	19	8	2	1	49	49	-8	6	1	16	7	-5	9	1	15	21
1	5	0	31	34	7	11	0	18	21	10	2	1	204	200	-6	6	1	26	9	-1	9	1	16	17
3	5	0	30	36	9	11	0	16	11	12	2	1	39	37	-4	6	1	38	40	1	9	1	21	26
5	5	0	33	35	0	12	0	256	254	-7	3	1	17	15	-2	6	1	46	38	3	9	1	16	17

OBSERVED AND CALCULATED STRUCTURE FACTORS FOR   DISORDERED WODGINITE. Alabama

H	K	L	FO	FC	H	K	L	FO	FC	H	K	L	FO	FC	H	K	L	FO	FC	H	K	L	FO	FC
9	9	1	19	16	-1	15	1	18	13	6	2	2	203	196	3	5	2	19	20	-8	10	2	46	43
-10	10	1	140	127	1	15	1	15	11	8	2	2	41	42	5	5	2	24	33	-6	10	2	131	129
-8	10	1	39	34	3	15	1	15	13	10	2	2	106	102	9	5	2	16	19	-4	10	2	32	34
-6	10	1	214	207	0	16	1	137	119	-11	3	2	23	17	-10	6	2	197	200	-2	10	2	172	178
-4	10	1	38	37	-12	0	2	190	183	-9	3	2	28	27	-8	6	2	48	49	0	10	2	54	56
-2	10	1	273	274	-10	0	2	71	70	-7	3	2	28	28	-6	6	2	341	356	2	10	2	173	173
0	10	1	49	48	-8	0	2	319	320	-5	3	2	37	40	-4	6	2	90	91	4	10	2	48	49
2	10	1	251	264	-6	0	2	42	33	-3	3	2	51	48	-2	6	2	465	456	6	10	2	119	123
4	10	1	43	40	-4	0	2	601	598	-1	3	2	48	45	0	6	2	97	91	8	10	2	24	21
6	10	1	204	204	-2	0	2	256	238	1	3	2	44	42	2	6	2	447	455	-5	11	2	19	18
8	10	1	25	27	0	0	2	577	562	3	3	2	42	47	4	6	2	69	70	-3	11	2	19	25
10	10	1	112	116	2	0	2	65	24	5	3	2	32	38	6	6	2	281	318	-1	11	2	18	23
-9	11	1	13	6	4	0	2	580	562	7	3	2	30	27	8	6	2	53	59	1	11	2	18	22
-5	11	1	20	21	6	0	2	141	136	9	3	2	26	23	10	6	2	181	181	3	11	2	27	29
5	11	1	17	17	8	0	2	298	285	11	3	2	16	13	5	7	2	15	6	7	11	2	18	17
-8	12	1	27	25	10	0	2	26	28	-12	4	2	91	87	-10	8	2	26	23	9	11	2	22	10
-2	12	1	50	50	12	0	2	173	160	-10	4	2	33	30	-8	8	2	88	91	-8	12	2	179	158
0	12	1	41	44	-11	1	2	18	14	-8	4	2	160	165	-6	8	2	16	15	-6	12	2	48	44
4	12	1	30	10	-7	1	2	24	22	-6	4	2	53	52	-4	8	2	183	178	-4	12	2	209	211
6	12	1	34	34	-5	1	2	17	19	-4	4	2	259	246	-2	8	2	70	70	-2	12	2	40	41
8	12	1	26	24	-3	1	2	18	23	-2	4	2	53	54	0	8	2	148	141	0	12	2	238	249
-5	13	1	22	22	-1	1	2	17	19	0	4	2	315	306	2	8	2	35	33	2	12	2	63	58
-3	13	1	27	29	1	1	2	22	15	2	4	2	71	74	4	8	2	164	166	4	12	2	207	201
-1	13	1	26	22	3	1	2	17	21	4	4	2	217	234	6	8	2	42	44	6	12	2	31	30
1	13	1	18	18	7	1	2	17	25	6	4	2	37	33	8	8	2	76	82	8	12	2	145	141
5	13	1	18	21	11	1	2	19	11	8	4	2	145	147	-9	9	2	14	14	5	13	2	15	9
7	13	1	17	19	-12	2	2	24	25	10	4	2	33	28	-7	9	2	23	29	-2	14	2	73	63
-6	14	1	150	138	-10	2	2	105	108	12	4	2	83	74	-5	9	2	25	24	2	14	2	74	71
-4	14	1	50	46	-6	2	2	230	224	-9	5	2	16	20	-3	9	2	25	23	-3	15	2	21	12
-2	14	1	194	181	-4	2	2	75	71	-7	5	2	18	17	-1	9	2	30	23	1	15	2	19	16
0	14	1	49	45	-2	2	2	281	273	-5	5	2	26	30	1	9	2	31	32	3	15	2	15	13
2	14	1	179	176	0	2	2	48	37	-3	5	2	32	30	3	9	2	31	30	-11	1	3	15	13
4	14	1	38	35	2	2	2	275	280	-1	5	2	36	37	5	9	2	24	24	-9	1	3	21	24
6	14	1	132	132	4	2	2	31	26	1	5	2	31	31	7	9	2	14	15	-7	1	3	20	25

OBSERVED AND CALCULATED STRUCTURE FACTORS FOR   DISORDERED WODGINITE. Alabama

H	K	L	FO	FC	H	K	L	FO	FC	H	K	L	FO	FC	H	K	L	FO	FC	H	K	L	FO	FC
-5	1	3	38	36	-11	5	3	18	15	2	8	3	63	69	0	14	3	40	38	-1	3	4	38	41
-3	1	3	25	34	-9	5	3	14	13	4	8	3	242	262	2	14	3	151	143	1	3	4	31	33
-1	1	3	33	35	-7	5	3	21	24	6	8	3	48	50	-10	0	4	32	34	3	3	4	22	25
1	1	3	39	44	-5	5	3	25	27	8	8	3	144	157	-8	0	4	255	248	5	3	4	23	27
3	1	3	31	36	-1	5	3	29	32	10	8	3	31	38	-6	0	4	108	102	7	3	4	22	21
5	1	3	29	32	1	5	3	28	24	-9	9	3	15	14	-4	0	4	406	393	-10	4	4	22	27
9	1	3	22	19	3	5	3	25	28	-3	9	3	18	13	-2	0	4	49	35	-8	4	4	118	125
11	1	3	12	10	7	5	3	13	14	3	9	3	16	13	0	0	4	366	380	-6	4	4	29	37
-12	2	3	34	34	9	5	3	14	9	9	9	3	18	9	2	0	4	123	135	-4	4	4	168	178
-10	2	3	200	208	11	5	3	18	17	-8	10	3	28	25	4	0	4	350	359	-2	4	4	54	55
-8	2	3	47	55	-8	6	3	17	13	-6	10	3	168	172	6	0	4	32	31	0	4	4	200	197
-6	2	3	290	305	-6	6	3	40	36	-4	10	3	39	39	8	0	4	202	195	2	4	4	42	40
-4	2	3	79	83	-4	6	3	18	17	-2	10	3	218	223	10	0	4	53	48	4	4	4	150	158
-2	2	3	442	453	0	6	3	21	14	0	10	3	38	38	-11	1	4	16	13	6	4	4	36	38
0	2	3	97	89	2	6	3	32	20	2	10	3	215	213	-9	1	4	15	9	8	4	4	105	102
2	2	3	397	416	4	6	3	18	14	4	10	3	38	36	-5	1	4	19	7	10	4	4	23	18
4	2	3	70	78	6	6	3	24	23	6	10	3	146	154	-3	1	4	16	22	-7	5	4	14	12
6	2	3	276	279	10	6	3	14	1	8	10	3	19	21	3	1	4	16	19	-1	5	4	23	24
8	2	3	49	45	-9	7	3	15	17	-7	11	3	15	2	7	1	4	17	17	1	5	4	27	28
10	2	3	181	167	-7	7	3	28	22	-3	11	3	13	13	-10	2	4	87	89	3	5	4	15	15
12	2	3	32	28	-5	7	3	31	31	5	11	3	16	9	-8	2	4	42	40	9	5	4	20	17
-7	3	3	18	18	-3	7	3	25	30	-6	12	3	16	15	-6	2	4	151	160	-10	6	4	159	163
3	3	3	16	21	-1	7	3	26	33	-4	12	3	43	47	-4	2	4	19	19	-8	6	4	52	58
-10	4	3	41	37	1	7	3	36	37	-2	12	3	17	13	-2	2	4	189	183	-6	6	4	247	263
-8	4	3	253	260	3	7	3	26	31	2	12	3	21	17	0	2	4	50	47	-4	6	4	52	58
-6	4	3	50	55	5	7	3	17	20	4	12	3	44	33	2	2	4	177	184	-2	6	4	296	321
-4	4	3	283	288	7	7	3	20	24	6	12	3	19	14	4	2	4	30	33	0	6	4	73	76
-2	4	3	73	76	9	7	3	16	14	-5	13	3	20	13	6	2	4	130	133	2	6	4	295	304
0	4	3	446	480	-10	8	3	36	35	-3	13	3	21	23	8	2	4	14	16	4	6	4	64	60
2	4	3	75	71	-8	8	3	178	188	-1	13	3	23	23	10	2	4	79	67	6	6	4	215	224
4	4	3	243	251	-6	8	3	55	59	1	13	3	23	21	-9	3	4	20	20	8	6	4	36	38
6	4	3	46	50	-4	8	3	273	281	3	13	3	15	15	-7	3	4	19	26	-3	8	4	70	74
8	4	3	232	226	-2	8	3	67	66	5	13	3	16	14	-5	3	4	26	23	-6	8	4	37	35
10	4	3	34	30	0	8	3	283	291	-2	14	3	150	144	-3	3	4	30	30	-4	8	4	121	125

OBSERVED AND CALCULATED STRUCTURE FACTORS FOR   DISORDERED WODGINITE. Alabama

H	K	L	FO	FC	H	K	L	FO	FC	H	K	L	FO	FC	H	K	L	FO	FC	H	K	L	FO	FC
0	8	4	102	104	-9	1	5	21	17	-7	5	5	20	18	-4	10	5	29	32	5	3	6	13	13
2	8	4	44	44	-7	1	5	18	18	-5	5	5	20	18	-2	10	5	152	147	-6	4	6	28	30
4	8	4	112	116	-5	1	5	24	24	-1	5	5	14	17	0	10	5	27	32	-4	4	6	117	110
6	8	4	14	7	-3	1	5	31	28	1	5	5	15	19	2	10	5	142	141	-2	4	6	32	32
8	8	4	56	57	-1	1	5	20	25	3	5	5	16	15	4	10	5	27	24	0	4	6	120	111
-7	9	4	16	16	1	1	5	21	23	5	5	5	17	13	-6	0	6	49	48	2	4	6	33	32
-5	9	4	16	20	3	1	5	19	21	7	5	5	20	17	-4	0	6	209	203	4	4	6	104	95
-3	9	4	29	28	5	1	5	22	24	-8	6	5	18	19	-2	0	6	62	62	6	4	6	26	22
-1	9	4	20	18	9	1	5	18	13	-6	6	5	19	5	0	0	6	266	259	-5	5	6	14	13
1	9	4	21	20	-8	2	5	38	35	-2	6	5	22	17	2	0	6	50	56	-3	5	6	20	13
3	9	4	19	21	-6	2	5	232	225	0	6	5	17	19	4	0	6	158	168	1	5	6	18	16
5	9	4	18	15	-4	2	5	73	71	2	6	5	20	11	6	0	6	38	39	3	5	6	13	12
-6	10	4	101	100	-2	2	5	269	262	-7	7	5	17	17	-7	1	6	17	16	5	5	6	15	14
-4	10	4	46	46	0	2	5	59	59	-5	7	5	18	19	-1	1	6	14	11	-4	6	6	52	48
-2	10	4	131	135	2	2	5	244	252	-3	7	5	23	24	1	1	6	13	7	-2	6	6	210	199
0	10	4	34	37	4	2	5	47	52	-1	7	5	21	23	7	1	6	13	5	0	6	6	48	49
2	10	4	117	120	6	2	5	177	178	1	7	5	18	17	-6	2	6	86	83	2	6	6	192	179
4	10	4	35	32	8	2	5	39	38	3	7	5	27	25	-4	2	6	25	24	4	6	6	45	42
6	10	4	87	88	-7	3	5	14	2	5	7	5	18	17	-2	2	6	124	121	-2	8	6	13	14
-3	11	4	15	17	-8	4	5	154	156	7	7	5	19	13	0	2	6	29	27	0	8	6	101	91
-1	11	4	24	21	-6	4	5	26	28	-6	8	5	41	45	2	2	6	100	100	2	8	6	15	12
1	11	4	15	15	-4	4	5	243	243	-4	8	5	170	181	6	2	6	78	73	-3	1	7	18	15
3	11	4	16	16	-2	4	5	84	82	-2	8	5	46	49	-7	3	6	16	15	-1	1	7	18	17
5	11	4	15	14	0	4	5	230	224	0	8	5	201	202	-5	3	6	24	22	1	1	7	16	16
-4	12	4	166	167	2	4	5	24	22	2	8	5	55	53	-3	3	6	23	19	-2	2	7	160	145
-2	12	4	49	48	4	4	5	211	211	4	8	5	167	158	-1	3	6	22	20	0	2	7	45	44
0	12	4	184	181	6	4	5	53	57	6	8	5	41	32	1	3	6	25	24	2	2	7	149	136
2	12	4	33	32	8	4	5	125	119	5	9	5	17	12	3	3	6	23	21	0	4	7	142	126
4	12	4	151	147																				

OBSERVED AND CALCULATED STRUCTURE FACTORS FOR BICROLITE (SMP-4), Tanco Pegmatite

H	K	L	FO	FC		H	K	L	FO	FC		H	K	L	FO	FC		H	K	L	FO	FC		H	K	L	FO	FC
1	1	1	467	474		0	6	6	80	79		4	6	8	22	13		7	9	9	113	113		3	7	11	132	134
2	2	2	1127	1128		2	6	6	650	656		6	6	8	25	4		0	2	10	40	37		5	7	11	139	140
1	1	3	439	441		4	6	6	69	71		0	8	8	461	460		2	2	10	519	523		1	9	11	131	130
1	3	3	257	254		6	6	6	514	526		4	8	8	449	450		2	4	10	27	26		3	9	11	124	113
3	3	3	506	500		1	1	7	279	277		6	8	8	32	17		4	4	10	23	9		0	0	12	337	335
0	0	4	861	855		1	3	7	320	324		8	8	8	301	302		0	6	10	70	75		2	2	12	24	16
2	2	4	71	56		3	3	7	188	192		1	1	9	239	239		2	6	10	441	436		0	4	12	414	411
0	4	4	1023	1032		1	5	7	244	249		1	3	9	249	256		4	6	10	31	21		4	4	12	355	351
2	4	4	26	13		3	5	7	213	217		3	3	9	174	173		6	6	10	366	363		4	6	12	31	10
4	4	4	765	765		5	5	7	227	233		1	5	9	196	202		0	10	10	33	22		6	6	12	33	25
1	1	5	254	233		1	7	7	194	198		3	5	9	186	191		2	10	10	329	311		0	8	12	314	300
1	3	5	331	317		3	7	7	254	254		5	5	9	195	193		4	10	10	41	45		1	1	13	163	165
3	3	5	343	357		5	7	7	200	203		1	7	9	173	170		1	1	11	155	151		1	3	13	130	124
1	5	5	353	349		7	7	7	146	143		3	7	9	203	207		1	3	11	177	183		3	3	13	177	174
3	5	5	253	263		0	0	8	765	769		5	7	9	166	163		3	3	11	197	196		1	5	13	134	131
5	5	5	199	202		2	2	8	61	67		7	7	9	125	129		1	5	11	193	185		3	5	13	145	143
0	2	6	90	87		0	4	8	602	615		1	9	9	149	151		3	5	11	162	161		2	2	14	335	309
2	2	6	816	931		2	4	8	37	14		3	9	9	155	163		5	5	11	130	131		2	4	14	23	10
2	4	6	70	13		4	4	8	551	565		5	9	9	136	143		1	7	11	151	149						

OBSERVED AND CALCULATED STRUCTURE FACTORS FOR CESSTIBTANTITE. Tanco Pegm.

H	K	L	FO	FC	H	K	L	FO	FC	H	K	L	FO	FC	H	K	L	FO	FC	H	K	L	FO	FC
1	1	1	375	415	2	6	6	698	718	0	8	8	531	541	2	4	10	49	48	1	9	11	188	195
0	2	2	75	55	4	6	6	131	129	2	8	8	43	62	4	4	10	39	14	3	9	11	170	181
2	2	2	1191	1201	6	6	6	608	604	4	8	8	514	515	0	6	10	111	122	0	0	12	430	438
1	1	3	455	455	1	1	7	288	286	6	8	8	57	51	2	6	10	494	510	2	2	12	29	4
1	3	3	198	212	1	3	7	392	368	8	8	8	402	378	4	6	10	31	9	0	4	12	489	495
3	3	3	576	549	3	3	7	213	212	1	1	9	274	257	6	6	10	458	437	4	4	12	431	413
0	0	4	892	892	1	5	7	279	287	1	3	9	320	314	2	8	10	27	15	2	6	12	32	7
0	4	4	1127	1124	3	5	7	243	240	3	3	9	206	197	4	8	10	27	32	4	6	12	27	33
2	4	4	47	32	5	5	7	275	264	1	5	9	262	269	6	8	10	57	62	6	6	12	58	57
4	4	4	819	823	1	7	7	215	232	3	5	9	216	218	0	10	10	42	17	0	8	12	372	364
1	1	5	330	322	3	7	7	319	310	5	5	9	256	245	2	10	10	385	383	2	8	12	36	50
1	3	5	300	299	5	7	7	264	257	1	7	9	216	217	4	10	10	66	83	1	1	13	217	225
3	3	5	409	395	7	7	7	200	207	3	7	9	269	270	1	1	11	235	234	1	3	13	175	180
1	5	5	369	352	0	0	8	852	861	5	7	9	227	233	1	3	11	228	227	3	3	13	237	233
3	5	5	313	312	2	2	8	69	49	7	7	9	177	181	3	3	11	266	257	1	5	13	171	181
5	5	5	278	259	0	4	8	655	668	1	9	9	172	190	1	5	11	246	243	3	5	13	192	206
0	2	6	154	147	2	4	8	42	42	3	9	9	224	238	3	5	11	219	220	5	5	13	181	175
2	2	6	923	906	4	4	8	636	643	5	9	9	184	204	5	5	11	180	196	1	7	13	193	200
2	4	6	31	34	2	6	8	25	23	7	9	9	158	164	1	7	11	189	207	0	2	14	31	21
4	4	6	37	31	4	6	8	35	36	0	2	10	50	35	3	7	11	168	188	2	2	14	409	380
0	6	6	92	80	6	6	8	38	8	2	2	10	611	595	5	7	11	179	196					

OBSERVED AND CALCULATED STRUCTURE FACTORS FOR   CESSTIBTANTITE (h,0-1) Kola Peninsula   PAGE   1

H	K	L	FO	FC		H	K	L	FO	FC		H	K	L	FO	FC		H	K	L	FO	FC		H	K	L	FO	FC
1	1	1	393	390		6	6	6	451	441		4	8	8	365	362		4	4	10	62	23		1	9	11	137	152
0	2	2	85	75		1	1	7	271	267		8	8	8	241	228		0	6	10	98	115		3	9	11	127	141
2	2	2	1126	1115		1	3	7	358	363		1	1	9	247	242		2	6	10	354	354		0	0	12	296	291
1	1	3	482	480		3	3	7	214	202		1	3	9	280	286		4	6	10	59	10		0	4	12	353	338
1	3	3	199	203		1	5	7	268	274		3	3	9	183	176		6	6	10	293	288		4	4	12	283	272
3	3	3	600	571		3	5	7	209	217		1	5	9	234	231		4	8	10	81	36		2	6	12	48	4
0	0	4	742	761		5	5	7	230	238		3	5	9	188	188		6	8	10	62	61		4	6	12	51	34
0	4	4	1023	1025		1	7	7	197	198		5	5	9	206	216		2	10	10	242	242		6	6	12	54	49
4	4	4	662	661		3	7	7	294	288		1	7	9	180	189		4	10	10	62	64		0	8	12	228	232
1	1	5	339	340		5	7	7	219	218		3	7	9	224	233		1	1	11	198	200		2	8	12	51	31
1	3	5	289	285		7	7	7	159	166		5	7	9	171	187		1	3	11	186	187		1	1	13	167	170
3	3	5	384	391		0	0	8	708	718		7	7	9	137	139		3	3	11	215	214		1	3	13	134	135
1	5	5	352	349		2	2	8	71	53		1	9	9	146	142		1	5	11	194	207		3	3	13	194	188
3	5	5	292	298		0	4	8	499	505		3	9	9	173	172		3	5	11	171	178		1	5	13	128	125
5	5	5	259	255		4	4	8	486	488		5	9	9	148	145		5	5	11	145	149		3	5	13	143	145
0	2	6	161	164		2	6	8	57	26		7	9	9	108	114		1	7	11	160	148		5	5	13	113	108
2	2	6	758	765		4	6	8	51	48		0	2	10	52	31		3	7	11	125	132		1	7	13	146	153
0	6	6	91	62		0	8	8	381	382		2	2	10	436	437		5	7	11	122	141		2	2	14	260	241
2	6	6	558	563		2	8	8	62	57		2	4	10	68	52		7	7	11	121	119		2	4	14	51	22
4	6	6	127	142																									